Detection of Higgs Bosons of the Minimal Supersymmetric Standard Model at Hadron Supercolliders

A DISSERTATION SUBMITTED TO THE GRADUATE DIVISION OF THE UNIVERSITY OF HAWAII IN PARTIAL FULFILLMENT OF THE REQUIREMENTS FOR THE DEGREE OF

DOCTOR OF PHILOSOPHY

IN

PHYSICS

MAY 1995

By

Michael Andrew Bisset

Dissertation Committee:

Xerxes R. Tata, Chairperson
James R. Gaines
Michael W. Peters
Sandip Pakvasa
Lawrence J. Wallen

Acknowledgements

To begin with, I would like to thank my boss, Xerxes Tata, for his infinite (well, almost infinite) patience in putting up with me over the years, as well as his guidance in all aspects of physics. I would also like to express my sincere thanks to Howard Baer for the tremendous amount of help he has given me during my research career. And also to Chung Kao, who has (politely) found more bugs in my computer programs than I'd care to mention, and thus saved me from screwing up even more things than I actually did. Among their many contributions to this work, Howie gave me the continuum ino production and ino to lepton branching ratio programs used in this work, and Chung sent me his SM background program which was incorporated into my analysis of the signals in Chapter 4. I am very grateful for these as well as the countless other assists and encouragements coming my way from Florida.

I feel *very* lucky to have taken courses from excellent instructors here at the University of Hawaii. Sandip Pakvasa suffered with me as his student in almost every course I took during my first two years here. When I was not baffling him with my slow-wittedness, Tom Weiler, Mike Peters, and Jim Gaines stepped in and shared some of the punishment. Then Xerxes got his turn with me, teaching me much of what I know about quantum field theory. I'd also like to thank Lenny Freed and John Stimson for giving excellent zoology courses I attended (while I should have been working) and Stephen Fleming for helping immensely in my Chinese language studies. They kept me from becoming more narrow-minded than I am. Professor Peters also deserves my thanks for suggesting many useful improvements to this work, and Professor Learned has my gratitude for looking out for the graduate students in this department, and Kalpana Kallianpur has my appreciation for keeping Xerxes from spending 24 hours a day in his office. I would also like to credit the many good students that I have taught in my classes over the years. I hope they learned from me a fraction of what I learned from them. I also thank Caroline Chong, Glenna

Sumiye, Margie Kidani, Josephine Asselin, and all the other secretaries and office workers who have tried to keep me out of trouble during my stay here.

I'd like to express my sincere thanks to the many gradute students who have truly made my stay in this department something I will always remember fondly. My fellow particle theory students, Andy Acker, Alakabha Datta, and John Sender, have been wonderful comrades from whom I have learned much, though not nearly as much as I should have. I am indebted to Andy Acker for giving me much of the software used in generating this thesis. John Sender also deserves very special thanks for dealing for me with some of the mysteries of PAW on short notice at the last minute. And I also thank Alakabha Datta for his role as part-time ambulance driver and full-time friend, and for not eating too much when we go out for Chinese food. I am also much obliged to the department's resident computer wizards, Ralph Becker-Szendy, John Flanagan, Gary McGrath, Antonio Querubin, John Sender, Diane Ibaraki, and especially Everett Chong for all the help they have offered me in dealing with these binary critters.

I'd also like to extend a great big mahalo to Cary Yoshikawa and Siu Lung (Roger) Kwok for befriending me when I first came to Hawaii and for remaining good friends ever since — and for helping me to acclimate to the Hawaiian style, and giddy giddy, and all that da kine stuff. I'd also like to say thanks to my friend and sometimes roommate Anupam Misra who is certainly one of the nicest persons I've ever had the pleasure to know. I'd also like to express my gratitude to Daniela Paluselli, Shinji Kondo, Jeff Bolesta, "Venki" Venkateswaran, John Balderston, John Flanagan, Everett Chong, Tony Querubin, Gargi Raina, Jörn Reise, Thomas Wöhrmann, Ralph Becker-Szendy, Linda Kelly, Jake Hudson, Den-ke Yang, Ri-ci Yu, Yaser Rehem, John Clem, and Wendy Asato for all the good times we've had, and all that we've gone through together. I am also beholden to Jake Hudson for giving me the space heater from Haleakela without which I would never have made it throught the frigid, bone-chilling nights studying in Watanabe Hall. I'd also like to thank the newer crop of students, Peruzan Dadbeh, Wenyan Ding, Patrick Greene, Dave Johnson, Atsuko Kibayashi, Derrick Kong, Jing Liu, Lingjun Pan,

Dean Takemori, and Chris Young for the fun we've had together; I wish you all the best of luck during your stay here. And finally to Wenhua Xu goes my very special thanks for a wonderful year I will always remember.

I'd also like to acknowledge Professors Gibor Basri and Ivan King of the Berkeley Astronomy Department who were helpful and supportive at a critical time. And also my old friend Richard Webb, I sometimes wonder what has become of you. My sister Lori also has my gratitude for her support, and for giving my parents something to occupy their thoughts with other than what their crazy son is doing.

This thesis is dedicated first and formost to my parents, Werdan and Esther Bisset, who have been an unceasing source of support throughout my life and my long collegiate career. They have always encouraged me to pursue whatever I wish to even if it must seem at times that I have gone completely nuts. For this I can never thank them enough. This thesis is dedicated second and almost as much to my boss, friend, and forever *Fearless Leader*, depicted on one of his more pedestrian days on the following page, whose energy and drive to study physics still amazes me. He can even outlast the Energizer Bunny. In fact, it is no exaggeration at all to say that he makes the Energizer Bunny look like a tranquilized slug. Lastly and leastly, this thesis is dedicated to all the other Arthur Dent-types like yours truly out there who can never quite find their towels.

This work was supported in part (sometimes grudgingly) by the U.S. Department of Energy.

Figure 0.0: **Da Boss:** Super*symmetry*man.
Superman's supersymmetric spartner.
Known by day as the not-always-so mild-mannered
Professor Xerxes R. Tata.

Abstract

The detectability of the various Higgs bosons of the Minimal Supersymmetric Standard Model (MSSM) at future supercolliders is investigated. Regions in the MSSM parameter space in which the well-known signals $H \rightarrow Z^0Z^0, Z^0Z^{0*} \rightarrow 4\ell$ ($\ell = e$ or μ) and $H \rightarrow \gamma\gamma$ should be observable at the LHC hadron supercollider are delineated. Regions excluded by the LEP e^+e^- collider along with those that can be probed using the upgraded LEP II collider are also mapped out. It is concluded that there is a 'hole' in the MSSM parameter space for higher values of $\tan\beta$ and $100\,\text{GeV} \lesssim m_{H_p} \lesssim 250\,\text{GeV}$ in which a Higgs boson will be detectable neither at the LHC nor at LEP II.

The sensitivity of this result to other MSSM input parameters, especially those affecting the masses of the charginos and neutralinos is examined. When Higgs boson decays to charginos and neutralinos are kinematically accessible, the rates for the signals mentioned above are reduced. However, new signal modes from Higgs bosons decaying into sparticles are found. The decay channel $H_p, H_h \rightarrow \widetilde{Z}_2\widetilde{Z}_2 \rightarrow 4\ell + \not{E}_T$ seems particularly promising. This signal along with other possible signals are studied to determine whether or not they might be able to fill in all or part of the 'hole.' Also described is the potential of these new signals, when added to the well-established signals previously noted, to enable the observation of two or more Higgs bosons for a given set of MSSM input parameters. Detection of more than one type of Higgs boson would clearly establish the existence of an extended Higgs sector as required by supersymmetry.

Contents

List of Tables

List of Figures

Pithy Quote

There is a theory which states that if ever anyone discovers exactly what the Universe is for and why it is here, it will instantly disappear and be replaced by something even more bizarre and inexplicable.

There is another which states that this has already happened.

Douglas Adams,
The Restaurant at the End of the Universe [1]

Chapter 0

The story so far [1]:
In the beginning the Universe was created.
This has made a lot of people very angry and been widely regarded as a bad move.

Many races believe that it was created by some sort of god, though the Jatravartid people of Viltvodle VI believe that the Universe was in fact sneezed out of the nose of a being called the Great Green Arkleseizure.

The Jatravartids, who live in perpetual fear of the time they call the Coming of the Great White Handkerchief, are small blue creatures with more than fifty arms each, who are therefore unique in being the only race in history to have invented the aerosol deodorant before the wheel.

However, the Great Green Arkleseizure Theory is not widely accepted outside Viltvodle VI and so, the Universe being the puzzling place it is, other explanations are constantly being sought.

This work purports to examine one small element which will hopefully someday be incorporated into an alternative theory. Whether this alternative theory, or some other theory not compatible with this work, or the Great Green Arkleseizure Theory is in fact the correct description of how and why the Universe works the way it does remains to be seen.
But we should have fun trying to find out!!! ☺

Chapter 1

Introduction

... skipping ahead a bit

The symmetry-breaking sector of modern gauge theories is probably the least understood, and therefore perhaps the most interesting facet of these models which heuristically at least describe the current experimental situation so very well. In the Weinberg-Salam-Glashow model [2,3,4], electroweak symmetry breaking results in the spontaneous breakdown of $SU(2)_L \times U(1)_Y$ into the $U(1)_{em}$ symmetry group of electrodynamics, with the concommitant acquisition of mass by the $W^{\pm}$ and Z^0 gauge bosons of the weak force. This is most parsimoniously facilitated by the introduction of a single $SU(2)_L$ doublet of complex spin zero fields which acquires a non-zero vacuum expectation value. The tell-tale residue of this so-called Standard Model (SM) dynamical mechanism is the existence of a single elementary spin-zero particle, since dubbed the Higgs boson, in the physical spectrum. The existence of a Higgs boson or of multiple Higgs bosons or of something that can perform the same function as Higgs bosons is essential in the formulation of an acceptable gauge theory of high energy physics. The search to discover such a particle or particles, and thus unravel the mystery that currently shrouds the symmetry-breaking sector, has become the high energy equivalent to the quest for the Holy Grail.

Thus, in the footsteps of such intrepid explorers as Monty Python and Indiana Jones, high energy physicists have embarked upon the planning and construction of supercollider accelerators which will hopefully provide us with the information needed to determine the components of the symmetry-breaking sector. Arguments from unitarity and perturbation theory [5,6] indicate that the SM Higgs boson must have a mass $\lesssim 1\,\mathrm{TeV}$. By demanding that the running Higgs boson self-coupling remains perturbative all the way up to the GUT scale, the Higgs boson mass can be even further restricted to $m_H \lesssim 220\,\mathrm{GeV}$ [7,8]. Thus a hadron supercollider

with a CMS energy in the tens of TeV might be expected to be able to provide conclusive evidence for the existence or non-existence of a Higgs boson if distinctive enough signatures for a Higgs boson can be found. The same is true for a e^+e^- supercollider with a CMS energy of $\sim$1 TeV. In fact, the latter machine would probably be superior to a hadron supercollider, but plans for an e^+e^- supercollider are much more sketchy and the ability to meet the technological requirements far less certain (see [9] for more information). It is the purpose of this work to evaluate the potential of a hadron supercollider, or, more specifically, the $\sqrt{s} = 14$ GeV LHC machine which is proposed for construction at CERN, to discover the Higgs bosons of the minimal supersymmetric extension of the Standard Model (MSSM).

An aspect of the SM Higgs sector which is disagreeable to many theorists is the need for fine-tuning. The radiative correction (δm_H^2) to the mass squared of the SM Higgs boson is quadradically divergent at the one-loop level as the internal momentum within the loop goes to infinity. This is in contrast to spin-$\frac{1}{2}$ and spin-1 particles whose masses are protected from such disastrously large corrections by chiral and gauge symmetries, respectively. There is no such symmetry known that protects the mass of a spin-0 Higgs boson, and thus a correction of order $\delta m_H^2 \sim g^2\Lambda^2$ should be expected. Here g is a dimensionless coupling constant which is extispiciously taken as $g^2 \sim \mathcal{O}(1)$ to avoid introducing a hierarchy among the dimensionless constants in the theory, and Λ is the energy scale at which the the loop momenta should be cut off due to the expression beyond this point of salient additional degrees of freedom or form factors not predicted by the SM. Thus, to lowest order in perturbation theory, the mass of a Higgs boson is expected to be

$$m_H^2 = m_0^2 + \delta m_H^2 \approx m_0^2 + g^2\Lambda^2 \tag{1.1}$$

where m_0 is the bare Higgs boson mass parameter in the Lagrangian. In grand unified models, $\Lambda \sim \mathcal{O}(M_{GUT} \approx 10^{15}\,\text{GeV})$, the scale at which GUT boson exchanges become significant, and in all reasonable models $\Lambda < \mathcal{O}(M_{Planck} \approx 10^{19}\,\text{GeV})$, since at this scale gravitational interactions not incorporated into the SM become comparable in strength to the SM gauge interactions. If we take $\Lambda \sim M_{GUT}$, then to get $m_H \lesssim 1$ TeV as is needed for agreement with the measured electroweak scale,

m_0 must be adjusted such that the two terms in Eqn. (1.1) cancel to within $\sim 10^{-24}\%$. This shocking cancellation must continue order by order in perturbation theory. While this exquisitely precise counter-balancing is not theoretically forbidden, it is generally regarded as a repellant feature of the SM picture of the electroweak symmetry-breaking sector, and a strong motivation to consider models with more elaborate symmetry-breaking mechanisms.

Several general avenues have been investigated for escaping the fine-tuning problem of the SM. It could be that perturbative expansion breaks down because the symmetry-breaking sector becomes strongly coupled at $\Lambda \lesssim 1\,\text{TeV}$. This may lead to the formation of resonance states at the TeV scale of new elementary fields added to the Lagrangian. Ideas like Technicolor [10,11] proceed from this supposition; however, to date it has not been possible to generate a satisfactory, phenomenologically acceptable model by this means. The other principal option considered to escape the SM fine-tuning dilemma is to keep the symmetry-breaking sector weakly-coupled but add new particles to the loops which offset the offensive SM contributions. The only known realization of a weakly-coupled electroweak symmetry-breaking sector without fine-tuning problems is weak scale low energy supersymmetry (reviewed in Refs. [12,13,14,15]) which will now be considered.

The proposed solution of supersymmetry (SUSY) to the fine-tuning problem is that for each SM boson (or fermion) contributing to a quadradically-divergent loop diagram there is a new fermion (or boson), the supersymmetric partner of the SM particle, which contributes in an opposing fashion. This is conceivable since bosonic and fermionic loops contribute to δm_H^2 with opposite signs. To attain the required cancellation in a plausible way, the masses and couplings of the SM fermions (bosons) and their boson (fermion) partners — known as sparticles — must be related. Such a symmetry is called a supersymmetry and differs from all other known symmetries, such as Lorentz space-time invariance or gauge invariances, which do not relate the properties of fermions to those of bosons in any way. In exact, unbroken SUSY, the particle and sparticle masses and couplings are exactly equal (aside from Clebsch-Gordon factors). This is immediately ruled out on phenomenological grounds by,

say, the failure to observe a boson with the same mass and other characteristics as an electron. However, SUSY need not remain unbroken to relieve the fine-tuning difficulty; all that is required is that the mass gap between the SM particles and their sparticle superpartners remain small enough so that $\delta m_H^2 \lesssim (1\,\mathrm{TeV})^2$; *i.e.*,

$$m^2_{sparticle} - m^2_{SMparticle} \lesssim (1\,\mathrm{TeV})^2 \quad . \tag{1.2}$$

Thus if SUSY is the answer to the fine-tuning dilemma, then sparticle masses are expected to be at or below the TeV scale, and within the range of the proposed supercolliders. The ways in which supersymmetry can be broken to produce this mass gap are restricted by requirements of gauge invariance and renormalizability. These are compiled in Ref. [16] and include chiral scalar mass terms (inputs are squark and slepton masses, $m_{\tilde{f}_L}$ and $m_{\tilde{f}_R}$), gaugino mass terms (inputs are soft SUSY-breaking gaugino masses, μ_1, μ_2, μ_3), and trilinear sfermionic interactions (inputs are the A-terms). From a phenomenological point of view, these terms are introduced *ad hoc* into the Minimal Supersymmetric Standard Model (MSSM) Lagrangian; the justification for this residing with some more encompassing theory manifest at a much higher energy scale (such as the GUT scale).

The MSSM is the simplest possible supersymmetric extension of the SM. For each SM chiral fermion (left- and right-handed quarks and leptons), f_i, there is a bosonic superpartner, $\tilde{f}_i$, with the same internal quantum numbers, except for the R-parity quantum number. Since all known spin-1 fundamental particles are force-propagating gauged bosons, it is preferable to make the superpartner sfermions (squarks and sleptons) have spin-0. The SM spin-1 gauge bosons have spin-$\frac{1}{2}$ Majorana fermion superpartners. For the color $SU(3)_C$ octet gluons, $\vec{g^\mu}$, there are eight gluinos, $\tilde{g}$'s; for the $SU(2)_L$ and $U(1)_Y$ gauge fields, $\vec{W}^\mu$ and B^μ, respectively, there are also corresponding spin-$\frac{1}{2}$ gauginos, $\vec{\tilde{\lambda}} = (\tilde{\lambda}_1, \tilde{\lambda}_2, \tilde{\lambda}_3)$ and $\tilde{\lambda}_0$, respectively. (And presumably for the spin-2 graviton there is a spin-$\frac{3}{2}$ gravitino though this will not be used in this work.) Again, all the sparticles listed have exactly the same internal quantum numbers as their SM partners save for the quantum number associated with R-parity. The full complement of particles comprising the MSSM particle spectrum is illustrated in Table 1.1.

Table 1.1:

Particle Content of the

Minimal Supersymmetric Standard Model

SM Particles	*Superpartner Sparticles*	with *EW Symmetry Breaking*
leptons $\begin{pmatrix}\nu_e\\ e^-\end{pmatrix}_L, e_R^-,$ $\begin{pmatrix}\nu_\mu\\ \mu^-\end{pmatrix}_L, \mu_R^-,$ $\begin{pmatrix}\nu_\tau\\ \tau^-\end{pmatrix}_L, \tau_R^-$	*sleptons* $\begin{pmatrix}\widetilde{\nu_{e_L}}\\ \widetilde{e_L^-}\end{pmatrix}, \widetilde{e_R^-},$ $\begin{pmatrix}\widetilde{\nu_{\mu_L}}\\ \widetilde{\mu_L^-}\end{pmatrix}, \widetilde{\mu_R^-},$ $\begin{pmatrix}\widetilde{\nu_{\tau_L}}\\ \widetilde{\tau_L^-}\end{pmatrix}, \widetilde{\tau_R^-}$	acquire mass via Yukawa interactions with Higgs bosons*
quarks $\begin{pmatrix}u\\ d\end{pmatrix}_L, u_R, d_R,$ $\begin{pmatrix}c\\ s\end{pmatrix}_L, c_R, s_R,$ $\begin{pmatrix}t\\ b\end{pmatrix}_L, t_R, b_R$	*squarks* $\begin{pmatrix}\widetilde{u_L}\\ \widetilde{d_L}\end{pmatrix}, \widetilde{u_R}, \widetilde{d_R},$ $\begin{pmatrix}\widetilde{c_L}\\ \widetilde{s_L}\end{pmatrix}, \widetilde{c_R}, \widetilde{s_R},$ $\begin{pmatrix}\widetilde{t_L}\\ \widetilde{b_L}\end{pmatrix}, \widetilde{t_R}, \widetilde{b_R}$	

gauge bosons

B^μ

$\vec{W}^\mu = (W_1^\mu, W_2^\mu, W_3^\mu)$ → break $SU(2)_L \times U(1)_Y$ to $U(1)_{em}$ → γ, $W^\pm$, Z^0

gluon $= g$ (octet)

(spin-2 *graviton*)

gauginos

$\tilde{\lambda}_0$

$\vec{\tilde{\lambda}} = (\tilde{\lambda}_1, \tilde{\lambda}_2, \tilde{\lambda}_3)$

gluino $= \tilde{g}$ (octet)

(spin-$\frac{3}{2}$ *gravitino*)

Higgs scalars

$\mathrm{H} = \begin{pmatrix}h^+\\ h^0\end{pmatrix}_{L\,(\underline{\mathbf{2}}\,\mathrm{rep})}$

$\mathrm{H}' = \begin{pmatrix}h'^-\\ h'^0\end{pmatrix}_{L\,(\underline{\mathbf{2}}^*\,\mathrm{rep})}$

→ $H^\pm$, H_p, H_ℓ, H_h

higgsinos

$\begin{pmatrix}\tilde{h}^+\\ \tilde{h}^0\end{pmatrix}_{L\,(\underline{\mathbf{2}}\,\mathrm{rep})}$

$\begin{pmatrix}\tilde{h}'^-\\ \tilde{h}'^0\end{pmatrix}_{L\,(\underline{\mathbf{2}}^*\,\mathrm{rep})}$

charginos

$\widetilde{W_1}^\pm$, $\widetilde{W_2}^\pm$

neutralinos

$\widetilde{Z}_1, \widetilde{Z}_2, \widetilde{Z}_3, \widetilde{Z}_4$

*sfermions also have soft SUSY-breaking mass terms

R-parity can be defined as a mutiplicative quantum number, R, which is either $+1$ or -1. Conservation of R-parity is something akin to conservation of SUSY-ness. A sparticle has the opposite R-parity as its SM partner. All the SM particles are assigned $R = +1$, while all the sparticles are given $R = -1$. So conservation of R-parity would forbid a sparticle from decaying into two SM particles, for example. Thus the SUSY-ness present originally cannot disappear. This has very important implications since it would mean the lightest $R = -1$ sparticle must be stable. Such a particle is known as the "lightest supersymmetric particle", or LSP for short, and its features will be further elaborated upon in Chapter 2. In the MSSM, R-parity is conserved. However, it is possible to construct valid supersymmetric theories with gauge-invariant interactions that do not conserve R-parity, for instance a squark decaying into two sleptons. Note that such an interaction would violate both baryon (B) and lepton (L) number conservation. In fact the R-parity of a particle may be defined as

$$R = (-1)^{3B+L+2S} \tag{1.3}$$

where S is the spin of the particle in units of $\hbar$. Violating baryon or lepton number conservation often leads to phenomenologically absurd models, where for instance all the protons in the Universe decay away in a few hours, thus it is easiest simply to add the extra constraint of R-parity conservation and assume that all such interactions are absent. Nonetheless, it should be emphasized that is is possible to construct R-parity violating theories consistent with current experimental constraints.

A way of insuring that the Lagrangian of a SUSY theory obey R-parity conservation and not allow interaction terms like the one just described is to demand that the superpotential used to generate the Lagrangian (see Eqn. (A.1) of Appendix A) contain only terms with an even number of "ordinary" superfields. Somewhat heuristically, a superfield is a bag into which can be tossed a particle and its sparticle superpartner, which then act as a unit within the superfield formalism. It is analogous to treating the proton and neutron together as a nucleon in the strong isospin formalism. The superpotential, which generates non-gauge interactions in the Lagrangian, is a function of superfields. An "ordinary" superfield is one whose fermionic component has $R = +1$.

So quark/squark and lepton/slepton superfields are both "ordinary," thus a quark-slepton-slepton interaction is not allowed. But a Higgs boson-slepton-slepton interaction is allowed since a Higgs boson/higgsino superfield is not ordinary. But, then, we already knew that Higgs fields are anything but ordinary!

In addition to enabling electroweak symmetry breaking, in the SM one complex $SU(2)_L$ doublet of Higgs fields with a vacuum expectation value is sufficient to provide mass terms to all the SM fermions via Yukawa interactions. This is possible since it is permissible to use the Higgs doublet to generate $SU(2)_L$ and $U(1)_Y$ invariant Yukawa interactions for one component of a SM fermion weak isodoublet, and the complex conjugate of the same Higgs doublet to generate singlet Yukawa terms for the other component of the weak isodoublet. Thus mass terms for both the up-type and down-type quarks can be generated with just a single doublet of Higgs fields. On the contrary, the Yukawa terms in the MSSM Lagrangian stem from the superpotential (see Eqn. (A.2) of Appendix A) which must be a function of only left- or right-chiral superfields. So a Higgs doublet superfield and its complex conjugate, which have opposite chiralities, cannot both be included in the superpotential to generate all the required Yukawa interaction terms since this would violate supersymmetry. Therefore, a minimum of two Higgs doublets which acquire vacuum expectation values are necessary in a SUSY model. The MSSM has the minimal two Higgs doublets: the $Y = +1$ doublet H with a vacuum expectation value (or vev for short) of v gives rise to the mass terms for the up-type quarks, and the $Y = -1$ doublet H$'$ whose vev is v' gives rise to the mass terms for the down-type quarks and the charged leptons. After spontaneous electroweak symmetry breaking, these two doublets also give rise to five physical Higgs particles: two charged particles, $H^{\pm} \equiv H_{ch}$, and three neutral particles. This is to be compared with the single physical Higgs particle of the SM.

The following nomenclature is employed for the three neutral Higgs bosons: the lightest CP-even particle is termed the light Higgs boson, H_ℓ; the heavier CP-even particle is called the heavy Higgs boson, H_h; and a CP-odd boson is known as the pseudoscalar Higgs boson, H_p. The latter is something of a misnomer since, *if* par-

ity were conserved, all the MSSM Higgs bosons would have $P = +1$, with $C = +1$ for H_ℓ and H_h while $C = -1$ for H_p. (This last assignment is required for consistency with the other imaginary components of the original complex Higgs fields. These other imaginary components go into making up the so-called Goldstone boson which in turn goes into the longitudinal component of the $C = -1$ Z^0 gauge boson via spontaneous symmetry breaking.) When interactions with chiral fermions are added to the theory, C and P are no longer separately conserved; but, CP is to a very good approximation still a valid quantum number. Thus H_ℓ and H_h are referred to as CP-even particles while H_p is labeled CP-odd. The C and P quantum numbers for a fermion-antifermion pair are given by $P = (-1)^{L+1}$ and $C = (-1)^{L+S}$, thus $CP = (-1)^{S+1}$ for the pair. For spin-$\frac{1}{2}$ fermions and antifermions, the total spin of such a pair must be $S = 0$ or 1. So coupling a fermion-anti-fermion pair to the CP-even H_ℓ or H_h requires $S = 1$ for the pair, while coupling to the CP-odd H_p boson needs $S = 0$ for the pair. Since the spins of the Higgs bosons are zero, $J = L \oplus S$ for the fermion-antifermion pair must be zero. Since CP is assumed to be conserved, in the case of the $CP = +1$ Higgs boson coupling the pair must have $L = 1$, and thus $P = +1$ for the pair. For the coupling to the $CP = -1$ Higgs boson, L must be zero for the pair and thus they must have $P = -1$. Hence the origin of the term "pseudoscalar" Higgs boson — it actually acquires its name from the parity the fermion-antifermion pair.

Put more succinctly, in the MSSM Lagrangian the couplings of the CP-even Higgs bosons to the SM fermions are of the form $\bar{f} f H_{\ell,h} = (\bar{f}_L f_R + \bar{f}_R f_L) H_{\ell,h}$; this Dirac bilinear has $P = +1$ and $C = +1$ yielding $CP = +1$ for the bilinear and thus $CP = +1$ for the entire term. The couplings of the CP-odd so-called pseudoscalar Higgs boson to SM fermions are of the form $\bar{f} \gamma_5 f H_p = (\bar{f}_L f_R - \bar{f}_R f_L) H_p$; for the Dirac bilinear here $P = -1$ and $C = +1$ yielding $CP = -1$ for the bilinear and thus $CP = +1$ for the entire term. The Higgs boson that couples to the $P = -1$ bilinear is given the name "pseudoscalar." Note that each term in the Lagrangian has $CP = +1$ so that this is a conserved quantity.

The mass spectrum of the MSSM Higgs bosons is worked out in detail in Appendix A both at tree-level and including radiative corrections from the third generation of heavy quarks and their squark superpartners. Figures 1.1 through 1.4 illustrate how the masses of the various Higgs bosons are related, and how they vary with the both top quark and stop squark masses. Plots are shown for relatively high (1 TeV) and relatively low (300 GeV) input squark masses. The squark masses, especially the stop masses, are seen to have a modest effect on $m_{H_{ch}}$ and m_{H_h} (recall m_{H_p} is input), and a fairly significant effect on m_{H_ℓ}. It is certainly true that these masses are considerably more sensitive to the top quark mass, as seen in Figure 1.1 (radiative corrections are roughly proportional to m_t^4), than to the stop squark masses; however, in keeping with what will be a focus of the rest of this work, the sometimes overlooked dependence on the stop masses is depicted here. (It should perhaps also be noted that there is a lot more freedom in the choice of squark mass inputs than there is in adjusting the top quark mass. Hopefully, the CDF and D0 experimenters at Fermilab will further accentuate this situation soon.)

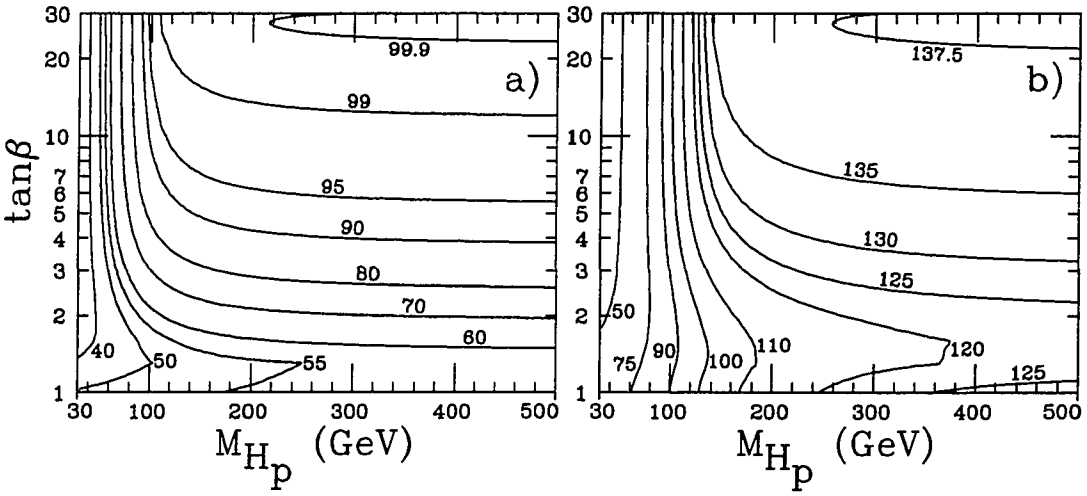

Figure 1.1: Contours for the mass of the light Higgs boson, m_{H_ℓ}, in GeV, in the m_{H_p} *vs.* $\tan\beta$ plane.
For plot a), $m_t = 125\,\text{GeV}$, and for plot b), $m_t = 200\,\text{GeV}$. In both plots, $m_{\tilde{g}} = -\mu = 1000\,\text{GeV} \doteq m_{\tilde{q}}$. See the captions to Figs. 2.2 and 2.4 for a complete listing of the other MSSM input parameters.

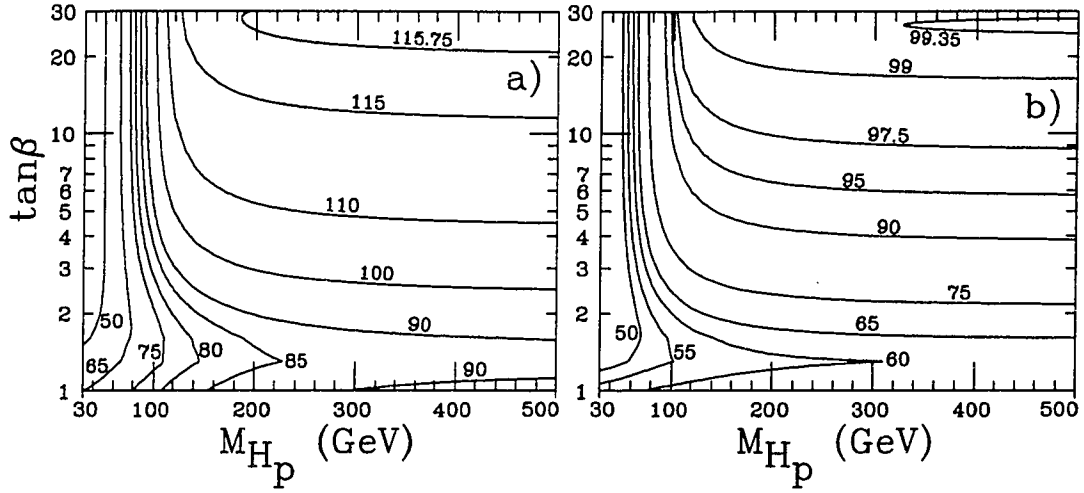

Figure 1.2: Contours for the mass of the light Higgs boson, m_{H_ℓ}, in GeV, in the m_{H_p} *vs.* $\tan\beta$ plane; $m_t = 165\,\text{GeV}$ for both plots.
For plot a), $m_{\tilde{g}} = -\mu = 1000\,\text{GeV} \doteq m_{\tilde{q}}$ and for plot b), $m_{\tilde{g}} = -\mu = 300\,\text{GeV} \doteq m_{\tilde{q}}$. Again, see the captions to Figs. 2.2 and 2.4 for a complete listing of the other MSSM input parameters.

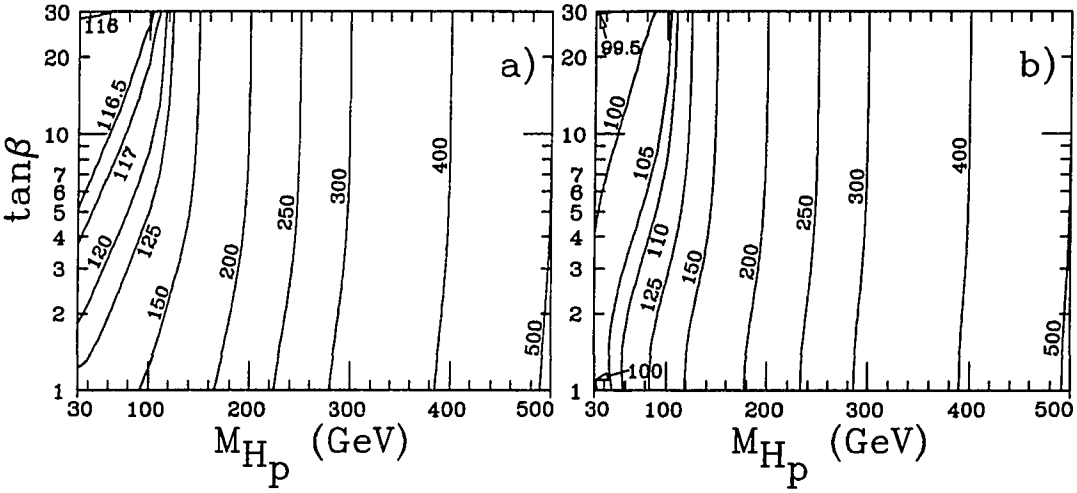

Figure 1.3: Contours for the mass of the heavy Higgs boson, m_{H_h}, in GeV, in the m_{H_p} *vs.* $\tan\beta$ plane; $m_t = 165\,\text{GeV}$ for both plots.
For plot a), $m_{\tilde{g}} = -\mu = 1000\,\text{GeV} \doteq m_{\tilde{q}}$ and for plot b), $m_{\tilde{g}} = -\mu = 300\,\text{GeV} \doteq m_{\tilde{q}}$. Again, see the captions to Figs. 2.2 and 2.4 for a complete listing of the other MSSM input parameters.

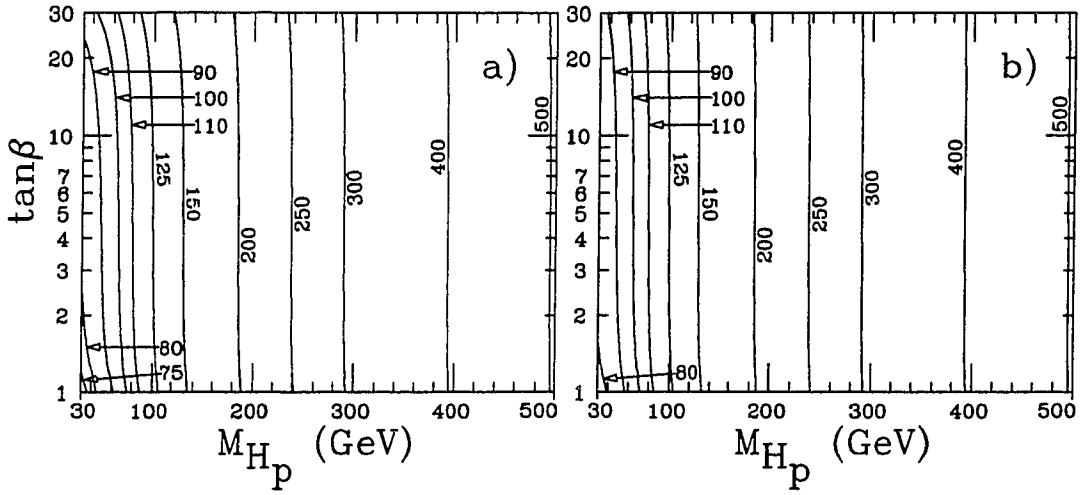

Figure 1.4: Contours for the mass of the charged Higgs boson, $m_{H_{ch}}$, in GeV, in the m_{H_p} *vs.* $\tan\beta$ plane; $m_t = 165\,\mathrm{GeV}$ for both plots.
For plot a), $m_{\tilde{g}} = -\mu = 1000\,\mathrm{GeV} \doteq m_{\tilde{q}}$ and for plot b), $m_{\tilde{g}} = -\mu = 300\,\mathrm{GeV} \doteq m_{\tilde{q}}$. See the captions to Figs. 2.2 and 2.4 for a complete listing of the other MSSM input parameters.

Couplings of the MSSM Higgs bosons to SM particles are related to those of a SM Higgs by MSSM angle factors consisting of the various combinations of the angles β and α given in Table 1.2, where $\tan\beta = v/v'$ is the ratio of the vacuum expectation values of the two Higgs doublets, and α is the scalar Higgs mixing angle required to diagonalize the scalar sector Higgs mass matrix (the latter is defined in Appendix A).

As with the quarks, leptons, and gauge bosons, the Higgs bosons must have superpartners. These are the spin-$\frac{1}{2}$ Majorana higgsinos, $\tilde{h}^+$, $\tilde{h}^0$, $\tilde{h}'^-$, and $\tilde{h}'^0$ (where the charges indicated are those of the left chiral components for the charged Majorana fields). With electroweak symmetry breaking these can mix with the $\vec{\tilde{\lambda}}$ and $\tilde{\lambda}_0$ gauginos having the same electric charge. (The leptons could also participate in this mixing if lepton numbers were not conserved, as is the case in some R-parity violating models. R-parity conservation and the concommitant requirement of lepton number conservation is the justification for keeping the leptons out of the

Table 1.2: MSSM mixing angle factors in the couplings of the Higgs bosons. Thus for instance the MSSM partial decay widths for the processes indicated at the top are
$|\text{MSSM mixing angle factor}|^2 \times \text{SM partial decay width}$.

	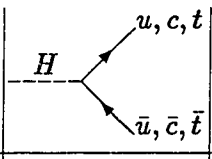	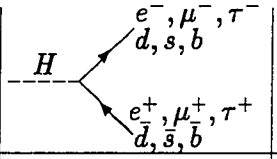	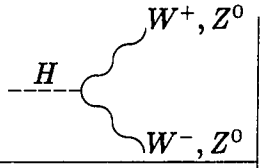
H_ℓ	$\frac{\cos\alpha}{\sin\beta}$	$\frac{\sin\alpha}{\cos\beta}$	$\sin(\beta+\alpha)$
H_h	$-\frac{\sin\alpha}{\sin\beta}$	$\frac{\cos\alpha}{\cos\beta}$	$\cos(\beta+\alpha)$
H_p	$-i\gamma_5\cot\beta$	$-i\gamma_5\tan\beta$	0

blender into which the gauginos and higgsinos are tossed to make the charginos and newtralinos.) In the MSSM, the $SU(2)_L$ and $U(1)_Y$ gauginos and higgsinos mix to form chargino, $\widetilde{W}_i$, and neutralino, $\widetilde{Z}_i$, mass eigenstates. The mass terms for the Lagrangian can be obtained by inserting the gaugino and higgsino fields into the third line Eqn. (A.1) of Appendix A, the general expression for a supersymmetric Lagrangian, and then adding the higgsino mixing term from the superpotential and allowable soft supersymmetric breaking gaugino mass terms. For the charged sector the resulting terms may be written as

$$[\bar{\tilde{\lambda}} \quad \bar{\tilde{\chi}}]\left(\mathcal{M}_{charge}P_L + \mathcal{M}^T_{charge}P_R\right)\begin{bmatrix}\tilde{\lambda}\\ \tilde{\chi}\end{bmatrix} \quad , \tag{1.4}$$

where $\tilde{\lambda}$ and $\tilde{\chi}$ are Dirac spinors which annihilate particles of definite charge ($Q=-1$) composed from the Majorana spinors,

$$\tilde{\lambda} = \tfrac{1}{\sqrt{2}}(\tilde{\lambda}_1 + i\tilde{\lambda}_2) \ , \qquad \chi = P_L\tilde{h}'^- - P_R\tilde{h}^+ \ . \tag{1.5}$$

Here P_L (P_R) is the chirality operator for the left- (right-) handed states. The charged mass matrix is given by

$$\mathcal{M}_{charge} = \begin{bmatrix} \mu_2 & -gv' \\ -gv & 2m_1 \end{bmatrix} \ , \tag{1.6}$$

where $2m_1$ is the supersymmetric higgsino mixing term from the superpotential (see Eqn. (A.2)), and μ_2 is the soft SUSY-breaking $SU(2)_L$ gaugino mass. The neutral gaugino-higgsino sector mass terms can similarly be written as

$$[\,\bar{\tilde{h}}^0 \quad \bar{\tilde{h}}'^0 \quad \bar{\tilde{\lambda}}_3 \quad \bar{\tilde{\lambda}}_0\,]\left(\mathcal{M}_{neutral}P_L + \mathcal{M}_{neutral}P_R\right)\begin{bmatrix} \tilde{h}^0 \\ \tilde{h}'^0 \\ \tilde{\lambda}_3 \\ \tilde{\lambda}_0 \end{bmatrix} \ , \tag{1.7}$$

with the neutral mass matrix given by

$$\mathcal{M}_{neutral} = \begin{bmatrix} 0 & -2m_1 & -\frac{gv}{\sqrt{2}} & \frac{g'v}{\sqrt{2}} \\ -2m_1 & 0 & \frac{gv'}{\sqrt{2}} & -\frac{g'v'}{\sqrt{2}} \\ -\frac{gv}{\sqrt{2}} & \frac{gv'}{\sqrt{2}} & \mu_2 & 0 \\ \frac{g'v}{\sqrt{2}} & -\frac{g'v'}{\sqrt{2}} & 0 & \mu_1 \end{bmatrix} \tag{1.8}$$

Here μ_1 is the soft SUSY-breaking $U(1)_Y$ gaugino mass. The diagonalization of $\mathcal{M}_{charge}$ and $\mathcal{M}_{neutral}$ will yield the eigenvectors of the charginos and neutralinos, respectively, in terms of the gauginos and higgsinos as well as the mass eigenvalues. (The details of this are left to Appendix B in the section describing the decays of the Higgs bosons into charginos and neutralinos.) The results are two pairs of physical charginos, which will be labelled $\widetilde{W}_1^{\pm}$ and $\widetilde{W}_2^{\pm}$ ($m_{\widetilde{W}_1} < m_{\widetilde{W}_2}$), and four physical neutralinos, denoted by $\widetilde{Z}_i$, i = 1-4 ($m_{\widetilde{Z}_i} < m_{\widetilde{Z}_j}$ if $i < j$).

Assuming low energy SUSY is embedded within a GUT framework with canonical kinetic terms for the gauge fields, the soft SUSY-breaking gaugino masses generated by radiative corrections may be related to one another by

$$\mu_1 = \frac{5}{3}\tan^2\theta_w\,\mu_2 \ , \qquad \mu_2 = \frac{\alpha_2}{\alpha_3}\mu_3 = -\frac{\alpha_{em}}{\alpha_s \sin^2\theta_w} m_{\tilde{g}} \ , \tag{1.9}$$

where in the second equation above $m_{\tilde{g}} \equiv m_{\tilde{g}}(M_{Z^0}) = |\mu_3|$ is the $\overline{\rm MS}$ gluino running mass at the momentum scale $q = M_{Z^0}$, and the strong coupling constant, $\alpha_s \equiv \alpha_s(M_{Z^0})$, is also evaluated at the Z^0 mass. The $\overline{\rm MS}$ gluino pole mass is then related to the physical gluino mass via the relations described in Ref. [17]. Thus, assuming a GUT structure, all the soft SUSY-breaking gaugino masses may be determined from the gluino mass which is then a basic parameter of the theory. This framework will be assumed throughout the rest of this work.

As previously noted, soft SUSY-breaking squark and slepton masses are also called for in the model to avoid the phenomenological embarrassment of degenerate SM particle and sparticle masses. In the least adorned, most economical supergravity models, SUSY-breaking generates a common mass for the sfermions at the SUSY-breaking scale. This degeneracy is then broken when these masses are evolved down to the electroweak-breaking scale. At this lower scale, the sleptons are expected to be substantially lighter than the squarks if the gluino and squark masses are fairly close to each other. In terms of the squark and gluino masses, the slepton masses can be written as (see, *e.g.*, [18] for further discussion):

$$\begin{aligned} m^2_{\tilde{\ell}_L} &= m^2_{\tilde{q}} - 0.73 m^2_{\tilde{g}} - 0.27 M^2_{Z^0} \cos 2\beta \,, \\ m^2_{\tilde{\ell}_R} &= m^2_{\tilde{q}} - 0.78 m^2_{\tilde{g}} - 0.23 M^2_{Z^0} \cos 2\beta \,, \\ m^2_{\tilde{\nu}_L} &= m^2_{\tilde{q}} - 0.73 m^2_{\tilde{g}} + 0.5 M^2_{Z^0} \cos 2\beta \,, \end{aligned} \tag{1.10}$$

where $m^2_{\tilde{q}}$ is the squark mass squared averaged over the different squark flavors. The soft SUSY-breaking slepton masses are seen to remain fairly close to each other. A similar conclusion is reached for the soft SUSY-breaking squark masses at the electroweak scale, except perhaps the stop squarks which may be expected to be somewhat lighter than the other soft SUSY-breaking squark masses due to their larger Yukawa couplings. Consistent with these supergravity-inspired predictions, input sfermion parameters for this work will be taken as a common squark mass for the first two generations, $m_{\tilde{q}}$ (which is then used in Eqns. (1.10) to determine the slepton masses), the mass of the left stop squark, $m_{\tilde{t}_L}$ (which then fixes the left bottom squark mass by the $SU(2)_L$ invariance), and the mass of the right top squark, $m_{\tilde{t}_R}$. The sbottom squark masses are taken as $m_{\tilde{b}_L} = m_{\tilde{t}_L}$ and, to simplify

matters, $m_{\tilde{b_R}} = m_{\tilde{q}}$. Note that the term "left stop squark," for example, refers to the superpartner to the left-handed chiral top quark state. The physical sfermion masses are further altered by intra-flavor mixing as described in the appendices — this can lead to a significantly lower mass for one of the stop mass eigenstates.

Another necessary input parameter is the ratio of the vacuum expectation values for the two Higgs doublets, $\tan\beta = v/v'$, defined by Eqn. (A.12). Perturbative limits on the top-bottom-charged Higgs boson Yukawa couplings along with limits from $b \rightarrow s\gamma$ [19,20] and B_d-$\overline{B_d}$ mixing [19,20,21] studies restrict $\tan\beta$ to

$$0.4 < \tan\beta < 120 \tag{1.11}$$

If one also assumes a common SUSY-breaking mass scale at the grand-unification point as predicted by supergravity models, this is further restricted to [22]

$$1 < \tan\beta < \frac{m_t}{m_b} \lesssim 40 \tag{1.12}$$

One of the Higgs boson masses, taken here to be the mass of the pseudoscalar Higgs boson, m_{H_p}, must also be input. Also needed is the supersymmetric higgsino mixing mass from the superpotential, $2m_1 \equiv -\mu$ (note that these two notations are in common use: this work uses $2m_1$ in equations in conformity with the notation of previous work using the same parameter definitions, but μ when plotting quantites in agreement with the more common notation from the literature), and the coefficients of the soft SUSY-breaking trilinear sfermion terms, A_f, as described in Appendix A (A_t and A_b, which can be important in determining the physical masses and intra-flavor mixings of the $\tilde{t}$- and $\tilde{b}$-squarks, are input but often taken to be zero for simplicity; the other A-terms are phenomenologically irrelevant). The radiative corrections to the masses of the Higgs bosons place restrictions on combinations of A_t, $2m_1$, and $\tan\beta$ by requiring that the light Higgs boson mass not be driven negative. And lastly all the input parameters to the SM must be given. Of these inputs two, m_t and $\alpha_s(M_{Z^0})$, come associated with a substantial degree of uncertainty.

Now all the needed ingredients to specify all quantites within the MSSM model (with the added conditions described above) have been elucidated. A summary of the input parameters is given in Table 1.3 . The stage is now set to examine the consequences of the MSSM model framework upon the future experimental studies at a hadron supercollider.

The outline for the rest of this work is as follows: In Chapter 2 the capabilities of the e^+e^- LEP collider are evaluated. Regions of parameter space where a MSSM Higgs boson should be detectable at both LEP and the soon to be completed LEP II are mapped out to give an indication of the degree of complementarity of LEP with a hadron supercollider, as well as to show what regions of parameter space will be left for the hadron supercollider to probe. Chapter 3 discusses the production mechanisms and rates for the neutral MSSM Higgs bosons at a hadron supercollider. Chapter 4 then examines the decays of the Higgs bosons into the SM modes known to provide viable signatures in a hadron collider environment. Next Chapter 5 examines the decays of Higgs bosons into sparticles, especially decays into the neutralinos and charginos. Chapter 6 describes some other proposals for searching for MSSM Higgs bosons and provides a summary of the overall MSSM parameter space coverage possible using the signal modes analyzed in the previous chapters. Also included are two appendices. Appendix A gives a derivation of the MSSM Higgs boson masses as well as the important H_h-H_ℓ-H_ℓ vertex including radiative corrections from the third generation of quarks and squarks. This calculation is unique to this work. Appendix B gives a compendium of the partial decay widths for MSSM Higgs bosons including all tree-level decay modes and also QCD corrections to the fermionic decays and numerous important one-loop decays. This is presented in a consistent notation at the level of sophistication used in generating the figures and other results given in this work. The formulæ presented in Appendix B are not original to this work.

Table 1.3: Summary of MSSM input parameters
(using some constraints from GUT & supergravity models)

Symbol	Name	Significance
$\tan\beta = \frac{v}{v'}$	Ratio of vacuum expectation values of two Higgs doublets	• masses of MSSM Higgs bosons • Higgs bosons int$^{\underline{n}}$ couplings • masses & int$^{\underline{n}}$'s of $\widetilde{W}$'s & $\widetilde{Z}$'s • relation $M_W^2 = \frac{1}{2}g^2(v^2+v'^2)$ makes ratio of vev's the unfixed quantity rather than the individual vev's
m_{H_p}	Pseudoscalar Higgs boson mass	• masses of all MSSM Higgs bosons fully determined *at tree-level* by m_{H_p} & $\tan\beta$
$m_{\tilde{g}}$	Physical gluino mass	• determines all other soft SUSY-breaking gaugino masses • determines slepton masses in conjunction with $m_{\tilde{q}}$ & $\tan\beta$ • masses & int$^{\underline{n}}$'s of $\widetilde{W}$'s & $\widetilde{Z}$'s
$\mu = -2m_1$	Supersymmetric higgsino mixing mass	• involved in Higgs boson masses via radiative corrections • masses & int$^{\underline{n}}$'s of $\widetilde{W}$'s & $\widetilde{Z}$'s • intraflavor mixing of sfermions
$m_{\tilde{q}}$	1^{st} & 2^{nd} generation rms squark mass	• masses of sleptons
$m_{\tilde{t_L}}$	left stop mass	• $m_{\tilde{b_L}} = m_{\tilde{t_L}}$ from $SU(2)_L$ invariance
$m_{\tilde{t_R}}$	right stop mass	• $m_{\tilde{t_L}}$, $m_{\tilde{t_R}}$, $m_{\tilde{b_L}}$ & $m_{\tilde{b_R}}$ involved in Higgs boson masses via radiative corrections
A_t, A_b	A-terms (coefficients of soft SUSY-breaking trilinear sfermionic int$^{\underline{n}}$'s)	• intraflavor mixing of sfermions • involved in Higgs boson masses via radiative corrections
m_t	top quark mass	• very important for radiative corrections to Higgs boson masses
⇑ ⇑ SM inputs with considerable uncertainty ⇓ ⇓		• important in determining B.R.'s of Higgs bosons to key decay modes • important for SM backgrounds
$\alpha_s(M_Z^0)$	strong int$^{\underline{n}}$ coupling constant at Z^0 mass scale	• used along with $m_{\tilde{g}}$ in determining SUSY-breaking gaugino masses which in turn are used to determine • masses & int$^{\underline{n}}$'s of $\widetilde{W}$'s & $\widetilde{Z}$'s

Chapter 2

Higgs Bosons at e^+e^- Machines

2.1 Introduction

While the subject of this work is MSSM Higgs boson detection at hadron colliders rather than at e^+e^- machines, it is nonetheless crucial to examine the capabilities of the leptonic machines. It is important to see which areas of the MSSM parameter space can be mapped out by the LEP and SLC e^+e^- machines currently operating in order to find out what regions of this space will already be excluded prior to the start-up of a hadron supercollider. Only then can the value of a hadron machine's reach be meaningfully assessed. It is also of interest to see what region of parameter space may be probed by the LEP II machine scheduled to go into operation at CERN sometime in the next couple of years. An investigation of the e^+e^- colliders will determine to what extent a hadron collider such as the proposed LHC machine at CERN will complement the attributes of the e^+e^- machines now or soon-to-be in operation and to what extent a hadron collider will merely duplicate their capabilities.

This chapter is intended to be a somewhat summary overview, and not an in-depth study of the detection of Higgs bosons at e^+e^- machines. Only a very brief discussion of the MSSM Higgs boson production at e^+e^- colliders will be given. (See Sopczak[23] for a more thorough investigation of MSSM Higgs boson detection at LEP.) The purpose is only to point out the regions of the MSSM parameter space excluded by searches at LEP for Higgs bosons as well as other supersymmetric particles. The individual proposed MSSM signals will be described and the regions each excludes delineated. Then these regions will be combined to give the overall region excluded by LEP which can be superimposed on the event rates from a hadron supercollider. An indication of the LEP II potential will also be included.

2.2 Restrictions from Higgs Boson Production

At LEP, a SM Higgs boson may be produced when a Z^0 decays into a Higgs boson and an off-shell Z^{0*}, $e^+e^- \rightarrow Z^0 \rightarrow H_{SM}Z^{0*}$. The Z^{0*} will then decay into a pair of fermions (quarks or leptons). This same bremsstrahlung process (also known as the Bjorken process) can produce the light Higgs boson, H_ℓ, of the MSSM. The heavy Higgs boson, H_h, is of course too heavy to be produced on-shell, and radiation of a pseudoscalar Higgs boson, H_p, is forbidden by its CP-odd nature. However, due to the existence of this CP-odd Higgs boson in the MSSM, decay of a Z^0 into a pair of Higgs bosons is allowed, $e^+e^- \rightarrow Z^0 \rightarrow H_\ell H_p$. (Production of a pair of CP-even or CP-odd Higgs bosons, $H_\ell H_\ell$, $H_h H_h$, or $H_p H_p$ is forbidden by Bose-Einstein statistics; and the mass of the heavy Higgs precludes consideration of $H_h H_p$ pair production for an on-shell Z^0.) Thus in the MSSM, we are left with the two production mechanisms shown below in Figure 2.1.

The limit on the mass of the SM Higgs boson resulting from the negative search results of the four experiments at LEP [24],

$$m_{H_{SM}} > 63.5\,\mathrm{GeV} \quad , \tag{2.1}$$

can be used to exclude regions of MSSM parameter space due to non-observation of the bremsstrahlung process, $e^+e^- \rightarrow Z^0 \rightarrow H_\ell Z^{0*}$. This is done by taking into

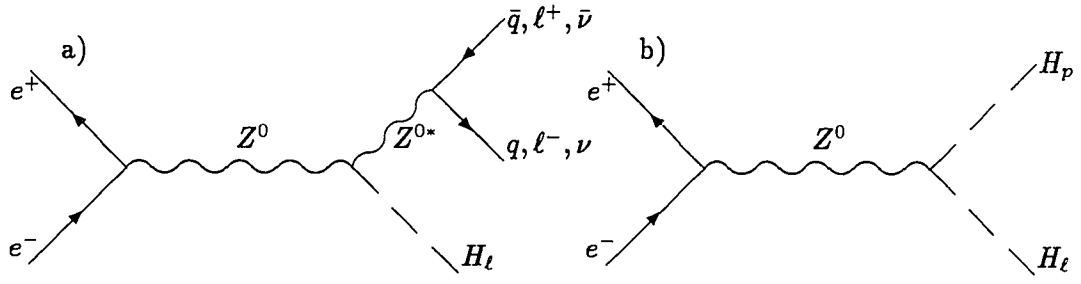

Figure 2.1: Feynman diagrams for MSSM Higgs boson production from Z^0 decays
a) Bremsstrahlung production of a light Higgs boson
b) Pair production of a light Higgs boson and a pseudoscalar Higgs boson

account the MSSM angle factors that must be included in the coupling between H_ℓ and the gauge bosons (see Table 1.2); for $m_{H_\ell} = m_{H_{SM}}$,

$$\Gamma(Z^0 \to H_\ell Z^{0*}) = \sin^2(\alpha+\beta)\Gamma(Z^0 \to H_{SM} Z^{0*}) \quad . \tag{2.2}$$

The partial decay width for the production of an $H_\ell H_p$ pair is given by

$$\begin{aligned}\Gamma(Z^0 \to H_\ell H_p) &= \cos^2(\alpha+\beta)\frac{g^2 M_{Z^0}}{192\pi\cos^2\theta_W}\lambda^{\frac{3}{2}}\Big(1, \frac{m^2_{H_\ell}}{M^2_{Z^0}}, \frac{m^2_{H_p}}{M^2_{Z^0}}\Big) \\ &= \cos^2(\alpha+\beta)\frac{\Gamma(Z^0 \to \nu\bar{\nu})}{2}\lambda^{\frac{3}{2}}\Big(1, \frac{m^2_{H_\ell}}{M^2_{Z^0}}, \frac{m^2_{H_p}}{M^2_{Z^0}}\Big) \quad . \end{aligned} \tag{2.3}$$

Here $\lambda(a,b,c) = a^2+b^2+c^2-2ab-2bc-2ac$. We see from the MSSM angle factors in Eqn. (2.2) and Eqn. (2.3) that these two process are roughly complementary. The non-observation of the decay $Z^0 \to H_p H_\ell$ in the sample of more than 7 million Z^0 events collected by the LEP experiments thus far [25] can be used to set the branching fraction for this process to be $B.F.(Z^0 \to H_\ell H_p) <$ few $\times 10^{-6}$. The regions of parameter space excluded by this requirement are found to coincide with those delineated by requiring $m_{H_p} + m_{H_\ell} > M_{Z^0}$.

Figures 2.2 and 2.3 show the regions of the MSSM parameter space which are excluded by these restrictions. What is shown is actually curves delineated what regions of the partameter space would be excluded *if* the limit on the mass of the SM Higgs boson had a given value (given by the label next to the curve). Thus some of the "excluded" regions shown (delineated for example by the $m_{H_{SM}} = 65\,\text{GeV}$ curve or the $m_{H_{SM}} = 70\,\text{GeV}$ curve) are now only potentially excluded regions. For Figure 2.2, the higgsino mixing parameter, $\mu = -2m_1$, and the squark and gluino masses have all been made large, so all the sparticle masses are large too. If these parameter values are lowered, they can affect the Higgs boson masses through the radiative corrections; this in turn will alter the Z^0 to Higgs boson branching ratios. Other sparticles, such as the neutralinos and charginos may also become light enough for the Z^0 to decay into them, which can conceivably also reduce the decay rates into Higgs bosons. Figure 2.3 shows the regions excluded when the values of these MSSM input parameters are lowered. The excluded regions grow in size, due mainly to the lowering of the mass of the light Higgs boson incorporating the radiative corrections.

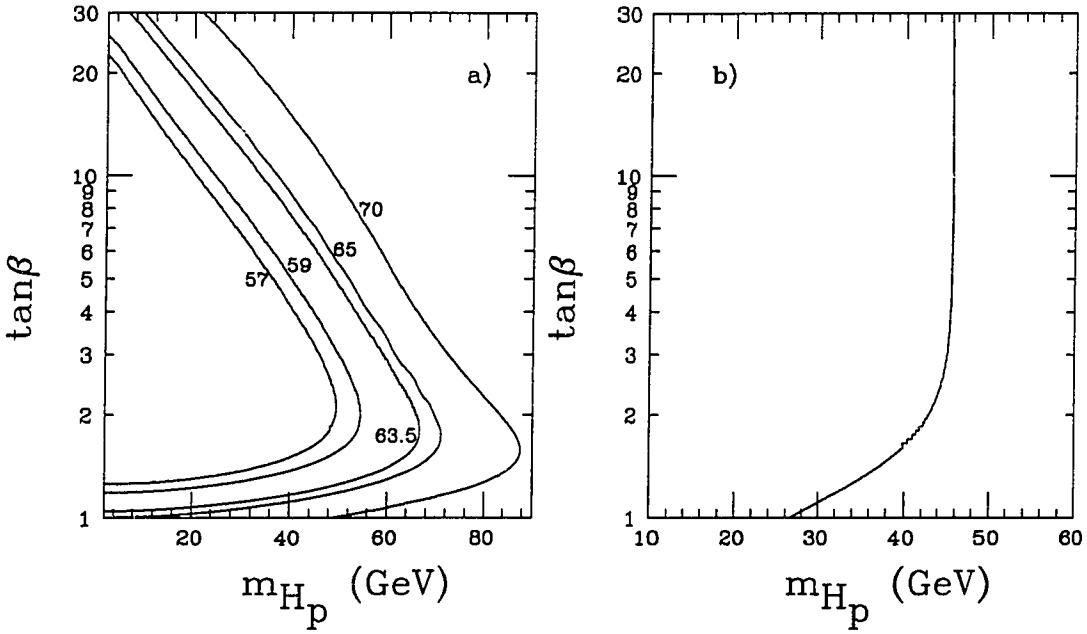

Figure 2.2: LEP excluded region from searches for Higgs bosons.
a) B.R.$(Z^0 \to Z^{0*}H_\ell)$ is too large. The number associated with each curve gives the limit on the mass of a SM Higgs boson used in deriving that curve. The current limit on $m_{H_{SM}}$ is taken as 63.5 GeV.
b) B.R.$(Z^0 \to H_pH_\ell) \geq 2 \times 10^{-6}$, corresponding to $m_{H_p} + m_{H_\ell} < M_{Z^0}$.
For each curve, the region excluded is to the *left* of that curve.
MSSM input parameters: $m_{\tilde{g}} = -\mu = 1000\,\text{GeV} \doteq m_{\tilde{q}}$ (actually, $m_{\tilde{q}}$ is set 0.35 GeV above $m_{\tilde{g}}$ to avoid computational problems — the symbol $\doteq$ will be used to signify this), $m^2_{\tilde{q}} - m^2_{\tilde{t}_L} = 50\,\text{GeV}^2$, $m^2_{\tilde{q}} - m^2_{\tilde{t}_R} = 100\,\text{GeV}^2$, $A_t = A_b = 0$, $M_{Z^0} = 91.19\,\text{GeV}$, $m_t = 165\,\text{GeV}$, $m_b = 5\,\text{GeV}$.
(The small steps or wiggles seen in some curves are artifacts of the generating program.)

Figure 2.3: (see next page) Plots for $m_{\tilde{g}} = -\mu = 300\,\text{GeV} \doteq m_{\tilde{q}}$.
All other parameters as in Figure 2.2 .
a) B.R.$(Z^0 \to Z^{0*}H_\ell)$ is too large. b) B.R.$(Z^0 \to H_pH_\ell) \geq 2 \times 10^{-6}$.
c) B.R.$(Z^0 \to Z^{0*}H_\ell)$ is too large: more complete plot with insert for low values of $\tan\beta$. If a number appears twice, the excluded region is *in between*. For the 57, 59, and 60 GeV curves, the excluded region is to the *left* of the curve. For the 63.5, 65, and 70 GeV curves, the excluded region is *below* the curve.
d) B.R.$(Z^0 \to Z^{0*}H_\ell)$ is too large: plotted vs. μ for $m_{H_p} = 250\,\text{GeV}$. All other parameters as in other plots. The region excluded is *below* each curve. Thus for this case of lower sparticle masses there is now a region around $\tan\beta \sim 1$ excluded for $m_{H_p} \approx 250\,\text{GeV}$ and low to moderate values of μ.

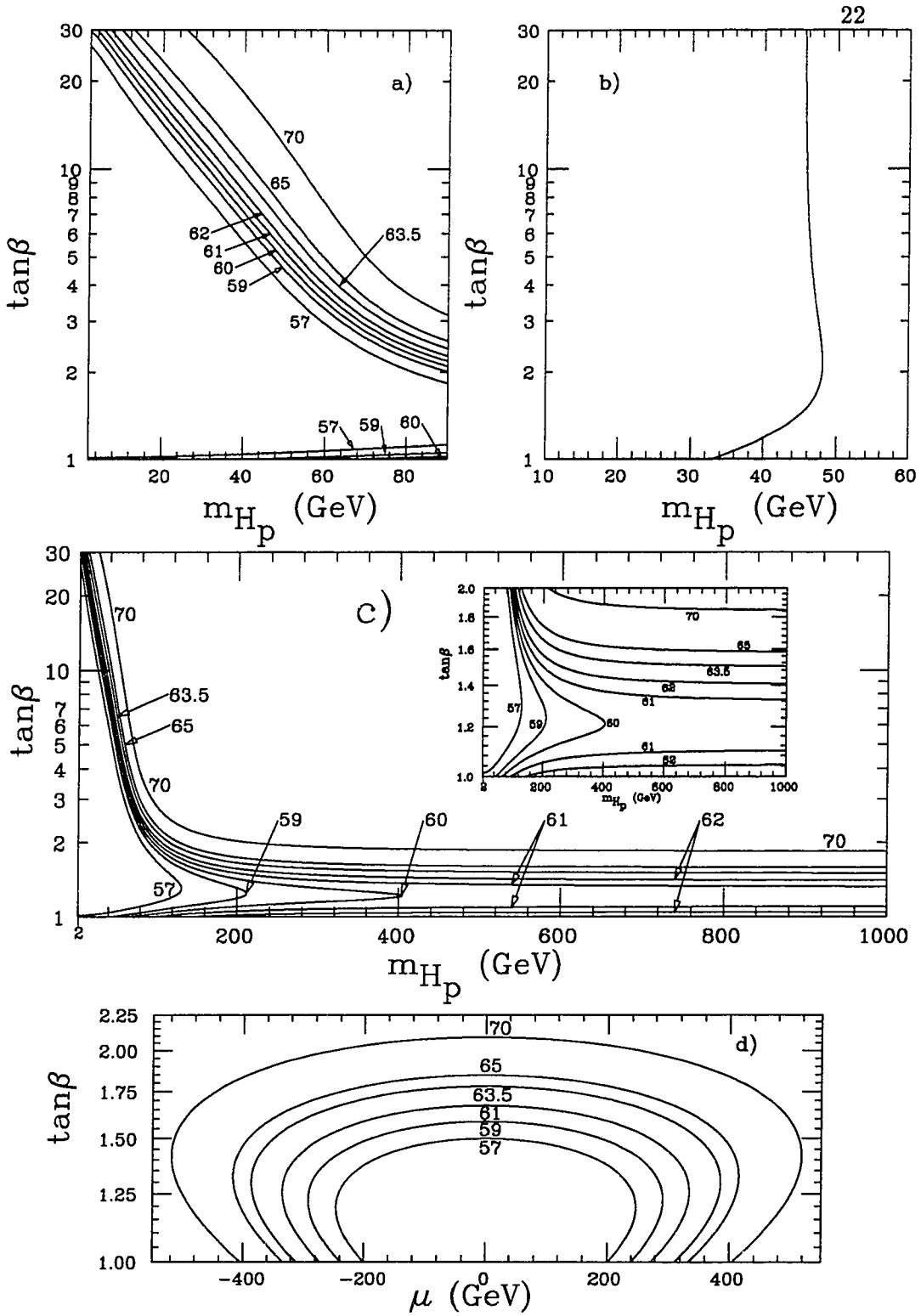

Figure 2.3: LEP excluded region from searches for Higgs bosons with low values of MSSM sparticle input parameters. See last page for more details.

2.3 Restrictions from Sparticle Production

The MSSM input parameters are further constrained by the failure to detect any sparticles among the decay products of the Z^0's studied at LEP. Since the masses and couplings of the neutralinos and charginos are fixed by the MSSM input parameters $m_{\tilde{g}}$, μ, and $\tan\beta$, such negative search results place restrictions upon these parameters.

The negative outcome of the search for charginos at LEP [26], together with the large value of the coupling constant between charginos and the Z^0 [27-29], essentially requires that

$$m_{\widetilde{W}_1} > \frac{1}{2} M_{Z^0} \quad . \tag{2.4}$$

The MSSM parameter region excluded by this restriction is shown in Figure 2.4. Note that in plot b) where the input gluino and squark masses are set low $m_{\widetilde{W}_1} < 90\,\mathrm{GeV}$ for much of the allowed parameter region.

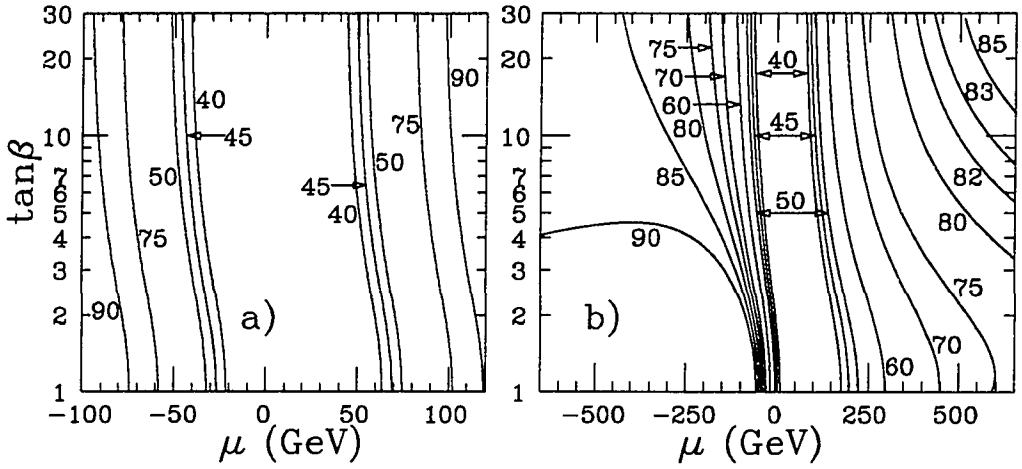

Figure 2.4: Mass of the lighter chargino.
MSSM input parameters: $m_{H_p} = 250\,\mathrm{GeV}$, $m^2_{\tilde{q}} - m^2_{\tilde{t}_L} = 50\,\mathrm{GeV}^2$, $m^2_{\tilde{q}} - m^2_{\tilde{t}_R} = 100\,\mathrm{GeV}^2$, $A_t = A_b = 0$, $m_t = 165\,\mathrm{GeV}$, $m_b = 5\,\mathrm{GeV}$, $M_{Z^0} = 91.19\,\mathrm{GeV}$, $\sin^2\theta_w = 0.23$, $\alpha_s(M_{Z^0}) = 0.118$, $\alpha_{em} = 1/128$, and in plot a) $m_{\tilde{g}} = 1000\,\mathrm{GeV} \doteq m_{\tilde{q}}$,
while in plot b) $m_{\tilde{g}} = 300\,\mathrm{GeV} \doteq m_{\tilde{q}}$.

Restrictions on neutralino masses are more difficult to set. Explicit mass limits on the heavier neutralinos generally assume that these decay directly to the LSP (lightest supersymmetric particle), which is taken to be the lightest neutralino, $\tilde{Z}_1$, ignoring the possibility of more complicated cascade decays. It is more useful for our purpose to look at the restriction placed on the overall neutralino production rate by an unsuccessful search for neutralino events in Z^0 decays. Based on a sample size of only around 10^4 Z^0 decays, LEP experimenters concluded [30-32] that $B.F.(Z^0 \rightarrow \tilde{Z}_1\tilde{Z}_2)$ + $B.F.(Z^0 \rightarrow \tilde{Z}_2\tilde{Z}_2)$ was at most a few times 10^{-4}. In view of the vastly larger sample of reconstructed Z^0's available today the requirement: $B.F.(Z^0 \rightarrow \tilde{Z}_i\tilde{Z}_j) < 5 \times 10^{-5}$ where i and j are not both equal to one, seems warranted. For the higher sparticle input masses used for plot a) of Figure 2.5, any improvement in the branching ratio bound below $\approx 10^{-4}$ does not noticeably alter the excluded region at all. For the lower sparticle input masses of plot b), the excluded region is slightly sensitive to the limit set on the branching ratio; however, further improvement in the experimental bound will not significantly increase the amount of parameter space excluded in this case either.

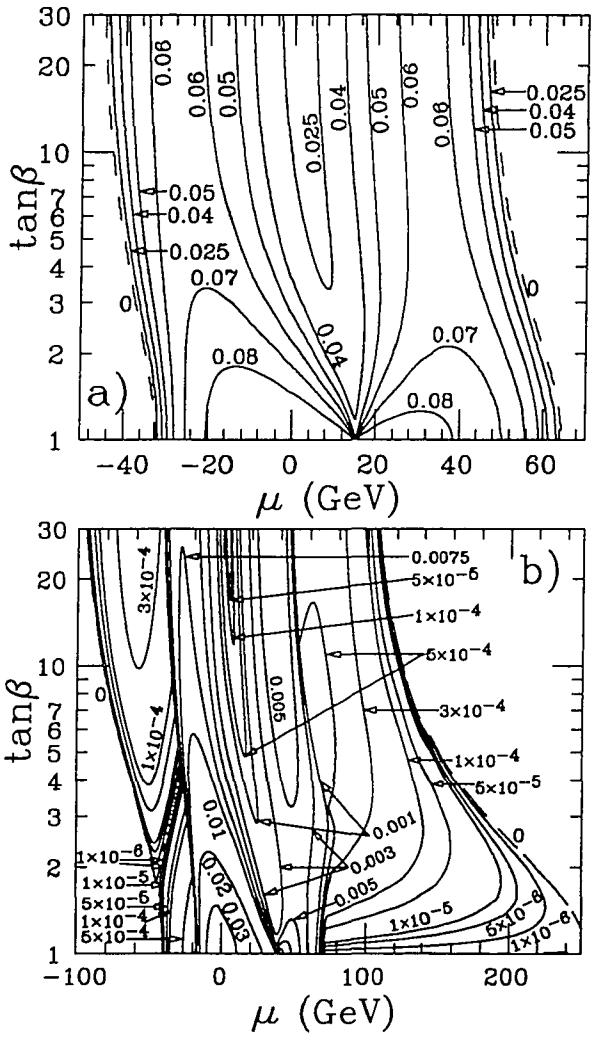

Figure 2.5: $B.F.(Z^0 \rightarrow \tilde{Z}_i\tilde{Z}_j)$ with i and j not both one.
a) high sparticle masses as in Fig. 2.4 a);
and b) lower sparticle masses as in Fig. 2.4 b).

2.4 Restrictions from Study of the Z^0 Width

The precise LEP measurements of the Z^0 total decay width and invisible decay widths[33]

$$\Gamma_{Z^0} = 2496.9 \pm 3.8\,\text{MeV} \quad \text{and} \quad \Gamma_{Z^0 invisible} = 499.4 \pm 3.5\ \text{MeV} \quad , \qquad (2.5)$$

respectively, can be used to set limits on the contributions to these quantities from as-of-yet undiscovered sparticles once lower bounds from purely SM channels are given. The SM contribution to Γ_{Z^0} will depend on the values used for the top quark mass, the strong coupling constant, and the SM Higgs mass (in decreasing order of importance). This introduces some uncertainty into the SM lower bounds. For $m_H(SM) \leq 1\,\text{TeV}$ and $\alpha_s(M_{Z^0}) \geq 0.111$, Figure 6 of Ref. [34] yields a lower bound of $\Gamma_{Z^0}(SM) > 2468\,\text{MeV}$ for $m_t \geq 90\,\text{GeV}$. If we take the DØ 95% C.L. lower limit on the top quark mass[35], 131 GeV, then the lower bound from [34] becomes $\Gamma_{Z^0}(SM) > 2474\,\text{MeV}$. And if we consider the tentative CDF measurements which fit a top quark mass of $174 \pm 10\ ^{+13}_{-12}$ GeV[36], then from [34] we obtain $\Gamma_{Z^0}(SM) > 2481\,\text{MeV}$ for $m_t \geq 164\,GeV$ and $\Gamma_{Z^0}(SM) > 2484\,\text{MeV}$ for $m_t \geq 174\,GeV$. The LEP measurement together with the SM lower bound leads to a 95% C.L. upper bound on the contribution of new particles to the total decay width of the Z^0 of

$$\Delta\Gamma_{Z^0} < 2496.9\,\text{MeV} + 1.64(3.8\,\text{MeV}) - 2468\,\text{MeV} = 35\,\text{MeV}$$
$$\text{for} \quad m_t \geq 90\,\text{GeV}; \qquad (2.6a)$$

$$\text{and} \quad \Delta\Gamma_{Z^0} < 29\,\text{MeV} \quad \text{for} \quad m_t \geq 131\,\text{GeV}, \qquad (2.6b)$$

$$< 22\,\text{MeV} \quad \text{for} \quad m_t \geq 164\,\text{GeV}, \qquad (2.6c)$$

$$< 19\,\text{MeV} \quad \text{for} \quad m_t \geq 174\,\text{GeV}. \qquad (2.6d)$$

Schaile [37], for $m_t \geq 90\,\text{GeV}$, $\alpha_s(M_{Z^0}) \geq 0.117$, and $m_H(SM) \leq 1\,\text{TeV}$, gives an even stricter limit of $\Delta\Gamma_{Z^0} < 13\,\text{MeV}$. Curves for the limits for the excluded regions for various values of $\Delta\Gamma_{Z^0}$ are shown in Figure 2.6. It can be seen that it virtually does not matter which of the above values is selected for the possible parameter choices displayed. For definiteness and to be conservative $\Delta\Gamma_{Z^0} < 35\,\text{MeV}$ will be

used hereinafter. Note that according to the figure the amount of parameter space excluded only increases significantly for $\Delta\Gamma_{Z^0}$'s well below any reasonable curerent bound selected. It should also be noted that only the standard deviation of the statistical error for the LEP Z^0 width measurement was considered in obtaining this number. Systematic errors were completely neglected. Clearly, when the systematic errors become comparable or larger than the statistical errors this becomes a very questionable procedure and a more careful analysis is then necessary.

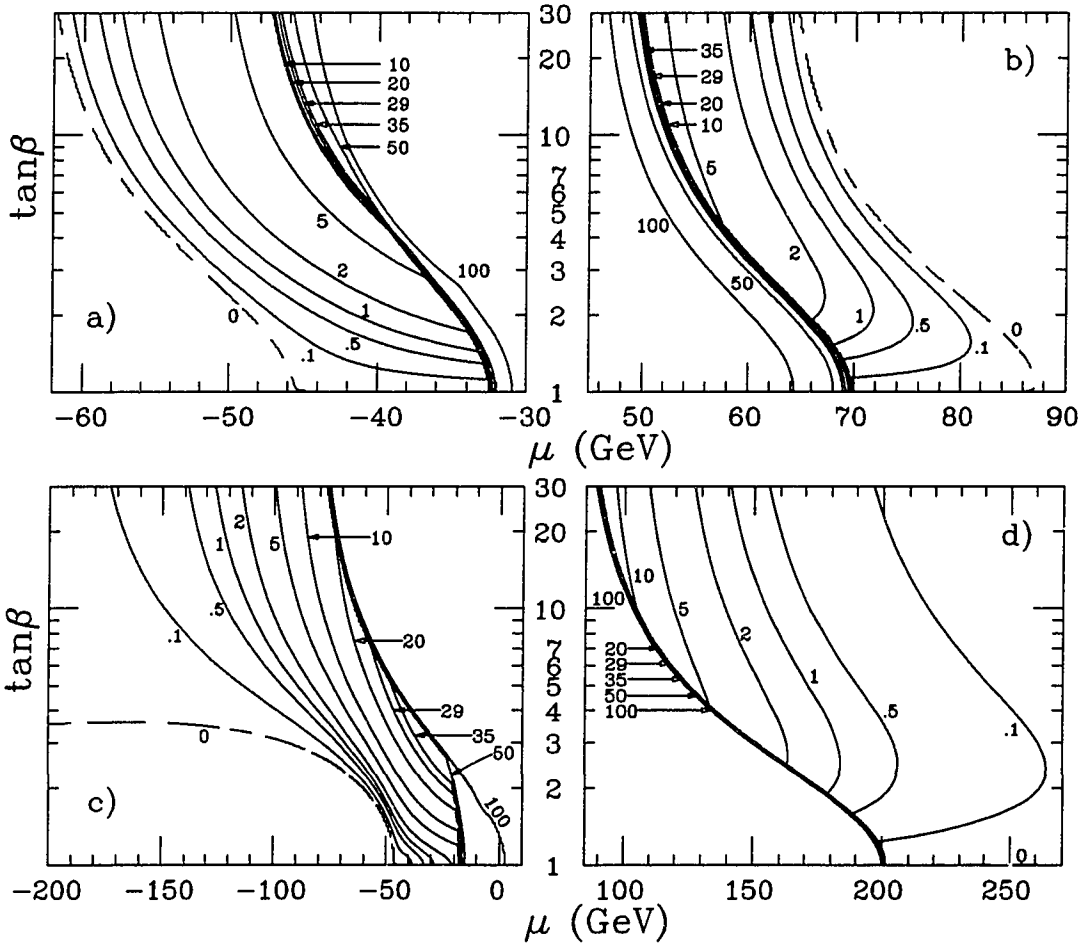

Figure 2.6: MSSM parameter region excluded by LEP's Z^0 total width measurement & the SM prediction. Number by each curve is $\Delta\Gamma_{Z^0}$ value (in MeV) used to generate that curve.
Excluded region is region *between* the two plots shown; *i.e.*, to the right of a curve in plots a) and c) and to the left of a curve in plots b) and d). For plots a) and b) $m_{\tilde{g}} = 1000\,\text{GeV} \doteq m_{\tilde{q}}$; for plots c) and d) $m_{\tilde{g}} = 300\,\text{GeV} \doteq m_{\tilde{q}}$. Other parameters as in Fig. 2.4 .

The restriction from the full Z^0 width measurement limits the allowable production of all sparticles that couple to the Z^0. In contrast to this, a restriction from the measured partial decay width of the Z^0 into particles which leave the detector without being detected serves to limit the rate of the decay of the Z^0 into a pair of LSP's, which in the MSSM, due to R-parity conservation, exhibit the same behavior in a detector as that of a SM neutrino. The SM contribution to $\Gamma_{Z^0 invisible}$ will also be dependent on the top quark mass, but the dependence is not as strong as in the case of the full Γ_{Z^0} (see Langacker [38]), and a SM lower bound of $\Gamma_{Z^0 invisible}(SM) > 499\,\mathrm{MeV}$ can be set. Then by an analogous procedure to the one given before, a 95% C.L. upper bound on the contribution of new neutral weakly-interacting particles to the invisible decay width of the Z^0, $\Delta\Gamma_{Z^0 invisible} < 6\,\mathrm{MeV}$, is obtained. The same caveat mentioned above concerning systematic errors also applies here, and the small value of $\Delta\Gamma_{Z^0 invisible}$ obtained thus makes its reliability somewhat doubtful. Figure 2.7 shows the region of the MSSM parameter space excluded by this measurement.

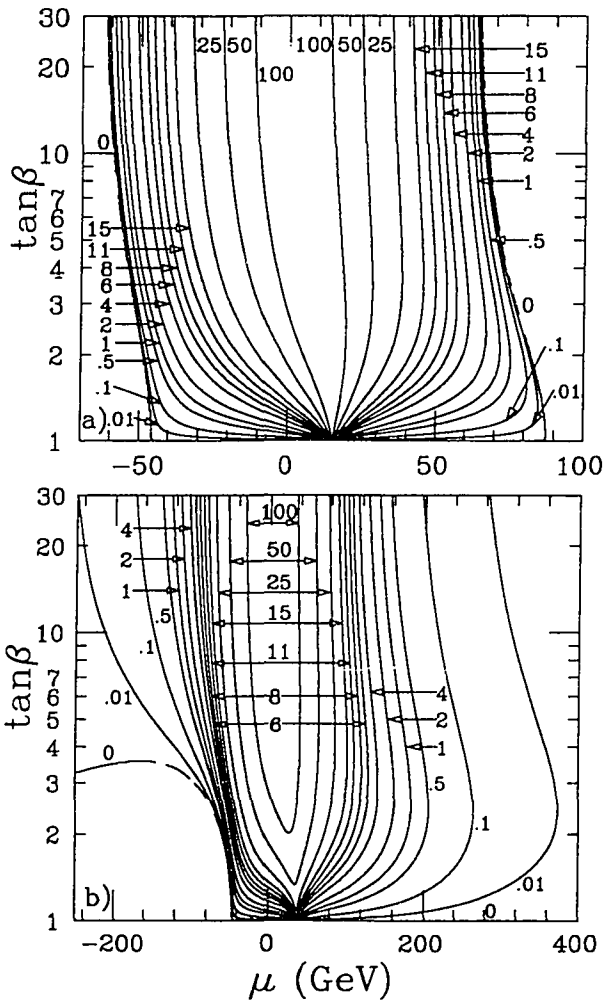

Figure 2.7: Excluded region from LEP's Z^0 invisible decay width measurement; numbers are $\Delta\Gamma_{Z^0 invisible}$ in MeV. Excluded region is *between* two labels of the same value. a) high sparticle masses as in Fig. 2.4 a); and b) lower sparticle masses as in Fig. 2.4 b).

Since cosmological constraints also demand that the LSP be neutral, as well as colorless, an additional requirement for a physically acceptable theory is that

$$m_{\widetilde{W}_1} > m_{\widetilde{Z}_1} \quad . \tag{2.7}$$

Figure 2.8 shows the MSSM parameter region excluded by this requirement. By comparison with Figure 2.4, it is seen that usually the constraint (2.4) will provide the tighter restriction.

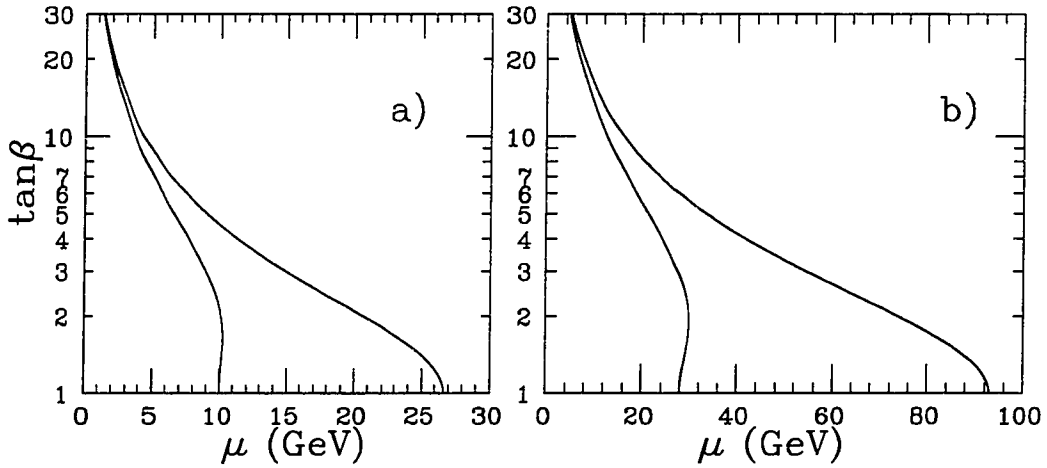

Figure 2.8: Region where mass of lighter chargino is less than the mass of the lightest neutralino ($m_{\widetilde{W}_1} < m_{\widetilde{Z}_1}$).
MSSM input parameters same as for Figure 2.4
with $m_{\tilde{g}} = 1000\,\text{GeV} \doteq m_{\tilde{q}}$ in plot a)
and $m_{\tilde{g}} = 300\,\text{GeV} \doteq m_{\tilde{q}}$ in plot b). The regions under and between the curves are excluded.

Squarks and sleptons, which could also contribute to Γ_{Z^0} if they were light enough to be produced in Z^0 decays, are too heavy to be so produced for most acceptable MSSM parameter sets. The failure to observe charged sleptons at LEP in general leads to the restriction [31,39-43]

$$m_{\tilde{l}^\pm} > 45\,\text{GeV} \quad . \tag{2.8}$$

The same limit will be assumed for squarks [44,45]. For reviews of the sfermion mass limits from LEP see [15,46]. These limits are somewhat sensitive to the LSP mass (for direct searches) and the $Z^0\widetilde{f}_1\overline{\widetilde{f}_1}$ coupling, which could accidently vanish with sfermion mixing (especially for stops). This restriction will generally not be significant for the heavier gluino, squark, and slepton masses we will be considering.

However, considerable intra-flavor mixing in the third generation of fermions may result in a very low stop squark or stau slepton mass. (See Eqns. (A.113) and the following special cases in Appendix A.) This could push these physical sfermion masses into the restricted region even though the input MSSM parameters are well above the LEP mass limits. Thus we see in Figure 2.9a) the mass of the lighter $\tilde{\tau}$-slepton moves into the LEP excluded region at the upper corners of the plot.

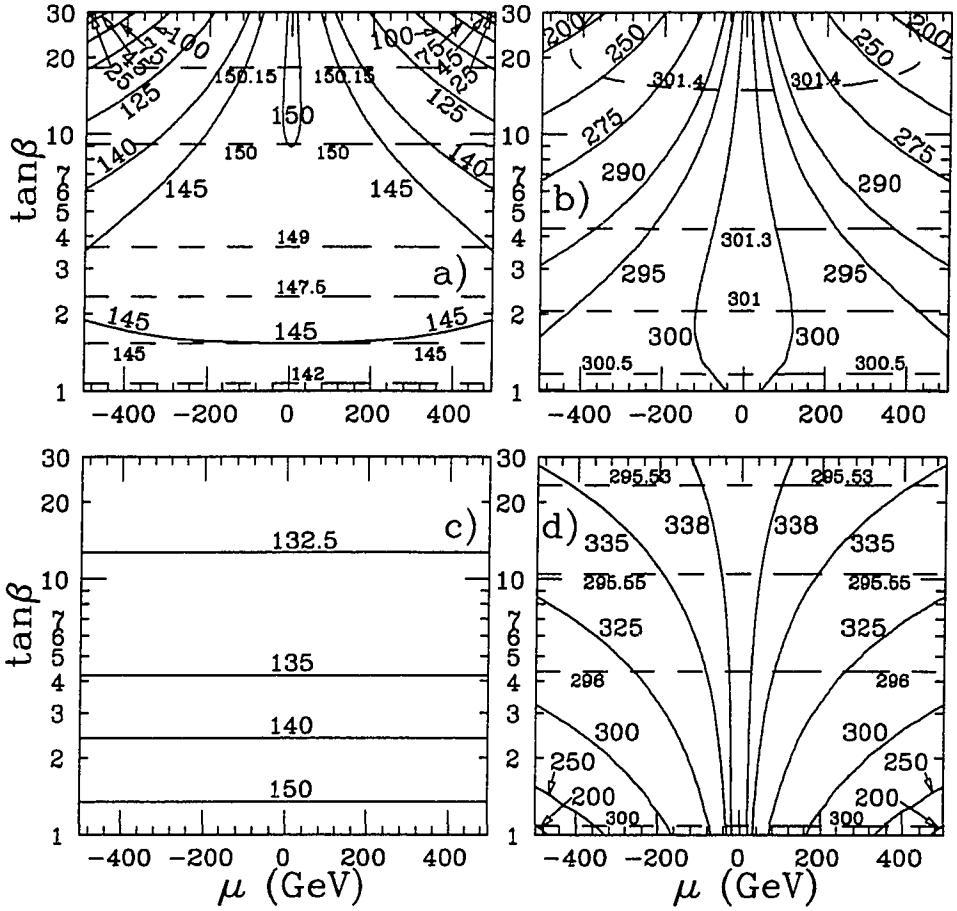

Figure 2.9: Masses (in GeV) of some of the sfermions for the case where $m_{\tilde{g}} = 300\,\text{GeV} \doteq m_{\tilde{q}}$ (other MSSM input parameters as in Figure 2.4).
Plot a) shows lighter $\tilde{\tau}$-slepton masses, $m_{\tilde{\tau}_1}$ (solid curves & larger labels), and lighter $\tilde{e}$-slepton masses, $m_{\tilde{e}_1}$ (dashed curves & smaller labels).
Plot b) shows lighter $\tilde{b}$-squark masses, $m_{\tilde{b}_1}$ (solid curves & larger labels), and lighter $\tilde{d}$-squark masses, $m_{\tilde{d}_1}$ (dashed curves & smaller labels).
Plot c) shows sneutrino masses.
Plot d) shows lighter $\tilde{t}$-squark masses, $m_{\tilde{t}_1}$ (solid curves & larger labels), and lighter $\tilde{u}$-squark masses, $m_{\tilde{u}_1}$ (dashed curves & smaller labels).

Note also that even if the input squark and slepton masses are roughly degenerate, the physical masses may be spread over a considerable range when the input values are fairly low. The slepton masses are also seen to be far less than the squark masses as a consequence of using Eqns. (1.10). This will prove to be very significant in the evaluation of the leptonic branching ratios for decaying neutralinos as will be discussed in Chapter 4. Finally, it should also be mentioned that light stop squark masses can decrease the value of the light Higgs boson mass through radiatively-induced corrections and thus increase the region of MSSM parameter space excluded by consideration of the Higgs boson production processes (2.2) and (2.3).

2.5 Combined Restrictions from LEP

To recapitulate, the following experimental limits are assumed: to generate an excluded region in the m_{H_p} *vs.* $\tan\beta$ plane, the lower bound on the SM Higgs boson mass is taken as $m_{H_{SM}} \geq 63.5\,\text{GeV}$. If the MSSM sparticle input parameters are low enough, searches for Higgs bosons also yield an excluded region in the μ *vs.* $\tan\beta$ plane for $m_{H_p} \simeq 250\,\text{GeV}$. Other constraints leading to excluded regions in this plane include a lower limit on the lighter chargino mass of 45 GeV and an upper limit on the branching ratio of the Z^0 into neutralinos other than just the lightest one of 5×10^{-5}. The latter value is probably somewhat conservative in view of the increasing number of Z^0's accummulated by LEP. Similarly, conservative values of $\Delta\Gamma_{Z^0} \leq 35\,\text{MeV}$ and $\Delta\Gamma_{Z^0 invisible} \leq 11\,\text{MeV}$ are adopted for the allowable contributions of sparticles to the Z^0 total width and invisible width, respectively. Inspection of Figures 2.5-2.7 show that the region excluded is fairly insensitive to the exact values used for these last three quantities. In fact, as these figures show, even very strict limits which seem experimentally inconceivable at this time generally do not add much to the parameter-space coverage obtained as experiments close in on the kinematical boundaries (shown by dashed curves and labelled by zeros in the figures). The total region excluded by the six constraints described above are shown in Figures 2.10 and 2.11. These will appear as blackened-in regions in many of the plots in the subsequent chapters.

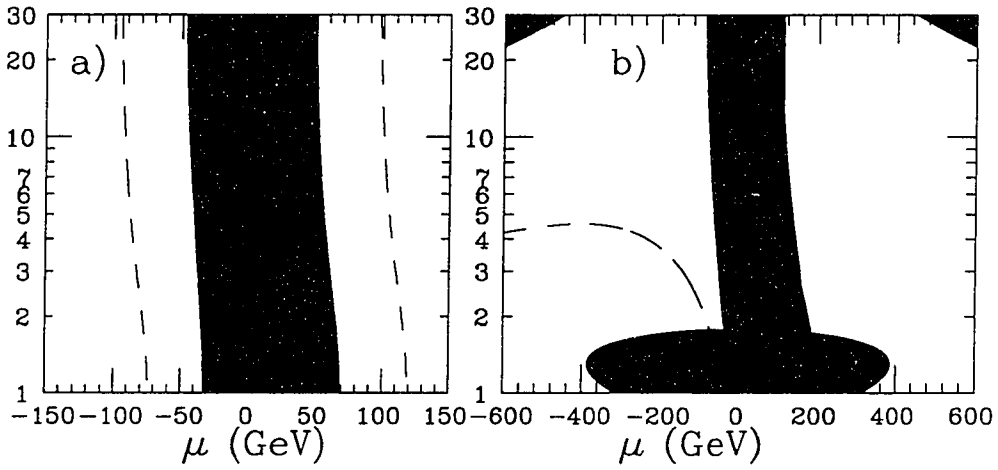

Figure 2.10: Restrictions from LEP in the μ *vs.* $\tan\beta$ plane.
MSSM input parameters: $m_{H_p} = 250\,\mathrm{GeV}$, $m^2_{\tilde{q}} - m^2_{\tilde{t}_L} = 50\,\mathrm{GeV}^2$, $m^2_{\tilde{q}} - m^2_{\tilde{t}_R} = 100\,\mathrm{GeV}^2$, $A_t = A_b = 0$, $m_t = 165\,\mathrm{GeV}$, $m_b = 5\,\mathrm{GeV}$, $M_{Z^0} = 91.19\,\mathrm{GeV}$, $\sin^2\theta_w = 0.23$, $\alpha_s(M_{Z^0}) = 0.118$, $\alpha_{em} = 1/128$, and in plot a) $m_{\tilde{g}} = 1000\,\mathrm{GeV} \doteq m_{\tilde{q}}$,
while in plot b) $m_{\tilde{g}} = 300\,\mathrm{GeV} \doteq m_{\tilde{q}}$.
$m_{\widetilde{W}_1} > 90\,\mathrm{GeV}$ outside of the dashed curves in plot a), and below and to the left of the dashed curve in b) — this gives some indication of the potential reach of LEP II.

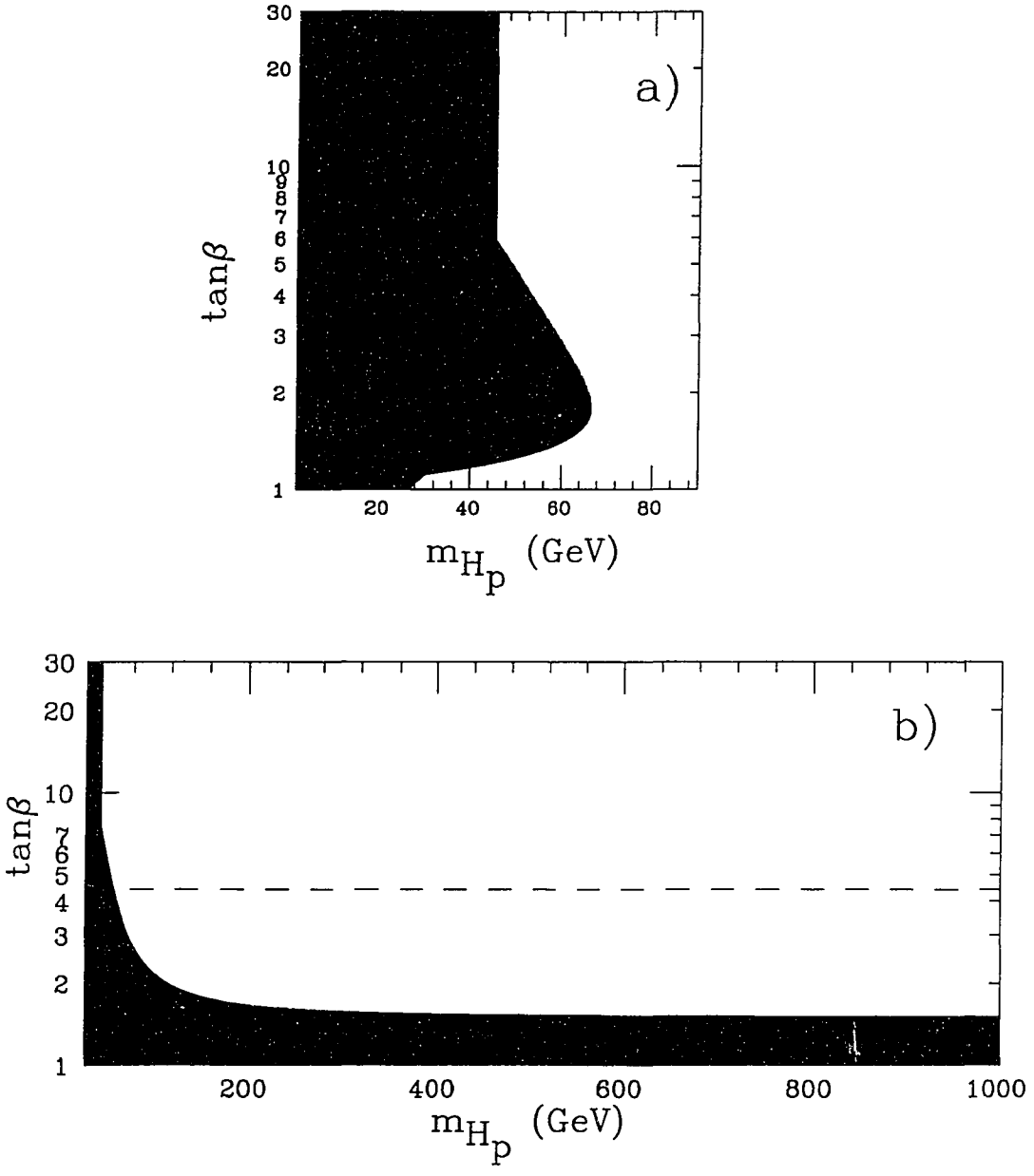

Figure 2.11: Restrictions from LEP in the m_{H_p} *vs.* $\tan\beta$ plane.
In plot a), $m_{\tilde{g}} = -\mu = 1000\,\mathrm{GeV} \doteq m_{\tilde{q}}$,
while in plot b) $m_{\tilde{g}} = -\mu = 300\,\mathrm{GeV} \doteq m_{\tilde{q}}$.
Other MSSM input parameters as in Figure 2.10.

In plot b) $m_{\widetilde{W}_1} > 90\,\mathrm{GeV}$ below the dashed line.

2.6 Potential Restrictions from LEP II

The exact operating parameters for the duration of the second phase of the LEP accelerator are still unclear. Thus, as in Ref. [47], optimistic and conservative projections for the reach of LEP II will be given. For the former, a CMS energy of $\sqrt{s} = 190\,\text{GeV}$ is taken, together with a lower limit of 0.05 pb for an observable cross-section for either of the Higgs boson production processes. For the latter, a CMS energy of $\sqrt{s} = 175\,\text{GeV}$ is taken, together a lower limit of 0.2 pb for an observable cross-section. This conservative scenario is represented by the solid curves in the plots of Figure 2.12, while the optimistic scenario is represented by dashed curves.

In additon to the $H_\ell Z^0$ and $H_p H_\ell$ Higgs boson production mechanisms already discussed, the analogous modes involving the heavy Higgs boson, $H_h Z^0$ and $H_p H_h$, are also detectable in rather limited regions of the parameter space at the higher energy of LEP II. It should be noted from the plots of Fig. 2.12 that the heavy Higgs boson production modes do not increase the reach of LEP II. Still, detecting more than one type of Higgs boson is of vital importance in establishing the existence of an extended Higgs sector; but, the H_h production signals only offer that possibility in a few small patches of the available parameter space.

Notice that if the top quark is sufficiently heavy and the stop squarks are sufficiently light, the failure to observe any Higgs boson signal at LEP II will not provide any bound at all upon the allowable values for $\tan\beta$. The sensitivity to these quantities comes about through their effects of the radiative corrections to the mass of the light Higgs boson. As can be easily by studying Eqns. (A.143-145) of Appendix A, the results are more sensitive to m_t than to the mass of the $\tilde{t}$-squarks. Nonetheless, as the plots in Fig. 2.12 demonstrate, changes in the values of the stop squark masses can significantly affect the predicted reach of LEP II. It should also be noted that as the absolute value of the stop A-term, $|A_t|$, is made very large, the mass of lighter physical stop, $m_{\tilde{t}_1}$, exhibits a sudden and drastic reduction (see Eqn. (A.117)); m_{H_ℓ} shows a similar though somewhat less pronounced behavior. For Fig. 2.12, A_t was set equal to zero for all plots. Thus, even if the stop mass inputs, $m_{\tilde{t}_L}$

and $m_{\tilde{t_R}}$, are quite high, a large value of $|A_t|$, $|A_t| \sim$ 2-3$m_{\tilde{q}}$, can make the left-hand plots of Fig. 2.12 look more like the right-hand plots of Fig. 2.12. However, the dependence on A_t tends to be fairly slight when it is only allowed to vary through more moderate values.

The range of chargino masses examined will also be extended by LEP II. Though the onset of W^+W^-–pair production may make isolation and identification of the chargino signals more difficult, it is still expected that LEP II will be able to discover any chargino whose mass is below the beam energy by more than a few GeV [48,49]. This is also in spite of the possibility that the chargino decays may become more complicated than the simple $\widetilde{W}_1 \rightarrow f f' \tilde{Z}_1$ which may be expected at LEP I. With a heavier chargino, cascade decay with the chargino initially decaying into a heavier neutralino (such as $\tilde{Z}_2$) which then decays to the LSP might become kinematically accessible. As a rough estimate, it will be assumed that chargino masses up to $m_{\widetilde{W}_1} = 90\,\mathrm{GeV}$ will be probed by LEP II. This condition is represented in the plots of Figures 2.10 and 2.11 as dashed curves.

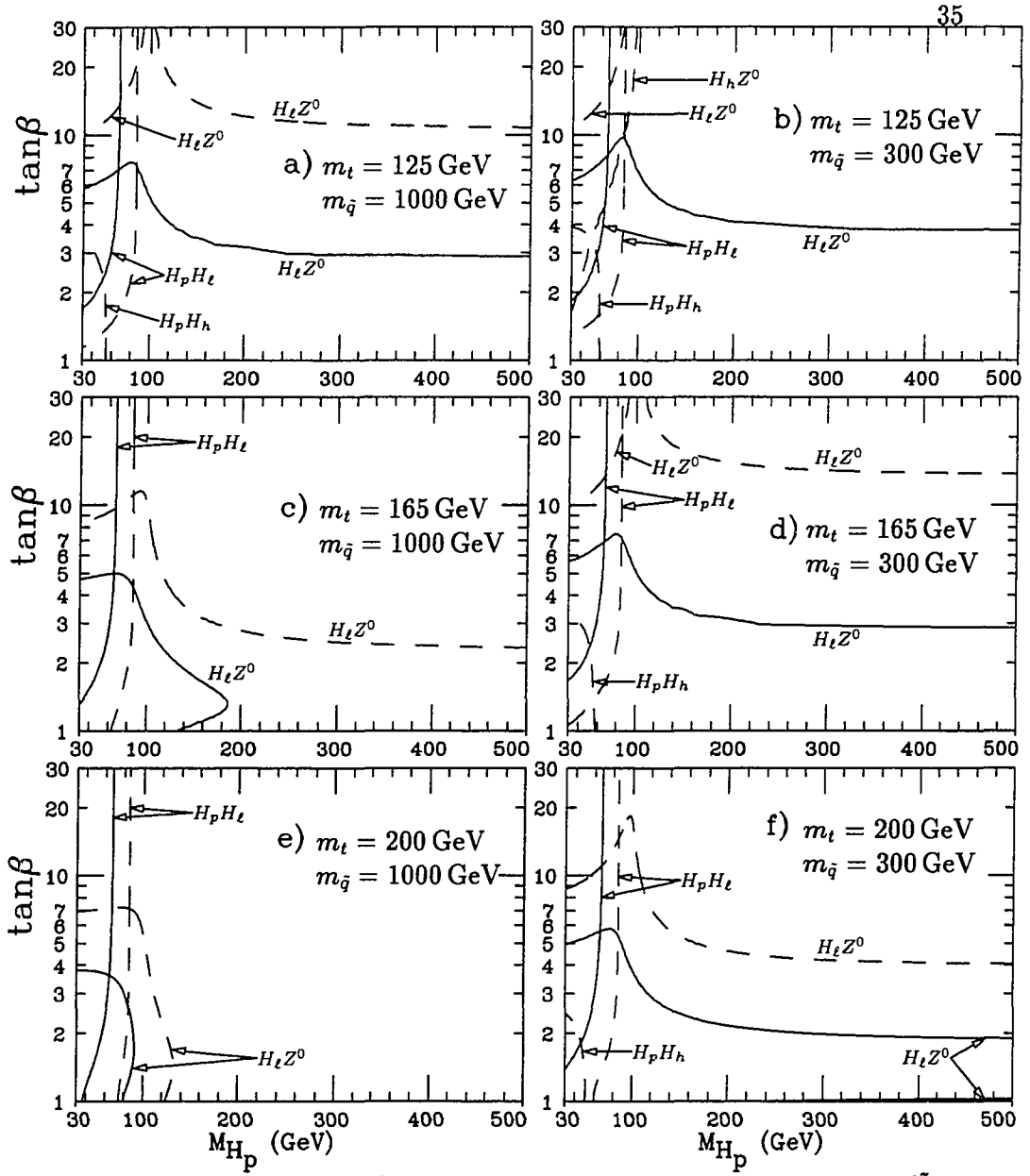

Figure 2.12: Potential reach of LEP II for different values of m_t and $m_{\tilde{q}}$ ($\tilde{t}$-squark masses are determined from $m_{\tilde{q}}$ via $m^2_{\tilde{t}_L} = m^2_{\tilde{q}} - 100\,\mathrm{GeV}^2$ and $m^2_{\tilde{t}_R} = m^2_{\tilde{q}} - 50\,\mathrm{GeV}^2$ — so $m_{\tilde{t}_L}$ and $m_{\tilde{t}_R}$ do not differ much from $m_{\tilde{q}}$.) Solid (dashes) curves are for the conservative (optimistic) estimate of the LEP II capabilities. (See last page for details.) Potential excluded regions are generally *below* the curves and/or to the *left* of the curves. Exceptions to this are in b) where the $H_\ell Z^0$ signal in the optimistic case would exclude all but the upper left-hand corner, and in f) where in the conservative case a small sliver of parameter space around $\tan\beta \simeq 1$ for higher values of m_{H_p} would remain unexcluded by the $H_\ell Z^0$ signal.

Chapter 3

Higgs Boson Production

There are several means of producing Higgs bosons at hadron supercolliders. For a SM Higgs Boson in the intermediate mass range $M_{Z^0} < m_H < 2M_W$, production via gluon fusion dominates. This actually occurs through the quark loop diagram shown in Fig. 3.1a). In the MSSM, squark loop diagrams are also present, as shown in Fig. 3.1b),c). The formula for the cross-section for Higgs production via gluon fusion at a hadron collider of CMS energy $\sqrt{s}$ is given by (see, *e.g.*, Ref. [50]):

$$\sigma(pp \to gg \to H\,X) = \Gamma(H \to gg)\,\frac{\pi^2}{8m_H^3}\tau \int_\tau^1 \frac{dx}{x}\, D_{g/p}\Big(x, m_H^2\Big)\, D_{g/p}\Big(\tfrac{\tau}{x}, m_H^2\Big) \quad (3.1)$$

where $\tau = \frac{m_H^2}{s}$ and $D_{g/p}(x, Q^2)$ is the gluon distribution function for the proton. Here $\Gamma(H \to gg)$ will include the contributions from squark loops for CP-even Higgs bosons within the MSSM (which may be significant if the squarks are not too heavy). An expression for $\Gamma(H \to gg)$ is given in Appendix B. The rest of Eqn. (3.1) will be the same in the case of the MSSM as for the SM case.

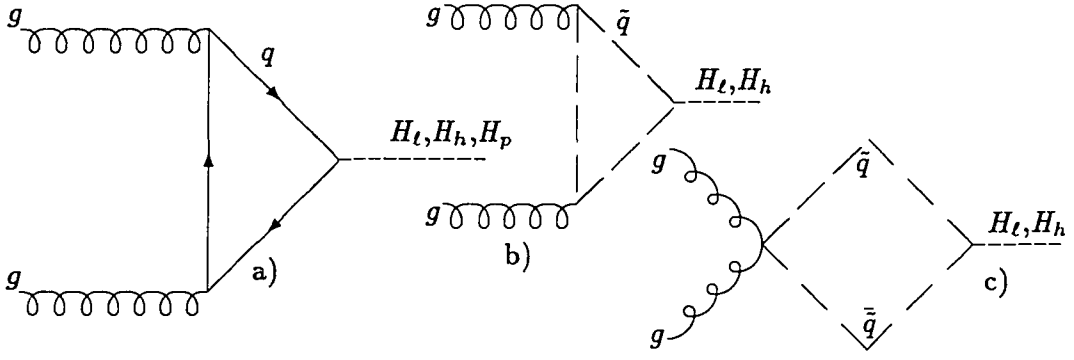

Figure 3.1: Diagrams for the production of Higgs bosons by gluon fusion via a) a quark loop and b), c) squark loops. (Incoming protons and all spectator partons are omitted in these diagrams as well as in all other diagrams in this chapter.)

There are a number of parametrizations for $D_{g/p}(x, Q^2)$ available, and it is of interest to see how much the production cross-section is influenced by which structure function set is employed. Within the MSSM, the decay width of a Higgs boson into a pair of gluons, $\Gamma(H \to gg)$, will be dependent upon which Higgs boson we are considering, and will also intoduce numerous MSSM input parameters into the calculation of the cross-section. These have nothing to do with the distribution functions we wish to compare. Thus it makes the comparison more general to consider the ratio $\sigma(pp \to gg \to H)/\Gamma(H \to gg)$. Then the only important inputs are the Higgs mass itself and SM parameters, including the top and bottom quark masses, This is done is Fig. 3.2. It is apparent that all the parametrizations shown yield similar results, and the choice of structure functions is not a major consideration here.

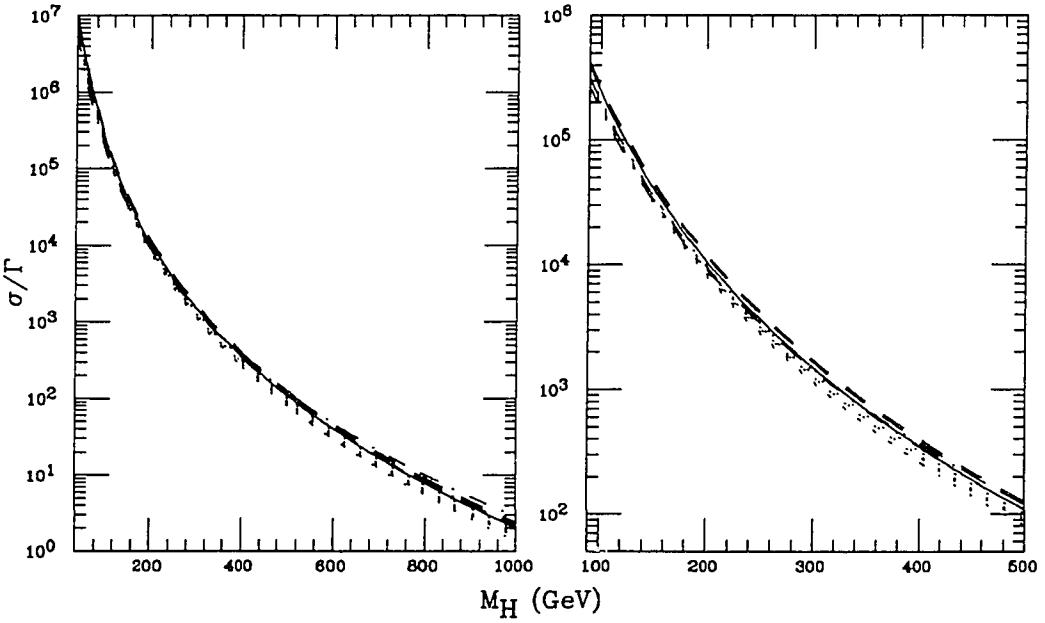

Figure 3.2: $\sigma(p\,p \to H$via gluon fusion$)/\Gamma(H \to g\,g)$ for various parton distribution sets ($\sqrt{s}$ = 14 TeV). The solid line (in the middle) is Owens Set 1.1. Dashes (generally high) are EHLQ sets 1 and 2, and dotdashes (high for large m_H) are HMRS sets EMC and BCDMS. Dots (generally low) are CTEQ sets 1M, 1MS, 1ML, 1D, and 1L. The bottom quark mass is set to 5 GeV. See Refs. [51-55] for information on the parton distribution sets.

Not included in Eqn. (3.1) are QCD corrections to the gluon fusion process from diagrams with extra gluons as indicated in Fig. 3.3 below. This has been studied (for quark loops) by Spira, Djouadi, Graudenz, and Zerwas [56,57], who found that these corrections are generally positive, increasing production cross-sections by up to factors of around two. (Dawson, Kauffman, and Schaffer [58-61] have obtained very similar results.) These corrections were found to depend only weakly on the Higgs boson masses; however, they were strongly dependent on the value of $\tan\beta$. Since these corrections have not been incorporated into the production rates given here and used in the rest of this work, the production rates given can be expected to be an under-estimate of the actual MSSM rates, and are thus somewhat conservative.

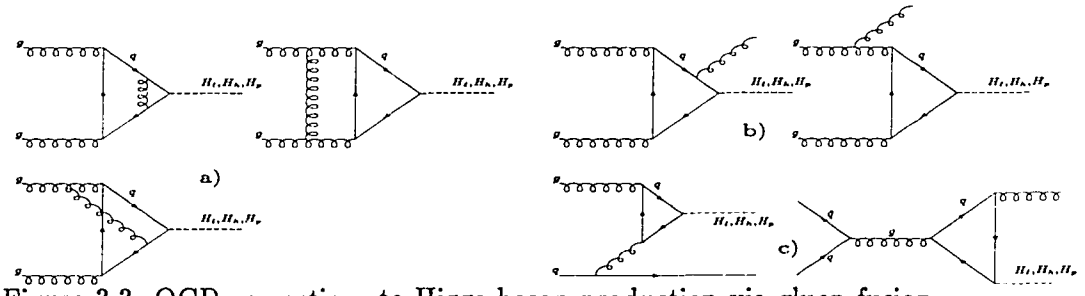

Figure 3.3: QCD corrections to Higgs boson production via gluon fusion
a) virtual corrections b) radiation of real gluons c) production via gq and $q\bar{q}$ collisions

Higgs bosons can also be produced via fusion of the quark partons of the colliding protons. Generally, these cross-sections will be considerably smaller than that from gluon fusion. However, in the MSSM, the bottom quark Yukawa coupling is inversely proportional to $\cos\beta$, and thus, for large values of $\tan\beta$, $\Gamma(H \to b\bar{b})$ can be enhanced substantially. This may make the production of Higgs bosons via $b\bar{b}$-fusion, as shown in Fig. 3.4, comparable to that from gluon fusion. The cross-section for Higgs production via $b\bar{b}$ fusion is given by [62]:

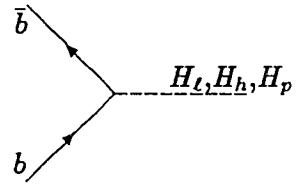

Figure 3.4: Simple 2→1 Higgs boson production via $b\,\bar{b}$ fusion

$$\sigma(pp \to b\bar{b} \to H\,X) = \frac{\Gamma'(H \to b\bar{b})}{\lambda^{\frac{1}{2}}(1, \frac{m_b^2}{m_H^2}, \frac{m_b^2}{m_H^2})} \frac{16\pi^2}{m_H^3} \frac{1}{4}\frac{1}{9} \times F_{DW}\,\tau \int_\tau^1 \frac{dx}{x}\left[D_{b/p}\left(x, m_H^2\right) D_{\bar{b}/p}\left(\tfrac{\tau}{x}, m_H^2\right) + (b \leftrightarrow \bar{b})\right] \tag{3.2}$$

where $D_{b/p}(x, Q^2)$ is the bottom-quark distribution function for the proton. An expression for $\Gamma'(H \rightarrow b\bar{b})$ is given in Appendix B. The factor F_{DW} is a fit to the results of Ref. [63] designed to incorporate the full 2→3 process $gg \rightarrow b\bar{b}H$, as depicted in Fig. 3.5, into the 2→1 $b\bar{b}$ fusion mechanism. The incorporation of the

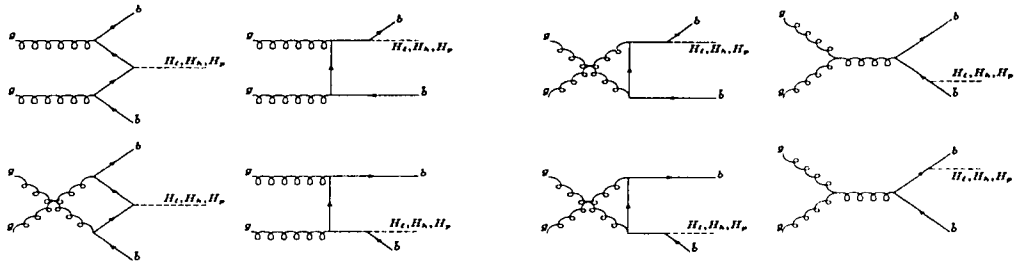

Figure 3.5: Diagrams contributing to the process $gg \rightarrow b\bar{b}H$

2→3 process was found to lower the Higgs production rate from $b\bar{b}$ fusion. From Fig. 10 of Dicus and Willenbrock [63], the following parametrization is obtained:

$$F_{DW} = \left[16.2 \; - \; 4.28 \log\left(\frac{m_H}{q}\right) \; + \; 0.31\left[\log\left(\frac{m_H}{q}\right)\right]^2\right]^{-1} \quad . \tag{3.3}$$

Here $q = 1$ GeV. Fig. 3.6 below shows a plot of F_{DW}.

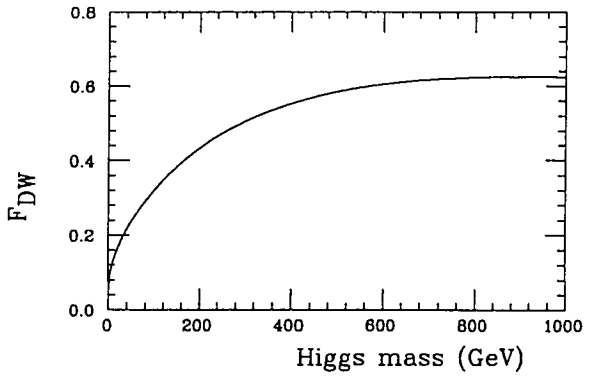

Figure 3.6: Correction factor F_{DW} to account for 2→3 processes.

As with the gluon distribution function, there are a number of parametrizations for $D_{b/p}(x, Q^2)$ available. A comparison of various parametrizations analogous to that given in Fig. 3.2 for gluon fusion is given in Fig. 3.7 on the next page for $b\bar{b}$ fusion. Here we find the selection of a set of structure functions is somewhat more significant than it was for gluon fusion.

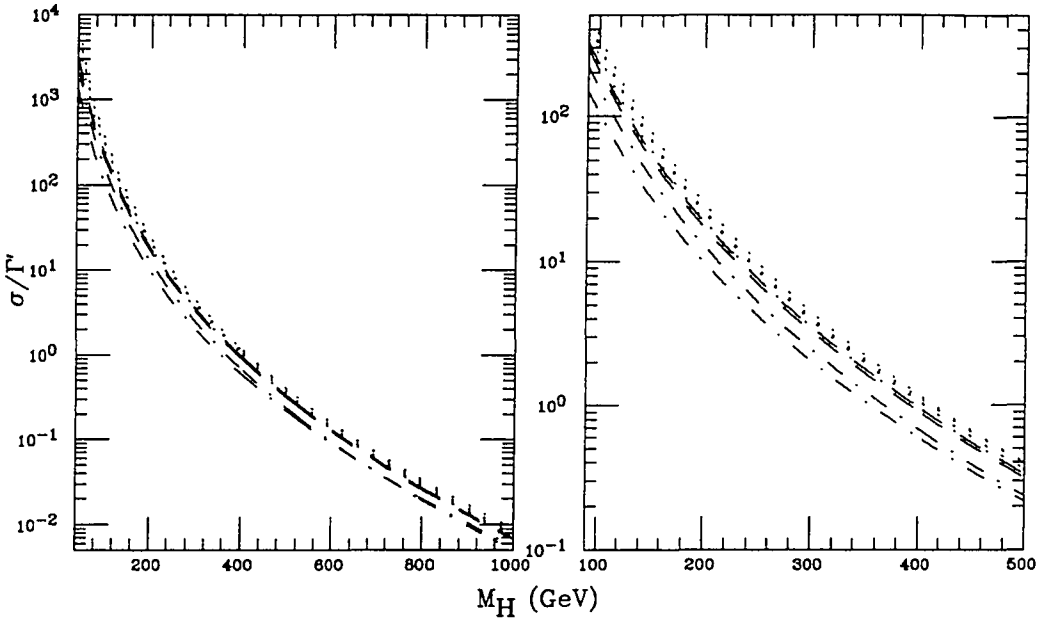

Figure 3.7: $\sigma(pp \rightarrow H$via $b\bar{b}$ fusion$)/\Gamma'(H \rightarrow b\bar{b})$ for various parton distribution sets ($\sqrt{s}$ = 14 TeV). Dashes (in the middle) are EHLQ sets 1 and 2, dotdashes (lower) are HMRS sets EMC and BCDMS. Dots (higher) are CTEQ sets 1M, 1MS, 1ML, 1D, and 1L. The bottom quark mass is set to 5 GeV. See Refs. [51-55] for information on the parton distribution sets.

For the case of a heavy SM Higgs boson, $m_H >> 2M_W$, production via gauge boson fusion dominates. However, for heavy neutral MSSM Higgs bosons, this rate is usually small, due to unfavorable mixing angles in the coupling of heavy Higgs boson, H_h, to the gauge bosons (to see this note Table 1.2 and Figure 4.2) and the lack of any tree level coupling of the pseudoscalar Higgs boson to the gauge bosons.

Another mechanism for producing MSSM Higgs bosons at hadron colliders is via decay chains resulting from the direct production of gluinos or squarks. It may be possible to use some of the defining characteristics of such supersymmetric events to substantially reduce the backgrounds to such events. The merits of this alternative production mechanism unique to supersymmetry will be discussed further in Chapter 6.

The production cross-sections from gluon fusion and $b\bar{b}$ fusion are added to give the total cross-section rates used in this work. These are shown in the m_{H_p} vs. $\tan\beta$ plane for the neutral MSSM Higgs bosons in Figures 3.8-3.12 on the following pages. This is for a proton-proton collider with $\sqrt{s} = 14\,\text{TeV}$, which is roughly the energy proposed for the LHC collider to be constructed at CERN. In these figures the EHLQ set 1 parton distributions are used (this set will be used throughout the rest of this work). It should be noted that Higgs bosons produced via the decay of other Higgs boson species, such as the light Higgs bosons from $H_h \rightarrow H_\ell H_\ell$ or the pseudoscalar Higgs boson from $H_h \rightarrow H_p Z^0$, are not included in these rates. The LEP excluded region discussed in Ch. 2 appears as a blacked-out region at the left-hand side of each plot.

From Fig. 3.8 for H_ℓ, we see that the production rate remains fairly constant for a given $\tan\beta$ when m_{H_p} is above 200 GeV or so. It also does not vary much as $\tan\beta$ is changed in this region. This is principally due to the fact that the light Higgs boson mass has become saturated at very close to its upper limit and thus is almost unchanging in this region. The production rates for the heavy Higgs boson and the pseudoscalar Higgs boson fall off markedly as m_{H_p} increases, dropping below 1 pb for m_{H_p} above 400 or 500 GeV (as can be seen in Figs. 3.9 and 3.11). Thus the mass zone below this (shown in more detail in Figures 3.10 and 3.12) will be the main region of interest. Based on Figures 3.9 and 3.11, pseudoscalar Higgs masses above 500 GeV will be neglected for H_h and H_p signals. Note that for high $\tan\beta$ and low m_{H_p}, the pseudoscalar Higgs boson production rate can be considerably larger than the heavy Higgs boson rate. This is due in part to the fact that m_{H_h} is a fair bit larger than m_{H_p} in this area of parameter space. Production rates for all the neutral Higgs boson types generally increase with increasing $\tan\beta$. The most significant contribution of the $b\bar{b}$-fusion production mode is in the high $\tan\beta$ region ($\tan\beta \gtrsim 12$) for $100\,\text{GeV} \lesssim m_{H_p} \lesssim 200\,\text{GeV}$ (basically the intermediate mass region), where the $b\bar{b}$-fusion production rate for heavy and pseudoscalar Higgs bosons is approximately equal to the production rate from gluon fusion.

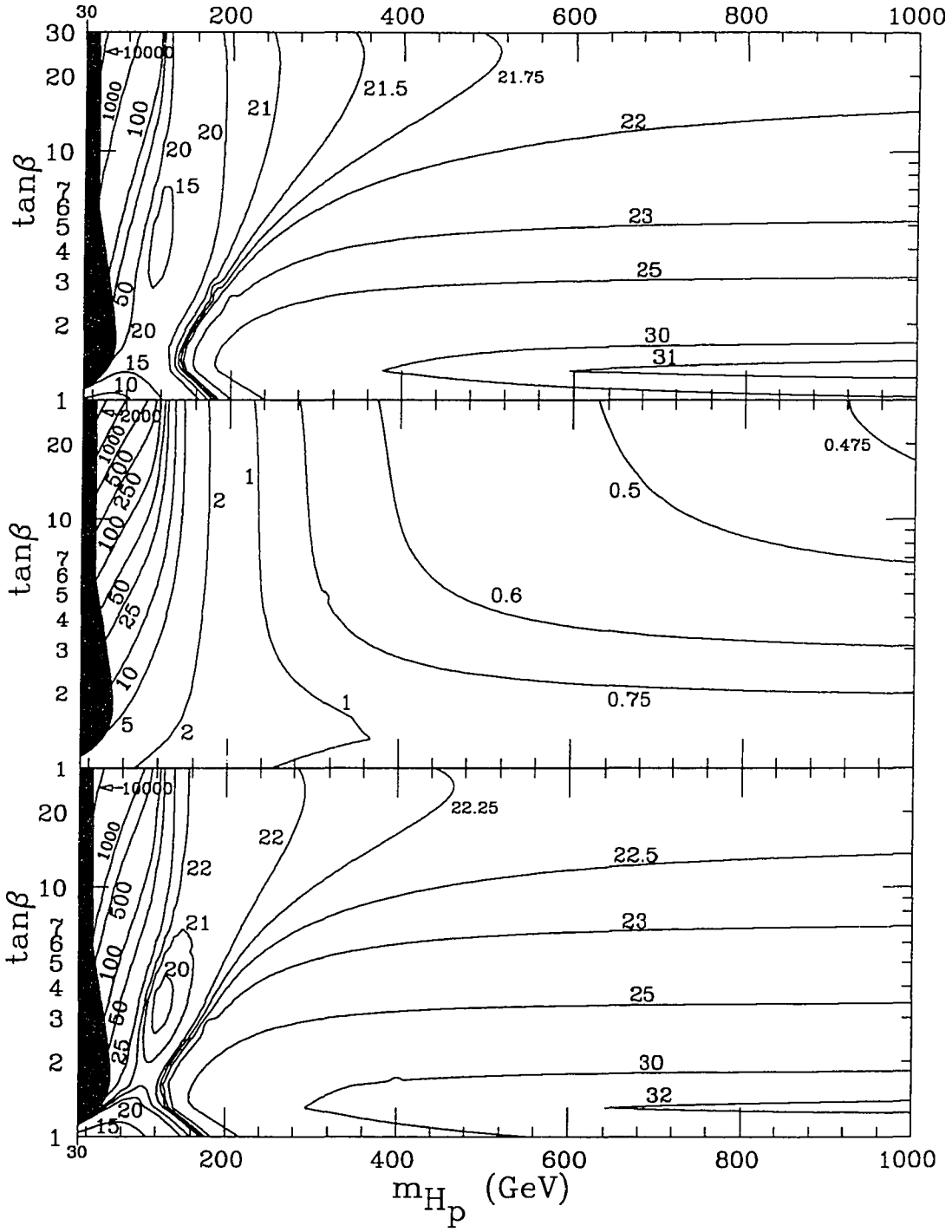

Figure 3.8: Light Higgs boson production (in pb) at pp collider via gluon fusion (upper), $b\bar{b}$-fusion (center), and combined (lower); $\sqrt{s} = 14\,\text{TeV}$. Also: $m_{\tilde{g}} = -\mu = 1000\,\text{GeV} \doteq m_{\tilde{q}}$, $m^2_{\tilde{q}} - m^2_{\tilde{t}_L} = 50\,\text{GeV}^2$, $m^2_{\tilde{q}} - m^2_{\tilde{t}_R} = 100\,\text{GeV}^2$, $A_t = A_b = 0$, $m_t = 165\,\text{GeV}$, $m_b = 5\,\text{GeV}$.

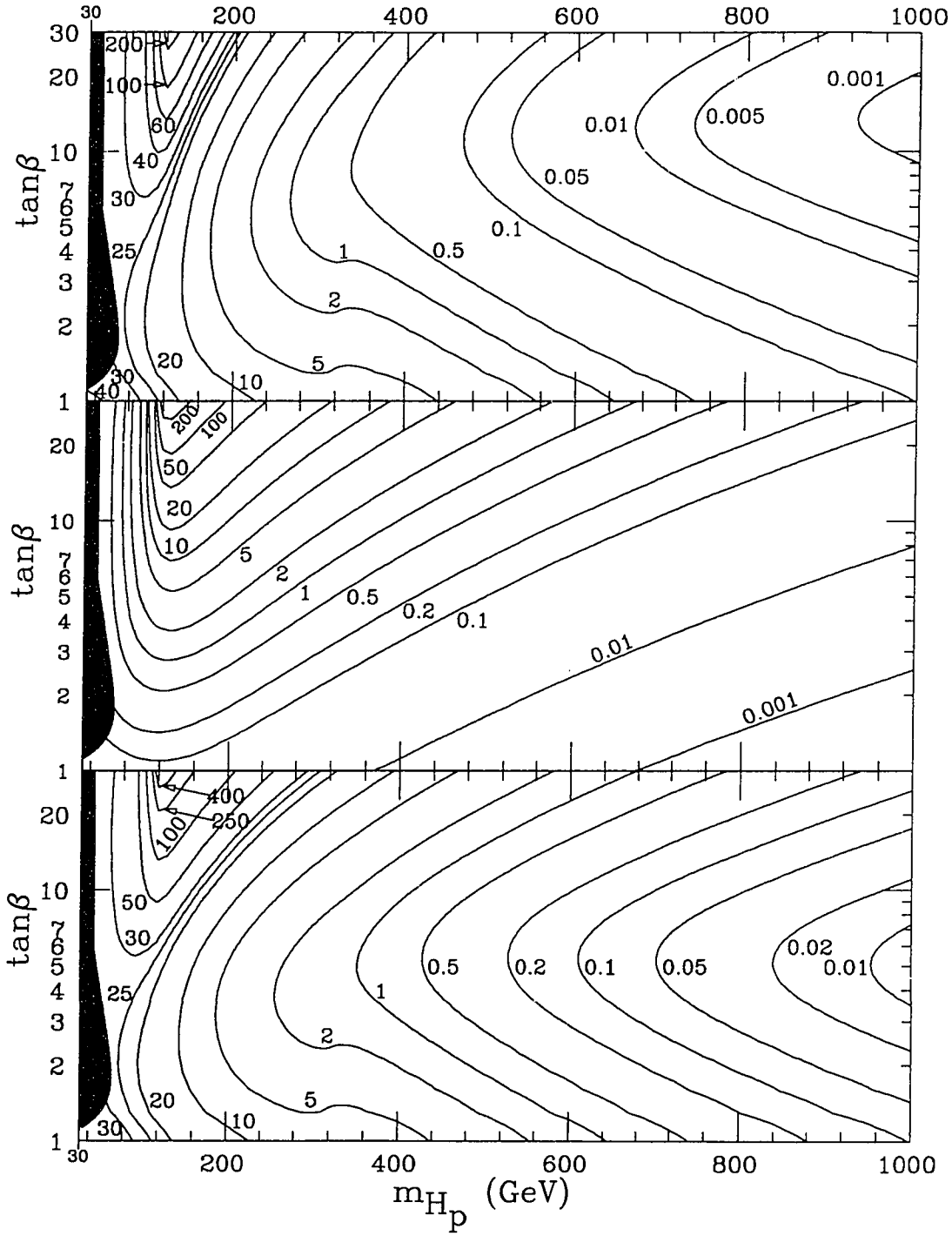

Figure 3.9: Heavy Higgs boson production (in pb) via gluon fusion (upper), $b\bar{b}$-fusion (center), and combined (lower). Other parameters are the same as those cited in Fugure 3.10.

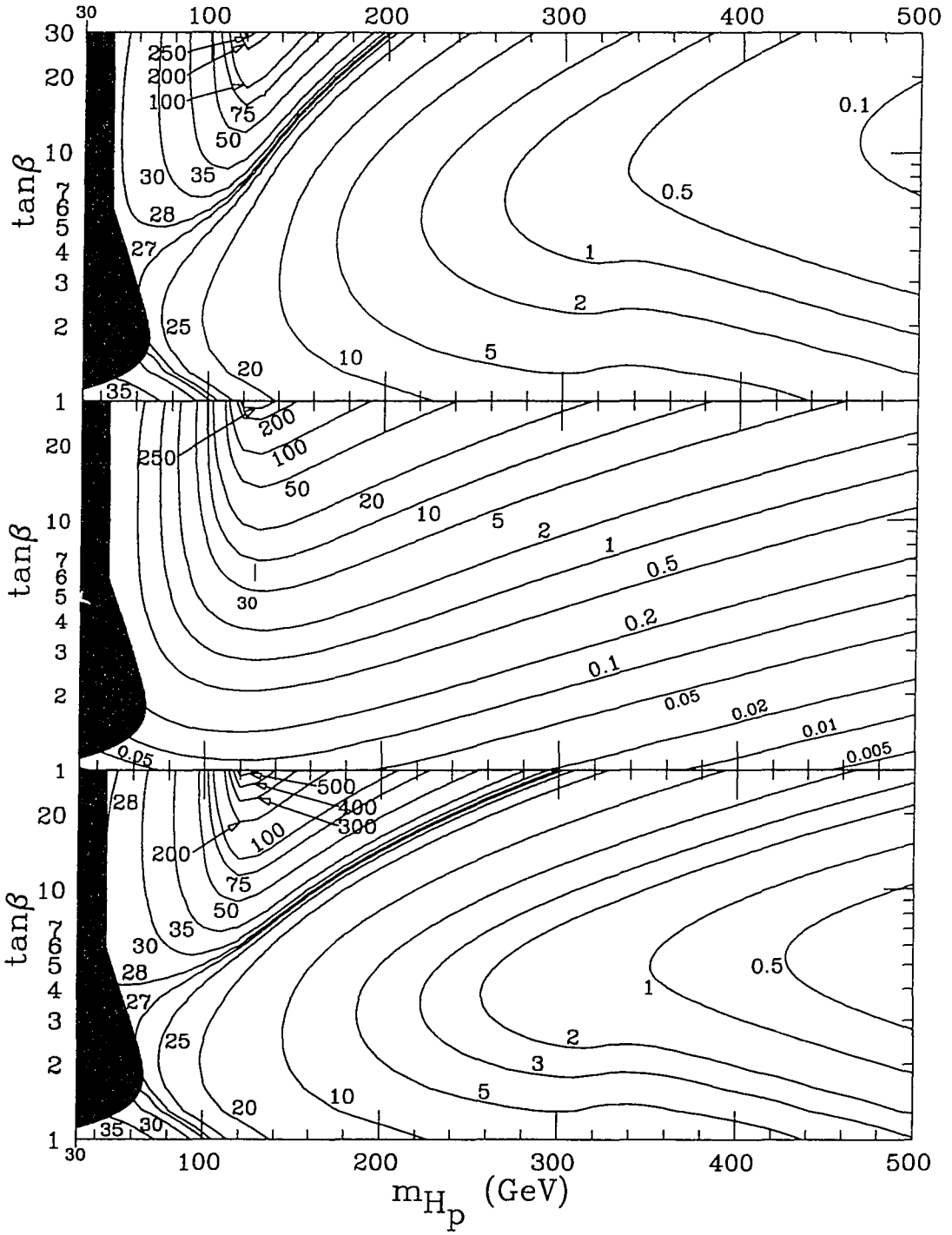

Figure 3.10: Heavy Higgs boson production (in pb) via gluon fusion (upper), $b\bar{b}$-fusion (center), and combined (lower) — a closer look at the lower mass region. Other parameters are the same as those cited in Fugure 3.8.

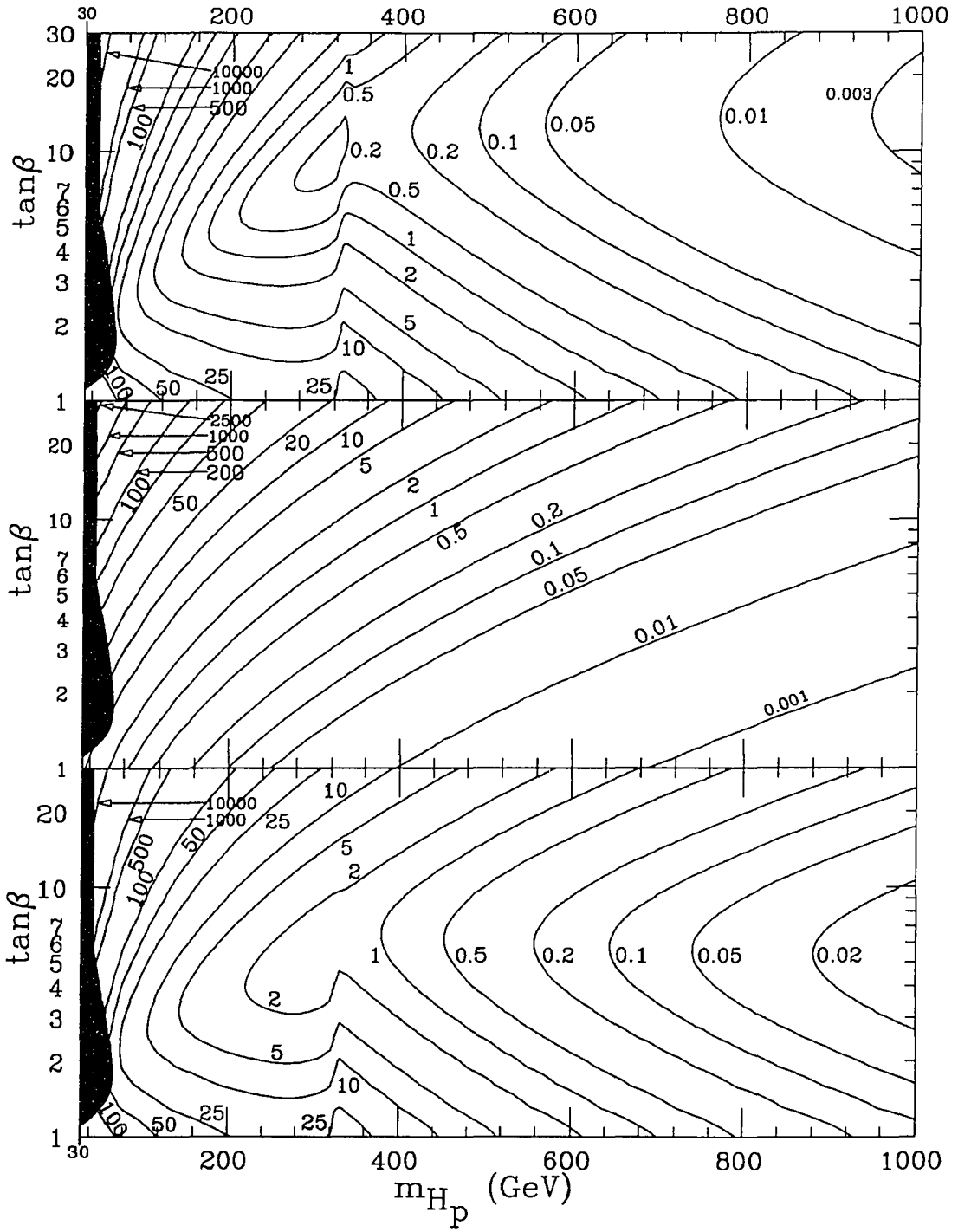

Figure 3.11: Pseudoscalar Higgs boson production (in pb) via gluon fusion (upper), $b\bar{b}$-fusion (center), and combined (lower). Other parameters are the same as those cited in Fugure 3.8.

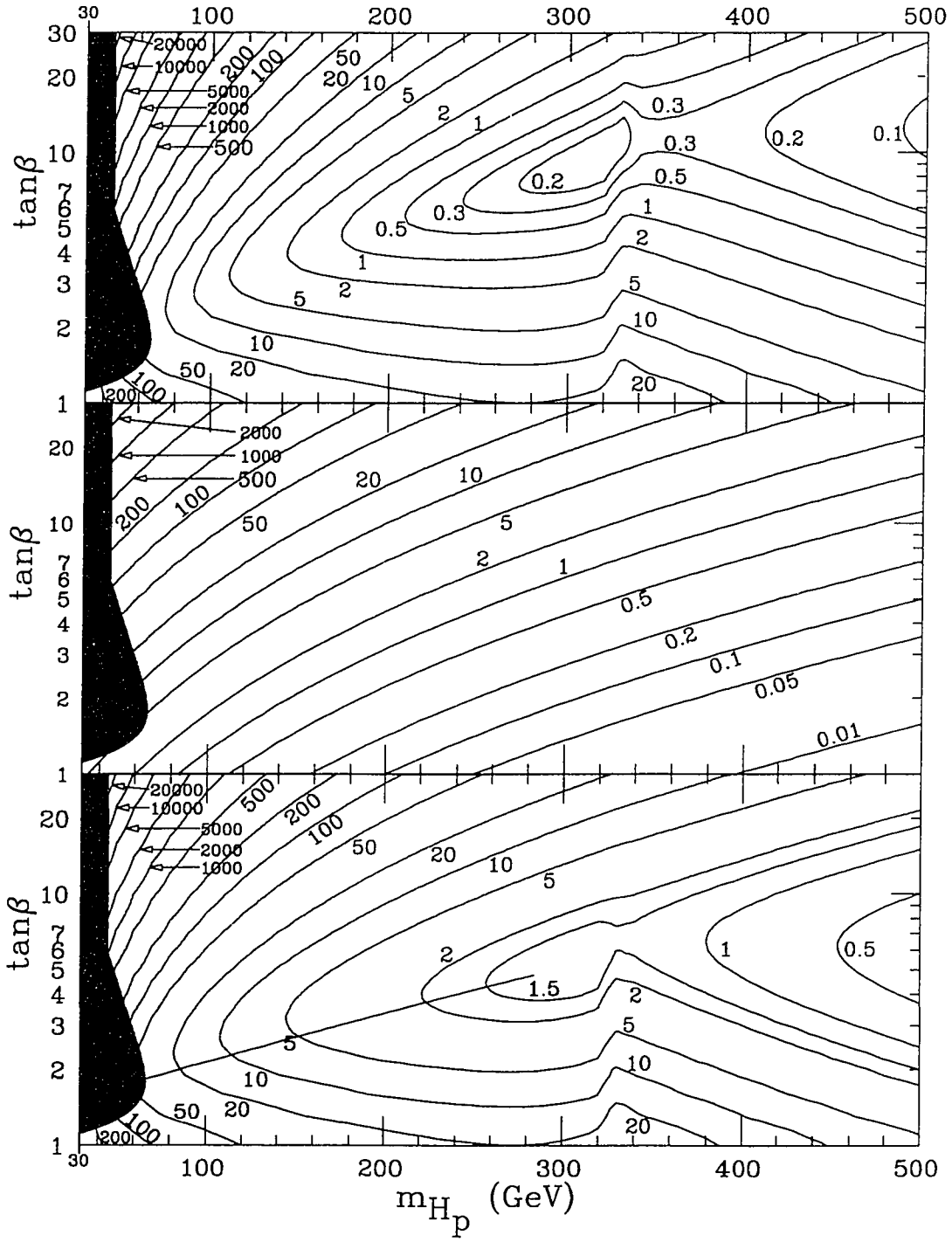

Figure 3.12: Pseudoscalar Higgs boson production (in pb) via gluon fusion (upper), $b\bar{b}$-fusion (center), and combined (lower) — a closer look at the lower mass region. Other parameters are the same as those cited in Fugure 3.8.

For the preceeding plots, the MSSM input parameters were chosen such that sparticle masses are quite large. Lowering the sparticle masses does not alter the plots very much. The main effect of lowering the sparticle masses is to lower the light and heavy Higgs boson masses for a given pseudoscalar Higgs mass. This is due to the radiative corrections derived in Appendix A. The mass of the light Higgs boson is more sensitive to the squark masses, while the heavy Higgs boson mass is only perceptibly affected in the low mass region. Since the abscissa for the plots is m_{H_p}, the figures of the production rate of the pseudoscalar Higgs boson are then expected to be unaltered by the lowering of the sparticle masses. It is also conceivable that the less massive squarks could make the squark loop contributions to $\Gamma(H \rightarrow gg)$ more significant; however, this is not an important factor in the changes seen here. Figures 3.13a and 3.13b on the next page may be compared to the lower plots of Figures 3.8 and 3.10 to see the effects on the Higgs boson production rates from lowering the sparticle masses. Since the pseudoscalar Higgs production rate is virtually unchanged, it is not shown here.

The dependence on μ was tested for $m_{H_p} \sim 250\,\mathrm{GeV}$ (with the other MSSM parameters set as in the figures) and found to be only very slight.

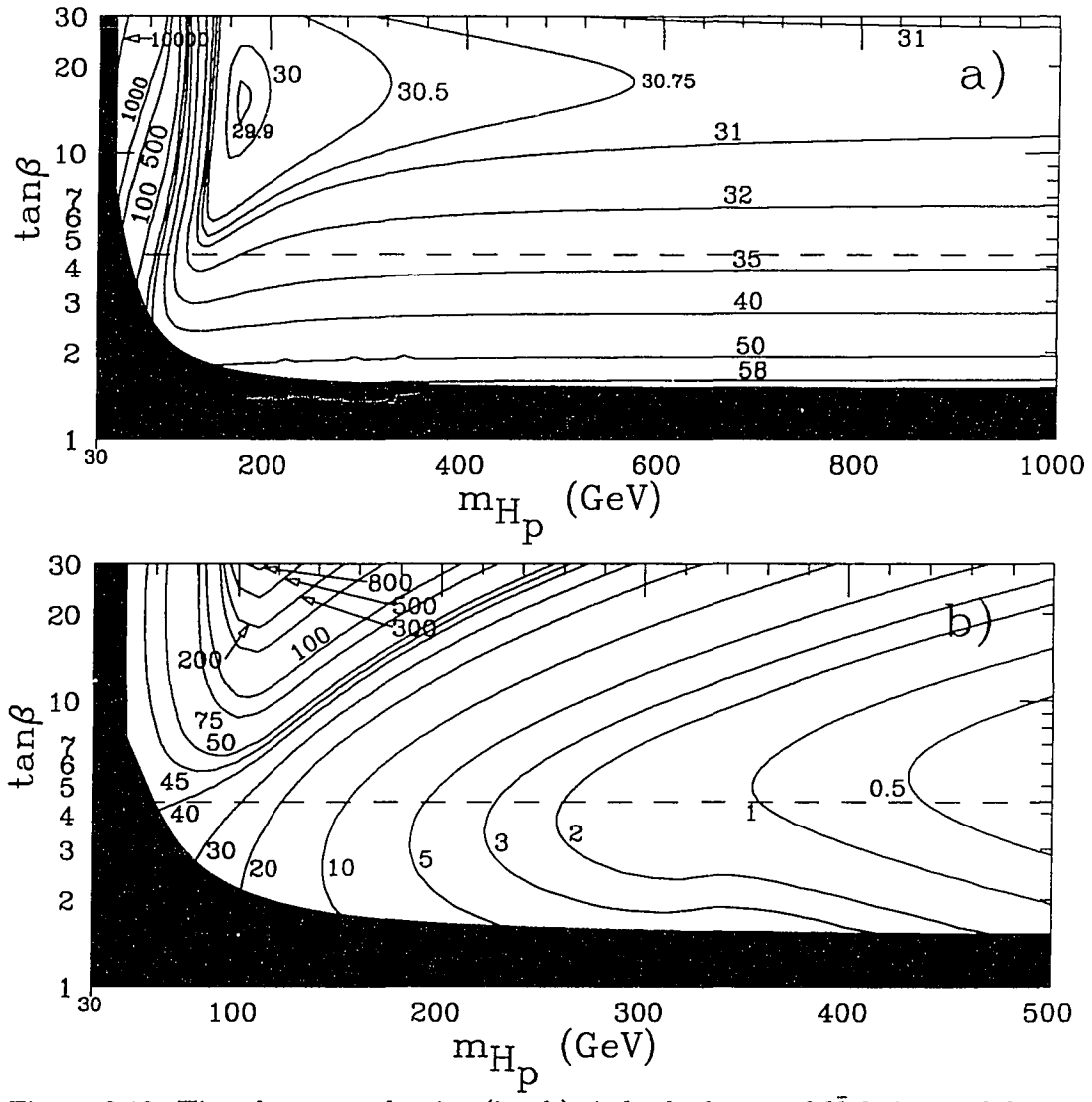

Figure 3.13: Higgs boson production (in pb) via both gluon and $b\bar{b}$-fusion with lower sparticle masses.
a) light Higgs boson production b) heavy Higgs boson production
With: $m_{\tilde{g}} = -\mu = 300\,\text{GeV} \doteq m_{\tilde{q}}$, and other parameters as in Fig. 3.8.
Above dashed line $m_{\tilde{W}_1} < 90\,\text{GeV}$.

Chapter 4

Higgs Boson Decays to SM Particles

In the SM, if the Higgs boson is heavier than $2M_W$ or $2M_{Z^0}$, then it decays mostly into W^+W^-, Z^0Z^0, and, to a lesser extent, into $t\bar{t}$ pairs (if the latter are kinematically accessible). A lighter SM Higgs boson, in the intermediate mass range ($M_{Z^0} < m_H < 2M_W$), decays mainly into the heaviest available fermion anti-fermion pair. Figure 4.1 on the next page displays the branching ratios for the various decay modes of a SM Higgs boson. The decay rates of a Higgs boson into leptons or quarks are proportional to the square of the SM fermion mass (see Appendix B), and thus the branching ratio for a Higgs boson going into a pair of the lighter leptons or quarks is vanishingly small. Rates for decays to quarks of the third generation (b or t) may be significant; however, the production of these relatively heavy SM fermions via either SM or MSSM Higgs boson decays is difficult to separate from the QCD background at a hadron collider. Exceptions to this may occur when the Higgs boson is produced in association with another heavy particle or particles such as a W, Z^0, or $t\bar{t}$ pair (more will be said about this in Chapter 6). Furthermore, rapid decays of the heavy fermions into lighter quarks and leptons accompanied by jets also make identification of events containing a given heavy SM fermion problematical.

The familiar way to escape the QCD background difficulties encountered with the colored quarks and the tiny rates from the diminutive leptons is to instead look at Higgs boson decays into pairs of colorless massive gauge bosons. These electroweak interactions have low jet activity and so are easier to identify and distinguish from the SM backgrounds. The decay of a Higgs boson into a pair of Z^0's which in turn both decay leptonically into electrons or muons provides the classic gold-plated sig-

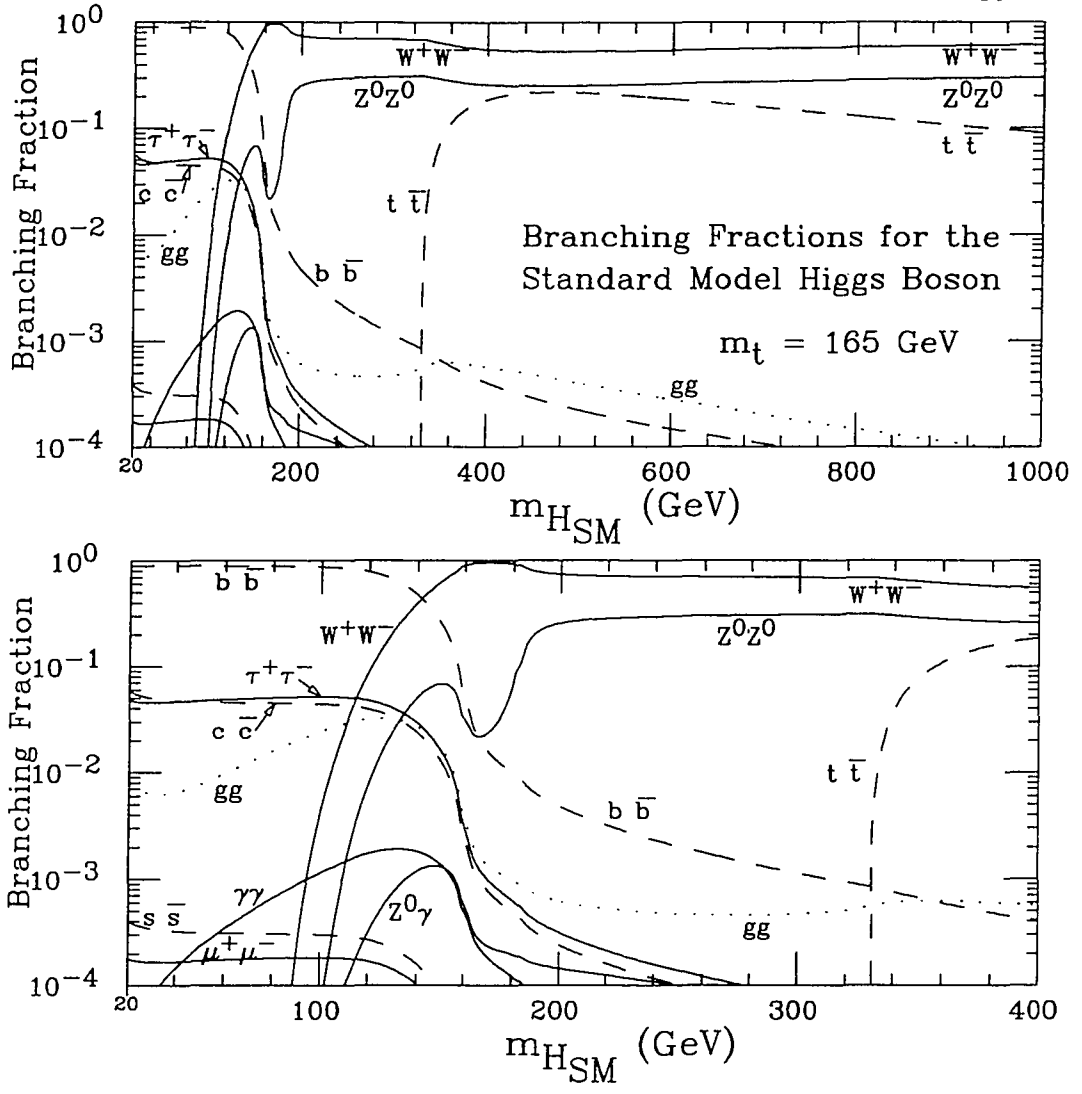

Figure 4.1: Branching ratios for a SM Higgs boson.
With: $M_{Z^0} = 91.19\,\text{GeV}$, $\sin^2\theta_w = 0.23$, $M_W = M_{Z^0}\cos\theta_w$ $\Gamma_{Z^0} = 2.4969\,\text{MeV}$, $\Gamma_W = 2.076\,\text{MeV}$, $m_t = 165\,\text{GeV}$, $m_b = 5\,\text{GeV}$, $m_\tau = 1.7769\,\text{GeV}$, $\Lambda_{QCD4} = 177\,\text{MeV}$.
(These same SM parameter values are used throughout this work unless otherwise noted.)

nature for Higgs production. It can be used to search for a SM Higgs boson as heavy as 800 GeV [64]. However, in the MSSM, the situation is generally far less favorable. This is due to the MSSM mixing angle factors which must be included in a Higgs boson's coupling to a pair of gauge bosons (see Table 2 of Chapter 1). The couplings of the light Higgs boson and heavy Higgs boson to a gauge boson pair are

proportional to $\sin(\alpha+\beta)$ and $\cos(\alpha+\beta)$, respectively. So we see from Fig. 4.2 that as m_{H_h} grows with m_{H_p}, the heavy Higgs boson's coupling angle factor becomes very small, while the light Higgs boson's coupling angle factor approaches one. ($H \to W^+W^-, Z^0Z^0$ rates are proportional to the square of this factor.) Thus, if the heavy Higgs boson is sufficiently massive, then it is decoupled from the gauge boson pairs while the light Higgs boson's coupling is about the same as that of a SM Higgs boson.

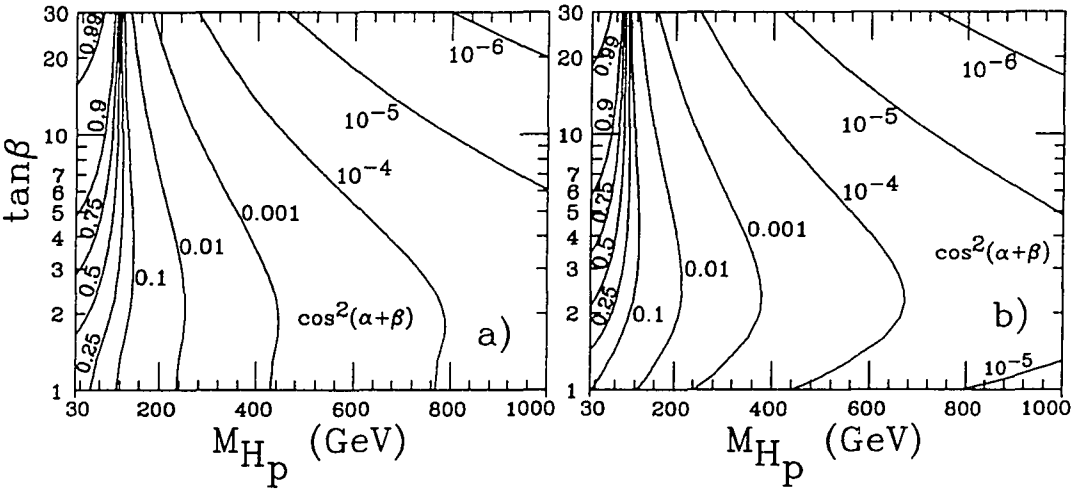

Figure 4.2: MSSM angle factor entering heavy Higgs boson decays to gauge bosons: $\Gamma(H_h \to Z^0Z^0) = \cos^2(\alpha+\beta)\Gamma(H_{SM} \to Z^0Z^0)$
$m_{\tilde{g}} = -\mu = 1000\,\text{GeV} \doteq m_{\tilde{q}}$ for plot a), and $m_{\tilde{g}} = -\mu = 300\,\text{GeV} \doteq m_{\tilde{q}}$ for plot b). Other MSSM input parameters as in Fig. 2.4 .

The situation for the pseudoscalar Higgs boson is even worse, since at tree level there is no coupling to either Z^0Z^0 or W^+W^- pairs. A coupling can be generated at the one-loop level. However, the rate for $H_p \to Z^0Z^0$ is almost always quite small [65], and so the gold-plated mode is potentially useful only in very limited regions of the MSSM parameter space. The situation appears optimal when $\tan\beta \lesssim 1$ and $m_{H_p} \sim 2m_t$, but even in this case a 4σ signal is not obtainable at the LHC [65]. This very skimpy rate will be neglected here, along with all other effects beyond tree-level in the decays of the MSSM Higgs bosons to W's or Z's. Thus only such decays for the neutral scalars H_ℓ and H_h will be considered.

Of course for one of these Higgs bosons to decay into a pair of gauge bosons, the Higgs boson must be sufficiently massive. As the mass of the Higgs boson is raised to approach the W^+W^- or Z^0Z^0 threshold, three-body decays via WW^* or ZZ^* become important, and their inclusion is necessary to give the correct threshold behavior. Figure 4.1 (see lower plot) illustrates their importance for a $m_H \sim 150\,\mathrm{GeV}$ intermediate mass Higgs boson. Note how the curve labeled W^+W^- turns on considerably before $2M_W \simeq 160\,\mathrm{GeV}$. These off-shell decays are dealt with in the manner formulated by Keung and Marciano [66] and described more fully in Appendix B.

Figures 4.3a) and 4.4a) show the branching fraction of the heavy Higgs boson into a pair of Z^0's. This is then convoluted with the heavy Higgs boson production rate (from Chapter 3) and the branching ratio of the Z^0 into electrons and muons (taken as 0.0672 [33]) to yield contour plots b) for $\sigma(H_h \to Z^0Z^0 \to 2\times\ell^+\ell^-)$, where $\ell = e$ or μ. As with Higgs boson decays to the heavy quarks, QCD backgrounds unfortunately make the more abundant hadronic decays of the Z^0 unusable. Finally, a region of expected detectability of this signal after background subtraction is shown in c). For this an integrated luminosity of $50\,\mathrm{fb}^{-1}$ is assumed. This is between the high luminosity option of $100\,\mathrm{fb}^{-1}/\mathrm{yr}$ (corresponding to one year running at a luminosity of $10^{34}\,\mathrm{cm}^{-2}\mathrm{s}^{-1}$) and the low luminosity option of $10\,\mathrm{fb}^{-1}/\mathrm{yr}$ which have been discussed [67] for the LHC.

Also incorporated is a detection efficiency for the signal estimated as in Ref. [68]. The estimation is based on values given in the SDC literature [69-71], some of which are in turn based on the results of a CDF analysis [72]. The electron and muon efficiencies within the detector acceptance are taken to be 85% for the first lepton from a Z^0 or $W^\pm$, and 95% for a second lepton from the Z^0 (the increase for the second lepton is due to relaxed identification cuts) (see Sec. 5.1 of [69], Sec. 4.1 of [70], or Sec. 3.1 of [71]). Each lepton is also required to be isolated, which is taken to mean that there is less than 5 GeV of energy in a cone of radius $\Delta R = \sqrt{\Delta\eta^2 + \Delta\phi^2} = 0.3$, where η is the pseudorapidity, around the lepton's direction (see Sec. 4.2 of [70] or Sec. 3.2.1 of [71]; Ref. [69] quotes a stricter cut of

$\Delta R = 0.7$). This cut results in a loss of about 5% of the identified leptons (see Sec. 4.2 of [70]). In addition, all four leptons must be within the detectors range for good momentum resolution, estimated as $|\eta| < 2.5$ for SDC (see Sec. 3.1 of [69], Sec. 3.2.1 of [70], or Secs. 1.2,2.1 of [71]). If the direction of each lepton was arbitrary, this would result in an efficiency of about 64%. Ref. [68] gives a value of approximately 70% for the four leptons from $H \rightarrow Z^0 Z^0 \rightarrow \ell^+\ell^-\ell'^+\ell'^-$, regardless of the value of m_H. Combining the values above gives an overall event efficiency of

$$\epsilon = (0.85 \times 0.95)^2 \times (0.95)^4 \times 0.7 \simeq 0.37 \ .$$

As in Ref. [68], the value $\epsilon = 0.35$ has been adopted here.

Since a Higgs boson does not have an appreciable width on the scale of a realistic detector's mass resolution capability, all of the signal events will lie within a "signal region" of $m_H \pm \Delta m$, where Δm is fixed by detector specifications. It is clearly best to make Δm as small as is possible, since in so doing only background is eliminated with no loss in signal (except of course for mismeasured signal events which are more likely to fall outside a more restricted region). Optimistic values of $\Delta m(4\ell) = 2.2\,\mathrm{GeV}$ for $m(4\ell) = 200\,\mathrm{GeV}$ and $\Delta m(4\ell) = 5.1\,\mathrm{GeV}$ for $m(4\ell) = 400\,\mathrm{GeV}$ are quoted in Ref. [68], along with conservative values of $\Delta m(4\ell) = 4.8\,\mathrm{GeV}$ for $m(4\ell) = 200\,\mathrm{GeV}$ and $\Delta m(4\ell) = 14.0\,\mathrm{GeV}$ for $m(4\ell) = 400\,\mathrm{GeV}$. Though a stringent demand upon a detector, the optimistic values appear technically feasible and are utilized here. The four leptons are thus further required to reconstruct the mass of the parent Higgs boson within a resolution Δm given by

$$\Delta m(4\ell) = 2.2\,\mathrm{GeV} \ + \ 0.0145 \times [m(4\ell) - 200]\,\mathrm{GeV} \quad , \tag{4.1}$$

which is obtained from a linear interpolation (or extrapolation) of the optimistic values. Actually, the mass resolution for four muons is expected to be about twice as good as that for four electrons (Ref. [71], Sec. 3.2.2); but, for simplicity, the same resolution function, given by Eqn. (4.1), is used here for all three possibilities ($4e$, 4μ, and $2e2\mu$).

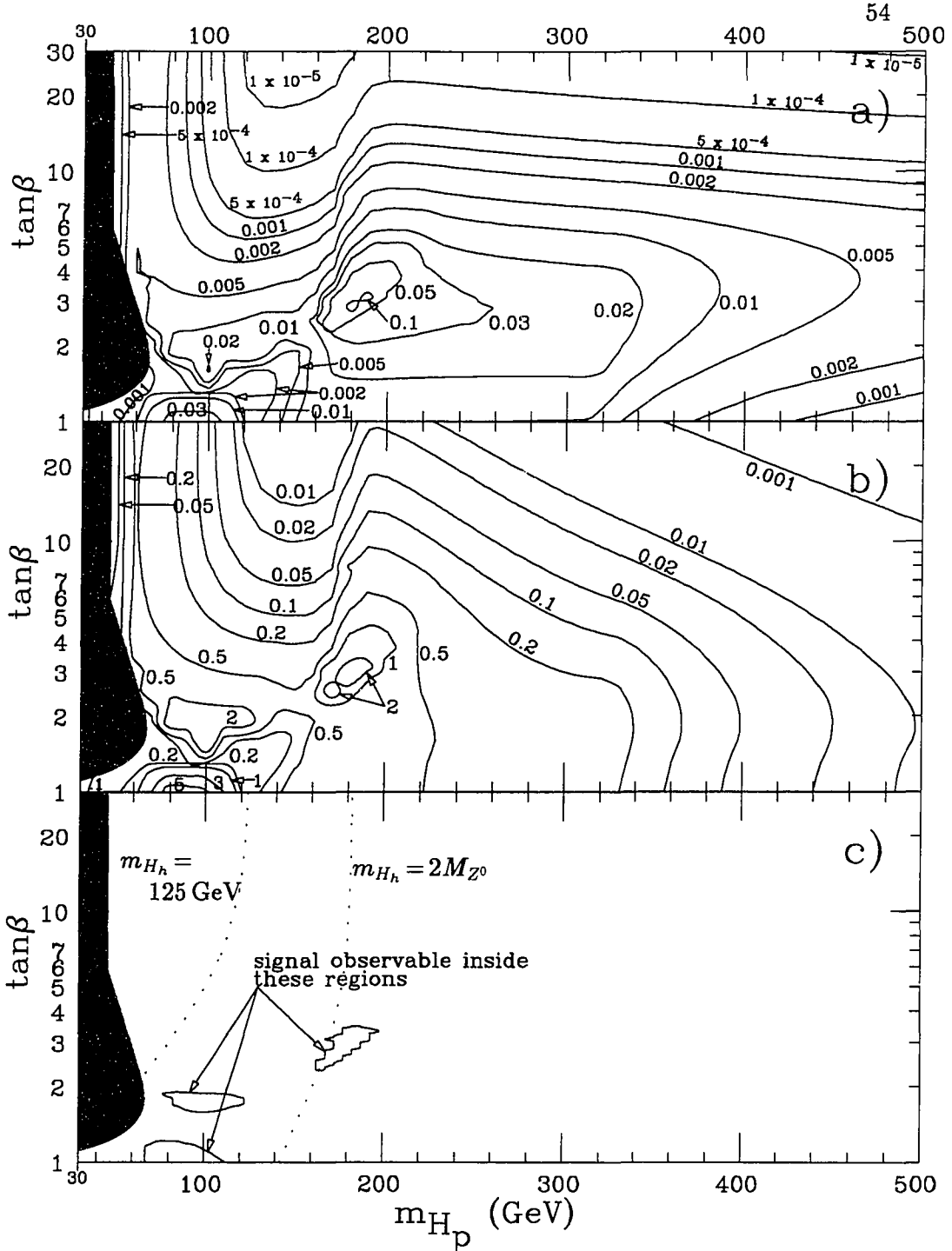

Figure 4.3: "Gold-plated" signal for H_h. a) $BR(H_h \to Z^0Z^0, Z^0Z^{0*})$; b) $\sigma(pp \to H_h \to Z^0Z^0, Z^0Z^{0*} \to 2 \times \ell^+\ell^-)$, where $\ell = e$ or μ. Curves are labeled in fb. c) Region of detectability for this signal. MSSM parameters as in Fig. 3.8 of Chapter 3, with $m_{\tilde{g}} = -\mu = 1000\,\text{GeV} \doteq m_{\tilde{q}}$ and $\sqrt{s} = 14\,\text{TeV}$.

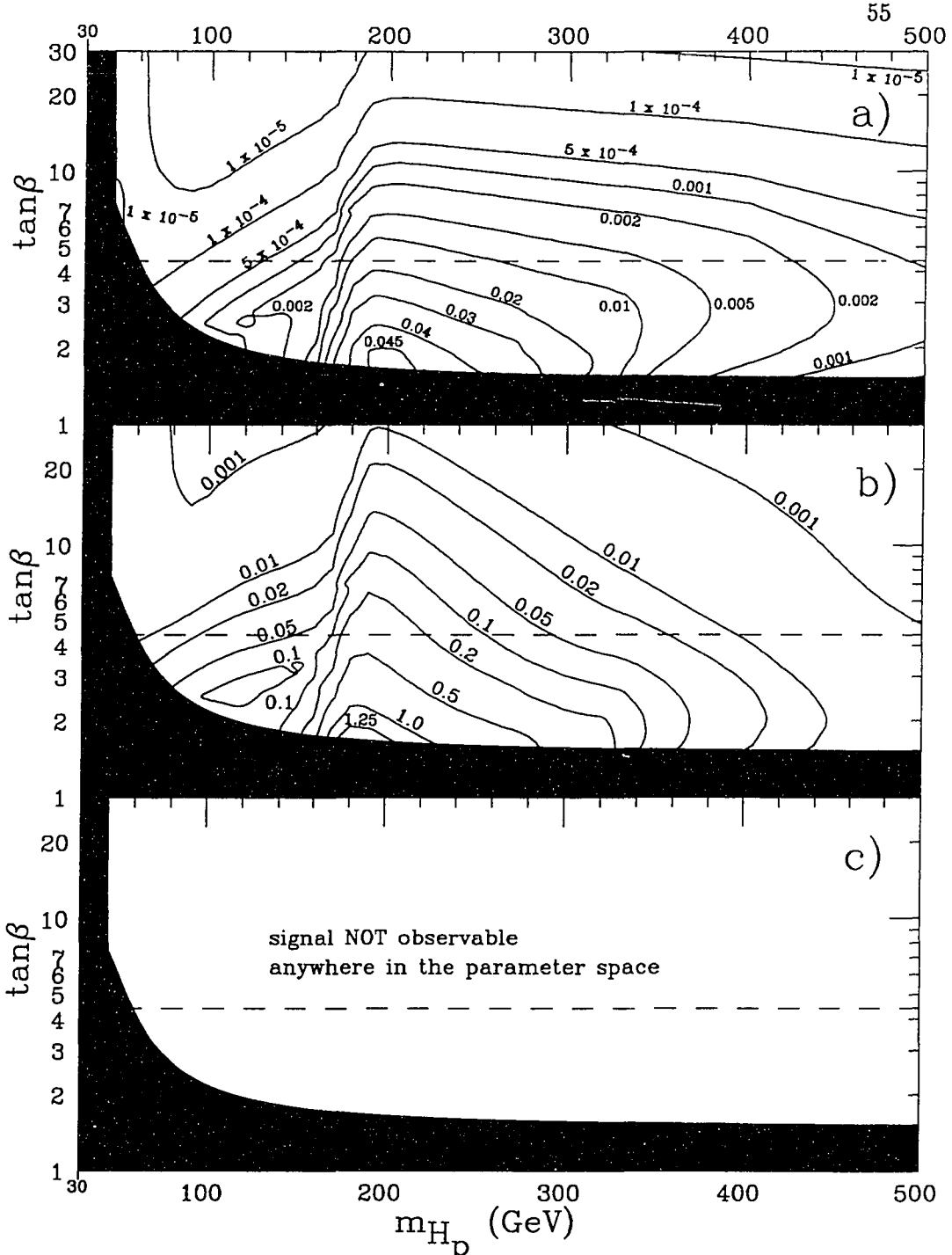

Figure 4.4: "Gold-plated" signal for H_h. a) $BR(pp \to H_h \to Z^0Z^0, Z^0Z^{0*})$; b) $\sigma(pp \to H_h \to Z^0Z^0, Z^0Z^{0*} \to 2 \times \ell^+\ell^-)$, where $\ell = e$ or μ. Curves are labeled in fb. c) Region of detectability for this signal. MSSM parameters as in Fig. 3.13 of Chapter 3, with $m_{\tilde{g}} = -\mu = 300\,\text{GeV} \doteq m_{\tilde{q}}$ and $\sqrt{s} = 14\,\text{TeV}$.

Figures 4.5 and 4.6 are the analogous illustrations for the gold-plated decay of the light Higgs boson (which decays into one real and one virtual Z^0). Here we see a drastic reduction in the high $\tan\beta$, high m_{H_p} values for the $H_\ell \to Z^0 Z^{0*}$ branching ratio when the values of the SUSY inputs $m_{\tilde{g}}$, $m_{\tilde{q}}$, and $\mu = -2m_1$ are lowered. As shown in Chapter 1, the mass of the light Higgs boson decreases as the $\tilde{t}$-squark masses are lowered due to the effects of radiative corrections. Requiring the Z^{0*} to be more off the mass-shell sharply reduces the rate for this decay. Looking at the heavy Higgs boson figures, we also see a decrease of roughly a factor of 2 in the $H_h \to Z^0 Z^0$ branching ratio when the MSSM inputs are lowered. Yet over most of the MSSM parameter space pictured, the mass of the heavy Higgs boson is not significantly affected by the radiative corrections. As will be explored in the next chapter, this decline is mainly due to the opening up of new channels to sparticles (charginos and neutralinos) since the sparticle masses also drop (some quite a bit) along with the MSSM input values.

For a heavier Higgs boson ($m_H > 2M_{Z^0}$), the main background to the gold-plated signal arises from continuum production of a pair of Z^0's from tree-level $q\bar{q}$-fusion or from a gluon pair via a quark loop [73,74], with both Z^0's decaying into electrons or muons. If $m(4\ell)$ from such a process happens to fall within Δm (as given by Eqn. (4.1)) of m_H, then it will be indistinguishable from the Higgs decay signal event sought.

For an intermediate mass Higgs boson decaying into an on mass-shell Z^0 and an off mass-shell Z^{0*}, the SM background stems from continuum $Z^0 Z^{0*}$ and continuum $Z^0\gamma^*$ production where the γ^* converts to a lepton pair. But the rate for the former was found to be quite modest [75] while events from the later are strongly concentrated around $m(\gamma^*) = 0$ and can be removed by imposing a mass cut on the dileptons from the virtual photon. Cutting events with dilepton masses below a certain threshold means that we are restricting $m(Z^{0*})$ from being too small. Again we follow the findings of the SDC study group: Ref. [69], Sec. 2.2 sets a lower limit of about 140 GeV; Ref. [70], Sec. 4.2 states that a 125 GeV Higgs boson should be detectable by this signal after about 2 years, running at the nominal luminosity of 10^{33} cm^{-2}s^{-1}; and Ref. [71], Sec. 3.2.2 says that a 130 GeV Higgs boson will have

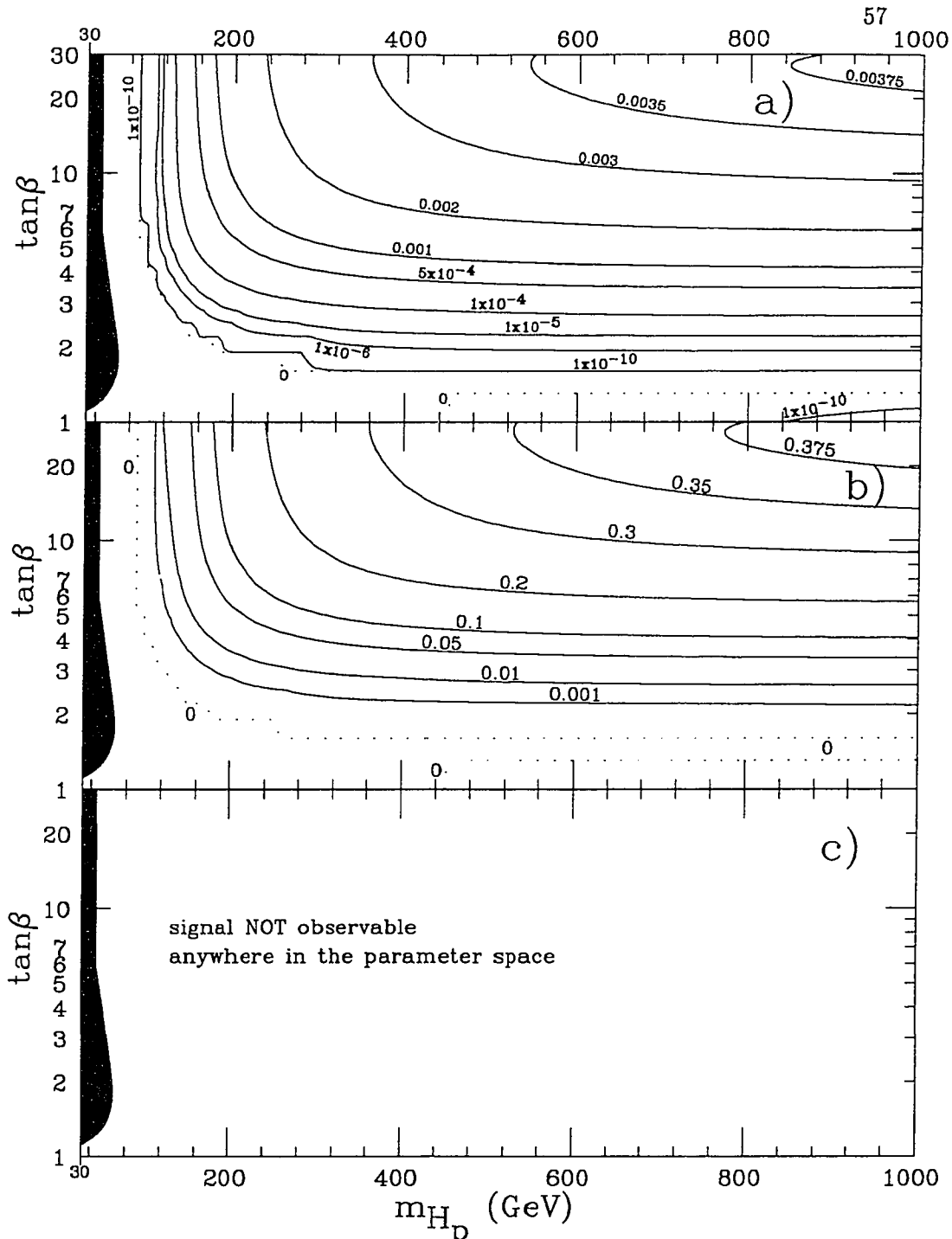

Figure 4.5: "Gold-plated" signal for H_ℓ. a) $BR(H_\ell \to Z^0 Z^{0*})$; b) $\sigma(pp \to H_\ell \to Z^0 Z^{0*} \to 2 \times \ell^+\ell^-)$, where $\ell = e$ or μ. Curves are labeled in fb. c) Region of detectability for this signal. MSSM parameters as in Fig. 3.8 of Chapter 3, with $m_{\tilde{g}} = -\mu = 1000\,\text{GeV} \doteq m_{\tilde{q}}$ and $\sqrt{s} = 14\,\text{TeV}$.

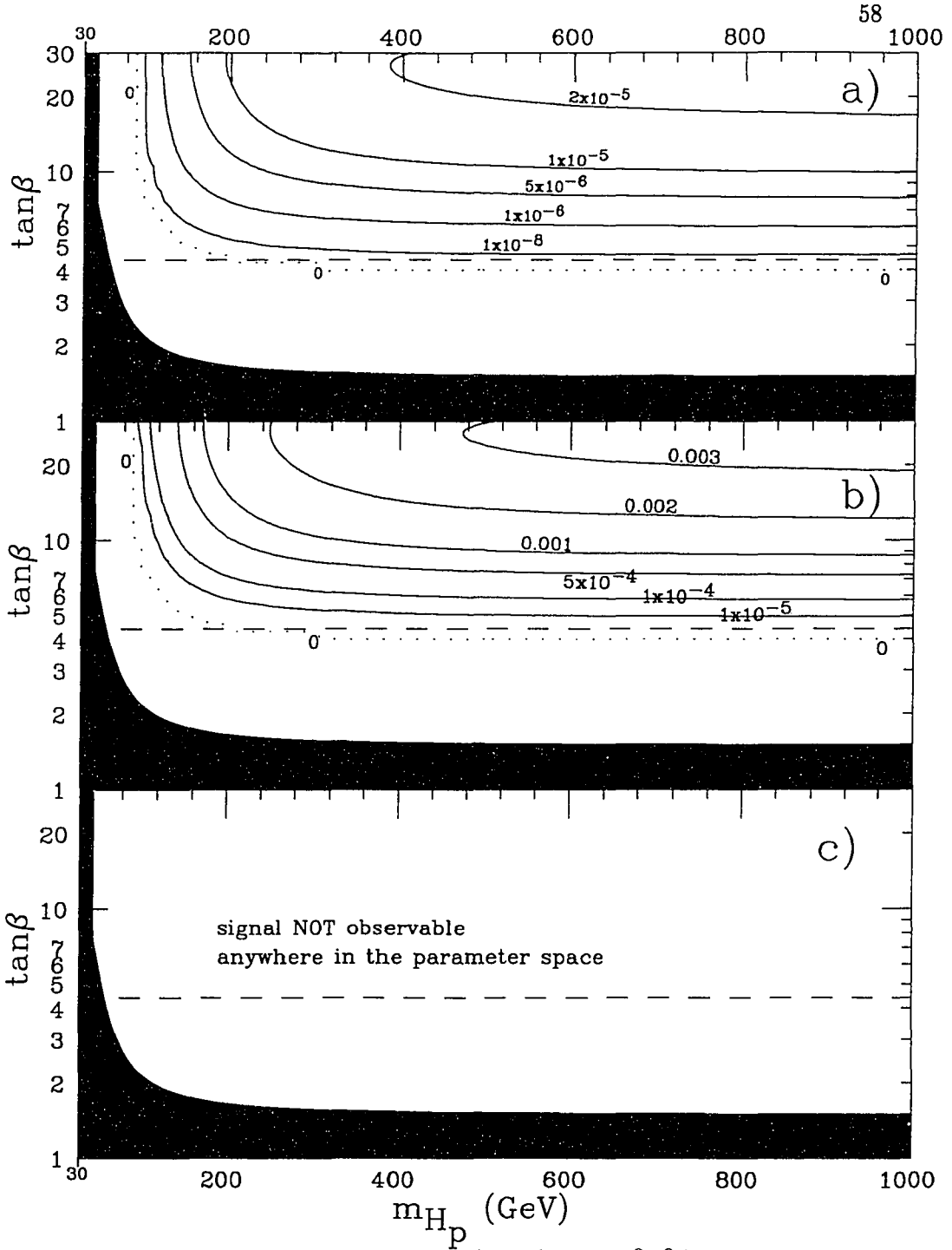

Figure 4.6: "Gold-plated" signal for H_ℓ. a) $BR(H_\ell \to Z^0 Z^{0*})$; b) $\sigma(pp \to H_\ell \to Z^0 Z^{0*} \to 2 \times \ell^+\ell^-)$, where $\ell = e$ or μ. Curves are labeled in fb. c) Region of detectability for this signal. MSSM parameters as in Fig. 3.13 of Chapter 3, with $m_{\tilde{g}} = -\mu = 300\,\text{GeV} \doteq m_{\tilde{q}}$ and $\sqrt{s} = 14\,\text{TeV}$.

an "unambiguous" signal after one year, while a 120 GeV requires several years to yield a "convincing" signal. Here, the 4ℓ signal is only considered for $m_H > 125$ GeV.

Our criterion for observability of a signal is that the 99% confidence level upper limit on the background is smaller than the corresponding 99% confidence level lower limit on the signal and background combined. This translates into

$$L(\sigma_s + \sigma_b) - 2.32\sqrt{L(\sigma_s + \sigma_b)} > L\sigma_b + 2.32\sqrt{L\sigma_b} \tag{4.2}$$

which may be rewritten as

$$\sigma_s > \frac{(2.32)^2}{L}\left[1 + \frac{2\sqrt{L\sigma_b}}{2.32}\right] \tag{4.3}$$

where L is the integrated luminosity, σ_s is the cross-section of the signal, and σ_b is the background cross-section in the signal region of $m_H \pm \Delta m$. This background cross-section is shown in Figure 4.8a). Note that for $\sigma_b \gg \sigma_s$, Eqn. (4.2) reduces to $L\sigma_s > 4.64\sqrt{L\sigma_b}$, which is the commonly adopted measure of statstical significance; in a more general case with smaller backgrounds employing Eqn. (4.2) can yield somewhat different results from the standard $\frac{signal\ events}{\sqrt{noise\ events}}$ diagnostic. This Gaussian approximation to the probability distribution is valid so long as the number of two-photon events is large. For this reason, as well as to guard against experimental misidentified events or fluke occurrences of very rare backgrounds, a minimum of 25 signal events for an integrated luminosity of 50 fb^{-1} is also demanded.

It is tempting to try to utilize the more prolific hadronic decay modes of the gauge bosons, but this leads back to the difficulties with SM backgrounds that rendered the heavy SM fermion Higgs decay modes unuseable. Modes where both gauge bosons decay hadronically appear pretty hopeless; however, decays where one of the gauge bosons decays leptonically merit some attention. The branching ratios for $H \to Z^0Z^0 \to \ell^+\ell^- + 2\,jets$ and $H \to W^+W^- \to \ell\nu + 2\,jets$ are, respectively, about 20 and 150 times that for $H \to Z^0Z^0 \to 4\ell$. Rather complicated analyses [76-78], mainly for the SSC (see also Sec. 3.2.3 of [71]), outlining a number of cuts on the data suggest that the background might be sufficiently reducible to yield a signal for the SM Higgs boson in the high mass region ($m_{H_{SM}} \simeq 800$ GeV or above). An LHC simulation [79,80] reached a similar conclusion, provided that the integrated

luminosity was large enough ($> 100\,\mathrm{fb}^{-1}$). In the MSSM however, due to the unfavorable MSSM mixing angle factor that is involved in such a case, these mixed hadronic and leptonic decay modes are not considered a viable source for signals.

In the SM, the dileptonic decay $H \rightarrow Z^0Z^0 \rightarrow \ell^+\ell^- + \nu\bar{\nu}$, whose rate is six times that of the four lepton decay mode, has also been considered as a means of extending Higgs detection capability (compared with that of the gold-plated signal alone) to higher Higgs masses ($\gtrsim 800\,\mathrm{GeV}$) where detection is hampered by the low Higgs boson production rate (see Sec 3.2.3 of Ref. [71] and Ref. [80]). But, again, the smallness of the MSSM angle factor for such high Higgs boson masses eliminates all hope of using this tactic in the MSSM. However, this means of detecting a lower mass MSSM Higgs boson (say, $m_{H_h} < 300\,\mathrm{GeV}$) may warrant some attention.

As can be seen from the figures, detection of an MSSM Higgs boson via its decays to Z^0's and W's is only possible for H_h in very limited regions of parameter space. This could make discovery of Higgs bosons, especially ones whose masses fall in the intermediate mass range ($M_{Z^0} < m_H < 2M_W$), extremely difficult at a hadron collider. Since the difficulty in discovering an MSSM Higgs boson in the intermediate mass range is more a matter of the poor signal-to-background ratio than of insufficient production rate, some rare decay processes which are particularly free from backgrounds might offer viable alternative discovery modes.

Several studies [75,81-84] have shown that the Higgs boson of the Standard Model may be detected at a hadron supercollider such as the LHC via the decay $H_{SM} \rightarrow \gamma\gamma$, provided the detector resolution is good enough [85]. For the $H \rightarrow Z^0Z^0$ decay, it was noted that the the decay width of the Higgs boson is much smaller than the the four-lepton invariant mass resolution of a realistic detector. In the case of $H \rightarrow \gamma\gamma$ decays, the analogous statement holds for the two-photon mass resolution. So to keep backgrounds down to the low level required, excellent electromagnetic calorimetry capable of measuring the two-photon mass with a precision of 1-2% is essential. The ATLAS LHC detector group does claim [86] (as did the GEM SSC detector group [87]) that a mass resolution of better than $\pm 1\%$ is obtainable, hence the value $\pm 1\%$ is adopted here.

The SM Higgs boson decay into a pair of photons is a loop decay mediated by quarks, leptons, or W-bosons. Two-photon decays for supersymmetric Higgs bosons were first computed back in 1986 [88,89], and the decay rates for MSSM Higgs bosons (without radiative corrections) were subsequently computed [90,91]. Inclusion of radiative corrections to the masses of the Higgs bosons in the analysis of potential collider signals has also more recently been accomplished [47,92-95]. In addition to the quark, lepton, and W-boson loops present in the SM case, in the MSSM loops from charginos are present for both the CP-even and the CP-odd neutral Higgs bosons and loops from squarks, sleptons, and charged Higgs bosons are also present for the CP-even Higgs bosons. The latter loops, as well as loops with W-bosons, are absent for the CP-odd pseudoscalar Higgs boson. (See Appendix B for more details.)

The principal background to the $H \rightarrow \gamma\gamma$ signal comes from two-photon continuum production via quark and gluon fusion. The latter is produced by the box diagram process shown in Figure 4.7b). For this gg contribution to the $\gamma\gamma$ background, the squared matrix elements given in Ref. [96] are employed in generating a predicted background rate. Although gluon fusion is suppressed by two powers of α_s relative to $q\bar{q}$ fusion, gluon fusion is nevertheless of equal or even greater importance than $q\bar{q}$ fusion, with their differential cross-sections (for a center-of-mass frame scattering angle of 90°) being roughly equal [97]. This is primarily due to the high gluon luminosity at a hadron supercollider, and also to a larger amplitude than might be expected and a coherent summing of the effects from the quark flavors in the box diagram [97]. The gluon fusion cross-section is also dependent on the mass of the top quark, since it will contribute as one of the flavors in the loop, whereas for $m_H < 2m_t$, the $q\bar{q}$ fusion rate is independent of the top quark mass. However, the m_t dependence of the gluon fusion cross-section is very weak for $m_t \geq 100\,\mathrm{GeV}$.

Most of the photons from these background QCD processes are produced along the beam direction and can be removed by a cut, $\cos\theta^* < 0.8$ ($\theta^* < 37°$), on the scattering angle of the photon in the rest frame of the Higgs boson. Since the photons from decays of a spinless Higgs boson are isotropic in this center-of-mass frame, this cut results in only a 20% reduction in the signal. Because the amplitude

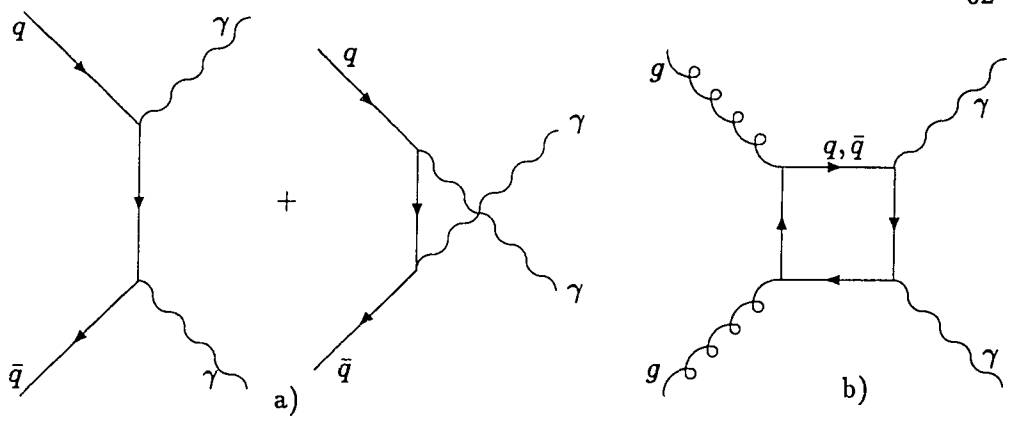

Figure 4.7: Background photon pair production processes:
a) $q\bar{q}$-fusion and b) gluon fusion via a quark loop.
(There are 6 box diagrams for the 3! permutations of the external legs. Three of these are independent.) [97]

of the background $gg \rightarrow \gamma\gamma$ process has no t- or u-channel poles, it is less concentrated along the beam axis than the brehmsstrahlung photons from $q\bar{q}$ fusion, which are expected to be mostly produced along the $q\bar{q}$ direction. Thus the $gg \rightarrow \gamma\gamma$ background is actually a larger source of large-angle photon pairs. Nonetheless, the afore-mentioned cut on the center of mass scattering angle does also remove a large percentage of this background.

A subsequent cut on higher rapidities for the two-photon rest frame relative to the laboratory frame has been shown to further reduce the $q\bar{q}$ background relative to the signal, though not the gg background which has the same rapidity distribution as a Higgs boson produced via gluon fusion. However, the improvement in the signal to background ratio obtained by adopting a rapidity cut (optimally of about $|y| < 3$ [97]) is not great and it does cut down the absolute number of signal events passing the cuts, possibly lowering it below the minimum number acceptable in some parameter space regions. Therefore, such a cut is not employed here.

Isolation and jet-veto cuts are also absolutely crucial to reduce the QCD background contamination [98], and eliminate events where either or both of the photons are radiated off jets and carry a substantial fraction of the jet energy [99]. Bearing in mind the angular distribution cut and the stringent demands for identifiability, it is clearly more important for a detector searching for an intermediate mass Higgs

boson to have high resolution for the invariant mass of photon pairs, as discussed earlier, to decrease the size of the "signal region" (and thus the background) and good γ *vs. jet* discrimination capabilites (at about the 10^{-4} level) than it is for the detector to provide hermetic coverage; in particular, the ability to detect photons at small angles or large rapidities is not extremely important for this search. It should be emphasized again that the extent of the detectable region is crucially dependent on the amount of reducible γ + jet and 2jet backgrounds that sneak in through mis-identification of jets as photons.

Figures 4.9a)-4.14a) show the branching fractions for the decays of the neutral Higgs bosons into photon pairs. These is then convoluted with the Higgs boson production rates to give the b) plots. The c) plots show the expected detectability region using the criterion of Eqn. (4.3) for what signifies an identifiable Higgs boson mass bump on top of the $\gamma\gamma$ continuum background, the cross-section of which is shown in Fig. 4.8b). The 25 event minimum specified for the $H \rightarrow Z^0Z^0$ signal is also again required. The detector is assumed to have excellent electromagnetic calorimetry, with $\Delta m = 0.02 m_{\gamma\gamma}$ as already specified, where Δm here is analogous to the one defined for the $H \rightarrow Z^0Z^0$ decays.

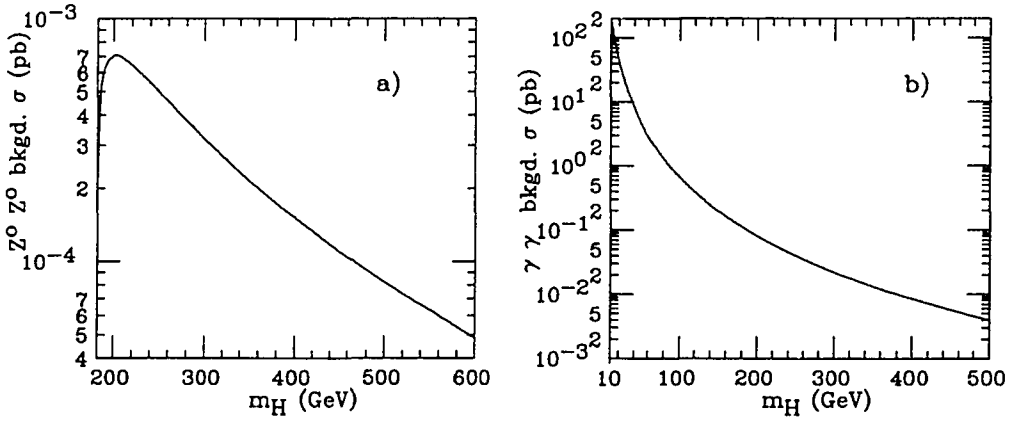

Figure 4.8: Estimated SM backgrounds to the a) $H \rightarrow Z^0Z^0$ and b) $H \rightarrow \gamma\gamma$ signals. Using the criterion described in this chapter. ($\sqrt{s} = 14\,\mathrm{TeV}$)

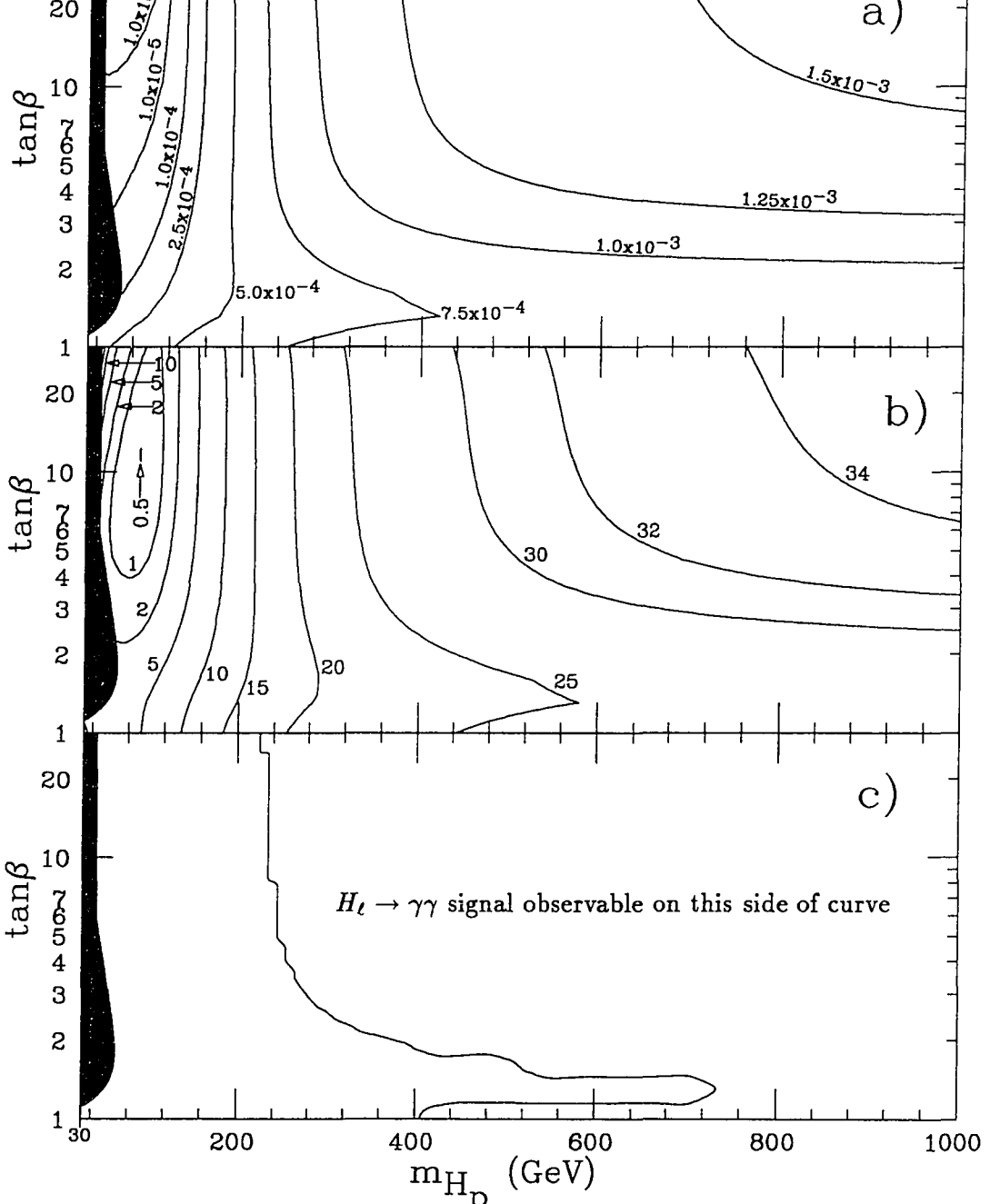

Figure 4.9: The $\gamma\gamma$ signal for H_ℓ. a) $B\tilde{R}(H_\ell \to \gamma\gamma)$;
b) $\sigma(pp \to H_\ell \to \gamma\gamma)$. Curves are labeled in fb.
c) Region of detectability for this signal.
MSSM parameters as in Fig. 3.8 of Chapter 3, with
$m_{\tilde{g}} = -\mu = 1000\,\text{GeV} \doteq m_{\tilde{q}}$ and $\sqrt{s} = 14\,\text{TeV}$.

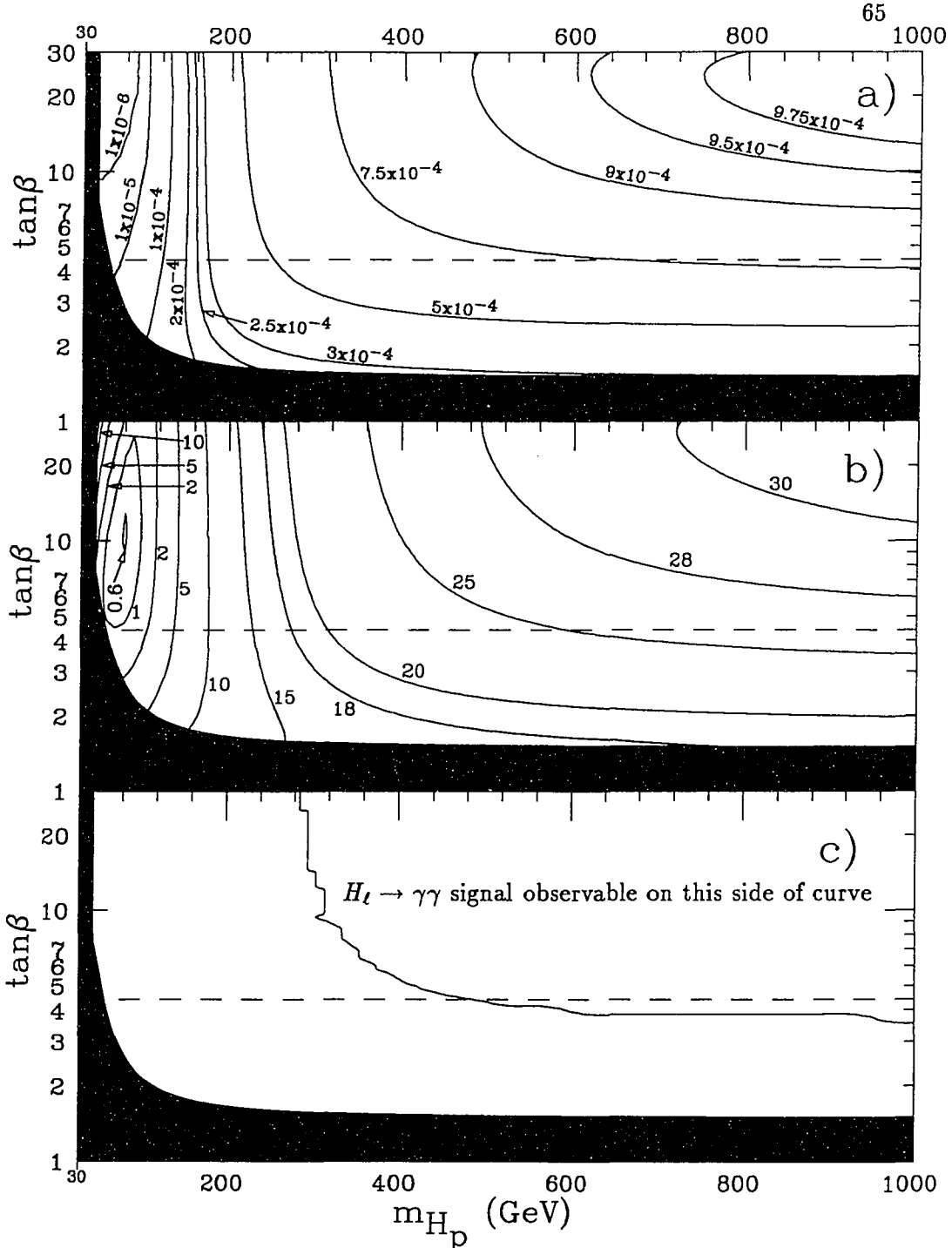

Figure 4.10: The $\gamma\gamma$ signal for H_ℓ. a) $BR(H_\ell \to \gamma\gamma)$;
b) $\sigma(pp \to H_\ell \to \gamma\gamma)$. Curves are labeled in fb.
c) Region of detectability for this signal.
MSSM parameters as in Fig. 3.8 of Chapter 3, with
$m_{\tilde{g}} = -\mu = 300\,\text{GeV} \doteq m_{\tilde{q}}$ and $\sqrt{s} = 14\,\text{TeV}$.

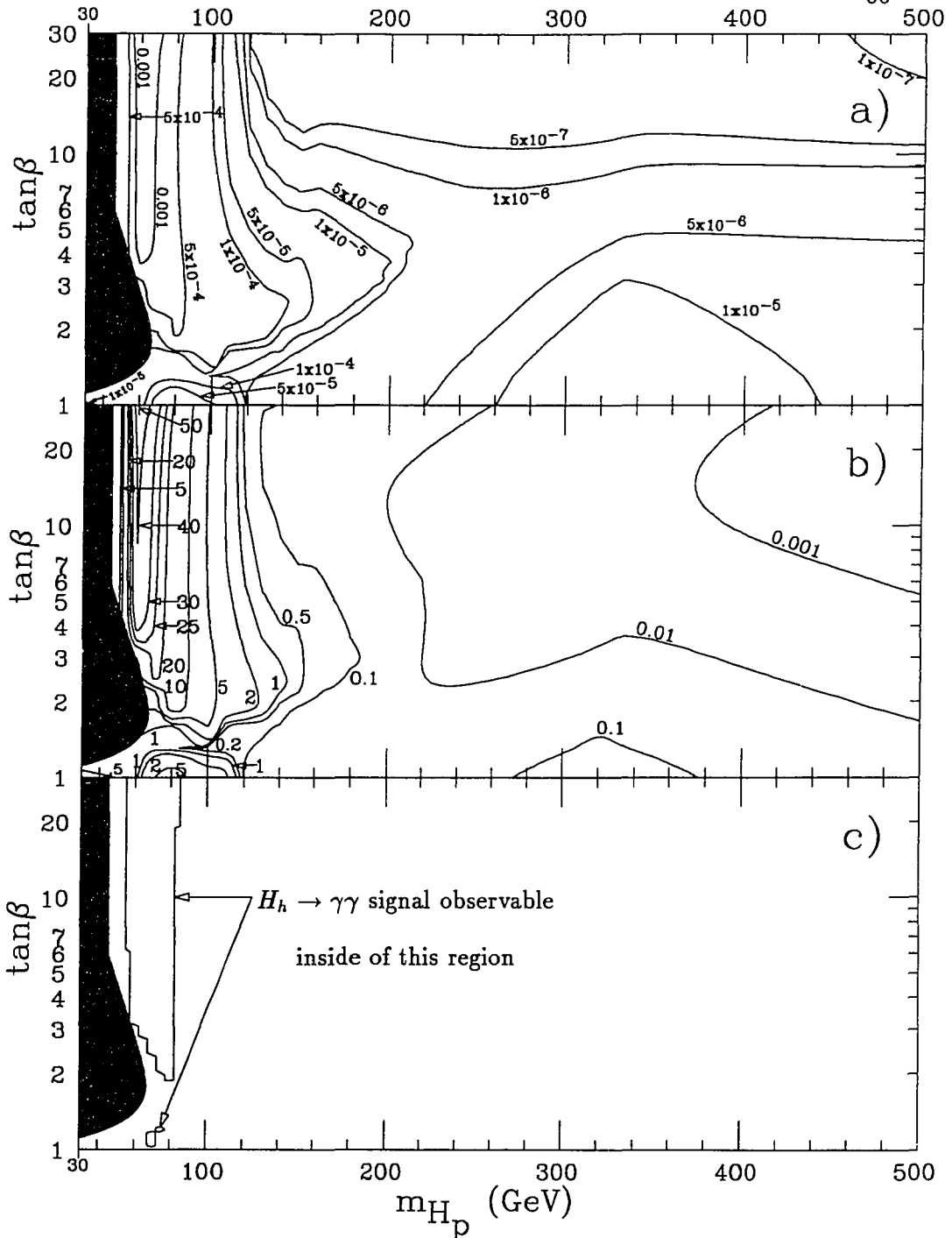

Figure 4.11: The $\gamma\gamma$ signal for H_h. a) $BR(H_h \to \gamma\gamma)$;
b) $\sigma(pp \to H_h \to \gamma\gamma)$. Curves are labeled in fb.
c) Region of detectability for this signal.
MSSM parameters as in Fig. 3.8 of Chapter 3, with
$m_{\tilde{g}} = -\mu = 1000\,\text{GeV} \doteq m_{\tilde{q}}$ and $\sqrt{s} = 14\,\text{TeV}$.

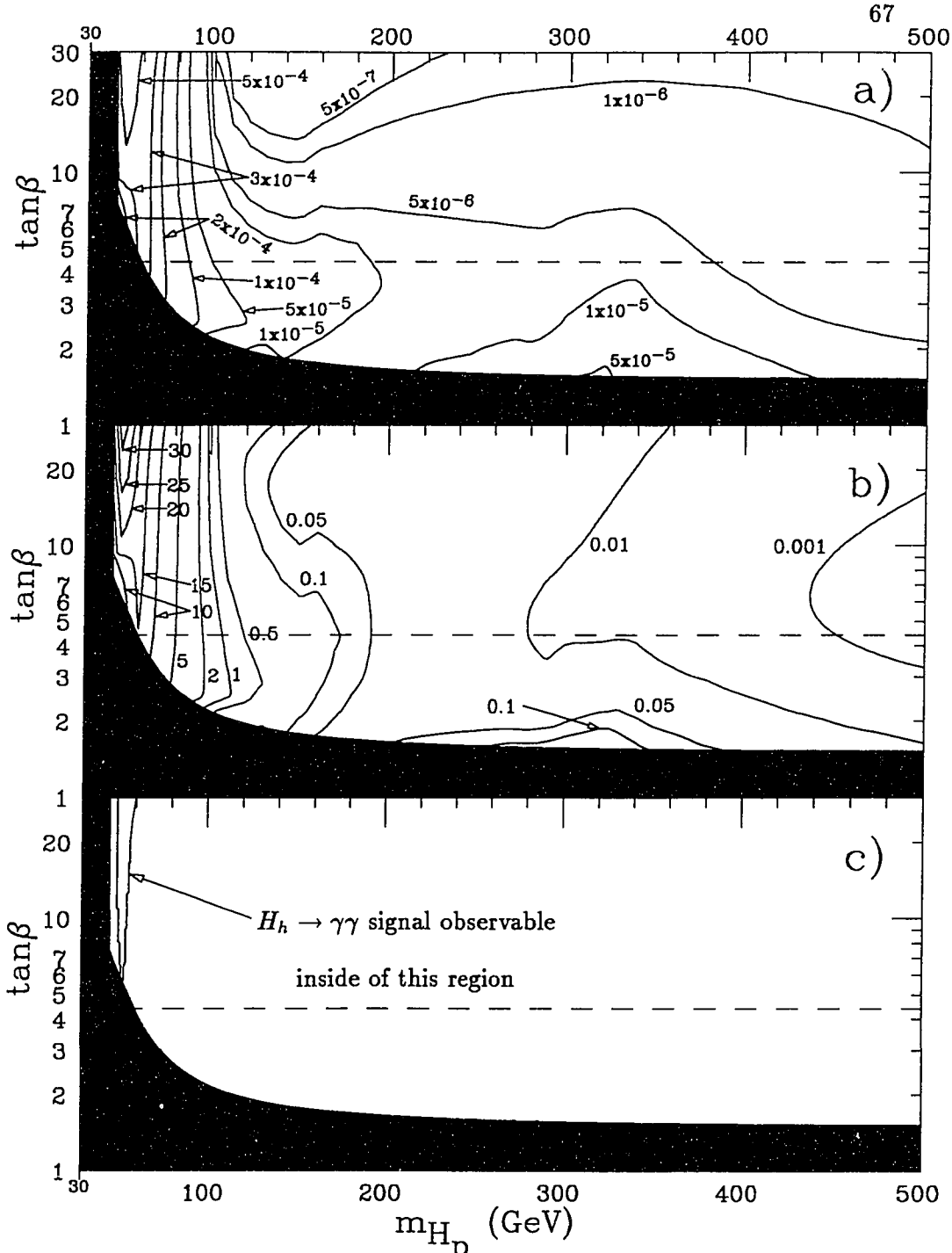

Figure 4.12: The $\gamma\gamma$ signal for H_h. a) $BR(H_h \to \gamma\gamma)$;
b) $\sigma(pp \to H_h \to \gamma\gamma)$. Curves are labeled in fb.
c) Region of detectability for this signal.
MSSM parameters as in Fig. 3.8 of Chapter 3, with
$m_{\tilde{g}} = -\mu = 300\,\text{GeV} \doteq m_{\tilde{q}}$ and $\sqrt{s} = 14\,\text{TeV}$.

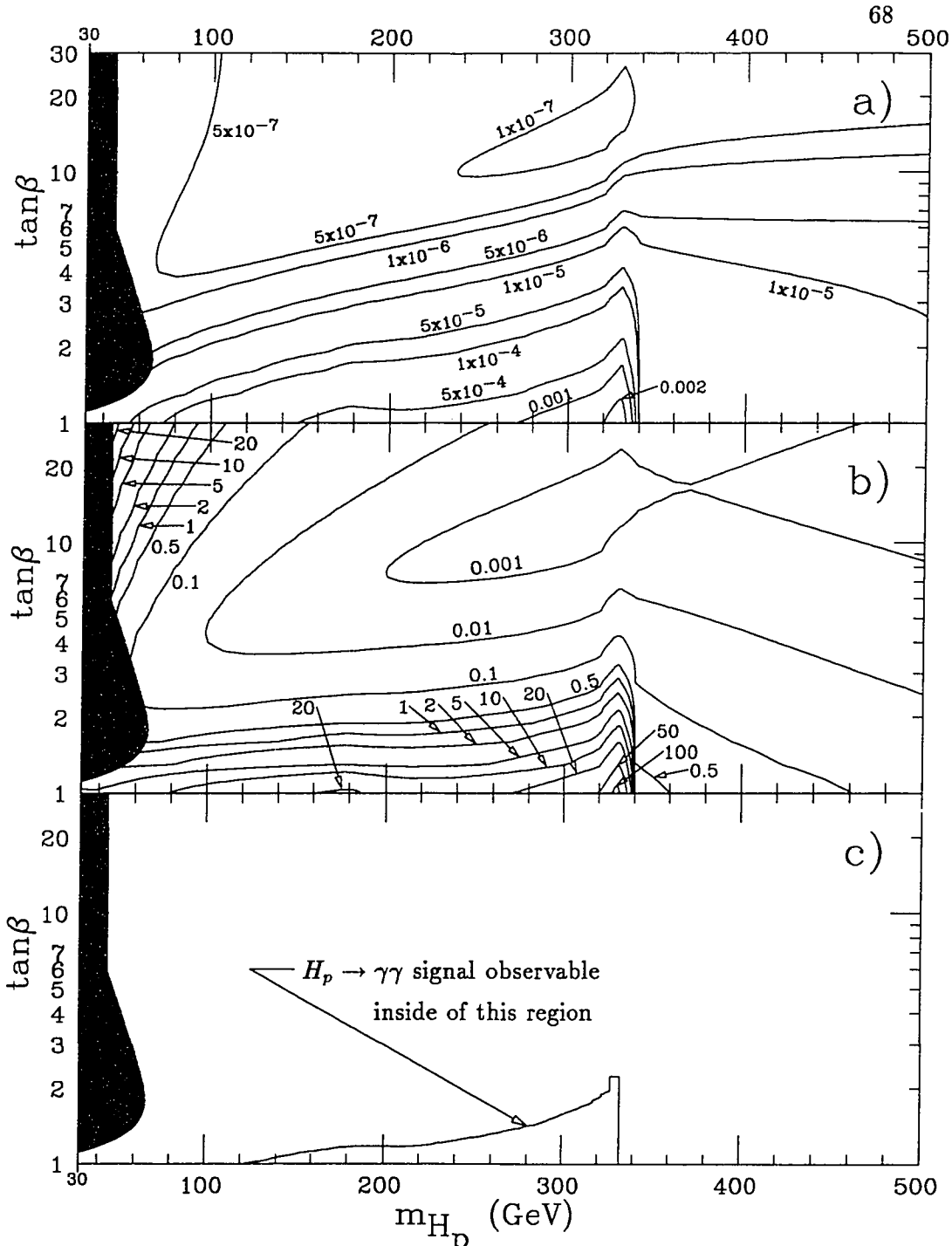

Figure 4.13: The $\gamma\gamma$ signal for H_p. a) $BR(H_p \to \gamma\gamma)$;
b) $\sigma(pp \to H_p \to \gamma\gamma)$. Curves are labeled in fb.
c) Region of detectability for this signal.
MSSM parameters as in Fig. 3.8 of Chapter 3, with
$m_{\tilde{g}} = -\mu = 1000\,\text{GeV} \doteq m_{\tilde{q}}$ and $\sqrt{s} = 14\,\text{TeV}$.

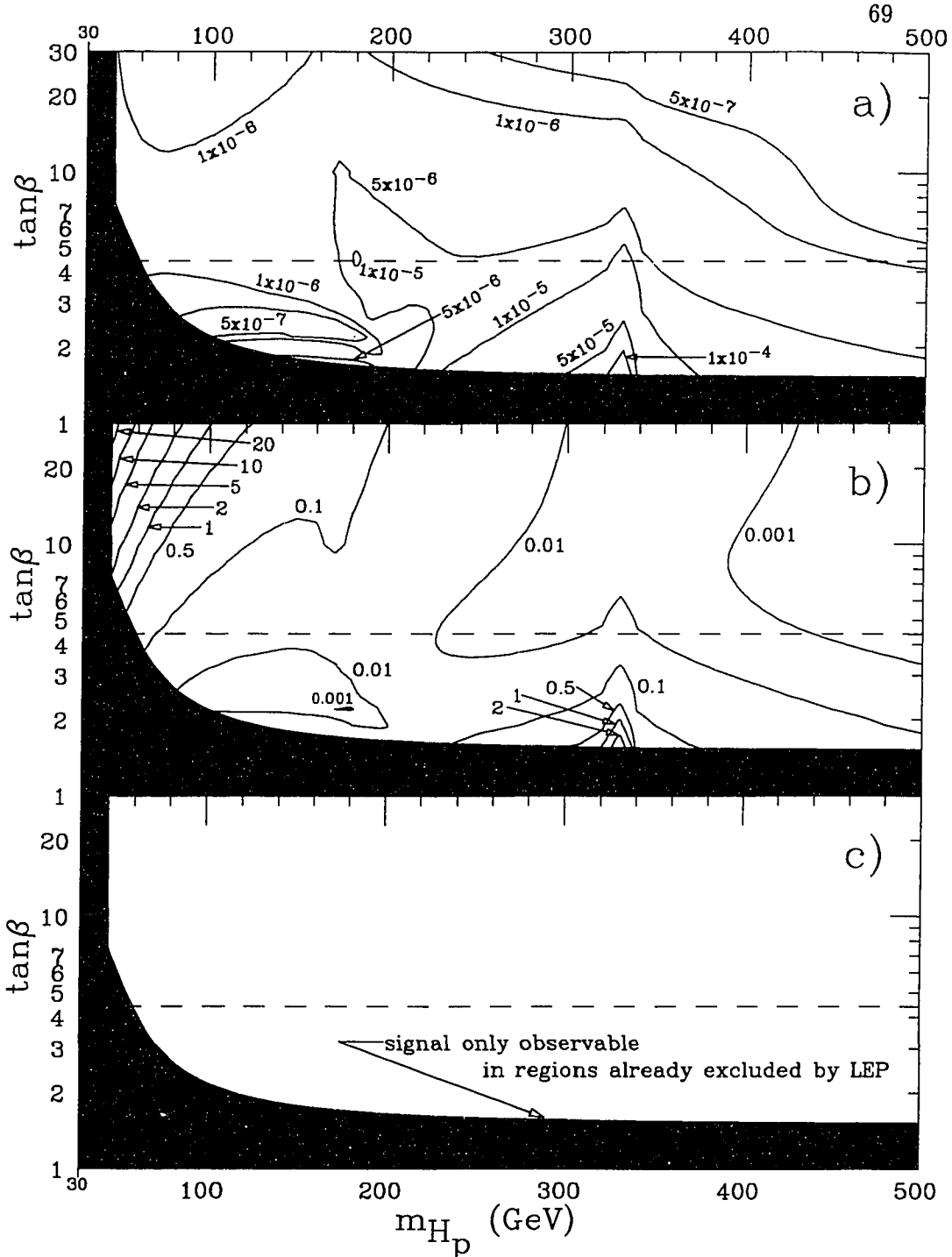

Figure 4.14: The $\gamma\,\gamma$ signal for H_p. a) $BR(H_p \to \gamma\gamma)$;
b) $\sigma(pp \to H_p \to \gamma\gamma)$. Curves are labeled in fb.
c) Region of detectability for this signal.
MSSM parameters as in Fig. 3.8 of Chapter 3, with
$m_{\tilde{g}} = -\mu = 1000\,\mathrm{GeV} \doteq m_{\tilde{q}}$ and $\sqrt{s} = 14\,\mathrm{TeV}$.

The calculation of the $H \to \gamma\gamma$ signal rate ignores interference between the $gg \to H \to \gamma\gamma$ signal process and the $gg \to \gamma\gamma$ QCD background process. This can only be large when the loop amplitudes for the two-photon decays of the Higgs bosons develop large imaginary parts [97]. However, this only occurs when the Higgs boson decay width becomes large, *i.e.*, when the corresponding tree-level two-body decay rates ($H_h, H_\ell \to W^+W^-$, $H_p \to t\bar{t}$) also become substantial; these large tree-level decay widths strongly suppress the $\gamma\gamma$ branching fraction, making the signal unobservable. So it is safe to neglect such interference in the region of interest ($m_{H_h} < 2M_W$, $m_{H_p} < 2m_t$).

It should also be noted that the photons from $q\bar{q}$ and gg fusion form a smooth continuous background (with only small statistical fluctuations) about the mass bin centered at $m(\gamma\gamma) = m_H$. One is thus not completely reliant upon theoretical computations of the background, in assessing the significance of the signal. The theoretical background estimates could be faulty if, for example, the gluon structure function used is inaccurate.

Finally, it should be added that QCD radiative corrections to both the $H \to \gamma\gamma$ decays (studied for the MSSM in Ref. [100], and for the SM with some discussion of the MSSM in Ref. [101]) and the $H \to Z^0Z^0$ decays (studied within the MSSM in Refs. [102,168]) have been neglected. For $H_{SM} \to \gamma\gamma$, QCD corrections were generally found to be $\lesssim$30% everywhere in the allowed MSSM parameter space, except where there is an accidental vanishing of the uncorrected width due to destructive interference between the W and quark loops [100], and for $H_p \to \gamma\gamma$ when $m_{H_p} \approx 2m_t$ [103]. (These studies neglected chargino and squark loops.)

The QCD radiative corrections to $\Gamma(H_h \to Z^0Z^0)$ were found [102,168] to increase the partial decay width for a given m_{H_h}, with the amount of the increase growing as m_{H_h} was increased. For the relatively low values of m_{H_h} in the region of the pockets of detectability for the "gold-plated" signal in Figure 4.3, the increase was roughly a factor of two for degenerate squarks with $m_{\tilde{q}} = 1000\,\text{GeV}$ and no squark mixing (*i.e.*, $A_t = A_b = \mu = 0$) [102]. This droped to only a $\sim$30% increase when squark masses are lowered to 300 GeV. From a complete one-loop renormalization scheme approximation technique, Ref. [168] obtained results that

agree fairly well with the one-loop effective potential technique used in Ref. [102] for $M_{H_h} \lesssim 500\,\mathrm{GeV}$ and $m_{\tilde{q}} = 1000\,\mathrm{GeV}$, but were considerably larger for higher values of m_{H_h}. Almost no dependence on $\tan\beta$ was seen by Ref. [102] if there was no squark mixing. However Ref. [168] does not agree with this, noting that the correction is largely determined by the top quark Yukawa coupling. Thus, the correction decreases with increasing $\tan\beta$ (see Table 1.2). If $|\mu|$ and/or $|A_t|$ were made large, then both references agree that the results were very sensitive to $\tan\beta$, μ, and A_t. For $m_{\tilde{t_1}} \simeq 300\,\mathrm{GeV}$, $m_{\tilde{t_2}} \simeq 600\,\mathrm{GeV}$, and $\tan\beta = 20$, the partial decay width was found to vary between roughly an order of magnitude larger and about an order of magnitude smaller than the uncorrected width depending on the values of μ and A_t. But for $\tan\beta = 2$, the variation was more moderate, ranging roughly from no change to an increase of something like a factor of 4-5 relative to the uncorrected width. The QCD correction also increased somewhat as m_t is increased.

Looking again at Z^0Z^0 modes for the case of high SUSY inputs, as illustrated by the c) plots of Figures 4.3, and 4.5, the "gold-plated" Z^0Z^0 is found to actually be somewhat tarnished, only providing a viable signal for the heavy Higgs boson, H_h, in a smattering of regions with lowish $\tan\beta$ and $m_{H_p} \lesssim 200\,\mathrm{GeV}$. Previous work [47,93,95,104] found a somewhat more substantial reach for this signal; however this was found to be diminished substantially by competition from the $H_h \to H_\ell H_\ell$ decay channel in this region of parameter space. This in turn is partly due to the large radiative corrections found for the H_h-H_ℓ-H_ℓ vertex (these corrections are calculated in Appendix A using the effective potential technique, and are larger than found previously, in part due to the larger than expected effect of the D-terms).

The $H_h \to \gamma\gamma$ signal shown in Fig. 4.11c) carves out a narrow slice of detectability for $50\,\mathrm{GeV} \lesssim m_{H_p} \lesssim 80\,\mathrm{GeV}$ and $\tan\beta \gtrsim 2.5$; and the $H_p \to \gamma\gamma$ signal of Fig. 4.13c) provides a detectable zone for $\tan\beta \lesssim 1.2$ for m_{H_p} values from $\sim$120 GeV to $\sim$350 GeV, with a broadening up to $\tan\beta \simeq 2.2$ just below the $t\bar{t}$ threshhold. The $H_\ell \to \gamma\gamma$ signal, shown in Fig. 4.9c), provides good coverage for higher vales of m_{H_p}, except for low $\tan\beta$ values between 1 and 2. It should be cautioned though that the location of the boundary for the $H_\ell \to \gamma\gamma$ detectable region is fairly sensitive

to the mass of the light Higgs boson. As shown in Fig. 1.2, a small change in m_{H_ℓ} can correspond to a large shift in position in the m_{H_p} *vs.* $\tan\beta$ plane. Also, as indicated in Fig. 4.8b), for $m_{H_\ell} \sim 100\,\mathrm{GeV}$, a small change in the mass of the light Higgs boson can significantly alter the expected amount of SM background from continuum $\gamma\gamma$ production (note the logarithmic scale for this plot). Thus, a slight change in the criterion for detectability can notably change the minimum value of m_{H_ℓ} needed to meet this requirement, assuming that the signal production rate does not change much (Fig. 4.9b) indicates this is a pretty good assumption). And even a modest change in m_{H_ℓ} can in turn markedly displace the location of such a borderline case in the m_{H_p} *vs.* $\tan\beta$ plane.

Putting all these modes together to give an overall picture of the parameter space that can be searched will be postponed until after consideration of other possible signal modes, including those from Higgs boson decays to sparticles, have been discussed in Chapters 5 and 6. Scanning the c) plots of Figures 4.5, 4.10, 4.12, and 4.14, it is immediately apparent that the detectable regions diminish in in size when the MSSM sparticle input values ($m_{\tilde{g}}$, $m_{\tilde{q}}$, and $\mu = -2m_1$) are lowered. In fact, the $H_h \rightarrow Z^0Z^0$ detectability region disappears entirely, and the $H_p \rightarrow \gamma\gamma$ favored region is greatly diminished and now falls in the area exluded by LEP searchs for Higgs bosons.

In summary, the gold-plated $H_h \rightarrow Z^0Z^0 \rightarrow 4\ell$ signal and the $H \rightarrow \gamma\gamma$ signals, the conventional, well-accepted Higgs boson signatures, are found to be serviceable only in limited regions of the MSSM parameter space. The fact that the rates drop when the values of $m_{\tilde{g}}$, $m_{\tilde{q}}$, and μ are lowered is again suggestive of the opening up of new supersymmetric decay modes of the Higgs bosons. It is thus beneficial to investigate whether or not this is indeed the case; and, if so, whether or not new signals from these decays of the Higgs bosons to sparticles can mitigate the diminishing of the conventional signatures from the decays of the Higgs bosons to SM particles, or even open up new regions of parameter space to experimental scrutiny.

Chapter 5

Higgs Boson Decays to Sparticles

Many studies in the past (see [47,92-95] for examples) have assigned high values to some of the MSSM input parameters, including $m_{\tilde{g}}$, $m_{\tilde{q}}$, and sometimes $2m_1 = -\mu$, specifically to render the sparticle decay modes of the Higgs bosons unimportant. Yet there is no justification for imposing this condition. The discussion on LEP constraints in Chapter 2 showed that the experimental lower bounds on most uncolored sparticle masses hover around $\frac{1}{2}M_{Z^0}$ (the LSP is even less restricted). Gluino and squark mass lower limits from the Fermilab TEVATRON experiments are also currently well under 200 GeV. Thus it is not necessary to raise the MSSM inputs such as $m_{\tilde{g}}$, $m_{\tilde{q}}$, and $\mu = -2m_1$ to around the TeV scale to conform with experimental results. In addition, grand unified models within the supergravity framework constructed to preserve the gauge hierarchy and to be consistent with constraints from accelerator experiments, limits on proton decay, and the demands of cosmology generally find that sparticle masses are well below 1 TeV[18,105-111]. In particular, the masses of the lighter charginos, $\widetilde{W_1}^{\pm}$, and neutralinos, $\widetilde{Z_1}$ and $\widetilde{Z_2}$, are frequently $\sim$100 GeV [107,108,110], and thus may well be kinematically accessible for Higgs boson decays.

When sparticle masses are sufficiently low, there is no reason to expect that the Higgs bosons will not decay via these supersymmetric modes. In fact, the SUSY decay modes of the Higgs bosons into charginos and neutralinos, which occur via gauge couplings, may dominate the Yukawa-coupling mediated $H \rightarrow b\bar{b}$ decay (which is proportional to the square of the b-quark mass) and the MSSM-mixing-angle-suppressed $H \rightarrow W^+W^-, Z^0Z^0$ modes. Thus if $b\bar{b}$, W^+W^-, and Z^0Z^0 are the principal SM decay products of a Higgs boson, then for appropriate choices of the

MSSM inputs charginos and neutralinos may actually have the largest branching fractions of any of the Higgs boson decay modes. The branching fractions of these supersymmetric decay modes were first systematically studied in Refs. [112-115]. However, the effects of radiative corrections to the Higgs boson masses were not included therein.

Figures 5.1 through 5.4 show in the μ *vs.* $\tan\beta$ plane the branching fractions of the various types of Higgs bosons into all kinds of sparticles, taking into account the radiative corrections to the Higgs boson masses from top and bottom Yukawa interactions. Here the pseudoscalar Higgs boson mass is taken to be 250 GeV. The SUSY decays are seen to be very important for the $m_{\tilde{g}} = 300\,\mathrm{GeV} \doteq m_{\tilde{q}}$ case in contrast to the $m_{\tilde{g}} = 1000\,\mathrm{GeV} \doteq m_{\tilde{q}}$ case (not shown) where the sparticle decays are insignificant. Thus, the branching fractions for the SUSY decays of H_h, H_p, and $H^{\pm}$ generally increase if $m_{\tilde{g}}$ is lowered. Figures 5.5 thourgh 5.7 in the m_{H_p} *vs.* $\tan\beta$ plane further indicate that the sparticle mode branching fractions for these Higgs bosons tend to increase as m_{H_p} is increased. Though this is interrupted for the pseudoscalar and charged Higgs bosons by the opening of the $H_p \to t\bar{t}$ and $H^+ \to t\bar{b}$ decays, respectively. The following additonal features of the lower sparticle mass figures merit attention:

- Decays of even the light Higgs boson to sparticles can have significant rates. Over much of the region where this is true, all or at least the overwhelming preponderence of these decays are to $\widetilde{Z}_1\widetilde{Z}_1$ which count as invisible decays. There are however areas where the visible $\widetilde{Z}_2\widetilde{Z}_1$ decay mode is also significant. Finally, note that if a chargino is not observed at LEP II, then Figure 5.1 predicts that the light Higgs boson decay modes into sparticles will be at best very meager (at least for this choice of $m_{\tilde{g}}$ and m_t).
- The sparticle branching fractions of the heavier Higgs bosons can indeed by quite large over a significant region of the parameter space not investigable at either LEP or LEP II (the latter is the region below the dashed line which denotes $m_{\widetilde{W}_1} = 90\,\mathrm{GeV}$). Note in some of these regions the sparticle decay branching fractions are in excess of 50% for all of the heavier MSSM Higgs bosons (H_h, H_p, and $H^{\pm}$).

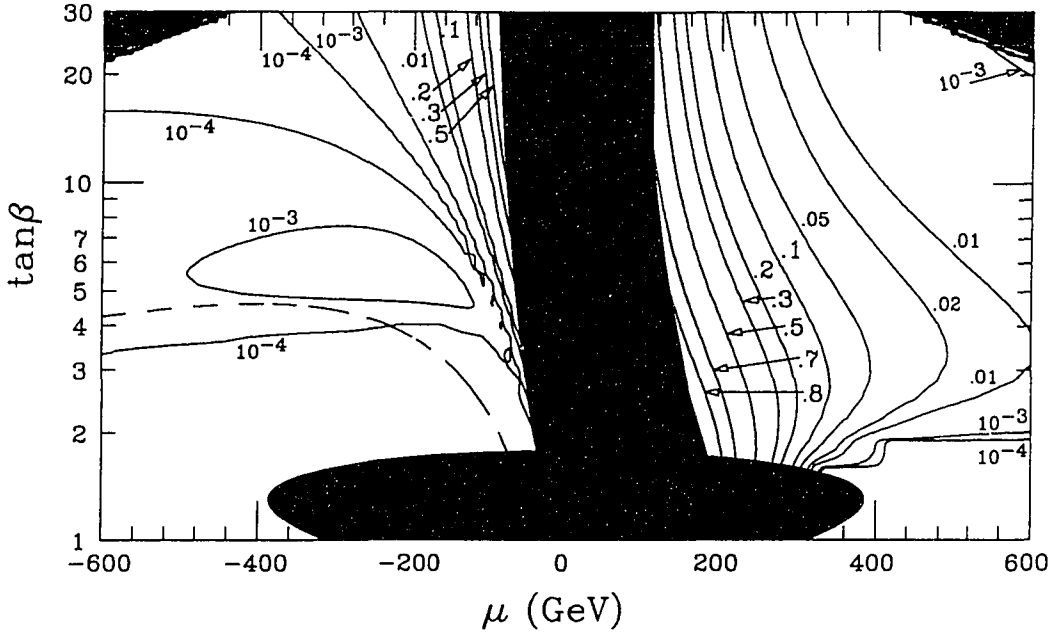

Figure 5.1: Branching fraction of H_ℓ into all types of sparticles, including (if kinematically accessible) charginos, neutralinos, and sfermions. Here $m_{\tilde{g}} = 300\,\text{GeV} \doteq m_{\tilde{q}}$. Other MSSM input parameters as in Figure 2.10.

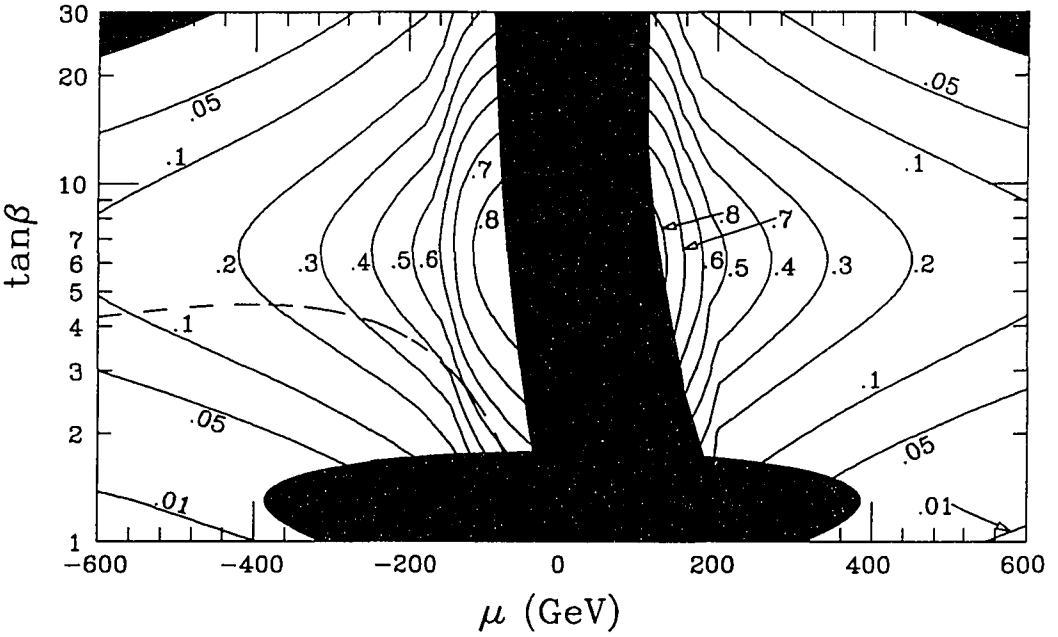

Figure 5.2: Branching fraction of H^+ or H^- into all types of sparticles, including (if kinematically accessible) charginos, neutralinos, and sfermions. Here $m_{\tilde{g}} = 300\,\text{GeV} \doteq m_{\tilde{q}}$. Other MSSM input parameters as in Figure 2.10.

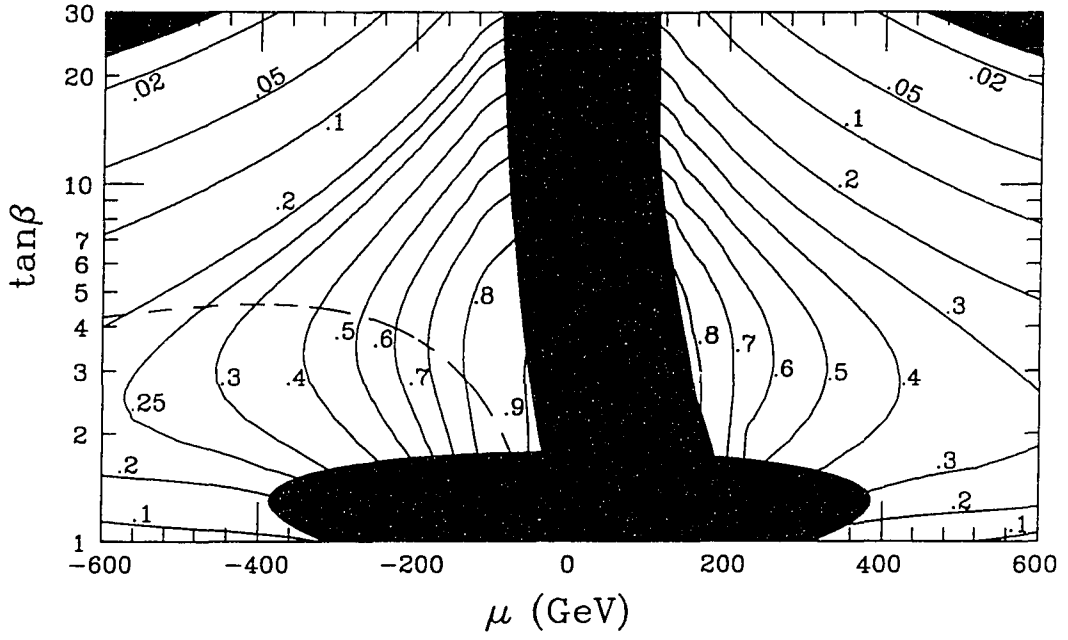

Figure 5.3: Branching fraction of H_h into all types of sparticles, including (if kinematically accessible) charginos, neutralinos, and sfermions. Here $m_{\tilde{g}} = 300\,\mathrm{GeV} \doteq m_{\tilde{q}}$. Other MSSM input parameters as in Figure 2.10.

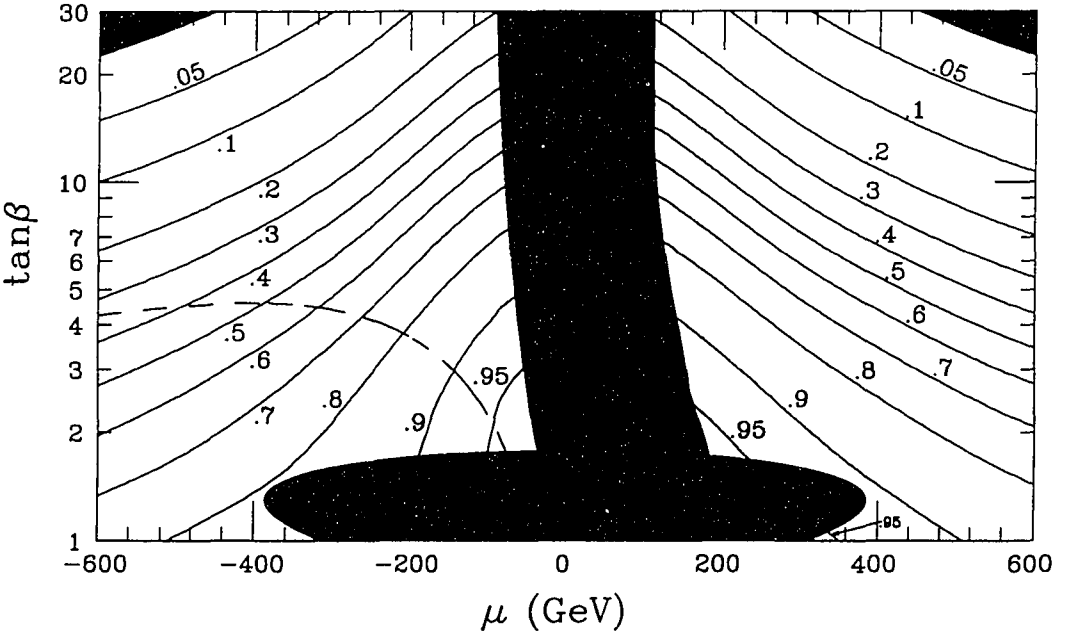

Figure 5.4: Branching fraction of H_p into all types of sparticles, including (if kinematically accessible) charginos, neutralinos, and sfermions. Here $m_{\tilde{g}} = 300\,\mathrm{GeV} \doteq m_{\tilde{q}}$. Other MSSM input parameters as in Figure 2.10.

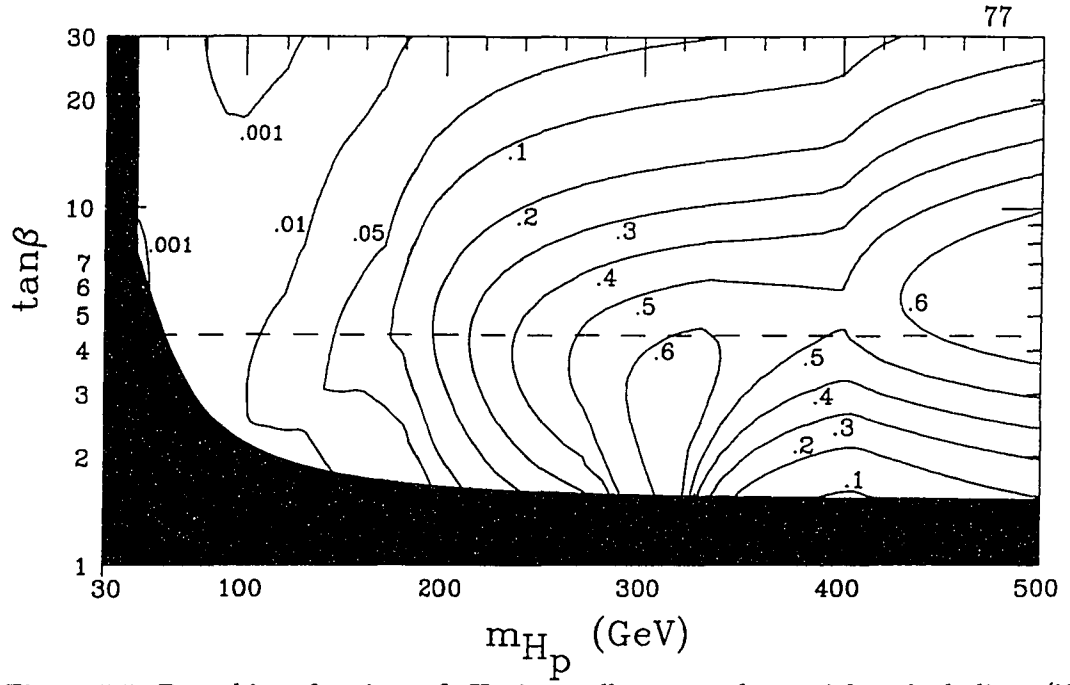

Figure 5.5: Branching fraction of H_h into all types of sparticles, including (if kinematically accessible) charginos, neutralinos, and sfermions. Here $m_{\tilde{g}} = -\mu = 300\,\mathrm{GeV} \doteq m_{\tilde{q}}$. Other MSSM input parameters as in Figure 2.10.

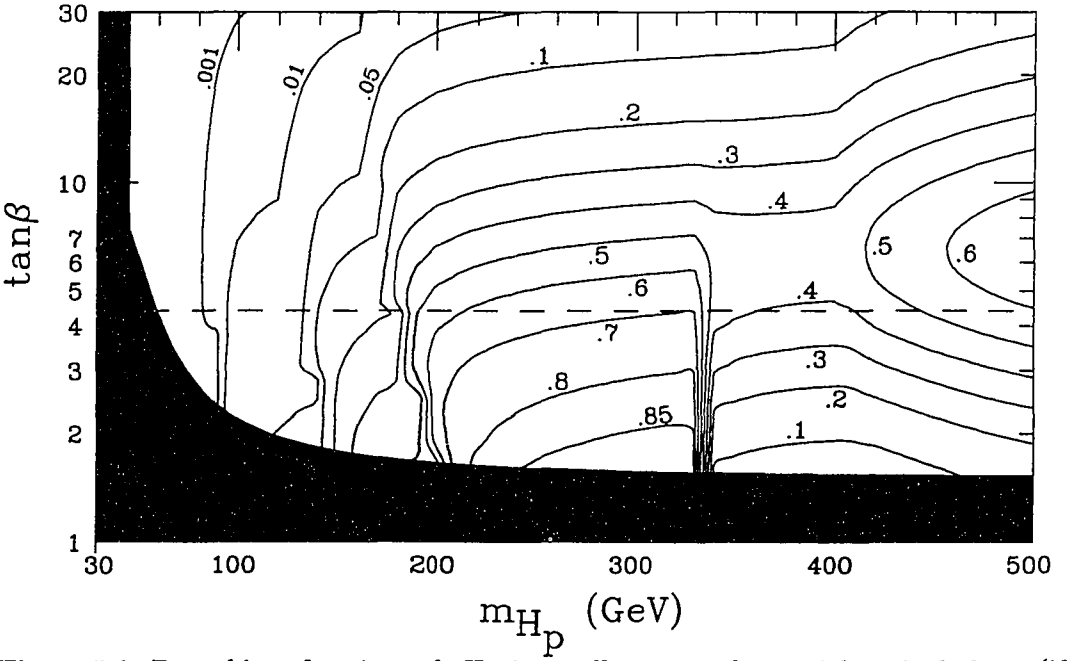

Figure 5.6: Branching fraction of H_p into all types of sparticles, including (if kinematically accessible) charginos, neutralinos, and sfermions. Here $m_{\tilde{g}} = -\mu = 300\,\mathrm{GeV} \doteq m_{\tilde{q}}$. Other MSSM input parameters as in Figure 2.10.

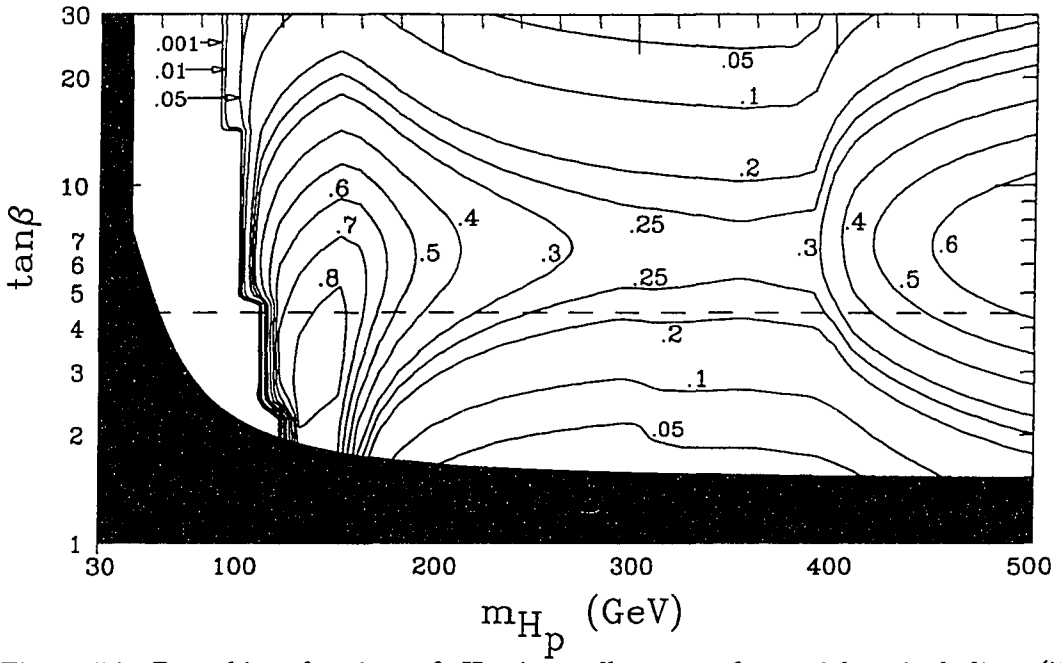

Figure 5.7: Branching fraction of H_{ch} into all types of sparticles, including (if kinematically accessible) charginos, neutralinos, and sfermions. Here $m_{\tilde{g}} = -\mu = 300\,\mathrm{GeV} \doteq m_{\tilde{q}}$. Other MSSM input parameters as in Figure 2.10.

In summary, it can be seen from these figures that there are regions of the MSSM parameter space consistent with all existing experimental constraints where branching fractions for the decay of Higgs bosons into neutralinos and charginos are substantial. Rates for the conventional SM decay signatures for the Higgs bosons will be reduced from what was otherwise expected in these regions, in agreement with what was found in the previous chapter. However, it is correspondingly also true that rates for the supersymmetric decay modes of the Higgs bosons then will be considerable, and it is possible that these will yield new signals for Higgs boson production.

In examining the chargino and neutralino decay modes of the Higgs bosons for new signatures for Higgs bosons, it is necessary to also consider how the charginos and neutralinos in turn decay. Consistent with the MSSM assumption of R-parity conservation, charginos and neutralinos must decay into lighter charginos, neutralinos or sfermions. Baryon and lepton number conservation further restrict the allowable two-body decays to:

$$\widetilde{W_2}^{\pm} \rightarrow \widetilde{W_1}^{\pm} + Z^0 \tag{5.1a}$$

$$\rightarrow \widetilde{W_1}^{\pm} + H \qquad (H = H_\ell,\ H_h, \text{ or } H_p) \tag{5.1b}$$

$$\widetilde{W_i}^{\pm} \rightarrow \widetilde{Z_j} + W^{\pm} \tag{5.1c}$$

$$\rightarrow \widetilde{Z_j} + H^{\pm} \tag{5.1d}$$

$$\rightarrow \widetilde{f_L} + \overline{f'} \quad \rightarrow f' + \overline{\widetilde{f_L}} \tag{5.1e}$$

$$\left.\begin{array}{l} \rightarrow \widetilde{t_R} + \overline{f'} \\ \rightarrow f' + \overline{\widetilde{t_R}} \end{array}\right\} \text{via Yukawa coupling of higgsino component} \tag{5.1f}$$

$$\widetilde{Z_i} \rightarrow \widetilde{W_j}^{\pm} + W^{\mp} \tag{5.1g}$$

$$\rightarrow \widetilde{W_j}^{\pm} + H^{\mp} \tag{5.1h}$$

$$\rightarrow \widetilde{Z_j} + Z^0 \tag{5.1i}$$

$$\rightarrow \widetilde{Z_j} + H \qquad (H = H_\ell,\ H_h, \text{ or } H_p) \tag{5.1j}$$

$$\rightarrow \widetilde{Z_j} + \gamma \qquad \text{(via loop diagram)} \tag{5.1k}$$

$$\rightarrow \widetilde{f_L} + \overline{f} \quad \rightarrow f + \overline{\widetilde{f_L}} \tag{5.1l}$$

$$\rightarrow \widetilde{f_R} + \overline{f} \quad \rightarrow f + \overline{\widetilde{f_R}} \tag{5.1m}$$

Formulæ for partial decay widths of all these decays are found in Ref. [116].

The gauge bosons in the neutralino and chargino decays may be real (if the decay is kinematically allowed) or virtual. In the latter case the charginos and neutralinos will decay via three body modes mediated by these off mass-shell gauge bosons or off mass-shell sfermions:

$$\widetilde{W_i}^{\pm} \rightarrow \widetilde{W_j}^{\pm} + f\overline{f} \tag{5.2a}$$

$$\rightarrow \widetilde{Z_j} + f'\overline{f} \tag{5.2b}$$

$$\widetilde{Z_i} \rightarrow \widetilde{W_j}^{\pm} + f'\overline{f} \tag{5.2c}$$

$$\rightarrow \widetilde{Z_j} + f\overline{f} \tag{5.2d}$$

(Recall from Chapter 2 that LEP sparticle production and Z^0 width constraints tend to rule out decay chains where the virtual Z^{0*} with a mass below M_{Z^0} in turn decays to the lightest charginos or neutralinos – the LSP's.) Generally, if they are kinematically accessible, the tree-level two-body decay modes of (5.1) will dominate the three-body decay modes of (5.2). Thus typically only the lighter charginos, $\widetilde{W_1}^{\pm}$, and the second lightest neutralino, $\widetilde{Z_2}$, have significant three-body decay branching fractions, whereas the heavier charginos, $\widetilde{W_2}^{\pm}$, and neutralinos, $\widetilde{Z_3}$ and $\widetilde{Z_4}$, typically produce events containing real gauge or Higgs bosons [116,117].

It is also possible for the three-body decay modes of (5.2) to be mediated by a Higgs boson or a sfermion. Since the amplitudes of the Higgs boson mediated decays are proportional to the fermion Yukawa couplings, the contributions from these processes are negligible. Whether or not sfermion mediated decays are important depends stongly on the mass of the sfermion involved. In the case of the lighter charginos, virtual W exchange is the dominant mechanism for the three-body decay if $m_{\tilde{f}} \gtrsim M_W$ [118] and $|\mu|$ is not extremely large. This being the case, the lighter charginos are expected to decay into $\widetilde{Z_1}$, the LSP, and a fermion pair with a leptonic branching fraction of about 11% per lepton family (which is just the branching fraction for leptonic W decays).

The situation for the $\widetilde{Z_2}$ decays is more complicated since this decay is frequently not dominated by a virtual Z^{0*} mediator. The Z^0 couples only to the higgsino components of the neutralinos, so that the Z^0-$\widetilde{Z_1}$-$\widetilde{Z_2}$ coupling can be strongly suppressed for some choices of the MSSM input parameters. This occurs when both of the lighter neutralinos are predominantly gaugino-like, which occurs when $|\mu| = |2m_1|$ is much larger than the soft SUSY-breaking $SU(2)_L$ and $U(1)_Y$ gaugino masses (μ_1 and μ_2 of Eqn. (1.8)), which themselves are determined from the gluino mass in the GUT-inspired framework assumed here. In terms of the MSSM inputs employed here, this then means $m_{\tilde{g}} \lesssim |\mu|$. (It might be noted that $|\mu| \simeq m_{\tilde{g}}$ is in fact predicted by supergravity models with radiative electroweak symmetry breaking [14,108,111].) In contrast, the W–$\widetilde{Z_1}$–$\widetilde{W_1}$ coupling receives contributions from both the higgsino *and* the $SU(2)_L$ gaugino components of the sparticles, and so the W-mediated three-

body decay of the lighter charginos can only be suppressed if the $\widetilde{Z}_1$ is a pure $U(1)_Y$ gaugino, which occurs only if $|\mu|$ is quite large. This leads to the relative insensitivity to the MSSM inputs of the lighter charginos' decay modes indicated in the previous paragraph. (The radiative decay $\widetilde{Z}_2 \to \widetilde{Z}_1\gamma$ of (5.1), which is mediated by sfermion-fermion and gaugino-gauge boson loops, may have a comparable branching ratio to these three-body tree-level decays. This generally occurs if one of the neutralinos is photino-like and the other is higgsino-like so that both the Z^{0*}- and the sfermion-mediated decay channels are suppressed since the photino does not couple to the Z^0 and the higgsino does not couple to the sfermion, or if the two neutralinos are higgsino-like and nearly degenerate in mass so that gauge boson mediated three-body decay is more phase space limited than the radiative two-body decay.)

If the virtual Z^{0*} contribution is indeed suppressed for the three-body $\widetilde{Z}_2$ decays, then the contribution of even a relatively heavy sfermion can be significant, and the branching ratios for the decays of the $\widetilde{Z}_2$ become very sensitive to the sfermion mass spectrum. According to Eqns. (1.9), sleptons can be considerably lighter than squarks if the gluino and squark masses are about the same. This then would strongly enhance the slepton-mediated leptonic decay of $\widetilde{Z}_2$ relative to the squark-mediated hadronic decays, and can significantly affect the overall leptonic decay rate of the $\widetilde{Z}_2$ for $|\mu| \gg m_{\tilde{g}} \simeq m_{\tilde{q}}$ [167].

This last conclusion is important for the study of Higgs boson detection techniques at hadron supercolliders since the most promising signatures for Higgs bosons at hadron colliders involve purely leptonic final states. Purely hadronic decay modes of the Higgs bosons have monstrous backgrounds from multi-jet production, while mixed leptonic-hadronic decays have daunting backgrounds from heavy flavor (including $t\bar{t}$) production. Invisible Higgs boson decay modes which could occur if a Higgs boson decays via $H \to \widetilde{Z}_1\widetilde{Z}_1$ or $H \to \widetilde{Z}_1\widetilde{Z}_2 \to \nu\bar{\nu}\widetilde{Z}_1\widetilde{Z}_1$ might lead to a missing $\not{E}_T$ signal (or in associated production processes where the Higgs boson is produced along with a gluon, a Z^0, or a $W^\pm$). But this would have to be distinguished from Z^0Z^0 production where both (or one) of the Z^0's decay to neutrinos and other MSSM sources of $\not{E}_T$. This leads one to consider final states with charged leptons.

Final states with only a single charged lepton have large SM backgrounds from $W \to e\nu_e$, $\mu\nu_\mu$, $\tau\nu_\tau$, so this leaves decay chains which have multi-charged-lepton final states as the optimal subset of the neutralino and chargino Higgs boson decays to investigate for new signatures for the Higgs bosons.

First contemplate investigating final states with two charged leptons. The dilepton (plus $\not{E}_T$) signal largely comes from

$$H_{h,p} \to \widetilde{Z}_2 \widetilde{Z}_1 \to \ell^+\ell^- \widetilde{Z}_1 \widetilde{Z}_1 \ , \tag{5.3a}$$

$$\text{and} \qquad H_{h,p} \to \widetilde{W}_1^{\,+} \widetilde{W}_1^{\,-} \to \ell^+\nu\ell^-\bar{\nu}\widetilde{Z}_1\widetilde{Z}_1, \ell^+\nu\ell'^-\bar{\nu}\widetilde{Z}_1\widetilde{Z}_1 \ , \tag{5.3b}$$

where $\ell, \ell' = e$ or μ (the term "lepton" will be used to a mean muon or an electron, but not a tau, in this chapter). Within the SM, W^+W^- and $t\bar{t}$ production can also lead to dilepton events with missing transverse energy. Decays of the heavier Higgs bosons to the heavier charginos ($\widetilde{W}_2^{\pm}$) or neutralinos ($\widetilde{Z}_3$,$\widetilde{Z}_4$) or to sfermions might also produce final states with two charged leptons plus $\not{E}_T$; however, these processes tend to be sub-dominant, and for simplicity will be neglected here. In addition, decays to a pair of the lighter stop mass eigenstate $H \to \tilde{t}_1\bar{\tilde{t}}_1$ as well as continuum stop pair production would also produce dilepton events accompanied by jets. As has been recently pointed out [119-122], a very light stop squark with $m_{\tilde{t}_1} \lesssim 100$ GeV is not experimentally ruled out. However, decays of neutralinos and charginos are more likely to produce hadronically quiet events than squark decays (or top quark decays, unless $m_t \simeq M_W$, which now appears to be ruled out experimentally); and thus chargino and neutralino decays seem better candidates for an initial study.

The leptons from the decay of $\widetilde{Z}_2$ in (5.3a) are always of the same flavor and are kinematically constrained to satisfy the condition $m(\ell^+\ell^-) < m_{\widetilde{Z}_2} - m_{\widetilde{Z}_1}$, features that may be useful in separating the signal from backgrounds. On the other hand, the leptons from the decays of the $\widetilde{W}_1$'s in (5.3b) can have mixed flavors (that is, $e^\pm\mu^\mp$) and are generally expected to have a broad invariant mass distribution which only cuts off at $m(2\ell) = m_{H_{h,p}} - 2m_{\widetilde{Z}_1}$.

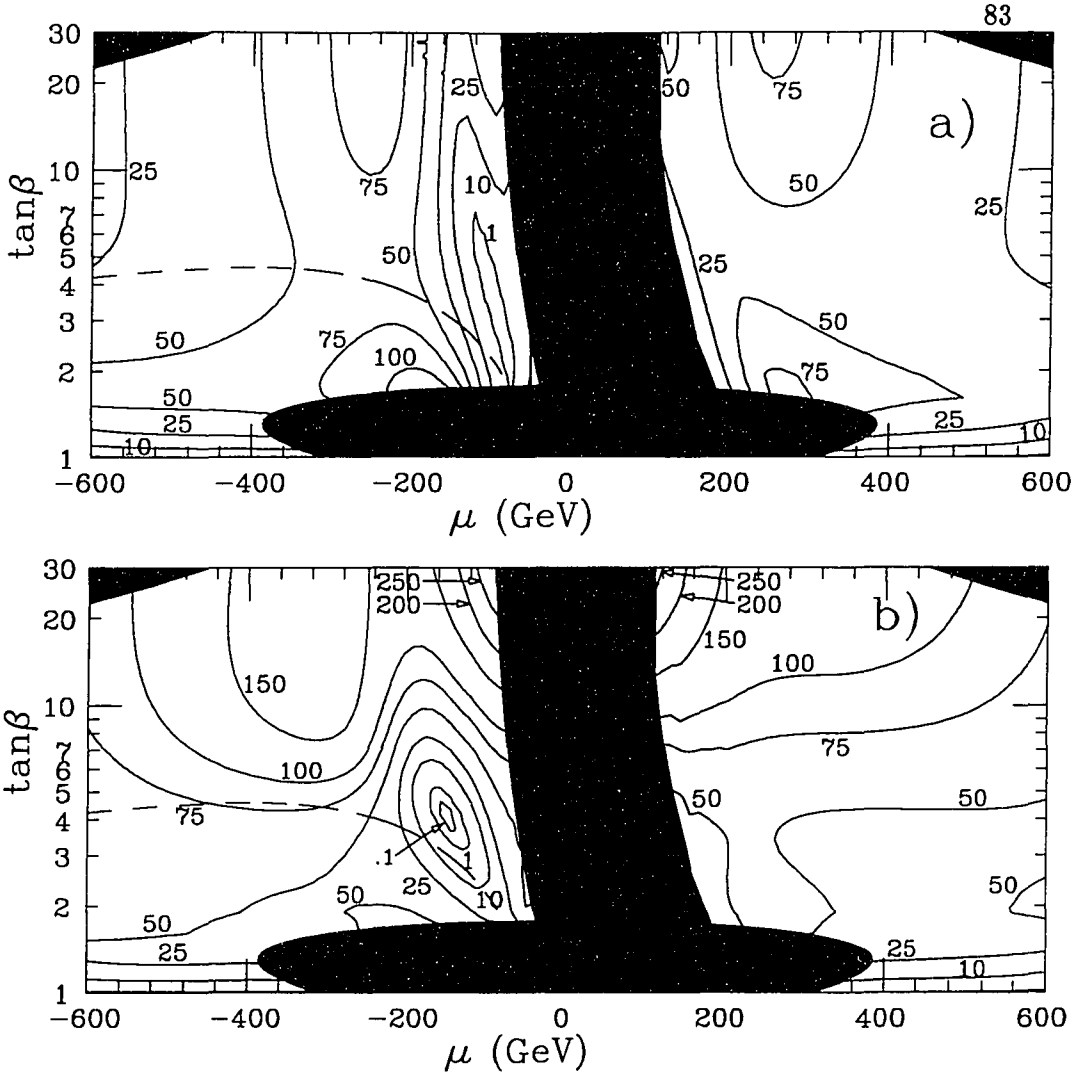

Figure 5.8: a) $\sigma(pp \to H_h \to \widetilde{Z}_2\widetilde{Z}_1 \to \ell^+\ell^- + \not{E}_T)$,
b) $\sigma(pp \to H_h \to \widetilde{W}_1\widetilde{W}_1 \to \ell^+\ell^- + \not{E}_T)$.
Labels in fb; $\sqrt{s} = 14\,\text{TeV}$.
Here: $m_{\tilde{g}} = 300\,\text{GeV} \doteq m_{\tilde{q}}$, with other parameters as in Fig. 3.8.

Figures 5.8-5.11 give LHC cross-sections for dilepton events from H_h decays and H_p decays, respectively, as described in (5.3). Note that the dilepton rates from $H_h, H_p \to \widetilde{W}_1^+\widetilde{W}_1^-$ tend to be larger than those from $H_h, H_p \to \widetilde{Z}_2\widetilde{Z}_1$ for high values of $\tan\beta$. In other regions of parameter space the cross-sections of the two decay channels are fairly comparable (within a factor of two or so). The figures also show that the dilepton rate from H_p is usually larger than that from the H_h.

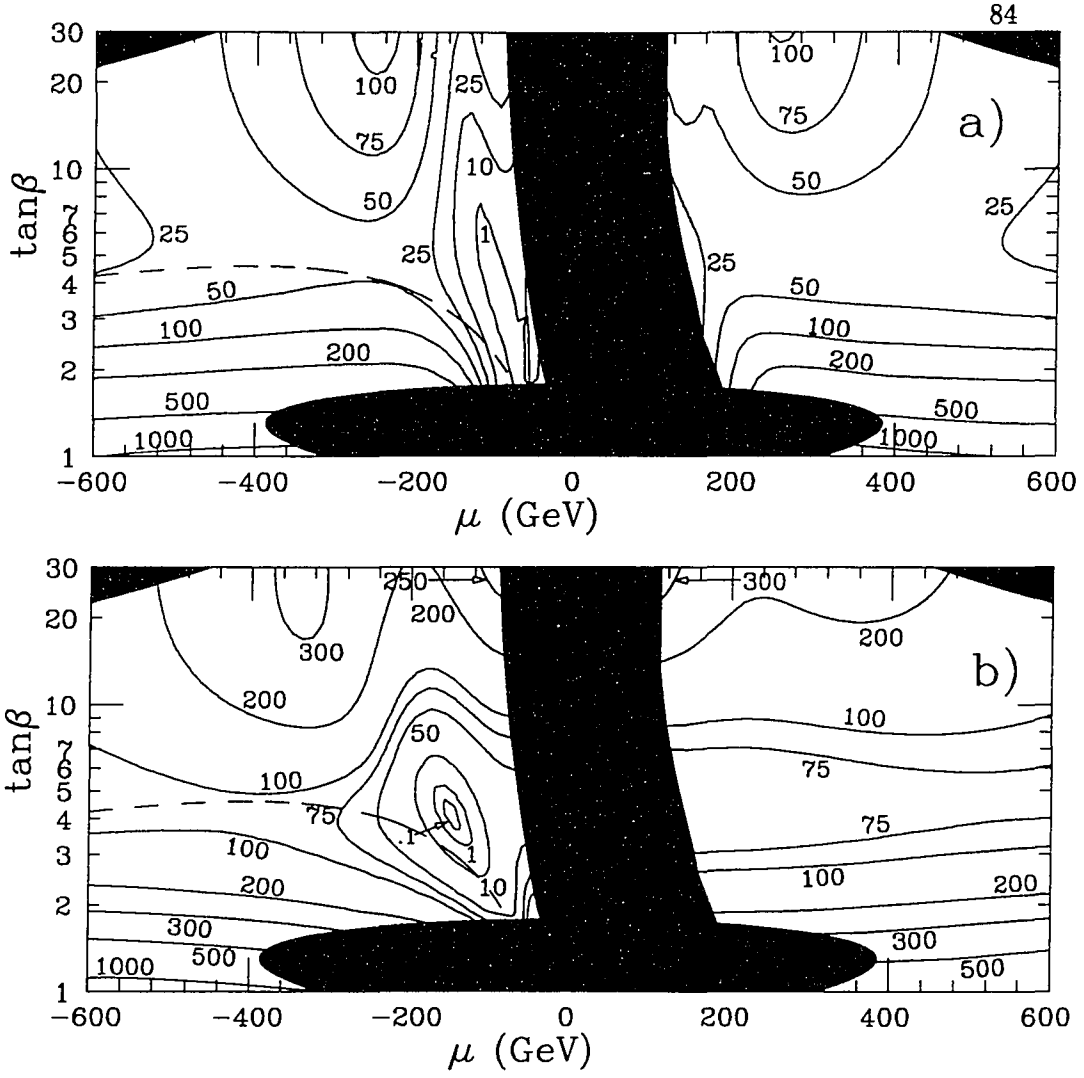

Figure 5.9: a) $\sigma(pp \to H_p \to \widetilde{Z}_2\widetilde{Z}_1 \to \ell^+\ell^- + \not{E}_T)$,
b) $\sigma(pp \to H_p \to \widetilde{W}_1\widetilde{W}_1 \to \ell^+\ell^- + \not{E}_T)$.
Labels in fb; $\sqrt{s} = 14\,\text{TeV}$.
Here: $m_{\tilde{g}} = -\mu = 300\,\text{GeV} \doteq m_{\tilde{q}}$, with other parameters as in Fig. 3.8.

There exist both SM and SUSY backgrounds to the $\ell\bar{\ell} + \not{E}_T$ Higgs boson signal. The dominant SM background to hadronically quiet dilepton events is from W^+W^- pair production. At the $\sqrt{s} = 14\,\text{GeV}$ LHC the W^+W^- cross-section is about 70-75 pb, which would lead to a $\sim$3 pb dilepton + $\not{E}_T$ SM background cross-section (note that this background can also yield mixed lepton flavor final states). Direct production of chargino and neutralino pairs will also provide a background as illus-

trated in Figure 5.12. The SUSY direct production background is much larger than the Higgs boson decay signal cross-section only for small values of μ, which mostly fall in the LEP excluded region (see Figure 2.10). For $|\mu| \geq 200\,\mathrm{GeV}$, the background from direct $\widetilde{Z}_1\widetilde{Z}_2$ production is frequently small, whereas the background from direct $\widetilde{W}_1\widetilde{W}_1$ production can be as high as several picobarns, making identification of a dilepton signal from Higgs boson decays difficult.

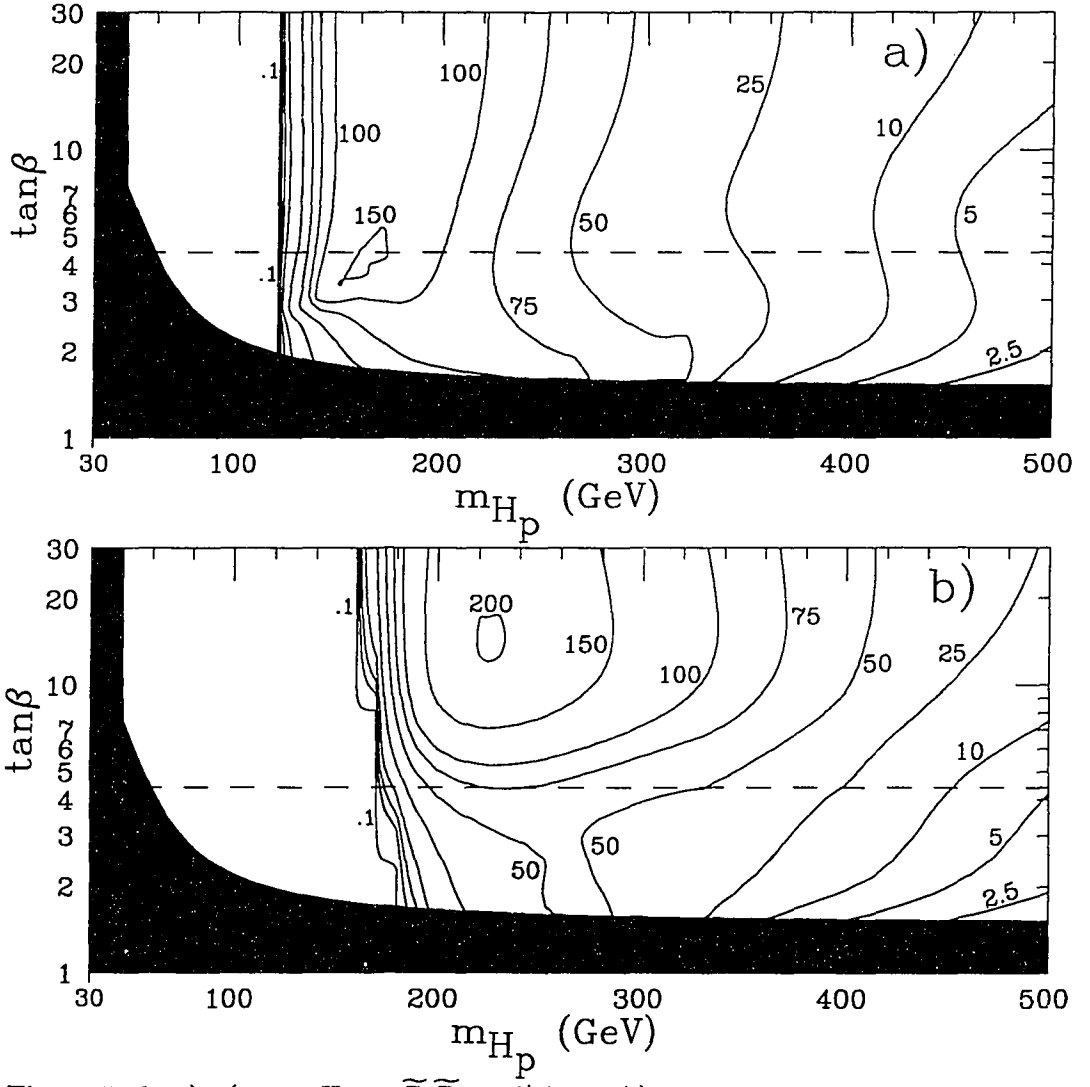

Figure 5.10: a) $\sigma(pp \to H_h \to \widetilde{Z}_2\widetilde{Z}_1 \to \ell^+\ell^- + \not{E}_T)$,
b) $\sigma(pp \to H_h \to \widetilde{W}_1\widetilde{W}_1 \to \ell^+\ell^- + \not{E}_T)$.
Labels in fb; $\sqrt{s} = 14\,\mathrm{TeV}$. Here: $m_{\tilde{g}} = -\mu = 300\,\mathrm{GeV} \doteq m_{\tilde{q}}$, with other parameters as in Fig. 3.8.

As with the dilepton invariant mass distribution from the Higgs boson decay to neutralinos mentioned previously, the $m(\ell^+\ell^-)$ mass distribution from direct $\widetilde{Z}_1\widetilde{Z}_2$ production will also be bounded by $m_{\widetilde{Z}_2} - m_{\widetilde{Z}_1}$. The $m(\ell^+\ell^-)$ distribution from direct chargino and W-boson production will be broad, again just like the dilepton invariant mass distribution from the Higgs boson decay to charginos. The significant size of the backgrounds and the inability to distinguish the background invariant

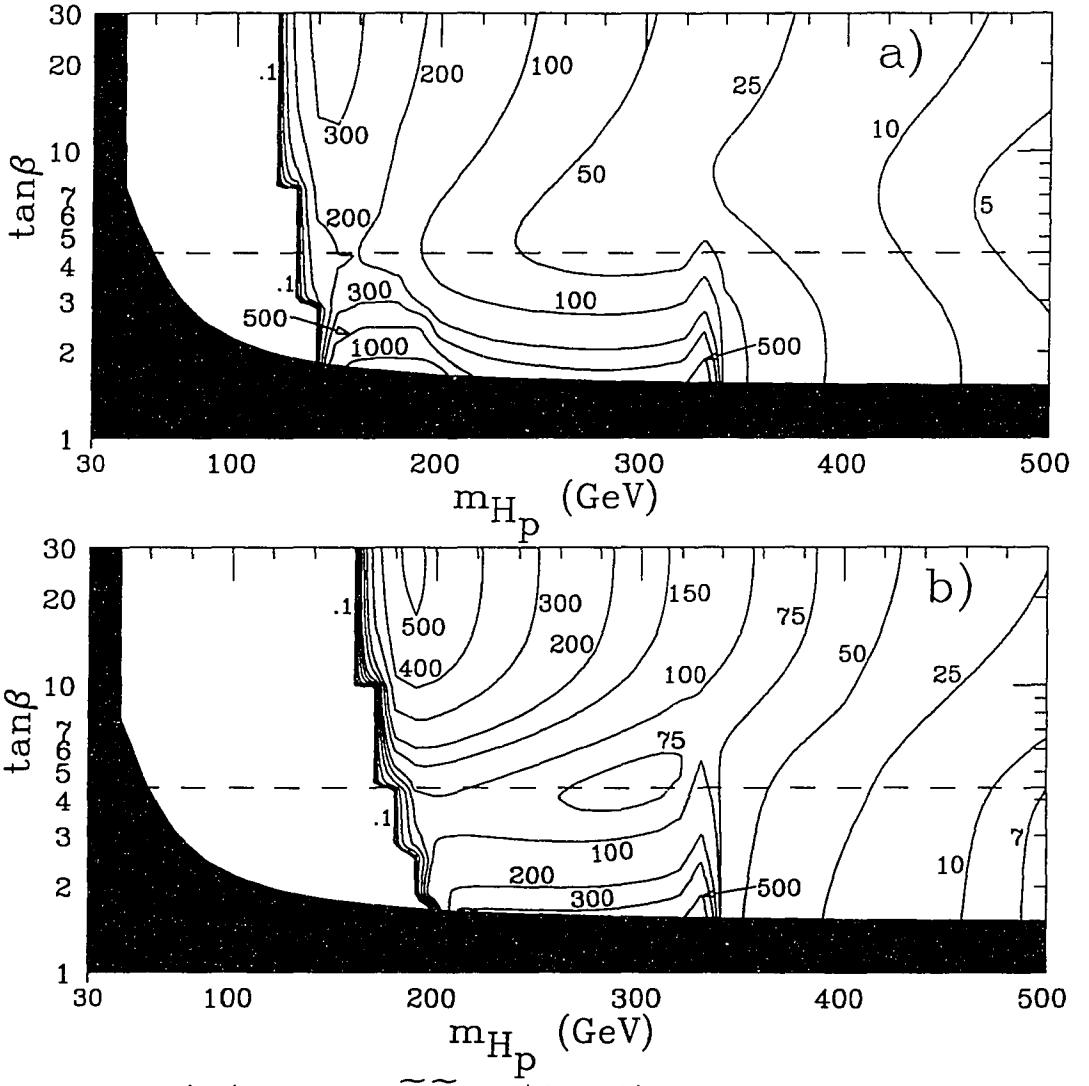

Figure 5.11: a) $\sigma(pp \to H_p \to \widetilde{Z}_2\widetilde{Z}_1 \to \ell^+\ell^- + \not{E}_T)$,
b) $\sigma(pp \to H_p \to \widetilde{W}_1\widetilde{W}_1 \to \ell^+\ell^- + \not{E}_T)$.
Labels in fb; $\sqrt{s} = 14\,\text{TeV}$. Here: $m_{\tilde{g}} = -\mu = 300\,\text{GeV} \doteq m_{\tilde{q}}$, with other parameters as in Fig. 3.8.

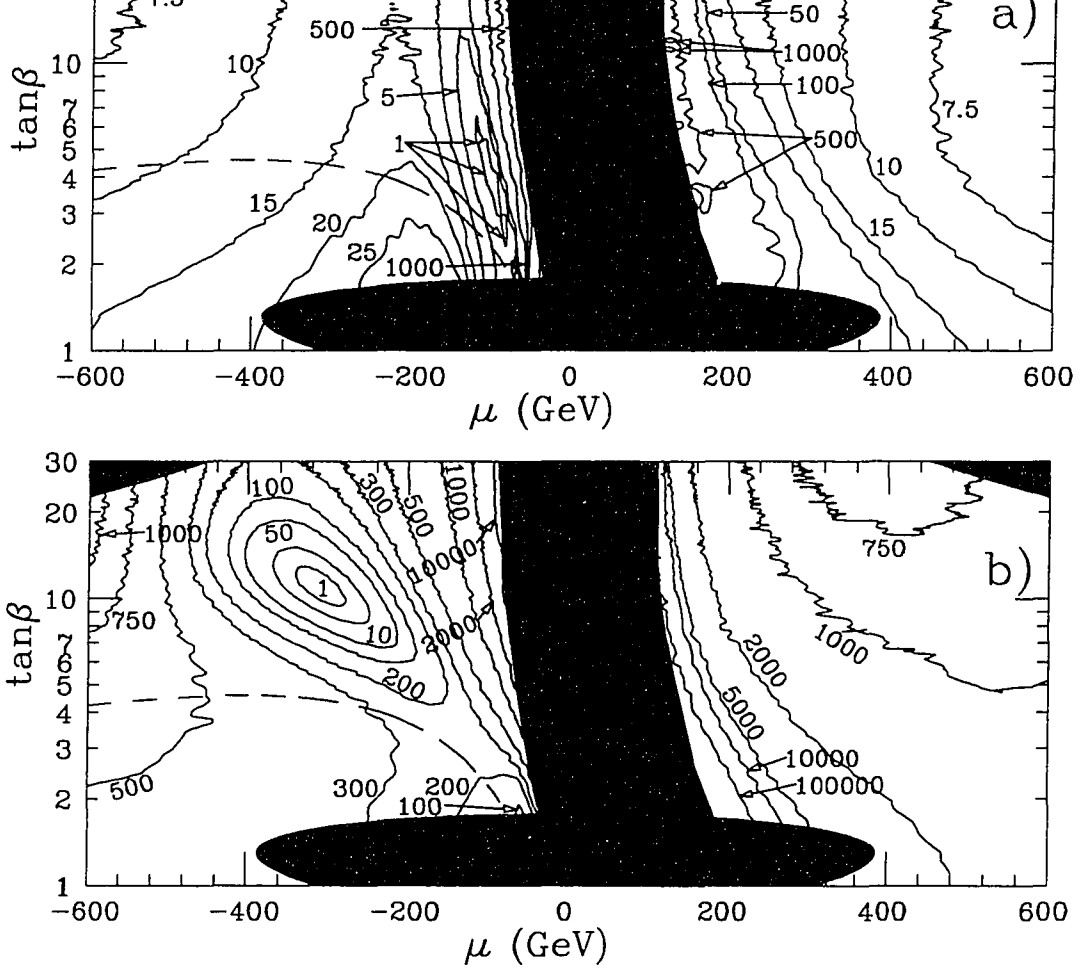

Figure 5.12: a) $\sigma(pp \to \widetilde{Z}_2\widetilde{Z}_1 \to \ell^+\ell^- + \not{E}_T)$, b) $\sigma(pp \to \widetilde{W}_1\widetilde{W}_1 \to \ell^+\ell^- + \not{E}_T)$. Labels in fb; $\sqrt{s} = 14\,\text{TeV}$. Here: $m_{\tilde{g}} = 300\,\text{GeV} \doteq m_{\tilde{q}}$ and $m_{H_p} = 250\,\text{GeV}$, with other parameters as in Fig. 3.8.

mass distributions from the signal invariant mass distribution make discovery of Higgs boson sparticle decays difficult in the dilepton channel, though perhaps some distortion of the low end of the $m(\ell^+\ell^-)$ distribution contributed by a Higgs boson whose mass is not too large could be detected, hopefully confirming signals seen in more promising channels.

Continuing the progression towards higher lepton multiplicities, the next class of signal-events to study are trilepton ($+ \not{E}_T$) signals from Higgs boson decays. One possible source for such events is the charged Higgs decay

$$H^{\pm} \rightarrow \widetilde{W_1}^{\pm} \widetilde{Z_2} \tag{5.4}$$

If the mass of the charged Higgs boson is low enough, then it could be produced in top quark decays and subsequently decay into a neutralino and a chargino, resulting in trileptonic top quark decays,

$$t \rightarrow bH^{\pm} \rightarrow b\widetilde{W_1}\widetilde{Z_2} \rightarrow b + 3\ell + \not{E}_T, b + 2\ell + \ell' + \not{E}_T \ , \tag{5.5}$$

where the missing transverse energy comes from both LSP's and ν_τ. Felcini [123] concluded that even with stringent requirements to cleanly tag $t\bar{t}$ events, $\gtrsim 2500$ such tagged events can be expected at the LHC for an integrated luminosity of $10\,\mathrm{fb}^{-1}$. Therefore, rare top quark decay modes with branching fractions in excess of $\sim 10^{-3}$ might be discernible if their characteristics provide sufficient discrimination between them and other top quark decay modes. *Three* somewhat high p_T leptons would certainly set $t \rightarrow H^+b \rightarrow \widetilde{W_1}^+ \widetilde{Z_2} b$ events apart from the common SM $t \rightarrow W^+b$ decays for which a *single* high p_T isolated lepton is normally expected. Actually, $t\bar{t}$ events can be tagged using the *two* lepton $e\mu$ SM top quark decays to fairly cleanly identify one top quark [123]. Events thus selected can then be scrutinized for trileptonic decays of the other top quark. Unfortunately, the two LSP's produced will absorb a good fraction of the top quark rest mass energy, making the trilepton energy spectrum fairly soft. Figure 5.13 illustrates the expected branching ratios for trileptonic top decays via a charged Higgs boson going into a chargino and a neutralino. Note that lower values for μ (and/or $m_{\tilde{g}}$) are required to make the chargino and neutralino masses sufficently low so that $H^{\pm} \rightarrow \widetilde{W_1}^{\pm} \widetilde{Z_2}$ is kinematically allowed (recall $m_{H_{ch}} \lesssim m_t - m_b$ is also necessary). The invariant mass of the two leptons from the $\widetilde{Z_2}$ decay will have a cut-off at $m_{\widetilde{Z_2}} - m_{\widetilde{Z_1}}$, while the overall trilepton invariant mass distribution must terminate at $m_{H_{ch}} - 2m_{\widetilde{Z_1}}$. Therefore, in addition to providing evidence both for the existence of a charged Higgs boson and for its supersymmetric decays to sparticles, these trileptonic events

may provide a means of measuring the mass of the charged Higgs boson, assuming the mass of one of the light neutralinos ($\widetilde{Z}_1$ or $\widetilde{Z}_2$) is known and sufficient statistics are available.

If $m_{H_{ch}} > m_t$, then charged Higgs bosons cannot be produced by top quark decays, and a collection of tagging top quark decays can no longer be used as a culled set of events less replete with SM backgrounds in which to search for evidence of the charged Higgs boson. Nonetheless, the $H^{\pm} \to \widetilde{W_1}^{+}\widetilde{Z}_2$ decays in this case still may merit investigation, especially since there really are no good signatures known for a heavier charged Higgs boson. (It should also be noted that a heavier charged Higgs boson is favored by $b \to s\gamma$ studies [19,124,125].) Yet backgrounds from both SM processes and direct $\widetilde{W_1}^{\pm}\widetilde{Z}_2$ may indeed prove insurmountable if events are not restricted to identified top quark decays [126]. If the charged Higgs boson is produced in association with a top quark, as expected in the process $gb \to H^{-}t$, one might even hope to pick up one (or more) additional lepton from the top quark decay, yielding a four-lepton event topology.

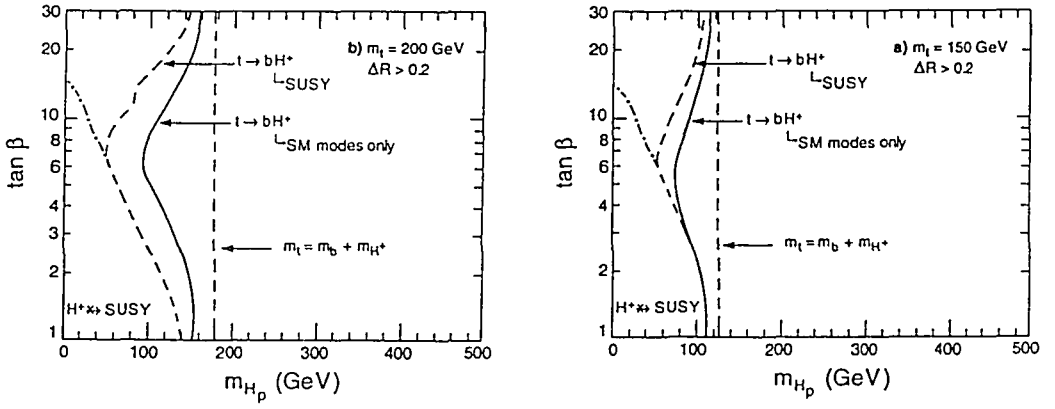

Figure 5.13: Branching ratio for $t \to bH^{+} \to b\widetilde{W_1}^{+}\widetilde{Z}_2 \to b + 3\ell + \not{E}_T$ with $m_t = 150\,\text{GeV}$ in a) and $m_t = 200\,\text{GeV}$ in b).
$m_{\tilde{g}} = 400\,\text{GeV}$ and $\mu = -70\,\text{GeV}$. The region to the left of the dot-dashed curve is where charged Higgs decays to sparticles are kinematically not allowed; the verticle dashed line is the phase space limit for $t \to bH^{+}$.

A more promising way to get four-lepton events from supersymmetric decays of the MSSM Higgs bosons is through decays of the heavier neutral Higgs bosons to a pair of $\widetilde{Z}_2$ neutralinos,

$$H_h, H_p \rightarrow \widetilde{Z}_2\widetilde{Z}_2 \rightarrow \ell^+\ell^-\widetilde{Z}_1 + \ell'^+\ell'^-\widetilde{Z}_1 \quad . \tag{5.6}$$

(Note that Higgs boson decays to the heavier neutralinos or charginos can also lead to four isolated leptons plus $\not{E}_T$; however, these decays tend to be far less important than (5.6) for Higgs boson masses of interest, and for simplicity will be neglected here.) Figures 5.14 through 5.19 show the cross-sections for the processes (5.6) plotted in the m_{H_p} *vs.* $\tan\beta$ plane, the $\mu = -2m_1$ *vs.* $\tan\beta$ plane, and the the $m_{\tilde{q}}$ *vs.* $\tan\beta$ plane. From the m_{H_p} *vs.* $\tan\beta$ plots, we see that the $H_p \rightarrow 4\ell$ cross-section exceeds 500 fb for small values of $\tan\beta$ and $m_{H_p} \sim 300$ GeV, just below threshold for $H_p \rightarrow t\bar{t}$ decay whereas the corresponding cross-section from H_h does not exceed 100 fb. Over a wide range of parameters, away from $\tan\beta = 1$, the two processes give comparable cross-sections. The large difference between the scalar and pseudoscalar contributions to the signal for small values of $\tan\beta$ mainly comes from the difference in their SUSY branching fractions [104]. The signal from the decays of H_p and H_h are also separately larger than 5 fb for 200 GeV $< m_{H_p} <$ 400 GeV. Since H_h and H_p are expected to be roughly degenerate over the range of masses where the signal is significant, this corresponds to a total of 250-25,000 4ℓ events at the LHC before any selection cuts, assuming a data sample with 50 fb^{-1}. Interestingly, the signal has a larger rate in the region below the dashed line, where the lighter chargino is heavier than 90 GeV, which again is taken to roughly represent the supersymmetry reach of LEP II (Note that this region is rather sensitive to the precise value of the chargino mass reach that is assumed). The Higgs bosons H_ℓ and H_p may themselves be directly accessible at LEP II though (see Fig. 2.12).

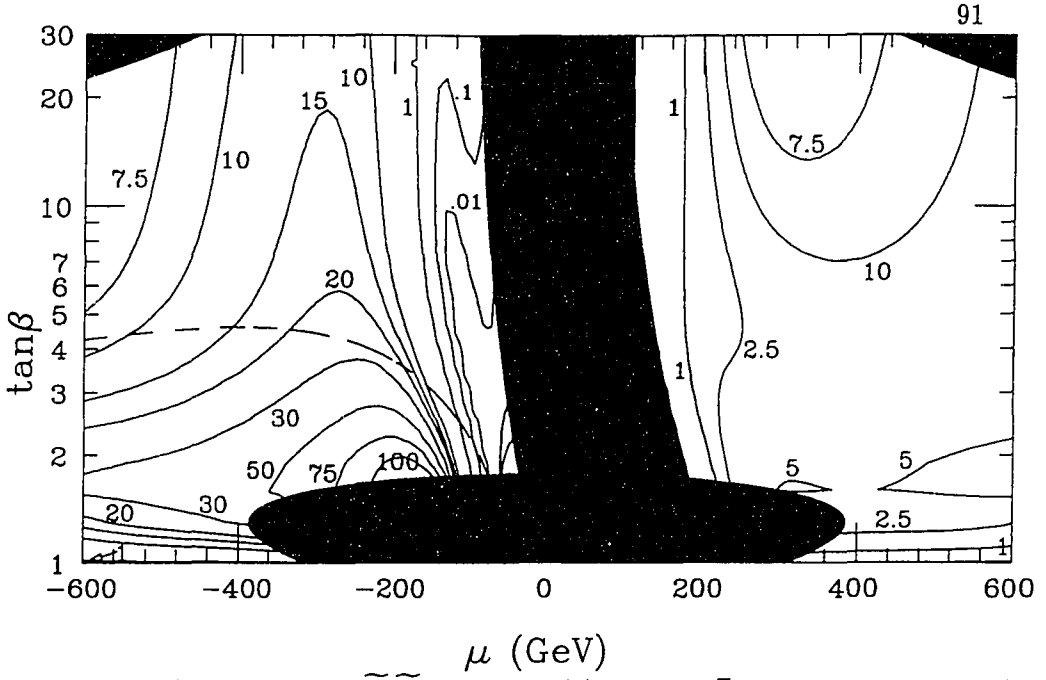

Figure 5.14: $\sigma(pp \to H_h \to \widetilde{Z}_2\widetilde{Z}_2 \to 4\ell + \not{E}_T)$ in fb, $\sqrt{s} = 14\,\text{TeV}$. Recall that the region above the dashed line corresponds to $m_{\widetilde{W}_1} < 90\,\text{GeV}$, the approximate reach of LEP II for charginos. Here $m_{H_p} = 250\,\text{GeV}$, $m_{\tilde{g}} = 300\,\text{GeV} \doteq m_{\tilde{q}}$. Other MSSM input parameters as in Figure 2.10.

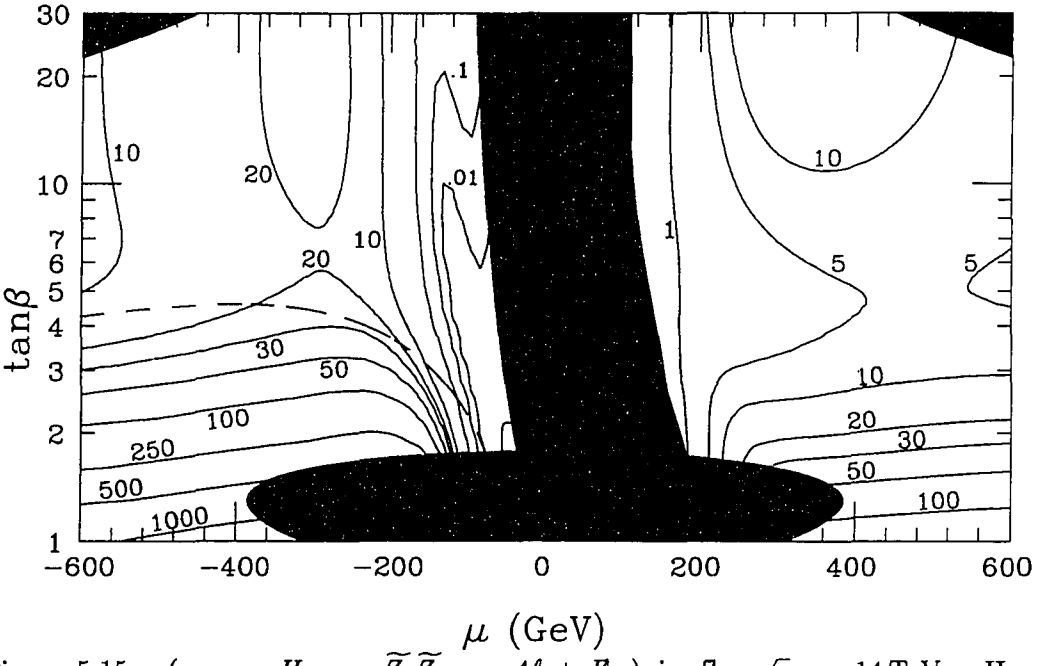

Figure 5.15: $\sigma(pp \to H_p \to \widetilde{Z}_2\widetilde{Z}_2 \to 4\ell + \not{E}_T)$ in fb, $\sqrt{s} = 14\,\text{TeV}$. Here $m_{H_p} = 250\,\text{GeV}$, $m_{\tilde{g}} = 300\,\text{GeV} \doteq m_{\tilde{q}}$. Other MSSM input parameters as in Figure 2.10.

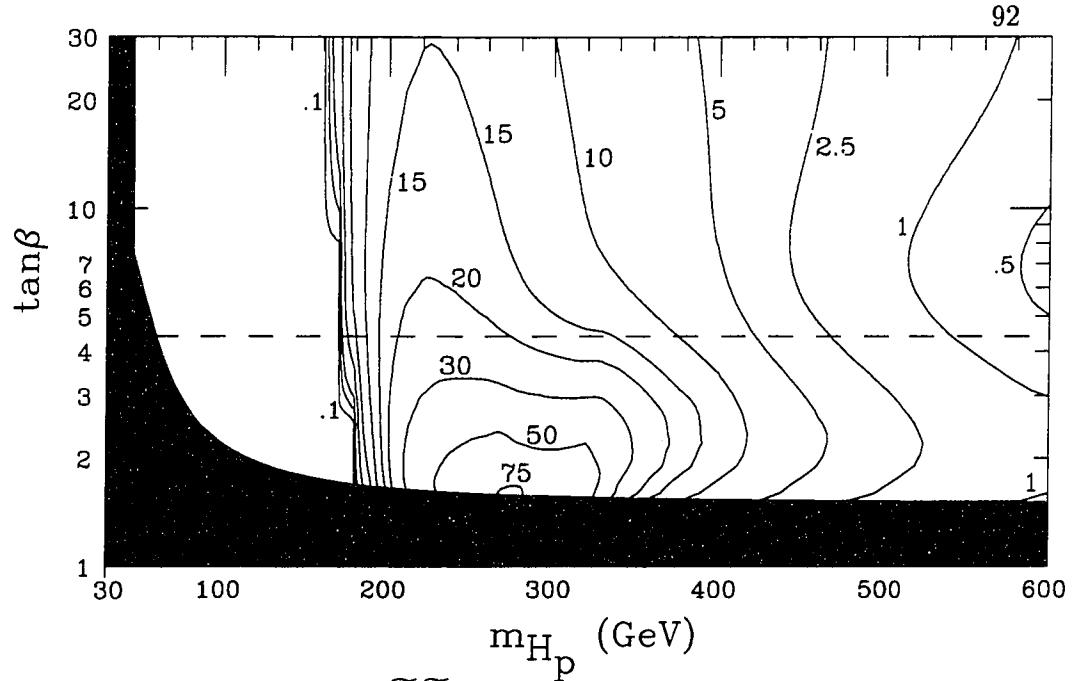

Figure 5.16: $\sigma(pp \to H_h \to \widetilde{Z}_2\widetilde{Z}_2 \to 4\ell + \not{E}_T)$ in fb, $\sqrt{s} = 14\,\text{TeV}$. Recall that the region above the dashed line corresponds to $m_{\widetilde{W}_1} < 90\,\text{GeV}$, the approximate reach of LEP II for charginos.
$m_{\tilde{g}} = -\mu = 300\,\text{GeV} \doteq m_{\tilde{q}}$. Other MSSM input parameters as in Figure 2.10.

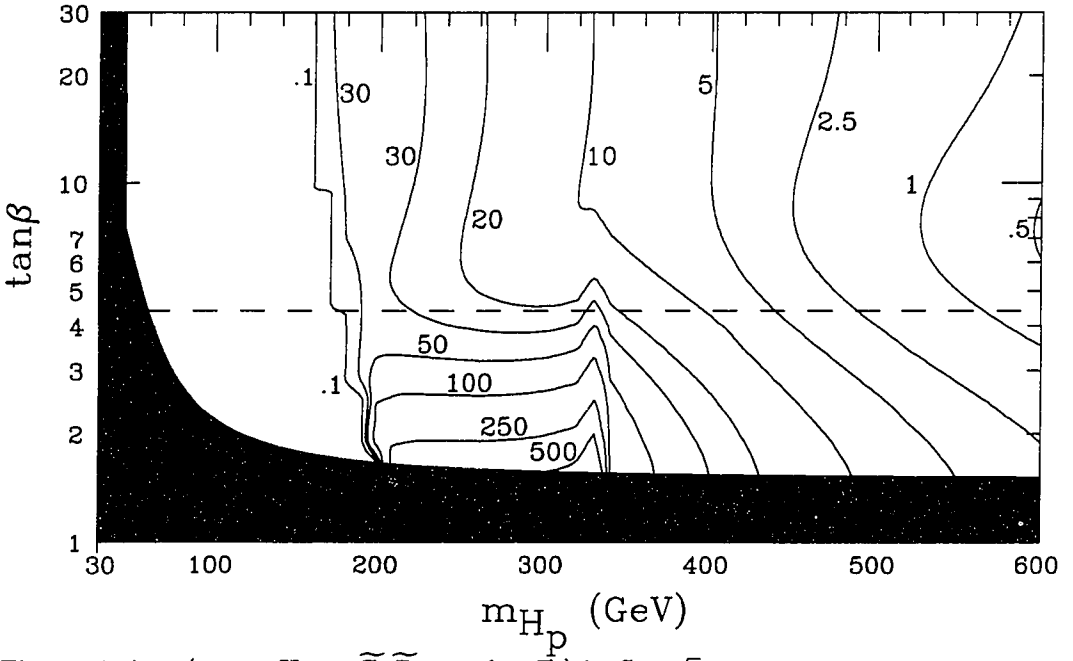

Figure 5.17: $\sigma(pp \to H_p \to \widetilde{Z}_2\widetilde{Z}_2 \to 4\ell + \not{E}_T)$ in fb, $\sqrt{s} = 14\,\text{TeV}$.
$m_{\tilde{g}} = -\mu = 300\,\text{GeV} \doteq m_{\tilde{q}}$. Other MSSM input parameters as in Figure 2.10.

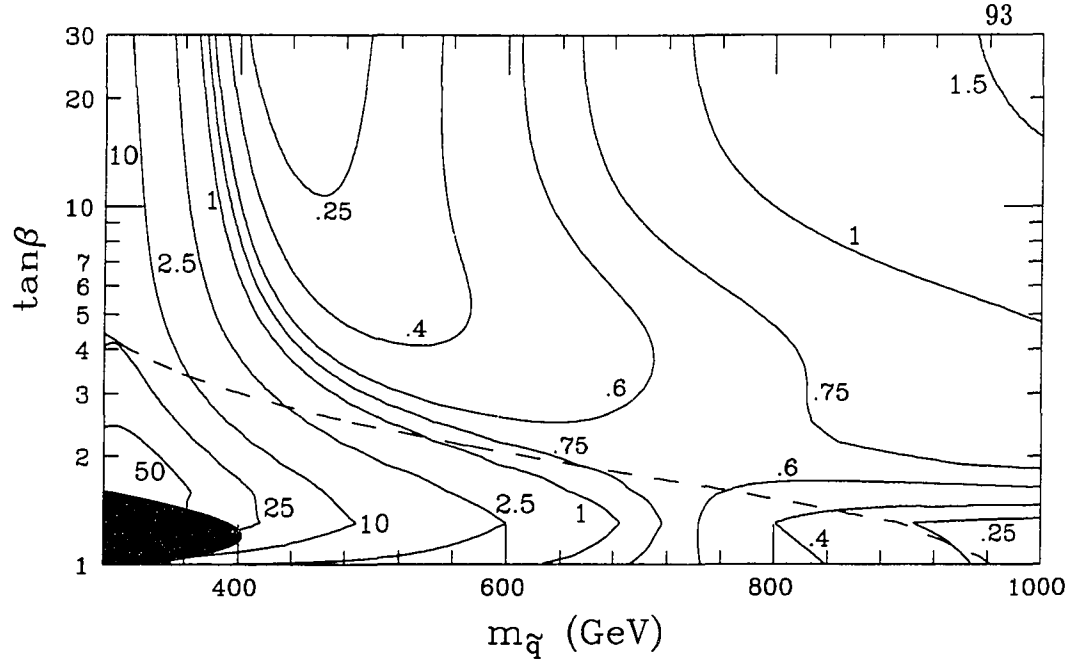

Figure 5.18: $\sigma(pp \to H_h \to \widetilde{Z}_2\widetilde{Z}_2 \to 4\ell + \not{E}_T)$ in fb, $\sqrt{s} = 14\,\text{TeV}$. The region above the dashed line corresponds to $m_{\widetilde{W}_1} < 90\,\text{GeV}$. The darkened-in LEP excluded area is where $Z^0 \to H_\ell Z^{0*}$ should have been seen at LEP. $m_{\tilde{g}} = -\mu = 300\,\text{GeV}$ and $m_{H_p} = 250\,\text{GeV}$. Other MSSM input parameters as in Figure 2.10.

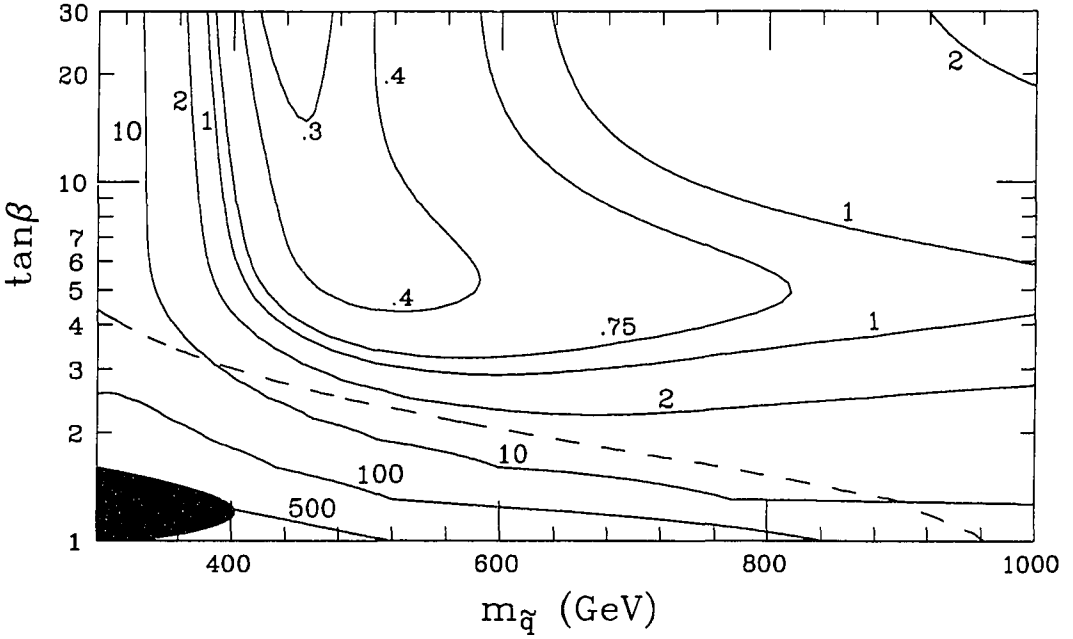

Figure 5.19: $\sigma(pp \to H_p \to \widetilde{Z}_2\widetilde{Z}_2 \to 4\ell + \not{E}_T)$ in fb, $\sqrt{s} = 14\,\text{TeV}$. $m_{\tilde{g}} = -\mu = 300\,\text{GeV}$ and $m_{H_p} = 250\,\text{GeV}$. Other MSSM input parameters as in Figure 2.10.

Notice from the the $\mu = -2m_1$ *vs.* $\tan\beta$ plots that the signal is small for small values of $|\mu|$. It is however comforting to see that the 4ℓ signal rate appears to be observable for $|\mu| \simeq m_{\tilde{g}}$ as expected in supergravity models with radiative EW symmetry breaking. Also notice that the pseudoscalar Higgs boson again tends to give a larger signal than the heavy scalar, and further, that the signal is significantly larger if μ is chosen to be negative.

Finally, in the $m_{\tilde{q}}$ *vs.* $\tan\beta$ plots, it can be seen that the 4ℓ cross-section rapidly drops off as $m_{\tilde{q}}$ increases from $m_{\tilde{g}}$ to larger values. This illustrates the aforementioned effect on the neutralino branching fractions of lowering the sfermion masses, and in particular the slepton masses which can be considerably lighter than those of the squarks (see Eqn. (1.9)). For values of $\tan\beta \gtrsim 5$, the cross-sections also show a slow increase for rather large squark masses. The increase in the cross-sections for large values of $m_{\tilde{q}}$ comes from interference between various amplitudes. Note the signal does have an observable rate even if squarks are significantly heavier than gluinos. The fact that the signal cross-section is largest below the dashed line where the chargino is likely to be undetectable at LEP II is also a worthy of note. In addition to these plots the 4ℓ cross-section dependence on the sfermion A-parameters was checked and found to be relatively minor unless new decay channels open up. This is especially important when considering the variation of the signal with A_t, since $H \to \tilde{t}_1\bar{\tilde{t}}_1$ decays become kinematically accessible when $|A_t|$ becomes very large The signal dependence on the precise value of m_t was also found to be small, again except when the threshold for a new decay is crossed. Finally, the variation of the signal with $m_{\tilde{g}}$ was investigated. For $m_{H_p} = 250$ GeV, and $m_{\tilde{g}} = -\mu \doteq m_{\tilde{q}}$, the signal exceeds 5 fb for gluinos as heavy as 350-400 GeV. This is reasonable since then $m_{\widetilde{Z}_2} \simeq m_{\tilde{g}}/3$ is approaching the kinematic boundary for $H_p \to \widetilde{Z}_2\widetilde{Z}_2$ decays. Overall, the rates sometimes quite impressive, with hundreds or even thousands of signal events per year anticipated for some MSSM parameter choices. However, it should be kept in mind that total rates are being shown here; the actual signal will be reduced once experimental cuts and detector efficiencies are incorporated. The severity of the backgrounds also needs to be investigated.

Within the SM, backgrounds arise from the leptonic decays of the $W^{\pm}$ and Z^0 gauge bosons, and also from top quark decays. The leading SM source of hadronically quiet 4ℓ events is Z^0Z^0 production followed by the leptonic decay of both Z^0's. However, such events are expected to have very little $\not{E}_T$ associated with them. Furthermore, mass reconstruction of the Z^0 can be used to veto these events by removing events in which leptons of the same flavor but opposite sign reconstruct the Z^0 mass within ± 8 GeV. To verify this, ten thousand Z^0Z^0 events were generated using the ISAJET program package [127] and the Z^0's were all forced to decay leptonically. No events survived this dilepton mass cut, resulting in an upper bound on the resulting 4ℓ background cross-section from this source of about 0.003 fb. This cut will also remove a large part of the signal if the decay $\widetilde{Z}_2 \rightarrow \widetilde{Z}_1 Z^0$ is kinematically accessible. Fortunately, this two-body decay is not open in parameter regions in which the signal is substantial, so very little signal is lost through imposition of this cut. This leaves $4W$ production as the main SM background to the signal. Electroweak multi-W production rates are dependent upon the nature of the Higgs sector; notwithstanding this complication, a simulation showed the trilepton cross-section from $3W$ production at the LHC to be $\sim$2 fb [128], and so the rate for 4ℓ events from $4W$ production should be negligible. The leptons from W decays also should tend to be much harder than those from the Higgs boson decays to neutralinos owing to the sizeable mass of the LSP, so suitable $p_T(\ell)$ and $\not{E}_T$ cuts should be able to enhance the signal relative to this background. The subject of what constitutes an optimal experimental set of cuts will be discussed in more detail shortly. If one of the leptons from a signal event is very soft and/or escapes identification, the the signal can be seen as a three lepton event which has the $3W$ production background just mentioned.

Another SM process that should be considered as a potential background is $t\bar{t}$ production, which will have an enormous cross-section at the LHC. This process can produce 4-lepton events if the leptons from the daughter bottom quarks are accidentally isolated. However, an ISAJET simulation of 300,000 $t\bar{t}$ events with forced top decays failed to yield any events with four isolated leptons, giving a background limit from this source of $\sigma(t\bar{t}) < 4$ fb [62]. Other top-quark related

backgrounds arise from $t\bar{t}t\bar{t}$ and $t\bar{t}Z^0$ production. But the latter can be removed using the Z^0-mass-reconstruction veto, and all these top quark backgounds can be greatly reduced by vetoing events with a central jet. Also, $4t$ production has been estimated to yield a 4ℓ cross-section of only around 0.05 fb at the LHC [129]. No other SM backgrounds to the 4 lepton signal from Higgs boson decays to sparticles were identifiable. Still, supersymmetric sparticle backgrounds within the MSSM must also be taken into account. The continuum production of $\widetilde{Z}_2$ pairs can yield the same signal as the sought-after Higgs boson decays. While the detection of these continuum neutralino pairs would in itself be very exciting, it is interesting to ask whether $\widetilde{Z}_2\widetilde{Z}_2$ production via H_h and H_p decays is distinguishable from the direct continuum production of $\widetilde{Z}_2$'s which, in effect, is the background to the Higgs signal. Continuum $\widetilde{Z}_2\widetilde{Z}_2$ production occurs in $q\bar{q}$ annihilation via s-channel Z^0 exchange or via t- or u-channel squark exchange. This background is not reducible by any experimental cuts, and so the continuum $\widetilde{Z}_2\widetilde{Z}_2$ production rate should be compared with that from Higgs boson decays to see if the latter yields a significant rate enhancement or skews the energy spectrum of the events for the overall $\widetilde{Z}_2\widetilde{Z}_2$ production rate, which will be the quantity measured. Toward this end, the cross-section for 4ℓ production via continuum $\widetilde{Z}_2\widetilde{Z}_2$ production is shown in Figure 5.20 below. While the continuum production cross-section is sensitive to the squark mass it is only mildly sensitive to $\tan\beta$ over the region where the cross-section is significant. The continuum $\widetilde{Z}_2\widetilde{Z}_2$ cross-section is seen to be generally comparable to, or smaller than, the Higgs boson decay cross-sections in Figures 5.14 and 5.15.

It should also be noted that direct continuum production of the heavier neutralinos ($\widetilde{Z}_3$ and $\widetilde{Z}_4$) will not form an irreducible background to the signal since $\widetilde{Z}_3$ and $\widetilde{Z}_4$ usually decay via the two-body decay modes of (5.1) — this is true for $m_{\tilde{g}} = -\mu$ and also from many other choices of μ — and 4ℓ events from these processes can be removed by the Z^0 mass reconstruction cut.

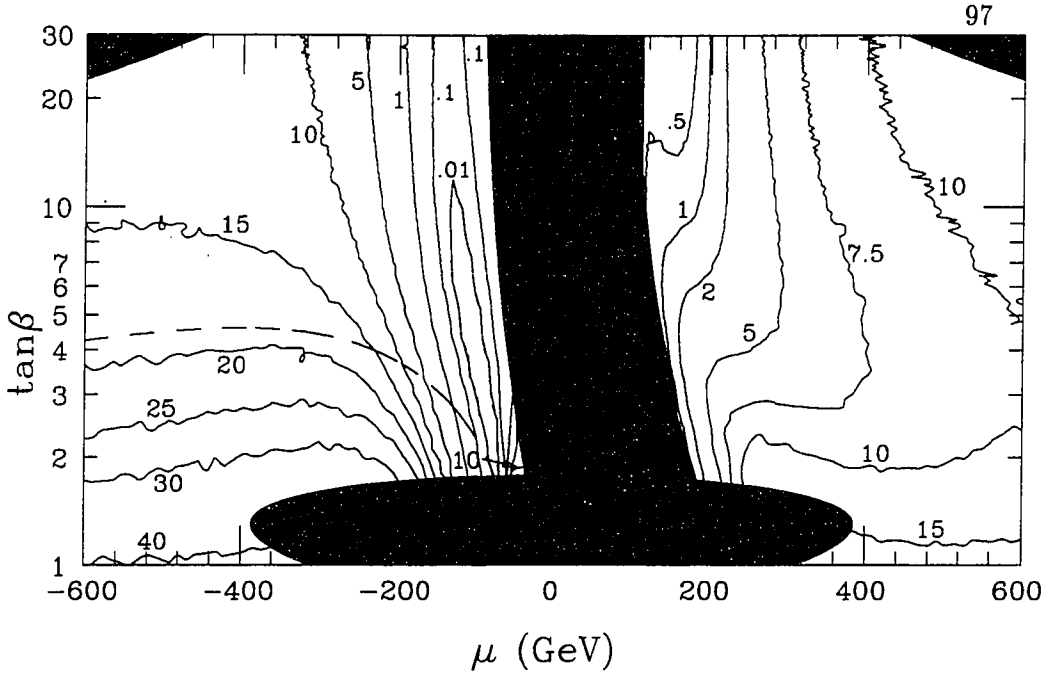

Figure 5.20: $\sigma(pp \to \widetilde{Z}_2\widetilde{Z}_2 \to 4\ell + \not{E}_T)$ in fb, $\sqrt{s} = 14\,\text{TeV}$. $m_{\tilde{g}} = 300\,\text{GeV}$ and $m_{H_p} = 250\,\text{GeV}$. Other MSSM input parameters as in Figure 2.10.

ISAJET 7.07 was again used to simulate the 4ℓ Higgs boson signal. Since explicit SUSY Higgs production has not yet been incorporated into this code, production of H_h or H_p was simulated by decaying the SM Higgs scalar into a $\widetilde{Z}_2\widetilde{Z}_2$ pair and forcing the SUSY decay mode; the total cross-section is then normalized to the results of Fig. 5.14-5.19.

The toy calorimeter simulation package ISAPLT was employed to model detector effects. The calorimetry with cell size was taken as $\Delta\eta \times \Delta\phi = 0.1 \times 0.1$, extending between $-5 < \eta < 5$ in pseudorapidity. The electromagnetic energy resolution is taken to be $10\%/\sqrt{E_T} \oplus 0.01$, while hadronic resolution is taken as $50\%/\sqrt{E_T} \oplus 0.03$ for $|\eta| < 3$, and $100\%/\sqrt{E_T} \oplus 0.07$ for $3 < |\eta| < 5$, where $\oplus$ denotes addition in quadrature. Jets are coalesced within cones of $R = \sqrt{\Delta\eta^2 + \Delta\phi^2} = 0.7$ using the ISAJET routine GETJET. Hadronic clusters with $E_T > 50$ GeV are labelled as jets. Muons and electrons are classified as isolated if they have $p_T > 10$ GeV, $|\eta(\ell)| < 2.5$, and the visible activity within a cone of $R = 0.3$ about the lepton direction is less than $E_T(\text{cone}) = 2$ GeV.

The following cuts designed to select signal events while vetoing SM backgrounds from ZZ and $t\bar{t}$ production were then imposed:

- require *two* isolated leptons with $p_T(\ell) > 20$ GeV to trigger the event,
- require *two* more isolated leptons with $p_T(\ell) > 10$ GeV,
- require all opposite sign but same flavor dilepton pairs to have invariant mass $m(\ell^+\ell^-) < 80\,\text{GeV}$ or $m(\ell^+\ell^-) > 100\,\text{GeV}$,
- require number of jets $n(\text{jets}) = 0$.

A cut on $\not{E}_T$ could be considered instead of the above dilepton mass cut. However, the $\not{E}_T$ spectrum from the signal is not so hard, while forward jet production and energy mis-measurement in Z^0Z^0 events can lead to substantial $\not{E}_T$, so that the dilepton mass cut is preferrable to an $\not{E}_T$ cut in rejecting background while preserving signal. To give some idea of what fraction of the signal events will fail these cuts, Figure 5.21 shows the p_T distributions of the four leptons (ranked according to p_T) along with the $\not{E}_T$ distribution from the decay $H_p \to \widetilde{Z}_2\widetilde{Z}_2$ for a particular representative choice of MSSM input parameters. Note that the fastest lepton almost always has $p_T > 20\,\text{GeV}$ as the trigger cut requires. We also see that, as expected, there will be a considerable number of signal events with low p_T leptons which fail the second cut given above, so that the capability of detecting low-p_T leptons can enhance the signal obtained.

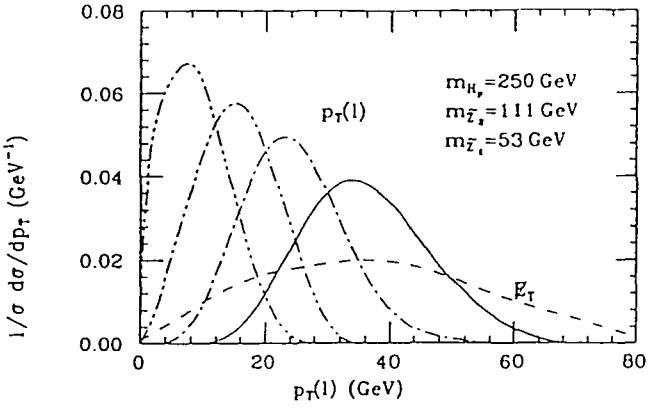

Figure 5.21: Plot of the distribution in p_T for the four leptons from $H_p \to \widetilde{Z}_2\widetilde{Z}_2 \to 4\ell + \not{E}_T$, where leptons are ordered from largest to smallest p_T. The $\not{E}_T$ distribution is also shown. MSSM parameters: $m_{H_p} = 250\,\text{GeV}$, $m_{\tilde{g}} = 400\,\text{GeV}$, $\mu = -100\,\text{GeV}$, and $\tan\beta = 2$.

It should be stressed that there are no significant SM backgrounds even before the last cut. Backgrounds involving Z^0's are efficiently removed by the $m(\ell^+\ell^-)$ cut. The main SM physics background would then be expected to come from $4t$ production which, as mentioned earlier, gives only a tiny 4ℓ cross-section at the LHC, even before acceptance cuts. The last cut which removes about 40% (70%) of the signal for a Higgs mass around 200 GeV (400 GeV) has been imposed to separate neutralino production from the cascade decays of gluinos and squarks [130] which can also produce multilepton events at observable rates.

To exemplify the impact of the cuts on the 4ℓ signal, Table 5.1 shows these cross-sections for illustrative choices of m_{H_p} and $\tan\beta$. The contributions from H_h and H_p decays have been combined since these are expected to lead to kinematically similar events. Also listed are the continuum backgrounds from direct $\widetilde{Z}_2\widetilde{Z}_2$ production for the same choices of parameters. The following points are worth noting.

- For the choice of parameters in the table, the signal exceeds the background for m_{H_p} up to somewhat beyond 300 GeV, where $t\bar{t}$ decays may become accessible. Also, the cross-section corresponds to an event rate of 100-1000 events after cuts in a $50\,\mathrm{fb}^{-1}$ data sample, compared to a continuum background of 50-100 events.
- The signal efficiency varies between 5 and 10 percent depending on the model parameters.

Table 5.1: Cross-sections in fb at LHC for $4\ell + \not{E}_T$ events from supersymmetric processes, with $m_{\tilde{g}} = -\mu = 300\,\mathrm{GeV} \doteq m_{\tilde{q}}$, and $A_t = 0$.

process	m_{H_p}	$\tan\beta$	$m_{\widetilde{Z}_2}$	$m_{\widetilde{Z}_1}$	$\sigma(4\ell)$	$\sigma(cut)$	effic.	χ^2 (12 d.f.)
$H_h, H_p \to 4\ell$	200	2	97.3	45.5	230	26	11%	18036
$H_h, H_p \to 4\ell$	300	2	"	"	260	23	9%	1024
$H_h, H_p \to 4\ell$	400	2	"	"	37	2.4	6.5%	23
$\widetilde{Z}_2\widetilde{Z}_2 \to 4\ell$	–	2	"	"	27	2.8	10%	–
$H_h, H_p \to 4\ell$	200	10	83.4	42.8	44	2.4	5.5%	528
$H_h, H_p \to 4\ell$	300	10	"	"	26	1.4	5.4%	32
$H_h, H_p \to 4\ell$	400	10	"	"	10	0.5	5%	4.5
$\widetilde{Z}_2\widetilde{Z}_2 \to 4\ell$	–	10	"	"	10	0.8	8%	–

It should, of course, be kept in mind that the SUSY parameters are not known, and that the total background (and signal) rate could be considerably different (even for similar values of $m_{\widetilde{Z}_2}$) from our estimate in the Table. An excess of the 4ℓ events relative to the background in Table I would, therefore, not clearly indicate a Higgs boson signal. As an alternative discriminator to an absolute rate measurement, analysis of the invariant mass distribution of the four leptons to see if this differs between continuum $\widetilde{Z}_2\widetilde{Z}_2$ production and $\widetilde{Z}_2\widetilde{Z}_2$ production via Higgs boson decays is one possibility. Signal events must have $m(4\ell) < m_H - 2m_{\widetilde{Z}_1}$, while the background should exhibit a rather broad distribution. Since these distributions are determined by the Higgs boson and neutralino masses, we expect them to be relatively insensitive to variations in model parameters that result in similar values of m_H, $m_{\widetilde{Z}_1}$ and $m_{\widetilde{Z}_2}$.

Figure 5.22 depicts these distributions for the signal plus background (solid) and the $\widetilde{Z}_2\widetilde{Z}_2$ continuum-only "background" (dashed) for the six cases in Table I. For the smaller values of m_{H_p}, the solid histograms are dominated by the signal and differ considerably from the dashed background histograms (note the log scale). As anticipated above, the solid and dashed lines indeed coincide for $m(4\ell) > m_{H_p} - 2m_{\widetilde{Z}_1}$. In order to decide whether the solid and dashed histograms are indeed distinguishable, the total χ^2 was computed for the difference between these two histogram, *normalized to the same number of events*, with the event number given by the signal plus background cross-section times an integrated luminosity of 50 pb^{-1}. Here twelve 20 GeV bins between $m(4\ell) = 60$ GeV and $m(4\ell) = 300$ GeV were used. There were about 1100, 900 and 600 events for $m_{H_p} = 200$, 300 and 400 GeV (after cuts) for the $\tan\beta = 2$ case, and about 550 events for each value of m_{H_p} for $\tan\beta = 10$. The resulting total χ^2 is shown in the last column of Table 5.1. For $m_{H_p} \lesssim 300\,\text{GeV}$, the distributions are apparently sufficiently different that the solid line is unlikely to be a chance fluctuation of the continuum background (for $\chi^2 > 26.2$, this probability is smaller than 1%).

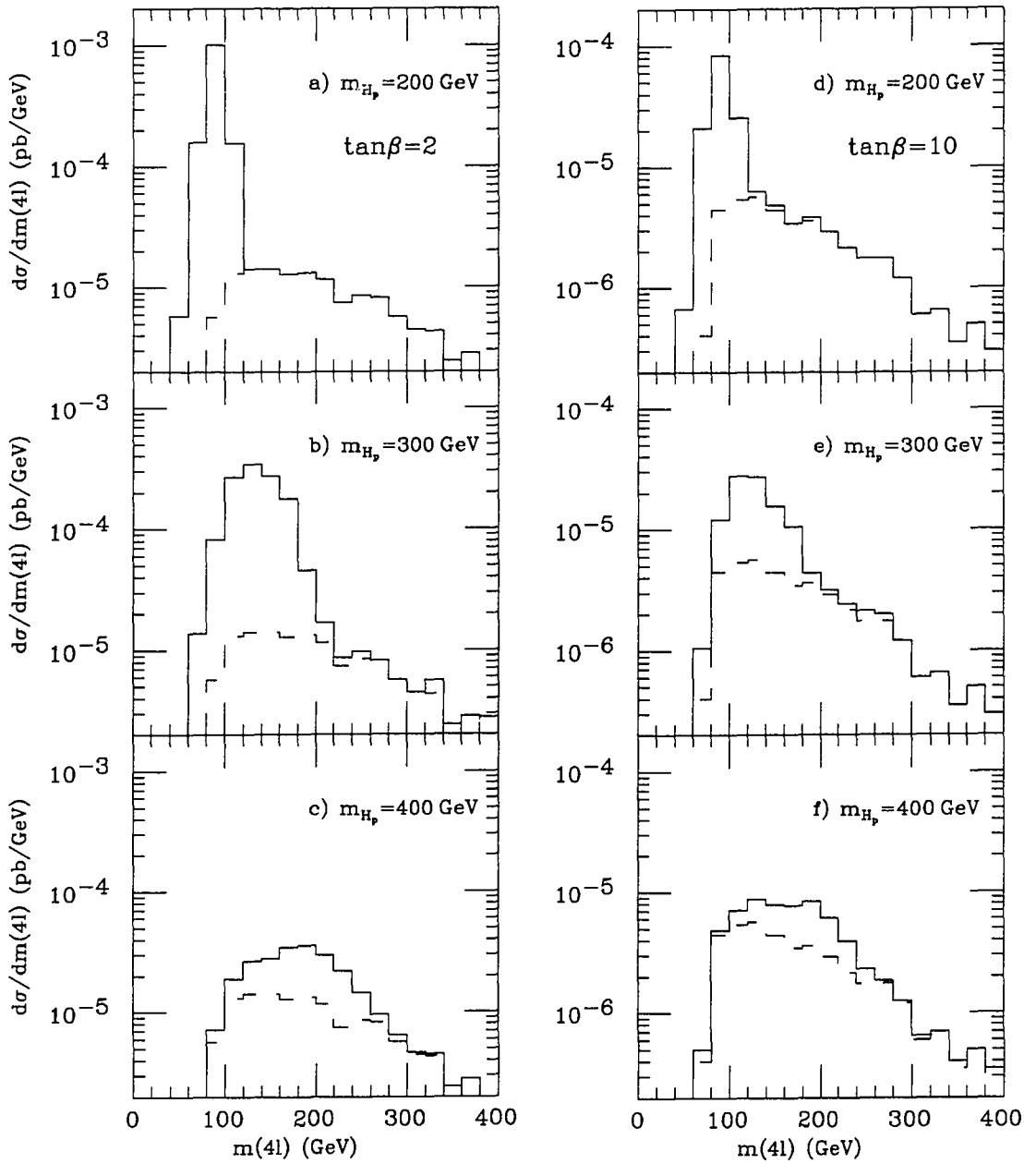

Figure 5.22: Distribution in $m(4\ell)$ after cuts from signal plus background (solid), and background (dashes) for $pp \to H_p, H_h \to \widetilde{Z}_2\widetilde{Z}_2 \to 4\ell + \not{E}_T$ production for $\tan\beta = 2$ (left) and $\tan\beta = 10$ (right) and $m_{H_p} = 200\,\text{GeV}$ (upper), 300 GeV (middle), and 400 GeV (lower).
Other MSSM parameters as in Figure 3.8.

A few caveats are in order though:

- Despite the fact that the solid and dashed histograms have been normalized to have the same number of events, whether or not they are distinguishable clearly depends on the relative number of Higgs initiated and continuum $\widetilde{Z}_2\widetilde{Z}_2$ events. Here, the rate as given by the MSSM for the values of parameters motivated by supergravity models was utilized.
- For the first two cases in Table 5.1, the number of events in the simulation is comparable to the expected number in a data sample of $50\,\mathrm{fb}^{-1}$. The computation of the total χ^2 can thus be expected to be a reasonable reflection of the experimental situation. For the $\tan\beta = 10$ case, with $m_{H_p} = 200\,\mathrm{GeV}$ ($300\,\mathrm{GeV}$), the signal cross-section is much smaller so that about $200\,\mathrm{fb}^{-1}$ ($400\,\mathrm{fb}^{-1}$) of integrated luminosity need to be collected in order that the fluctuations in the simulation are of comparable magnitude to those in the data. Thus while $50\,\mathrm{fb}^{-1}$ of data may suffice to enable one to distinguish the Higgs signal from continuum $\widetilde{Z}_2\widetilde{Z}_2$ production for smaller values of $\tan\beta$, integrated luminosities of 200-400 fb^{-1} may be necessary if $\tan\beta$ is large.
- Note that here only the shape of the 4ℓ mass distribution has been employed to try to untangle the Higgs signal from continuum $\widetilde{Z}_2\widetilde{Z}_2$ production without any regard for rate or other event shape variables. It would be interesting to explore whether other distributions serve as better discriminators of the Higgs from the continuum background.

Another potential use of the invariant mass distribution of the leptons is as a means of measuring the neutralino mass. This is possible by looking at mixed-flavor decays such as $H_h \to \widetilde{Z}_2\widetilde{Z}_2 \to e^+e^-\mu^+\mu^-$. The four-lepton invariant mass distribution will again cut off at $m(e^+e^-\mu^+\mu^-) = m_{H_h} - 2m_{\widetilde{Z}_1}$, while the like-flavor dilepton energy spectrums will cut off at $m(e^+e^-) = m(\mu^+\mu^-) = m_{\widetilde{Z}_2} - m_{\widetilde{Z}_1}$. If the mass of the Higgs boson can be determined from its $\gamma\gamma$ or Z^0Z^0 decay modes, then a study of these invariant mass distributions can yield both $m_{\widetilde{Z}_1}$ and $m_{\widetilde{Z}_2}$. The endpoints of the distributions will of course be somewhat smeared by effects from the finite experimental energy resolution; however, good resolution should enable a fairly precise mass determination for the neutralinos. This is of considerable signif-

icance since neutralino masses can otherwise be very difficult to measure, even at an e^+e^- collider (since here a neutralino's production rate may be suppressed if its coupling to Z^0 is small).

In summary, cross-sections for four-lepton final states from $H_{h,p} \rightarrow \widetilde{Z}_2\widetilde{Z}_2$ decays have been found to be as large as 500 fb for ranges of model parameters allowed by all known experimental data. (It is also worth noting that, before experimental cuts, the signal exceeds 10 fb over a large region of parameter space where there may be no visible SUSY signal even at LEP II.) There appear to be no significant SM backgrounds to this signal. Thus the detection of four lepton events at such rates will be a signal for new physics. However, its identification as a Higgs boson signal requires that it be separable from continuum $\widetilde{Z}_2\widetilde{Z}_2$ production. The cross-section for the latter was in fact found to be significantly smaller than that of the signal over a wide range of supergravity-inspired MSSM parameter sets. The shape of the four-lepton invariant mass distribution may also serve to discriminate the Higgs signal from continuum neutralino production provided $m_{H_p} \lesssim 2m_t$. For low values of $\tan\beta$ an integrated luminosity of $50\,\text{fb}^{-1}$ is sufficient for this discrimination, but an integrated luminosity of 200-400 fb^{-1} is required if $\tan\beta = 10$. In passing, it can also be noted that this Higgs signal is relatively insensitive to variations in the A_t-parameter. The efficiency with which this signal may be detected is shown in Table 5.1, for cuts typical of LHC detectors. This is typically 5-10%, so that the cross-sections in Figures 5.14-5.19 correspond to 25-1000 events in an experimental data sample of $50\,\text{fb}^{-1}$. The parameter space region where the neutralino decays of SUSY Higgs bosons ought to be observable can be summarized as

- $2m_t > m_{H_p} > 2m_{\widetilde{Z}_2} \simeq 2m_{\tilde{g}}/3$,
- $m_{H_p} \sim 200 - 350\,\text{GeV}$,
- $m_{\tilde{q}} \sim m_{\tilde{g}}$ so that $m_{\tilde{\ell}} \ll m_{\tilde{q}}$ and $|\mu| \sim m_{\tilde{g}} \lesssim 500\,\text{GeV}$

How this correlates with the regions favorably-inclined to searches for MSSM Higgs boson decays to SM particles will be discussed in Chapter 6 which will bring togeter the results of the LEP and LEP II analyses, the Z^0Z^0 and $\gamma\gamma$ signal modes (as well as other proposed signals from decays to SM particles), and the sparticle signals to present an overall picture of our capability to probe the MSSM symmetry-breaking Higgs sector with the LEP II / LHC combination.

Chapter 6

An Overview of Search Prospects for MSSM Higgs Bosons

The purpose of this final chapter is to give an overview of the prospects for detecting MSSM Higgs bosons via any of the suggested discovery channels at the proposed LHC hadron collider or the LEP e^+e^- machine now in operation or at its energy upgrade, LEP II, now under construction. Basically, this chapter is divided into two parts. First a compendium of other MSSM Higgs boson signals not covered in the previous chapters is presented. The analysis of these signals is not as polished and exhaustive as the studies of the signatures discussed in Chapters 2 and 4, so the conclusions of these studies should be regarded as somewhat preliminary. Thus, the regions of MSSM parameter space for which they provide coverage is not extremely well-defined. It is the aim of this discussion to indicate the aspects of these signals that require further attention and study.

The second part of this chapter then maps out the overall coverage of the MSSM parameter space possible using the Higgs boson signatures described in detail in Chapters 2, 4, and 5. The combined results are presented in the m_{H_p} *vs.* $\tan\beta$ plane, with discussion of the dependence on other MSSM input parameters. In particular, the effects of lowering the sparticle masses from around the TeV scale to values allowing them to participate meaningfully in Higgs boson decays are described. Since the other proposed Higgs boson signals from the first half of this chapter are not as well-studied, they are not included in this assessment of the MSSM parameter-space coverage of a hadron supercollider; however, their potential impact on the findings is outlined. The crucial questions that will need to be addressed by the conclusions

drawn are

- Are there any regions of the MSSM parameter space for which none of the established Higgs boson signals is viable?
- What regions, if any, of the parameter space offer the prospect of detecting more than one type of Higgs boson? Such an observation of more than one type of Higgs boson would demonstrate conclusively that the symmetry-breaking Higgs sector is non-minimal and non-SM.

6.1 Survey of Alternative Higgs Boson Signals

6.1.1 Neutral Higgs Boson Decays to τ's

The search for the Higgs bosons via their decays to $\tau^+\tau^-$ pairs is very difficult due to the very high rate for continuum Drell-Yan $\tau^+\tau^-$ production as well τ production via $t\bar{t}$ and W^+W^- pairs. Aspects of the signal topology also hinder analysis. First of all, the τ leptons are not seen directly since they decay too rapidly. Thus their presence must be indirectly inferred, and, if required, their kinematic parameters must be reconstructed from their decay products. The presence of neutrinos and the accompanying $\not\!\!E_T$ or $\not\!\!p_T$ in these decay products precludes searching for a mass bump on top of the continuum background as is proposed for the $\gamma\gamma$ and $Z^0Z^0 \rightarrow \ell^+\ell^-\ell^+\ell^-$ channels. The latter difficulty is somewhat alleviated for relativistic $\tau^+\tau^-$ pairs recoiling against hard jets (or hadrons from QCD radiation). This would be the case, for example, if the τ-pair were produced by a decaying Higgs boson with large transverse momentum balanced by a jet [82]. Detailed Monte Carlo studies by Unal *et. al.* [131] using the PYTHIA event generator [132] have shown that Higgs bosons are if fact typically produced with relatively large p_T's. They found that the transverse momentum of a Higgs boson with $m_H \sim 200\,\mathrm{GeV}$ produced either via gluon fusion or $b\bar{b}$-fusion (recall from Chapter 3 that the latter is often very significant for high values of $\tan\beta$) is $\sim$50 GeV. This method was found to agree with a theoretical computation using leading log resummation of soft gluons at low p_T and an α_s perturbative calculation at high p_T [133]. If there is suf-

ficient p_T, then the approximation [134,135]:

$$p_\nu^{(1)} \frac{\vec{p}_{\ell,T}^{(1)}}{E_\ell^{(1)}} + p_\nu^{(2)} \frac{\vec{p}_{\ell,T}^{(2)}}{E_\ell^{(2)}} = \not{p}_T \tag{6.1}$$

becomes viable for reconstructing the transverse energy of the neutrinos. This could then be added to the visible energy of the decay products of the τ-lepton pair to obtain the invariant mass of the pair. In Eqn. (6.1), $\vec{p}_{\ell,T}^{(i)}$ and $E_\ell^{(i)}$ are the lepton transverse momenta and energies, respectively, and $p_\nu^{(i)}$ are the total transverse momenta of the neutrinos coming from each of the τ's.

The detectability of the τ-pair decay signal was studied at the LHC for a SM Higgs boson by DiLella [134]. Higgs boson masses of 100 GeV and 140 GeV were tested; for these cases, an $m(\tau^+\tau^-)$ resolution of about 11% and 13%, respectively, is reported using mixed decay mode events (one of the τ's decays to an electron and the other to a muon) and assuming calorimetry coverage out to a rapidity of 5. If coverage is only out to a rapidity of 3, then the resolution drops to 20% or so. Looking at the background from the sources mentioned above within mass bins of 40 GeV centered on the Higgs boson masses, the conclusion was reached that it is virtually impossible to detect a Higgs boson signal in this manner, with signal to background ratios on the order of $\sim 10^{-3}$ reported. Another preliminary study [135] showed that the dominant background from $t\bar{t}$ production to ee, $e\mu$, or $\mu\mu$ events could be considerably reduced by taking advantage of the energetic jets (coming from the b-quarks) accompanying these events. This was done by making a cut allowing only one jet above a specified E_T cut in a sample event. The price paid of course is a reduction in the number of signal events, with the resulting number being somewhat marginal in this SM study. It should also be noted that the study chose a very optimal case where $m_t = 200$ GeV so that b-quark jets tended to be quite energetic.

The branching fraction for $\tau^+\tau^- \rightarrow e + \mu + 4\nu$'s is about 6.4%. That for $\tau^+\tau^- \rightarrow e$ or μ + hadrons + 3ν's is about 45.8%, and that for $\tau^+\tau^- \rightarrow$ hadrons + 2ν's is about 41.2%. So if τ's decaying via hadronic modes modes can be cleanly identified, then the resolution of the $m(\tau^+\tau^-)$ measurement can be significantly

improved. Suggestions about how to recognize 'τ-jets' through their narrowness, low multiplicity (charged-track content), and invariant mass have been discussed in Refs. [136] and [137] in connection with the τ decays of the W gauge boson. The basic need is for calorimeters to be very accurate. Generally this is thought of as a means of making identification of electrons and photons as clean as possible, rejecting pions and other singly charged hadrons for instance. But this can also be used in "reverse" to identify singly-charged hadrons or jets with a very low multiplicity and angular spread. A singly-charged hadron is basically the extreme case, and in the real world of finite experimental resolutions this is equivalent to a very skinny jet. About 48% of τ's do in fact decay into a single charged hadron (with accompanying neutral particles). The $\not{E}_T$ from accompanying neutrinos can also be used as a handle. But there are still stupendous QCD backgrounds associated with an all-hadronic final state. So recent studies [131,138] have demanded that one of the τ's decay into an electron or muon. Nevertheless, even allowing for the identifiction of 'τ-jets' with a reasonable efficiency, in the SM the absolute event rate after cuts is just too low to be seen over the background.

This situation within the MSSM framework, however, can be quite different. The branching fractions of H_h and H_p to τ-lepton pairs can be significantly enhanced for higher values of $\tan\beta$ by the MSSM angle mixing factors as can be seen from Table 1.2 (see also Eqns. (B.6) and (B.9) for the $H \to \tau^+\tau^-$ tree-level partial decay widths), yielding a $\tau^+\tau^-$ signal rate well above SM expectations. For Higgs boson masses around a couple hundred GeV, Kunszt and Zwirner [47] have found that cross-sections for $pp \to H_h, H_p \to \tau^+\tau^-$ can be enhanced over the analogous process for a SM Higgs boson by a factor of up to 100-1000 for $m_H \sim 200\,\mathrm{GeV}$. It should however be borne in mind that only high p_T Higgs bosons might detectable by this method. Thus the useful cross-section will be pared down somewhat from the $H_h \to \tau^+\tau^-$ and $H_p \to \tau^+\tau^-$ total cross-sections. The same MSSM enhancement factor will also boost the $H_p \to \mu^+\mu^-$ decay rate. Muons are much easier to detect than τ-leptons, but their branching fraction is suppressed by a factor of roughly $(\frac{m_\mu}{m_\tau})^2$ relative to that of the τ-leptons. Nevertheless, a preliminary look [139] suggests that a signal might be obtainable for high values of $\tan\beta$.

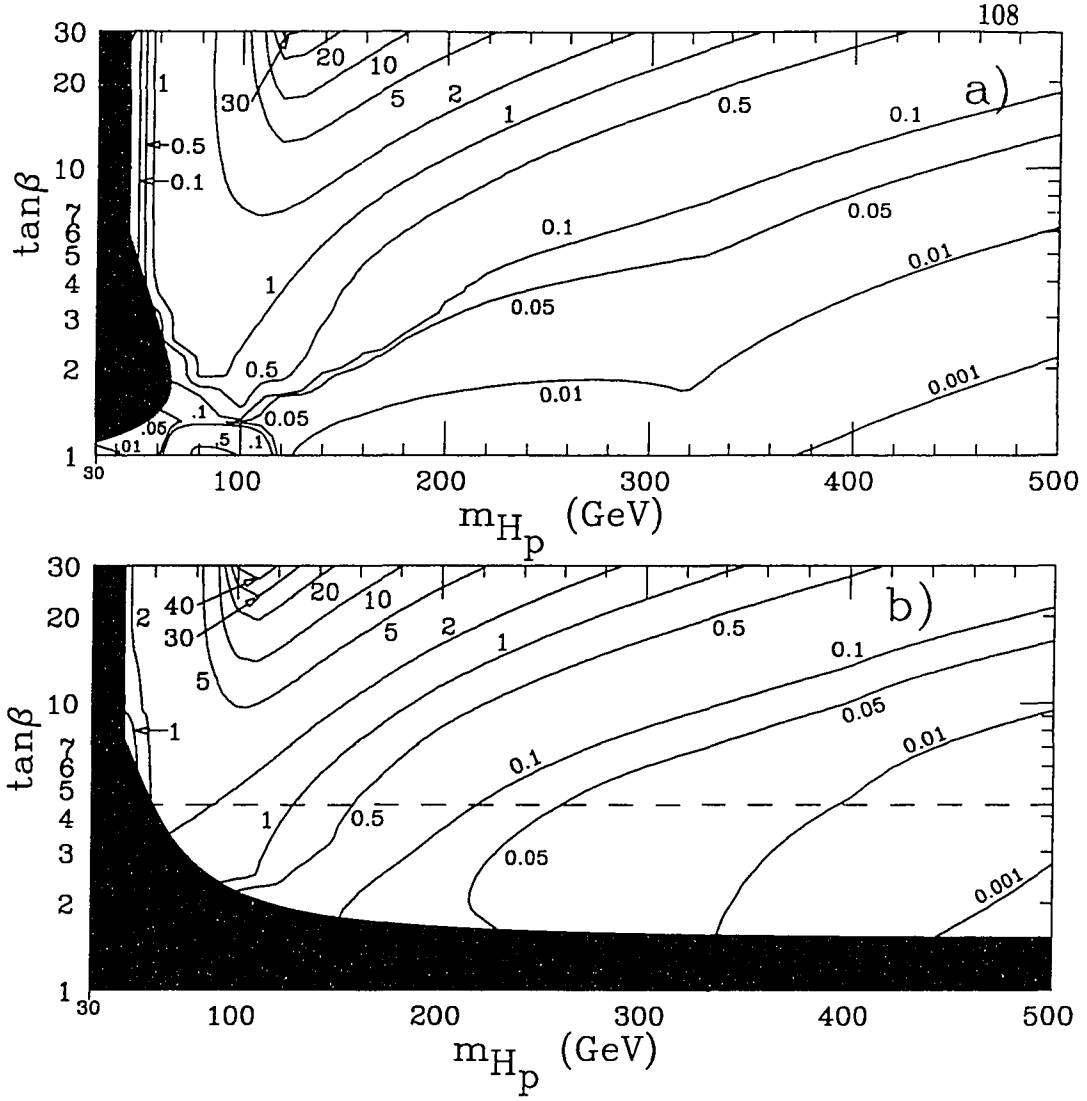

Figure 6.1: $\sigma(pp \to H_h \to \tau^+\tau^-)$ (in pb) without any selection cuts. $\sqrt{s} = 14\,\text{TeV}$.
With: $m_{\tilde{g}} = -\mu = 1000\,\text{GeV} \doteq m_{\tilde{q}}$ in plot a),
and $m_{\tilde{g}} = -\mu = 300\,\text{GeV} \doteq m_{\tilde{q}}$ in plot b),
(other parameters as in Fig. 3.8)

The next question is when are cross-sections in fact large enough to afford detection of a signal above the large background. A preliminary LHC study [140] using the mixed $\tau^+\tau^-$ decay channel ℓ + 'τ-jet' reported a sensitivity to $\sigma(pp \to H_{SM} \to \tau^+\tau^-)$ down to $\sim$10 pb for $m_{H_{SM}} \sim 100\,\text{GeV}$ and $\sim$1 pb for $m_{H_{SM}} \sim 400\,\text{GeV}$. This can be compared with the MSSM cross-sections shown in Figures 6.1 and 6.2, where *no p_T cut has been made on the Higgs boson* (so these values are over-estimates). Lowering the sparticle masses does not significantly affect this signal, which is viable

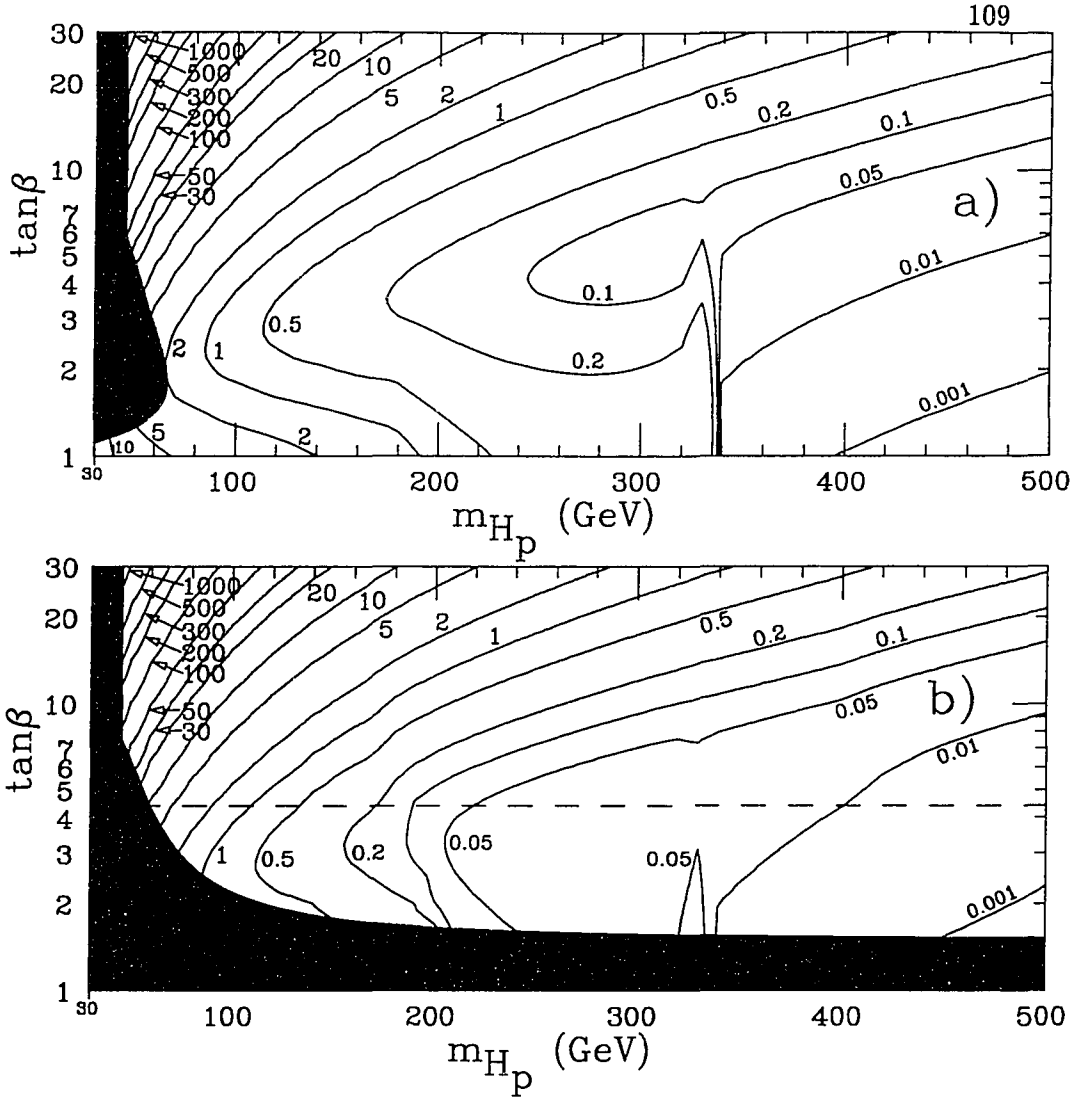

Figure 6.2: $\sigma(pp \to H_p \to \tau^+\tau^-)$ (in pb) without any selection cuts. $\sqrt{s} = 14\,\text{TeV}$.
With: $m_{\tilde{g}} = -\mu = 1000\,\text{GeV} \doteq m_{\tilde{q}}$ in plot a),
and $m_{\tilde{g}} = -\mu = 300\,\text{GeV} \doteq m_{\tilde{q}}$ in plot b),
(other parameters as in Fig. 3.8)

in a region of parameter space where decays to sparticles are unimportant (see Figs. 5.6 and 5.7). From these raw $\tau^+\tau^-$ production rates, it seems fair to conclude that a search for H_h and H_p via their decays to $\tau^+\tau^-$ pairs will be able to exclude a high $\tan\beta$, low m_{H_p} region of the MSSM parameter space. The uncertainty in the percentage of Higgs bosons with sufficient p_T should be resolved to insure an accurate detectable region is mapped out. Also, one should add the caveat that this is a fairly tricky signal to disentangle from the relevant backgrounds, and running

the supercollider at higher luminosities can unravel the picture presented here. DiLella in the study mentioned above in fact does state that a luminosity higher than $10\,\mathrm{fb}^{-1}$/year will invalidate his results.

Finally, it might be mentioned that, even if it is feasible, using a microvertex detector to detect τ vertices probably will not be helpful since it is more likely to find b's from background $t\bar{t}$ of $b\bar{b}$ events since the b-quark lifetime is $\simeq 3$ times longer. Thus the signal to background ratio will actually be reduced [131].

6.1.2 Charged Higgs Boson Decays to τ's & Lepton Non-universality

If the charged Higgs bosons are light enough, they may be produced in the decays of the top quark, as was already pointed out in the discussion on trileptonic signals from SUSY decay modes of the Higgs bosons in Chapter 5. For $\tan\beta \gtrsim \frac{3m_c^2}{m_\tau^2} \sim 2$, the charged Higgs bosons will decay largely into τ-leptons, $H^+ \to \tau^+\nu_\tau$ (assuming no SUSY decay modes with favorable couplings are kinematically accessible). Thus production of charged Higgs bosons in top quark decays is signaled by an excess of τ-leptons over and above the rate expected from the usual SM decay chain $t \to bW^+$, $W^+ \to \tau^+\nu_\tau$. Now consider the quantity $R_{\tau\ell}$ defined by

$$R_{\tau\ell} \equiv \frac{B.R.(t \to \tau^+\nu_\tau b)}{B.R.(t \to \ell\nu_\ell b)} = 1 + \frac{B.R.(t \to H^+b)\,B.R.(H^+ \to \tau^+\nu_\tau)}{B.R.(t \to W^+b)\,B.R.(W^+ \to \ell\nu_\ell)} \equiv 1 + \Delta R_{\tau\ell}\,, \tag{6.2}$$

where $\ell = e$ or μ. $R_{\tau\ell}$ is expected to be one in the SM due to the universality of the W-boson couplings to the leptons. Thus any deviation, $\Delta R_{\tau l} \neq 0$, serves as a measure of the charged Higgs decay mode of the t-quark.

The τ-leptons are again supposed to be identified via their hadronic decays. This has been carefully studied for the LHC by Felcini [123] by starting with a sample of tagged $t\bar{t}$ events (defined by an $e\mu$ sample with $p_T(e) > 75\,\mathrm{GeV}$ and $p_T(\mu) > 25\,\mathrm{GeV}$ from b-quark daughter of the same top quark) and determining the ratio, N_τ/N_μ,

of the number of decays where the other t-quark in the $t\bar{t}$ pair decays into a muon or a tau. This can be written as [123]

$$R_{\tau\mu} = A\frac{N_\tau}{N_\mu} + B \tag{6.3a}$$

$$\text{where} \qquad A = \frac{\epsilon_{W^+\to\mu^+}}{B.R.(\tau^+ \to \text{hadrons})\epsilon_{H^+\to\tau^+}} \ , \tag{6.3b}$$

$$\text{and} \qquad B = 1 - \frac{\epsilon_{W^+\to\tau^+}}{\epsilon_{H^+\to\tau^+}} \ . \tag{6.3c}$$

Here $\epsilon_{...}$ is the experimental efficiency for the detection of the particular process. The variance of $R_{\tau\mu}$ is given by $A^2 N_\tau \frac{(N_\tau + N_\mu)}{N_\mu^3}$. For $m_t = 200\,GeV$, Felcini [123] has estimated that $\epsilon_{W\to\mu} = 94\%$ and $\epsilon_{W\to\tau} B.R.(\tau \to hadrons) = 35\%$. To obtain these values a simulation of 2389 tagged $t\bar{t}$ events corresponding to an integrated luminosity of 10 fb^{-1} at the LHC was generated and analyzed. This study also found that, for $m_{H_{ch}} = 150\,\text{GeV}$, $\frac{\epsilon_{H^+\to\tau^+}}{\epsilon_{W^+\to\tau^+}} = 1.5$. Since $R_{\tau\mu}$ is not distributed as a Gaussian, a criterion for observability of the $t \to bH^+$ signal can be obtained by requiring that $R_{\tau\mu}$ deviates from its SM value of unity by at least four times the variance. At the LHC, for the m_t and $m_{H_{ch}}$ values given above and assuming an integrated luminosity of $10\,\text{fb}^{-1}$, this indicates there will be an observable signal if $\frac{\Delta R_{\tau\mu}}{R_{\tau\mu}} > 0.32$. A couple of caveats should be pointed out though:

- There are additional systematic uncertainties from errors in tracking efficiency (which affects the number of detected charged tracks), and energy resolution of the calorimeter. Both of these can affect the number of detected τ's and are not taken into account by the simple statistical approach just outlined.
- The efficiency of τ detection decreases with $m_{H_{ch}}$, so that if H^+ is considerably lighter, the τ detection efficiency may be considerably overestimated.

Spin effects do tend to favor the harder pion spectrum from the decays of τ's in H^+ decays compared to those from W^+ decays [141], and this can lead to a higher detection efficiency for τ's from Higgs decays as opposed to those from W-boson decays. However, in view of the uncertainties just noted, and to be conservative $\frac{\epsilon_{H^+\to\tau}}{\epsilon_{W\to\tau}} = 1$ will be used. In this case, the expression for the fractional variance of

$R_{\tau\mu}$ simply reduces to $\sqrt{\frac{1}{N_\mu}+\frac{1}{N_\tau}}$. In the SM, $N_\mu \sim 250$, $N_\tau \sim 100$ for tagged top events per $10\,\mathrm{fb}^{-1}$ at the LHC, so that the requirement for a detectable signal at the LHC reduces to $\Delta R_{\tau\mu} > 0.48$. For the LHC operating at the high design luminosity of $100\,\mathrm{fb}^{-1}$/year, the ten times larger $t\bar{t}$ sample implies that $\Delta R_{\tau\mu} > 0.15$ would be observable, while $50\,\mathrm{fb}^{-1}$ predicts that $\Delta R_{\tau\mu} > 0.215$ would be observable. In view of the simplicity of our estimates, we will take $\Delta R_{\tau\mu} = 0.48$ to be the limit of observability. This is illustrated in Figure 6.3 for $m_t = 150\,\mathrm{GeV}$ and $m_t = 200\,\mathrm{GeV}$.

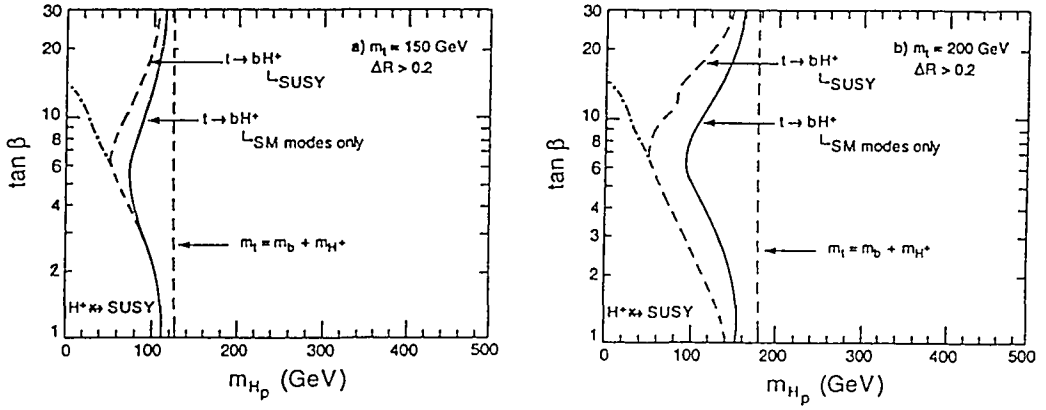

Figure 6.3: Observable region for seeing lepton non-universality in the top quark decay $t \to bH^+$ followed by $H^+ \to \tau^+\nu_\tau$ with $m_t = 150\,\mathrm{GeV}$ in a) and $m_t = 200\,\mathrm{GeV}$ in b).
$\Delta R > 0.2$ to the left of the solid curve if $m_{\tilde{g}} = \mu = 1000\,\mathrm{GeV} \doteq m_{\tilde{q}}$, and to the left of the dashed curve if $m_{\tilde{g}} = 400\,\mathrm{GeV}$, $\mu = -70\,\mathrm{GeV}$, and $m_{\tilde{q}} = 1000\,\mathrm{GeV}$, in which case the SUSY decay modes of H^+ are open, and so the fraction decaying to τ's is reduced.
The region to the left of the dot-dashed curve is where all the SUSY decay modes of the H^+ are closed. And finally, the vertical dashes line indicated the phase space limit for $t \to bH^+$

The harder pion spectrum from a charged Higgs boson as compared to that of the W (about twice as hard if the $m_{H_{ch}} \simeq M_W$; *i.e.*, the average p_T of the pion coming from a charged Higgs boson is about twice that on a pion coming from a W-boson [141]) can also be used as a signature of charged Higgs production if one can obtain a clean sample of τ's produced in $t\bar{t}$ decays. It also clearly suggests cuts that could be made on the minimum p_T of the π's (supplemented for higher charged Higgs masses, $m_{H_{ch}} \simeq m_t$, by a maximum p_T cut on accompanying b-quark jets from

the t-quark decays). This distinction between spin-1 W's and spin-0 charged Higgs bosons is a result of the spin polarization of the τ-leptons owing to the existence of only left-handed ν_τ's and right-handed $\overline{\nu_\tau}$'s, which restricts the allowable $W^\pm$ and $H^\pm$ decays to

$$H^+ \to \tau_L^+ \nu_{\tau L}\,, \qquad H^- \to \tau_R^- \overline{\nu_{\tau R}} \tag{6.4a}$$

$$\text{and} \qquad W^+ \to \tau_R^+ \nu_{\tau L}\,, \qquad W^- \to \tau_L^- \overline{\nu_{\tau R}}\ . \tag{6.4b}$$

Simple angular momentum conservation then shows for instance that $\tau_L^- \to \nu_{\tau L}\pi^-$ favors a π^- moving backward in the rest frame of the decaying τ (where the direction is relative to the τ's direction in the laboratory reference frame) and thus slower in the laboratory reference frame while $\tau_R^- \to \nu_{\tau L}\pi^-$ favors the spin-0 π^- moving forward in the rest frame of the decaying τ and thus faster in the laboratory reference frame. Analogous arguments may be made for the τ-lepton decays to spin-1 ρ mesons. Such momentum distribution patterns among the decay products of chiral leptons have been studied extensively for many years [142-145]. The difference in the expected distributions from τ_L^- and τ_R^- implies that a measurement of the τ-lepton polarization by measuring the momentum distribution of the decaying pions can also yield a signature of the charged Higgs boson — it could even be used as a mass measurement if $\tan\beta$ was known [141]. This has been shown to be a more sensitive test for the presence of a charged Higgs boson then the lepton non-universality diagnostic [146], requiring fewer events and lower statistics to establish a conclusion. LEP has recently used a similar technique to measure τ-lepton polarization to a precision of $\pm 5\%$ [147]. The charged Higgs signal at the LHC from τ-lepton polarization has been investigated by D.P. Roy [141,148] considering both the angular and p_T distributions of the resulting pions (see also the SSC study by Barnett *et. al.* [149-151]). He found favorable signal to background ratios after appropriate cuts for all values of $\tan\beta$ and for $m_{H_{ch}} \lesssim m_t - 20\,\text{GeV}$. The crucial question that remains to be addressed with this technique is then the efficiency of selecting top-quark decays to τ-leptons when the τ's then decay to pions, and the amount of contamination at a hadron supercollider due to the huge rate for other pion-producing processes.

6.1.3 Associated Production — $\ell\gamma\gamma$ Signals

When a Higgs boson is produced in association with either a W-boson or a $t\bar{t}$ pair, it is possible to obtain an $\ell\gamma\gamma$ final state, where the photon pair is from the decay of the Higgs boson and the extra isolated lepton is from the decay of the associated W-boson or top quark. It has been pointed out [47,93] that this signal has a higher signal to physics background ratio than one that includes all $\gamma\gamma$ pairs produced in Higgs boson decays, regardless of whether or not an isolated lepton is also produced. This has lead some authors [93] to suggest that the $\ell\gamma\gamma$ mode is superior to the inclusive $\gamma\gamma$ mode for detecting a Higgs boson, and that a Higgs signal will probably first be detected in the $\ell\gamma\gamma$ mode and then later confirmed in the inclusive $\gamma\gamma$ channel [93].

Parton-level simulations [81,152-154] for a SM Higgs boson with a mass of about 100 GeV show it will typically yield about 12 and 15 $\ell\gamma\gamma$ events via WH_{SM} and $t\bar{t}H_{SM}$ production modes, respectively, at the LHC for an integrated luminosity of $100\,\mathrm{fb}^{-1}$. This is after taking into account lepton and photon detection efficiencies of ~70-75% and *losses* of ~30% due to acceptances. For almost all choices of the MSSM input parameters, the production rate for MSSM Higgs bosons will be even smaller than in the SM [47]. The only exception to this noted in Ref. [47] was for m_{H_p} near the $2m_t$ threshold and $\tan\beta \simeq 1$, and in this case the rate is still too small to allow detection.

The total irreducible background in the above simulations was found to be 20-30% the size of the signal, and to be dominated by contributions from continuum $\gamma\gamma$ production (as discussed in Chapter 4) accompanied by W or $t\bar{t}$ production. There are also many sources of reducible background, for example from $\gamma\gamma$ continuum production associted with $b\bar{b}$ production where a lepton from one of the b decays is accidentally isolated. As with the inclusive $\gamma\gamma$ mode, the mis-identification of jets as photons is also a source of background. With signal rates that are so pitifully small, there is little room for error in the determination of the correct background subtraction. Yet this determination should prove much more worrisome in the $\ell\gamma\gamma$

case than in the inclusive $\gamma\gamma$ case, since in the latter there is a smooth continuum background outside of the resonance region. As noted in Chapter 4, this diminishes the importance of uncertanties in a theoretical calculation of the background stemming for instance from attempts at estimating higher-order QCD processes or the proton structure functions. For the case of $\ell\gamma\gamma$, a background calculation that goes beyond the parton level certainly seems necessary.

Thus perhaps the best summary of the situation is that a Higgs boson "signal" may (or may not) be seen first in the $\ell\gamma\gamma$ mode, but it will be difficult to know how much significance to assign to a result with $\sim$10 events per $100\,\mathrm{fb}^{-1}$.

6.1.4 Associated Production with b-quark Tagging

If it is possible to tag b-quark jets reasonably cleanly and with a reasonable efficiency, then several other Higgs boson signals become feasible. The Technical Design Report of the Solenoidal Detector Collaboration [71] gave an expected b-tagging efficiency of their proposed vertex detector of $\sim$0.2 for jet p_T's of around 25 GeV and an efficiency of $\sim$0.4 for jet p_T's around 200 GeV, with p_T = 40-100 GeV jets having efficiencies around 0.3. The percentage of other jets mis-identified as b-quark jets was given as $\sim$1%. It should most definitely be kept in mind though that these numbers were estimated for detector operation at the SSC, not at the higher luminosity environment proposed for LHC, where multiple events per crossing are much more likely.

As Figure 4.1 shows, a SM Higgs boson with a mass below $2M_W$ almost always decays into a $b\bar{b}$ pair. So if the b-quarks can be tagged this is certainly a logical decay mode to consider as a potential source of signals. Unfortunately, the QCD production rate for $b\bar{b}$ pairs at a hadron supercollider is enormous, and there is no hope of picking out a signal for Higgs boson decay. This again suggests looking at associated production processes. If a Higgs boson is produced in association with a $t\bar{t}$ pair, or a $b\bar{b}$ pair, then an $H \to b\bar{b}$ decay would result in an event with four b-quark jets. Backgrounds to this are far more modest.

$H_{SM} \rightarrow b\bar{b}$ associated with a leptonically-decaying W or Z^0 gauge boson has also been studied [155] for the LHC and found to yield potentially viable signals for $80\,\mathrm{GeV} < m_{H_{SM}} < 120\,\mathrm{Gev}$. (Interestingly, a study [156] for a $\sqrt{s} = 2\,\mathrm{TeV}$, high luminosity $p\bar{p}$ collider reached a similar conclusion with $M_{Z^0} < m_{H_{SM}} < 130\,\mathrm{Gev}$ and $H \rightarrow \tau^+\tau^-$ produced in association with a gauge boson decaying into jets. Even $b\bar{b}H \rightarrow b\bar{b}\mu^+\mu^-$ has recently been explored for the LHC [139].)

It should first be noted that attempts to generate a signal from

$$t\ \bar{t}\ H_{SM} \rightarrow b\ell^+\nu\ \bar{b}\ell^-\bar{\nu}\ b\bar{b} \tag{6.5}$$

without b-tagging by demanding that the top-quark decay to e or μ and looking for a bump in the invariant mass spectrum of the two jets provided at best extremely marginal results due to the fierce backgrounds from $t\bar{t}$ events associated with $Z^0 \rightarrow q\bar{q}$, or continuum gg or $q\bar{q}$ jet production. (The $t\bar{t}gg$ background is the largest in the $t\bar{t} + 2\,\mathrm{jet}$ channel.) To beat down these backgrounds using b-quark tagging, at least 3 b's must be tagged [157]. Unfortunately, according to the b-tagging efficiency estimates just given, this removes about 97% of the signal events. Trying in addition to tag both leptons was found to leave no observable signal; thus, detection of a single lepton was required in the study in Ref. [157]. The results of this study are given in Table 6.1 on the following page which is taken from this source. Note that with a b-tagging efficiency of 30% and a miss-tagging frequency of 1% a 5σ confidence level signal is obtained with $< 100\,\mathrm{fb}^{-1}$ of integrated luminosity if $m_{H_{SM}} \lesssim 100\,\mathrm{GeV}$, assuming $m_t \simeq 180\,\mathrm{GeV}$. The amount of integrated luminosity required increases as $m_{H_{SM}}$ increases (note that this is opposite to the trend seen in the $H_\ell \rightarrow \gamma\gamma$ signal) but decreases as m_t increases (it is better that m_t be large so that the b-quark jets from the top decays are not too weak). Demanding that all four b-quark jets be tagged was also found to reduce the size of the data sample required to confirm a signal.

These SM results were then applied to the case of MSSM Higgs bosons by taking into account the relevant MSSM mixing angle factors of Table 1.2 [158]. The crucial observation is that for virtually any choice of the parameter pair $(m_{H_p}, \tan\beta)$, either

Table 6.1: Number of $100\,\mathrm{fb}^{-1}$ years (signal event rate) at the LHC required for a 5σ confidence level signal in four cases: I), II) — tagging 3 b-quark jets with $(e_{b-tag}, e_{mis-tag}) = (30\%, 1\%)$, $(40\%, 0.5\%)$; and III), IV) — tagging 4 b-quark jets with $(e_{b-tag}, e_{mis-tag}) = (30\%, 1\%)$, $(40\%, 0.5\%)$.
From Dai, Gunion, and Vega [157]

Case	$m_t \backslash m_{H_{SM}}$	80	100	120	140
I	110	1.5(407)	2.4(488)	6.0(654)	27.2(1146)
	140	0.8(365)	2.0(600)	3.5(621)	21.7(1338)
	180	0.2(102)	0.6(210)	1.8(373)	12.5(963)
II	110	0.4(229)	0.6(283)	1.5(368)	6.6(662)
	140	0.2(179)	0.4(291)	0.8(323)	4.7(690)
	180	0.1(62)	0.1(109)	0.4(195)	2.3(422)
III	110	6.4(145)	9.9(151)	22.4(204)	111.9(395)
	140	2.0(99)	3.3(112)	7.5(139)	44.3(303)
	180	0.7(43)	1.2(49)	2.9(74)	18.8(176)
IV	110	1.3(92)	2.4(116)	5.6(160)	28.7(321)
	140	0.3(51)	0.7(71)	1.8(103)	10.5(227)
	180	0.1(25)	0.3(35)	0.6(48)	3.9(114)

$B.R.(H_\ell \to b\bar{b})$ or $B.R.(H_h \to b\bar{b})$ will be large and SM-like. Then, assuming that whichever Higgs boson type is SM-like is light enough, the results from the SM study can be carried over to the MSSM. This was indeed found to be the case, with the role of SM-like Higgs boson switching from H_h to H_ℓ as m_{H_p} grows above $\sim$110 GeV. A recent study [159] further indicates that the $t\bar{t}H$, $W^{\pm}H$, and $b\bar{b}H$ associated production modes are to some degree complementary, and can cover much of the available parameter space, given an integrated luminosity $\gtrsim 100\,\mathrm{fb}^{-1}$ and good b-tagging capabilities, $(e_{b-tag}, e_{mis-tag}) = (30\%, 1\%)$. The results are quite sensitive to these values. Further, it is claimed that they are insensitive to the sparticle mass scales. The results are encouraging, but still preliminary, and as usual dependent on b-tagging and/or τ-lepton identification proficiencies.

6.1.5 Searching for Higgs Bosons in SUSY Events

Another possibility is to pre-select events having characteristics associated with sparticle production, namely $\not{E}_T$, and search for Higgs bosons within this set of events. This was investigated by Baer, Bisset, Tata, and Woodside [160] for the cascade decays of gluinos and squarks, sparticles expected to be copiously produced at the LHC. A previous study [130] had shown that it should be possible to identify such SUSY events in several channels such as events with $\not{E}_T$, same-sign dilepton $+\not{E}_T$ events, $n\ell + jets + \not{E}_T$ events ($n \geq 3$, leptons isolated and with high p_T), and n_1 high p_T $Z^0 + n_2\ell + jets + \not{E}_T$ ($n_1 = 1, 2$; $n_2 = 0, 1$; Z^0('s) decays leptonically. These signals are produced when the gluino or squark decays into charginos or neutralinos via the processes (assuming $m_{\tilde{g}} < m_{\tilde{q}}$):

$$\widetilde{q_L}, \widetilde{q_R} \rightarrow q\tilde{g} \tag{6.6a}$$

$$\widetilde{q_L}, \widetilde{q_R} \rightarrow q\widetilde{Z_i} \tag{6.6b}$$

$$\widetilde{q_L} \rightarrow q'\widetilde{W_j} \tag{6.6c}$$

$$\tilde{g} \rightarrow q\bar{q}^* \rightarrow q\bar{q}\widetilde{Z_i} \tag{6.7a}$$

$$\tilde{g} \rightarrow q\bar{q}^* \rightarrow q\bar{q}'\widetilde{W_j} \tag{6.7b}$$

Usually charginos or heavier neutralinos (*i.e.*, other than the LSP, $\widetilde{Z_1}$) are thus produced; they then decay via the modes listed in (5.1) and (5.2), producing the aforementioned leptonic and Z^0 signatures. This earlier study assumed the heavier MSSM Higgs bosons (H_h,H_p, and $H^{\pm}$ — collectively referred to as "Non-Standard Model" or NSM Higgs bosons since the other MSSM Higgs boson, H_ℓ is expected to usually mimic H_{SM} if m_{H_p} is large enough) have masses on the order of several hundred GeV.

If, on the other hand, NSM Higgs bosons are lighter, $m_{H_{NSM}} \lesssim 2M_W$, then processes like (5.1b), (5.1d), (5.1h), and (5.1j) open up for the NSM Higgs bosons. Since such Higgs bosons in the intermediate mass range usually decay via $b\bar{b}$ (or $t\bar{b}$ or $\tau^+\nu_\tau$ for H^+) into jets, the opening of such channels can be expected to reduce

the rate of the multilepton and Z^0 signals for SUSY production which mainly arise from the competing decays (5.1a), (5.1c), (5.1g), (5.1i), and (5.2). However, the study [160] showed that the $\not{E}_T$, same-sign dilepton, and trilepton signatures for SUSY were in fact relatively insensitive to low NSM Higgs boson masses, and that these signals remained viable for the identification of SUSY at the LHC.

Since these SUSY signals are still detectable, one can then ask if it is possible to use these SUSY signatures as triggers for NSM Higgs boson events. That is, can the discovery of NSM Higgs bosons ride piggy-back on the discovery of SUSY? The reach of this method is somewhat complementary to that of the SUSY Higgs boson decays discussed in Chapter 5. Here the neutralinos and charginos decay into the Higgs bosons rather than the other way around, so these sparticles should be heavier than the Higgs bosons. The gluinos or squarks which decay into the neutralinos and charginos need to be heavier still. Thus the prospects for using this methodology improve if the MSSM sparticle inputs are raised to higher values, as shown in Figure 6.4a) for gluino decays to NSM Higgs bosons.

The branching fraction for gluino cascade decays to NSM Higgs bosons were found to go as high as 60% for MSSM input parameter sets not excluded by LEP measurements (see Chapter 2) or TEVATRON gluino searches [161]. This branching fraction was also found to exceed 20-25% for a wide range of parameters. A branching fraction of 25% implies that, on the average, there is a NSM Higgs boson in half of the gluino or squark pair events. As illustrated in Figure 6.4c), this rate drops rapidly as $m_{H^+} = \sqrt{m_{H_p}^2 + M_W^2}$ is raised (note: raddiative corrections to H^+ due to b-quark Yukawa coupling were not included in this study, so the above tree-level relation holds in this approximation).

Branching fractions of $\widetilde{u_L}$ and $\widetilde{d_L}$ were also found to be very substantial for some parameter choices, but the branching ratios for $\widetilde{u_R}$ and $\widetilde{d_R}$ were found to be $\lesssim$1% except for a very limited region of parameters. The latter small branching ratio is due to the fact that for $m_{\tilde{g}} \gg |2m_1|$, $\widetilde{Z}_4$, the heaviest neutralino and thus the best prospect for decaying to intermediate mass Higgs bosons, is mostly an $SU(2)_L$ gaugino. (This can be seen from the structure of the matrix in Eqn. (1.8) using the

relations of Eqns. (1.9).) Therefore, $\widetilde{Z}_4$ does not couple very much to the $SU(2)_L$ singlet $\widetilde{q_R}$. (For $m_{\tilde{g}} \ll |2m_1|$, $\widetilde{Z}_4$ is mainly a higgsino and has only small gaugino couplings.) The $SU(2)_L$ doublet charginos also couple only weakly to $\widetilde{q_R}$ via very suppressed Yukawa interactions (which were neglected in this work). Thus the charginos and heavier neutralinos likely to produce NSM Higgs bosons among their daughter products have little coupling to $\widetilde{q_R}$'s; the latter are therefore not likely to have NSM Higgs bosons in their decays. The above results assume the squarks are degenerate in mass, so that two-body decays of a squark into a lighter squark and a Higgs boson are ruled out. This assumption may be questionable for the third generation squarks which have large Yukawa couplings.

To identify the MSSM Higgs bosons produced in identified SUSY events via the $H_h \to Z^0 Z^0$ ($Z^0 \to e^+e^-$ or $\mu^+\mu^-$) mode is probably impossible, and the $H_{\ell,h,p} \to \gamma\gamma$ modes (accompanied by jets and $\not{E}_T$) only looks promising for a very limited range of the MSSM parameters. This leaves us to consider the dominant $b\bar{b}$ and $t\bar{b}$ or $\tau^+\nu_\tau$ decay modes. *If* it is possible to identify b-jets (within the experimental acceptance) with an efficiency of 50% per jet, the presence of a relatively light H_h or H_p will be signaled by a significant increase in the average multiplicity of B hadrons in the SUSY events. The increase in b-multiplicity expected when m_{H_p} is reduced from $\sim$500 GeV to $\sim$60 GeV cannot be attributed to variation of either $\tan\beta$ or $2m_1$ [160].

Searching for lepton non-universality in the same-sign dilepton and trilepton SUSY events as a signal for charged Higgs boson production might also be possible if high p_T, isolated τ-leptons can be identified in these multijet + $\not{E}_T$ events. Since the neutral Higgs bosons decay mainly into $b\bar{b}$ pairs, excess τ-leptons are expected to come charged Higgs boson decays, which go into τ-leptons almost 90% of the time if $m_{H^+} < m_t + m_b$ (and sparticle decay modes are closed). Also note that since H^+ and H^- are equally likely to be produced in gluino decays, τ pairs from charged leptons are as likely to be like sign as opposite sign. An SSC simulation [160] with $m_{\tilde{g}}$, $m_{\tilde{q}}$, m_t, $\mu = -2m_1$, $\tan\beta$) = (1 TeV, 1.1 TeV, 140 GeV, -150 GeV, 5) found after cuts a 6σ τ excess in the trilepton channel and an even greater excess in the same-sign dilepton channel for m_{H^+} just below the $H^+ \to t\bar{b}$ threshold. Lowering m_{H_p} down to the LEP limits magnifies this exceess still more.

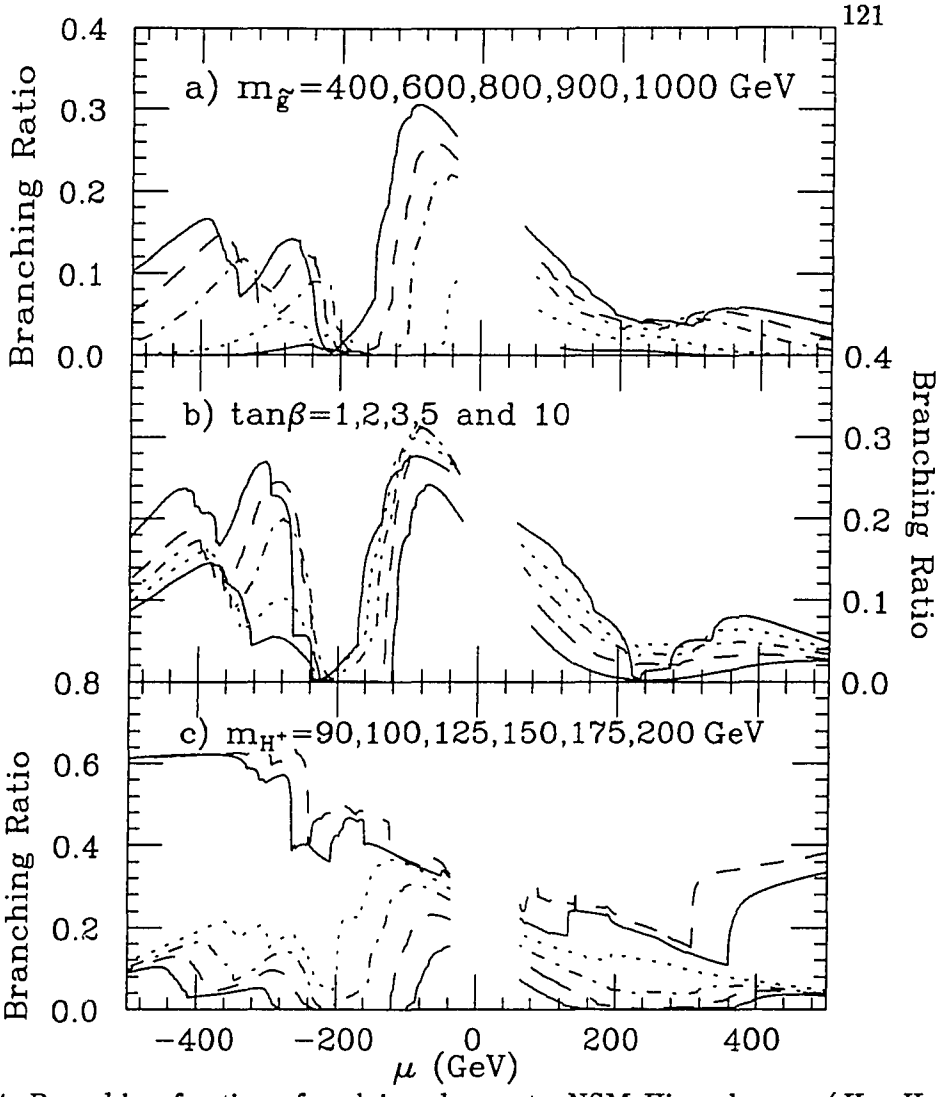

Figure 6.4: Branching fractions for gluino decays to NSM Higgs bosons (H_h, H_p, and $H^{\pm}$), *vs.* μ. Unless otherwise noted, the default values for the MSSM parameters are $m_{\tilde{g}} = 1000\,\text{GeV} \doteq m_{\tilde{q}}$, $m_{H_{ch}} = 150\,\text{GeV}$ and $\tan\beta = 4$; also set is $m_t = 140\,\text{GeV}$. In a), curves are for $m_{\tilde{g}} = 400\,\text{GeV}$ (lower solid), 600 GeV (dots), 800 GeV (dot-dash), 900 GeV (dashes), and 1000 GeV (upper solid). In plot b) curves are $\tan\beta = 1$ (solid - largest for $\mu \sim -500\,\text{GeV}$, smallest for $\mu \sim 500\,\text{GeV}$), $\tan\beta = 2$ (dashes), $\tan\beta = 3$ (dot-dash), $\tan\beta = 5$ (dots), and $\tan\beta = 10$ (other solid). In plot c), curves are $m_{H^+} = 90\,\text{GeV}$ (upper dashes), 100 GeV (upper solid), 125 GeV (dots), 150 GeV (dot-dash), 175 GeV (lower dashes), and 200 GeV (lower solid). The blanked-out region around the middle of each plot is excluded by LEP. For this figure, $m^2_{H^{\pm}} = m^2_{H_p} + M^2_W$ (tree-level only).

The idea of searching for Higgs bosons using a set of LHC events already enhanced by selecting for SUSY-like characteristics still needs a great deal more analysis and study. As with several of the other proposed discovery channels for Higgs bosons that have been discussed in this chapter, the usefulness of this method will depend on the capabilities of the detector to identify τ-leptons from their decay products and b-quark jets. Complete detector simulations will be required to fully establish the feasibility of using these Higgs detection modes.

6.2 Conclusions & Outlook

Figure 6.5 displays the regions of the $m_{H_p} - \tan\beta$ plane where the "gold-plated" $H \to Z^0Z^0, Z^0Z^{0*} \to 4\ell$ signal and the $H \to \gamma\gamma$ signals are observable using the criterion established in Chapter 4 with $m_{\tilde{g}} = -\mu = 1\,\text{TeV} \doteq m_{\tilde{q}}$; Figure 6.6 is the analagous picture this time assuming $m_{\tilde{g}} = -\mu = 300\,\text{GeV} \doteq m_{\tilde{q}}$. The integrated luminosity is taken to be 50 fb^{-1}. Unless otherwise indicated, the label for a given signal in these figures appears on the side of the boundary where that signal is observable. A summary of the MSSM Higgs boson detection signals displayed in these figures is given in Table 6.2 on the following page. These figures are further dissected in Figures 6.7 through 6.14 through the use of shading. The black region in all figures denotes the range of parameters excluded by experiments at LEP while the regions below the lines marked LEP190 and LEP175 can be probed in experiments at LEP II with optimistic ($\sigma(H_\ell H_p)$ or $\sigma(H_\ell Z) > 0.05\,\text{pb}$, $\sqrt{s} = 190$ GeV) and pessimistic ($\sigma(H_\ell H_p)$ or $\sigma(H_\ell Z) > 0.2\,\text{pb}$, $\sqrt{s} = 175$ GeV) scenarios for performance of the LEP collider in its LEP II phase. Also roughly indicated by the crosses and open circles in Figure 6.6 is the region an excess in the $4\ell + \not{E}_T$ mode from the supersymmetric Higgs boson decays $H_{h,p} \to \widetilde{Z}_2\widetilde{Z}_2 \to 4\ell + 2\widetilde{Z}_1$ should be observable. The crosses signify points where the Higgs decay signal was found to be distinguishable from continuum neutralino production via the invarant mass spectrum of the leptons while the open circles are at locations where about 250 to 400 fb^{-1} of integrated luminosity will be required to make this distinction.

Table 6.2: Summary of Processes Important in MSSM Higgs Boson Identification.

Process	Signature	General Region of detectability
at hadron supercollider		
main well-established signals:		
• $H_h \to Z^0 Z^0 \to 4\ell$ "gold-plated" signal	4 charged leptons 2 lepton pairs reconstruct M_{Z^0}	patches in low $\tan\beta$, low m_{H_p} high sparticle masses; these small pockets
• $H_h \to Z^0 Z^{0*} \to 4\ell$ • $H_\ell \to Z^0 Z^{0*} \to 4\ell$	4 charged leptons 1 lepton pair reconstructs M_{Z^0}	for H_h are largely for $m_{H_h} < 2M_{Z^0}$; not useful for H_ℓ see Figs. 4.3,4.4
•$H_\ell \to \gamma\gamma$ •$H_h \to \gamma\gamma$ •$H_p \to \gamma\gamma$	reconstruct 2-γ invariant mass	higher m_{H_p} Figs. 4.9,10 low m_{H_p} Figs. 4.11,12 low $\tan\beta$ Figs. 4.13,14
Other signals:		
• $H_h \to \tau^+\tau^-$ • $H_p \to \tau^+\tau^-$	identify τ-jets or τ leptonic decays	high $\tan\beta$, low m_{H_p} see Figs. 6.1,2
• $t\bar{t}H, b\bar{b}H \to 4b$'s • $WH \to b\bar{b}\ell\nu$	dependent on b-jet tagging capabilities	lower m_H see Table 6.1
• $H_h \to \widetilde{Z}_2\widetilde{Z}_2 \to 4\ell + \not{E}_T$ • $H_p \to \widetilde{Z}_2\widetilde{Z}_2 \to 4\ell + \not{E}_T$	4 charged leptons & missing E_T	low sparticle masses $m_{H_p} \sim 200 - 350$ GeV see Figs. 5.14-20,23
at LEP II e^+e^- machine		
• $Z^{0*} \to H_\ell Z^0$ • $Z^{0*} \to H_p H_\ell$	identify Higgs boson via $b\bar{b}$ decay *etc.*	low $\tan\beta$ low m_{H_p} see Fig. 2.12

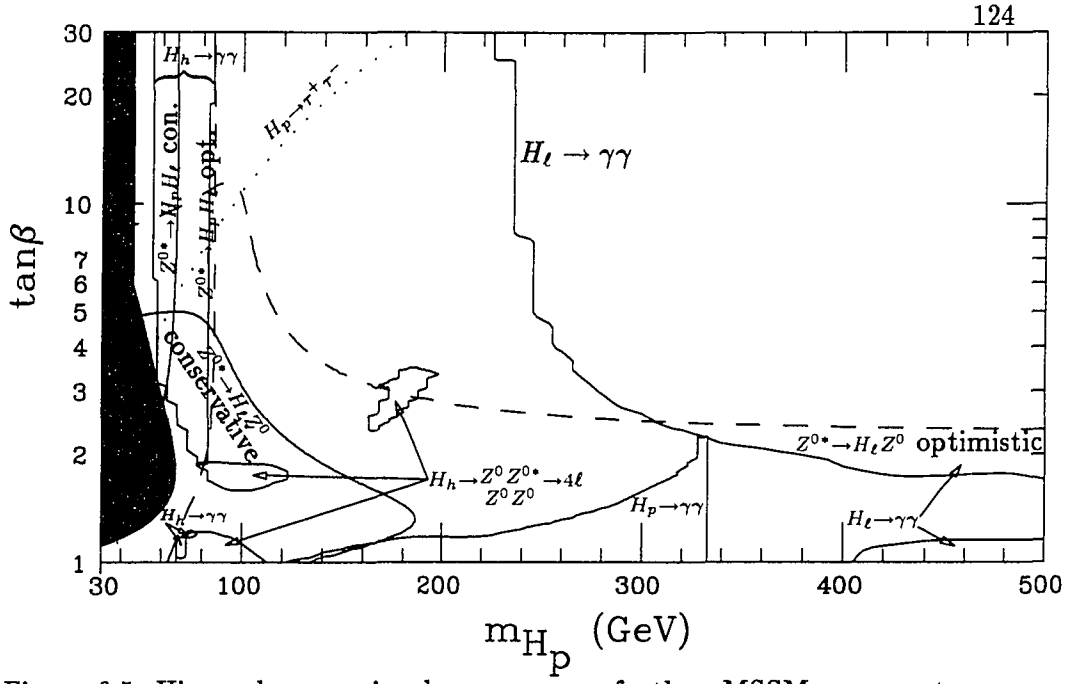

Figure 6.5: Higgs boson signal coverage of the MSSM parameter space. $m_{\tilde{g}} = -\mu = 1000\,\text{GeV} \doteq m_{\tilde{q}}$. Other MSSM input parameters as in Figure 2.10.

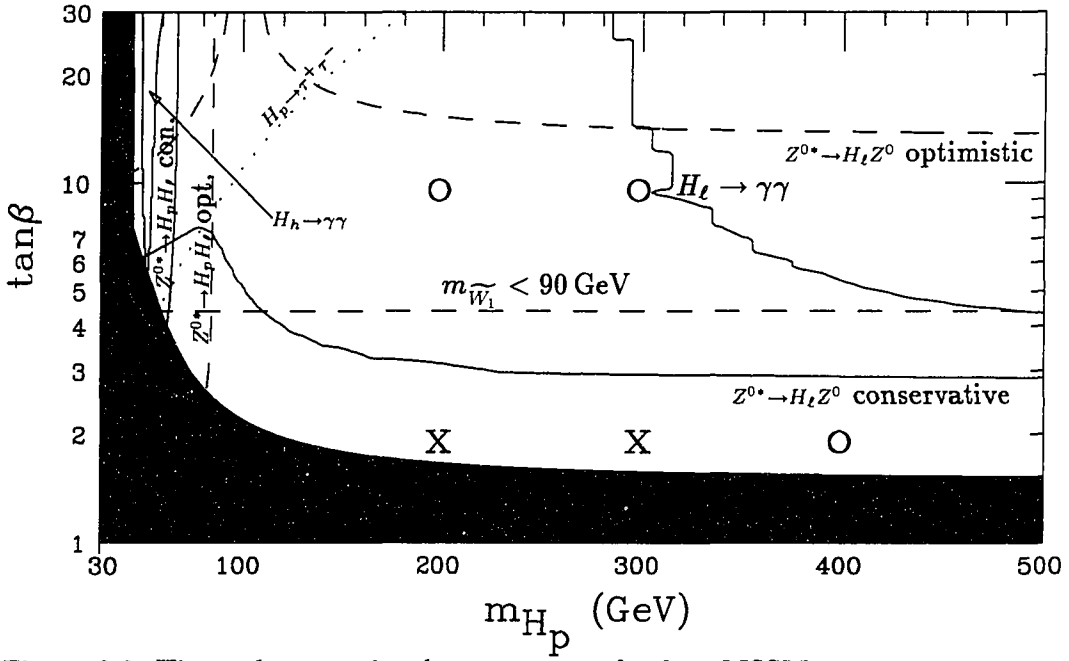

Figure 6.6: Higgs boson signal coverage of the MSSM parameter space. $m_{\tilde{g}} = -\mu = 300\,\text{GeV} \doteq m_{\tilde{q}}$. Other MSSM input parameters as in Figure 2.10.

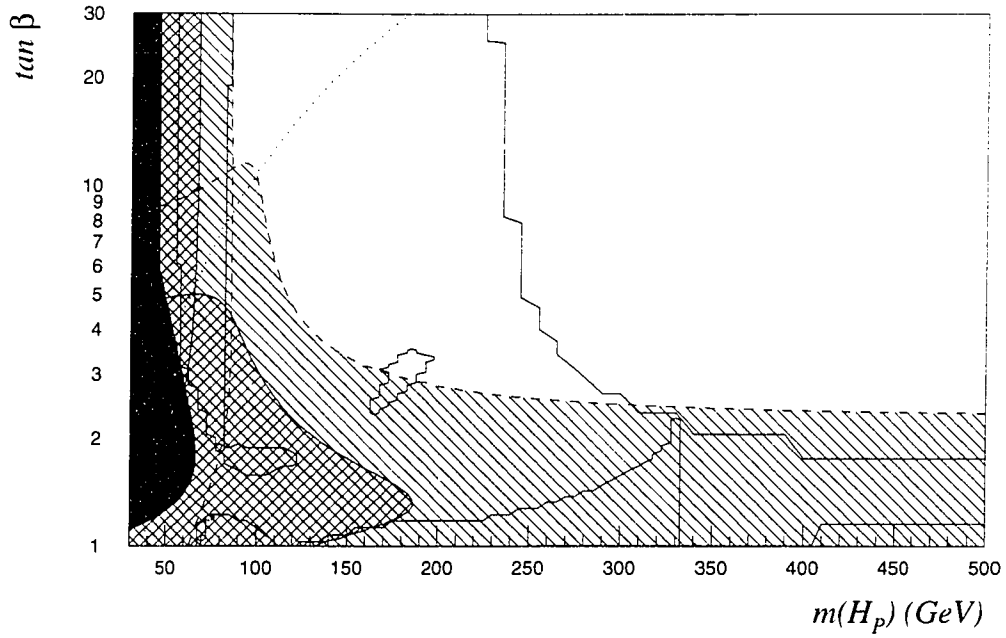

Figure 6.7: LEP II discovery reach for MSSM Higgs bosons. The diagonally shaded regions are covered assuming the optimistic LEP II capabilities, while the cross-hatched regions are covered using the conservative estimate. $m_{\tilde{g}} = -\mu = 1000\,\mathrm{GeV} \doteq m_{\tilde{q}}$. Other MSSM input parameters as in Figure 2.10.

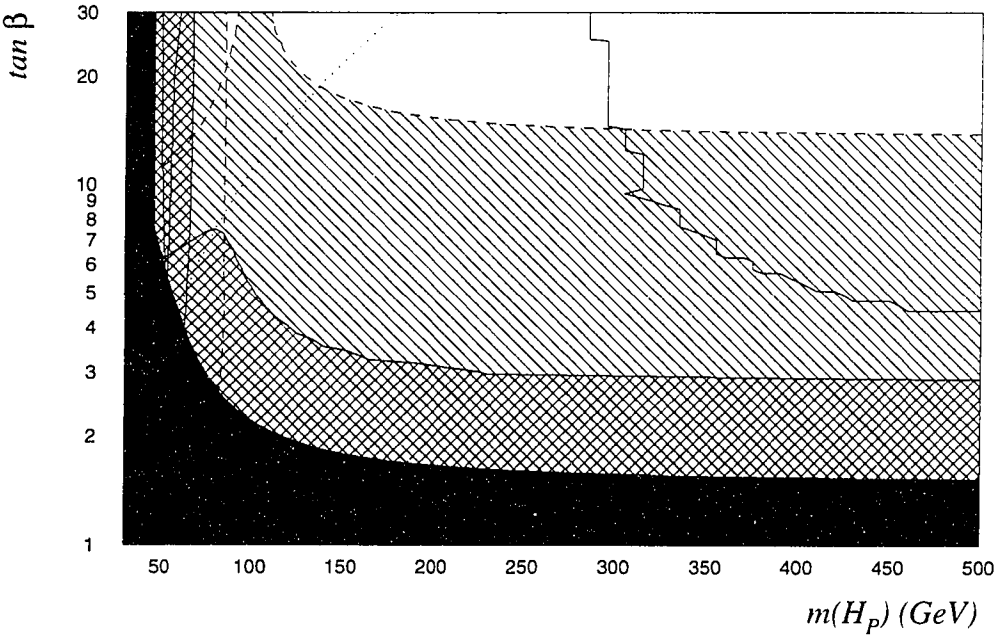

Figure 6.8: LEP II discovery reach for MSSM Higgs bosons.
$m_{\tilde{g}} = -\mu = 300\,\mathrm{GeV} \doteq m_{\tilde{q}}$. See Figure 6.7 above for explanation.

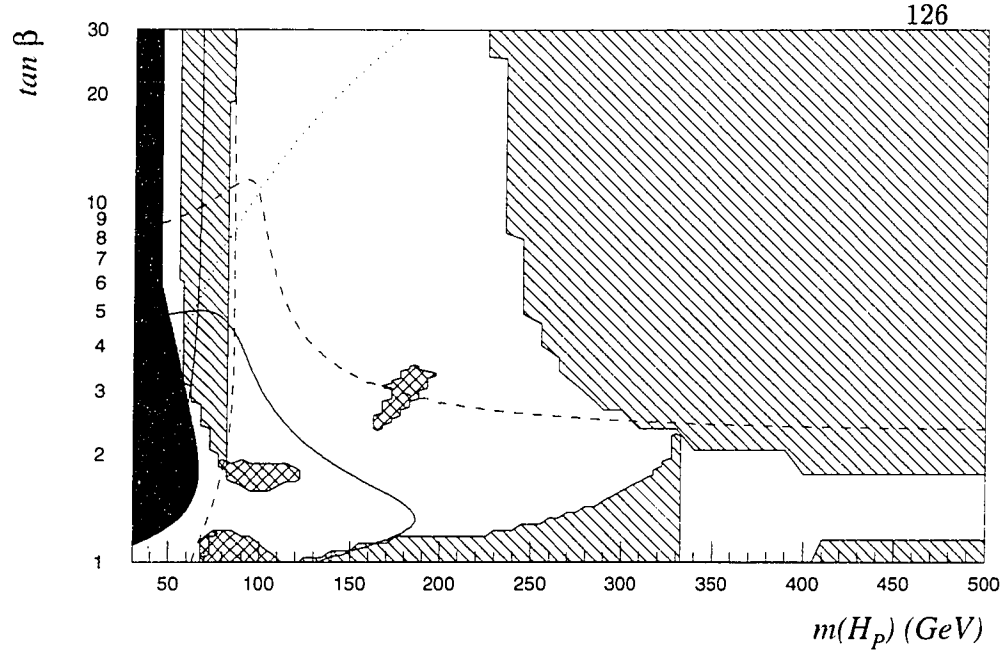

Figure 6.9: LHC discovery reach for MSSM Higgs bosons, considering only the well-established $H_h \to Z^0Z^0, Z^0Z^{0*} \to 4\ell$ (cross-hatched regions) and $H_\ell, H_h, H_p \to \gamma\gamma$ (diagonally shaded regions) signatures. $m_{\tilde{g}} = -\mu = 1000\,\text{GeV} \doteq m_{\tilde{q}}$. Other MSSM input parameters as in Figure 2.10.

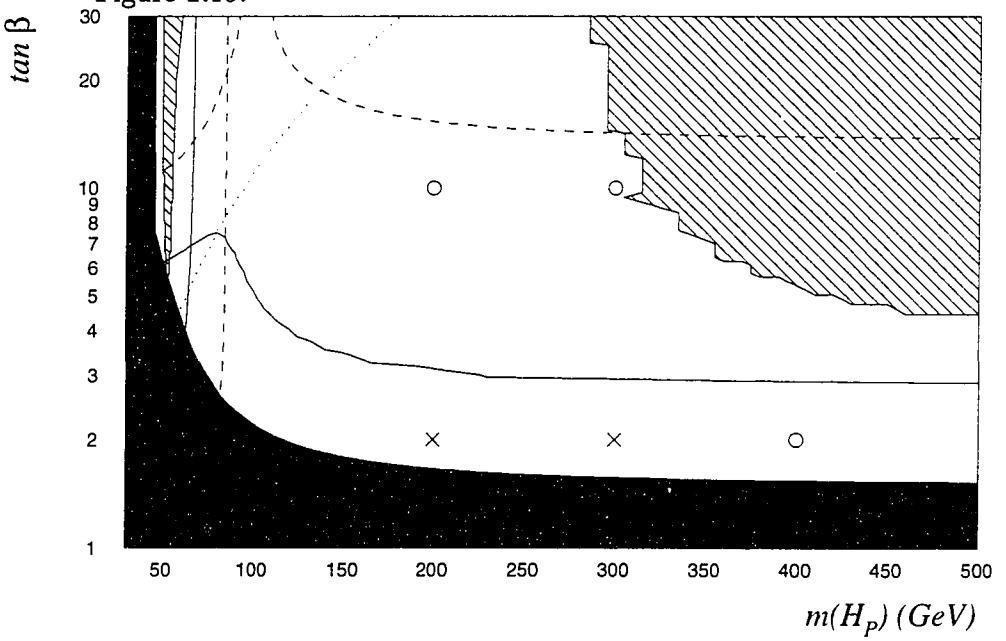

Figure 6.10: LHC discovery reach for MSSM Higgs bosons, considering only $H_h \to Z^0Z^0, Z^0Z^{0*} \to 4\ell$ (no detectable regions) and $H_\ell, H_h, H_p \to \gamma\gamma$ (diagonally shaded regions) signatures. $m_{\tilde{g}} = -\mu = 300\,\text{GeV} \doteq m_{\tilde{q}}$. Other MSSM input parameters as in Figure 2.10.

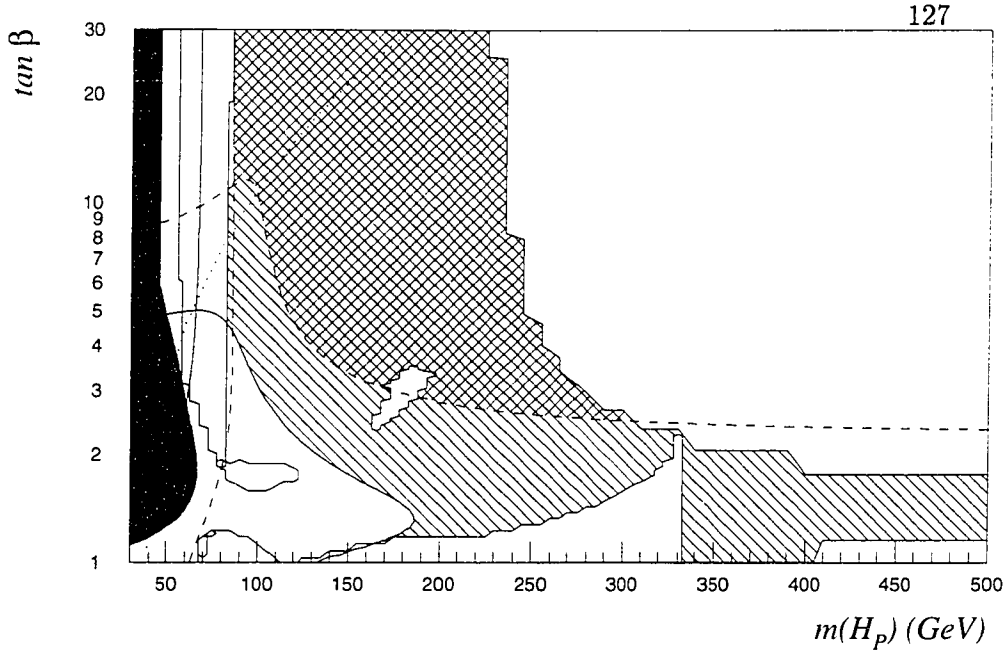

Figure 6.11: The "hole" in which no MSSM Higgs boson is detectable at either LEP II or the LHC. It encompassses the cross-hatched region for optimistic LEP II capabilities, and expands to include the diagonally shaded regions when conservative LEP II characteristics are assumed. $m_{\tilde{g}} = -\mu = 1000\,\mathrm{GeV} \doteq m_{\tilde{q}}$. Other MSSM input parameters as in Figure 2.10.

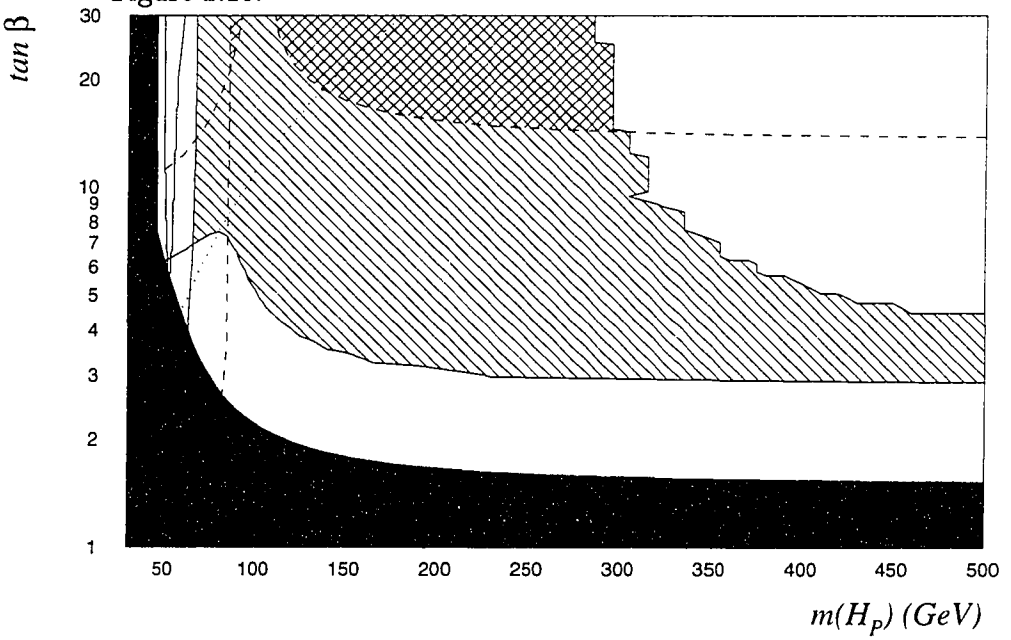

Figure 6.12: The "hole" in which no MSSM Higgs boson is detectable at either LEP II or the LHC. $m_{\tilde{g}} = -\mu = 300\,\mathrm{GeV} \doteq m_{\tilde{q}}$. See Figure 6.10 above for further explanation.

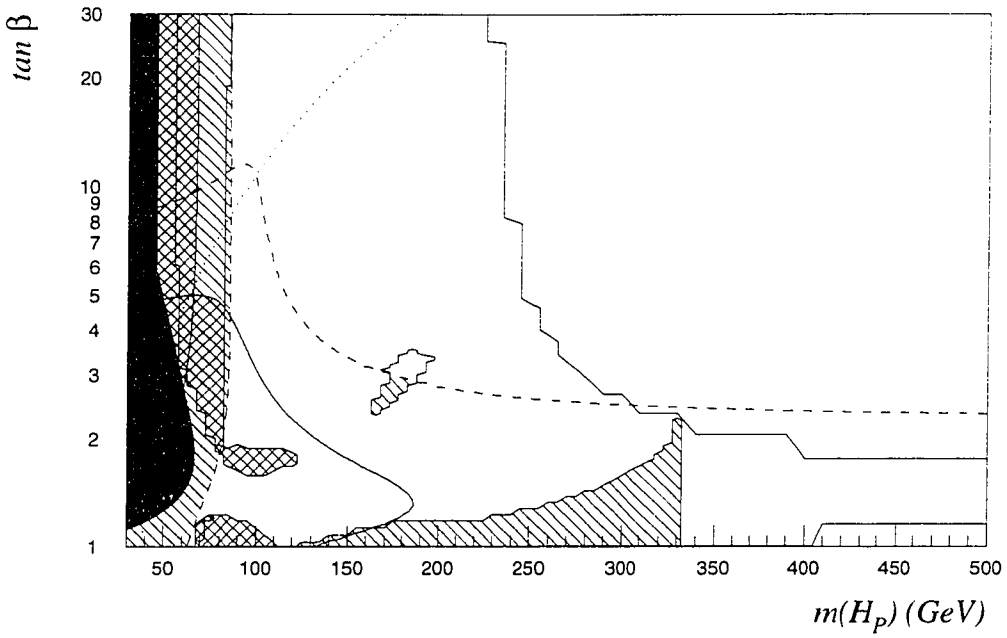

Figure 6.13: Regions where > 1 MSSM Higgs boson type observable at LEP II and/or LHC. The cross-hatched regions assume conservative LEP II operating capabilities, while the diagonally shaded regions require the more optimistic LEP II features. $m_{\tilde{g}} = -\mu = 1000\,\mathrm{GeV} \doteq m_{\tilde{q}}$. Other MSSM input parameters as in Figure 2.10.

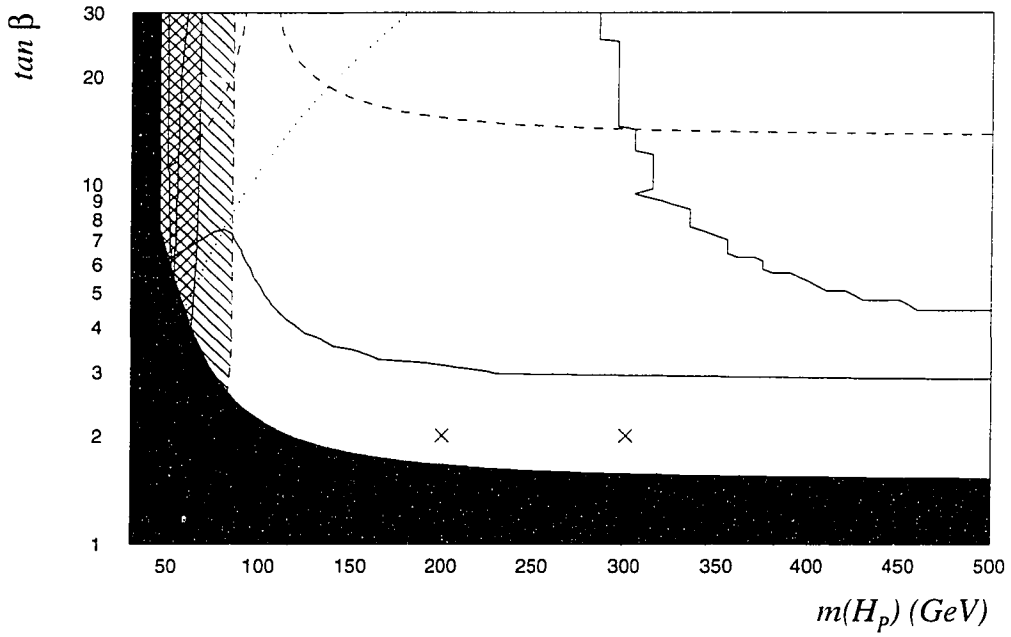

Figure 6.14: Regions where > 1 MSSM Higgs boson type observable at LEP II and/or LHC. $m_{\tilde{g}} = -\mu = 300\,\mathrm{GeV} \doteq m_{\tilde{q}}$. See Figure 6.12 above for further explanation.

Several aspects of these figures deserve some elaboration:

- The $H_h \to 4\ell$ mode is only viable with high MSSM inputs in quite limited regions of the parameter space. It is hampered by the $H_h \to H_\ell H_\ell$ decay which can be the overwhelmingly-dominant decay mode of the heavy Higgs boson in this zone, as illustrated in Figure 6.15. This latter decay receives

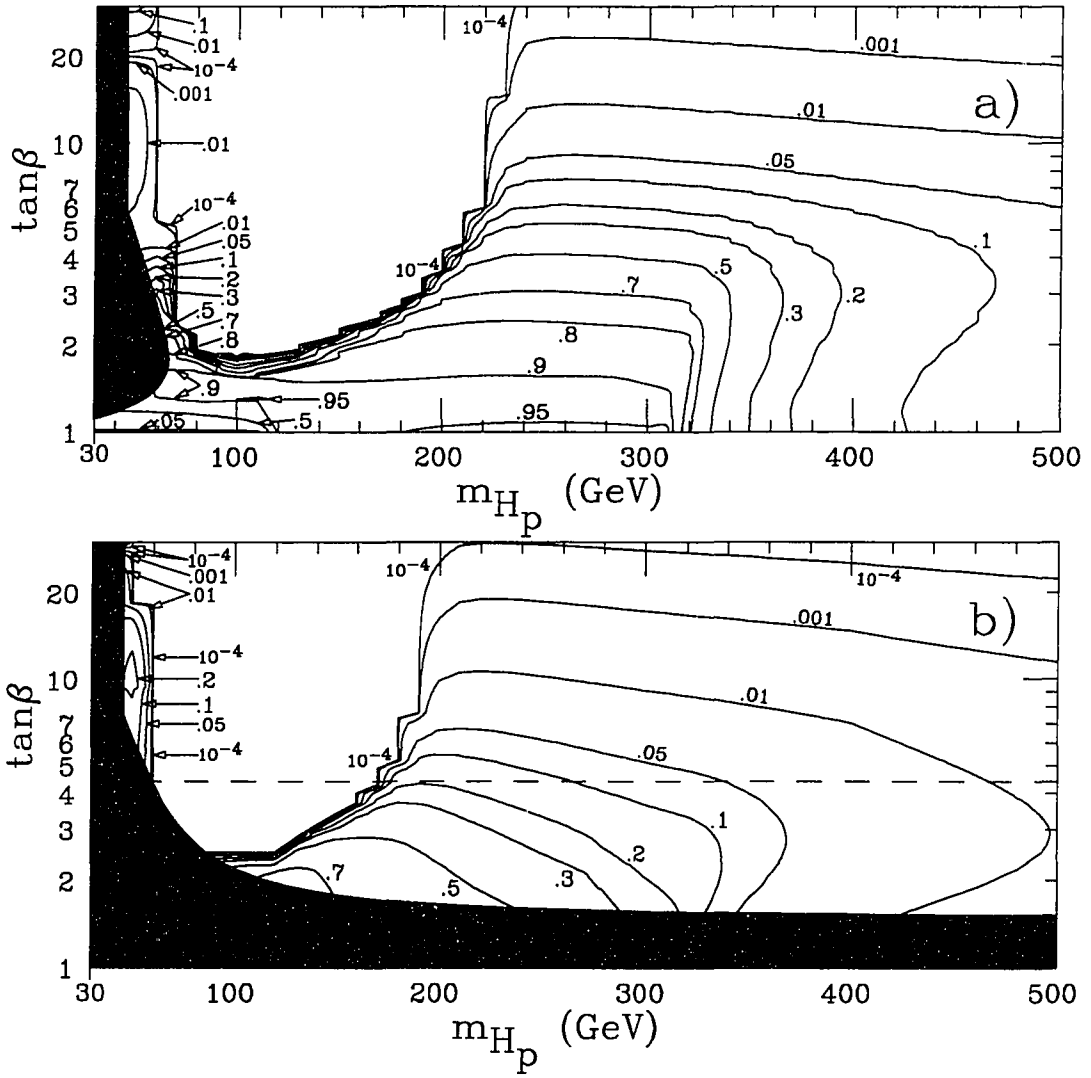

Figure 6.15: $B.R.(H_h \to H_\ell H_\ell)$. The U-shaped region where the branching ratio goes to zero corresponds to where $m_{H_h} < 2m_{H_\ell}$. The sharp edges seen here are an artifact of the grid size used in making the contour plot. MSSM parameters: $m_{\tilde{g}} = -\mu = 1000\,\text{GeV} \doteq m_{\tilde{q}}$ in plot a), and $m_{\tilde{g}} = -\mu = 300\,\text{GeV} \doteq m_{\tilde{q}}$ in plot b). (Other parameters as in Fig. 3.8.)

very significant radiative corrections and was probably under-estimated in previous analyses, leading to a larger detectability zone for the "gold-plated" signal than that depicted here.

- The $H_\ell \to \gamma\gamma$ signal would be essentially unobservable over the whole plane in Figure 6.5 if a data sample of "just" $30\,\text{fb}^{-1}$ was assumed. This is a reflection of the fact that the position of this contour is extremely sensitive to the assumptions about the detector. In addition, QCD corrections to both the Higgs boson production and decay (as noted in Chapters 3 and 4, respectively) not incorporated into the $\gamma\gamma$ analysis may noticeably displace this contour. In addition, the high branching ratio for the decay $H_h \to H_\ell H_\ell$ in the low $\tan\beta$ and moderate to low m_{H_p} region will enhance the $H_\ell \to \gamma\gamma$ signal region in this area. Preliminary analysis shows that, for the case of high sparticle masses ($m_{\tilde{g}} = -\mu = 1000\,\text{GeV} \doteq m_{\tilde{q}}$), the $H_\ell \to \gamma\gamma$ signal region is extended to include a narrow strip of $1 \lesssim \tan\beta \lesssim 1.2$ for $m_{H_p} \gtrsim 125\,\text{GeV}$, and a bar-shaped region of $1 \lesssim \tan\beta \lesssim 2$ and $300\,\text{GeV} \lesssim m_{H_p} \lesssim 325\,\text{GeV}$. This could be significant since it overlaps with about 50% of the $H_p \to \gamma\gamma$ signal region. However, events with H_ℓ's coming from H_h decays are expected to have different characteristics from those from direct H_ℓ production owing to the relatively high p_T an H_ℓ from a decaying H_h is likely to have. Therefore, light Higgs bosons produced via $H_h \to H_\ell H_\ell$ (or via $H_p \to H_\ell Z^0$ or via $H^\pm \to H_\ell W^\pm$) are *not* included in the cross-section that goes into determining the $H_\ell \to \gamma\gamma$ signal region shown.
- The shaded regions in Figures 6.11 and 6.12 are where none of the neutral Higgs bosons of the MSSM are detectable at either the LHC via the 4ℓ and $\gamma\gamma$ modes or at LEP II. This is known colloquially as the "hole." Note that $m_{\widetilde{W}_1} < 90\,\text{GeV}$ throughout much of the 'hole' region in Figure 6.12. If $m_{\widetilde{W}_1} < 90\,\text{GeV}$, then the lighter chargino should be detectable at LEP II.
- The cross-hatched region actually shrinks in going from Figure 6.11 to Figure 6.12 where the sparticle decay channels are significant. This is somewhat misleading because this shrinkage is due to the upward movement of the LEP190 curve. More conservative assumptions about the performance of LEP, as illus-

trated by the LEP175 curve, considerably increase the region where there is no signal either at LEP II, or at the LHC.

- As described at the end of Chapter 2, increasing the value of $|A_t|$, the soft SUSY-breaking triliear coupling for the stop squarks, from its arbitrarily-chosen default value of zero can lower the LEP190 curve considerably. This is due to an increase in m_{H_ℓ} from the radiative corrections, and the corresponding suppression of the cross section for ZH_ℓ production: for $A_t = 400\,\mathrm{GeV}$ or $A_t = -700\,\mathrm{GeV}$, the LEP190 curve roughly follows the LEP175 curve in the figure. Thus, the "hole" in Figure 6.12 may be considerably larger than indicated by the cross-hatched region even with optimistic assumptions about the performance of LEP II.
- The main reason for the change in the $H_\ell \to \gamma\gamma$ boundary when the parameters are altered from 1 TeV to 300 GeV is *not* the opening of the SUSY decays of H_ℓ. The shift occurs primarily because the Higgs mass is lowered due to smaller radiative corrections, pushing it to a lower mass where the $\gamma\gamma$ continuum background is larger — see Figure 4.8b).

Finally, notice that the region of parameters where the signal from two different Higgs bosons is simultaneously detectable is greatly reduced with lowered sparticle masses. It should also be noted that other studies analyzing basically the same signals (47,93,95) also find a "hole" in roughly the same parameter-space location.

One way around the dilemma of the "hole" and the lack of sufficient overlap among the signals of the assorted Higgs boson species is the construction of a $\sim$500 GeV e^+e^- linear collider. Such a machine would be ideal for searching for Higgs bosons whose masses are at most somewhat below the beam energy. Naturally, the e^+e^- machine would be free of the associated QCD noise and initial state uncertainty inherent in a hadron collider. For a recent review of the Higgs boson detection prospects of a 500 GeV e^+e^- linear collider, see the review of Janot [162] from the Waikaloa conference on the study of such an accelerator. It should however be noted that thoughts about such a machine are still in the exploratory phase, and an actual operating device is quite a ways over the horizon as of yet. This would nevertheless be the definitive machine for exploring the MSSM Higgs sector.

As noted in Section 6.1 of this Chapter, at a hadron collider there are other MSSM Higgs boson decay modes which have been proposed as candidates to fill in all or part of the hole. Most notable among these are Higgs boson decays to $b\bar{b}$-pairs accompanied by $t\bar{t}$ production and H_h and H_p decays to τ-pairs. The difficulties with these signals have been discussed in some detail. One can draw from Figures 6.1 and 6.2 a fair idea of what is the potential reach of the $\tau^+\tau^-$ signal. Taking as a guide the 10 pb sensitivity for $m_H \sim 100\,\mathrm{GeV}$ noted in Refs. [47,140], $H_p \to \tau^+\tau^-$ should be observable in the high $\tan\beta$ regions above the dotted curves in Figures 6.5 and 6.6. (Note: for $m_{H_\ell} + M_{Z^0} < m_{H_P} < 2m_t$, $H_\ell \to \tau^+\tau^-$ accompanied by $Z^0 \to \ell^+\ell^-$ might be observable for *low* $\tan\beta$ values, $\tan\beta \lesssim 2-3$ [163].) The $b\bar{b}$ associated production modes have the potential of filling in the entire "hole" region (and then some). Ref. [159] states that at least one, and usually two or three $H \to b\bar{b}$ associated production modes are detectable throughout the parameter space covered by the "hole," given the usual caveats concerning the need for an substantial integrated luminosity and good b-tagging qualities. It is especially important to note that these signals become more pronounced as the mass of the Higgs boson decreases, which is just the opposite of the case for the $\gamma\gamma$ signal. But it is also equally important, if not more important, to caution that obtaining a signal from this process is wholly dependent on the detector having very good b-tagging capabilities. In the high-luminosity environment of LHC, this may not be possible.

In addition to these Higgs boson decays to SM particles, SUSY decays of Higgs bosons are also detectable well into the "hole" region if LEP II is operated at about 175 GeV. Although this is not obvious from the figure, this may also be the case with optimistic assumptions about the performance of LEP II, since, as was mentioned in Section 2.8, even the optimistic LEP II observability curve essentially follows the LEP 175 curve if $|A_t|$ is large, while the Higgs boson to neutralinos signal is relatively insensitive to variations in A_t.

Further use of the additional rich spectrum of sparticles provided with SUSY in the quest to unravel the mysteries of the symmetry-breaking sector should remain the source for a great many studies in the future. If low energy supersymmetry does

indeed describe our Universe, then an extended Higgs sector is obligatory. Up to now, the focus has been on showing conclusively that a Higgs boson, any type of Higgs boson, can be detected. Hopefully a Higgs boson will be discovered, either at the LEP or at the LHC, through one of the channels outlined in this work. Though the vexing doubts concerning the "hole" in the parameter space, in which there is no incontrovertible signal predicted, cast a cloud over this somewhat optimistic outlook — it is at least encouraging to note that there are decay modes to both SM particles and sparticles which may fill in this gap.

Setting aside for the moment the unwelcome contingency of all the MSSM Higgs bosons slipping through the cracks and into the "hole," after a Higgs boson is discovered, attention will then shift to the search for additional Higgs boson species (as well as to the measurement of the discovered Higgs boson's couplings). It is very unlikely that measuring the rate from the discovery channel of the first Higgs boson will enable physicists to piece together the structure of the electroweak symmetry-breaking sector, or even conclude that a supersymmetric theory is valid (recall that for many choices of the MSSM parameters, H_ℓ does a very good imitation of a SM Higgs boson). Discovering the other Higgs bosons predicted by supersymmetry seems mandatory. Yet examining Figures 6.13 and 6.14 illustrates that there are very few regions of overlap for the conventional signals from the SM decays of the MSSM Higgs bosons. Ref. [159] indicated significant regions of overlap will exist if the b-tagging associated production signals can be exploited to the degree contemplated. In addition, the myriad of possiblities opened up through full use of the MSSM sparticle spectrum offers great prospects for clarifying the situation. For a great many choices of the MSSM input parameters, including those inspired by supergravity and GUT theories, there will be neutralinos and charginos with masses light enough to be accessible for the decays of the heavier Higgs boson species. Since the light Higgs boson is the only Higgs boson species detectable by the convention SM signals displayed in Figures 6.5 and 6.6 over large regions of the MSSM parameter space, sparticle decay signals from the heavier MSSM Higgs boson species could greatly increase the amount of parameter space in which there are overlapping signals.

In Chapter 5, this work began the investigation into these supersymmetric decay modes of the MSSM Higgs bosons. The main conclusions obtained thus far are that:

- If open, the supersymmetric decay modes of the Higgs bosons can appreciably cut into the parameter space that would have been searchable via the conventional SM decay modes if the Higgs bosons to sparticles decays were all closed.
- New signals can exist from the heavier neutral Higgs bosons decaying into neutralinos which in turn decay leptonically. In particular, the decay chains,

$$H_h, H_p \rightarrow \widetilde{Z}_2\widetilde{Z}_2 \rightarrow 4\,\text{charged leptons} + 2\,\widetilde{Z}_1\,(\Rightarrow \not{E}_T) \quad ,$$

  stand out conspicuously above the SM backgrounds over a large patch of the MSSM parameter space, including part of the "hole" region. This new signal region also overlaps with the region in which the light Higgs boson is detectable via its SM decays at LHC or LEP II.

Future work in this area will probably yield more signal modes. While none of these may be dramatic, taken as a whole they can probably aid significantly in teasing out the exact structure of the electroweak symmetry-breaking sector of the MSSM. The usefulness of the Higgs boson to spartcles decay modes should also be further investigated within the additional contraints imposed by supergravity and GUT theories. Since μ and m_{H_p} are determined in a supergravity theory; that is, they are not free parameters, the amount of parameter phase space in greatly reduced. This should tend to favor the possibility that some rather definite predictions can be made [164].

The supersymmetric decay modes of the charged Higgs bosons also merit further attention. The existence of charged Higgs bosons is a crucial prediction of an extended Higgs sector, and discovery of a charged Higgs boson would provide clear, unequivocal proof for an extended sector. Yet the most uncontestable signal we have for a charged Higgs boson is via top decays, which is clearly only valid for rather low values of $m_{H_{ch}}$. Such values are already disfavored by $b \rightarrow s\,\gamma$ measurements. Supersymmetric decay modes, on the other hand, will only open up if the charged Higgs boson is sufficiently heavy. Thus they might offer an avenue for the detection

of a charged Higgs bosons thoughout much of MSSM parameter space. (Studies of the main SM decay mode for a heavy charged Higgs boson, $H^+ \to t\bar{b}$, have been performed, and they suggest signals for $gb \to tH^-$ [165] or $gg \to H^-t\bar{b} + H^+b\bar{t}$ [166] might be discernable in some regions of the MSSM parameter space, given adequate b-tagging capabilities.) In addition, associated production modes, which have already received considerable attention in connection with the b-quark and $\ell\gamma\gamma$ Higgs boson signals, have yet to be investigated for the supersymmetric decay modes. Since the branching fractions of the Higgs bosons to sparticles can in fact be quite high, as seen in Figures 5.1-5.7, there is some chance that signals can be obtained from these production channels despite the large drop in the production rates over the inclusive Higgs boson production processes. In particular, the associated production of a charged Higgs boson with top quarks or gauge bosons makes possible four lepton signals similar to those studied for the neutral Higgs bosons. In fact, the main production mode of the charged Higgs boson, $gb \to tH^-$, leads to an associated top quark. More study of this process seems warranted, and will soon be underway.

Appendix A

MSSM Higgs Masses & Couplings

A.1 The Scalar Potential — Tree-Level

The most general Lagrangian compatible with supersymmetry is of the form (see [15] and references therein):

$$\begin{aligned}
\mathcal{L} \;=\; & \sum_i (D_\mu \mathcal{S}_i)^\dagger (D^\mu \mathcal{S}_i) \;+\frac{i}{2}\sum_i \overline{\psi}_i \not{D}\psi_i \\
& -\frac{1}{4}\sum_A F_{\mu\nu A}F^{\mu\nu}{}_A \;+\frac{i}{2}\sum_A \overline{\lambda}_A \not{D}\lambda_A \\
& -\sqrt{2}\sum_i \left[\mathcal{S}_i^\dagger (t_A)\overline{\psi}_i \frac{1-\gamma_5}{2}\lambda_A \;+\; \text{h.c.}\right] \\
& -\frac{1}{2}\sum_A \left[\sum_i \mathcal{S}_i^\dagger t_A \mathcal{S}_i \;+\xi_A\right]^2 \\
& -\sum_i \left|\frac{\partial f}{\partial S_i}\right|^2_{S=\mathcal{S}} \\
& -\frac{1}{2}\sum_{i,j}\left\{\overline{\psi}_i\left[\frac{1-\gamma_5}{2}\right]\left[\frac{\partial^2 f}{\partial S_i\,\partial S_j}\right]_{S=\mathcal{S}}\psi_j \;+\; \text{h.c.}\right\} \;. \qquad \text{(A.1)}
\end{aligned}$$

The Higgs sector of the Minimal Supersymmetric Standard Model (MSSM) is composed of two doublet scalar fields $\mathrm{H} = \begin{pmatrix} h^+ \\ h^0 \end{pmatrix}$ and $\mathrm{H}' = \begin{pmatrix} h'^- \\ h'^0 \end{pmatrix}$, where H′ is a representation $\underline{\mathbf{2}}^*$ SU(2) doublet, and so the corresponding $\underline{\mathbf{2}}$ doublet is $\begin{pmatrix} -h'^0 \\ h'^- \end{pmatrix}$. Here h^+, h^0, h'^-, and h'^0 are all complex scalar fields. With these definitions, the superpotential, f, for the MSSM is of the form (see [15]):

$$\begin{aligned}
f \;=\; & -2m_1(\hat{h}^0\hat{h}'^0 + \hat{h}^+\hat{h}'^-) \;+f_u(\hat{u}\hat{h}^0 - \hat{d}\hat{h}^+)\hat{U}^c \\
& +f_d(\hat{u}\hat{h}'^- + \hat{d}\hat{h}'^0)\hat{D}^c \;+f_e(\hat{\nu}\hat{h}'^- + \hat{e}\hat{h}'^0)\hat{E}^c \;+\ldots \;. \qquad \text{(A.2)}
\end{aligned}$$

Here the hats above the fields signify that these are superfields. From this we may derive the scalar potential for the case of the MSSM. This is done below and is also used as an opportunity to introduce some notation to be used for the MSSM parameters.

We begin by considering the scalar interactions from the fourth line above. For the U(1) terms we have,

$$\begin{aligned}
[\quad] &= (h^{+*} \quad h^{0*})\, g' \frac{Y}{2} \begin{pmatrix} h^+ \\ h^0 \end{pmatrix} + (-h'^{0*} \quad h'^{-*})\, g' \frac{Y'}{2} \begin{pmatrix} -h'^0 \\ h'^- \end{pmatrix} + 0 \\
&= \frac{g'}{2}\Big((|h^+|^2 + |h^0|^2) - (|h'^0|^2 + |h'^-|^2)\Big)
\end{aligned}$$

where the Fayet-Iliopoulos term [169], ξ_A, has been set to zero by choice ($\xi_A = 0$ if the MSSM is embedded in a GUT theory). Thus for the U(1) terms we have

$$\mathcal{V}_{U(1)} = \frac{1}{2}\frac{g'^2}{4}\Big[|h^+|^2 + |h^0|^2 - |h'^0|^2 - |h'^-|^2\Big]^2 = \frac{g'^2}{8}\Big[|\mathrm{H}|^2 - |\mathrm{H}'|^2\Big]^2 \quad . \text{(A.3)}$$

For the SU(2) component,

$$[\quad] = (h^{+*} \quad h^{0*})\, t_a \begin{pmatrix} h^+ \\ h^0 \end{pmatrix} + (-h'^{0*} \quad h'^{-*})\, t_a \begin{pmatrix} -h'^0 \\ h'^- \end{pmatrix} \quad ,$$

where $2t_a$ are the Pauli spin matices times the SU(2) coupling constant. Thus,

$$\begin{aligned}
\sum_a [\quad]^2 = \sum_a \Big\{ & (h^{+*} \quad h^{0*})\, t_a \begin{pmatrix} h^+ \\ h^0 \end{pmatrix} (h^{+*} \quad h^{0*})\, t_a \begin{pmatrix} h^+ \\ h^0 \end{pmatrix} \\
& + 2(h^{+*} \quad h^{0*})\, t_a \begin{pmatrix} h^+ \\ h^0 \end{pmatrix} (-h'^{0*} \quad h'^{-*})\, t_a \begin{pmatrix} -h'^0 \\ h'^- \end{pmatrix} \\
& + (-h'^0 \quad h'^-)\, t_a \begin{pmatrix} -h'^0 \\ h'^- \end{pmatrix} (-h'^{0*} \quad h'^{-*})\, t_a \begin{pmatrix} -h'^0 \\ h'^- \end{pmatrix} \Big\} \quad .
\end{aligned}$$

And so

$$\begin{aligned}
\mathcal{V}_{SU(2)} = \frac{g^2}{8}\Big\{ & (h^{+*}h^0 + h^{0*}h^+)^2 - 2(h^{+*}h^0 + h^{0*}h^+)(h'^{0*}h'^- + h'^{-*}h'^0) \\
& + (h'^{0*}h'^- + h'^{-*}h'^0)^2 - (-h^{+*}h^0 + h^{0*}h^+)^2 \\
& - 2(-h^{+*}h^0 + h^{0*}h^+)(h'^{0*}h'^- - h'^{-*}h'^0) - (h'^{0*}h'^- - h'^{-*}h'^0)^2 \\
& + (|h^+|^2 - |h^0|^2)^2 + 2(|h^+|^2 - |h^0|^2)(|h'^0|^2 - |h'^-|^2) \\
& + (|h'^0|^2 - |h'^-|^2)^2 \Big\}
\end{aligned}$$

$$= \frac{g^2}{8}\Big\{(|h^+|^2 - |h^0|^2 + |h'^0|^2 - |h'^-|^2)^2 + 4|h^+|^2|h^0|^2 + 4|h'^0|^2|h'^-|^2 - 4(h^{+*}h'^{-*}h^0h'^0 + h^{0*}h'^{0*}h^+h'^-)\Big\} \quad . \tag{A.4}$$

Contributions also arise from the superpotential terms in line five of Eqn. (A.1). Specifically, for $f_h = -2m_1(\hat{h}^0\hat{h}'^0 + \hat{h}^+\hat{h}'^-)$,

$$\left.\frac{\partial f_h}{\partial \hat{h}^0}\right|_{\hat{h}=h} = -2m_1h'^0 \quad \left.\frac{\partial f_h}{\partial \hat{h}'^0}\right|_{\hat{h}=h} = -2m_1h^0$$
$$\left.\frac{\partial f_h}{\partial \hat{h}^+}\right|_{\hat{h}=h} = -2m_1h'^- \quad \left.\frac{\partial f_h}{\partial \hat{h}'^-}\right|_{\hat{h}=h} = -2m_1h^+ \tag{A.5}$$

$$\Longrightarrow \quad \left|\tfrac{\partial f_h}{\partial \hat{h}^0}\right|^2_{\hat{h}=h} = (2m_1)^2|h'^0|^2 \quad \left|\tfrac{\partial f_h}{\partial \hat{h}'^0}\right|^2_{\hat{h}=h} = (2m_1)^2|h^0|^2$$
$$\left|\tfrac{\partial f_h}{\partial \hat{h}^+}\right|^2_{\hat{h}=h} = (2m_1)^2|h'^-|^2 \quad \left|\tfrac{\partial f_h}{\partial \hat{h}'^-}\right|^2_{\hat{h}=h} = (2m_1)^2|h^+|^2$$

$$\text{This yields} \qquad \mathcal{V}_{sp} = (2m_1)^2\Big(|h^0|^2 + |h'^0|^2 + |h^+|^2 + |h'^-|^2\Big) \tag{A.6}$$

Finally, we must consider contributions from soft supersymmetry breaking terms [16]. These are resticted to be gauge-invariant terms of mass dimension three or lower. The allowable dimension-two terms are just

$$\bar{m}_1^2\begin{pmatrix} h^{+*} & h^{0*}\end{pmatrix}\begin{pmatrix} h^+ \\ h^0\end{pmatrix} = \bar{m}_1^2(|h^0|^2 + |h^+|^2)$$
$$\bar{m}_2^2\begin{pmatrix} -h'^{0*} & h'^{-*}\end{pmatrix}\begin{pmatrix} -h'^0 \\ h'^-\end{pmatrix} = \bar{m}_2^2(|h'^0|^2 + |h'^-|^2) \tag{A.7}$$
$$-\bar{m}_{12}^2\begin{pmatrix} h^+ & h^0\end{pmatrix}\epsilon_{ij}\begin{pmatrix} -h'^0 \\ h'^-\end{pmatrix} + \text{h.c.} = \bar{m}_{12}^2(h^+h'^- + h^0h'^0 + \text{h.c.})$$

where $\epsilon_{21} = -\epsilon_{12} = 1$ and $\epsilon_{11} = \epsilon_{22} = 0$ (to contract doublets in a gauge-invariant fashion). The dimension-three terms are just the cubic terms of the superpotential f plus their hermitian conjugates. But since none of the cubic terms in f is composed solely of Higgs fields, these do not contribute to the potential. Thus the soft supersymmetry breaking contribution to the scalar potential is

$$\mathcal{V}_{soft} = \bar{m}_1^2(|h^0|^2 + |h^+|^2) + \bar{m}_2^2(|h'^0|^2 + |h'^-|^2) + \bar{m}_{12}^2(h^+h'^- + h^0h'^0 + \text{h.c.}) \tag{A.8}$$

Now we may add $\mathcal{V}_{sp}$ plus $\mathcal{V}_{soft}$ to obtain

$$\begin{aligned}\mathcal{V}_{sp} + \mathcal{V}_{soft} &= (\bar{m}_1^2 + (2m_1)^2)(|h^0|^2 + |h^+|^2) + (\bar{m}_2^2 + (2m_1)^2)(|h'^0|^2 + |h'^-|^2) \\ &\quad + \bar{m}_{12}^2(h^+h'^- + h^0h'^0 + \text{h.c.}) \\ &= m^2(|h^0|^2 + |h^+|^2) + m'^2(|h'^0|^2 + |h'^-|^2) \\ &\quad + \bar{m}_{12}^2(h^+h'^- + h^0h'^0 + \text{h.c.}) \quad , \end{aligned} \tag{A.9}$$

where $m^2 \equiv \bar{m}_1^2 + (2m_1)^2$ and $m'^2 \equiv \bar{m}_2^2 + (2m_1)^2$.

Putting all the contributions together yields

$$\begin{aligned}\mathcal{V}_{tree} &= m^2(|h^0|^2 + |h^+|^2) + m'^2(|h'^0|^2 + |h'^-|^2) \\ &\quad + \bar{m}_{12}^2(h^+h'^- + h^0h'^0 + \text{h.c.}) \\ &\quad + \frac{g^2}{8}\Big\{(|h^+|^2 - |h^0|^2 + |h'^0|^2 - |h'^-|^2)^2 + 4|h^+|^2|h^0|^2 + 4|h'^0|^2|h'^-|^2 \\ &\quad - 4(h^{+*}h'^{-*}h^0h'^0 + h^{0*}h'^{0*}h^+h'^-)\Big\} \\ &\quad + \frac{g'^2}{8}\Big[|h^+|^2 + |h^0|^2 - |h'^0|^2 - |h'^-|^2\Big]^2 \quad . \end{aligned} \tag{A.10}$$

A.2 Tree-level Higgs Masses

The masses for the MSSM Higgs may now be calculated from the scalar potential. First we define

$$h = \frac{1}{\sqrt{2}}(h_R + ih_I) \qquad h' = \frac{1}{\sqrt{2}}(h'_R + ih'_I) \tag{A.11}$$

where h_R, h_I, h'_R, and $h'_I \in \Re$. The minimum of the scalar potential is at

$$\langle \mathrm{H} \rangle = \begin{pmatrix} 0 \\ v \end{pmatrix} \qquad \langle \mathrm{H}' \rangle = \begin{pmatrix} 0 \\ v' \end{pmatrix} \tag{A.12}$$

where v and v' are non-negative real numbers (using the gauge freedom, we can pick the arbitrary phases of the complex Higgs fields to guarantee this). Thus $\langle h_R \rangle = \sqrt{2}v$, $\langle h'_R \rangle = \sqrt{2}v'$, and $\langle h_I \rangle = \langle h'_I \rangle = \langle h^+ \rangle = \langle h'^- \rangle = 0$. This defines the vacuum expectation values (*vev*'s) for the Higgs fields. We can further make the standard definition of the ratio of the expectation values as $\tan\beta = \frac{v}{v'}$.

The formula for the elements of the squared mass matrix now takes the form

$$M_{ij} = \left.\frac{\partial^2 \mathcal{V}}{\partial h_i \partial h_j}\right|_{vev} , \tag{A.13}$$

where h_i, h_j are h_R, h'_R for the scalar Higgs bosons and h_I, h'_I for the pseudoscalar. First we calculate the second derivatives of $\mathcal{V}_{tree}$ with respect to h_I and h'_I:

$$\begin{aligned}\frac{\partial \mathcal{V}_{tree}}{\partial h_I} &= m^2 h_I - \bar{m}_{12}^2 h'_I \\ &+ \tfrac{-1}{4} g^2 \{ h_I (|h'^0|^2 - |h^0|^2 - |h^+|^2 - |h'^-|^2) \\ &\qquad + \sqrt{2} i (h^{+*} h'^{-*} h'^0 - h'^{0*} h^+ h^-) \} \\ &+ \tfrac{1}{4} g'^2 \{ h_I (|h^0|^2 - |h'^0|^2 + |h^+|^2 - |h'^-|^2) \} \quad , \end{aligned} \tag{A.14}$$

and

$$\begin{aligned}\frac{\partial \mathcal{V}_{tree}}{\partial h'_I} &= m'^2 h'_I - \bar{m}_{12}^2 h_I \\ &+ \tfrac{-1}{4} g^2 \{ h'_I (|h^0|^2 - |h'^0|^2 - |h^+|^2 - |h'^-|^2) \\ &\qquad + \sqrt{2} i (h^{+*} h'^{-*} h^0 - h^{0*} h^+ h^-) \} \\ &+ \tfrac{-1}{4} g'^2 \{ h'_I (|h^0|^2 - |h'^0|^2 + |h^+|^2 - |h'^-|^2) \} \quad . \end{aligned} \tag{A.15}$$

But since we have already chosen $\langle h_I \rangle = \langle h'_I \rangle = 0$,

$$\left.\frac{\partial \mathcal{V}_{tree}}{\partial h_I}\right|_{vev} = \left.\frac{\partial \mathcal{V}_{tree}}{\partial h'_I}\right|_{vev} = 0 \tag{A.16}$$

automatically, yielding no constraining equations. For the second derivatives,

$$\begin{aligned}\frac{\partial^2 \mathcal{V}_{tree}}{\partial {h_I}^2} &= m^2 + \tfrac{-1}{4} g^2 \{ |h'^0|^2 - |h^0|^2 - |h^+|^2 - |h'^-|^2 - {h_I}^2 \} \\ &+ \tfrac{-1}{4} g'^2 \{ -|h^0|^2 + |h'^0|^2 - |h^+|^2 + |h'^-|^2 - {h_I}^2 \} \quad , \end{aligned} \tag{A.17}$$

and

$$\begin{aligned}\frac{\partial^2 \mathcal{V}_{tree}}{\partial {h'_I}^2} &= m'^2 + \tfrac{-1}{4} g^2 \{ |h^0|^2 - |h'^0|^2 - |h^+|^2 - |h'^-|^2 - {h'_I}^2 \} \\ &+ \tfrac{-1}{4} g'^2 \{ |h^0|^2 - |h'^0|^2 + |h^+|^2 - |h'^-|^2 - {h'_I}^2 \} \quad , \end{aligned} \tag{A.18}$$

and finally

$$\begin{aligned}\frac{\partial^2 \mathcal{V}_{tree}}{\partial h_I \partial h'_I} &= -\bar{m}_{12}^2 - \tfrac{1}{4}(g^2 + g'^2) h_I h'_I \\ &+ \tfrac{1}{4} g^2 \{ h^+ h'^- + h^{+*} h'^{-*} \} \quad . \end{aligned} \tag{A.19}$$

$$\Longrightarrow \left.\frac{\partial^2 \mathcal{V}_{tree}}{\partial h_I^2}\right|_{vev} = m^2 + \tfrac{1}{4}(g^2+g'^2)(v^2-v'^2)$$
$$\left.\frac{\partial^2 \mathcal{V}_{tree}}{\partial h_I'^2}\right|_{vev} = m'^2 - \tfrac{1}{4}(g^2+g'^2)(v^2-v'^2)$$
$$\left.\frac{\partial^2 \mathcal{V}_{tree}}{\partial h_I \partial h_I'}\right|_{vev} = -\bar{m}_{12}^2 \qquad \text{(A.20)}$$

Now for the derivatives with respect to h_R and h'_R:

$$\begin{aligned}\frac{\partial \mathcal{V}_{tree}}{\partial h_R} &= m^2 h_R - \bar{m}_{12}^2 h'_R \\ &\quad + \tfrac{-1}{4} g^2 \{ h_R(|h'^0|^2 - |h^0|^2 - |h^+|^2 - |h'^-|^2) \\ &\qquad + \sqrt{2}(h^{+*} h'^{-*} h'^0 + h'^{0*} h^+ h^-)\} \\ &\quad + \tfrac{1}{4} g'^2 \{ h_R(|h^0|^2 - |h'^0|^2 + |h^+|^2 - |h'^-|^2)\} \quad , \qquad \text{(A.21)}\end{aligned}$$

and

$$\begin{aligned}\frac{\partial \mathcal{V}_{tree}}{\partial h'_R} &= m'^2 h'_R - \bar{m}_{12}^2 h_R \\ &\quad + \tfrac{-1}{4} g^2 \{ h'_R(|h^0|^2 - |h'^0|^2 - |h^+|^2 - |h'^-|^2) \\ &\qquad + \sqrt{2}(h^{+*} h'^{-*} h^0 + h^{0*} h^+ h^-)\} \\ &\quad + \tfrac{-1}{4} g'^2 \{ h'_R(|h^0|^2 - |h'^0|^2 + |h^+|^2 - |h'^-|^2)\} \quad . \qquad \text{(A.22)}\end{aligned}$$

Notice that if we were to disregard the terms containing h^+ and h'^-, which is perfectly permissible since we are only interested in the values of the derivatives of $\mathcal{V}$ at the minimum where $\langle h^+ \rangle = \langle h'^- \rangle = 0$, then

$$\begin{aligned}\frac{\partial \mathcal{V}_{tree}}{\partial h_R} &\leftrightarrow \frac{\partial \mathcal{V}_{tree}}{\partial h'_R} \text{ when } h_R \leftrightarrow h'_R \\ \frac{\partial \mathcal{V}_{tree}}{\partial h_R} &\leftrightarrow \frac{\partial \mathcal{V}_{tree}}{\partial h_I} \text{ when } h_R \leftrightarrow h_I \qquad \text{(A.23)}\end{aligned}$$

In addition, since the minimum of the potential by definition occurs where the values of the Higgs fields are set equal to their *vev*'s, this is an extremum, and

$$\begin{aligned}\left.\frac{\partial \mathcal{V}_{tree}}{\partial h_R}\right|_{vev} &= \sqrt{2}v\left\{m^2 + \bar{m}_{12}^2 \cot\beta + \tfrac{1}{4}(g^2+g'^2)(v^2-v'^2)\right\} = 0 \quad , \\ \left.\frac{\partial \mathcal{V}_{tree}}{\partial h'_R}\right|_{vev} &= \sqrt{2}v'\left\{m'^2 + \bar{m}_{12}^2 \tan\beta - \tfrac{1}{4}(g^2+g'^2)(v^2-v'^2)\right\} = 0 \quad . \text{(A.24)}\end{aligned}$$

Thus we have the conditions:

$$m^2 + \bar{m}_{12}^2 \cot\beta \;+\; \tfrac{1}{4}(g^2+g'^2)(v^2-v'^2) = 0 \qquad \text{(A.25)}$$

$$\text{and} \qquad m'^2 + \bar{m}_{12}^2 \tan\beta \;-\; \tfrac{1}{4}(g^2+g'^2)(v^2-v'^2) = 0 \quad . \qquad \text{(A.26)}$$

For the second derivatives,

$$\begin{aligned}\frac{\partial^2 \mathcal{V}_{tree}}{\partial {h_R}^2} \;&=\; m^2 \;+\; \tfrac{-1}{4}g^2\{|h'^0|^2 - |h^0|^2 - |h^+|^2 - |h'^-|^2 - {h_R}^2\} \\ &+\; \tfrac{-1}{4}g'^2\{-|h^0|^2 + |h'^0|^2 - |h^+|^2 + |h'^-|^2 - {h_R}^2\} \quad , \qquad \text{(A.27)}\end{aligned}$$

$$\begin{aligned}\text{and} \quad \frac{\partial^2 \mathcal{V}_{tree}}{\partial {h'_R}^2} \;&=\; m'^2 \;+\; \tfrac{-1}{4}g^2\{|h^0|^2 - |h'^0|^2 - |h^+|^2 - |h'^-|^2 - {h'_R}^2\} \\ &+\; \tfrac{-1}{4}g'^2\{|h^0|^2 - |h'^0|^2 + |h^+|^2 - |h'^-|^2 - {h'_R}^2\} \quad , \qquad \text{(A.28)}\end{aligned}$$

$$\begin{aligned}\text{and finally} \quad \frac{\partial^2 \mathcal{V}_{tree}}{\partial h_R \partial h'_R} \;&=\; \bar{m}_{12}^2 \;-\; \tfrac{1}{4}(g^2+g'^2)h_R h'_R \\ &-\; \tfrac{1}{4}g^2\{h^+ h'^- + h^{+*} h'^{-*}\} \quad . \qquad \text{(A.29)}\end{aligned}$$

$$\begin{aligned}\Longrightarrow \quad \left.\frac{\partial^2 \mathcal{V}_{tree}}{\partial {h_R}^2}\right|_{vev} \;&=\; m^2 \;+\; \tfrac{1}{4}(g^2+g'^2)(3v^2-v'^2) \\ \left.\frac{\partial^2 \mathcal{V}_{tree}}{\partial {h'_R}^2}\right|_{vev} \;&=\; m'^2 \;-\; \tfrac{1}{4}(g^2+g'^2)(v^2-3v'^2) \\ \left.\frac{\partial^2 \mathcal{V}_{tree}}{\partial h_R \partial h'_R}\right|_{vev} \;&=\; \bar{m}_{12}^2 - \tfrac{1}{2}vv'(g^2+g'^2) \qquad \text{(A.30)}\end{aligned}$$

Now subtracting zero from these expressions by applying the conditions from Eqns. (A.25) and (A.26) to the first two of these expressions yields:

$$\begin{aligned}\left.\frac{\partial^2 \mathcal{V}_{tree}}{\partial {h_R}^2}\right|_{vev} = \left.\frac{\partial^2 \mathcal{V}_{tree}}{\partial {h_R}^2}\right|_{vev} - \frac{1}{\sqrt{2}v}\left.\frac{\partial \mathcal{V}_{tree}}{\partial h_R}\right|_{vev} \;&=\; -\bar{m}_{12}^2 \cot\beta \;+\; \frac{v^2}{2}(g^2+g'^2) \\ \left.\frac{\partial^2 \mathcal{V}_{tree}}{\partial {h'_R}^2}\right|_{vev} = \left.\frac{\partial^2 \mathcal{V}_{tree}}{\partial {h'_R}^2}\right|_{vev} - \frac{1}{\sqrt{2}v'}\left.\frac{\partial \mathcal{V}_{tree}}{\partial h'_R}\right|_{vev} \;&=\; -\bar{m}_{12}^2 \tan\beta \;+\; \frac{v'^2}{2}(g^2+g'^2) \\ \left.\frac{\partial^2 \mathcal{V}_{tree}}{\partial h_R \partial h'_R}\right|_{vev} \;&=\; \bar{m}_{12}^2 - \frac{vv'}{2}(g^2+g'^2) \qquad \text{(A.31)}\end{aligned}$$

Further, applying Eqns. (A.25) and (A.26) to Eqns. (A.20) yields:

$$\begin{aligned}
\left.\frac{\partial^2 \mathcal{V}_{tree}}{\partial {h_I}^2}\right|_{vev} &= \left.\frac{\partial^2 \mathcal{V}_{tree}}{\partial {h_I}^2}\right|_{vev} - \left.\frac{1}{\sqrt{2}v}\frac{\partial \mathcal{V}_{tree}}{\partial h_R}\right|_{vev} &= -\bar{m}_{12}^2 \cot\beta \\
\left.\frac{\partial^2 \mathcal{V}_{tree}}{\partial {h'_I}^2}\right|_{vev} &= \left.\frac{\partial^2 \mathcal{V}_{tree}}{\partial {h'_I}^2}\right|_{vev} - \left.\frac{1}{\sqrt{2}v'}\frac{\partial \mathcal{V}_{tree}}{\partial h'_R}\right|_{vev} &= -\bar{m}_{12}^2 \tan\beta \\
& \left.\frac{\partial^2 \mathcal{V}_{tree}}{\partial h_I \partial h'_I}\right|_{vev} &= -\bar{m}_{12}^2
\end{aligned} \tag{A.32}$$

The tree level masses of the neutral Higgs bosons may now be determined by diagonalizing the appropriate Higgs mass squared matrix. The matrix has the form

$$\begin{pmatrix} A & B \\ B & C \end{pmatrix} \tag{A.33}$$

And so the eigenvalues are found from

$$\begin{vmatrix} \lambda - A & -B \\ -B & \lambda - C \end{vmatrix} = \lambda^2 - (A+C)\lambda + AC - B^2 = 0$$

$$\begin{aligned}
\Longrightarrow \lambda &= \frac{1}{2}\left[(A+C) \pm \sqrt{(A+C)^2 + 4(AC - B^2)}\right] \\
&= \frac{1}{2}\left[(A+C) \pm \sqrt{(A-C)^2 + 4B^2}\right]
\end{aligned} \tag{A.34}$$

For the imaginary parts of the Higgs fields, which are associated with the so-called pseudoscalar Higgs boson (see Chapter 1 for the rationale behind this appellation),

$$\mathcal{M}_{H_p^2}^{tree} = \begin{bmatrix} \left.\frac{\partial^2 \mathcal{V}_{tree}}{\partial {h_I}^2}\right|_{vev} & \left.\frac{\partial^2 \mathcal{V}_{tree}}{\partial h_I \partial h'_I}\right|_{vev} \\ \left.\frac{\partial^2 \mathcal{V}_{tree}}{\partial h_I \partial h'_I}\right|_{vev} & \left.\frac{\partial^2 \mathcal{V}_{tree}}{\partial {h'_I}^2}\right|_{vev} \end{bmatrix} = \begin{bmatrix} -\bar{m}_{12}^2 \cot\beta & -\bar{m}_{12}^2 \\ -\bar{m}_{12}^2 & -\bar{m}_{12}^2 \tan\beta \end{bmatrix} \tag{A.35}$$

$$\text{Then} \qquad \det(\lambda \mathcal{I} - \mathcal{M}_{H_p^2}^{tree}) = \lambda[\lambda + \bar{m}_{12}^2(\tan\beta + \cot\beta)] = 0$$

$$\Longrightarrow \lambda = 0 \quad \text{or} \quad \lambda = \frac{-\bar{m}_{12}^2}{\sin\beta\cos\beta} = \frac{-2\bar{m}_{12}^2}{\sin 2\beta} \quad . \tag{A.36}$$

The Goldstone mode which was "eaten" to give mass to the Z^0 gauge boson is thus uncovered along with the mass of the pseudoscalar Higgs boson:

$$m_{Goldstone^0} = 0 \quad \text{and} \quad m^2_{H_p} = \frac{-2\bar{m}^2_{12}}{\sin 2\beta} \quad . \tag{A.37}$$

The corresponding eigenvectors are readily found to be

$$\mathcal{G}^0 = h_I \sin\beta - h'_I \cos\beta \tag{A.38}$$

$$\Phi_p = h_I \cos\beta + h'_I \sin\beta \tag{A.39}$$

Plugging the expression for $m^2_{H_p}$ into the CP-even squared mass matrix terms gives:

$$\begin{aligned} A &= -\bar{m}^2_{12}\cot\beta + \frac{v^2}{2}(g^2+g'^2) = m^2_{H_p}\cos^2\beta + m^2_{Z^0}\sin^2\beta \\ B &= \bar{m}^2_{12} - \frac{vv'}{2}(g^2+g'^2) = -(m^2_{H_p} + m^2_{Z^0})\sin\beta\cos\beta \\ C &= -\bar{m}^2_{12}\tan\beta + \frac{v'^2}{2}(g^2+g'^2) = m^2_{H_p}\sin^2\beta + m^2_{Z^0}\cos^2\beta \end{aligned} \tag{A.40}$$

$$\Rightarrow A + C = m^2_{H_p} + m^2_{Z^0} \ , \quad AC - 4B^2 = m^2_{H_p} m^2_{Z^0}\cos^2 2\beta \quad , \tag{A.41}$$

where $m^2_{Z^0} = \frac{1}{2}(g^2+g'^2)\sum vev\text{'s} = \frac{1}{2}(g^2+g'^2)(v^2+v'^2)$ (with the definition of the vev's given above, which differs from that in Halzen and Martin[170] - Eqns. (15.15) and (15.21)) and $\sin^2\beta = \frac{v^2}{v^2+v'^2}$, $\cos^2\beta = \frac{v'^2}{v^2+v'^2}$, have been used. Thus,

$$\mathcal{M}^{tree}_{H^2_\ell, H^2_h} = \begin{bmatrix} \left.\frac{\partial^2 \mathcal{V}_{tree}}{\partial h_R{}^2}\right|_{vev} & \left.\frac{\partial^2 \mathcal{V}_{tree}}{\partial h_R \partial h'_R}\right|_{vev} \\ \left.\frac{\partial^2 \mathcal{V}_{tree}}{\partial h_R \partial h'_R}\right|_{vev} & \left.\frac{\partial^2 \mathcal{V}_{tree}}{\partial h'_R{}^2}\right|_{vev} \end{bmatrix}$$

$$= \begin{bmatrix} m^2_{H_p}\cos^2\beta + m^2_{Z^0}\sin^2\beta & -(m^2_{H_p} + m^2_{Z^0})\sin\beta\cos\beta \\ -(m^2_{H_p} + m^2_{Z^0})\sin\beta\cos\beta & m^2_{H_p}\sin^2\beta + m^2_{Z^0}\cos^2\beta \end{bmatrix} \tag{A.42}$$

$$\text{And so} \qquad \det(\lambda\mathcal{I} - \mathcal{M}^{tree}_{H^2_\ell, H^2_h}) = 0$$

$$\Longrightarrow m^2_{H_h}, m^2_{H_\ell} = \frac{1}{2}[m^2_{H_p} + m^2_{Z^0} \pm \sqrt{(m^2_{H_p} + m^2_{Z^0})^2 + 4m^2_{H_p} m^2_{Z^0}\cos^2 2\beta}\,] \tag{A.43}$$

A.3 Tree-level Scalar Higgs Mixing angle α

For the two CP-even neutral Higgs bosons, referred to as the light and heavy Higgs bosons, we may define a mixing angle α, following the convention of [116], by

$$\begin{aligned} H_\ell &= (h_R - \sqrt{2}v)\cos\alpha + (h'_R - \sqrt{2}v')\sin\alpha \\ H_h &= -(h_R - \sqrt{2}v)\sin\alpha + (h'_R - \sqrt{2}v')\cos\alpha \end{aligned} \tag{A.44}$$

(with $0 \leq \alpha \leq \frac{\pi}{2}$) defining the contribution of the Higgs doublet coupling to the up-type quarks, H, to the physical light Higgs boson, H_ℓ, etc. This will then go into determining the coupling strengths and thus the decay widths of the physical Higgs bosons to the various quarks and leptons and their supersymmetric partners as well as the neutralinos and charginos. Inverting the equations above gives

$$\begin{aligned} h_R &= H_\ell \cos\alpha - H_h \sin\alpha + \sqrt{2}v \\ h'_R &= H_\ell \sin\alpha + H_h \cos\alpha + \sqrt{2}v' \quad , \end{aligned} \tag{A.45}$$

$$\Rightarrow \frac{\partial \mathcal{V}}{\partial H_\ell} = \Big(\frac{\partial h_R}{\partial H_\ell}\frac{\partial}{\partial h_R} + \frac{\partial h'_R}{\partial H_\ell}\frac{\partial}{\partial h'_R}\Big)\mathcal{V} = \cos\alpha \frac{\partial \mathcal{V}}{\partial h_R} + \sin\alpha \frac{\partial \mathcal{V}}{\partial h'_R} \tag{A.46}$$

$$\frac{\partial^2 \mathcal{V}}{\partial {H_\ell}^2} = \cos^2\alpha \frac{\partial^2 \mathcal{V}}{\partial h_R} + 2\cos\alpha\sin\alpha \frac{\partial^2 \mathcal{V}}{\partial h_R \partial h'_R} + \sin^2\alpha \frac{\partial^2 \mathcal{V}}{\partial {h'_R}^2} \tag{A.47}$$

$$\frac{\partial^2 \mathcal{V}}{\partial H_h^2} = \sin^2\alpha \frac{\partial^2 \mathcal{V}}{\partial h_R} - 2\cos\alpha\sin\alpha \frac{\partial^2 \mathcal{V}}{\partial h_R \partial h'_R} + \cos^2\alpha \frac{\partial^2 \mathcal{V}}{\partial {h'_R}^2} \tag{A.48}$$

Then $\left.\frac{\partial^2 \mathcal{V}}{\partial H_\ell^2}\right|_{vev} = m^2_{H_\ell}$ and $\left.\frac{\partial^2 \mathcal{V}}{\partial H_h^2}\right|_{vev} = m^2_{H_h}$ leads to

$$\begin{aligned} m^2_{H_\ell} &= A\cos^2\alpha + 2B\sin\alpha\cos\alpha + C\sin^2\alpha \\ m^2_{H_h} &= A\sin^2\alpha - 2B\sin\alpha\cos\alpha + C\cos^2\alpha \end{aligned}$$

$$\Rightarrow m^2_{H_h} - m^2_{H_\ell} = -(A - C)\cos 2\alpha - 2B\sin 2\alpha \quad ; \tag{A.49}$$

and solving this for $\sin 2\alpha$ gives

$$\sin 2\alpha = \frac{-2B}{\sqrt{(A-C)^2+4B^2}} = \frac{-2B}{m_{H_h}^2 - m_{H_\ell}^2}$$
$$\cos 2\alpha = \frac{-(A-C)}{\sqrt{(A-C)^2+4B^2}} = \frac{-(A-C)}{m_{H_h}^2 - m_{H_\ell}^2}$$

$$\Rightarrow \quad \tan 2\alpha = \frac{2B}{A-C} \tag{A.50}$$

$$\begin{aligned} \Longrightarrow \quad \tan\alpha &= \frac{1}{2b}\Big[-(A-C) + \sqrt{(A-C)^2+4B^2}\Big] \\ &= \frac{1}{2b}\Big[-(A-C) + m_{H_h}^2 - m_{H_\ell}^2\Big] \end{aligned} \tag{A.51}$$

A comparison of these equations to those on page 197 of *The Higgs Hunter's Guide*[64] (HHG) yields the following identifications:

Table A.1

This work	*Higgs Hunter's Guide*
A	$\mathcal{M}_{22}$
B	$\mathcal{M}_{12}$
C	$\mathcal{M}_{11}$
m_{H_ℓ}	m_{h^0}
m_{H_h}	m_{H^0}
α	$-\alpha$

For the tree-level case,

$$\tan\alpha = \frac{(m_{H_p}^2 - m_{Z^0}^2)\cos 2\beta - \sqrt{(m_{H_p}^2 + m_{Z^0}^2)^2 + 4m_{H_p}^2 m_{Z^0}^2 \cos^2 2\beta}}{(m_{H_p}^2 + m_{Z^0}^2)\sin 2\beta} \tag{A.52}$$

A.4 Tree-level Charged Higgs Boson Mass

To find the mass of the charged Higgs bosons, the derivatives of $\mathcal{V}_{tree}$, Eqn. (A.10), with respect to the charged complex scalar fields must be calculated:

$$\begin{aligned}\frac{\partial \mathcal{V}_{tree}}{\partial h^+} &= m^2 h^{+*} + \bar{m}_{12}^2 h'^- \\ &+ \tfrac{1}{4}g^2\{h^{+*}(|h'^0|^2 + |h^0|^2 + |h^+|^2 - |h'^-|^2) - 2h^{0*}h'^{0*}h'^-\} \\ &+ \tfrac{1}{4}g'^2\{h^{+*}(|h^0|^2 - |h'^0|^2 + |h^+|^2 - |h'^-|^2)\} \quad , \end{aligned} \tag{A.53}$$

$$\begin{aligned}\frac{\partial \mathcal{V}_{tree}}{\partial h'^-} &= m'^2 h'^{-*} + \bar{m}_{12}^2 h^+ \\ &+ \tfrac{1}{4}g^2\{h'^{-*}(|h'^0|^2 + |h^0|^2 - |h^+|^2 + |h'^-|^2) - 2h^{0*}h'^{0*}h^+\} \\ &+ \tfrac{-1}{4}g'^2\{h'^{-*}(|h^0|^2 - |h'^0|^2 + |h^+|^2 - |h'^-|^2)\} \quad , \end{aligned} \tag{A.54}$$

$$\Longrightarrow \left.\frac{\partial \mathcal{V}_{tree}}{\partial h^+}\right|_{vev} = \left.\frac{\partial \mathcal{V}_{tree}}{\partial h'^-}\right|_{vev} = 0 \tag{A.55}$$

$$\begin{aligned}\frac{\partial^2 \mathcal{V}_{tree}}{\partial h^+ \partial h^{+*}} &= m^2 + \tfrac{1}{4}g^2(|h^0|^2 + |h'^0|^2 + 2|h^+|^2 - |h'^-|^2) \\ &+ \tfrac{1}{4}g'^2(|h^0|^2 - |h'^0|^2 + 2|h^+|^2 - |h'^-|^2) \end{aligned} \tag{A.56}$$

$$\begin{aligned}\frac{\partial^2 \mathcal{V}_{tree}}{\partial h'^- \partial h'^{-*}} &= m'^2 + \tfrac{1}{4}g^2(|h^0|^2 + |h'^0|^2 - |h^+|^2 + 2|h'^-|^2) \\ &+ \tfrac{-1}{4}g'^2(|h^0|^2 - |h'^0|^2 + |h^+|^2 - 2|h'^-|^2) \end{aligned} \tag{A.57}$$

$$\frac{\partial^2 \mathcal{V}_{tree}}{\partial h^+ \partial h'^-} = \bar{m}_{12}^2 - \tfrac{1}{2}g^2 h^{0*}h'^{0*} - \tfrac{1}{4}(g^2 + g'^2)h^{+*}h'^{-*} \tag{A.58}$$

$$\frac{\partial^2 \mathcal{V}_{tree}}{\partial h^{+*} \partial h'^{-*}} = \bar{m}_{12}^2 - \tfrac{1}{2}g^2 h^0 h'^0 + \tfrac{1}{4}(g^2 + g'^2)h^+ h'^- \tag{A.59}$$

$$\begin{aligned}\Longrightarrow \left.\frac{\partial^2 \mathcal{V}_{tree}}{\partial h^+ \partial h^{+*}}\right|_{vev} &= m^2 + \tfrac{g^2}{4}(v^2 + v'^2) + \tfrac{g'^2}{4}(v^2 - v'^2) \\ \left.\frac{\partial^2 \mathcal{V}_{tree}}{\partial h'^- \partial h'^{-*}}\right|_{vev} &= m'^2 + \tfrac{g^2}{4}(v^2 + v'^2) - \tfrac{g'^2}{4}(v^2 - v'^2) \\ \left.\frac{\partial^2 \mathcal{V}_{tree}}{\partial h^+ \partial h'^-}\right|_{vev} &= \left.\frac{\partial^2 \mathcal{V}_{tree}}{\partial h^{+*} \partial h'^{-*}}\right|_{vev} = \bar{m}_{12}^2 - \tfrac{g^2}{2}vv' \end{aligned} \tag{A.60}$$

Now applying Eqns. (A.25) and (A.26) to the above expressions yields:

$$\left.\frac{\partial^2\mathcal{V}_{tree}}{\partial h^+\partial h^{+*}}\right|_{vev} = \left.\frac{\partial^2\mathcal{V}_{tree}}{\partial h^+\partial h^{+*}}\right|_{vev} - \left.\frac{1}{\sqrt{2}v}\frac{\partial\mathcal{V}_{tree}}{\partial h_R}\right|_{vev} = -\bar{m}_{12}^2\cot\beta + \frac{g^2}{2}v'^2$$

$$\left.\frac{\partial^2\mathcal{V}_{tree}}{\partial h'^-\partial h'^{-*}}\right|_{vev} = \left.\frac{\partial^2\mathcal{V}_{tree}}{\partial h'^-\partial h'^{-*}}\right|_{vev} - \left.\frac{1}{\sqrt{2}v'}\frac{\partial\mathcal{V}_{tree}}{\partial h'_R}\right|_{vev} = -\bar{m}_{12}^2\tan\beta + \frac{g^2}{2}v^2$$

$$\left.\frac{\partial^2\mathcal{V}_{tree}}{\partial h^+\partial h'^-}\right|_{vev} = \left.\frac{\partial^2\mathcal{V}_{tree}}{\partial h^{+*}\partial h'^{-*}}\right|_{vev} = \bar{m}_{12}^2 - \frac{g^2}{2}vv' \quad \text{(A.61)}$$

(Note here that one could define the quantities h^- and h'^+ such that $h^- = h^{+*}$ and $h'^+ = h'^{-*}$; however, to avoid confusion it seems better to refrain from this: fields denoted with a plus sign will always be from the H doublet and those denoted with a minus sign will always be from the H′ doublet.) The charged Higgs mass squared matrix is thus

$$\mathcal{M}_{H_{ch}^2}^{tree} = \begin{bmatrix} \left.\frac{\partial^2\mathcal{V}_{tree}}{\partial h^+\partial h^{+*}}\right|_{vev} & \left.\frac{\partial^2\mathcal{V}_{tree}}{\partial h^+\partial h'^-}\right|_{vev} \\ \left.\frac{\partial^2\mathcal{V}_{tree}}{\partial h^{+*}\partial h'^{-*}}\right|_{vev} & \left.\frac{\partial^2\mathcal{V}_{tree}}{\partial h'^-\partial h'^{-*}}\right|_{vev} \end{bmatrix} = \begin{bmatrix} -\bar{m}_{12}^2\cot\beta + \frac{g^2v'^2}{2} & \bar{m}_{12}^2 - \frac{g^2vv'}{2} \\ \bar{m}_{12}^2 - \frac{g^2vv'}{2} & -\bar{m}_{12}^2\tan\beta + \frac{g^2v^2}{2} \end{bmatrix} \quad \text{(A.62)}$$

This is very similar to $\mathcal{M}_{H_p^2}^{tree}$ of Eqn. (A.35), differing only by the addition of the terms proportional to the SU(2) coupling constant and in the signs of the off-diagonal elements. Then

$$\det(\lambda\mathcal{I} - \mathcal{M}_{H_{ch}^2}^{tree}) = \lambda[\lambda + \bar{m}_{12}^2(\tan\beta + \cot\beta - \tfrac{1}{2}g^2(v^2 + v'^2))] = 0$$

$$\Longrightarrow \lambda = 0 \quad \text{or} \quad \lambda = \frac{-\bar{m}_{12}^2}{\sin\beta\cos\beta} + \frac{g^2}{2}(v^2 + v'^2) = m_{H_p}^2 + m_W^2 \quad , \quad \text{(A.63)}$$

where Eqn. (A.37) has been used, along with the relation

$$m_W^2 = m_{Z^0}^2\cos^2\theta_W = m_{Z^0}\frac{g^2}{(g+g')^2} = \tfrac{1}{2}g^2\sum vev\text{'s} = \tfrac{1}{2}g^2(v^2 + v'^2) \quad \text{(A.64)}$$

(as before with $m_{Z^0}^2$, this is with the definition of the vev's used here). The charged Goldstone mode which was "eaten" to give mass to the $W^\pm$ gauge bosons is thus uncovered along with the mass of the charged Higgs bosons ($H_{ch} = H^+$ or H^-):

$$m_{Goldstone^+} = 0 \quad \text{and} \quad m_{H_{ch}}^2 = m_{H_p}^2 + m_W^2 \quad . \quad \text{(A.65)}$$

The corresponding eigenvectors are

$$\mathcal{G}^+ = h^+\sin\beta + h'^{-*}\cos\beta \quad \text{(A.66)}$$

$$\Phi_{ch} = h^+\cos\beta - h'^{-*}\sin\beta \quad \text{(A.67)}$$

A.5 Radiative Corrections: Effective Potential Approximation

It was recognized several years ago that loops involving top quarks and $\tilde{t}$-squarks could lead to significant radiative corrections to the masses of the MSSM Higgs bosons [171-173]. The corrections to the mass of the light Higgs boson were found to be proportional to $m_t^4 \log\left(\frac{m_{\tilde{t}}^4}{m_t^4}\right)$. This is of great phenomenological significance since the tree-level relations of Eqn. (A.43) imply that

$$m_{H_\ell} \leq \min(M_{Z^0}, m_{H_p})|\cos 2\beta| \leq M_{Z^0} \tag{A.68a}$$

$$m_{H_h} \geq M_{Z^0} \tag{A.68b}$$

$$m_{H_{ch}} \geq M_W \tag{A.68c}$$

As can be seen in Figures 1.1 and 1.2 of Chapter 1, these corrections are sufficient to push the mass of the light Higgs boson above M_{Z^0}, and beyond the reach of the LEP II collider soon to be in operation at CERN (see Figure 2.12 of Chapter 2). Previous studies of the corrections to the MSSM Higgs boson masses had either neglected to consider a heavy top quark [174], or had concentrated on calculating sum rules among the Higgs boson masses rather than individual masses [175,176]. A large number of studies have been done since the discovery of the large top-stop sector corrections, and the scope of the corrections calculated has grown both in completeness and in complexity. Several methods of calculating the radiative corrections to the MSSM Higgs bosons have been employed. These can be roughly classified as renormalization-group equation techniques [177-184], summing of relevant Feynman diagrams to one-loop order [172,175,176,185-194], or effective potential approximations [47,171,173,178,181,195-203]. The list of references presented here covers a significant amount of the work being done on radiative corrections to the MSSM Higgs boson masses; however, it is by no means exhaustive. See Dabelstein [193] for a brief description of these techniques; results from the different techniques are compared in various places, see for example Brignole [190,191].

The effective potential method will be employed here. Notable weaknesses of this technique include neglecting the q^2-dependence of the relevant diagrams and omitting the gaugino-higgsino sector altogether. The correction to $\mathcal{V}$ in the one-loop effective potential approximation has the form [204-206]:

$$\Delta\mathcal{V} = \frac{1}{64\pi^2}\mathrm{Tr}[M^4 \log M^2 - (m^\dagger m)^2 \log(m^\dagger m)] \qquad \text{(A.69)}$$

Here M and m are the classical field-dependent "mass" matrices which reduce to the fermion and boson mass matrices, respectively, when the classical fields are set equal to their *vev*'s — m and M will hereafter be referred to simply though somewhat loosely as the fermion (or quark) and sfermion (or squark) "mass" matrices, respectively; technically the mass matrices are actually $m|_{vev}$ and $M|_{vev}$. An arbitrary mass scale (Q) required to make the arguments of the logarithms dimensionless has been suppressed in Eqn. (A.69) and in numerous equations to follow. More will be said about this after Eqn. (A.140) and again after Eqn. (A.143).

First a brief mathematical interlude: suppose $\mathcal{M}$ is some $N \times N$ diagonalizable matrix, and $f(\mathcal{M})$ is some function of $\mathcal{M}$. Then for some state ket $|v>$,

$$f(\mathcal{M})|v> = f(\mathcal{M})\sum_i v_i|e_i> = \sum_i f(\mathcal{M})v_i|e_i>$$

where $|e_i>$ are the eigenkets of the matrix $\mathcal{M}$, which form a complete set enabling us to expand $|v>$ in terms of them, $|v> = \sum_i v_i|e_i> \Rightarrow v_i = <e_i|v>$. Now taking a power series expansion of $f(\mathcal{M})$, $f(\mathcal{M}) = \sum_j c_j\mathcal{M}^j$ leads to

$$\begin{aligned} f(\mathcal{M})|v> &= \sum_i(\sum_j c_j\mathcal{M}^j)v_i|e_i> = \sum_i\sum_j v_i c_j(\mathcal{M}^j|e_i>) \\ &= \sum_i\sum_j v_i c_j(\lambda_i^j|e_i>) = \sum_i v_i(\sum_j c_j\lambda_i^j)|e_i> = \sum_i v_i f(\lambda_i)|e_i> \end{aligned}$$

where λ_i are the eigenvalues of the matrix $\mathcal{M}$, and thus, $\mathcal{M}|e_i> = \lambda_i|e_i>$ and $\mathcal{M}^j|e_i> = \lambda_i^j|e_i>$ for any positive integer j. Now substituting the expression for v_i yields

$$f(\mathcal{M})|v> = \sum_i f(\lambda_i)|e_i><e_i|v> \quad ; \qquad \text{(A.70)}$$

$$\text{and so} \qquad f(\mathcal{M}) = \sum_i f(\lambda_i)|e_i><e_i| \quad . \qquad \text{(A.71)}$$

Now the trace is the same in both the diagonalized and the original undiagonalized bases (i.e., the trace is invariant under changes of bases, the trace is equal to the sum of the eigenvalues). This can be seen at once from the cyclic property of the trace, $\mathrm{Tr}(\mathcal{M}' = P^{-1}\mathcal{M}P) = \mathrm{Tr}(\mathcal{M}P^{-1}P) = \mathrm{Tr}(\mathcal{M})$. Therefore, I am free to choose the diagonal basis and use in Eqn. (A.69)

$$\mathrm{Tr}(f(\mathcal{M})) = \sum_i f(\lambda_i) \quad . \tag{A.72}$$

A.6 Top/Bottom "Mass" Matrix

The form of the fermion "mass" matrix, m, may be found from the last line of Eqn. (A.1) using the f given in Eqn. (A.2). Only the third generation of quarks will be considered here, and any inter-generational mixing will be neglected. In terms of the third generation of quarks, f may be written as

$$f = -2m_1(\hat{h}^0\hat{h}'^0 + \hat{h}^+\hat{h}'^-) + f_t(\hat{t}\hat{h}^0 - \hat{b}\hat{h}^+)\hat{T}^c + f_b(\hat{t}\hat{h}'^- + \hat{b}\hat{h}'^0)\hat{B}^c \tag{A.73}$$

where f_t and f_b are the top and bottom Yukawa couplings, respectively. According to Eqn. (A.1), derivatives of f with respect to the various superfields are needed:

$$\frac{\partial f}{\partial \hat{T}^c} = f_t(\hat{t}\hat{h}^0 - \hat{b}\hat{h}^+) \qquad \frac{\partial f}{\partial \hat{B}^c} = f_b(\hat{t}\hat{h}'^- + \hat{b}\hat{h}'^0)$$
$$\frac{\partial f}{\partial \hat{t}} = f_t\hat{T}^c\hat{h}^0 + f_b\hat{B}^c\hat{h}'^- \qquad \frac{\partial f}{\partial \hat{b}} = -f_t\hat{T}^c\hat{h}^+ + f_b\hat{B}^c\hat{h}'^0) \tag{A.74}$$

$$\Rightarrow \quad \frac{\partial^2 f}{\partial \hat{T}^c \partial \hat{t}} = f_t\hat{h}^0 \quad \Rightarrow \left.\frac{\partial^2 f}{\partial \hat{T}^c \partial \hat{t}}\right|_{\hat{h}^0 = h^0} = f_t h^0 \tag{A.75}$$

$$\frac{\partial^2 f}{\partial \hat{B}^c \partial \hat{b}} = f_b\hat{h}'^0 \quad \Rightarrow \left.\frac{\partial^2 f}{\partial \hat{B}^c \partial \hat{b}}\right|_{\hat{h}'^0 = h'^0} = f_b h'^0 \tag{A.76}$$

$$\frac{\partial^2 f}{\partial \hat{T}^c \partial \hat{b}} = -f_t\hat{h}^+ \quad \Rightarrow \left.\frac{\partial^2 f}{\partial \hat{T}^c \partial \hat{b}}\right|_{\hat{h}^+ = h^+} = f_t h^+ \tag{A.77}$$

$$\frac{\partial^2 f}{\partial \hat{B}^c \partial \hat{t}} = f_b\hat{h}'^- \quad \Rightarrow \left.\frac{\partial^2 f}{\partial \hat{B}^c \partial \hat{t}}\right|_{\hat{h}'^- = h'^-} = f_b h'^- \tag{A.78}$$

with the same expressions holding for the derivatives taken in the opposite order. The quark third generation part of the potential, which gives the top & bottom Yukawa interactions, can now be written as

$$\begin{aligned}\mathcal{V}_{Yuk} &= \tfrac{1}{2}\bar{t}\frac{1-\gamma_5}{2}f_t h^0 T + \tfrac{1}{2}\bar{T}\frac{1-\gamma_5}{2}f_t h^0 t - \tfrac{1}{2}\bar{b}\frac{1-\gamma_5}{2}f_t h^+ T - \tfrac{1}{2}\bar{T}\frac{1-\gamma_5}{2}f_t h^+ b \\ &+\tfrac{1}{2}\bar{t}\frac{1-\gamma_5}{2}f_b h'^- B + \tfrac{1}{2}\bar{B}\frac{1-\gamma_5}{2}f_b h'^- t + \tfrac{1}{2}\bar{b}\frac{1-\gamma_5}{2}f_b h'^0 B \\ &+\tfrac{1}{2}\bar{B}\frac{1-\gamma_5}{2}f_b h'^0 b + \text{h.c.} \quad . \end{aligned} \tag{A.79}$$

In the above equations, t, b, T, and B are four-component Majorana spinors. The Majorana property $\psi = C\bar{\psi}^T$, can be used to write Eqn. (A.79) in terms of Dirac spinors, t^D and b^D, where

$$t^D = \tfrac{1}{2}(1-\gamma_5)t^D + \tfrac{1}{2}(1+\gamma_5)t^D \equiv t_L^D + t_R^D \quad . \tag{A.80}$$

The associated two-component Weyl spinors are t_L and t_R where $t^D = \begin{pmatrix} t_R \\ t_L \end{pmatrix}$ and $t_L^D = \tfrac{1}{2}(1-\gamma_5)t^D = \begin{pmatrix} 0 \\ t_L \end{pmatrix}$, $\quad t_R^D = \tfrac{1}{2}(1+\gamma_5)t^D = \begin{pmatrix} t_R \\ 0 \end{pmatrix}$.

Aside: let $\psi = \begin{pmatrix} \phi_R \\ \phi_L \end{pmatrix}$, be a four-component Majorana spinor, with ϕ_L and ϕ_R two-component Weyl spinors. Then $\bar{\psi}^T = \psi^\dagger\gamma_0 = \begin{pmatrix} \phi_L^* \\ \phi_R^* \end{pmatrix}$ in the Dirac-Pauli representation, in which $C = i\gamma_2\gamma_0 = i\begin{pmatrix} \sigma_2 & 0 \\ 0 & -\sigma_2 \end{pmatrix}$. And so if $\psi = C\bar{\psi}^T$, then

$$\begin{pmatrix} \phi_R \\ \phi_L \end{pmatrix} = i\begin{pmatrix} \sigma_2 & 0 \\ 0 & -\sigma_2 \end{pmatrix}\begin{pmatrix} \phi_L^* \\ \phi_R^* \end{pmatrix} = \begin{pmatrix} i\sigma_2\phi_L^* \\ -i\sigma_2\phi_R^* \end{pmatrix} \tag{A.81}$$

So the Majorana condition is equivalent to

$$\phi_R = i\sigma_2\phi_L^* \;,\; \phi_L = -i\sigma_2\phi_R^* \quad \Leftrightarrow \quad \psi_R = C\gamma_0\psi_L^* \tag{A.82}$$

where ψ_L and ψ_R are four-component spinors analogous to t_L^D and t_R^D above. A couple useful relations are

$$\bar{\psi}t_L^D = (\,\phi_L^* \quad \phi_R^*\,)\begin{pmatrix} 0 \\ t_L \end{pmatrix} = \phi_R^* t_L = \bar{\psi}_R t_L^D \;, \tag{A.83}$$

$$\text{and} \qquad \bar{\psi} t_R^D = (\, \phi_L^* \quad \phi_R^* \,) \begin{pmatrix} t_R \\ 0 \end{pmatrix} = \phi_L^* t_R = \bar{\psi}_L t_R^D \ . \tag{A.84}$$

Two further useful properties of Majorana spinors are

$$\bar{\psi}\chi = \bar{\chi}\psi \qquad \text{and} \qquad \bar{\psi}\gamma_5\chi = \bar{\chi}\gamma_5\psi \quad , \tag{A.85}$$

where ϕ and χ are Majorana spinors. The first relation is proved in Ref. [15] following which the second can readily be worked out. Using Eqn. (A.82), the four component Majorana spinors may now be constructed,

$$t = \begin{pmatrix} i\sigma_2 t_L^* \\ t_L \end{pmatrix} \qquad T = \begin{pmatrix} t_R \\ -i\sigma_2 t_R^* \end{pmatrix} \tag{A.86}$$

with analogous expressions for the bottom quark Majorana spinors. Note that this is in agreement with

$$\tfrac{1}{2}(1-\gamma_5)t = t_L^D \qquad \text{and} \qquad \tfrac{1}{2}(1+\gamma_5)T = t_R^D \ . \tag{A.87}$$

Consider the first two terms (plus their hermitian conjugates) in $\mathcal{V}_{Yuk}$, Eqn. (A.79):

$$\begin{aligned} \mathcal{V}_{Yuk} \ = \ & \tfrac{1}{2} f_t h^0 \bar{t} \tfrac{1}{2}(1-\gamma_5)T \ + \ \tfrac{1}{2} f_t h^{0*} \bar{T} \tfrac{1}{2}(1+\gamma_5)t \\ & + \tfrac{1}{2} f_t h^0 \bar{T} \tfrac{1}{2}(1-\gamma_5)t \ + \ \tfrac{1}{2} f_t h^{0*} \bar{t} \tfrac{1}{2}(1+\gamma_5)T + \ldots \ , \end{aligned} \tag{A.88}$$

(where the even terms above are the hermitian conjugates of the odd terms). Now using the relations in Eqn. (A.85) on the first two terms, this can be rewritten as

$$\begin{aligned} \mathcal{V}_{Yuk} \ = \ & \tfrac{1}{2} f_t h^0 \bar{T} \tfrac{1}{2}(1-\gamma_5)t \ + \ \tfrac{1}{2} f_t h^{0*} \bar{t} \tfrac{1}{2}(1+\gamma_5)T \\ & + \tfrac{1}{2} f_t h^0 \bar{T} \tfrac{1}{2}(1-\gamma_5)t \ + \ \tfrac{1}{2} f_t h^{0*} \bar{t} \tfrac{1}{2}(1+\gamma_5)T \ + \ \ldots \ . \end{aligned} \tag{A.89}$$

Now noting Eqn.(A.87), this can be written as

$$\begin{aligned} \mathcal{V}_{Yuk} \ &= \ \tfrac{1}{2} f_t h^0 \bar{t_R^D} t_L^D \ + \ \tfrac{1}{2} f_t h^{0*} \bar{t_L^D} t_R^D \ + \ \tfrac{1}{2} f_t h^0 \bar{t_R^D} t_L^D \ + \ \tfrac{1}{2} f_t h^{0*} \bar{t_L^D} t_R^D \ + \ \ldots \\ &= \ f_t h^0 \bar{t_R^D} t_L^D \ + \ f_t h^{0*} \bar{t_L^D} t_R^D \ + \ \ldots \\ &= \ f_t h^0 \bar{t^D} \tfrac{1}{2}(1-\gamma_5) t^D \ + \ f_t h^{0*} \bar{t^D} \tfrac{1}{2}(1+\gamma_5) t^D \ + \ \ldots \ . \end{aligned} \tag{A.90}$$

Thus, employing the same steps on the other terms, Eqn. (A.79) may be rewritten as

$$\begin{aligned}\mathcal{V}_{Yuk} &= f_t h^0 t^{\bar{D}} \tfrac{1}{2}(1-\gamma_5) t^D + f_t h^{0*} t^{\bar{D}} \tfrac{1}{2}(1+\gamma_5) t^D \\ &\quad - f_t h^+ t^{\bar{D}} \tfrac{1}{2}(1-\gamma_5) b^D - f_t h^{+*} b^{\bar{D}} \tfrac{1}{2}(1+\gamma_5) t^D \\ &\quad + f_b h'^- b^{\bar{D}} \tfrac{1}{2}(1-\gamma_5) t^D + f_b h'^{-*} t^{\bar{D}} \tfrac{1}{2}(1+\gamma_5) b^D \\ &\quad + f_b h'^0 b^{\bar{D}} \tfrac{1}{2}(1-\gamma_5) b^D + f_b h'^{0*} b^{\bar{D}} \tfrac{1}{2}(1+\gamma_5) b^D \quad . \end{aligned} \tag{A.91}$$

The quark "mass" matrix is now given by

$$\mathcal{M}_{qk} = \tfrac{1}{2}(1-\gamma_5) m + \tfrac{1}{2}(1+\gamma_5) m^\dagger \quad , \tag{A.92}$$

$$\text{where} \quad m = \begin{bmatrix} f_t h^0 & f_b h'^- \\ -f_t h^+ & f_b h'^0 \end{bmatrix} \quad \text{and} \quad m^\dagger = \begin{bmatrix} f_t h^{0*} & -f_t h^{+*} \\ f_b h'^{-*} & f_b h'^{0*} \end{bmatrix} \quad , \tag{A.93}$$

$$\text{and so} \quad m^\dagger m = \begin{bmatrix} f_t^2(|h^0|^2 + |h'^-|^2) & f_t f_b (h^{0*} h'^- - h^{+*} h'^0) \\ f_t f_b (h'^{-*} h^0 - h'^{0*} h^+) & f_b^2(|h'^0|^2 + |h'^-|^2) \end{bmatrix} \quad . \tag{A.94}$$

The eigenvalues for this matrix are:

$$\begin{aligned}\lambda_1, \lambda_2 &= \tfrac{1}{2}\Big\{ f_t^2(|h^0|^2 + |h^+|^2) + f_b^2(|h'^0|^2 + |h'^-|^2) \\ &\quad \pm \Big[f_t^4(|h^0|^2 + |h^+|^2)^2 + f_b^4(|h'^0|^2 + |h'^-|^2)^2 \\ &\quad + 2 f_t^2 f_b^2 (|h^0|^2 |h'^-|^2 + |h^+|^2 |h'^0|^2 - |h^0|^2 |h'^0|^2 - |h^+|^2 |h'^-|^2 \\ &\quad - 2h^{0*} h'^{0*} h^+ h'^- - 2h^{+*} h'^{-*} h^0 h'^0) \Big]^{\frac{1}{2}} \Big\} \end{aligned} \tag{A.95}$$

$$\equiv \zeta \pm \eta \tag{A.96}$$

Note that when the fields are set equal to their *vev*'s,
$\zeta|_{vev} = \frac{1}{2}(f_t^2 v^2 + f_b^2 v'^2) = \frac{1}{2}(m_t^2 + m_b^2)$ and $\eta|_{vev} = \frac{1}{2}(f_t^2 v^2 - f_b^2 v'^2) = \frac{1}{2}(m_t^2 - m_b^2)$.

$$\text{Thus} \quad \lambda_1|_{vev} = f_t^2 v^2 = m_t^2 \quad \text{and} \quad \lambda_2|_{vev} = f_b^2 v'^2 = m_b^2 \quad . \tag{A.97}$$

Inserting these results into Eqn. (A.69) yields

$$\begin{aligned}\Delta\mathcal{V}_{qk} &= -\frac{N_c}{64\pi^2} \mathrm{Tr}(m^\dagger m)^2 \log(m^\dagger m) = -\frac{3 \cdot 4}{64\pi^2} \left[\lambda_1^2 \log \lambda_1 + \lambda_2^2 \log \lambda_2 \right] \\ &= -\frac{3}{16\pi^2} \left[(\zeta+\eta)^2 \log(\zeta+\eta) + (\zeta-\eta)^2 \log(\zeta-\eta) \right] \end{aligned} \tag{A.98}$$

where the number of colors is $N_c = 3$ and the extra factor of four is due to the trace over the Lorentz-space indices of the Dirac field. From Eqn. (A.98) expressions for the derivatives at the minimum are easily derived:

$$\frac{1}{\sqrt{2}v}\frac{\partial(\Delta\mathcal{V}_{qk})}{\partial h_R}\bigg|_{vev} = \frac{-3f_t^2m_t^2}{16\pi^2}\left[2\log(m_t^2) + 1\right] \quad \text{(A.99)}$$

$$\frac{1}{\sqrt{2}v'}\frac{\partial(\Delta\mathcal{V}_{qk})}{\partial h'_R}\bigg|_{vev} = \frac{-3f_b^2m_b^2}{16\pi^2}\left[2\log(m_b^2) + 1\right] \quad \text{(A.100)}$$

$$\frac{\partial(\Delta\mathcal{V}_{qk})}{\partial h_I}\bigg|_{vev} = \frac{\partial(\Delta\mathcal{V}_{qk})}{\partial h'_I}\bigg|_{vev} = 0 \quad \text{(A.101)}$$

$$\frac{\partial(\Delta\mathcal{V}_{qk})}{\partial h^+}\bigg|_{vev} = \frac{\partial(\Delta\mathcal{V}_{qk})}{\partial h'^-}\bigg|_{vev} = \frac{\partial(\Delta\mathcal{V}_{qk})}{\partial h^{+*}}\bigg|_{vev} = \frac{\partial(\Delta\mathcal{V}_{qk})}{\partial h'^{-*}}\bigg|_{vev} = 0 \quad \text{(A.102)}$$

$$\frac{\partial^2(\Delta\mathcal{V}_{qk})}{\partial h_R^2}\bigg|_{vev} = \frac{-3f_t^2m_t^2}{16\pi^2}\left[6\log(m_t^2) + 7\right]$$

$$\frac{\partial^2(\Delta\mathcal{V}_{qk})}{\partial h'^2_R}\bigg|_{vev} = \frac{-3f_b^2m_b^2}{16\pi^2}\left[6\log(m_b^2) + 7\right]$$

$$\frac{\partial^2(\Delta\mathcal{V}_{qk})}{\partial h_I^2}\bigg|_{vev} = \frac{-3f_t^2m_t^2}{16\pi^2}\left[2\log(m_t^2) + 1\right]$$

$$\frac{\partial^2(\Delta\mathcal{V}_{qk})}{\partial h'^2_I}\bigg|_{vev} = \frac{-3f_b^2m_b^2}{16\pi^2}\left[2\log(m_b^2) + 1\right]$$

$$\frac{\partial^2(\Delta\mathcal{V}_{qk})}{\partial h_R\partial h'_R}\bigg|_{vev} = \frac{\partial^2(\Delta\mathcal{V}_{qk})}{\partial h_I\partial h'_I}\bigg|_{vev} = 0$$

$$\frac{\partial^2(\Delta\mathcal{V}_{qk})}{\partial h^+\partial h^{+*}}\bigg|_{vev} = \frac{-3f_t^2}{16\pi^2}(m_t^2+m_b^2)\left[\log(m_t^2m_b^2) + \frac{m_t^4+m_b^4}{m_t^4-m_b^4}\log\left(\frac{m_t^2}{m_b^2}\right) + 1\right]$$

$$\frac{\partial^2(\Delta\mathcal{V}_{qk})}{\partial h'^-\partial h'^{-*}}\bigg|_{vev} = \frac{-3f_b^2}{16\pi^2}(m_t^2+m_b^2)\left[\log(m_t^2m_b^2) + \frac{m_t^4+m_b^4}{m_t^4-m_b^4}\log\left(\frac{m_t^2}{m_b^2}\right) + 1\right]$$

$$\frac{\partial^2(\Delta\mathcal{V}_{qk})}{\partial h^+\partial h'^-}\bigg|_{vev} = \frac{\partial^2(\Delta\mathcal{V}_{qk})}{\partial h^{+*}\partial h'^{-*}}\bigg|_{vev} = \frac{3f_tf_bm_tm_b}{16\pi^2}\left[\log(m_t^2m_b^2) + \frac{m_t^2+m_b^2}{m_t^2-m_b^2}\log\left(\frac{m_t^2}{m_b^2}\right) + 1\right]$$

Now since the minimum of the *complete* potential occurs when the Higgs fields are set equal to their *vev*'s, Eqns. (A.24) must be modified by adding the quark terms. This leads to expressions analogous to Eqns. (A.31), (A.32), and (A.61) for the second derivatives of the quark correction to the scalar potential.

$$\left.\frac{\partial^2(\Delta\mathcal{V}_{qk})}{\partial {h_R}^2}\right|_{vev} = \left.\frac{\partial^2(\Delta\mathcal{V}_{qk})}{\partial {h_R}^2}\right|_{vev} - \frac{1}{\sqrt{2}v}\left.\frac{\partial(\Delta\mathcal{V}_{qk})}{\partial h_R}\right|_{vev} = \frac{-3f_t^2m_t^2}{16\pi^2}\left[4\log(m_t^2) + 6\right]$$

$$\left.\frac{\partial^2(\Delta\mathcal{V}_{qk})}{\partial {h'_R}^2}\right|_{vev} = \left.\frac{\partial^2(\Delta\mathcal{V}_{qk})}{\partial {h'_R}^2}\right|_{vev} - \frac{1}{\sqrt{2}v'}\left.\frac{\partial(\Delta\mathcal{V}_{qk})}{\partial h'_R}\right|_{vev} = \frac{-3f_b^2m_b^2}{16\pi^2}\left[4\log(m_b^2) + 6\right]$$

$$\left.\frac{\partial^2(\Delta\mathcal{V}_{qk})}{\partial h_R\partial h'_R}\right|_{vev} = 0 \qquad \text{(A.103)}$$

$$\left.\frac{\partial^2(\Delta\mathcal{V}_{qk})}{\partial {h_I}^2}\right|_{vev} = \left.\frac{\partial^2(\Delta\mathcal{V}_{qk})}{\partial {h_I}^2}\right|_{vev} - \frac{1}{\sqrt{2}v}\left.\frac{\partial(\Delta\mathcal{V}_{qk})}{\partial h_R}\right|_{vev} = 0$$

$$\left.\frac{\partial^2(\Delta\mathcal{V}_{qk})}{\partial {h'_I}^2}\right|_{vev} = \left.\frac{\partial^2(\Delta\mathcal{V}_{qk})}{\partial {h'_I}^2}\right|_{vev} - \frac{1}{\sqrt{2}v'}\left.\frac{\partial(\Delta\mathcal{V}_{qk})}{\partial h'_R}\right|_{vev} = 0$$

$$\left.\frac{\partial^2(\Delta\mathcal{V}_{qk})}{\partial h_I\partial h'_I}\right|_{vev} = 0 \qquad \text{(A.104)}$$

$$\left.\frac{\partial^2(\Delta\mathcal{V}_{qk})}{\partial h^+\partial h^{+*}}\right|_{vev} = \left.\frac{\partial^2(\Delta\mathcal{V}_{qk})}{\partial h^+\partial h^{+*}}\right|_{vev} - \frac{1}{\sqrt{2}v}\left.\frac{\partial(\Delta\mathcal{V}_{qk})}{\partial h_R}\right|_{vev}$$

$$= \frac{-3f_t^2m_b^2}{16\pi^2}\left[\log(m_t^2m_b^2) + 1 + \frac{m_t^2+m_b^2}{m_t^2-m_b^2}\log\left(\frac{m_t^2}{m_b^2}\right)\right]$$

$$\left.\frac{\partial^2(\Delta\mathcal{V}_{qk})}{\partial h'^-\partial h'^{-*}}\right|_{vev} = \left.\frac{\partial^2(\Delta\mathcal{V}_{qk})}{\partial h'^-\partial h'^{-*}}\right|_{vev} - \frac{1}{\sqrt{2}v'}\left.\frac{\partial(\Delta\mathcal{V}_{qk})}{\partial h'_R}\right|_{vev}$$

$$= \frac{-3f_b^2m_t^2}{16\pi^2}\left[\log(m_t^2m_b^2) + 1 + \frac{m_t^2+m_b^2}{m_t^2-m_b^2}\log\left(\frac{m_t^2}{m_b^2}\right)\right]$$

$$\left.\frac{\partial^2(\Delta\mathcal{V}_{qk})}{\partial h^+\partial h'^-}\right|_{vev} = \left.\frac{\partial^2(\Delta\mathcal{V}_{qk})}{\partial h^{+*}\partial h'^{-*}}\right|_{vev} = \frac{3f_tf_bm_tm_b}{16\pi^2}\left[\log(m_t^2m_b^2) + 1 + \frac{m_t^2+m_b^2}{m_t^2-m_b^2}\log\left(\frac{m_t^2}{m_b^2}\right)\right]$$

(A.105)

A.7 Stop/Sbottom "Mass" Matrix

The terms of the sfermion "mass" matrix M are derived from lines four and five of Eqn. (A.1). Using the expression for the superpotential, f, in Eqn. (A.73), we find

$$\begin{aligned}
\frac{\partial f}{\partial \hat{h}^0} &= -2m_1\hat{h'}^0 + f_t\hat{t}\hat{T}^c \;\Rightarrow\; \left.\frac{\partial f}{\partial \hat{h}^0}\right|_{S=\mathcal{S}} = -2m_1 h'^0 + f_t\widetilde{t_L}\widetilde{t_R}^* \\
\frac{\partial f}{\partial \hat{h'}^0} &= -2m_1\hat{h}^0 + f_b\hat{b}\hat{B}^c \;\Rightarrow\; \left.\frac{\partial f}{\partial \hat{h'}^0}\right|_{S=\mathcal{S}} = -2m_1 h^0 + f_b\widetilde{b_L}\widetilde{b_R}^* \\
\frac{\partial f}{\partial \hat{h}^+} &= -2m_1\hat{h'}^- - f_t\hat{b}\hat{T}^c \;\Rightarrow\; \left.\frac{\partial f}{\partial \hat{h}^+}\right|_{S=\mathcal{S}} = -2m_1 h'^- - f_t\widetilde{b_L}\widetilde{t_R}^* \\
\frac{\partial f}{\partial \hat{h'}^-} &= -2m_1\hat{h}^+ + f_b\hat{t}\hat{B}^c \;\Rightarrow\; \left.\frac{\partial f}{\partial \hat{h'}^-}\right|_{S=\mathcal{S}} = -2m_1 h^+ + f_b\widetilde{t_L}\widetilde{b_R}^*
\end{aligned} \tag{A.106}$$

$$\begin{aligned}
\Longrightarrow \left|\left.\frac{\partial f}{\partial \hat{h}^0}\right|_{S=\mathcal{S}}\right|^2 &= (2m_1)^2|h'^0|^2 + f_t^2|\widetilde{t_L}|^2|\widetilde{t_R}|^2 - 2m_1 h'^0 f_t\widetilde{t_L}^*\widetilde{t_R} - 2m_1 h'^{0*} f_t\widetilde{t_L}\widetilde{t_R}^* \\
\left|\left.\frac{\partial f}{\partial \hat{h'}^0}\right|_{S=\mathcal{S}}\right|^2 &= (2m_1)^2|h^0|^2 + f_b^2|\widetilde{b_L}|^2|\widetilde{b_R}|^2 - 2m_1 h^0 f_b\widetilde{b_L}^*\widetilde{b_R} - 2m_1 h^{0*} f_b\widetilde{b_L}\widetilde{b_R}^* \\
\left|\left.\frac{\partial f}{\partial \hat{h}^+}\right|_{S=\mathcal{S}}\right|^2 &= (2m_1)^2|h'^-|^2 + f_t^2|\widetilde{b_L}|^2|\widetilde{t_R}|^2 + 2m_1 h'^- f_t\widetilde{b_L}^*\widetilde{t_R} + 2m_1 h'^{-*} f_t\widetilde{b_L}\widetilde{t_R}^* \\
\left|\left.\frac{\partial f}{\partial \hat{h'}^-}\right|_{S=\mathcal{S}}\right|^2 &= (2m_1)^2|h^+|^2 + f_b^2|\widetilde{t_L}|^2|\widetilde{b_R}|^2 - 2m_1 h^+ f_b\widetilde{t_L}^*\widetilde{b_R} - 2m_1 h^{+*} f_b\widetilde{t_L}\widetilde{b_R}^*
\end{aligned} \tag{A.107}$$

Stop and sbottom mass terms can be picked out from Eqns. (A.107), yielding

$$\begin{aligned}
\mathcal{V}_{sq} \ni\; & -2m_1 f_t h'^0\widetilde{t_R}\widetilde{t_L}^* - 2m_1 f_b h^0\widetilde{b_R}\widetilde{b_L}^* + 2m_1 f_t h'^-\widetilde{t_R}\widetilde{b_L}^* - 2m_1 f_b h^+\widetilde{b_R}\widetilde{t_L}^* \\
& + \text{h.c.}
\end{aligned} \tag{A.108}$$

Additional sfermion mass terms come from taking derivatives of the superpotential with respect to chiral superfields – see Eqns. (A.74). This yields:

$$\begin{aligned}
\mathcal{V}_{sq} \ni\; & (f_t^2|h^0|^2 + f_b^2|h'^-|^2)|\widetilde{t_L}|^2 + (f_t^2|h^+|^2 + f_b^2|h'^0|^2)|\widetilde{b_L}|^2 \\
& - (f_t^2 h^0 h^{+*} - f_b^2 h'^- h'^{0*})\widetilde{t_L}\widetilde{b_L}^* - (f_t^2 h^+ h^{0*} - f_b^2 h'^0 h'^{-*})\widetilde{b_L}\widetilde{t_L}^* \\
& + f_t^2(|h^0|^2 + |h^+|^2)|\widetilde{t_R}|^2 + f_b^2(|h'^0|^2 + |h'^-|^2)|\widetilde{b_R}|^2 \\
& + f_t f_b(h^0 h'^{-*} - h^+ h'^{0*})\widetilde{b_R}\widetilde{t_R}^* + f_t f_b(h'^- h^{0*} - h'^0 h^{+*})\widetilde{t_R}\widetilde{b_R}^*
\end{aligned} \tag{A.109}$$

There are also the so-called D-terms arising from line five of Eqn. (A.1). For the U(1) terms,

$$\begin{aligned}
[\quad] \;=\; & (h^{+*} \quad h^{0*})\, g' \frac{Y}{2} \begin{pmatrix} h^+ \\ h^0 \end{pmatrix} \;+\; (-h'^{0*} \quad h'^{-*})\, g' \frac{Y'}{2} \begin{pmatrix} -h'^0 \\ h'^- \end{pmatrix} \\
& + \; (\widetilde{t_L}^* \quad \widetilde{b_L}^*)\, g' \frac{Y_L}{2} \begin{pmatrix} \widetilde{t_L} \\ \widetilde{t_R} \end{pmatrix} \;+\; g' \frac{Y_R}{2} \widetilde{t_R}^* \widetilde{t_R} \;+\; g' \frac{Y_R}{2} \widetilde{b_R}^* \widetilde{b_R} \;+\; 0 \\
\\
= \; & \tfrac{1}{2} g' \Big[(|h^+|^2 + |h^0|^2) \;-\; (|h'^0|^2 + |h'^-|^2) \\
& + \; \tfrac{1}{3}(|\widetilde{t_L}|^2 + |\widetilde{b_L}|^2) \;+\; \tfrac{-4}{3}|\widetilde{t_R}|^2 \;+\; \tfrac{2}{3}|\widetilde{b_R}|^2 \Big] \quad ,
\end{aligned}$$

where the Fayet-Iliopoulos term, ξ_A, has again been set to zero by choice. Upon squaring, cross-terms betweeen the Higgs fields and the squark fields will lead to mass terms for the squarks when the Higgs fields are set equal to their *vev*'s. The following terms are thus obtained:

$$\mathcal{V}_{sq} \;\ni\; g'^2 (|h^+|^2 + |h^0|^2 - |h'^-|^2 - |h'^0|^2) \Big[\tfrac{1}{12}|\widetilde{t_L}|^2 \;-\; \tfrac{1}{3}|\widetilde{t_R}|^2 \;+\; \tfrac{1}{12}|\widetilde{b_L}|^2 \;+\; \tfrac{1}{6}|\widetilde{b_R}|^2 \Big] \tag{A.110}$$

For the SU(2) component,

$$[\quad] \;=\; (h^{+*} \quad h^{0*})\, t_a \begin{pmatrix} h^+ \\ h^0 \end{pmatrix} \;+\; (-h'^{0*} \quad h'^{-*})\, t_a \begin{pmatrix} -h'^0 \\ h'^- \end{pmatrix} \;+\; (\widetilde{t_L}^* \quad \widetilde{b_L}^*)\, t_a \begin{pmatrix} \widetilde{t_L} \\ \widetilde{t_R} \end{pmatrix}.$$

Thus,

$$\begin{aligned}
\sum_a [\quad]^2 \;=\; & \sum_a \Big\{ 2 (h^{+*} \quad h^{0*})\, t_a \begin{pmatrix} h^+ \\ h^0 \end{pmatrix} (\widetilde{t_L}^* \quad \widetilde{b_L}^*)\, t_a \begin{pmatrix} \widetilde{t_L} \\ \widetilde{t_R} \end{pmatrix} \\
& + \; 2 (-h'^{0*} \quad h'^{-*})\, t_a \begin{pmatrix} -h'^0 \\ h'^- \end{pmatrix} (\widetilde{t_L}^* \quad \widetilde{b_L}^*)\, t_a \begin{pmatrix} \widetilde{t_L} \\ \widetilde{t_R} \end{pmatrix} \;+\; \cdots \Big\}.
\end{aligned}$$

where the cross-terms leading to squark mass terms are shown. And so

$$\begin{aligned}
\mathcal{V}_{sq} \;\ni\; & g^2 \Big[\tfrac{1}{2}(h^{0*} h^+ - h'^{-*} h'^0) \widetilde{t_L}^* \widetilde{b_L} \;+\; \tfrac{1}{2}(h^{+*} h^0 - h'^{0*} h'^-) \widetilde{b_L}^* \widetilde{t_L} \\
& + \; \tfrac{1}{4}(|h^+|^2 - |h^0|^2 + |h'^0|^2 - |h'^-|^2)(|\widetilde{t_L}|^2 \;-\; |\widetilde{b_L}|^2) \Big]
\end{aligned} \tag{A.111}$$

Finally, we must consider soft supersymmetry breaking terms. The allowable dimension-two terms are

$$m_{\widetilde{L}}(\widetilde{t_L}^* \quad \widetilde{b_L}^*)\begin{pmatrix}\widetilde{t_L}\\ \widetilde{b_L}\end{pmatrix} = m_{\widetilde{L}}(|\widetilde{t_L}|^2 + |\widetilde{b_L}|^2)\,,\ m_{\widetilde{t_R}}|\widetilde{t_R}|^2\,,\ \text{and}\ m_{\widetilde{b_R}}|\widetilde{b_R}|^2\,. \quad \text{(A.112)}$$

The dimension-three soft supersymmetry breaking terms are found from the superpotential f. From the last two terms of Eqn. (A.73), we find

$$\mathcal{V}_{soft} \ni A_t f_t(\widetilde{t_L}h^0 - \widetilde{b_L}h^+)\widetilde{t_R}^* + A_b f_b(\widetilde{t_L}h'^- + \widetilde{b_L}h'^0)\widetilde{b_R}^* + \text{h.c.}\,, \quad \text{(A.113)}$$

where A_t and A_b are inputs with the dimension of mass. In general, they are referred to as A-terms.

Collecting all the terms from Eqns. (A.108)-(A.113), the squark mass squared matrix may now be written as

$$\mathcal{V}_{sq} = \tilde{q}\mathcal{M}^2_{sq}\tilde{q}^* = [\widetilde{t_L}\ \ \widetilde{t_R}\ \ \widetilde{b_L}\ \ \widetilde{b_R}]\begin{bmatrix}\mathrm{M}_{11} & \mathrm{M}_{12} & \mathrm{M}_{13} & \mathrm{M}_{14}\\ \mathrm{M}_{21} & \mathrm{M}_{22} & \mathrm{M}_{23} & \mathrm{M}_{24}\\ \mathrm{M}_{31} & \mathrm{M}_{32} & \mathrm{M}_{33} & \mathrm{M}_{34}\\ \mathrm{M}_{41} & \mathrm{M}_{42} & \mathrm{M}_{43} & \mathrm{M}_{44}\end{bmatrix}\begin{bmatrix}\widetilde{t_L}^*\\ \widetilde{t_R}^*\\ \widetilde{b_L}^*\\ \widetilde{b_R}^*\end{bmatrix} \quad \text{(A.114)}$$

where:

$$\begin{aligned}
\mathrm{M}_{11} &= m^2_{\widetilde{L}} + f_t^2|h^0|^2 + f_b^2|h'^-|^2 \\
&\quad + \tfrac{g^2}{4}(|h^+|^2 - |h^0|^2 + |h'^0|^2 - |h'^-|^2) + \tfrac{g'^2}{12}(|h^+|^2 + |h^0|^2 - |h'^0|^2 - |h'^-|^2)\\
\mathrm{M}_{22} &= m^2_{\widetilde{t_R}} + f_t^2(|h^0|^2 + |h'^+|^2) - \tfrac{g'^2}{3}(|h^+|^2 + |h^0|^2 - |h'^0|^2 - |h'^-|^2)\\
\mathrm{M}_{33} &= m^2_{\widetilde{L}} + f_t^2|h^+|^2 + f_b^2|h'^0|^2 \\
&\quad - \tfrac{g^2}{4}(|h^+|^2 - |h^0|^2 + |h'^0|^2 - |h'^-|^2) + \tfrac{g'^2}{12}(|h^+|^2 + |h^0|^2 - |h'^0|^2 - |h'^-|^2)\\
\mathrm{M}_{44} &= m^2_{\widetilde{b_R}} + f_b^2(|h'^0|^2 + |h'^-|^2) + \tfrac{g'^2}{6}(|h^+|^2 + |h^0|^2 - |h'^0|^2 - |h'^-|^2)\\
\mathrm{M}_{12} &= \mathrm{M}^*_{21} = -2m_1 f_t h'^{0*} - A_t f_t h^0\\
\mathrm{M}_{34} &= \mathrm{M}^*_{43} = -2m_1 f_b h^{0*} - A_b f_b h'^0\\
\mathrm{M}_{13} &= \mathrm{M}^*_{31} = -f_t^2 h^0 h^{+*} + f_b^2 h'^- h'^{0*} + \tfrac{g^2}{2}(h^{+*}h^0 - h'^{0*}h'^-)\\
\mathrm{M}_{14} &= \mathrm{M}^*_{41} = -2m_1 f_b h^{+*} - A_b f_b h'^-\\
\mathrm{M}_{23} &= \mathrm{M}^*_{32} = 2m_1 f_t h'^- + A_t^* f_t h^{+*}\\
\mathrm{M}_{24} &= \mathrm{M}^*_{42} = f_t f_b(h'^- h^{0*} - h'^0 h^{+*})\quad . \qquad \text{(A.115)}
\end{aligned}$$

This is in agreement with the formulæ of Eqn. (4) of Brignole *et al.* [198] if the following identifications are made:

Table A.2

This work	Brignole *et al.*
$m_{\tilde{L}}$	m_Q
$m_{\tilde{t_R}}$, $m_{\tilde{b_R}}$	m_U, m_D
f_t, f_b	h_t, h_b
$-2m_1$	μ
h^+, h^0	H_2^+, H_2^0
h'^-, h'^0	H_1^0, $-H_1^-$
A_t, A_b	$-A_t$, $-A_b$ (assumes real A-terms)

Note that the H_1 doublet of [198] is a representation $\underline{\mathbf{2}}$ SU(2) doublet whereas the H′ used here is a $\underline{\mathbf{2}}^*$ SU(2) doublet. This accounts for the extra minus sign in the comparison above.

Now in order to apply Eqn. (A.72) to the sfermion sector, the eigenvalues of the above 4×4 matrix must be found. For the case of the neutral Higgs bosons, this can be considerably simplified by noting that all terms proportional to a charged Higgs field may be dropped. This is because $\langle h^+ \rangle = \langle h'^- \rangle = 0$, and if we only take derivatives with respect to the neutral fields then terms with charged field dependence will be set to zero at the minimum. This of course will not work for the case of the charged Higgs, which will be considered later. Dropping the terms proportional to the charged Higgs fields leaves $\mathcal{M}^2_{sq}$ in block diagonal form, decoupling the stop and sbottom sectors, which have the following eigenvalues:

$$\begin{aligned}\lambda_t \;=\; & \tfrac{1}{2}(m^2_{\tilde{L}} + m^2_{\tilde{t_R}}) \;+\; f_t^2|h^0|^2 \;+\; \tfrac{1}{8}(g^2+g'^2)(|h'^0|^2 - |h^0|^2) \\ & \pm \left\{ \frac{1}{4}\left[(m^2_{\tilde{L}} - m^2_{\tilde{t_R}}) \;+\; \tfrac{1}{4}(g^2 - \tfrac{5}{3}g'^2)(|h'^0|^2 - |h^0|^2)\right]^2 \right. \\ & \qquad \left. + f_t^2(2m_1 h'^0 + A_t^* h^{0*})(2m_1 h'^{0*} + A_t h^0) \right\}^{\frac{1}{2}} \qquad \text{(A.116)}\end{aligned}$$

$$\lambda_b = \tfrac{1}{2}(m^2_{\tilde{L}} + m^2_{\tilde{b}_R}) + f_b^2|h'^0|^2 - \tfrac{1}{8}(g^2+g'^2)(|h'^0|^2 - |h^0|^2)$$
$$\pm \left\{ \frac{1}{4}\left[(m^2_{\tilde{L}} - m^2_{\tilde{b}_R}) - \tfrac{1}{4}(g^2 - \tfrac{1}{3}g'^2)(|h'^0|^2 - |h^0|^2)\right]^2 \right.$$
$$\left. + f_b^2(2m_1 h^0 + A_b^* h'^{0*})(2m_1 h^{0*} + A_b h'^0) \right\}^{\frac{1}{2}} \quad , \text{(A.117)}$$

and at the minimum,

$$m^2_{\tilde{t}_2}, m^2_{\tilde{t}_1} \equiv \lambda_t|_{vev} = \tfrac{1}{2}(m^2_{\tilde{L}} + m^2_{\tilde{t}_R}) + f_t^2 v^2 + \tfrac{1}{8}(g^2+g'^2)(v'^2 - v^2)$$
$$\pm \left\{ \frac{1}{4}\left[(m^2_{\tilde{L}} - m^2_{\tilde{t}_R}) + \tfrac{1}{4}(g^2 - \tfrac{5}{3}g'^2)(v'^2 - v^2)\right]^2 \right.$$
$$\left. + f_t^2(2m_1 v' + A_t v)(2m_1 v' + A_t^* v) \right\}^{\frac{1}{2}}$$
$$= \tfrac{1}{2}(m^2_{\tilde{L}} + m^2_{\tilde{t}_R}) + m_t^2 + \tfrac{1}{4}m^2_{Z^0}\cos 2\beta$$
$$\pm \left\{ \frac{1}{4}\left[(m^2_{\tilde{L}} - m^2_{\tilde{t}_R}) + \tfrac{1}{6}(8m_W^2 - 5m^2_{Z^0})\cos 2\beta\right]^2 \right.$$
$$\left. + m_t^2(2m_1 \cot\beta + A_t)(2m_1 \cot\beta + A_t^*) \right\}^{\frac{1}{2}} \quad \text{(A.118)}$$
$$\equiv \tfrac{1}{2}\alpha_t \pm D_t^{\frac{1}{2}} \quad \text{(A.119)}$$

Thus $\alpha_t = m^2_{\tilde{t}_2} + m^2_{\tilde{t}_1}$ and $D_t^{\frac{1}{2}} = \frac{1}{2}(m^2_{\tilde{t}_2} - m^2_{\tilde{t}_1})$.

$$m^2_{\tilde{b}_2}, m^2_{\tilde{b}_1} \equiv \lambda_b|_{vev} = \tfrac{1}{2}(m^2_{\tilde{L}} + m^2_{\tilde{b}_R}) + f_b^2 v'^2 - \tfrac{1}{8}(g^2+g'^2)(v'^2 - v^2)$$
$$\pm \left\{ \frac{1}{4}\left[(m^2_{\tilde{L}} - m^2_{\tilde{b}_R}) - \tfrac{1}{4}(g^2 - \tfrac{1}{3}g'^2)(v'^2 - v^2)\right]^2 \right.$$
$$\left. + f_b^2(2m_1 v + A_b v')(2m_1 v + A_b^* v') \right\}^{\frac{1}{2}}$$
$$= \tfrac{1}{2}(m^2_{\tilde{L}} + m^2_{\tilde{b}_R}) + m_b^2 - \tfrac{1}{4}m^2_{Z^0}\cos 2\beta$$
$$\pm \left\{ \frac{1}{4}\left[(m^2_{\tilde{L}} - m^2_{\tilde{b}_R}) - \tfrac{1}{12}(4m_W^2 - m^2_{Z^0})\cos 2\beta\right]^2 \right.$$
$$\left. + m_b^2(2m_1 \tan\beta + A_b)(2m_1 \tan\beta + A_b^*) \right\}^{\frac{1}{2}} \quad \text{(A.120)}$$
$$\equiv \tfrac{1}{2}\alpha_b \pm D_b^{\frac{1}{2}} \quad \text{(A.121)}$$

So $\alpha_b = m^2_{\tilde{b}_2} + m^2_{\tilde{b}_1}$ and $D_b^{\frac{1}{2}} = \frac{1}{2}(m^2_{\tilde{b}_2} - m^2_{\tilde{b}_1})$. Also note that $m_{\tilde{t}_1} < m_{\tilde{t}_2}$, and $m_{\tilde{b}_1} < m_{\tilde{b}_2}$.

Here values for the "mixed" stop and sbottom masses, $m_{\tilde{t_1}}$, $m_{\tilde{t_2}}$, $m_{\tilde{b_1}}$, $m_{\tilde{b_2}}$, are given for some special limiting cases:

$f_b = m_b = 0$

$m_{\tilde{t_1}}$, $m_{\tilde{t_2}}$ unaffected, see Eqn. (A.118), $\quad m_{\tilde{b_1}} = m_{\tilde{b_R}}$, $\quad m_{\tilde{b_2}} = m_{\tilde{L}}$.

(Here it is assumed that the right "bare" stop or sbottom mass is lighter than the left bare mass, as predicted by supergravity models.)

no D-terms in sfermion mass matrix, ($g = g' = 0$ in Eqn.(A.115)).

$$m^2_{\tilde{t_2}}, m^2_{\tilde{t_1}} = \tfrac{1}{2}(m^2_{\tilde{L}} + m^2_{\tilde{t_R}}) + m_t^2 \pm \left\{ \tfrac{1}{4}(m^2_{\tilde{L}} - m^2_{\tilde{t_R}})^2 + m_t^2(2m_1 \cot\beta + A_t)^2 \right\}^{\frac{1}{2}}$$

$$m^2_{\tilde{b_2}}, m^2_{\tilde{b_1}} = \tfrac{1}{2}(m^2_{\tilde{L}} + m^2_{\tilde{t_R}}) + m_b^2 \pm \left\{ \tfrac{1}{4}(m^2_{\tilde{L}} - m^2_{\tilde{b_R}})^2 + m_b^2(2m_1 \tan\beta + A_b)^2 \right\}^{\frac{1}{2}}$$

no D-terms, degenerate bare stop or sbottom masses

$$m^2_{\tilde{t_2}}, m^2_{\tilde{t_1}} = m^2_{\tilde{L}} + m_t^2 \pm m_t|2m_1 \cot\beta + A_t|$$
$$m^2_{\tilde{b_2}}, m^2_{\tilde{b_1}} = m^2_{\tilde{L}} + m_b^2 \pm m_b|2m_1 \tan\beta + A_b|$$

no D-terms, $2m_1 = A_t = A_b = 0$

$$m^2_{\tilde{t_1}} = m^2_{\tilde{t_R}} + m_t^2\,, \quad m^2_{\tilde{t_2}} = m^2_{\tilde{L}} + m_t^2$$
$$m^2_{\tilde{b_1}} = m^2_{\tilde{b_R}} + m_b^2\,, \quad m^2_{\tilde{b_2}} = m^2_{\tilde{L}} + m_b^2$$

From Eqns. (A.69) and (A.72),

$$\Delta\mathcal{V}_{sq} = \frac{2 \cdot N_c}{64\pi^2} \sum_i \lambda_i^2 \log\lambda_i = \frac{2 \cdot 3}{64\pi^2} \sum_{i=1,2} \left[{\lambda_{t_i}}^2 \log\lambda_{t_i} + {\lambda_{b_i}}^2 \log\lambda_{b_i} \right] \qquad \text{(A.122)}$$

where the first factor of 2 comes from the fact that the squark fields are complex. Now the derivatives of the eigenvalues of the sfermion mass matrix, Eqns. (A.116) and (A.117), must be found. It is convenient to define several quantites that appear repeatedly in the expressions:

$$g_+^2 \equiv g^2 + g'^2 \quad g_t^2 \equiv g^2 - \tfrac{5}{3}g'^2 \quad g_b^2 \equiv g^2 - \tfrac{1}{3}g'^2 \qquad \text{(A.123)}$$

$$[T0] \equiv \left[(m^2_{\tilde{L}} - m^2_{\tilde{t_R}}) + \frac{g_t^2}{4}(v'^2 - v^2) \right] \quad [B0] \equiv \left[(m^2_{\tilde{L}} - m^2_{\tilde{b_R}}) - \frac{g_b^2}{4}(v'^2 - v^2) \right] \qquad \text{(A.124)}$$

The A-terms, A_t and A_b, which are allowed to be complex, are written as $A \equiv \Re e\{A\} + i\Im m\{A\}$. Then:

$$\frac{1}{\sqrt{2}v}\frac{\partial\lambda_t}{\partial h_R}\bigg|_{vev} = f_t^2 - \tfrac{g_+^2}{8} \pm \frac{1}{2D_t{}^{\frac{1}{2}}}\Big\{f_t^2(|A_t|^2 + 2m_1\Re e\{A_t\}\cot\beta) - \tfrac{g_t^2}{8}[T0]\Big\}$$

$$\frac{1}{\sqrt{2}v'}\frac{\partial\lambda_t}{\partial h'_R}\bigg|_{vev} = \tfrac{g_+^2}{8} \pm \frac{1}{2D_t{}^{\frac{1}{2}}}\Big\{f_t^2 2m_1(2m_1 + \Re e\{A_t\}\tan\beta) + \tfrac{g_t^2}{8}[T0]\Big\}$$

$$\frac{1}{\sqrt{2}v}\frac{\partial\lambda_b}{\partial h_R}\bigg|_{vev} = \tfrac{g_+^2}{8} \pm \frac{1}{2D_b{}^{\frac{1}{2}}}\Big\{f_b^2 2m_1(2m_1 + \Re e\{A_b\}\cot\beta) + \tfrac{g_b^2}{8}[B0]\Big\}$$

$$\frac{1}{\sqrt{2}v'}\frac{\partial\lambda_b}{\partial h'_R}\bigg|_{vev} = f_b^2 - \tfrac{g_+^2}{8} \pm \frac{1}{2D_b{}^{\frac{1}{2}}}\Big\{f_b^2(|A_b|^2 + 2m_1\Re e\{A_b\}\cot\beta) - \tfrac{g_b^2}{8}[B0]\Big\}$$

$$\frac{\partial\lambda_t}{\partial h_I}\bigg|_{vev} = \pm\frac{1}{\sqrt{2}D_t{}^{\frac{1}{2}}}(-f_t m_t 2m_1\Im m\{A_t\}\cot\beta)$$

$$\frac{\partial\lambda_t}{\partial h'_I}\bigg|_{vev} = \pm\frac{1}{\sqrt{2}D_t{}^{\frac{1}{2}}}(-f_t m_t 2m_1\Im m\{A_t\})$$

$$\frac{\partial\lambda_b}{\partial h_I}\bigg|_{vev} = \pm\frac{1}{\sqrt{2}D_b{}^{\frac{1}{2}}}(-f_b m_b 2m_1\Im m\{A_b\})$$

$$\frac{\partial\lambda_b}{\partial h'_I}\bigg|_{vev} = \pm\frac{1}{\sqrt{2}D_b{}^{\frac{1}{2}}}(-f_b m_b 2m_1\Im m\{A_b\}\tan\beta)$$

Now for the second derivatives:

$$\frac{\partial^2\lambda_t}{\partial h_R^2}\bigg|_{vev} = f_t^2 - \tfrac{g_+^2}{8} \pm \frac{1}{2D_t{}^{\frac{1}{2}}}\Big\{f_t^2|A_t|^2 - \tfrac{g_t^2}{8}[T0] + \tfrac{g_t^4v^2}{16}\Big\} \pm \frac{-1}{2D_t{}^{\frac{3}{2}}}\Big\{f_t m_t\Big[2m_1\Re e\{A_t\}\cot\beta + |A_t|^2\Big] - \tfrac{g_t^2 v}{8}[T0]\Big\}^2$$

$$\frac{\partial^2\lambda_t}{\partial h_R'^2}\bigg|_{vev} = \tfrac{g_+^2}{8} \pm \frac{1}{2D_t{}^{\frac{1}{2}}}\Big\{f_t^2(2m_1)^2 + \tfrac{g_t^2}{8}[T0] + \tfrac{g_t^4v'^2}{16}\Big\} \pm \frac{-1}{2D_t{}^{\frac{3}{2}}}\Big\{f_t m_t 2m_1\Big[2m_1\cot\beta + \Re e\{A_t\}\Big] + \tfrac{g_t^2 v'}{8}[T0]\Big\}^2$$

$$\frac{\partial^2\lambda_t}{\partial h_R\partial h'_R}\bigg|_{vev} = \pm\frac{1}{2D_t{}^{\frac{1}{2}}}\Big\{f_t^2 2m_1\Re e\{A_t\} - \tfrac{g_t^4 vv'}{16}\Big\} \pm \frac{-1}{2D_t{}^{\frac{3}{2}}}\Big\{f_t m_t\Big[2m_1\Re e\{A_t\}\cot\beta + |A_t|^2\Big] - \tfrac{g_t^2 v}{8}[T0]\Big\} \cdot \Big\{f_t m_t 2m_1\Big[2m_1\cot\beta + \Re e\{A_t\}\Big] + \tfrac{g_t^2 v'}{8}[T0]\Big\}$$

The expression for $\left.\frac{\partial^2\lambda_b}{\partial h_R^2}\right|_{vev}$ is obtained from that for $\left.\frac{\partial^2\lambda_t}{\partial h_R'^2}\right|_{vev}$ by the set of substitutions $(v', v, f_t, g_t, A_t, D_t, [T0]) \longrightarrow (v, v', f_b, g_b, A_b, D_b, [B0])$. The expression for $\left.\frac{\partial^2\lambda_b}{\partial h_R'^2}\right|_{vev}$ is obtained from that for $\left.\frac{\partial^2\lambda_t}{\partial h_R^2}\right|_{vev}$, and the expression for $\left.\frac{\partial^2\lambda_b}{\partial h_R \partial h_R'}\right|_{vev}$ is obtained from that for $\left.\frac{\partial^2\lambda_t}{\partial h_R \partial h_R'}\right|_{vev}$ by the same set of substitutions. Remember that $v \leftrightarrow v'$ means that $\cot\beta \leftrightarrow \tan\beta$.

$$\left.\frac{\partial^2\lambda_t}{\partial h_I^2}\right|_{vev} = f_t^2 - \tfrac{g_+^2}{8} \pm \frac{1}{2D_t^{\frac{1}{2}}}\left\{f_t^2|A_t|^2 - \tfrac{g_t^2}{8}[T0]\right\} \pm \frac{-f_t^4 v'^2}{2D_t^{\frac{3}{2}}}(2m_1)^2(\Im m\{A_t\})^2$$

$$\left.\frac{\partial^2\lambda_t}{\partial h_I'^2}\right|_{vev} = \tfrac{g_+^2}{8} \pm \frac{1}{2D_t^{\frac{1}{2}}}\left\{f_t^2(2m_1)^2 + \tfrac{g_t^2}{8}[T0]\right\} \pm \frac{-f_t^4 v^2}{2D_t^{\frac{3}{2}}}(2m_1)^2(\Im m\{A_t\})^2$$

$$\left.\frac{\partial^2\lambda_t}{\partial h_I \partial h_I'}\right|_{vev} = \pm\frac{-f_t^2}{2D_t^{\frac{1}{2}}}2m_1\Re e\{A_t\} \pm \frac{-f_t^4 vv'}{2D_t^{\frac{3}{2}}}(2m_1)^2(\Im m\{A_t\})^2$$

Expressions for the second derivatives of λ_b with respect to the imaginary components of the neutral Higgs fields may be obtained from the λ_t expressions by the same set of substitutions described for the second derivatives with respect to the real components of the Higgs fields.

Note that these formulæ are not valid if $D_t = 0$ and/or $D_b = 0$. This corresponds to the cases where the stop and/or sbottom mass eigenstates ($m_{\tilde{t}_1}, m_{\tilde{t}_2}$ and/or $m_{\tilde{b}_1}, m_{\tilde{b}_2}$) are degenerate. These will be dealt with later as special cases.

Otherwise, we find: $\left.\frac{1}{\sqrt{2}v}\frac{\partial(\Delta\mathcal{V}_{sq})}{\partial h_R}\right|_{vev} =$

$$\begin{aligned}
\frac{3}{32\pi^2}\Bigg\{&\Big\{(f_t^2 - \tfrac{g_+^2}{8})\alpha_t + f_t^2[2m_1\Re e\{A_t\}\cot\beta + |A_t|^2] - \tfrac{g_t^2}{8}[T0]\Big\}\Big[\log(m_{\tilde{t}_1}^2 m_{\tilde{t}_2}^2) + 1\Big] \\
&+ \Big\{2(f_t^2 - \tfrac{g_+^2}{8})D_t^{\frac{1}{2}} + \frac{\alpha_t}{2D_t^{\frac{1}{2}}}\Big[f_t^2[2m_1\Re e\{A_t\}\cot\beta + |A_t|^2] - \tfrac{g_t^2}{8}[T0]\Big]\Big\}\log\left(\frac{m_{\tilde{t}_2}^2}{m_{\tilde{t}_1}^2}\right) \\
&+ \Big\{\tfrac{g_+^2}{8}\alpha_b + f_b^2 2m_1\left[2m_1 + \Re e\{A_b\}\cot\beta\right] + \tfrac{g_b^2}{8}[B0]\Big\}\Big[\log(m_{\tilde{b}_1}^2 m_{\tilde{b}_2}^2) + 1\Big] \\
&+ \Big\{\tfrac{g_+^2}{4}D_b^{\frac{1}{2}} + \frac{\alpha_b}{2D_b^{\frac{1}{2}}}\Big[f_b^2 2m_1\left[2m_1 + \Re e\{A_b\}\cot\beta\right] + \tfrac{g_b^2}{8}[B0]\Big]\Big\}\log\left(\frac{m_{\tilde{b}_2}^2}{m_{\tilde{b}_1}^2}\right)\Bigg\}
\end{aligned} \tag{A.125}$$

The expression for $\frac{1}{\sqrt{2}v'}\frac{\partial(\Delta\mathcal{V}_{sq})}{\partial h'_R}\Big|_{vev}$ is obtained from Eqn. (A.125) for $\frac{1}{\sqrt{2}v}\frac{\partial(\Delta\mathcal{V}_{sq})}{\partial h_R}\Big|_{vev}$ by the set of substitutions

$$(v', f_t, g_t, A_t, \alpha_t, D_t, [T0], m_{\tilde{t}_1}, m_{\tilde{t}_2}) \longleftrightarrow (v, f_b, g_b, A_b, \alpha_b, D_b, [B0], m_{\tilde{b}_1}, m_{\tilde{b}_2}) \quad . \tag{A.126}$$

$$\frac{\partial(\Delta\mathcal{V}_{sq})}{\partial h_I}\Big|_{vev} = \frac{-3\sqrt{2}(2m_1)}{32\pi^2}\Big\{ f_t m_t \Im m\{A_t\}\cot\beta\Big[\log(m^2_{\tilde{t}_1}m^2_{\tilde{t}_2}) + 1 + \frac{\alpha_t}{2D_t^{\frac{1}{2}}}\log\Big(\frac{m^2_{\tilde{t}_2}}{m^2_{\tilde{t}_1}}\Big)\Big] + f_b m_b \Im m\{A_b\}\Big[\log(m^2_{\tilde{b}_1}m^2_{\tilde{b}_2}) + 1 + \frac{\alpha_b}{2D_b^{\frac{1}{2}}}\log\Big(\frac{m^2_{\tilde{b}_2}}{m^2_{\tilde{b}_1}}\Big)\Big]\Big\} \tag{A.127}$$

The expression for $\frac{\partial(\Delta\mathcal{V}_{sq})}{\partial h'_I}\Big|_{vev}$ is obtained from the one above for $\frac{\partial(\Delta\mathcal{V}_{sq})}{\partial h_I}\Big|_{vev}$ by the set of substitutions (A.126).

$$\begin{aligned}
\frac{\partial^2(\Delta\mathcal{V}_{sq})}{\partial h_R^2}\Big|_{vev} = \\
&\frac{3}{32\pi^2}\Big\{ \Big\{4v^2(f_t^2-\tfrac{g_+^2}{8})^2 + \alpha_t(f_t^2-\tfrac{g_+^2}{8}) + f_t^2|A_t|^2 - \tfrac{g_t^2}{8}[T0] + \tfrac{v^2g_t^4}{16}\Big\} \\
&\qquad\qquad \cdot \Big[\log(m^2_{\tilde{t}_1}m^2_{\tilde{t}_2}) + 1\Big] \\
&+ 8v^2(f_t^2-\tfrac{g_+^2}{8})^2 + \frac{2v^2}{D_t}\Big[f_t^2[2m_1\Re e\{A_t\}\cot\beta + |A_t|^2] - \tfrac{g_t^2}{8}[T0]\Big]^2 \\
&+ \frac{1}{2D_t^{\frac{1}{2}}}\Big[(8m_t^2 - v^2g_+^2)\Big\{f_t^2[2m_1\Re e\{A_t\}\cot\beta + |A_t|^2] - \tfrac{g_t^2}{8}[T0]\Big\} \\
&\qquad + 4(f_t^2-\tfrac{g_+^2}{8})D_t + \alpha_t(f_t^2|A_t|^2 - \tfrac{g_t^2}{8}[T0] + \tfrac{v^2g_t^4}{16}) \\
&\qquad - \frac{v^2\alpha_t}{D_t}\Big[f_t^2[2m_1\Re e\{A_t\}\cot\beta + |A_t|^2] - \tfrac{g_t^2}{8}[T0]\Big]^2\Big]\log\Big(\frac{m^2_{\tilde{t}_2}}{m^2_{\tilde{t}_1}}\Big) \\
&+ \Big\{\tfrac{v^2g_+^4}{16} + \tfrac{g_+^2}{8}\alpha_b + f_b^2(2m_1)^2 + \tfrac{g_b^2}{8}[B0] + \tfrac{v^2g_b^4}{16}\Big\}\Big[\log(m^2_{\tilde{b}_1}m^2_{\tilde{b}_2}) + 1\Big] \\
&+ \tfrac{v^2g_+^4}{8} + \frac{2v^2}{D_b}\Big[f_b^2(2m_1)[2m_1 + \Re e\{A_b\}\cot\beta] + \tfrac{g_b^2}{8}[B0]\Big]^2 \\
&+ \frac{1}{2D_b^{\frac{1}{2}}}\Big[v^2g_+^2\Big\{f_b^2(2m_1)[2m_1 + \Re e\{A_b\}\cot\beta] + \tfrac{g_b^2}{8}[B0]\Big\} + \tfrac{g_+^2}{2}D_b \\
&\qquad + \alpha_b\Big\{-\frac{v^2}{D_b}\Big[f_b^2(2m_1)[2m_1 + \Re e\{A_b\}\cot\beta] + \tfrac{g_b^2}{8}[B0]\Big]^2 \\
&\qquad\qquad + f_b^2(2m_1)^2 + \tfrac{g_b^2}{8}[B0] + \tfrac{v^2g_b^4}{16}\Big\}\Big]\log\Big(\frac{m^2_{\tilde{b}_2}}{m^2_{\tilde{b}_1}}\Big)\Big\}
\end{aligned} \tag{A.128}$$

Analogous to what we've seen before, the expression for $\left.\frac{\partial^2(\Delta\mathcal{V}_{sq})}{\partial h_R'^2}\right|_{vev}$ may be obtained from Eqn. (A.128) for $\left.\frac{\partial^2(\Delta\mathcal{V}_{sq})}{\partial h_R^2}\right|_{vev}$ via the set of substitutions (A.126).

$$
\begin{aligned}
&\left.\frac{\partial^2(\Delta\mathcal{V}_{sq})}{\partial h_R \partial h_R'}\right|_{vev} = \\
&\frac{3}{32\pi^2}\Bigg\{ \Big\{ \tfrac{vv'g_+^2}{2}(f_t^2 - \tfrac{g_+^2}{8}) - \tfrac{vv'g_t^2}{16} + f_t^2(2m_1)\Re e\{A_t\}\Big\}\Big[\log(m_{\tilde{t}_1}^2 m_{\tilde{t}_2}^2) + 1\Big] \\
&\quad + vv'g_+^2(f_t^2 - \tfrac{g_+^2}{8}) + \frac{2vv'}{D_t}\Big[f_t^2(2m_1\Re e\{A_t\}\cot\beta + |A_t|^2) - \tfrac{g_t^2}{8}[T0]\Big] \\
&\qquad\qquad \cdot \Big[f_t^2(2m_1)(2m_1 + \Re e\{A_t\}\tan\beta) + \tfrac{g_t^2}{8}[T0]\Big] \\
&\quad + \frac{1}{2D_t^{\frac{1}{2}}}\Bigg[4vv'(f_t^2 - \tfrac{g_+^2}{8})\Big[f_t^2(2m_1)(2m_1 + \Re e\{A_t\}\tan\beta) + \tfrac{g_t^2}{8}[T0]\Big] \\
&\qquad + \tfrac{vv'g_+^2}{2}\Big[f_t^2(2m_1\Re e\{A_t\}\cot\beta + |A_t|^2) - \tfrac{g_t^2}{8}[T0]\Big] \\
&\qquad - \frac{vv'\alpha_t}{D_t}\Big[f_t^2(2m_1\Re e\{A_t\}\cot\beta + |A_t|^2) - \tfrac{g_t^2}{8}[T0]\Big] \\
&\qquad\qquad \cdot \Big[f_t^2(2m_1)(2m_1 + \Re e\{A_t\}\tan\beta) + \tfrac{g_t^2}{8}[T0]\Big] \\
&\qquad\qquad + \alpha_t\Big(f_t^2(2m_1)\Re e\{A_t\} - \tfrac{vv'g_t^4}{16}\Big)\Bigg]\log\left(\frac{m_{\tilde{t}_2}^2}{m_{\tilde{t}_1}^2}\right) \\
&\quad + \Big\{\tfrac{vv'g_+^2}{2}(f_b^2 - \tfrac{g_+^2}{8}) - \tfrac{vv'g_b^2}{16} + f_b^2(2m_1)\Re e\{A_b\}\Big\}\Big[\log(m_{\tilde{b}_1}^2 m_{\tilde{b}_2}^2) + 1\Big] \\
&\quad + vv'g_+^2(f_b^2 - \tfrac{g_+^2}{8}) + \frac{2vv'}{D_b}\Big[f_b^2(2m_1)(2m_1 + \Re e\{A_b\}\cot\beta) + \tfrac{g_b^2}{8}[B0]\Big] \\
&\qquad\qquad \cdot \Big[f_b^2(2m_1\Re e\{A_b\}\tan\beta + |A_b|^2) - \tfrac{g_b^2}{8}[B0]\Big] \\
&\quad + \frac{1}{2D_b^{\frac{1}{2}}}\Bigg[4vv'(f_b^2 - \tfrac{g_+^2}{8})\Big[f_b^2(2m_1)(2m_1 + \Re e\{A_b\}\cot\beta) + \tfrac{g_b^2}{8}[B0]\Big] \\
&\qquad + \tfrac{vv'g_b^2}{2}\Big[f_b^2(2m_1\Re e\{A_b\}\tan\beta + |A_b|^2) - \tfrac{g_b^2}{8}[B0]\Big] \\
&\qquad - \frac{vv'\alpha_b}{D_b}\Big[f_b^2(2m_1)(2m_1 + \Re e\{A_b\}\cot\beta) + \tfrac{g_b^2}{8}[B0]\Big] \\
&\qquad\qquad \cdot \Big[f_b^2(2m_1\Re e\{A_b\}\tan\beta + |A_b|^2) - \tfrac{g_b^2}{8}[B0]\Big] \\
&\qquad\qquad + \alpha_b\Big(f_b^2(2m_1)\Re e\{A_b\} - \tfrac{vv'g_b^4}{16}\Big)\Bigg]\log\left(\frac{m_{\tilde{b}_2}^2}{m_{\tilde{b}_1}^2}\right)\Bigg\}
\end{aligned}
\tag{A.129}
$$

$$\left.\frac{\partial^2(\Delta\mathcal{V}_{sq})}{\partial h_I^2}\right|_{vev} = \frac{3}{32\pi^2}\Bigg\{\Big\{\alpha_t(f_t^2-\tfrac{g_+^2}{8}) + f_t^2|A_t|^2 - \tfrac{g_t^2}{8}[T0]\Big\}\Big[\log(m_{\tilde{t}_1}^2 m_{\tilde{t}_2}^2) + 1\Big]$$
$$+ \frac{2f_t^4 v'^2}{D_t}(2m_1)^2(\Im m\{A_t\})^2$$
$$+ \frac{1}{2D_t^{\frac{1}{2}}}\Bigg[4(f_t^2-\tfrac{g_+^2}{8})D_t - \frac{f_t^4 v'^2\alpha_t}{D_t}(2m_1)^2(\Im m\{A_t\})^2$$
$$+ f_t^2\alpha_t|A_t|^2 - \tfrac{g_t^2}{8}\alpha_t[T0]\Bigg]\log\left(\frac{m_{\tilde{t}_2}^2}{m_{\tilde{t}_1}^2}\right)$$
$$+ \Big\{\alpha_b\tfrac{g_+^2}{8} + f_b^2(2m_1)^2 + \tfrac{g_b^2}{8}[B0]\Big\}\Big[\log(m_{\tilde{b}_1}^2 m_{\tilde{b}_2}^2) + 1\Big]$$
$$+ \frac{2f_b^4 v'^2}{D_b}(2m_1)^2(\Im m\{A_b\})^2$$
$$+ \frac{1}{2D_b^{\frac{1}{2}}}\Bigg[\frac{g_+^2}{2}D_b - \frac{f_b^4 v'^2\alpha_b}{D_b}(2m_1)^2(\Im m\{A_b\})^2$$
$$+ f_b^2\alpha_b(2m_1)^2 + \tfrac{g_b^2}{8}\alpha_b[B0]\Bigg]\log\left(\frac{m_{\tilde{b}_2}^2}{m_{\tilde{b}_1}^2}\right)\Bigg\} \tag{A.130}$$

Again, the expression for $\left.\frac{\partial^2(\Delta\mathcal{V}_{sq})}{\partial h_I'^2}\right|_{vev}$ is obtained from the one for $\left.\frac{\partial^2(\Delta\mathcal{V}_{sq})}{\partial h_I^2}\right|_{vev}$ via the set of substitutions (A.126).

$$\left.\frac{\partial^2(\Delta\mathcal{V}_{sq})}{\partial h_I\partial h_I'}\right|_{vev} = \frac{3}{32\pi^2}\Bigg\{-f_t^2(2m_1)\Re e\{A_t\}\Big[\log(m_{\tilde{t}_1}^2 m_{\tilde{t}_2}^2) + 1\Big]$$
$$+ \frac{2f_t^4 vv'}{D_t}(2m_1)^2(\Im m\{A_t\})^2$$
$$- \frac{f_t^2\alpha_t}{2D_t^{\frac{1}{2}}}(2m_1)\Big[\frac{f_t^2 vv'}{D_t}(2m_1)(\Im m\{A_t\})^2 + \Re e\{A_t\}\Big]\log\left(\frac{m_{\tilde{t}_2}^2}{m_{\tilde{t}_1}^2}\right)$$
$$- f_b^2(2m_1)\Re e\{A_b\}\Big[\log(m_{\tilde{b}_1}^2 m_{\tilde{b}_2}^2) + 1\Big]$$
$$+ \frac{2f_b^4 vv'}{D_b}(2m_1)^2(\Im m\{A_b\})^2$$
$$- \frac{f_b^2\alpha_b}{2D_b^{\frac{1}{2}}}(2m_1)\Big[\frac{f_b^2 vv'}{D_b}(2m_1)(\Im m\{A_b\})^2 + \Re e\{A_b\}\Big]\log\left(\frac{m_{\tilde{b}_2}^2}{m_{\tilde{b}_1}^2}\right)\Bigg\} \tag{A.131}$$

Now once again, just as we did for the quark correction to the potential in Eqns. (A.103) and (A.104), the fact that the minimum of the *complete* potential occurs when the Higgs fields are set equal to their *vev*'s must be taken into account by subtracting the first derivative expressions from the second derivative ones.

$$\left.\frac{\partial^2(\Delta\mathcal{V}_{sq})}{\partial {h_R}^2}\right|_{vev} = \left.\frac{\partial^2(\Delta\mathcal{V}_{sq})}{\partial {h_R}^2}\right|_{vev} - \frac{1}{\sqrt{2}v}\left.\frac{\partial(\Delta\mathcal{V}_{sq})}{\partial h_R}\right|_{vev}$$

$$\begin{aligned}
= \frac{3}{32\pi^2}\Bigg\{ & \Big\{4v^2(f_t^2-\tfrac{g_+^2}{8})^2 + \tfrac{v^2 g_t^4}{16} - f_t^2(2m_1)\Re e\{A_t\}\cot\beta\Big\}\Big[\log(m_{\tilde{t}_1}^2 m_{\tilde{t}_2}^2) + 1\Big] \\
& + 8v^2(f_t^2-\tfrac{g_+^2}{8})^2 + \frac{2v^2}{D_t}\Big[f_t^2[2m_1\Re e\{A_t\}\cot\beta + |A_t|^2] - \tfrac{g_t^2}{8}[T0]\Big]^2 \\
& + \frac{1}{2D_t^{\frac{1}{2}}}\Bigg[(8m_t^2 - v^2g_+^2)\Big\{f_t^2[2m_1\Re e\{A_t\}\cot\beta + |A_t|^2] - \tfrac{g_t^2}{8}[T0]\Big\} \\
& \qquad + \alpha_t\Big\{-\frac{v^2}{D_t}\Big[f_t^2[2m_1\Re e\{A_t\}\cot\beta + |A_t|^2] - \tfrac{g_t^2}{8}[T0]\Big]^2 \\
& \qquad\qquad - f_t^2(2m_1)\Re e\{A_t\}\cot\beta + \tfrac{v^2 g_t^4}{16}\Big\}\Bigg]\log\left(\frac{m_{\tilde{t}_2}^2}{m_{\tilde{t}_1}^2}\right) \\
& + \Big\{\tfrac{v^2(g_+^4+g_b^4)}{16} - f_b^2(2m_1)\Re e\{A_b\}\cot\beta\Big\}\Big[\log(m_{\tilde{b}_1}^2 m_{\tilde{b}_2}^2) + 1\Big] \\
& + \tfrac{v^2 g_+^4}{8} + \frac{2v^2}{D_b}\Big[f_b^2(2m_1)[2m_1 + \Re e\{A_b\}\cot\beta] + \tfrac{g_b^2}{8}[B0]\Big]^2 \\
& + \frac{1}{2D_b^{\frac{1}{2}}}\Bigg[v^2g_+^2\Big\{f_b^2(2m_1)[2m_1 + \Re e\{A_b\}\cot\beta] + \tfrac{g_b^2}{8}[B0]\Big\} \\
& \qquad + \alpha_b\Big\{-\frac{v^2}{D_b}\Big[f_b^2(2m_1)[2m_1 + \Re e\{A_b\}\cot\beta] + \tfrac{g_b^2}{8}[B0]\Big]^2 \\
& \qquad\qquad - f_b^2(2m_1)\Re e\{A_b\}\cot\beta + \tfrac{v^2 g_b^4}{16}\Big\}\Bigg]\log\left(\frac{m_{\tilde{b}_2}^2}{m_{\tilde{b}_1}^2}\right)\Bigg\}
\end{aligned} \tag{A.132}$$

$$\left.\frac{\partial^2(\Delta\mathcal{V}_{sq})}{\partial {h'_R}^2}\right|_{vev} = \left.\frac{\partial^2(\Delta\mathcal{V}_{sq})}{\partial {h'_R}^2}\right|_{vev} - \frac{1}{\sqrt{2}v'}\left.\frac{\partial(\Delta\mathcal{V}_{sq})}{\partial h'_R}\right|_{vev}$$

$$\begin{aligned}
= \frac{3}{32\pi^2}\Bigg\{ & \Big\{\tfrac{v'^2(g_+^4+g_t^4)}{16} - f_t^2(2m_1)\Re e\{A_t\}\tan\beta\Big\}\Big[\log(m^2_{\tilde{t}_1}m^2_{\tilde{t}_2}) + 1\Big] \\
& + \tfrac{v'^2 g_+^4}{8} + \frac{2v'^2}{D_t}\Big[f_t^2(2m_1)[2m_1 + \Re e\{A_t\}\tan\beta] + \tfrac{g_t^2}{8}[T0]\Big]^2 \\
& + \frac{1}{2D_t^{\frac{1}{2}}}\Bigg[v'^2 g_+^2\Big\{f_t^2(2m_1)[2m_1 + \Re e\{A_t\}\tan\beta] + \tfrac{g_t^2}{8}[T0]\Big\} \\
& \qquad + \alpha_t\Big\{-\frac{v'^2}{D_t}\Big[f_t^2(2m_1)[2m_1 + \Re e\{A_t\}\tan\beta] + \tfrac{g_t^2}{8}[T0]\Big]^2 \\
& \qquad\qquad - f_t^2(2m_1)\Re e\{A_t\}\tan\beta + \tfrac{v'^2 g_t^4}{16}\Big\}\Bigg]\log\left(\frac{m^2_{\tilde{t}_2}}{m^2_{\tilde{t}_1}}\right) \\
& + \Big\{4v'^2(f_b^2 - \tfrac{g_+^2}{8})^2 + \tfrac{v'^2 g_b^4}{16} - f_b^2(2m_1)\Re e\{A_b\}\tan\beta\Big\} \\
& \qquad\qquad \cdot \Big[\log(m^2_{\tilde{b}_1}m^2_{\tilde{b}_2}) + 1\Big] \\
& + 8v'^2(f_b^2 - \tfrac{g_+^2}{8})^2 + \frac{2v'^2}{D_b}\Big[f_b^2[2m_1\Re e\{A_b\}\tan\beta + |A_b|^2] - \tfrac{g_b^2}{8}[B0]\Big]^2 \\
& + \frac{1}{2D_b^{\frac{1}{2}}}\Bigg[(8m_b^2 - v'^2 g_+^2)\Big\{f_b^2[2m_1\Re e\{A_b\}\tan\beta + |A_b|^2] - \tfrac{g_b^2}{8}[B0]\Big\} \\
& \qquad + \alpha_b\Big\{-\frac{v'^2}{D_b}\Big[f_b^2[2m_1\Re e\{A_b\}\tan\beta + |A_b|^2] - \tfrac{g_b^2}{8}[B0]\Big]^2 \\
& \qquad\qquad - f_b^2(2m_1)\Re e\{A_b\}\tan\beta + \tfrac{v'^2 g_b^4}{16}\Big\}\Bigg]\log\left(\frac{m^2_{\tilde{b}_2}}{m^2_{\tilde{b}_1}}\right)\Bigg\}
\end{aligned} \tag{A.133}$$

Note that this expression can be obtained from the last equation via (A.126).

$$\left.\frac{\partial^2(\Delta\mathcal{V}_{sq})}{\partial {h_I}^2}\right|_{vev} = \left.\frac{\partial^2(\Delta\mathcal{V}_{sq})}{\partial {h_I}^2}\right|_{vev} - \frac{1}{\sqrt{2}v}\left.\frac{\partial(\Delta\mathcal{V}_{sq})}{\partial h_R}\right|_{vev}$$

$$\begin{aligned}
= \frac{3}{32\pi^2}\Bigg\{ & \Big\{ -f_t^2 \Re e\{A_t\}\cot\beta\left[\log(m_{\tilde{t}_1}^2 m_{\tilde{t}_2}^2) + 1\right] + \frac{2f_t^4 v'^2}{D_t}(2m_1)(\Im m\{A_t\})^2 \\
& - \frac{f_t^2\alpha_t}{2D_t^{\frac{1}{2}}}\left[\Re e\{A_t\}\cot\beta + \frac{f_t^2 v'^2}{D_t}(2m_1)(\Im m\{A_t\})^2\right]\log\left(\frac{m_{\tilde{t}_2}^2}{m_{\tilde{t}_1}^2}\right) \\
& - f_b^2 \Re e\{A_b\}\cot\beta\left[\log(m_{\tilde{b}_1}^2 m_{\tilde{b}_2}^2) + 1\right] + \frac{2f_b^4 v'^2}{D_b}(2m_1)(\Im m\{A_b\})^2 \\
& - \frac{f_b^2\alpha_b}{2D_b^{\frac{1}{2}}}\left[\Re e\{A_b\}\cot\beta + \frac{f_b^2 v'^2}{D_b}(2m_1)(\Im m\{A_b\})^2\right]\log\left(\frac{m_{\tilde{b}_2}^2}{m_{\tilde{b}_1}^2}\right)\Big\}
\end{aligned} \tag{A.134}$$

$$\left.\frac{\partial^2(\Delta\mathcal{V}_{sq})}{\partial {h'_I}^2}\right|_{vev} = \left.\frac{\partial^2(\Delta\mathcal{V}_{sq})}{\partial {h'_I}^2}\right|_{vev} - \frac{1}{\sqrt{2}v}\left.\frac{\partial(\Delta\mathcal{V}_{sq})}{\partial h'_R}\right|_{vev}$$

$$\begin{aligned}
= \frac{3}{32\pi^2}\Bigg\{ & \Big\{ -f_t^2 \Re e\{A_t\}\tan\beta\left[\log(m_{\tilde{t}_1}^2 m_{\tilde{t}_2}^2) + 1\right] + \frac{2f_t^4 v^2}{D_t}(2m_1)(\Im m\{A_t\})^2 \\
& - \frac{f_t^2\alpha_t}{2D_t^{\frac{1}{2}}}\left[\Re e\{A_t\}\tan\beta + \frac{f_t^2 v^2}{D_t}(2m_1)(\Im m\{A_t\})^2\right]\log\left(\frac{m_{\tilde{t}_2}^2}{m_{\tilde{t}_1}^2}\right) \\
& - f_b^2 \Re e\{A_b\}\tan\beta\left[\log(m_{\tilde{b}_1}^2 m_{\tilde{b}_2}^2) + 1\right] + \frac{2f_b^4 v^2}{D_b}(2m_1)(\Im m\{A_b\})^2 \\
& - \frac{f_b^2\alpha_b}{2D_b^{\frac{1}{2}}}\left[\Re e\{A_b\}\tan\beta + \frac{f_b^2 v^2}{D_b}(2m_1)(\Im m\{A_b\})^2\right]\log\left(\frac{m_{\tilde{b}_2}^2}{m_{\tilde{b}_1}^2}\right)\Big\}
\end{aligned} \tag{A.135}$$

Once again, Eqn. (A.135) may be obtained from Eqn. (A.134) using the substitutions (A.126).

A.8 Neutral Higgs Boson Masses with Radiative Corrections

We are now in a position to calculate the masses and mixing angle for the neutral Higgs bosons with radiative corrections included. But before we do this, we should take note of an extra restraint that exists due to the fact that $\frac{\partial(\Delta\mathcal{V}_{sq})}{\partial h_I}\Big|_{vev} \neq 0$ and $\frac{\partial(\Delta\mathcal{V}_{sq})}{\partial h'_I}\Big|_{vev} \neq 0$ in Eqn. (A.127)) without specifying and addition condition. In Eqn. (A.24) and also for the quark and squark corrections we have used the fact that the minimum of the potential occurs when the Higgs fields are set equal to their *vev*'s; *i.e.*,

$$\frac{\partial\mathcal{V}}{\partial h}\Big|_{vev} = 0 \qquad \frac{\partial\mathcal{V}}{\partial h'}\Big|_{vev} = 0 \quad . \tag{A.136}$$

This leads immediately to $\frac{\partial\mathcal{V}}{\partial h_R}\Big|_{vev} = 0$ and $\frac{\partial\mathcal{V}}{\partial h'_R}\Big|_{vev} = 0$, which is what we have used. But Eqns. (A.136) also require that $\frac{\partial\mathcal{V}}{\partial h_I}\Big|_{vev} = 0$ and $\frac{\partial\mathcal{V}}{\partial h'_I}\Big|_{vev} = 0$. Now since $\frac{\partial\mathcal{V}_{tree}}{\partial h_I}\Big|_{vev} = \frac{\partial(\Delta\mathcal{V}_{qk})}{\partial h_I}\Big|_{vev} = \frac{\partial\mathcal{V}_{tree}}{\partial h'_I}\Big|_{vev} = \frac{\partial(\Delta\mathcal{V}_{qk})}{\partial h'_I}\Big|_{vev} = 0$ (Eqns.(A.16) and (A.101)), we must also set $\frac{\partial(\Delta\mathcal{V}_{sq})}{\partial h_I}\Big|_{vev} = \frac{\partial(\Delta\mathcal{V}_{sq})}{\partial h'_I}\Big|_{vev} = 0$. This yields the following condition:

$$f_t^2 \Im m\{A_t\}\left[\log(m^2_{\tilde{t}_1} m^2_{\tilde{t}_2}) + 1 + \frac{m^2_{\tilde{t}_1} + m^2_{\tilde{t}_2}}{m^2_{\tilde{t}_2} - m^2_{\tilde{t}_1}} \log\left(\frac{m^2_{\tilde{t}_2}}{m^2_{\tilde{t}_1}}\right)\right] \tag{A.137}$$
$$+ f_b^2 \Im m\{A_b\}\left[\log(m^2_{\tilde{b}_1} m^2_{\tilde{b}_2}) + 1 + \frac{m^2_{\tilde{b}_1} + m^2_{\tilde{b}_2}}{m^2_{\tilde{b}_2} - m^2_{\tilde{b}_1}} \log\left(\frac{m^2_{\tilde{b}_2}}{m^2_{\tilde{b}_1}}\right)\right] = 0$$

Several things merit mentioning. First, if the A-terms are made real there is no extra condition. Second, since $\alpha_t, \alpha_b > 0$ for all reasonable choices of MSSM parameters and $m_{\tilde{t}_2} \geq m_{\tilde{t}_1}$, $m_{\tilde{b}_2} \geq m_{\tilde{b}_1}$, Eqn. (A.137) requires that if $\Im m\{A_t\} \neq 0$ ($\Im m\{A_b\} \neq 0$), then $\Im m\{A_b\} \neq 0$ ($\Im m\{A_t\} \neq 0$), and $\Im m\{A_t\}$ and $\Im m\{A_b\}$ must have opposite signs. Finally, we should note that this is a rather special case, since only the A-terms are allowed to be complex, (other coupling parameters such as $2m_1$, g, g', f_t, and f_b are assumed to be real — all of these could in principle be complex). Also, I am neglecting contributions from other sfermion flavors as well as from pure gauge boson and gaugino/higgsino interactions. Allowing other complex couplings (or *vev*'s) and including corrections from other sectors can make Eqn.

(A.137) more complicated. Also, restrictions on complex couplings from limits on CP violation and other conditions not considered here must be applied. We will not incorporate Eqn. (A.137) into subsequent formulæ (since we are primarily interested in cases in which the A-terms are real), but leave it as an auxilliary condition to be applied if the A-terms do have imaginary components, bearing in mind the caveat that several other couplings have been assumed to be real.

For the CP-odd squared pseudoscalar mass matrix, using Eqns. (A.32), (A.104), (A.131), (A.134), and (A.135), we obtain

$$\mathcal{M}_{H_p^2} = \begin{bmatrix} -\bar{m}_{rad}^2 \cot\beta & -\bar{m}_{rad}^2 \\ -\bar{m}_{rad}^2 & -\bar{m}_{rad}^2 \tan\beta \end{bmatrix} \tag{A.138}$$

which is just the tree-level form, Eqn. (A.35), with $\bar{m}_{12}^2$ replaced by $\bar{m}_{rad}^2$ where

$$\begin{aligned} \bar{m}_{rad}^2 \;=\; \bar{m}_{12}^2 \;+\; \frac{3(2m_1)}{32\pi^2}\Bigg\{ & f_t^2 \Re e\{A_t\}\Big[\log(m_{\tilde{t}_1}^2 m_{\tilde{t}_2}^2) \;+\; 1 \;+\; \frac{m_{\tilde{t}_1}^2 + m_{\tilde{t}_2}^2}{m_{\tilde{t}_2}^2 - m_{\tilde{t}_1}^2} \log\left(\frac{m_{\tilde{t}_2}^2}{m_{\tilde{t}_1}^2}\right)\Big] \\ & - \frac{f_t^4 vv'}{2D_t}(2m_1)(\Im m\{A_t\})^2 \left[4 - \frac{m_{\tilde{t}_1}^2 + m_{\tilde{t}_2}^2}{m_{\tilde{t}_2}^2 - m_{\tilde{t}_1}^2} \log\left(\frac{m_{\tilde{t}_2}^2}{m_{\tilde{t}_1}^2}\right)\right] \\ & + f_b^2 \Re e\{A_b\}\Big[\log(m_{\tilde{b}_1}^2 m_{\tilde{b}_2}^2) \;+\; 1 \;+\; \frac{m_{\tilde{b}_1}^2 + m_{\tilde{b}_2}^2}{m_{\tilde{b}_2}^2 - m_{\tilde{b}_1}^2} \log\left(\frac{m_{\tilde{b}_2}^2}{m_{\tilde{b}_1}^2}\right)\Big] \\ & - \frac{f_b^4 vv'}{2D_b}(2m_1)(\Im m\{A_b\})^2 \left[4 - \frac{m_{\tilde{b}_1}^2 + m_{\tilde{b}_2}^2}{m_{\tilde{b}_2}^2 - m_{\tilde{b}_1}^2} \log\left(\frac{m_{\tilde{b}_2}^2}{m_{\tilde{b}_1}^2}\right)\right]\Bigg\} \end{aligned} \tag{A.139}$$

The Goldstone mode is thus recovered with the mass of the pseudoscalar Higgs boson:

$$m_{Goldstone^0} = 0 \quad \text{and} \quad m_{H_p}^2 = \frac{-2\bar{m}_{rad}^2}{\sin 2\beta} \quad . \tag{A.140}$$

Notice that there are terms in $\bar{m}_{rad}^2$ and thus in $m_{H_p}^2$ which have logarithms whose arguments are not dimensionless. To make the arguments dimensionless, some arbitrary mass scale, Q, must be inserted into the problem, so, for example,

$$\log(m_{\tilde{t}_1} m_{\tilde{t}_2}) \;\Rightarrow\; \log\Big(\frac{m_{\tilde{t}_1} m_{\tilde{t}_2}}{Q^4}\Big) \; .$$

In practice, we will be inputting a pseudoscalar Higgs mass and then determining the masses of the other Higgs bosons just as we did in Eqns. (A.40) for the tree

level case. The dependence on the arbitrary mass scale Q may be expected to then disappear if the approximations that have gone into the calculation are discounted (this will be discussed further later).

Using the expression for $m^2_{H_p}$ to replace the $\bar{m}_{12}$ dependence, we finally arrive at the entries for the CP-even squared mass matrix. From Eqns. (A.31), (A.103), (A.132), (A.139), and (A.140), we obtain:

$$
\begin{aligned}
\left.\frac{\partial^2 \mathcal{V}}{\partial h_R^2}\right|_{vev} \;=\; & m^2_{H_p}\cos^2\beta \;+\; m^2_{Z^0}\sin^2\beta \\
& + \frac{3v^2}{32\pi^2}\Bigg\{ 4f_t^4 \log\!\left(\frac{m^2_{\tilde{t}_1} m^2_{\tilde{t}_2}}{m_t^4}\right) \;+\; \left(-f_t^2 g_+^2 + \tfrac{g_+^4+g_t^4}{16}\right)\log\!\left(\frac{m^2_{\tilde{t}_1} m^2_{\tilde{t}_2}}{Q^4}\right) \\
& \quad - \frac{8f_t^4\cot^2\beta}{(m^2_{\tilde{t}_2}-m^2_{\tilde{t}_1})^2}(2m_1)^2(\Im m\{A_t\})^2 \;-\; 3f_t^2 g_+^2 + \tfrac{3g_+^4+g_t^4}{16} \\
& \quad + \frac{8}{(m^2_{\tilde{t}_1}-m^2_{\tilde{t}_2})^2}\Big[f_t^2[2m_1\Re e\{A_t\}\cot\beta + |A_t|^2] \;-\; \tfrac{g_t^2}{8}[T0]\Big]^2 \\
& \quad + \frac{1}{(m^2_{\tilde{t}_2}-m^2_{\tilde{t}_1})}\Bigg[(8f_t^2 - g_+^2)\Big[f_t^2[2m_1\Re e\{A_t\}\cot\beta + |A_t|^2] \;-\; \tfrac{g_t^2}{8}[T0]\Big] \\
& \qquad + \frac{(m^2_{\tilde{t}_1}+m^2_{\tilde{t}_2})}{(m^2_{\tilde{t}_2}-m^2_{\tilde{t}_1})^2}\Big[-4\{f_t^2[2m_1\Re e\{A_t\}\cot\beta + |A_t|^2] \;-\; \tfrac{g_t^2}{8}[T0]\}^2 \\
& \qquad\quad + \tfrac{g_t^4}{16}(m^2_{\tilde{t}_2}-m^2_{\tilde{t}_1})^2 \;+\; 4f_t^4\cot^2\beta(2m_1)^2(\Im m\{A_t\})^2\Big]\Bigg]\log\!\left(\frac{m^2_{\tilde{t}_2}}{m^2_{\tilde{t}_1}}\right) \\
& \quad + \left(\tfrac{g_+^4+g_b^4}{16}\right)\log\!\left(\frac{m^2_{\tilde{b}_1} m^2_{\tilde{b}_2}}{Q^4}\right) \\
& \quad - \frac{8f_b^4\cot^2\beta}{(m^2_{\tilde{b}_2}-m^2_{\tilde{b}_1})^2}(2m_1)^2(\Im m\{A_b\})^2 \;+\; \tfrac{3g_+^4+g_b^4}{16} \\
& \quad + \frac{8}{(m^2_{\tilde{b}_2}-m^2_{\tilde{b}_1})^2}\Big[f_b^2(2m_1)[2m_1 + \Re e\{A_b\}\cot\beta] \;+\; \tfrac{g_b^2}{8}[B0]\Big]^2 \\
& \quad + \frac{1}{(m^2_{\tilde{b}_2}-m^2_{\tilde{b}_1})}\Bigg[g_+^2\Big[f_b^2(2m_1)[2m_1 + \Re e\{A_b\}\cot\beta] \;+\; \tfrac{g_b^2}{8}[B0]\Big] \\
& \qquad + \frac{(m^2_{\tilde{b}_2}+m^2_{\tilde{b}_1})}{(m^2_{\tilde{b}_2}-m^2_{\tilde{b}_1})^2}\Big[-4\{f_b^2(2m_1)[2m_1 + \Re e\{A_b\}\cot\beta] \;+\; \tfrac{g_b^2}{8}[B0]\}^2 \\
& \qquad\quad + \frac{g_b^4}{16}(m^2_{\tilde{b}_2}-m^2_{\tilde{b}_1})^2 \;+\; 4f_b^4\cot^2\beta(2m_1)^2(\Im m\{A_b\})^2\Big]\Bigg]\log\!\left(\frac{m^2_{\tilde{b}_2}}{m^2_{\tilde{b}_1}}\right)\Bigg\}
\end{aligned}
\tag{A.141}
$$

From Eqns. (A.31), (A.103), (A.133), (A.139), and (A.140), we obtain:

$$
\begin{aligned}
\left.\frac{\partial^2 \mathcal{V}}{\partial {h'_R}^2}\right|_{vev} &= m_{H_p}^2 \sin^2\beta \;+\; m_{Z^0}^2 \cos^2\beta \\
&+ \frac{3v^2}{32\pi^2}\Bigg\{ \left(\tfrac{g_+^4+g_t^4}{16}\right) \log\!\left(\frac{m_{\tilde{t}_1}^2 m_{\tilde{t}_2}^2}{Q^4}\right) \\
&\quad + \frac{8}{(m_{\tilde{t}_2}^2 - m_{\tilde{t}_1}^2)^2}\Big[f_t^2(2m_1)[2m_1 + \Re e\{A_b\}\tan\beta] \;+\; \tfrac{g_t^2}{8}[T0]\Big]^2 \\
&\quad - \frac{8 f_t^4 \tan^2\beta}{(m_{\tilde{t}_2}^2 - m_{\tilde{t}_1}^2)^2}(2m_1)^2(\Im m\{A_t\})^2 \;+\; \tfrac{3g_+^4+g_t^4}{16} \\
&\quad + \frac{1}{(m_{\tilde{t}_2}^2 - m_{\tilde{t}_1}^2)}\Bigg[g_+^2\Big[f_t^2(2m_1)[2m_1 + \Re e\{A_t\}\tan\beta] \;+\; \tfrac{g_t^2}{8}[T0]\Big] \\
&\qquad + \frac{(m_{\tilde{t}_2}^2 + m_{\tilde{t}_1}^2)}{(m_{\tilde{t}_2}^2 - m_{\tilde{t}_1}^2)^2}\Big[-4\{f_t^2(2m_1)[2m_1 + \Re e\{A_t\}\tan\beta] \;+\; \tfrac{g_t^2}{8}[T0]\}^2 \\
&\qquad + \tfrac{g_t^4}{16}(m_{\tilde{t}_2}^2 - m_{\tilde{t}_1}^2)^2 \;+\; 4f_t^4\tan^2\beta(2m_1)^2(\Im m\{A_t\})^2\Big]\Bigg] \log\!\left(\frac{m_{\tilde{t}_2}^2}{m_{\tilde{t}_1}^2}\right) \\
&\quad + 4f_b^4 \log\!\left(\frac{m_{\tilde{b}_1}^2 m_{\tilde{b}_2}^2}{m_b^4}\right) \;-\; 3f_b^2 g_+^2 + \tfrac{3g_+^4+g_b^4}{16} \\
&\quad + \left(-f_b^2 g_+^2 + \tfrac{g_+^4+g_b^4}{16}\right) \log\!\left(\frac{m_{\tilde{b}_1}^2 m_{\tilde{b}_2}^2}{Q^4}\right) \\
&\quad + \frac{8}{(m_{\tilde{b}_1}^2 - m_{\tilde{b}_2}^2)^2}\Big[f_b^2[2m_1 \Re e\{A_b\}\tan\beta + |A_b|^2] \;-\; \tfrac{g_b^2}{8}[B0]\Big]^2 \\
&\quad - \frac{8 f_b^4 \tan^2\beta}{(m_{\tilde{b}_2}^2 - m_{\tilde{b}_1}^2)^2}(2m_1)^2(\Im m\{A_b\})^2 \\
&\quad + \frac{1}{(m_{\tilde{b}_2}^2 - m_{\tilde{b}_1}^2)}\Bigg[(8f_b^2 - g_+^2)\Big[f_b^2[2m_1 \Re e\{A_b\}\tan\beta + |A_b|^2] \;-\; \tfrac{g_b^2}{8}[B0]\Big] \\
&\qquad + \frac{(m_{\tilde{b}_1}^2 + m_{\tilde{b}_2}^2)}{(m_{\tilde{b}_2}^2 - m_{\tilde{b}_1}^2)^2}\Big[-4\{f_b^2[2m_1 \Re e\{A_b\}\tan\beta + |A_b|^2] \;-\; \tfrac{g_b^2}{8}[B0]\}^2 \\
&\qquad + \tfrac{g_b^4}{16}(m_{\tilde{b}_2}^2 - m_{\tilde{b}_1}^2)^2 \;+\; 4f_b^4\tan^2\beta(2m_1)^2(\Im m\{A_b\})^2\Big]\Bigg] \log\!\left(\frac{m_{\tilde{b}_2}^2}{m_{\tilde{b}_1}^2}\right)\Bigg\}
\end{aligned}
\tag{A.142}
$$

Again we find Eqn. (A.142) is obtained from Eqn. (A.141) through the set of substitutions (A.126).

$$
\left.\frac{\partial^2 \mathcal{V}}{\partial h_R \partial h'_R}\right|_{vev} = (m^2_{H_p} + m^2_{Z^0})\sin\beta\cos\beta
$$

$$
+ \frac{3vv'}{32\pi^2}\Bigg\{ \Big(f_t^2\frac{g_+^2}{2} - \frac{g_+^4+g_t^4}{16}\Big)\log\Big(\frac{m^2_{\tilde{t}_1}m^2_{\tilde{t}_2}}{Q^4}\Big) + \tfrac{3}{2}f_t^2 g_+^2 - \tfrac{3g_+^4+g_t^4}{16}
$$

$$
+ \frac{8}{(m^2_{\tilde{t}_2}-m^2_{\tilde{t}_1})^2}\Big[\Big\{f_t^2(2m_1\Re e\{A_t\}\cot\beta + |A_t|^2) - \tfrac{g_t^2}{8}[T0]\Big\}
$$

$$
\cdot\Big\{f_t^2(2m_1)(2m_1+\Re e\{A_t\}\tan\beta) + \tfrac{g_t^2}{8}[T0]\Big\} + f_t^4(2m_1)^2(\Im m\{A_t\})^2\Big]
$$

$$
+ \frac{1}{(m^2_{\tilde{t}_2}-m^2_{\tilde{t}_1})}\Big[4(f_t^2-\tfrac{g_+^2}{8})\Big[f_t^2(2m_1)(2m_1+\Re e\{A_t\}\tan\beta) + \tfrac{g_t^2}{8}[T0]\Big]
$$

$$
+ \tfrac{g_+^2}{2}\Big[f_t^2(2m_1\Re e\{A_t\}\cot\beta + |A_t|^2) - \tfrac{g_t^2}{8}[T0]\Big]
$$

$$
- \frac{(m^2_{\tilde{t}_1}+m^2_{\tilde{t}_2})}{(m^2_{\tilde{t}_2}-m^2_{\tilde{t}_1})^2}\Big[4\Big\{f_t^2(2m_1\Re e\{A_t\}\cot\beta + |A_t|^2) - \tfrac{g_t^2}{8}[T0]\Big\}
$$

$$
\cdot\Big\{f_t^2(2m_1)(2m_1+\Re e\{A_t\}\tan\beta) + \tfrac{g_t^2}{8}[T0]\Big\}
$$

$$
+ \tfrac{g_t^4}{16}(m^2_{\tilde{t}_2}-m^2_{\tilde{t}_1})^2 + 4f_t^4(2m_1)^2(\Im m\{A_t\})^2\Big]\Big]\log\Big(\frac{m^2_{\tilde{t}_2}}{m^2_{\tilde{t}_1}}\Big)
$$

$$
+ \Big(f_b^2\tfrac{g_+^2}{2} - \tfrac{g_+^4+g_b^4}{16}\Big)\log\Big(\frac{m^2_{\tilde{b}_1}m^2_{\tilde{b}_2}}{Q^4}\Big) + \tfrac{3}{2}f_b^2 g_+^2 - \tfrac{3g_+^4+g_b^4}{16}
$$

$$
+ \frac{8}{(m^2_{\tilde{t}_2}-m^2_{\tilde{t}_1})^2}\Big[\Big\{f_b^2(2m_1)(2m_1+\Re e\{A_b\}\cot\beta) + \tfrac{g_b^2}{8}[B0]\Big\}
$$

$$
\cdot\Big\{f_b^2(2m_1\Re e\{A_b\}\tan\beta + |A_b|^2) - \tfrac{g_b^2}{8}[B0]\Big\} + f_b^4(2m_1)^2(\Im m\{A_b\})^2\Big]
$$

$$
+ \frac{1}{(m^2_{\tilde{b}_2}-m^2_{\tilde{b}_1})}\Big[4(f_b^2-\tfrac{g_+^2}{8})\Big[f_b^2(2m_1)(2m_1+\Re e\{A_b\}\cot\beta) + \tfrac{g_b^2}{8}[B0]\Big]
$$

$$
+ \tfrac{g_b^2}{2}\Big[f_b^2(2m_1\Re e\{A_b\}\tan\beta + |A_b|^2) - \tfrac{g_b^2}{8}[B0]\Big]
$$

$$
- \frac{(m^2_{\tilde{b}_1}+m^2_{\tilde{b}_2})}{(m^2_{\tilde{b}_2}-m^2_{\tilde{b}_1})^2}\Big[4\Big\{f_b^2(2m_1)(2m_1+\Re e\{A_b\}\cot\beta) + \tfrac{g_b^2}{8}[B0]\Big\}
$$

$$
\cdot\Big\{f_b^2(2m_1\Re e\{A_b\}\tan\beta + |A_b|^2) - \tfrac{g_b^2}{8}[B0]\Big\}
$$

$$
+ \tfrac{g_b^4}{16}(m^2_{\tilde{b}_2}-m^2_{\tilde{b}_1})^2 + 4f_b^4(2m_1)^2(\Im m\{A_b\})^2\Big]\Big\}\log\Big(\frac{m^2_{\tilde{b}_2}}{m^2_{\tilde{b}_1}}\Big)\Bigg\}
$$

(A.143)

Eqns. (A.141 – A.143) give the entries for the CP-even neutral Higgs squared mass matrix (A, C, and B of Eqn. (A.33), respectively). The light and heavy Higgs masses are now found by finding the eigenvalues of this matix. The resulting expressions for $m^2_{H_\ell}$ and $m^2_{H_h}$ are given by Eqn. (A.34). Plugging Eqns. (A.141 – A.143) into Equation (A.34) would result in very unwieldy expressions for the masses, and will not be done here. However, it is easy to do this numerically for a given choice of parameters. Similarly, the scalar Higgs mixing angle, α, can be found by substituting Eqns. (A.141 – A.143) into Eqn.(A.51).

Notice that in Eqns. (A.141 – A.143) the arbitrary mass Q must be added to make the arguments of some logarithms dimensionless. This arbitrariness would not be there if all relevant diagrams had been incorporated into our calculation. But, as has already been mentioned, gauge boson/Higgs and gaugino/higgsino/Higgs interactions have been neglected. Inclusion of these interactions in the calculation of the effective potential correction to the scalar potential would eliminate the need for the arbitrary mass in our expressions for the physical Higgs masses. All the offending logarithmic terms in Eqns. (A.141 – A.143) contain the gauge couplings g and g' which enter from the D-term contributions to the squark mass matrix. This must be the case if such terms are to be fixed by terms from the gauge boson and gaugino/higgsino sectors. The justification for including the D-terms contributions in the squark mass matrix while neglecting corection terms to the scalar potential from these other sectors is that some of the D-term contributions are proportional to the top quark coupling in addition to the gauge couplings ($\sim f_t^2 g^2$ for example), and these mixed terms can have a much larger effect than pure terms with only gauge couplings.

If the D-terms are all removed, and the A-terms are assumed to be real, the expressions simplify considerably. We obtain:

$$\left.\frac{\partial^2\mathcal{V}}{\partial h_R^2}\right|_{vev} = m_{H_p}^2\cos^2\beta + m_{Z^0}^2\sin^2\beta + \frac{3g^2}{16\pi^2 m_W^2}\left\{\frac{m_t^4}{\sin^2\beta}\left[\log\left(\frac{m_{\tilde{t}_1}^2 m_{\tilde{t}_2}^2}{m_t^4}\right) + \frac{2A_t(A_t+2m_1\cot\beta)}{m_{\tilde{t}_2}^2-m_{\tilde{t}_1}^2}\log\left(\frac{m_{\tilde{t}_2}^2}{m_{\tilde{t}_1}^2}\right)\right] + \frac{m_t^4}{\sin^2\beta}\left[\frac{A_t(A_t+2m_1\cot\beta)}{m_{\tilde{t}_2}^2-m_{\tilde{t}_1}^2}\right]^2\left[2 - \frac{m_{\tilde{t}_1}^2+m_{\tilde{t}_2}^2}{m_{\tilde{t}_2}^2-m_{\tilde{t}_1}^2}\log\left(\frac{m_{\tilde{t}_2}^2}{m_{\tilde{t}_1}^2}\right)\right] + \frac{m_b^4}{\cos^2\beta}\left[\frac{(2m_1)(A_b+2m_1\tan\beta)}{m_{\tilde{b}_2}^2-m_{\tilde{b}_1}^2}\right]^2\left[2 - \frac{m_{\tilde{b}_1}^2+m_{\tilde{b}_2}^2}{m_{\tilde{b}_2}^2-m_{\tilde{b}_1}^2}\log\left(\frac{m_{\tilde{b}_2}^2}{m_{\tilde{b}_1}^2}\right)\right]\right\} \tag{A.144}$$

$$\left.\frac{\partial^2\mathcal{V}}{\partial h_R'^2}\right|_{vev} = m_{H_p}^2\sin^2\beta + m_{Z^0}^2\cos^2\beta + \frac{3g^2}{16\pi^2 m_W^2}\left\{\frac{m_b^4}{\cos^2\beta}\left[\log\left(\frac{m_{\tilde{b}_1}^2 m_{\tilde{b}_2}^2}{m_b^4}\right) + \frac{2A_b(A_b+2m_1\tan\beta)}{m_{\tilde{b}_2}^2-m_{\tilde{b}_1}^2}\log\left(\frac{m_{\tilde{b}_2}^2}{m_{\tilde{b}_1}^2}\right)\right] + \frac{m_t^4}{\sin^2\beta}\left[\frac{2m_1(A_t+2m_1\cot\beta)}{m_{\tilde{t}_2}^2-m_{\tilde{t}_1}^2}\right]^2\left[2 - \frac{m_{\tilde{t}_1}^2+m_{\tilde{t}_2}^2}{m_{\tilde{t}_2}^2-m_{\tilde{t}_1}^2}\log\left(\frac{m_{\tilde{t}_2}^2}{m_{\tilde{t}_1}^2}\right)\right] + \frac{m_b^4}{\cos^2\beta}\left[\frac{A_b(A_b+2m_1\tan\beta)}{m_{\tilde{b}_2}^2-m_{\tilde{b}_1}^2}\right]^2\left[2 - \frac{m_{\tilde{b}_1}^2+m_{\tilde{b}_2}^2}{m_{\tilde{b}_2}^2-m_{\tilde{b}_1}^2}\log\left(\frac{m_{\tilde{b}_2}^2}{m_{\tilde{b}_1}^2}\right)\right]\right\} \tag{A.145}$$

$$\left.\frac{\partial^2\mathcal{V}}{\partial h_R\partial h_R'}\right|_{vev} = -(m_{H_p}^2 + m_{Z^0}^2)\sin\beta\cos\beta + \frac{3g^2}{16\pi^2 m_W^2}\left\{\frac{m_t^4}{\sin^2\beta}\frac{(2m_1)(A_t+2m_1\cot\beta)}{m_{\tilde{t}_2}^2-m_{\tilde{t}_1}^2}\left[\log\left(\frac{m_{\tilde{t}_2}^2}{m_{\tilde{t}_1}^2}\right) + \frac{A_t(A_t+2m_1\cot\beta)}{m_{\tilde{t}_2}^2-m_{\tilde{t}_1}^2}\left[2 - \frac{m_{\tilde{t}_1}^2+m_{\tilde{t}_2}^2}{m_{\tilde{t}_2}^2-m_{\tilde{t}_1}^2}\log\left(\frac{m_{\tilde{t}_2}^2}{m_{\tilde{t}_1}^2}\right)\right]\right] + \frac{m_b^4}{\cos^2\beta}\frac{(2m_1)(A_b+2m_1\tan\beta)}{m_{\tilde{b}_2}^2-m_{\tilde{b}_1}^2}\left[\log\left(\frac{m_{\tilde{b}_2}^2}{m_{\tilde{b}_1}^2}\right) + \frac{A_b(A_b+2m_1\tan\beta)}{m_{\tilde{b}_2}^2-m_{\tilde{b}_1}^2}\left[2 - \frac{m_{\tilde{b}_1}^2+m_{\tilde{b}_2}^2}{m_{\tilde{b}_2}^2-m_{\tilde{b}_1}^2}\log\left(\frac{m_{\tilde{b}_2}^2}{m_{\tilde{b}_1}^2}\right)\right]\right]\right\} \tag{A.146}$$

These formulæ are in agreement with Eqns. (21-25) in Ellis, Ridolfi, and Zwirner [197] (which uses the same conventions as Brignole *et. al.* [198] described in Table A.2; also note that the Δ of [197] equals $-2\bar{m}^2_{rad}$).

As was mentioned earlier, Eqns. (A.141 - A.146) are not valid for cases in which the stop and/or sbottom mass eigenstates are degenerate ($D_t = 0$ and/or $D_b = 0 \Leftrightarrow m_{\tilde{t_1}} = m_{\tilde{t_2}}$ and/or $m_{\tilde{b_1}} = m_{\tilde{b_2}}$). From Eqns. (A.118) and (A.124) (Eqns. (A.120) and (A.124)) we see that degenerate stop (sbottom) mass eigenstates occur when:
1) [T0] = 0 ([B0] = 0), which will happen for example when $m_{\tilde{L}} = m_{\tilde{t_R}}$ ($m_{\tilde{L}} = m_{\tilde{b_R}}$) and either $\tan\beta = 1$ or squark D-terms are neglected;
and
2) $A_t = \Re e\{A_t\} = 2m_1 \cot\beta$ ($A_b = \Re e\{A_b\} = 2m_1 \tan\beta$)
(The A-terms must be real since the other quantities are assumed to be real.) Expressions for these cases are found by taking the limit as 1) occurs and then setting condition 2) or vice versa (which was checked to yield the same result.) The following results were thus obtained (with squark D-terms left in):
If $m_{\tilde{t_1}} = m_{\tilde{t_2}}$, then replace

lines 2-7 of Eqn. (A.141) by

$$+\frac{3v^2}{32\pi^2}\left\{8f_t^4\log\left(\frac{m^2_{\tilde{t_1}}}{m_t^2}\right) + \left(-f_t^2g_+^2 + \tfrac{g_+^2+g_t^2}{16}\right)\left[\log\left(\frac{m^4_{\tilde{t_1}}}{Q^4}\right) + 3\right]\right. \quad \text{(A.147)}$$

lines 2-7 of Eqn. (A.142) by

$$+\frac{3v'^2}{32\pi^2}\left\{\left(\tfrac{g_+^2+g_t^2}{16}\right)\left[\log\left(\frac{m^4_{\tilde{t_1}}}{Q^4}\right) + 3\right]\right. \quad \text{(A.148)}$$

and lines 2-9 of Eqn. (A.143) by

$$+\frac{3vv'}{32\pi^2}\left\{\left(\tfrac{1}{2}f_t^2g_+^2 - \tfrac{g_+^2+g_t^2}{16}\right)\left[\log\left(\frac{m^4_{\tilde{t_1}}}{Q^4}\right) + 3\right]\right. \quad \text{(A.149)}$$

If $m_{\tilde{b_1}} = m_{\tilde{b_2}}$, then replace
lines 9-14 of Eqn. (A.141) by

$$+ \left(\tfrac{g_+^2+g_b^2}{16}\right)\left[\log\left(\frac{m_{\tilde{b}_1}^4}{Q^4}\right) + 3\right]\Bigg\} \tag{A.150}$$

lines 8-14 of Eqn. (A.142) by

$$+ 8f_b^4 \log\left(\frac{m_{\tilde{b}_1}^2}{m_b^2}\right) + \left(-f_b^2 g_+^2 + \tfrac{g_+^2+g_b^2}{16}\right)\left[\log\left(\frac{m_{\tilde{b}_1}^4}{Q^4}\right) + 3\right]\Bigg\} \tag{A.151}$$

and lines 10-17 of Eqn. (A.143) by

$$+ \left(\tfrac{1}{2}f_b^2 g_+^2 - \tfrac{g_+^2+g_b^2}{16}\right)\left[\log\left(\frac{m_{\tilde{b}_1}^4}{Q^4}\right) + 3\right]\Bigg\} \tag{A.152}$$

A.9 Corrections to Charged Higgs Boson Mass

When deriving the $\mathcal{M}_{sq}^2$ eigenvalues in our calculation of the neutral Higgs boson masses (Eqns. (A.116) and (A.117)), terms proportional to the charged Higgs fields were dropped. We now need to take derivatives of the scalar potential with respect to the charged Higgs fields, so dropping these terms is no longer permissible. This means that $\mathcal{M}_{sq}^2$ no longer has a 2×2 block diagonal form. To make calculating the eigenvales of the general 4×4 $\mathcal{M}_{sq}^2$ matrix, given by Eqns. (A.114) and (A.115), analytically tractable, the terms in the off-diagonal 2×2 blocks will be treated as perturbations to the matrix with just the 2×2 block diagonal elements. That is,

$$\mathcal{M}_{sq}{}^2 = \mathcal{M}_{sq}^{(0)2} + \delta\mathcal{M}_{sq}{}^2 \tag{A.153}$$

where $\mathcal{M}_{sq}^{(0)2} \equiv \begin{bmatrix} \mathrm{M}_{11} & \mathrm{M}_{12} & 0 & 0 \\ \mathrm{M}_{21} & \mathrm{M}_{22} & 0 & 0 \\ 0 & 0 & \mathrm{M}_{33} & \mathrm{M}_{34} \\ 0 & 0 & \mathrm{M}_{43} & \mathrm{M}_{44} \end{bmatrix}$ and $\delta\mathcal{M}_{sq}{}^2 \equiv \begin{bmatrix} 0 & 0 & \mathrm{M}_{13} & \mathrm{M}_{14} \\ 0 & 0 & \mathrm{M}_{23} & \mathrm{M}_{24} \\ \mathrm{M}_{31} & \mathrm{M}_{32} & 0 & 0 \\ \mathrm{M}_{41} & \mathrm{M}_{42} & 0 & 0 \end{bmatrix}$.

(A.154)

In fact, since the charged Higgs boson mass comes from the coefficient of the bilinear terms (at the minimum), and since this technique is correct and exact up to second order, using this technique does not entail any additional approximation in the calculation of the charged Higgs boson mass.

The eigenvalues of the matrix $\mathcal{M}^{(0)^2}_{sq}$ must first be calculated.

$$\begin{aligned}\lambda^{(0)}_{t_{2,1}} &= \tfrac{1}{2}(m^2_{\tilde{L}} + m^2_{\tilde{t}_R}) + f_t^2|h^0|^2 + \tfrac{1}{2}(f_t^2|h^+|^2 + f_b^2|h'^-|^2) \\ &\quad + \tfrac{1}{8}(g^2|h_2^{comb}|^2 - g'^2|h_1^{comb}|^2) \\ &\quad \pm \left\{ \frac{1}{4}\Big[(m^2_{\tilde{L}} - m^2_{\tilde{t}_R}) - (f_t^2|h^+|^2 - f_b^2|h'^-|^2) + \tfrac{1}{4}(g^2|h_2^{comb}|^2 + \tfrac{5}{3}g'^2|h_1^{comb}|^2)\Big]^2 \right. \\ &\quad \left. + f_t^2(2m_1h'^0 + A_t^* h^{0*})(2m_1h'^{0*} + A_t h^0) \right\}^{\frac{1}{2}} \qquad \text{(A.155)}\end{aligned}$$

$$\begin{aligned}\lambda^{(0)}_{b_{2,1}} &= \tfrac{1}{2}(m^2_{\tilde{L}} + m^2_{\tilde{b}_R}) + f_b^2|h'^0|^2 + \tfrac{1}{2}(f_t^2|h^+|^2 + f_b^2|h'^-|^2) \\ &\quad - \tfrac{1}{8}(g^2|h_2^{comb}|^2 - g'^2|h_1^{comb}|^2) \\ &\quad \pm \left\{ \frac{1}{4}\Big[(m^2_{\tilde{L}} - m^2_{\tilde{b}_R}) + (f_t^2|h^+|^2 - f_b^2|h'^-|^2) - \tfrac{1}{4}(g^2|h_2^{comb}|^2 + \tfrac{1}{3}g'^2|h_1^{comb}|^2)\Big]^2 \right. \\ &\quad \left. + f_b^2(2m_1h^0 + A_b^* h'^{0*})(2m_1h^{0*} + A_b h'^0) \right\}^{\frac{1}{2}}, \qquad \text{(A.156)}\end{aligned}$$

$$\begin{aligned}\text{where} \quad |h_1^{comb}|^2 &\equiv (|h^+|^2 + |h^0|^2 - |h'^-|^2 - |h'^0|^2) \\ \text{and} \quad |h_2^{comb}|^2 &\equiv (|h^+|^2 - |h^0|^2 - |h'^-|^2 + |h'^0|^2) \qquad \text{(A.157)}\end{aligned}$$

At the minimum, Eqns. (A.118) and (A.120) are still valid since $\langle h^+ \rangle = \langle h'^- \rangle = 0$:

$$m^2_{\tilde{t}_2}, m^2_{\tilde{t}_1} = \lambda^{(0)}_{t_{2,1}}|_{vev} \qquad \text{and} \qquad m^2_{\tilde{b}_2}, m^2_{\tilde{b}_1} = \lambda^{(0)}_{b_{2,1}}|_{vev} \quad . \qquad \text{(A.158)}$$

Next the derivatives of the unperturbed eigenvalues with respect to the charged Higgs fields will be calculated: It is again convenient to define several quantites that appear repeatedly in the expressions:

$$g_-^2 \equiv g^2 - g'^2 \quad g_t'^2 \equiv g^2 + \tfrac{5}{3}g'^2 \quad g_b'^2 \equiv g^2 + \tfrac{1}{3}g'^2 \qquad \text{(A.159)}$$

The quantities defined in Eqns. (A.119),(A.121), and (A.124) will also be employed. Note that once again, as with the neutral Higgs boson calculation, the following

formulæ are only valid if $D_t \neq 0$ and $D_b \neq 0$. The cases in which $D_t = 0$ and/or $D_b = 0$ will again be treated as special cases later.

$$\left.\frac{\partial\lambda_t^{(0)}}{\partial h^+}\right|_{vev} = \left.\frac{\partial\lambda_t^{(0)}}{\partial h^{+*}}\right|_{vev} = \left.\frac{\partial\lambda_t^{(0)}}{\partial h'^-}\right|_{vev} = \left.\frac{\partial\lambda_t^{(0)}}{\partial h'^{-*}}\right|_{vev} = 0$$
$$\left.\frac{\partial\lambda_b^{(0)}}{\partial h^+}\right|_{vev} = \left.\frac{\partial\lambda_b^{(0)}}{\partial h^{+*}}\right|_{vev} = \left.\frac{\partial\lambda_b^{(0)}}{\partial h'^-}\right|_{vev} = \left.\frac{\partial\lambda_b^{(0)}}{\partial h'^{-*}}\right|_{vev} = 0 \qquad \text{(A.160)}$$

$$\left.\frac{\partial^2\lambda_{t_{2,1}}^{(0)}}{\partial h^+\partial h^{+*}}\right|_{vev} = \tfrac{1}{2}f_t^2 + \tfrac{g_-^2}{8} \pm -\tfrac{1}{4}(f_t^2 - \tfrac{g_t'^2}{4})\frac{[T0]}{D_t^{\frac{1}{2}}} \qquad \text{(A.161)}$$

$$\left.\frac{\partial^2\lambda_{t_{2,1}}^{(0)}}{\partial h'^-\partial h'^{-*}}\right|_{vev} = \tfrac{1}{2}f_b^2 - \tfrac{g_-^2}{8} \pm \tfrac{1}{4}(f_b^2 - \tfrac{g_t'^2}{4})\frac{[T0]}{D_t^{\frac{1}{2}}} \qquad \text{(A.162)}$$

$$\left.\frac{\partial^2\lambda_{b_{2,1}}^{(0)}}{\partial h^+\partial h^{+*}}\right|_{vev} = \tfrac{1}{2}f_t^2 - \tfrac{g_-^2}{8} \pm \tfrac{1}{4}(f_t^2 - \tfrac{g_b'^2}{4})\frac{[B0]}{D_b^{\frac{1}{2}}} \qquad \text{(A.163)}$$

$$\left.\frac{\partial^2\lambda_{b_{2,1}}^{(0)}}{\partial h'^-\partial h'^{-*}}\right|_{vev} = \tfrac{1}{2}f_b^2 + \tfrac{g_-^2}{8} \pm -\tfrac{1}{4}(f_b^2 - \tfrac{g_b'^2}{4})\frac{[B0]}{D_b^{\frac{1}{2}}} \qquad \text{(A.164)}$$

$$\left.\frac{\partial^2\lambda_t^{(0)}}{\partial h^+\partial h'^-}\right|_{vev} = \left.\frac{\partial^2\lambda_t^{(0)}}{\partial h^{+*}\partial h'^{-*}}\right|_{vev} = \left.\frac{\partial^2\lambda_b^{(0)}}{\partial h^+\partial h'^-}\right|_{vev} = \left.\frac{\partial^2\lambda_b^{(0)}}{\partial h^{+*}\partial h'^{-*}}\right|_{vev} = 0 \qquad \text{(A.165)}$$

Note the expression for $\left.\frac{\partial^2\lambda_b^{(0)}}{\partial h'^-\partial h'^{-*}}\right|_{vev}$ $\left(\left.\frac{\partial^2\lambda_b^{(0)}}{\partial h^+\partial h^{+*}}\right|_{vev}\right)$ is obtained from that for $\left.\frac{\partial^2\lambda_t^{(0)}}{\partial h^+\partial h^{+*}}\right|_{vev}$ $\left(\left.\frac{\partial^2\lambda_t^{(0)}}{\partial h'^-\partial h'^{-*}}\right|_{vev}\right)$ by the set of substitutions $(f_t, f_b, g_t', D_t, [T0]) \longrightarrow (f_b, f_t, g_b', D_b, [B0])$.

Next expressions for the eigenvectors, $\vec{u}$, of $\mathcal{M}_{sq}^{(0)^2}$ will be given, where

$$(\lambda_{t,b}^{(0)}\mathcal{I} - \mathcal{M}_{sq}^{(0)^2})\vec{u} = \vec{0} \qquad \text{with} \qquad \vec{u} \equiv \begin{bmatrix} u1 \\ u2 \\ u3 \\ u4 \end{bmatrix} . \qquad \text{(A.166)}$$

For the stops,

$$\begin{bmatrix} \lambda_{t_{2,1}}^{(0)} - \mathrm{M}_{11} & -\mathrm{M}_{12} \\ -\mathrm{M}_{21} & \lambda_{t_{2,1}}^{(0)} - \mathrm{M}_{22} \end{bmatrix} \begin{bmatrix} u1_{t_{2,1}}^{(0)} \\ u2_{t_{2,1}}^{(0)} \end{bmatrix} = \begin{bmatrix} 0 \\ 0 \end{bmatrix} \qquad \text{(A.167)}$$

Thus, $$(\lambda_{t_{2,1}}^{(0)} - \mathrm{M}_{11})u1_{t_{2,1}}^{(0)} - \mathrm{M}_{12}u2_{t_{2,1}}^{(0)} = 0$$

and $$-\mathrm{M}_{21}u1_{t_{2,1}}^{(0)} - (\lambda_{t_{2,1}}^{(0)} - \mathrm{M}_{22})u2_{t_{2,1}}^{(0)} = 0$$

So the stop eigenvectors may be written as

$$\vec{u}^{(0)}_{t_{2,1}} = \frac{1}{\sqrt{|\mathrm{M}_{12}|^2 + |\lambda^{(0)}_{t_{2,1}} - \mathrm{M}_{11}|^2}} \begin{bmatrix} \mathrm{M}_{12} \\ (\lambda^{(0)}_{t_{2,1}} - \mathrm{M}_{11}) \\ 0 \\ 0 \end{bmatrix} \tag{A.168}$$

Similarly, for the sbottoms,

$$\begin{bmatrix} \lambda^{(0)}_{b_{2,1}} - \mathrm{M}_{33} & -\mathrm{M}_{34} \\ -\mathrm{M}_{43} & \lambda^{(0)}_{b_{2,1}} - \mathrm{M}_{44} \end{bmatrix} \begin{bmatrix} u3^{(0)}_{b_{2,1}} \\ u4^{(0)}_{b_{2,1}} \end{bmatrix} = \begin{bmatrix} 0 \\ 0 \end{bmatrix} \tag{A.169}$$

$$\begin{aligned} \text{Thus,} \qquad & (\lambda^{(0)}_{b_{2,1}} - \mathrm{M}_{33}) u3^{(0)}_{b_{2,1}} - \mathrm{M}_{34} u4^{(0)}_{b_{2,1}} = 0 \\ \text{and} \qquad & -\mathrm{M}_{43} u3^{(0)}_{b_{2,1}} - (\lambda^{(0)}_{b_{2,1}} - \mathrm{M}_{44}) u4^{(0)}_{b_{2,1}} = 0 \end{aligned}$$

And so the sbottom eigenvectors may be written as

$$\vec{u}^{(0)}_{b_{2,1}} = \frac{1}{\sqrt{|\mathrm{M}_{34}|^2 + |\lambda^{(0)}_{b_{2,1}} - \mathrm{M}_{33}|^2}} \begin{bmatrix} 0 \\ 0 \\ \mathrm{M}_{34} \\ (\lambda^{(0)}_{b_{2,1}} - \mathrm{M}_{33}) \end{bmatrix} \tag{A.170}$$

$$\begin{aligned} \text{Define} \quad N_{t_{2,1}} &\equiv \frac{1}{\sqrt{|\mathrm{M}_{12}|^2 + |\lambda^{(0)}_{t_{2,1}} - \mathrm{M}_{11}|^2}} \\ \text{and} \quad N_{b_{2,1}} &\equiv \frac{1}{\sqrt{|\mathrm{M}_{34}|^2 + |\lambda^{(0)}_{b_{2,1}} - \mathrm{M}_{33}|^2}} \; . \end{aligned} \tag{A.171}$$

One can then show that (see Eqns. (A.119), (A.121), and (A.124)):

$$\begin{aligned} N_{t_{2,1}}\Big|_{vev} &= \left\{ \tfrac{1}{4}\Big[(m^2_{\tilde{t}_2} - m^2_{\tilde{t}_1}) \mp [T0]\Big]^2 + m_t^2 [T1] \right\}^{-\frac{1}{2}} \\ N_{b_{2,1}}\Big|_{vev} &= \left\{ \tfrac{1}{4}\Big[(m^2_{\tilde{b}_2} - m^2_{\tilde{b}_1}) \mp [B0]\Big]^2 + m_b^2 [B1] \right\}^{-\frac{1}{2}} \end{aligned} \tag{A.172}$$

$$\begin{aligned} \text{where } [T1] &\equiv \Big[|A_t|^2 + (2m_1)^2 \cot^2\beta + 2(2m_1)\Re e\{A_t\} \cot\beta\Big] \\ \text{and } [B1] &\equiv \Big[|A_b|^2 + (2m_1)^2 \tan^2\beta + 2(2m_1)\Re e\{A_b\} \tan\beta\Big] \end{aligned} \tag{A.173}$$

So now the corrections to the eigenvalues of the matrix $\mathcal{M}_{sq}^{(0)^2}$ can be calculated. Assume for the moment that there are no degeneracies among the eigenvalues, which again demands that D_t and D_b are non-zero. Recall that the cases where $D_t = 0$ and/or $D_b = 0$ will be treated later as special cases. Accidental degeneracies, where one of the stop masses $(m_{\tilde{t}_2}, m_{\tilde{t}_1})$ equals one of the sbottom masses $(m_{\tilde{b}_2}, m_{\tilde{b}_1})$, but the two stop masses or the two sbottom masses themselves are not equal, will also invalidate the following derivation, but this remote possibility will be neglected. So without degeneracies, the first order corrections to the eigenvalues are

$$\delta\lambda_i^{(1)} \;=\; \langle u_i^{(0)} | \delta\mathcal{M}_{sq}{}^2 | u_i^{(0)} \rangle \;=\; 0 \quad . \tag{A.174}$$

Therefore the second order corrections need to be considered:

$$\delta\lambda_i^{(2)} \;=\; \sum_{j \neq i} \frac{|\langle u_i^{(0)} | \delta\mathcal{M}_{sq}{}^2 | u_j^{(0)} \rangle|^2}{\lambda_i^{(0)} - \lambda_j^{(0)}} \quad . \tag{A.175}$$

First note that all elements of $\delta\mathcal{M}_{sq}{}^2|_{vev}$ equal zero since each term in each element contains one of the charged Higgs fields. Thus,

$$\delta m_{\tilde{q}}^2 \;=\; \delta\lambda_i^{(2)}\Big|_{vev} = 0 \quad . \tag{A.176}$$

So the formulæ for the stop and sbottom masses, Eqns. (A.118) and (A.120) still remain unaltered, as already noted in Eqn. (A.158). On the other hand, if derivatives of Eqn. (A.175) are taken with respect to the charged Higgs fields, the resulting expressions need no longer equal zero at the minimum. This can lead to contributions that need to be added to Eqns. (A.160)–(A.165), for example,

$$\frac{\partial\lambda_i}{\partial h^+}\bigg|_{vev} \;\equiv\; \frac{\partial\lambda_i^{(0)}}{\partial h^+}\bigg|_{vev} + \frac{\partial(\delta\lambda_i^{(2)})}{\partial h^+}\bigg|_{vev} , \quad etc. \tag{A.177}$$

Because the 2×2 block diagonal elements of $\delta\mathcal{M}_{sq}{}^2$ are zero, we have for the stop and sbottom eigenvalue corrections:

$$\delta\lambda_{t_{2,1}}^{(2)} \;=\; \sum_{j=1,2} \frac{|\langle u_{t_{2,1}}^{(0)} | \delta\mathcal{M}_{sq}{}^2 | u_{b_j}^{(0)} \rangle|^2}{\lambda_{t_{2,1}}^{(0)} - \lambda_{b_j}^{(0)}} , \quad \delta\lambda_{b_{2,1}}^{(2)} \;=\; \sum_{j=1,2} \frac{|\langle u_{b_{2,1}}^{(0)} | \delta\mathcal{M}_{sq}{}^2 | u_{t_j}^{(0)} \rangle|^2}{\lambda_{b_{2,1}}^{(0)} - \lambda_{t_j}^{(0)}} \tag{A.178}$$

The four distinct matrix elements of the operator $\delta\mathcal{M}_{sq}{}^2$ *in the basis* $\{\vec{u}^{(0)}_{t_{2,1}}, \vec{u}^{(0)}_{b_{2,1}}\}$ that enter into the last two equations are:

$$\begin{aligned}\langle u^{(0)}_{t_{2,1}}|\delta\mathcal{M}_{sq}{}^2|u^{(0)}_{b_{2,1}}\rangle &= N_{t_{2,1}}N_{b_{2,1}}\Big\{\mathrm{M}_{13}\mathrm{M}^*_{12}\mathrm{M}_{34} + \mathrm{M}_{14}\mathrm{M}^*_{12}(\lambda^{(0)}_{b_{2,1}} - \mathrm{M}_{33}) \\ &\quad + \mathrm{M}_{23}(\lambda^{(0)*}_{t_{2,1}} - \mathrm{M}^*_{11})\mathrm{M}_{34} \\ &\quad + \mathrm{M}_{24}(\lambda^{(0)*}_{t_{2,1}} - \mathrm{M}^*_{11})(\lambda^{(0)}_{b_{2,1}} - \mathrm{M}_{33})\Big\} \qquad \text{(A.179)} \\ &\equiv N_{t_{2,1}}N_{b_{2,1}}C(\lambda^{(0)}_{t_{2,1}}, \lambda^{(0)}_{b_{2,1}}) \quad , \qquad \text{(A.180)}\end{aligned}$$

and of course, $\langle u^{(0)}_{b_2}|\delta\mathcal{M}_{sq}{}^2|u^{(0)}_{t_2}\rangle = \langle u^{(0)}_{t_2}|\delta\mathcal{M}_{sq}{}^2|u^{(0)}_{b_2}\rangle^*$, etc. Each term inside the curly brackets of Eqns. (A.179) is a product of three elements: the first is from $\delta\mathcal{M}_{sq}{}^2$, the second is from the stop eigenvector, and the third is from the sbottom eigenvector.

The first derivatives with respect to the charged Higgs fields of the eigenvalue corrections at the minimum are:

$$\left.\frac{\partial(\delta\lambda^{(2)}_i)}{\partial h^{ch}}\right|_{vev} = \sum_j \frac{1}{m^2_{\tilde{q}_i} - m^2_{\tilde{q}_j}} \left.\frac{\partial|\langle u^{(0)}_i|\delta\mathcal{M}_{sq}{}^2|u^{(0)}_j\rangle|^2}{\partial h^{ch}}\right|_{vev} \quad , \qquad \text{(A.181)}$$

where I have used Eqns. (A.160), and h^{ch} represents h^+, h'^-, h^{+*}, or h'^{-*}. However, as we see from Eqns. (A.179), each term in $\langle u^{(0)}_i|\delta\mathcal{M}_{sq}{}^2|u^{(0)}_j\rangle$ will contain one element of $\delta\mathcal{M}_{sq}{}^2$, and thus it will be proportional to one of the charged Higgs fields. Therefore, each term in $|\langle u^{(0)}_i|\delta\mathcal{M}_{sq}{}^2|u^{(0)}_j\rangle|^2$ will be proportional to two charged Higgs fields, and so

$$\left.\frac{\partial(\delta\lambda^{(2)}_i)}{\partial h^{ch}}\right|_{vev} = 0 \qquad \text{(A.182)}$$

since $\langle h^{ch}\rangle = h^{ch}|_{vev} = 0$. Thus, by Eqns. (A.160) and (A.182),

$$\left.\frac{\partial\lambda_i}{\partial h^{ch}}\right|_{vev} = 0 \quad . \qquad \text{(A.183)}$$

Then, using Eqn. (A.122), we find

$$\left.\frac{\partial(\Delta\mathcal{V}_{sq})}{\partial h^{ch}}\right|_{vev} = \frac{3}{32\pi^2}\sum_{i=1,2}\left[\lambda_{t_i}\frac{\partial\lambda_{t_i}}{\partial h^{ch}}(2\log\lambda_{t_i} + 1) + (t_i \to b_i)\right] = 0 \quad . \qquad \text{(A.184)}$$

We can also see though that the second derivatives with respect to the charged Higgs fields of the eigenvalue corrections at the minimum are not expected to be zero. We find, employing Eqns. (A.160), (A.179), and (A.180) and the information in this

paragraph,

$$\left.\frac{\partial^2(\delta\lambda_i^{(2)})}{\partial h^{ch1}\partial h^{ch2}}\right|_{vev} = \sum_j \frac{1}{(m_{q_i}^2 - m_{q_j}^2)^2}\left.\frac{\partial^2|\langle u_i^{(0)}|\delta\mathcal{M}_{sq}{}^2|u_j^{(0)}\rangle|^2}{\partial h^{ch1}\partial h^{ch2}}\right|_{vev} \tag{A.185}$$

$$= \sum_j \frac{N_{t_i}^2 N_{b_j}^2}{(m_{q_i}^2 - m_{q_j}^2)^2}\left.\frac{\partial^2|\mathcal{C}(\lambda_{t_{2,1}}^{(0)}, \lambda_{b_{2,1}}^{(0)})|^2}{\partial h^{ch1}\partial h^{ch2}}\right|_{vev} . \tag{A.186}$$

where $\left.\frac{\partial^2|\mathcal{C}(\lambda_{t_{2,1}}^{(0)}, \lambda_{b_{2,1}}^{(0)})|^2}{\partial h^{ch1}\partial h^{ch2}}\right|_{vev} =$

$$\begin{aligned}
&\Bigg\{\left[\frac{\partial \mathrm{M}_{13}}{\partial h^{ch1}}\frac{\partial \mathrm{M}_{13}^*}{\partial h^{ch2}} + \frac{\partial \mathrm{M}_{13}^*}{\partial h^{ch1}}\frac{\partial \mathrm{M}_{13}}{\partial h^{ch2}}\right]|\mathrm{M}_{12}|^2|\mathrm{M}_{34}|^2 \\
&+ \left[\frac{\partial \mathrm{M}_{13}}{\partial h^{ch1}}\frac{\partial \mathrm{M}_{14}^*}{\partial h^{ch2}} + \frac{\partial \mathrm{M}_{14}^*}{\partial h^{ch1}}\frac{\partial \mathrm{M}_{13}}{\partial h^{ch2}}\right]|\mathrm{M}_{12}|^2\mathrm{M}_{34}(\lambda_{b_j}^{(0)*} - \mathrm{M}_{33}^*) \\
&\quad + \left[\frac{\partial \mathrm{M}_{13}^*}{\partial h^{ch1}}\frac{\partial \mathrm{M}_{14}}{\partial h^{ch2}} + \frac{\partial \mathrm{M}_{14}}{\partial h^{ch1}}\frac{\partial \mathrm{M}_{13}^*}{\partial h^{ch2}}\right]|\mathrm{M}_{12}|^2\mathrm{M}_{34}^*(\lambda_{b_j}^{(0)} - \mathrm{M}_{33}) \\
&+ \left[\frac{\partial \mathrm{M}_{13}}{\partial h^{ch1}}\frac{\partial \mathrm{M}_{23}^*}{\partial h^{ch2}} + \frac{\partial \mathrm{M}_{23}^*}{\partial h^{ch1}}\frac{\partial \mathrm{M}_{13}}{\partial h^{ch2}}\right]\mathrm{M}_{12}^*|\mathrm{M}_{34}|^2(\lambda_{t_i}^{(0)} - \mathrm{M}_{11}) \\
&\quad + \left[\frac{\partial \mathrm{M}_{13}^*}{\partial h^{ch1}}\frac{\partial \mathrm{M}_{23}}{\partial h^{ch2}} + \frac{\partial \mathrm{M}_{23}}{\partial h^{ch1}}\frac{\partial \mathrm{M}_{13}^*}{\partial h^{ch2}}\right]\mathrm{M}_{12}|\mathrm{M}_{34}|^2(\lambda_{t_i}^{(0)*} - \mathrm{M}_{11}^*) \\
&+ \left[\frac{\partial \mathrm{M}_{13}}{\partial h^{ch1}}\frac{\partial \mathrm{M}_{24}^*}{\partial h^{ch2}} + \frac{\partial \mathrm{M}_{24}^*}{\partial h^{ch1}}\frac{\partial \mathrm{M}_{13}}{\partial h^{ch2}}\right]\mathrm{M}_{12}^*\mathrm{M}_{34}(\lambda_{t_i}^{(0)} - \mathrm{M}_{11})(\lambda_{b_j}^{(0)*} - \mathrm{M}_{33}^*) \\
&\quad + \left[\frac{\partial \mathrm{M}_{13}^*}{\partial h^{ch1}}\frac{\partial \mathrm{M}_{24}}{\partial h^{ch2}} + \frac{\partial \mathrm{M}_{24}}{\partial h^{ch1}}\frac{\partial \mathrm{M}_{13}^*}{\partial h^{ch2}}\right]\mathrm{M}_{12}\mathrm{M}_{34}^*(\lambda_{t_i}^{(0)*} - \mathrm{M}_{11}^*)(\lambda_{b_j}^{(0)} - \mathrm{M}_{33}) \\
&+ \left[\frac{\partial \mathrm{M}_{14}}{\partial h^{ch1}}\frac{\partial \mathrm{M}_{14}^*}{\partial h^{ch2}} + \frac{\partial \mathrm{M}_{14}^*}{\partial h^{ch1}}\frac{\partial \mathrm{M}_{14}}{\partial h^{ch2}}\right]|\mathrm{M}_{12}|^2|\lambda_{b_j}^{(0)*} - \mathrm{M}_{33}|^2 \\
&+ \left[\frac{\partial \mathrm{M}_{14}}{\partial h^{ch1}}\frac{\partial \mathrm{M}_{23}^*}{\partial h^{ch2}} + \frac{\partial \mathrm{M}_{23}^*}{\partial h^{ch1}}\frac{\partial \mathrm{M}_{14}}{\partial h^{ch2}}\right]\mathrm{M}_{12}^*\mathrm{M}_{34}^*(\lambda_{t_i}^{(0)} - \mathrm{M}_{11})(\lambda_{b_j}^{(0)} - \mathrm{M}_{33}) \\
&\quad + \left[\frac{\partial \mathrm{M}_{14}^*}{\partial h^{ch1}}\frac{\partial \mathrm{M}_{23}}{\partial h^{ch2}} + \frac{\partial \mathrm{M}_{23}}{\partial h^{ch1}}\frac{\partial \mathrm{M}_{14}^*}{\partial h^{ch2}}\right]\mathrm{M}_{12}\mathrm{M}_{34}(\lambda_{t_i}^{(0)*} - \mathrm{M}_{11}^*)(\lambda_{b_j}^{(0)*} - \mathrm{M}_{33}^*) \\
&+ \left[\frac{\partial \mathrm{M}_{14}}{\partial h^{ch1}}\frac{\partial \mathrm{M}_{24}^*}{\partial h^{ch2}} + \frac{\partial \mathrm{M}_{24}^*}{\partial h^{ch1}}\frac{\partial \mathrm{M}_{14}}{\partial h^{ch2}}\right]\mathrm{M}_{12}^*(\lambda_{t_i}^{(0)} - \mathrm{M}_{11})|\lambda_{b_j}^{(0)} - \mathrm{M}_{33}|^2 \\
&\quad + \left[\frac{\partial \mathrm{M}_{14}^*}{\partial h^{ch1}}\frac{\partial \mathrm{M}_{24}}{\partial h^{ch2}} + \frac{\partial \mathrm{M}_{24}}{\partial h^{ch1}}\frac{\partial \mathrm{M}_{14}^*}{\partial h^{ch2}}\right]\mathrm{M}_{12}(\lambda_{t_i}^{(0)*} - \mathrm{M}_{11}^*)|\lambda_{b_j}^{(0)} - \mathrm{M}_{33}|^2 \\
&+ \left[\frac{\partial \mathrm{M}_{23}}{\partial h^{ch1}}\frac{\partial \mathrm{M}_{23}^*}{\partial h^{ch2}} + \frac{\partial \mathrm{M}_{23}^*}{\partial h^{ch1}}\frac{\partial \mathrm{M}_{23}}{\partial h^{ch2}}\right]|\mathrm{M}_{34}|^2|\lambda_{t_i}^{(0)} - \mathrm{M}_{11}|^2 \\
&+ \left[\frac{\partial \mathrm{M}_{23}}{\partial h^{ch1}}\frac{\partial \mathrm{M}_{24}^*}{\partial h^{ch2}} + \frac{\partial \mathrm{M}_{24}^*}{\partial h^{ch1}}\frac{\partial \mathrm{M}_{23}}{\partial h^{ch2}}\right]\mathrm{M}_{34}|\lambda_{t_i}^{(0)} - \mathrm{M}_{11}|^2(\lambda_{b_j}^{(0)*} - \mathrm{M}_{33}^*) \\
&\quad + \left[\frac{\partial \mathrm{M}_{23}^*}{\partial h^{ch1}}\frac{\partial \mathrm{M}_{24}}{\partial h^{ch2}} + \frac{\partial \mathrm{M}_{24}}{\partial h^{ch1}}\frac{\partial \mathrm{M}_{23}^*}{\partial h^{ch2}}\right]\mathrm{M}_{34}^*|\lambda_{t_i}^{(0)} - \mathrm{M}_{11}|^2(\lambda_{b_j}^{(0)} - \mathrm{M}_{33}) \\
&+ \left[\frac{\partial \mathrm{M}_{24}}{\partial h^{ch1}}\frac{\partial \mathrm{M}_{24}^*}{\partial h^{ch2}} + \frac{\partial \mathrm{M}_{24}^*}{\partial h^{ch1}}\frac{\partial \mathrm{M}_{24}}{\partial h^{ch2}}\right]|\lambda_{t_i}^{(0)} - \mathrm{M}_{11}|^2|\lambda_{b_j}^{(0)} - \mathrm{M}_{33}|^2\Bigg\}\Bigg|_{vev}
\end{aligned} \tag{A.187}$$

Now the squark sector corrections to the charged Higgs mass squared matrix (whose tree-level form is given in Eqn. (A.62)) can be derived. The correction terms for the matrix elements are of the form:

$$\begin{aligned}
\left.\frac{\partial^2(\Delta\mathcal{V}_{sq})}{\partial h^{ch1}\partial h^{ch2}}\right|_{vev} &= \frac{3}{32\pi^2}\sum_{i=1,2}\left\{\left[\frac{\partial\lambda_{t_i}}{\partial h^{ch1}}\frac{\partial\lambda_{t_i}}{\partial h^{ch2}} + \lambda_{t_i}\frac{\partial^2\lambda_{t_i}}{\partial h^{ch1}\partial h^{ch2}}\right]\left[2\log\lambda_{t_i} + 1\right]\right. \\
&\qquad \left. + 2\frac{\partial\lambda_{t_i}}{\partial h^{ch1}}\frac{\partial\lambda_{t_i}}{\partial h^{ch2}} + (t_i \to b_i)\right\}\Bigg|_{vev} \\
&= \frac{3}{32\pi^2}\sum_{i=1,2}\left\{\left[\lambda_{t_i}\frac{\partial^2\lambda_{t_i}}{\partial h^{ch1}\partial h^{ch2}}\right]\left[2\log\lambda_{t_i} + 1\right]\right. \\
&\qquad \left. + (t_i \to b_i)\right\}\Bigg|_{vev} \quad \text{(using Eqn. (A.183))} \\
&= \frac{3}{32\pi^2}\sum_{i=1,2}\left\{\left[\left(\lambda_{t_i}^{(0)} + \delta\lambda_{t_i}^{(2)}\right)\left(\frac{\partial^2\lambda_{t_i}^{(0)}}{\partial h^{ch1}\partial h^{ch2}} + \frac{\partial^2(\delta\lambda_{t_i}^{(2)})}{\partial h^{ch1}\partial h^{ch2}}\right)\right]\right. \\
&\qquad \left. \cdot\left[2\log(\lambda_{t_i}^{(0)} + \delta\lambda_{t_i}^{(2)}) + 1\right] + (t_i \to b_i)\right\}\Bigg|_{vev} \\
&= \frac{3}{32\pi^2}\sum_{i=1,2}\left\{\left[\lambda_{t_i}^{(0)}\left(\frac{\partial^2\lambda_{t_i}^{(0)}}{\partial h^{ch1}\partial h^{ch2}} + \frac{\partial^2(\delta\lambda_{t_i}^{(2)})}{\partial h^{ch1}\partial h^{ch2}}\right)\right]\right. \qquad \text{(A.188)} \\
&\qquad \left. \cdot\left[2\log\lambda_{t_i}^{(0)} + 1\right] + (t_i \to b_i)\right\}\Bigg|_{vev}
\end{aligned}$$

where Eqn. (A.176) has been used in the last step above.

As was done for the neutral Higgs mass corrections, as well as for the tree level charged Higgs mass and quark sector charged Higgs mass correction, the fact that the minimum of the complete scalar potential occurs when the Higgs fields are set equal to their *vev*'s must again be accounted for by subtracting off the expressions for the first derivatives with respect to the appropriate neutral Higgs fields from the expressions for the second derivatives with respect to charged Higgs fields. This is so that the expression we obtain for the squark sector correction terms for $\mathcal{M}_{H^2_{ch}}$ will be in balance with those we have already obtained for the tree level terms (Eqns. (A.61)) and quark sector correction terms (Eqns. (A.105)).

$$\left.\frac{\partial^2(\Delta\mathcal{V}_{sq})}{\partial h^+\partial h^{+*}}\right|_{vev} = \left.\frac{\partial^2(\Delta\mathcal{V}_{sq})}{\partial h^+\partial h^{+*}}\right|_{vev} - \frac{1}{\sqrt{2}v}\frac{\partial(\Delta\mathcal{V}_{sq})}{\partial h_R}$$

$$= \frac{3}{32\pi^2}\sum_{i=1,2}\left\{\left[\lambda_{t_i}^{(0)}\left(\frac{\partial^2\lambda_{t_i}^{(0)}}{\partial h^+\partial h^{+*}} - \frac{1}{\sqrt{2}v}\frac{\partial\lambda_{t_i}^{(0)}}{\partial h_R}\right)\right]\left[2\log\lambda_{t_i}^{(0)}+1\right] + (t_i \to b_i)\right\}\Bigg|_{vev} \quad \text{(A.189a)}$$

$$+ \frac{3}{32\pi^2}\sum_{i=1,2}\left\{\left[\lambda_{t_i}^{(0)}\frac{\partial^2(\delta\lambda_{t_i}^{(2)})}{\partial h^+\partial h^{+*}}\left[2\log\lambda_{t_i}^{(0)}+1\right] + (t_i \to b_i)\right\}\right|_{vev} \quad \text{(A.189b)}$$

$$\left.\frac{\partial^2(\Delta\mathcal{V}_{sq})}{\partial h'^-\partial h'^{-*}}\right|_{vev} = \left.\frac{\partial^2(\Delta\mathcal{V}_{sq})}{\partial h'^-\partial h'^{-*}}\right|_{vev} - \frac{1}{\sqrt{2}v'}\frac{\partial(\Delta\mathcal{V}_{sq})}{\partial h'_R}$$

$$= \frac{3}{32\pi^2}\sum_{i=1,2}\left\{\left[\lambda_{t_i}^{(0)}\left(\frac{\partial^2\lambda_{t_i}^{(0)}}{\partial h'^-\partial h'^{-*}} - \frac{1}{\sqrt{2}v'}\frac{\partial\lambda_{t_i}^{(0)}}{\partial h'_R}\right)\right]\left[2\log\lambda_{t_i}^{(0)}+1\right] + (t_i \to b_i)\right\}\Bigg|_{vev} \quad \text{(A.190a)}$$

$$+ \frac{3}{32\pi^2}\sum_{i=1,2}\left\{\left[\lambda_{t_i}^{(0)}\frac{\partial^2(\delta\lambda_{t_i}^{(2)})}{\partial h'^-\partial h'^{-*}}\left[2\log\lambda_{t_i}^{(0)}+1\right] + (t_i \to b_i)\right\}\right|_{vev} \quad \text{(A.190b)}$$

For the off-diagonal elements of $\mathcal{M}_{H^2_{ch}}$, Eqns. (A.165) simplify the form of Eqn. (A.188) to

$$\left.\frac{\partial^2(\Delta\mathcal{V}_{sq})}{\partial h^+\partial h'^-}\right|_{vev} = \frac{3}{32\pi^2}\sum_{i=1,2}\left\{\lambda_{t_i}^{(0)}\frac{\partial^2(\delta\lambda_{t_i}^{(2)})}{\partial h^+\partial h'^-}\left[2\log\lambda_{t_i}^{(0)} + 1\right] + (t_i \to b_i)\right\}\Bigg|_{vev} \quad \text{(A.191)}$$

$$\left.\frac{\partial^2(\Delta\mathcal{V}_{sq})}{\partial h^{+*}\partial h'^{-*}}\right|_{vev} = \frac{3}{32\pi^2}\sum_{i=1,2}\left\{\lambda_{t_i}^{(0)}\frac{\partial^2(\delta\lambda_{t_i}^{(2)})}{\partial h^{+*}\partial h'^{-*}}\left[2\log\lambda_{t_i}^{(0)} + 1\right] + (t_i \to b_i)\right\}\Bigg|_{vev} \quad \text{(A.192)}$$

Writing out the terms in line (A.189a) gives:

$$\frac{3}{32\pi^2}\Bigg\{\Big\{-\tfrac{1}{2}(f_t^2-\tfrac{g^2}{2})(\alpha_t+[T0]) - f_t^2[2m_1\Re e\{A_t\}\cot\beta+|A_t|^2]\Big\}\Big[\log(m_{\tilde{t}_1}^2 m_{\tilde{t}_2}^2)+1\Big] + \Big\{-(f_t^2-\tfrac{g^2}{2})D_t^{\frac{1}{2}}\Big[1+\frac{\alpha_t[T0]}{4D_t}\Big] - \frac{\alpha_t f_t^2}{2D_t^{\frac{1}{2}}}[2m_1\Re e\{A_t\}\cot\beta+|A_t|^2]\Big\}\log\left(\frac{m_{\tilde{t}_2}^2}{m_{\tilde{t}_1}^2}\right) + \Big\{\tfrac{1}{2}(f_t^2-\tfrac{g^2}{2})(\alpha_b+[B0]) - f_b^2(2m_1)[2m_1+\Re e\{A_b\}\cot\beta]\Big\}\Big[\log(m_{\tilde{b}_1}^2 m_{\tilde{b}_2}^2)+1\Big] + \Big\{(f_t^2-\tfrac{g^2}{2})D_b^{\frac{1}{2}}\Big[1+\frac{\alpha_b[B0]}{4D_b}\Big] - \frac{\alpha_b f_b^2}{2D_b^{\frac{1}{2}}}(2m_1)[2m_1+\Re e\{A_b\}\cot\beta]\log\left(\frac{m_{\tilde{b}_2}^2}{m_{\tilde{b}_1}^2}\right)\Big\}\Bigg\} \tag{A.193}$$

Writing out the terms in line (A.190a) gives:

$$\frac{3}{32\pi^2}\Bigg\{\Big\{\tfrac{1}{2}(f_b^2-\tfrac{g^2}{2})(\alpha_t+[T0]) - f_t^2(2m_1)[2m_1+\Re e\{A_t\}\tan\beta]\Big\}\Big[\log(m_{\tilde{t}_1}^2 m_{\tilde{t}_2}^2)+1\Big] + \Big\{(f_b^2-\tfrac{g^2}{2})D_t^{\frac{1}{2}}\Big[1+\frac{\alpha_t[T0]}{4D_t}\Big] - \frac{\alpha_t f_t^2}{2D_t^{\frac{1}{2}}}(2m_1)[2m_1+\Re e\{A_t\}\tan\beta]\Big\}\log\left(\frac{m_{\tilde{t}_2}^2}{m_{\tilde{t}_1}^2}\right) + \Big\{-\tfrac{1}{2}(f_b^2-\tfrac{g^2}{2})(\alpha_b+[B0]) - f_b^2[(2m_1)\Re e\{A_b\}\tan\beta+|A_b|^2]\Big\}\Big[\log(m_{\tilde{b}_1}^2 m_{\tilde{b}_2}^2)+1\Big] + \Big\{-(f_b^2-\tfrac{g^2}{2})D_b^{\frac{1}{2}}\Big[1+\frac{\alpha_b[B0]}{4D_b}\Big] - \frac{\alpha_b f_b^2}{2D_b^{\frac{1}{2}}}[2m_1\Re e\{A_b\}\tan\beta+|A_b|^2]\log\left(\frac{m_{\tilde{b}_2}^2}{m_{\tilde{b}_1}^2}\right)\Big\}\Bigg\} \tag{A.194}$$

Notice that (A.194) may be obtained from (A.193) via the set of substitutions (A.126).

Using (A.193) above, along with Eqns. (A.61), (A.140), (A.139), and (A.105), the upper left element of the charged Higgs mass squared matrix (including radiative corrections) may be written in the form:

$$
\begin{aligned}
\left.\frac{\partial^2 \mathcal{V}}{\partial h^+ \partial h^{+*}}\right|_{vev} \;=\;& m_{H_p}^2 \cos^2\beta + \tfrac{1}{2} g^2 v'^2 \\
&+ \frac{3}{32\pi^2} \Bigg\{ \Big\{ -\tfrac{1}{2}(f_t^2 - \tfrac{g^2}{2})(\alpha_t + [T0]) - f_t^2 |A_t|^2 \Big\} \Big[\log\Big(\frac{m_{\tilde{t}_1}^2 m_{\tilde{t}_2}^2}{Q^4} \Big) + 1 \Big] \\
&\qquad + D_t^{\frac{1}{2}} \Big\{ -(f_t^2 - \tfrac{g^2}{2}) \Big[1 + \frac{\alpha_t [T0]}{4 D_t} \Big] - \frac{\alpha_t f_t^2}{2 D_t} |A_t|^2 \Big\} \log\Big(\frac{m_{\tilde{t}_2}^2}{m_{\tilde{t}_1}^2} \Big) \\
&\qquad + \Big\{ \tfrac{1}{2}(f_t^2 - \tfrac{g^2}{2})(\alpha_b + [B0]) - f_b^2 (2m_1)^2 \Big\} \Big[\log\Big(\frac{m_{\tilde{b}_1}^2 m_{\tilde{b}_2}^2}{Q^4} \Big) + 1 \Big] \\
&\qquad + D_b^{\frac{1}{2}} \Big\{ (f_t^2 - \tfrac{g^2}{2}) \Big[1 + \frac{\alpha_b [B0]}{4 D_b} \Big] - \frac{\alpha_b f_b^2}{2 D_b} (2m_1)^2 \Big\} \log\Big(\frac{m_{\tilde{b}_2}^2}{m_{\tilde{b}_1}^2} \Big) \\
&\qquad - \tfrac{1}{2} v'^2 (2m_1)^2 \Big\{ \frac{f_t^4 (\Im m\{A_t\})^2}{D_t} \Big[4 - \frac{\alpha_t}{2 D_t^{\frac{1}{2}}} \log\Big(\frac{m_{\tilde{t}_2}^2}{m_{\tilde{t}_1}^2} \Big) \Big] \\
&\qquad\qquad + \frac{f_b^4 (\Im m\{A_b\})^2}{D_b} \Big[4 - \frac{\alpha_b}{2 D_b^{\frac{1}{2}}} \log\Big(\frac{m_{\tilde{b}_2}^2}{m_{\tilde{b}_1}^2} \Big) \Big] \Big\} \\
&\qquad - 2 f_t^2 m_b^2 \Big[\log\Big(\frac{m_t^2 m_b^2}{Q^4} \Big) + 1 + \frac{m_t^2 + m_b^2}{m_t^2 - m_b^2} \log\Big(\frac{m_t^2}{m_b^2} \Big) \Big] \Bigg\} \\
&+ \quad \text{contribution from (A.189b)}
\end{aligned}
\tag{A.195}
$$

(Note that the arbitrary mass scale that is required to make the arguments of the logarithms dimensionless is written explicitely in the above equation.) Unfortunately, the contribution from (A.189b), *i.e.*, from the terms containing the second order corrections to the eigenvalues, is rather unwieldy. We will return to this shortly.

Using (A.194), again along with Eqns. (A.61), (A.140), (A.139), and (A.105), the lower right element of the charged Higgs mass squared matrix (including radiative corrections) may be written in the form:

$$\begin{aligned}
\left.\frac{\partial^2 \mathcal{V}}{\partial h'^- \partial h'^{-*}}\right|_{vev} &= m_{H_p}^2 \sin^2\beta + \tfrac{1}{2} g^2 v^2 \\
&+ \frac{3}{32\pi^2} \Bigg\{ \Big\{ \tfrac{1}{2}(f_b^2 - \tfrac{g^2}{2})(\alpha_t + [T0]) - f_t^2 (2m_1)^2 \Big\} \Big[\log\Big(\frac{m_{\tilde{t}_1}^2 m_{\tilde{t}_2}^2}{Q^4} \Big) + 1 \Big] \\
&\quad + D_t^{\frac{1}{2}} \Big\{ (f_b^2 - \tfrac{g^2}{2}) \Big[1 + \frac{\alpha_t [T0]}{4 D_t} \Big] - \frac{\alpha_t f_t^2}{2 D_t} (2m_1)^2 \Big\} \log\Big(\frac{m_{\tilde{t}_2}^2}{m_{\tilde{t}_1}^2} \Big) \\
&\quad + \Big\{ -\tfrac{1}{2}(f_b^2 - \tfrac{g^2}{2})(\alpha_b + [B0]) - f_b^2 |A_b|^2 \Big\} \Big[\log\Big(\frac{m_{\tilde{b}_1}^2 m_{\tilde{b}_2}^2}{Q^4} \Big) + 1 \Big] \\
&\quad + D_b^{\frac{1}{2}} \Big\{ -(f_b^2 - \tfrac{g^2}{2}) \Big[1 + \frac{\alpha_b [B0]}{4 D_b} \Big] - \frac{\alpha_b f_b^2}{2 D_b} |A_b|^2 \Big\} \log\Big(\frac{m_{\tilde{b}_2}^2}{m_{\tilde{b}_1}^2} \Big) \\
&\quad - \tfrac{1}{2} v^2 (2m_1)^2 \Big\{ \frac{f_t^4 (\Im m\{A_t\})^2}{D_t} \Big[4 - \frac{\alpha_t}{2 D_t^{\frac{1}{2}}} \log\Big(\frac{m_{\tilde{t}_2}^2}{m_{\tilde{t}_1}^2} \Big) \Big] \\
&\qquad + \frac{f_b^4 (\Im m\{A_b\})^2}{D_b} \Big[4 - \frac{\alpha_b}{2 D_b^{\frac{1}{2}}} \log\Big(\frac{m_{\tilde{b}_2}^2}{m_{\tilde{b}_1}^2} \Big) \Big] \Big\} \\
&\quad - 2 f_b^2 m_t^2 \Big[\log\Big(\frac{m_t^2 m_b^2}{Q^4} \Big) + 1 + \frac{m_t^2 + m_b^2}{m_t^2 - m_b^2} \log\Big(\frac{m_t^2}{m_b^2} \Big) \Big] \Bigg\} \\
&+ \quad \text{contribution from (A.190b)}
\end{aligned} \tag{A.196}$$

Eqn. (A.196) — excluding the contribution from (A.190b) which we will consider shortly — may be obtained from Eqn. (A.195) — again excluding the contribution from (A.189b) — via the set of substitutions (A.126).

The off diagonal elements are given by:

$$\left.\frac{\partial^2\mathcal{V}}{\partial h^+\partial h'^-}\right|_{vev} = -m_{H_p}^2\cos\beta\sin\beta + \tfrac{1}{2}g^2vv'$$
$$+\frac{3(2m_1)}{32\pi^2}\Bigg\{ f_t^2\Re e\{A_t\}\Big[\log\Big(\frac{m_{\tilde{t}_1}^2 m_{\tilde{t}_2}^2}{Q^4}\Big) + 1 + \frac{\alpha_t}{2D_t^{\frac{1}{2}}}\log\Big(\frac{m_{\tilde{t}_2}^2}{m_{\tilde{t}_1}^2}\Big)\Big]$$
$$- \frac{f_t^4 vv'}{2D_t}(2m_1)(\Im m\{A_t\})^2\Big[4 - \frac{\alpha_t}{D_t^{\frac{1}{2}}}\log\Big(\frac{m_{\tilde{t}_2}^2}{m_{\tilde{t}_1}^2}\Big)\Big]$$
$$+ f_b^2\Re e\{A_b\}\Big[\log\Big(\frac{m_{\tilde{b}_1}^2 m_{\tilde{b}_2}^2}{Q^4}\Big) + 1 + \frac{\alpha_b}{2D_b^{\frac{1}{2}}}\log\Big(\frac{m_{\tilde{b}_2}^2}{m_{\tilde{b}_1}^2}\Big)\Big]$$
$$- \frac{f_b^4 vv'}{2D_b}(2m_1)(\Im m\{A_b\})^2\Big[4 - \frac{\alpha_b}{D_b^{\frac{1}{2}}}\log\Big(\frac{m_{\tilde{b}_2}^2}{m_{\tilde{b}_1}^2}\Big)\Big]$$
$$+ 2f_t f_b m_t m_b\Big[\log\Big(\frac{m_t^2 m_b^2}{Q^4}\Big) + 1 + \frac{m_t^2+m_b^2}{m_t^2-m_b^2}\log\Big(\frac{m_t^2}{m_b^2}\Big)\Big] \Bigg\}$$

$$+ \quad \text{contribution from (A.191)} \tag{A.197}$$

The equation for $\left.\frac{\partial^2\mathcal{V}}{\partial h^{+*}\partial h'^{-*}}\right|_{vev}$ is the same as Eqn. (A.197) except that (A.192) replaces (A.191).

Now we must evaluate the contributions from the second order perturbative corrections to the eigenvalues. These corrections are given in Eqns. (A.189b), (A.190b), (A.191), and (A.192). In general, they can be written as

$$\frac{3}{32\pi^2}\sum_{i=1,2}\Big\{\lambda_{t_i}^{(0)}\frac{\partial^2(\delta\lambda_{t_i}^{(2)})}{\partial h^{ch1}\partial h^{ch2}}\Big[2\log\lambda_{t_i}^{(0)} + 1\Big] + (t_i\to b_i)\Big\}\Big|_{vev}$$
$$= \frac{3}{32\pi^2}\Bigg\{\sum_{i=1,2}2m_{\tilde{t}_i}^2 N_{t_i}^2\log\Big(\frac{m_{\tilde{t}_i}^2}{Q^2}\Big)\sum_{j=1,2}\frac{N_{b_j}^2}{(m_{\tilde{t}_i}^2-m_{\tilde{b}_j}^2)^2}\frac{\partial^2|\mathcal{C}(\lambda_{t_i}^{(0)},\lambda_{b_j}^{(0)})|^2}{\partial h^{ch1}\partial h^{ch2}}$$
$$+\sum_{j=1,2}2m_{\tilde{b}_j}^2 N_{b_j}^2\log\Big(\frac{m_{\tilde{b}_j}^2}{Q^2}\Big)\sum_{i=1,2}\frac{N_{t_i}^2}{(m_{\tilde{t}_i}^2-m_{\tilde{b}_j}^2)^2}\frac{\partial^2|\mathcal{C}(\lambda_{t_i}^{(0)},\lambda_{b_j}^{(0)})|^2}{\partial h^{ch1}\partial h^{ch2}}$$
$$+\sum_{i=1,2}\sum_{j=1,2}\frac{N_{t_i}^2 N_{b_j}^2(m_{\tilde{t}_i}^2+m_{\tilde{b}_j}^2)}{(m_{\tilde{t}_i}^2-m_{\tilde{b}_j}^2)^2}\frac{\partial^2|\mathcal{C}(\lambda_{t_i}^{(0)},\lambda_{b_j}^{(0)})|^2}{\partial h^{ch1}\partial h^{ch2}}\Bigg\}\Big|_{vev} \tag{A.198}$$

Formulæ for $N_{t_i}|_{vev}$ and $N_{b_j}|_{vev}$ are given in Eqns. (A.172) and (A.173), the stop and sbottom masses ($m^2_{\tilde{t}_i}$ and $m^2_{\tilde{b}_j}$) are again given by Eqns. (A.118) and (A.120), and expressions for the $\left.\frac{\partial^2|\mathcal{C}(\lambda^{(0)}_{t_i},\lambda^{(0)}_{b_j})|^2}{\partial h^{ch1}\partial h^{ch2}}\right|_{vev}$'s are found via Eqn. (A.187), and will be given in more explicit form below.

$$
\begin{aligned}
\left.\frac{\partial^2|\mathcal{C}(\lambda^{(0)}_{t_i},\lambda^{(0)}_{b_j})|^2}{\partial h^+\partial h^{+*}}\right|_{vev} \;=\; & (f_t^2-\tfrac{g^2}{2})m_t^2m_b^2\Big\{(f_t^2-\tfrac{g^2}{2})v^2[T1][B1] \\
& + 2(2m_1)\tan\beta[T1](2m_1\tan\beta+\Re e\{A_b\})(\tfrac{1}{2}[B0]+\eta_jD_b^{\frac{1}{2}}) \\
& - 2[B1](2m_1\Re e\{A_t\}\cot\beta+|A_t|^2)(\tfrac{1}{2}[T0]+\epsilon_iD_t^{\frac{1}{2}}) \\
& + 2\Big[(2m_1)^2+2m_1(\Re e\{A_t\}\tan\beta+\Re e\{A_b\}\cot\beta) \\
& \qquad +\Re e\{A_t\}\Re e\{A_b\}+\Im m\{A_t\}\Im m\{A_b\}\Big] \\
& \qquad \cdot(\tfrac{1}{2}[T0]+\epsilon_iD_t^{\frac{1}{2}})(\tfrac{1}{2}[B0]+\eta_jD_b^{\frac{1}{2}})\Big\} \\
& + f_t^2m_b^2|A_t|^2[B1](\tfrac{1}{2}[T0]+\epsilon_iD_t^{\frac{1}{2}})^2 \\
& + f_b^2m_t^2(2m_1)^2[T1](\tfrac{1}{2}[B0]+\eta_jD_b^{\frac{1}{2}})^2 \\
& + 2f_tf_bm_tm_b(2m_1)\Big\{(2m_1\cot\beta+\Re e\{A_t\})(\tfrac{1}{2}[B0]+\eta_jD_b^{\frac{1}{2}}) \\
& \quad -(2m_1)^2\Re e\{A_t\}+|A_t|^2(2m_1\tan\beta+\Re e\{A_b\}) \\
& \quad +2m_1\cot\beta(\Re e\{A_t\}\Re e\{A_b\}+\Im m\{A_t\}\Im m\{A_b\})\Big\} \\
& \qquad \cdot(\tfrac{1}{2}[T0]+\epsilon_iD_t^{\frac{1}{2}})(\tfrac{1}{2}[B0]+\eta_jD_b^{\frac{1}{2}}) \\
& - 2f_t^2m_b^2\Big[2m_1\Re e\{A_t\}\tan\beta+\Re e\{A_t\}\Re e\{A_b\} \\
& \qquad +\Im m\{A_t\}\Im m\{A_b\}\Big](\tfrac{1}{2}[T0]+\epsilon_iD_t^{\frac{1}{2}})^2(\tfrac{1}{2}[B0]+\eta_jD_b^{\frac{1}{2}}) \\
& + f_t^2m_b^2(\tfrac{1}{2}[T0]+\epsilon_iD_t^{\frac{1}{2}})^2(\tfrac{1}{2}[B0]+\eta_jD_b^{\frac{1}{2}})^2 \qquad \text{(A.199)}
\end{aligned}
$$

where $\epsilon_i = \begin{cases} +1 & \text{for } i=1 \\ -1 & \text{for } i=2 \end{cases}$ and $\eta_j = \begin{cases} +1 & \text{for } j=1 \\ -1 & \text{for } j=2 \end{cases}$

$$
\begin{aligned}
\left.\frac{\partial^2|\mathcal{C}(\lambda_{t_i}^{(0)},\lambda_{b_j}^{(0)})|^2}{\partial h'^{-}\partial h'^{-*}}\right|_{vev} = \;& (f_b^2-\tfrac{g^2}{2})m_t^2m_b^2\Big\{(f_b^2-\tfrac{g^2}{2})v'^2[T1][B1] \\
& + 2(2m_1)\cot\beta[B1](2m_1\cot\beta+\Re e\{A_t\})(\tfrac{1}{2}[T0]+\epsilon_i D_t^{\frac{1}{2}}) \\
& - 2[T1](2m_1\Re e\{A_b\}\tan\beta+|A_b|^2)(\tfrac{1}{2}[B0]+\eta_j D_b^{\frac{1}{2}}) \\
& + 2\Big[(2m_1)^2+2m_1(\Re e\{A_t\}\tan\beta+\Re e\{A_b\}\cot\beta) \\
& \qquad +\Re e\{A_t\}\Re e\{A_b\}+\Im m\{A_t\}\Im m\{A_b\}\Big] \\
& \qquad \cdot(\tfrac{1}{2}[T0]+\epsilon_i D_t^{\frac{1}{2}})(\tfrac{1}{2}[B0]+\eta_j D_b^{\frac{1}{2}})\Big\} \\
& + f_b^2m_t^2|A_b|^2[T1](\tfrac{1}{2}[B0]+\eta_j D_b^{\frac{1}{2}})^2 \\
& + f_t^2m_b^2(2m_1)^2[B1](\tfrac{1}{2}[T0]+\epsilon_i D_t^{\frac{1}{2}})^2 \\
& + 2f_tf_bm_tm_b(2m_1)\Big\{(2m_1\tan\beta+\Re e\{A_b\})(\tfrac{1}{2}[T0]+\epsilon_i D_t^{\frac{1}{2}}) \\
& \quad -(2m_1)^2\Re e\{A_b\}+|A_b|^2(2m_1\cot\beta+\Re e\{A_t\}) \\
& \quad +2m_1\tan\beta(\Re e\{A_t\}\Re e\{A_b\}+\Im m\{A_t\}\Im m\{A_b\})\Big\} \\
& \qquad \cdot(\tfrac{1}{2}[T0]+\epsilon_i D_t^{\frac{1}{2}})(\tfrac{1}{2}[B0]+\eta_j D_b^{\frac{1}{2}}) \\
& - 2f_b^2m_t^2\Big[2m_1\Re e\{A_b\}\cot\beta+\Re e\{A_t\}\Re e\{A_b\} \\
& \qquad +\Im m\{A_t\}\Im m\{A_b\}\Big](\tfrac{1}{2}[T0]+\epsilon_i D_t^{\frac{1}{2}})(\tfrac{1}{2}[B0]+\eta_j D_b^{\frac{1}{2}})^2 \\
& + f_b^2m_t^2(\tfrac{1}{2}[T0]+\epsilon_i D_t^{\frac{1}{2}})^2(\tfrac{1}{2}[B0]+\eta_j D_b^{\frac{1}{2}})^2 \qquad \text{(A.200)}
\end{aligned}
$$

Eqn. (A.200) may be obtained from Eqn. (A.199) via the set of substitutions (A.126), if the substitutions $[T1] \leftrightarrow [B1]$ and $\epsilon_i \leftrightarrow \eta_j$ are also performed.

$$\left.\frac{\partial^2|\mathcal{C}(\lambda_{t_i}^{(0)},\lambda_{b_j}^{(0)})|^2}{\partial h^+\partial h'^-}\right|_{vev} =$$

$$\begin{aligned}
&m_t^2 m_b^2\Big\{-vv'(f_t^2-\tfrac{g^2}{2})(f_b^2-\tfrac{g^2}{2})[T1][B1] \\
&\quad+\Big[(f_t^2-\tfrac{g^2}{2})\tan\beta(2m_1A_b\tan\beta+|A_b|^2) \\
&\qquad-(f_b^2-\tfrac{g^2}{2})(2m_1)(2m_1\tan\beta+A_b)\Big][T1](\tfrac{1}{2}[B0]+\eta_jD_b^{\frac{1}{2}}) \\
&\quad+\Big[(f_t^2-\tfrac{g^2}{2})(2m_1)(2m_1\cot\beta+A_t) \\
&\qquad-(f_b^2-\tfrac{g^2}{2})\cot\beta(2m_1A_t\cot\beta+|A_t|^2)\Big][B1](\tfrac{1}{2}[T0]+\epsilon_iD_t^{\frac{1}{2}}) \\
&\quad-\Big[(f_t^2-\tfrac{g^2}{2})\tan\beta\Big[(2m_1)^2+2m_1(A_t\tan\beta+A_b^*\cot\beta)+A_tA_b^*\Big] \\
&\qquad+(f_b^2-\tfrac{g^2}{2})\cot\beta\Big[(2m_1)^2+2m_1(A_t^*\tan\beta+A_b\cot\beta)+A_t^*A_b\Big]\Big] \\
&\qquad\qquad\cdot(\tfrac{1}{2}[T0]+\epsilon_iD_t^{\frac{1}{2}})(\tfrac{1}{2}[B0]+\eta_jD_b^{\frac{1}{2}})\Big\} \\
&-f_tf_bm_tm_b\Big\{(2m_1)^2\Big[(2m_1)^2+2m_1(A_t\tan\beta+A_b\cot\beta)+A_tA_b\Big] \\
&\qquad+A_tA_b\Big[(2m_1)^2+2m_1(A_t^*\tan\beta+A_b^*\cot\beta)+A_t^*A_b^*\Big] \\
&\qquad+\Big[2m_1(2m_1+A_t\tan\beta)-A_b(2m_1\cot\beta+A_t^*)\Big](\tfrac{1}{2}[B0]+\eta_jD_b^{\frac{1}{2}}) \\
&\qquad+\Big[2m_1(2m_1+A_b\cot\beta)-A_t(2m_1\tan\beta+A_b^*)\Big](\tfrac{1}{2}[T0]+\epsilon_iD_t^{\frac{1}{2}}) \\
&\qquad+(\tfrac{1}{2}[T0]+\epsilon_iD_t^{\frac{1}{2}})(\tfrac{1}{2}[B0]+\eta_jD_b^{\frac{1}{2}})\Big\}(\tfrac{1}{2}[T0]+\epsilon_iD_t^{\frac{1}{2}})(\tfrac{1}{2}[B0]+\eta_jD_b^{\frac{1}{2}}) \\
&+f_b^2m_t^2(2m_1)A_b[T1](\tfrac{1}{2}[B0]+\eta_jD_b^{\frac{1}{2}})^2+f_t^2m_b^2(2m_1)A_t[B1](\tfrac{1}{2}[T0]+\epsilon_iD_t^{\frac{1}{2}})^2
\end{aligned} \tag{A.201}$$

Note that the right-hand side of Eqn. (A.201) is in general complex if the A-terms are complex, as compared to the right-hand sides of Eqns. (A.199) and (A.200) which are always real whether or not the A-terms are complex. (This is as expected since $h^+h^{+*}=|h^+|^2$ and $h'^-h'^{-*}=|h'^-|^2$.) Also note that, as expected,

$$\left.\frac{\partial^2|\mathcal{C}(\lambda_{t_i}^{(0)},\lambda_{b_j}^{(0)})|^2}{\partial h^{+*}\partial h'^{-*}}\right|_{vev} = \left(\left.\frac{\partial^2|\mathcal{C}(\lambda_{t_i}^{(0)},\lambda_{b_j}^{(0)})|^2}{\partial h^+\partial h'^-}\right|_{vev}\right)^* \quad . \tag{A.202}$$

The necessary ingredients for calculating the mass of the charged Higgs boson are now all given. The charged Higgs mass squared matrix is

$$\mathcal{M}^{tree}_{H^2_{ch}} = \begin{bmatrix} \left.\frac{\partial^2 \mathcal{V}}{\partial h^+ \partial h^{+*}}\right|_{vev} & \left.\frac{\partial^2 \mathcal{V}}{\partial h^+ \partial h'^-}\right|_{vev} \\ \left.\frac{\partial^2 \mathcal{V}}{\partial h^{+*} \partial h'^{-*}}\right|_{vev} & \left.\frac{\partial^2 \mathcal{V}}{\partial h'^- \partial h'^{-*}}\right|_{vev} \end{bmatrix} \quad ; \tag{A.203}$$

$\left.\frac{\partial^2 \mathcal{V}}{\partial h^+ \partial h^{+*}}\right|_{vev}$ is given by Eqns. (A.195), (A.198), and (A.199); $\left.\frac{\partial^2 \mathcal{V}}{\partial h'^- \partial h'^{-*}}\right|_{vev}$ is given by Eqns. (A.196), (A.198), and (A.200); $\left.\frac{\partial^2 \mathcal{V}}{\partial h^+ \partial h'^-}\right|_{vev}$ is given by Eqns. (A.197), (A.198), and (A.201); and $\left.\frac{\partial^2 \mathcal{V}}{\partial h^{+*} \partial h'^{-*}}\right|_{vev}$ is given by Eqns. (A.197), (A.198), and (A.202). The eigenvalues of this matrix — see Eqn. (A.34) with $B^2 \Rightarrow |B|^2$ — give the masses of the charged Higgs boson, $m^2_{H_{ch}}$, and the would-be Goldstone boson. The resulting expression for $m^2_{H_{ch}}$ would be quite cumbersome and will not be given here. However, it is relatively easy to plug the formula cited above into Eqn. (A.34) and numerically calculate the eigenvalues for a given choice of input parameters. Many numerical tests have been performed, and the mass of the charged Goldstone mode was always found to be zero (within rounding errors of the computer).

Next we must deal with the special cases mentioned earlier where $D_t = 0 \Leftrightarrow m_{\tilde{t}_1} = m_{\tilde{t}_2}$ and/or $D_b = 0 \Leftrightarrow m_{\tilde{b}_1} = m_{\tilde{b}_2}$. We follow the same procedure as described on page 41. Note that if $D_t = 0$, then we require $\Im m\{A_t\} = 0$ as in condition 2) on page 41, and then Eqn. (A.137) requires that $\Im m\{A_b\} = 0$ as well. If $D_t = 0$ but $D_b \neq 0$, then the material within the large curly brackets of Eqn. (A.195) becomes

$$\begin{aligned} \left.\frac{\partial^2 \mathcal{V}}{\partial h^+ \partial h^{+*}}\right|_{vev} \ni \; & \Big\{ \Big\{ -(f_t^2 - \tfrac{g^2}{2}) m^2_{\tilde{t}_1} - f_t^2 (2m_1)^2 \cot^2\beta \Big\} \Big[\log\Big(\frac{m^4_{\tilde{t}_1}}{Q^4}\Big) + 1 \Big] \\ & - 2 f_t^2 (2m_1)^2 \cot^2\beta \\ & + \Big\{ \tfrac{1}{2}(f_t^2 - \tfrac{g^2}{2})(\alpha_b + [B0]) - f_b^2 (2m_1)^2 \Big\} \Big[\log\Big(\frac{m^2_{\tilde{b}_1} m^2_{\tilde{b}_2}}{Q^4}\Big) + 1 \Big] \\ & + D_b^{\frac{1}{2}} \Big\{ (f_t^2 - \tfrac{g^2}{2}) \Big[1 + \frac{\alpha_b [B0]}{4 D_b} \Big] - \frac{\alpha_b f_b^2}{2 D_b} (2m_1)^2 \Big\} \log\Big(\frac{m^2_{\tilde{b}_2}}{m^2_{\tilde{b}_1}}\Big) \\ & - 2 f_t^2 m_b^2 \Big[\log\Big(\frac{m_t^2 m_b^2}{Q^4}\Big) + 1 + \frac{m_t^2 + m_b^2}{m_t^2 - m_b^2} \log\Big(\frac{m_t^2}{m_b^2}\Big) \Big] \Big\} \end{aligned} \tag{A.204}$$

The inside of the big curly brackets of Eqn. (A.196) becomes:

$$\left.\frac{\partial^2\mathcal{V}}{\partial h'^{-}\partial h'^{-*}}\right|_{vev} \ni \Big\{ \Big\{\tfrac{1}{2}(f_b^2-\tfrac{g^2}{2})m^2_{\tilde{t}_1} - f_t^2(2m_1)^2\Big\}\Big[\log\Big(\frac{m^4_{\tilde{t}_1}}{Q^4}\Big)+1\Big] - 2f_t^2(2m_1)^2$$
$$+\Big\{-\tfrac{1}{2}(f_b^2-\tfrac{g^2}{2})(\alpha_b+[B0]) - f_b^2|A_b|^2\Big\}\Big[\log\Big(\frac{m^2_{\tilde{b}_1}m^2_{\tilde{b}_2}}{Q^4}\Big)+1\Big]$$
$$+D_b^{\frac{1}{2}}\Big\{-(f_b^2-\tfrac{g^2}{2})\Big[1+\frac{\alpha_b[B0]}{4D_b}\Big] - \frac{\alpha_b f_b^2}{2D_b}|A_b|^2\Big\}\log\Big(\frac{m^2_{\tilde{b}_2}}{m^2_{\tilde{b}_1}}\Big)$$
$$-2f_b^2m_t^2\Big[\log\Big(\frac{m_t^2m_b^2}{Q^4}\Big)+1+\frac{m_t^2+m_b^2}{m_t^2-m_b^2}\log\Big(\frac{m_t^2}{m_b^2}\Big)\Big]\Big\} \tag{A.205}$$

And the corresponding part of Eqn. (A.197) becomes:

$$\left.\frac{\partial^2\mathcal{V}}{\partial h^{+}\partial h'^{-}}\right|_{vev} \ni \Big\{ -f_t^2(2m_1)\cot\beta\Big[\log\Big(\frac{m^4_{\tilde{t}_1}}{Q^4}\Big)+3\Big]$$
$$+f_b^2\Re e\{A_b\}\Big[\log\Big(\frac{m^2_{\tilde{b}_1}m^2_{\tilde{b}_2}}{Q^4}\Big)+1+\frac{\alpha_b}{2D_b^{\frac{1}{2}}}\log\Big(\frac{m^2_{\tilde{b}_2}}{m^2_{\tilde{b}_1}}\Big)\Big]$$
$$+2f_tf_bm_tm_b\Big[\log\Big(\frac{m_t^2m_b^2}{Q^4}\Big)+1+\frac{m_t^2+m_b^2}{m_t^2-m_b^2}\log\Big(\frac{m_t^2}{m_b^2}\Big)\Big]\Big\} \tag{A.206}$$

Since the A-terms are real, $\left.\frac{\partial^2\mathcal{V}}{\partial h^{+}\partial h'^{-}}\right|_{vev} = \left.\frac{\partial^2\mathcal{V}}{\partial h^{+*}\partial h'^{-*}}\right|_{vev}$.
Now if $D_b = 0$ but $D_t \neq 0$, then curly bracket part of Eqn. (A.195) becomes

$$\left.\frac{\partial^2\mathcal{V}}{\partial h^{+}\partial h^{+*}}\right|_{vev} \ni \Big\{ \Big\{-\tfrac{1}{2}(f_t^2-\tfrac{g^2}{2})(\alpha_t+[T0]) - f_t^2|A_t|^2\Big\}\Big[\log\Big(\frac{m^2_{\tilde{t}_1}m^2_{\tilde{t}_2}}{Q^4}\Big)+1\Big]$$
$$+D_t^{\frac{1}{2}}\Big\{-(f_t^2-\tfrac{g^2}{2})\Big[1+\frac{\alpha_t[T0]}{4D_t}\Big] - \frac{\alpha_t f_t^2}{2D_t}|A_t|^2\Big\}\log\Big(\frac{m^2_{\tilde{t}_2}}{m^2_{\tilde{t}_1}}\Big)$$
$$+\Big\{\tfrac{1}{2}(f_t^2-\tfrac{g^2}{2})m^2_{\tilde{b}_1} - f_b^2(2m_1)^2\Big\}\Big[\log\Big(\frac{m^4_{\tilde{b}_1}}{Q^4}\Big)+1\Big] - 2f_b^2(2m_1)^2$$
$$-2f_t^2m_b^2\Big[\log\Big(\frac{m_t^2m_b^2}{Q^4}\Big)+1+\frac{m_t^2+m_b^2}{m_t^2-m_b^2}\log\Big(\frac{m_t^2}{m_b^2}\Big)\Big]\Big\} \tag{A.207}$$

The corresponding part of Eqn. (A.196) becomes:

$$\left.\frac{\partial^2\mathcal{V}}{\partial h'^{-}\partial h'^{-*}}\right|_{vev} \ni \Big\{ \Big\{\tfrac{1}{2}(f_b^2-\tfrac{g^2}{2})(\alpha_t + [T0]) - f_t^2(2m_1)^2\Big\}\Big[\log\Big(\frac{m^2_{\tilde{t}_1}m^2_{\tilde{t}_2}}{Q^4}\Big) + 1\Big]$$
$$+ D_t^{\frac{1}{2}}\Big\{(f_b^2-\tfrac{g^2}{2})\Big[1+\frac{\alpha_t[T0]}{4D_t}\Big] - \frac{\alpha_t f_t^2}{2D_t}(2m_1)^2\Big\}\log\Big(\frac{m^2_{\tilde{t}_2}}{m^2_{\tilde{t}_1}}\Big)$$
$$+ \Big\{-\tfrac{1}{2}(f_b^2-\tfrac{g^2}{2})m^2_{\tilde{b}_1} - f_b^2(2m_1)^2\tan^2\beta\Big\}\Big[\log\Big(\frac{m^4_{\tilde{b}_1}}{Q^4}\Big)+1\Big]$$
$$- 2f_b^2(2m_1)^2\tan^2\beta$$
$$- 2f_b^2m_t^2\Big[\log\Big(\frac{m_t^2m_b^2}{Q^4}\Big) + 1 + \frac{m_t^2+m_b^2}{m_t^2-m_b^2}\log\Big(\frac{m_t^2}{m_b^2}\Big)\Big]\Big\} \tag{A.208}$$

And for Eqn. (A.197) the curly-bracketed material becomes:

$$\left.\frac{\partial^2\mathcal{V}}{\partial h^{+}\partial h'^{-}}\right|_{vev} \ni \Big\{ f_t^2\Re e\{A_t\}\Big[\log\Big(\frac{m^2_{\tilde{t}_1}m^2_{\tilde{t}_2}}{Q^4}\Big) + 1 + \frac{\alpha_t}{2D_t^{\frac{1}{2}}}\log\Big(\frac{m^2_{\tilde{t}_2}}{m^2_{\tilde{t}_1}}\Big)\Big]$$
$$- f_b^2(2m_1)\tan\beta\Big[\log\Big(\frac{m^4_{\tilde{b}_1}}{Q^4}\Big)+3\Big]$$
$$+ 2f_tf_bm_tm_b\Big[\log\Big(\frac{m_t^2m_b^2}{Q^4}\Big) + 1 + \frac{m_t^2+m_b^2}{m_t^2-m_b^2}\log\Big(\frac{m_t^2}{m_b^2}\Big)\Big]\Big\} \tag{A.209}$$

Finally, in the very special case when $D_t = D_b = 0$. This is true *for instance* if $m_{\tilde{L}} = m_{\tilde{t}_R} = m_{\tilde{b}_R}$, and $2m_1 = A_t = A_b = 0$, and either $\tan\beta = 1$ or D-terms are neglected. In this case the curly bracket part of Eqn. (A.195) becomes

$$\left.\frac{\partial^2\mathcal{V}}{\partial h^{+}\partial h^{+*}}\right|_{vev} \ni \Big\{ \Big\{-\tfrac{1}{2}(f_t^2-\tfrac{g^2}{2})m^2_{\tilde{b}_1} - f_t^2(2m_1)^2\cot^2\beta\Big\}\Big[\log\Big(\frac{m^4_{\tilde{t}_1}}{Q^4}\Big)+1\Big]$$
$$+ \Big\{\tfrac{1}{2}(f_t^2-\tfrac{g^2}{2})m^2_{\tilde{b}_1} - f_b^2(2m_1)^2\Big\}\Big[\log\Big(\frac{m^4_{\tilde{b}_1}}{Q^4}\Big)+1\Big]$$
$$- 2(f_t^2\cot^2\beta - f_b^2)(2m_1)^2$$
$$- 2f_t^2m_b^2\Big[\log\Big(\frac{m_t^2m_b^2}{Q^4}\Big) + 1 + \frac{m_t^2+m_b^2}{m_t^2-m_b^2}\log\Big(\frac{m_t^2}{m_b^2}\Big)\Big]\Big\} \tag{A.210}$$

For Eqn. (A.196) the corresponding part becomes:

$$\left.\frac{\partial^2\mathcal{V}}{\partial h'^{-}\partial h'^{-*}}\right|_{vev} \ni \Bigg\{ \Big\{\tfrac{1}{2}(f_b^2-\tfrac{g^2}{2})m_{\tilde{t}_1}^2 - f_t^2(2m_1)^2\Big\}\Big[\log\Big(\frac{m_{\tilde{t}_1}^4}{Q^4}\Big)+1\Big] + \Big\{-\tfrac{1}{2}(f_b^2-\tfrac{g^2}{2})m_{\tilde{b}_1}^2 - f_b^2(2m_1)^2\tan^2\beta\Big\}\Big[\log\Big(\frac{m_{\tilde{b}_1}^4}{Q^4}\Big)+1\Big] - 2(f_t^2+f_b^2\tan^2\beta)(2m_1)^2 - 2f_b^2m_t^2\Big[\log\Big(\frac{m_t^2m_b^2}{Q^4}\Big)+1+\frac{m_t^2+m_b^2}{m_t^2-m_b^2}\log\Big(\frac{m_t^2}{m_b^2}\Big)\Big]\Bigg\} \tag{A.211}$$

And the portion of Eqn. (A.197) within the curly brackets becomes:

$$\left.\frac{\partial^2\mathcal{V}}{\partial h^{+}\partial h'^{-}}\right|_{vev} \ni \Bigg\{ -f_t^2(2m_1)\cot\beta\Big[\log\Big(\frac{m_{\tilde{t}_1}^4}{Q^4}\Big)+3\Big] - f_b^2(2m_1)\tan\beta\Big[\log\Big(\frac{m_{\tilde{b}_1}^4}{Q^4}\Big)+3\Big] + 2f_tf_bm_tm_b\Big[\log\Big(\frac{m_t^2m_b^2}{Q^4}\Big)+1+\frac{m_t^2+m_b^2}{m_t^2-m_b^2}\log\Big(\frac{m_t^2}{m_b^2}\Big)\Big]\Bigg\} \tag{A.212}$$

The contributions from (A.189b) to Eqn. (A.195), from (A.190b) to Eqn. (A.196), and from (A.191) to Eqn. (A.197), for the special cases must now be considered. For $D_t = 0$ and $D_b \neq 0$, Eqn. (A.198) becomes

$$\frac{3}{32\pi^2}\sum_{i=1,2}\left\{\lambda_{t_i}^{(0)}\frac{\partial^2(\delta\lambda_{t_i}^{(2)})}{\partial h^{ch1}\partial h^{ch2}}\Big[2\log\lambda_{t_i}^{(0)}+1\Big] + (t_i\to b_i)\right\}\Bigg|_{vev}$$
$$= \frac{3}{32\pi^2}\Bigg\{\sum_{j=1,2}\frac{N_{b_j}^2}{(m_{\tilde{t}_1}^2-m_{\tilde{b}_j}^2)^2}\Big[m_{\tilde{t}_1}^2\log\Big(\frac{m_{\tilde{t}_1}^2}{Q^2}\Big)+m_{\tilde{b}_j}^2\log\Big(\frac{m_{\tilde{b}_j}^2}{Q^2}\Big) + \tfrac{1}{2}(m_{\tilde{t}_1}^2+m_{\tilde{b}_j}^2)\Big]\sum_{i=1,2}\frac{\partial^2|\mathcal{C}(\lambda_{t_i}^{(0)},\lambda_{b_j}^{(0)})|^2}{\partial h^{ch1}\partial h^{ch2}}\Bigg|_{vev}\Bigg\} \tag{A.213}$$

In this special case:

$$\left.\frac{\partial^2|\mathcal{C}(\lambda_{t_i}^{(0)},\lambda_{b_j}^{(0)})|^2}{\partial h^+\partial h^{+*}}\right|_{vev} = m_b^2\Big[(f_t^2-\tfrac{g^2}{2})v+\epsilon_i f_t(2m_1)\cot\beta\Big]^2[B1]$$
$$+ f_b^2\Big[2m_1+\epsilon_i m_t\cot\beta\Big]^2(\tfrac{1}{2}[B0]+\eta_j D_b^{\frac{1}{2}})^2$$
$$+ 2m_b\Big[m_b(f_t^2-\tfrac{g^2}{2})+\epsilon_i f_t f_b(2m_1)\cot^2\beta\Big]$$
$$\cdot\ (2m_1\tan\beta+\epsilon_i m_t)(2m_1\tan\beta+A_b)$$
$$\cdot\ (\tfrac{1}{2}[B0]+\eta_j D_b^{\frac{1}{2}}) \qquad \text{(A.214)}$$

And so $$\sum_{i=1,2}\left.\frac{\partial^2|\mathcal{C}(\lambda_{t_i}^{(0)},\lambda_{b_j}^{(0)})|^2}{\partial h^+\partial h^{+*}}\right|_{vev} = 2m_b^2\Big[(f_t^2-\tfrac{g^2}{2})^2v^2+f_t^2(2m_1)^2\cot^2\beta\Big][B1]$$
$$+ 2f_b^2\Big[(2m_1)^2+m_t^2\cot^2\beta\Big](\tfrac{1}{2}[B0]+\eta_j D_b^{\frac{1}{2}})^2$$
$$+ 4m_b^2(2m_1)\Big[(f_t^2-\tfrac{g^2}{2})\tan\beta+f_t^2\cot\beta\Big]$$
$$\cdot\ (2m_1\tan\beta+A_b)(\tfrac{1}{2}[B0]+\eta_j D_b^{\frac{1}{2}})$$
$$\text{(A.215)}$$

$$\left.\frac{\partial^2|\mathcal{C}(\lambda_{t_i}^{(0)},\lambda_{b_j}^{(0)})|^2}{\partial h'^-\partial h'^{-*}}\right|_{vev} = m_b^2\Big[(f_b^2-\tfrac{g^2}{2})v'+\epsilon_i f_t(2m_1)\Big]^2[B1]$$
$$+ f_b^2\Big[\epsilon_i m_t-A_b\Big]^2(\tfrac{1}{2}[B0]+\eta_j D_b^{\frac{1}{2}})^2$$
$$+ 2m_b\Big[m_b(f_b^2-\tfrac{g^2}{2})+\epsilon_i f_t f_b(2m_1)\Big]$$
$$\cdot\ (\epsilon_i m_t-A_b)(2m_1\tan\beta+A_b)$$
$$\cdot\ (\tfrac{1}{2}[B0]+\eta_j D_b^{\frac{1}{2}}) \qquad \text{(A.216)}$$

And so $$\sum_{i=1,2}\left.\frac{\partial^2|\mathcal{C}(\lambda_{t_i}^{(0)},\lambda_{b_j}^{(0)})|^2}{\partial h'^-\partial h'^{-*}}\right|_{vev} = 2m_b^2\Big[(f_b^2-\tfrac{g^2}{2})^2v'^2+f_t^2(2m_1)^2\Big][B1]$$
$$+ 2f_b^2\Big[m_t^2+A_b^2\Big](\tfrac{1}{2}[B0]+\eta_j D_b^{\frac{1}{2}})^2$$
$$+ 4m_b\Big[f_t f_b m_t(2m_1)-(f_b^2-\tfrac{g^2}{2})m_b A_b\Big]$$
$$\cdot\ (2m_1\tan\beta+A_b)(\tfrac{1}{2}[B0]+\eta_j D_b^{\frac{1}{2}})$$
$$\text{(A.217)}$$

$$\left.\frac{\partial^2|\mathcal{C}(\lambda_{t_i}^{(0)},\lambda_{b_j}^{(0)})|^2}{\partial h^+\partial h'^-}\right|_{vev} = \left.\frac{\partial^2|\mathcal{C}(\lambda_{t_i}^{(0)},\lambda_{b_j}^{(0)})|^2}{\partial h^{+*}\partial h'^{-*}}\right|_{vev}$$
$$= -m_b^2\Big[(f_t^2-\tfrac{g^2}{2})v+\epsilon_i f_t(2m_1)\cot\beta\Big]$$
$$\cdot\Big[(f_b^2-\tfrac{g^2}{2})v'+\epsilon_i f_t(2m_1)\Big][B1]$$
$$+f_b^2(2m_1+\epsilon_i m_t\cot\beta)(A_b-\epsilon_i m_t)(\tfrac{1}{2}[B0]+\eta_j D_b^{\frac{1}{2}})^2$$
$$+f_b m_b\Big[(f_t^2-\tfrac{g^2}{2})vA_b-(f_b^2-\tfrac{g^2}{2})v'(2m_1)$$
$$-2m_t(2m_1)\cot\beta$$
$$-\epsilon_i f_t\Big(m_t^2+m_b^2+(2m_1)^2-m_W^2-(2m_1)A_b\cot\beta\Big)\Big]$$
$$\cdot(2m_1\tan\beta+A_b)(\tfrac{1}{2}[B0]+\eta_j D_b^{\frac{1}{2}}) \qquad \text{(A.218)}$$

$$\text{And so}\quad \sum_{i=1,2}\left.\frac{\partial^2|\mathcal{C}(\lambda_{t_i}^{(0)},\lambda_{b_j}^{(0)})|^2}{\partial h^+\partial h'^-}\right|_{vev} = -2m_b^2\Big[(f_t^2-\tfrac{g^2}{2})(f_b^2-\tfrac{g^2}{2})vv'$$
$$+f_t^2(2m_1)^2\cot\beta\Big][B1]$$
$$+2f_b^2(2m_1A_b-m_t^2\cot\beta)(\tfrac{1}{2}[B0]+\eta_j D_b^{\frac{1}{2}})^2$$
$$+2f_b m_b\Big[(f_t^2-\tfrac{g^2}{2})vA_b-(f_b^2-\tfrac{g^2}{2})v'(2m_1)$$
$$-2m_t(2m_1)\cot\beta\Big]$$
$$\cdot(2m_1\tan\beta+A_b)(\tfrac{1}{2}[B0]+\eta_j D_b^{\frac{1}{2}}) \qquad \text{(A.219)}$$

For $D_b=0$ and $D_t\neq 0$, Eqn. (A.198) becomes

$$\frac{3}{32\pi^2}\sum_{i=1,2}\left\{\lambda_{t_i}^{(0)}\frac{\partial^2(\delta\lambda_{t_i}^{(2)})}{\partial h^{ch1}\partial h^{ch2}}\Big[2\log\lambda_{t_i}^{(0)}+1\Big]+(t_i\to b_i)\right\}\Big|_{vev}$$
$$=\frac{3}{32\pi^2}\Bigg\{\sum_{i=1,2}\frac{N_{t_i}^2}{(m_{t_i}^2-m_{\tilde{b}_1}^2)^2}\Big[m_{t_i}^2\log\Big(\frac{m_{t_i}^2}{Q^2}\Big)+m_{\tilde{b}_1}^2\log\Big(\frac{m_{\tilde{b}_1}^2}{Q^2}\Big)$$
$$+\tfrac{1}{2}(m_{t_i}^2+m_{\tilde{b}_1}^2)\Big]\sum_{j=1,2}\left.\frac{\partial^2|\mathcal{C}(\lambda_{t_i}^{(0)},\lambda_{b_j}^{(0)})|^2}{\partial h^{ch1}\partial h^{ch2}}\right|_{vev}\Bigg\} \qquad \text{(A.220)}$$

In this special case:

$$\left.\frac{\partial^2|\mathcal{C}(\lambda_{t_i}^{(0)},\lambda_{b_j}^{(0)})|^2}{\partial h^+\partial h^{+*}}\right|_{vev} = m_t^2\Big[(f_t^2-\tfrac{g^2}{2})v+\eta_j f_b(2m_1)\Big]^2[T1] + f_t^2\Big[\eta_j m_b - A_t\Big]^2(\tfrac{1}{2}[T0]+\epsilon_i D_t^{\frac{1}{2}})^2 + 2m_t\Big[m_t(f_t^2-\tfrac{g^2}{2})+\eta_j f_t f_b(2m_1)\Big] \cdot (\eta_j m_b - A_t)(2m_1\cot\beta + A_t) \cdot (\tfrac{1}{2}[T0]+\epsilon_i D_t^{\frac{1}{2}}) \quad \text{(A.221)}$$

$$\text{And so } \sum_{j=1,2}\left.\frac{\partial^2|\mathcal{C}(\lambda_{t_i}^{(0)},\lambda_{b_j}^{(0)})|^2}{\partial h^+\partial h^{+*}}\right|_{vev} = 2m_t^2\Big[(f_t^2-\tfrac{g^2}{2})^2v^2+f_b^2(2m_1)^2\Big][T1] + 2f_t^2\Big[m_b^2+A_t^2\Big](\tfrac{1}{2}[T0]+\epsilon_i D_t^{\frac{1}{2}})^2 + 4m_t\Big[f_t f_b m_b(2m_1) - (f_t^2-\tfrac{g^2}{2})m_t A_t\Big] \cdot (2m_1\cot\beta + A_t)(\tfrac{1}{2}[T0]+\epsilon_i D_t^{\frac{1}{2}}) \quad \text{(A.222)}$$

$$\left.\frac{\partial^2|\mathcal{C}(\lambda_{t_i}^{(0)},\lambda_{b_j}^{(0)})|^2}{\partial h'^-\partial h'^{-*}}\right|_{vev} = m_t^2\Big[(f_b^2-\tfrac{g^2}{2})v'+\eta_j f_b(2m_1)\tan\beta\Big]^2[T1] + f_t^2\Big[2m_1+\eta_j m_b\tan\beta\Big]^2(\tfrac{1}{2}[T0]+\epsilon_i D_t^{\frac{1}{2}})^2 + 2m_t\Big[m_t(f_b^2-\tfrac{g^2}{2})+\eta_j f_t f_b(2m_1)\tan^2\beta\Big] \cdot (2m_1\cot\beta+\eta_j m_b)(2m_1\cot\beta + A_t) \cdot (\tfrac{1}{2}[T0]+\epsilon_i D_t^{\frac{1}{2}}) \quad \text{(A.223)}$$

$$\text{And so } \sum_{i=1,2}\left.\frac{\partial^2|\mathcal{C}(\lambda_{t_i}^{(0)},\lambda_{b_j}^{(0)})|^2}{\partial h'^-\partial h'^{-*}}\right|_{vev} = 2m_t^2\Big[(f_b^2-\tfrac{g^2}{2})^2v'^2+f_b^2(2m_1)^2\tan^2\beta\Big][T1] + 2f_t^2\Big[(2m_1)^2+m_b^2\tan^2\beta\Big](\tfrac{1}{2}[T0]+\epsilon_i D_t^{\frac{1}{2}})^2 + 4m_t^2(2m_1)\Big[(f_b^2-\tfrac{g^2}{2})\cot\beta + f_b^2\tan\beta\Big] \cdot (2m_1\cot\beta + A_t)(\tfrac{1}{2}[T0]+\epsilon_i D_t^{\frac{1}{2}}) \quad \text{(A.224)}$$

$$\begin{aligned}
\left.\frac{\partial^2|\mathcal{C}(\lambda_{t_i}^{(0)},\lambda_{b_j}^{(0)})|^2}{\partial h^+\partial h'^-}\right|_{vev} &= \left.\frac{\partial^2|\mathcal{C}(\lambda_{t_i}^{(0)},\lambda_{b_j}^{(0)})|^2}{\partial h^{+*}\partial h'^{-*}}\right|_{vev} \\
&= -m_t^2\Big[(f_b^2-\tfrac{g^2}{2})v'+\eta_j f_b(2m_1)\tan\beta\Big] \\
&\qquad\cdot\Big[(f_t^2-\tfrac{g^2}{2})v+\eta_j f_b(2m_1)\Big][T1] \\
&\quad + f_t^2(2m_1+\eta_j m_b\tan\beta)(A_t-\eta_j m_b)(\tfrac{1}{2}[T0]+\epsilon_i D_t^{\frac{1}{2}})^2 \\
&\quad + f_t m_t\Big[(f_b^2-\tfrac{g^2}{2})v'A_t \;-\; (f_t^2-\tfrac{g^2}{2})v(2m_1) \\
&\qquad - 2m_b(2m_1)\tan\beta \\
&\qquad - \eta_j f_b\Big(m_t^2+m_b^2+(2m_1)^2-m_W^2-(2m_1)A_t\tan\beta\Big)\Big] \\
&\qquad\cdot(2m_1\cot\beta+A_t)(\tfrac{1}{2}[T0]+\epsilon_i D_t^{\frac{1}{2}})
\end{aligned} \tag{A.225}$$

$$\begin{aligned}
\text{And so}\quad \sum_{i=1,2}\left.\frac{\partial^2|\mathcal{C}(\lambda_{t_i}^{(0)},\lambda_{b_j}^{(0)})|^2}{\partial h^+\partial h'^-}\right|_{vev} &= -2m_t^2\Big[(f_t^2-\tfrac{g^2}{2})(f_b^2-\tfrac{g^2}{2})vv' \\
&\qquad + f_b^2(2m_1)^2\tan\beta\Big][T1] \\
&\quad + 2f_t^2(2m_1A_t-m_b^2\tan\beta)(\tfrac{1}{2}[T0]+\epsilon_i D_t^{\frac{1}{2}})^2 \\
&\quad + 2f_t m_t\Big[(f_b^2-\tfrac{g^2}{2})v'A_t \;-\; (f_t^2-\tfrac{g^2}{2})v(2m_1) \\
&\qquad - 2m_b(2m_1)\tan\beta\Big] \\
&\qquad\cdot(2m_1\cot\beta+A_t)(\tfrac{1}{2}[T0]+\epsilon_i D_t^{\frac{1}{2}})
\end{aligned} \tag{A.226}$$

Finally, For $D_t = D_b = 0$, Eqn. (A.198) becomes

$$\begin{aligned}
&\frac{3}{32\pi^2}\sum_{i=1,2}\left\{\lambda_{t_i}^{(0)}\frac{\partial^2(\delta\lambda_{t_i}^{(2)})}{\partial h^{ch1}\partial h^{ch2}}\Big[2\log\lambda_{t_i}^{(0)}\;+\;1\Big] \quad + \quad (t_i\to b_i)\right\}\Bigg|_{vev} \\
&\quad = \frac{3}{32\pi^2}\Bigg\{\frac{1}{2(m_{\tilde{t}_i}^2-m_{\tilde{b}_1}^2)^2}\Big[m_{\tilde{t}_1}^2\log\Big(\frac{m_{\tilde{t}_1}^2}{Q^2}\Big)\;+\;m_{\tilde{b}_1}^2\log\Big(\frac{m_{\tilde{b}_1}^2}{Q^2}\Big) \\
&\qquad\qquad + \tfrac{1}{2}(m_{\tilde{t}_1}^2+m_{\tilde{b}_1}^2)\Big]\sum_{i,j=1,2}\left.\frac{\partial^2|\mathcal{C}(\lambda_{t_i}^{(0)},\lambda_{b_j}^{(0)})|^2}{\partial h^{ch1}\partial h^{ch2}}\right|_{vev}\Bigg\}
\end{aligned} \tag{A.227}$$

In this special case:

$$\left.\frac{\partial^2|\mathcal{C}(\lambda_{t_i}^{(0)},\lambda_{b_j}^{(0)})|^2}{\partial h^+\partial h^{+*}}\right|_{vev} = (f_t^2-\tfrac{g^2}{2})^2v^2 + (2m_1)^2(f_b^2-f_t^2\cot^2\beta) + f_t^2m_b^2$$
$$+ 2\epsilon_i(2m_1)m_t\cot\beta(f_t^2+f_b^2-\tfrac{g^2}{2})$$
$$+ 2\eta_j(2m_1)m_b\Big[(f_t^2-\tfrac{g^2}{2})\tan\beta + f_t^2\cot\beta\Big]$$
$$+ 2f_tf_b\epsilon_i\eta_j\Big[(f_t^2-\tfrac{g^2}{2})vv' + (2m_1)^2\cot\beta\Big] \quad \text{(A.228)}$$

$$\text{And so} \sum_{i,j=1,2}\left.\frac{\partial^2|\mathcal{C}(\lambda_{t_i}^{(0)},\lambda_{b_j}^{(0)})|^2}{\partial h^+\partial h^{+*}}\right|_{vev} = 4\Big[(f_t^2-\tfrac{g^2}{2})^2v^2 + f_t^2m_b^2$$
$$+ (2m_1)^2(f_b^2-f_t^2\cot^2\beta)\Big] \quad \text{(A.229)}$$

$$\left.\frac{\partial^2|\mathcal{C}(\lambda_{t_i}^{(0)},\lambda_{b_j}^{(0)})|^2}{\partial h'^-\partial h'^{-*}}\right|_{vev} = (f_b^2-\tfrac{g^2}{2})^2v'^2 + (2m_1)^2(f_t^2-f_b^2\tan^2\beta) + f_b^2m_t^2$$
$$+ 2\epsilon_i(2m_1)m_t\Big[(f_b^2-\tfrac{g^2}{2})\cot\beta + f_b^2\tan\beta\Big]$$
$$+ 2\eta_j(2m_1)m_b\tan\beta(f_t^2+f_b^2-\tfrac{g^2}{2})$$
$$+ 2f_tf_b\epsilon_i\eta_j\Big[(f_b^2-\tfrac{g^2}{2})vv' + (2m_1)^2\tan\beta\Big] \quad \text{(A.230)}$$

$$\text{And so} \sum_{i,j=1,2}\left.\frac{\partial^2|\mathcal{C}(\lambda_{t_i}^{(0)},\lambda_{b_j}^{(0)})|^2}{\partial h'^-\partial h'^{-*}}\right|_{vev} = 4\Big[(f_b^2-\tfrac{g^2}{2})^2v'^2 + f_b^2m_t^2$$
$$+ (2m_1)^2(f_t^2-f_b^2\tan^2\beta)\Big] \quad \text{(A.231)}$$

$$\left.\frac{\partial^2|\mathcal{C}(\lambda_{t_i}^{(0)},\lambda_{b_j}^{(0)})|^2}{\partial h^+\partial h'^-}\right|_{vev} = \left.\frac{\partial^2|\mathcal{C}(\lambda_{t_i}^{(0)},\lambda_{b_j}^{(0)})|^2}{\partial h^{+*}\partial h'^{-*}}\right|_{vev}$$
$$= -vv'\Big[(f_t^2-\tfrac{g^2}{2})(f_b^2-\tfrac{g^2}{2}) - f_t^2f_b^2\Big] - 2m_1(f_b^2\tan\beta + f_t^2\cot\beta)$$
$$- \epsilon_i(2m_1)m_t\Big[f_t^2+2f_b^2-\tfrac{g^2}{2}+(f_b^2-\tfrac{g^2}{2})\cot\beta\Big]$$
$$- \eta_j(2m_1)m_b\Big[2f_t^2+f_b^2-\tfrac{g^2}{2}+(f_t^2-\tfrac{g^2}{2})\tan\beta\Big]$$
$$+ f_tf_b\epsilon_i\eta_j\Big[m_t^2+m_b^2+2(2m_1)^2-m_W^2\Big] \quad \text{(A.232)}$$

$$\text{And so} \sum_{i=1,2}\left.\frac{\partial^2|\mathcal{C}(\lambda_{t_i}^{(0)},\lambda_{b_j}^{(0)})|^2}{\partial h^+\partial h'^-}\right|_{vev} = -4vv'\Big[(f_t^2-\tfrac{g^2}{2})(f_b^2-\tfrac{g^2}{2}) - f_t^2f_b^2\Big]$$
$$- 4(2m_1)(f_b^2\tan\beta + f_t^2\cot\beta)$$
$$\text{(A.233)}$$

A.10 Tree-Level Scalar Higgs Trilinear Interaction Coupling

For many choices of the MSSM input parameters, the decay of the heavy Higgs boson, H_h, into a pair of light Higgs bosons, H_ℓ, is kinematically allowed. Thus the coupling constant in the MSSM Lagrangian (so opposite sign to $\mathcal{V}$) for the H_h-H_ℓ-H_ℓ vertex , $\xi_{h\ell\ell}$ with $\mathcal{L} \ni \xi_{h\ell\ell} H_h H_\ell H_\ell$, is given by

$$\xi_{h\ell\ell} = -\frac{1}{2} \frac{\partial^3 \mathcal{V}}{\partial H_h \partial H_\ell \partial H_\ell}\bigg|_{vev} \quad . \tag{A.234}$$

Since this is often a significant decay mode for the heavy Higgs boson, it is of interest to see whether or not radiative corrections significantly affect the values of this vertex factor [47,168,207].

There are also other three-Higgs vertices within the MSSM which can be altered by radiative corrections. These other possible vertices are the H_h-H_p-H_p vertex, the H_ℓ-H_p-H_p vertex, and the H_h-H^+-H^- vertex. However, these other vertices are only of limited interest phenomenologically since the associated decays are kinematically forbidden for most experimentally allowable MSSM parameter sets. (See, however, Refs. [198,208] concerning the $H_\ell \to H_p H_p$ which can be open when $m_{H_p} < m_{H_\ell}/2$, which is possible with radiative corrections to m_{H_ℓ}. For $m_{H_\ell} \lesssim M_{Z^0}/2$, $H_\ell \to H_p H_p$ can compete with and even dominate over $H_\ell \to b\bar{b}$ and $H_\ell \to \tau^+\tau^-$ [207 and erratum]. LEP experimenters there have now searched for $Z^0 \to H_\ell H_p \to H_p H_p H_p$ events without success [23,209]. The allowable region for this channel will be probed by LEP, and it should not be important for supercollider searches.)

With the convention of Eqn. (A.44), and using the same procedure as Eqns. (A.45)-(A.47), we find:

$$\begin{aligned} \frac{\partial^3 \mathcal{V}}{\partial H_h \partial H_\ell \partial H_\ell}\bigg|_{vev} = \Bigg[& -\cos^2\alpha \sin\alpha \frac{\partial^3 \mathcal{V}}{\partial {h_R}^3} + \cos\alpha(\cos^2\alpha - 2\sin^2\alpha) \frac{\partial^3 \mathcal{V}}{\partial {h_R}^2 \partial h'_R} \\ & + \sin\alpha(2\cos^2\alpha - \sin^2\alpha) \frac{\partial^3 \mathcal{V}}{\partial h_R \partial {h'_R}^2} + \cos\alpha \sin^2\alpha \frac{\partial^3 \mathcal{V}}{\partial {h'_R}^3} \Bigg]\Bigg|_{vev} \end{aligned} \tag{A.235}$$

For the tree-level potential of Eqn. (A.10), the following results are obtained:

$$\left.\frac{\partial^3\mathcal{V}}{\partial {h_R}^3}\right|_{vev} = \tfrac{3\sqrt{2}}{4}v(g^2+g'^2) \qquad \left.\frac{\partial^3\mathcal{V}}{\partial {h'_R}^3}\right|_{vev} = \tfrac{3\sqrt{2}}{4}v'(g^2+g'^2)$$
$$\left.\frac{\partial^3\mathcal{V}}{\partial {h_R}^2\partial h'_R}\right|_{vev} = \tfrac{-\sqrt{2}}{4}v'(g^2+g'^2) \qquad \left.\frac{\partial^3\mathcal{V}}{\partial h_R\partial {h'_R}^2}\right|_{vev} = \tfrac{-\sqrt{2}}{4}v(g^2+g'^2) \quad \text{(A.236)}$$

Plugging these equations into Eqns. (A.234) and (A.235) gives ($\tan\theta_W = \frac{g'}{g}$):

$$\xi^{tree}_{htt} = \frac{g m_{Z^0}}{4\cos\theta_W}\Big[\cos 2\alpha\,\cos(\beta-\alpha) + 2\sin 2\alpha\,\sin(\beta-\alpha)\Big] \quad . \qquad \text{(A.237)}$$

A.11 Scalar Higgs Trilinear Interaction Coupling with Radiative Corrections

From the quark sector, Eqn. (A.98) yields

$$\left.\frac{\partial^3(\Delta\mathcal{V}_{qk})}{\partial {h_R}^3}\right|_{vev} = \frac{-3}{32\pi^2}2\sqrt{2}f_t^3 m_t\Big[6\log(m_t^2) + 13\Big] \qquad \text{(A.238)}$$

$$\left.\frac{\partial^3(\Delta\mathcal{V}_{qk})}{\partial {h'_R}^3}\right|_{vev} = \frac{-3}{32\pi^2}2\sqrt{2}f_b^3 m_b\Big[6\log(m_b^2) + 13\Big] \qquad \text{(A.239)}$$

$$\left.\frac{\partial^3(\Delta\mathcal{V}_{qk})}{\partial {h_R}^2\partial h'_R}\right|_{vev} = \left.\frac{\partial^3(\Delta\mathcal{V}_{qk})}{\partial h_R\partial {h'_R}^2}\right|_{vev} = 0 \qquad \text{(A.240)}$$

For the squark sector, we need to find the third derivatives with respect to the scalar Higgs fields of Eqn. (A.122), and to find these we need calculate the third derivatives with respect to the scalar Higgs fields of the stop and sbottom eigenvalues. (These eigenvalues are given by Eqns. (A.116) and (A.117).)

$$\left.\frac{\partial^3\lambda_t}{\partial {h_R}^3}\right|_{vev} = \pm\Bigg\{\frac{3\sqrt{2}g_t^4 v}{64 D_t^{\frac{1}{2}}} - \frac{3\sqrt{2}v}{4D_t^{\frac{3}{2}}}\Big[f_t^2\Big(|A_t|^2 + 2m_1\Re e\{A_t\}\cot\beta\Big) - \tfrac{g_t^2}{8}[T0]\Big] \cdot\Big[f_t^2|A_t|^2 - \tfrac{g_t^2}{8}[T0] + \tfrac{g_t^4 v^2}{16}\Big] + \frac{3\sqrt{2}v^3}{4D_t^{\frac{5}{2}}}\Big[f_t^2\Big(|A_t|^2 + 2m_1\Re e\{A_t\}\cot\beta\Big) - \tfrac{g_t^2}{8}[T0]\Big]^3\Bigg\} \qquad \text{(A.241)}$$

$$\left.\frac{\partial^3\lambda_t}{\partial {h_R}^2\partial h'_R}\right|_{vev} = \pm\left\{\frac{-\sqrt{2}g_t^4v'}{64D_t^{\frac{1}{2}}} - \frac{\sqrt{2}v}{2D_t^{\frac{3}{2}}}\left[f_t^2\left(|A_t|^2+2m_1\Re e\{A_t\}\cot\beta\right) - \frac{g_t^2}{8}[T0]\right]\right.$$
$$\cdot\left[f_t^2(2m_1)\Re e\{A_t\} - \frac{g_t^2vv'}{16}\right]$$
$$-\frac{\sqrt{2}v'}{4D_t^{\frac{3}{2}}}\left[f_t^2\left((2m_1)^2+2m_1\Re e\{A_t\}\tan\beta\right) + \frac{g_t^2}{8}[T0]\right]$$
$$\cdot\left[f_t^2|A_t|^2 - \frac{g_t^2}{8}[T0] + \frac{g_t^4v^2}{16}\right]$$
$$+\frac{3\sqrt{2}v^2v'}{4D_t^{\frac{5}{2}}}\left[f_t^2\left(|A_t|^2+2m_1\Re e\{A_t\}\cot\beta\right) - \frac{g_t^2}{8}[T0]\right]^2$$
$$\left.\cdot\left[f_t^2\left((2m_1)^2+2m_1\Re e\{A_t\}\tan\beta\right) + \frac{g_t^2}{8}[T0]\right]\right\} \tag{A.242}$$

$$\left.\frac{\partial^3\lambda_t}{\partial h_R\partial {h'_R}^2}\right|_{vev} = \pm\left\{\frac{-\sqrt{2}g_t^4v}{64D_t^{\frac{1}{2}}} - \frac{\sqrt{2}v'}{2D_t^{\frac{3}{2}}}\left[f_t^2\left((2m_1)^2+2m_1\Re e\{A_t\}\tan\beta\right) + \frac{g_t^2}{8}[T0]\right]\right.$$
$$\cdot\left[f_t^2(2m_1)\Re e\{A_t\} - \frac{g_t^4vv'}{16}\right]$$
$$-\frac{\sqrt{2}v}{4D_t^{\frac{3}{2}}}\left[f_t^2\left(|A_t|^2+2m_1\Re e\{A_t\}\cot\beta\right) - \frac{g_t^2}{8}[T0]\right]$$
$$\cdot\left[f_t^2(2m_1)^2 + \frac{g_t^2}{8}[T0] + \frac{g_t^4v'^2}{16}\right]$$
$$+\frac{3\sqrt{2}vv'^2}{4D_t^{\frac{5}{2}}}\left[f_t^2\left(|A_t|^2+2m_1\Re e\{A_t\}\cot\beta\right) - \frac{g_t^2}{8}[T0]\right]$$
$$\left.\cdot\left[f_t^2\left((2m_1)^2+2m_1\Re e\{A_t\}\tan\beta\right) + \frac{g_t^2}{8}[T0]\right]^2\right\} \tag{A.243}$$

$$\left.\frac{\partial^3\lambda_t}{\partial {h'_R}^3}\right|_{vev} = \pm\left\{\frac{3\sqrt{2}g_t^4v'}{64D_t^{\frac{1}{2}}} - \frac{3\sqrt{2}v'}{4D_t^{\frac{3}{2}}}\left[f_t^2\left((2m_1)^2+2m_1\Re e\{A_t\}\tan\beta\right) + \frac{g_t^2}{8}[T0]\right]\right.$$
$$\cdot\left[f_t^2(2m_1)^2 + \frac{g_t^2}{8}[T0] + \frac{g_t^4v'^2}{16}\right]$$
$$\left.+\frac{3\sqrt{2}v'^3}{4D_t^{\frac{5}{2}}}\left[f_t^2\left((2m_1)^2+2m_1\Re e\{A_t\}\tan\beta\right) + \frac{g_t^2}{8}[T0]\right]^3\right\} \tag{A.244}$$

$\left.\frac{\partial^3\lambda_b}{\partial {h_R}^3}\right|_{vev}$ may be obtained from $\left.\frac{\partial^3\lambda_t}{\partial {h_R}^3}\right|_{vev}$ by applying the set of substitutions (A.126), with analogous procedures holding for the other derivatives of λ_b. As we've seen before, these formulæ are not valid for $D_t = 0$ or $D_b = 0$ which will again be treated later as special cases.

It will again be helpful in making the following equations more manageable in size if a few new quantities are defined:

$$[At1] \equiv 2m_1 \Re e\{A_t\} \cot\beta + |A_t|^2 \qquad [At2] \equiv 2m_1(2m_1 + \Re e\{A_t\} \tan\beta) \tag{A.245}$$

$$[Ab1] \equiv 2m_1 \Re e\{A_b\} \tan\beta + |A_b|^2 \qquad [Ab2] \equiv 2m_1(2m_1 + \Re e\{A_b\} \cot\beta) \tag{A.246}$$

Now, from Eqn. (A.122),

$$\left.\frac{\partial^3(\Delta\mathcal{V}_{sq})}{\partial {h_R}^3}\right|_{vev} = \frac{3}{32\pi^2}\sum_{i=1,2}\left\{2\left[3\frac{\partial\lambda_{t_i}}{\partial h_R}\frac{\partial^2\lambda_{t_i}}{\partial {h_R}^2} + \lambda_{t_i}\frac{\partial^3\lambda_{t_i}}{\partial {h_R}^3}\right]\log\lambda_{t_i} + \frac{2}{\lambda_{t_i}}\left(\frac{\partial\lambda_{t_i}}{\partial h_R}\right)^3 + 9\frac{\partial\lambda_{t_i}}{\partial h_R}\frac{\partial^2\lambda_{t_i}}{\partial {h_R}^2} + \lambda_{t_i}\frac{\partial^3\lambda_{t_i}}{\partial {h_R}^3} + (t_i \to b_i)\right\}\Bigg|_{vev} \tag{A.247}$$

$$\left.\frac{\partial^3(\Delta\mathcal{V}_{sq})}{\partial h'_R \partial {h_R}^2}\right|_{vev} = \frac{3}{32\pi^2}\sum_{i=1,2}\left\{2\left[\frac{\partial\lambda_{t_i}}{\partial h'_R}\frac{\partial^2\lambda_{t_i}}{\partial {h_R}^2} + \frac{\partial\lambda_{t_i}}{\partial h_R}\frac{\partial^2\lambda_{t_i}}{\partial h'_R \partial h_R} + \lambda_{t_i}\frac{\partial^3\lambda_{t_i}}{\partial h'_R \partial {h_R}^2}\right]\log\lambda_{t_i} + \frac{2}{\lambda_{t_i}}\frac{\partial\lambda_{t_i}}{\partial h'_R}\left(\frac{\partial\lambda_{t_i}}{\partial h_R}\right)^2 + 3\frac{\partial\lambda_{t_i}}{\partial h'_R}\frac{\partial^2\lambda_{t_i}}{\partial {h_R}^2} + 6\frac{\partial\lambda_{t_i}}{\partial h_R}\frac{\partial^2\lambda_{t_i}}{\partial h'_R \partial h_R} + \lambda_{t_i}\frac{\partial^3\lambda_{t_i}}{\partial h'_R \partial {h_R}^2} + (t_i \to b_i)\right\}\Bigg|_{vev} \tag{A.248}$$

Expressions for $\left.\frac{\partial^3(\Delta\mathcal{V}_{sq})}{\partial {h'_R}^3}\right|_{vev}$ and $\left.\frac{\partial^3(\Delta\mathcal{V}_{sq})}{\partial h_R \partial {h'_R}^2}\right|_{vev}$ may be obtained from those above for $\left.\frac{\partial^3(\Delta\mathcal{V}_{sq})}{\partial {h_R}^3}\right|_{vev}$ and $\left.\frac{\partial^3(\Delta\mathcal{V}_{sq})}{\partial h'_R \partial {h_R}^2}\right|_{vev}$ by interchanging the roles of h_R and h'_R.

The above formulæ yield:

$$\left.\frac{\partial^3(\Delta\mathcal{V}_{sq})}{\partial {h_R}^3}\right|_{vev} =$$

$$\frac{9\sqrt{2}v}{32\pi^2}\Bigg\{ \Big[2(f_t^2-\tfrac{g_+^2}{8})^2+\tfrac{g_t^4}{32}\Big]\Big[\log\Big(\frac{m^2_{\tilde{t}_1}m^2_{\tilde{t}_2}}{Q^4}\Big)+1\Big] + 4(f_t^2-\tfrac{g_+^2}{8})^2$$
$$+\frac{1}{D_t^{\frac{1}{2}}}\Big\{(f_t^2-\tfrac{g_+^2}{8})\Big[f_t^2([At1]+|A_t|^2)-\tfrac{g_t^2}{8}[T0]+\tfrac{v^2g_t^4}{16}\Big]+\tfrac{g_t^4}{64}\alpha_t$$
$$-\frac{1}{D_t}(f_t^2[At1]-\tfrac{g_t^2}{8}[T0])\Big[\frac{\alpha_t}{4}(f_t^2|A_t|^2-\tfrac{g_t^2}{8}[T0]+\tfrac{v^2g_t^4}{16})$$
$$+(f_t^2-\tfrac{g_+^2}{8})v^2(f_t^2[At1]-\tfrac{g_t^2}{8}[T0])\Big]$$
$$+\frac{v^2\alpha_t}{4D_t^2}(f_t^2[At1]-\tfrac{g_t^2}{8}[T0])^3\Big\}\log\Big(\frac{m^2_{\tilde{t}_2}}{m^2_{\tilde{t}_1}}\Big)$$
$$+\frac{1}{D_t}(f_t^2[At1]-\tfrac{g_t^2}{8}[T0])\Big[f_t^2|A_t|^2-\tfrac{g_t^2}{8}[T0]+\tfrac{v^2g_t^4}{16}-\frac{v^2}{D_t}(f_t^2[At1]-\tfrac{g_t^2}{8}[T0])^2\Big]$$
$$+\frac{16v^2}{\alpha_t^2-4D_t}\Big\{\alpha_t(f_t^2-\tfrac{g_+^2}{8})\Big[\frac{1}{3}(f_t^2-\tfrac{g_+^2}{8})^2+\frac{1}{4D_t}(f_t^2[At1]-\tfrac{g_t^2}{8}[T0])^2\Big]$$
$$-(f_t^2[At1]-\tfrac{g_t^2}{8}[T0])\Big[(f_t^2-\tfrac{g_+^2}{8})^2+\frac{1}{12D_t}(f_t^2[At1]-\tfrac{g_t^2}{8}[T0])^2\Big]\Big\}$$
$$+\tfrac{1}{32}(g_+^4+g_b^4)\Big[\log\Big(\frac{m^2_{\tilde{b}_1}m^2_{\tilde{b}_2}}{Q^4}\Big)+1\Big]+\tfrac{g_+^4}{16}$$
$$+\frac{1}{D_b^{\frac{1}{2}}}\Big\{\tfrac{g_+^2}{8}\Big[f_b^2([Ab2]+(2m_1)^2)+\tfrac{g_b^2}{4}[B0]+\tfrac{v^2g_b^4}{16}\Big]+\tfrac{g_b^4}{64}\alpha_b$$
$$-\frac{1}{D_b}(f_b^2[Ab2]+\tfrac{g_b^2}{8}[B0])\Big[\frac{\alpha_b}{4}(f_b^2(2m_1)^2+\tfrac{g_b^2}{8}[B0]+\tfrac{v^2g_b^4}{16})$$
$$+\tfrac{g_+^2}{8}v^2(f_b^2[Ab2]+\tfrac{g_b^2}{8}[B0])\Big]$$
$$+\frac{v^2\alpha_b}{4D_b^2}(f_b^2[Ab2]+\tfrac{g_b^2}{8}[B0])^3\Big\}\log\Big(\frac{m^2_{\tilde{b}_2}}{m^2_{\tilde{b}_1}}\Big)$$
$$+\frac{1}{D_b}(f_b^2[Ab2]+\tfrac{g_b^2}{8}[B0])\Big[f_b^2(2m_1)^2+\tfrac{g_b^2}{8}[B0]+\tfrac{v^2g_b^4}{16}$$
$$-\frac{v^2}{D_b}(f_b^2[Ab2]+\tfrac{g_b^2}{8}[B0])^2\Big]$$
$$+\frac{v^2}{\alpha_b^2-4D_b}\Big\{\tfrac{g_+^2}{4}\alpha_b\Big[\frac{1}{3}\tfrac{g_+^2}{24}+\frac{2}{D_b}(f_b^2[Ab2]+\tfrac{g_b^2}{8}[B0])^2\Big]$$
$$-(f_b^2[Ab2]+\tfrac{g_b^2}{8}[B0])\Big[\tfrac{g_+^4}{4}+\frac{4}{3D_b}(f_b^2[Ab2]+\tfrac{g_b^2}{8}[B0])^2\Big]\Big\}\Bigg\} \tag{A.249}$$

$$\left.\frac{\partial^3(\Delta\mathcal{V}_{sq})}{\partial h_R'\partial {h_R}^2}\right|_{vev} = \frac{3\sqrt{2}v'}{32\pi^2}\Big\{ \text{ stop part } + \text{ sbottom part } \Big\} \qquad \text{(A.250)}$$

$$\begin{aligned}
\text{stop part } = \; & \Big[\tfrac{g_+^2}{4}(f_t^2-\tfrac{g_+^2}{8}) - \tfrac{g_t^4}{32}\Big]\Big[\log\Big(\frac{m_{\tilde{t}_1}^2 m_{\tilde{t}_2}^2}{Q^4}\Big) + 1\Big] + \tfrac{g_+^2}{2}(f_t^2-\tfrac{g_+^2}{8}) \\
& + \frac{1}{D_t^{\frac{1}{2}}}\Big\{ f_t^2(f_t^2-\tfrac{g_+^2}{8})(2m_1)(2m_1+3\Re e\{A_t\}\tan\beta) - \tfrac{g_t^4}{64}(\alpha_t+8m_t^2) \\
& \quad + \tfrac{1}{8}f_t^2(g_+^2|A_t|^2+g_t^2[T0]) + \tfrac{g_+^2 g_t^2}{32}(\tfrac{3g_t^2v^2}{4}-[T0]) \\
& \quad - \frac{1}{D_t}\Big[v^2(f_t^2[At1]-\tfrac{g_t^2}{8}[T0])\Big[2(f_t^2-\tfrac{g_+^2}{8})(f_t^2[At2]+\tfrac{g_t^2}{8}[T0]) \\
& \qquad + \tfrac{g_+^2}{8}(f_t^2[At1]-\tfrac{g_t^2}{8}[T0])\Big] \\
& \quad + \frac{\alpha_t}{4}\Big[2(f_t^2[At1]-\tfrac{g_t^2}{8}[T0])(f_t^2(2m_1)\Re e\{A_t\}\tan\beta-\tfrac{g_t^4v^2}{16}) \\
& \qquad + (f_t^2[At2]+\tfrac{g_t^2}{8}[T0])(f_t^2|A_t|^2-\tfrac{g_t^2}{8}[T0]+\tfrac{g_t^4v^2}{16})\Big]\Big] \\
& \quad + \frac{3v^2\alpha_t}{4D_t^2}(f_t^2[At1]-\tfrac{g_t^2}{8}[T0])^2(f_t^2[At2]+\tfrac{g_t^2}{8}[T0])\Big\}\log\Big(\frac{m_{\tilde{t}_2}^2}{m_{\tilde{t}_1}^2}\Big) \\
& + \frac{1}{D_t}\Big[2(f_t^2[At1]-\tfrac{g_t^2}{8}[T0])(f_t^2(2m_1)\Re e\{A_t\}\tan\beta-\tfrac{g_t^4v^2}{16}) \\
& \qquad + (f_t^2[At2]+\tfrac{g_t^2}{8}[T0])(f_t^2|A_t|^2-\tfrac{g_t^2}{8}[T0]+\tfrac{g_t^4v^2}{16})\Big] \\
& - \frac{3v^2}{D_t^2}(f_t^2[At1]-\tfrac{g_t^2}{8}[T0])^2(f_t^2[At2]+\tfrac{g_t^2}{8}[T0]) \\
& + \frac{8v^2}{\alpha_t^2-4D_t}\Big\{\alpha_t\Big[\frac{1}{D_t}(f_t^2[At1]-\tfrac{g_t^2}{8}[T0])\Big[(f_t^2-\tfrac{g_+^2}{8})(f_t^2[At2]+\tfrac{g_t^2}{8}[T0]) \\
& \qquad + \tfrac{g_+^2}{16}(f_t^2[At1]-\tfrac{g_t^2}{8}[T0])\Big] \\
& \qquad + \tfrac{g_+^2}{4}(f_t^2-\tfrac{g_+^2}{8})^2\Big] \\
& \quad - (f_t^2-\tfrac{g_+^2}{8})\Big[2(f_t^2-\tfrac{g_+^2}{8})(f_t^2[At2]+\tfrac{g_t^2}{8}[T0]) \\
& \qquad + \tfrac{g_+^2}{2}(f_t^2[At1]-\tfrac{g_t^2}{8}[T0])\Big] \\
& \quad - \frac{1}{2D_t}(f_t^2[At1]-\tfrac{g_t^2}{8}[T0])^2(f_t^2[At2]+\tfrac{g_t^2}{8}[T0])\Big\}
\end{aligned}$$

(A.250a)

$$
\begin{aligned}
\text{sbottom} \\ \text{part} \quad = \quad & \Big[\tfrac{g_+^2}{4}(f_b^2-\tfrac{g_+^2}{8})-\tfrac{g_b^4}{32}\Big]\Big[\log\Big(\frac{m^2_{\tilde{b}_1}m^2_{\tilde{b}_2}}{Q^4}\Big)+1\Big]+\tfrac{g_+^2}{2}(f_b^2-\tfrac{g_+^2}{8}) \\
& +\frac{1}{D_b^{\frac{1}{2}}}\Big\{ f_b^4(2m_1)^2+\tfrac{1}{8}f_b^2g_+^2(|A_b|^2+3(2m_1)\Re e\{A_b\}\tan\beta-(2m_1)^2) \\
& \qquad +\tfrac{1}{8}f_b^2g_b^2[B0]-\tfrac{g_+^2g_B^2}{32}(\tfrac{3g_b^2v^2}{4}+[B0])-\tfrac{g_b^4}{64}(\alpha_b-4m_b^2\tan^2\beta) \\
& \qquad -\frac{1}{D_b}\Big[v^2(f_b^2[Ab2]+\tfrac{g_b^2}{8}[B0])\Big[(f_b^2-\tfrac{g_+^2}{8})(f_b^2[Ab2]+\tfrac{g_b^2}{8}[B0]) \\
& \qquad\qquad +\tfrac{g_+^2}{4}(f_b^2[Ab1]-\tfrac{g_b^2}{8}[B0])\Big] \\
& \qquad +\frac{\alpha_b}{4}\Big[2(f_b^2[Ab2]+\tfrac{g_b^2}{8}[B0])(f_b^2(2m_1)\Re e\{A_b\}\tan\beta-\tfrac{g_b^4v^2}{16}) \\
& \qquad\qquad +(f_b^2[Ab1]-\tfrac{g_b^2}{8}[B0])(f_b^2(2m_1)^2+\tfrac{g_b^2}{8}[B0+\tfrac{g_b^4v^2}{16})\Big]\Big] \\
& \qquad +\frac{3v^2\alpha_b}{4D_b^2}(f_b^2[Ab1]-\tfrac{g_b^2}{8}[B0])(f_b^2[Ab2]+\tfrac{g_b^2}{8}[B0])^2\Big\}\log\Big(\frac{m^2_{\tilde{b}_2}}{m^2_{\tilde{b}_1}}\Big) \\
& +\frac{1}{D_b}\Big[2(f_b^2[Ab2]+\tfrac{g_b^2}{8}[B0])(f_b^2(2m_1)\Re e\{A_b\}\tan\beta-\tfrac{g_b^4v^2}{16}) \\
& \qquad\qquad +(f_b^2[Ab1]-\tfrac{g_b^2}{8}[B0])(f_b^2(2m_1)^2+\tfrac{g_b^2}{8}[B0+\tfrac{g_b^4v^2}{16})\Big] \\
& -\frac{3v^2}{D_b^2}(f_b^2[Ab1]-\tfrac{g_b^2}{8}[B0])(f_b^2[Ab2]+\tfrac{g_b^2}{8}[B0])^2 \\
& +\frac{4v^2}{\alpha_b^2-4D_b}\Big\{\alpha_b\Big[\frac{1}{D_b}(f_b^2[Ab2]+\tfrac{g_b^2}{8}[B0])\Big[(f_b^2-\tfrac{g_+^2}{8})(f_b^2[Ab2]+\tfrac{g_b^2}{8}[B0]) \\
& \qquad\qquad +\tfrac{g_+^2}{4}(f_b^2[Ab1]-\tfrac{g_b^2}{8}[B0])\Big] \\
& \qquad +\tfrac{g_+^4}{16}(f_b^2-\tfrac{g_+^2}{8})\Big] \\
& \qquad -g_+^2(f_b^2-\tfrac{g_+^2}{8})(f_b^2[Ab2]+\tfrac{g_b^2}{8}[B0]) \\
& \qquad -\tfrac{g_+^4}{16}(f_b^2[Ab1]-\tfrac{g_b^2}{8}[B0]) \\
& \qquad -\frac{1}{D_b}(f_b^2[Ab1]-\tfrac{g_b^2}{8}[B0])(f_b^2[Ab2]+\tfrac{g_b^2}{8}[B0])^2\Big\}
\end{aligned}
\tag{A.250b}
$$

The expression for $\frac{\partial^3(\Delta\mathcal{V}_{sq})}{\partial h_R'^3}\Big|_{vev}$ is obtained from Eqn. (A.249) for $\frac{\partial^3(\Delta\mathcal{V}_{sq})}{\partial h_R^3}\Big|_{vev}$ by the set of substitutions (A.126). Likewise, the expression for $\frac{\partial^3(\Delta\mathcal{V}_{sq})}{\partial h_R \partial h_R'^2}\Big|_{vev}$ is obtained from Eqn. (A.250) for $\frac{\partial^3(\Delta\mathcal{V}_{sq})}{\partial h_R' \partial h_R^2}\Big|_{vev}$ via the same set of substitutions. (Note that (A.126) also means that $[At1] \leftrightarrow [Ab1]$ and $[At2] \leftrightarrow [Ab2]$.)

To obtain the correction to the trilinear coupling, $\Delta\xi_{h\ell\ell}$, where

$$\xi_{h\ell\ell} = \xi_{h\ell\ell}^{tree} + \Delta\xi_{h\ell\ell} \quad , \tag{A.251}$$

the results from the quark and squark sectors must now be combined. Eqn. (A.240) tells us that the corrections from the mixed derivative terms comes only from the squark sector. When Eqn. (A.238) and Eqn. (A.249) are combined we find that all remaining logarithmic terms which depend on the arbitary mass scale Q are proportional to the gauge couplings. This is exactly the same as the case for the Higgs boson masses (see Section A.8 on the neutral Higgs masses for further discussion.) The final expression for $\Delta\xi_{h\ell\ell}$ is:

$$\begin{aligned}\Delta\xi_{h\ell\ell} \;=\; -2\Bigg[&-\cos^2\alpha\sin\alpha\frac{\partial^3(\Delta\mathcal{V}_{qk}+\Delta\mathcal{V}_{sq})}{\partial h_R^3} + \cos\alpha(\cos^2\alpha-2\sin^2\alpha)\frac{\partial^3(\Delta\mathcal{V}_{sq})}{\partial h_R^2\partial h_R'} \\ &+ \sin\alpha(2\cos^2\alpha-\sin^2\alpha)\frac{\partial^3(\Delta\mathcal{V}_{sq})}{\partial h_R\partial h_R'^2} + \cos\alpha\sin^2\alpha\frac{\partial^3(\Delta\mathcal{V}_{qk}+\Delta\mathcal{V}_{sq})}{\partial h_R'^3}\Bigg]\Bigg|_{vev}\end{aligned} \tag{A.252}$$

$\frac{\partial^3(\Delta\mathcal{V}_{sq})}{\partial h_R'\partial h_R^2}\Big|_{vev}$ is given by Eqn. (A.250) on the preceeding two pages and $\frac{\partial^3(\Delta\mathcal{V}_{qk}+\Delta\mathcal{V}_{sq})}{\partial h_R^3}\Big|_{vev}$ is given by Eqn. (A.253) on the next page; $\frac{\partial^3(\Delta\mathcal{V}_{sq})}{\partial h_R\partial h_R'^2}\Big|_{vev}$ and $\frac{\partial^3(\Delta\mathcal{V}_{qk}+\Delta\mathcal{V}_{sq})}{\partial h_R'^3}\Big|_{vev}$ are obtained from these via the set of substitutions (A.126). The squark D-term dependence has been left explicit in Eqns. (A.253) and (A.250); thus, the result for $\Delta\xi_{h\ell\ell}$ neglecting D-terms is obtained by dropping terms proportional to g_t, g_b, or g_+ in Eqns. (A.253) and (A.250), then using (A.126) as indicated above to obtain the remaining derivative terms, and substituting the resulting expressions into Eqn. (A.252). Note that the scalar Higgs mixing angle α must also be calculated with D-terms neglected.

$$\left.\frac{\partial^3(\Delta\mathcal{V}_{qk}+\Delta\mathcal{V}_{sq})}{\partial {h_R}^3}\right|_{vev} =$$

$$\frac{9\sqrt{2}v}{32\pi^2}\Bigg\{\; 2f_t^4\log\Big(\frac{m^2_{\tilde{t}_1}m^2_{\tilde{t}_2}}{m_t^4}\Big) + \Big[-\tfrac{g_+^2}{2}f_t^2 + \tfrac{g_+^4+g_t^4}{32}\Big]\Big[\log\Big(\frac{m^2_{\tilde{t}_1}m^2_{\tilde{t}_2}}{Q^4}\Big) + 3\Big]$$

$$+\frac{1}{D_t^{\frac{1}{2}}}\Big\{(f_t^2-\tfrac{g_+^2}{8})\Big[f_t^2([At1]+|A_t|^2) - \tfrac{g_t^2}{4}[T0] + \tfrac{v^2g_t^4}{16}\Big] + \tfrac{g_t^4}{64}\alpha_t$$

$$-\frac{1}{D_t}(f_t^2[At1]-\tfrac{g_t^2}{8}[T0])\Big[\frac{\alpha_t}{4}(f_t^2|A_t|^2 - \tfrac{g_t^2}{8}[T0] + \tfrac{v^2g_t^4}{16})$$

$$+(f_t^2-\tfrac{g_+^2}{8})v^2(f_t^2[At1]-\tfrac{g_t^2}{8}[T0])\Big]$$

$$+\frac{v^2\alpha_t}{4D_t^2}(f_t^2[At1]-\tfrac{g_t^2}{8}[T0])^3\Big\}\log\Big(\frac{m^2_{\tilde{t}_2}}{m^2_{\tilde{t}_1}}\Big) - \tfrac{8}{3}f_t^4 - \tfrac{g_t^4}{16}$$

$$+\frac{1}{D_t}(f_t^2[At1]-\tfrac{g_t^2}{8}[T0])\Big[f_t^2|A_t|^2 - \tfrac{g_t^2}{8}[T0] + \tfrac{v^2g_t^4}{16} - \frac{v^2}{D_t}(f_t^2[At1]-\tfrac{g_t^2}{8}[T0])^2\Big]$$

$$+\frac{16v^2}{\alpha_t^2-4D_t}\Big\{\alpha_t(f_t^2-\tfrac{g_+^2}{8})\Big[\frac{1}{3}(f_t^2-\tfrac{g_+^2}{8})^2 + \frac{1}{4D_t}(f_t^2[At1]-\tfrac{g_t^2}{8}[T0])^2\Big]$$

$$-(f_t^2[At1]-\tfrac{g_t^2}{8}[T0])\Big[(f_t^2-\tfrac{g_+^2}{8})^2 + \frac{1}{12D_t}(f_t^2[At1]-\tfrac{g_t^2}{8}[T0])^2\Big]\Big\}$$

$$+\tfrac{1}{32}(g_+^4+g_b^4)\Big[\log\Big(\frac{m^2_{\tilde{b}_1}m^2_{\tilde{b}_2}}{Q^4}\Big) + 1\Big] + \tfrac{g_+^4}{16}$$

$$+\frac{1}{D_b^{\frac{1}{2}}}\Big\{\tfrac{g_+^2}{8}\Big[f_b^2([Ab2]+(2m_1)^2) + \tfrac{g_b^2}{4}[B0] + \tfrac{v^2g_b^4}{16}\Big] + \tfrac{g_b^4}{64}\alpha_b$$

$$-\frac{1}{D_b}(f_b^2[Ab2]+\tfrac{g_b^2}{8}[B0])\Big[\frac{\alpha_b}{4}(f_b^2(2m_1)^2 + \tfrac{g_b^2}{8}[B0] + \tfrac{v^2g_b^4}{16})$$

$$+\tfrac{g_+^2}{8}v^2(f_b^2[Ab2]+\tfrac{g_b^2}{8}[B0])\Big]$$

$$+\frac{v^2\alpha_b}{4D_b^2}(f_b^2[Ab2]+\tfrac{g_b^2}{8}[B0])^3\Big\}\log\Big(\frac{m^2_{\tilde{b}_2}}{m^2_{\tilde{b}_1}}\Big)$$

$$+\frac{1}{D_b}(f_b^2[Ab2]+\tfrac{g_b^2}{8}[B0])\Big[f_b^2(2m_1)^2 + \tfrac{g_b^2}{8}[B0] + \tfrac{v^2g_b^4}{16}$$

$$-\frac{v^2}{D_b}(f_b^2[Ab2]+\tfrac{g_b^2}{8}[B0])^2\Big]$$

$$+\frac{v^2}{\alpha_b^2-4D_b}\Big\{\tfrac{g_+^2}{8}\alpha_b\Big[\tfrac{g_+^4}{12} + \frac{4}{D_b}(f_b^2[Ab2]+\tfrac{g_b^2}{8}[B0])^2\Big]$$

$$-(f_b^2[Ab2]+\tfrac{g_b^2}{8}[B0])\Big[\tfrac{g_+^4}{4} + \frac{4}{3D_b}(f_b^2[Ab2]+\tfrac{g_b^2}{8}[B0])^2\Big]\Big\}\Bigg\} \tag{A.253}$$

Finally, the special cases where either $D_t = 0$ and/or $D_b = 0$ must be considered. If $D_t = 0$, then lines 2-9 of Eqn. (A.253) are replaced by

$$\frac{9\sqrt{2}v}{32\pi^2}\Bigg\{ 2f_t^4 \log\Big(\frac{\alpha_t^2}{4m_t^4}\Big) - \tfrac{8}{3}f_t^4 + \Big[-\tfrac{g_+^2}{2}f_t^2 + \tfrac{g_+^4+g_t^4}{32}\Big]\Big[\log\Big(\frac{\alpha_t^2}{4Q^4}\Big) + 3\Big] + \frac{4}{\alpha_t}(f_t^2 - \tfrac{g_+^2}{8})\Big[f_t^2(2m_1)^2\cot^2\beta + \tfrac{4}{3}(f_t^2 - \tfrac{g_+^2}{8})^2 v^2 + \tfrac{g_t^4 v^2}{16}\Big] \tag{A.254}$$

And Eqn. (A.250a) is replaced by

$$\begin{aligned} \text{stop part} \;=\; & \Big[\tfrac{g_+^2}{4}(f_t^2 - \tfrac{g_+^2}{8})^2 - \tfrac{g_t^4}{32}\Big]\Big[\log\Big(\frac{\alpha_t^2}{4Q^4}\Big) + 3\Big] \\ & + \frac{4f_t^2(2m_1)^2}{\alpha_t}\Big[-2f_t^2 + \tfrac{g_+^2}{8}(2+\cot^2\beta)\Big] \\ & + \frac{v^2}{2\alpha_t}\Big[4g_+^2(f_t^2 - \tfrac{g_+^2}{8})^2 - g_t^4(f_t^2 - \tfrac{3g_+^2}{16})\Big] \end{aligned} \tag{A.255}$$

If $D_b = 0$, then lines 10-18 of Eqn. (A.253) are replaced by

$$+ \tfrac{1}{32}(g_+^4 + g_b^4)\Big[\log\Big(\frac{\alpha_b^2}{4Q^4}\Big) + 3\Big] + \frac{g_+^2}{2\alpha_b}\Big[f_b^2(2m_1)^2 + \tfrac{v^2}{16}(\tfrac{g_+^4}{3} + g_b^4)\Big]\Bigg\} \tag{A.256}$$

And Eqn. (A.250b) is replaced by

$$\begin{aligned} \begin{matrix}\text{sbottom}\\ \text{part}\end{matrix} \;=\; & \Big[\tfrac{g_+^2}{4}(f_b^2 - \tfrac{g_+^2}{8})^2 - \tfrac{g_b^4}{32}\Big]\Big[\log\Big(\frac{\alpha_b^2}{4Q^4}\Big) + 3\Big] \\ & + \frac{4f_b^2(2m_1)^2}{\alpha_b}\Big[f_b^2 - \tfrac{g_+^2}{8}(1+2\tan^2\beta)\Big] \\ & + \frac{v^2}{4\alpha_b}\Big[f_b^2(g_+^4 + g_b^4) - \tfrac{g_+^2}{8}(g_+^4 + 3g_b^4)\Big] \end{aligned} \tag{A.257}$$

The set of substitutions (A.126) may now be used to obtain the bottom/sbottom part of $\frac{\partial^3(\Delta\mathcal{V}_{qk}+\Delta\mathcal{V}_{sq})}{\partial h_R'^3}\Big|_{vev}$ when $D_b = 0$ from the top/stop part of $\frac{\partial^3(\Delta\mathcal{V}_{qk}+\Delta\mathcal{V}_{sq})}{\partial h_R^3}\Big|_{vev}$ when $D_t = 0$ given by the expression (A.254) above. Likewise, the stop part of $\frac{\partial^3(\Delta\mathcal{V}_{qk}+\Delta\mathcal{V}_{sq})}{\partial h_R'^3}\Big|_{vev}$ when $D_t = 0$ is obtained from the sbottom part of $\frac{\partial^3(\Delta\mathcal{V}_{qk}+\Delta\mathcal{V}_{sq})}{\partial h_R^3}\Big|_{vev}$ when $D_b = 0$ as given by the expression (A.255) using (A.126). The sbottom part of $\frac{\partial^3(\Delta\mathcal{V}_{sq})}{\partial h_R \partial h_R'^2}\Big|_{vev}$ when $D_b = 0$ is found from the stop part of $\frac{\partial^3(\Delta\mathcal{V}_{sq})}{\partial h_R' \partial h_R^2}\Big|_{vev}$ when $D_t = 0$ as given by Eqn. (A.256) via (A.126); and the stop part of $\frac{\partial^3(\Delta\mathcal{V}_{sq})}{\partial h_R \partial h_R'^2}\Big|_{vev}$ when $D_t = 0$ is found from the sbottom part of $\frac{\partial^3(\Delta\mathcal{V}_{sq})}{\partial h_R' \partial h_R^2}\Big|_{vev}$ when $D_b = 0$ as given by Eqn. (A.257) via (A.126).

Appendix B

Partial Decay Widths for MSSM Higgs Bosons

B.1 Introduction

In this appendix formulæ for the partial widths of all tree-level MSSM Higgs boson decays will be given. The majority of these formulæ are taken directly from the hand-written notes of Professor Xerxes R. Tata (though the author of course assumes full responsibility for any errors in transcription); the formulæ have also been published previously in various places. Equations for several higher-order decay processes important for the analysis done are also presented. Most results will be presented without any derivation. The purpose of this appendix is to provide a complete set of the equations used in the Higgs boson decay program. In addition, it is desirable to have all the Higgs boson decay formulæ given in one place in a notation consistent with that in the ISASUSY [127] part of ISAJET [210], a software program extensively used for phenomenological SUSY analyses.

B.2 Higgs Boson Decays to SM Fermions

The partial decay widths of the light Higgs boson into a pair of quarks or leptons is given at tree-level by

$$\Gamma(H_\ell \to u\bar{u}) = \frac{g^2}{32\pi} N_c \frac{\cos^2\alpha}{\sin^2\beta} \left(\frac{m_u}{M_W}\right)^2 m_{H_\ell} \left(1 - \frac{4m_u^2}{m_{H_\ell}^2}\right)^{\frac{3}{2}} \quad , \tag{B.1}$$

with analogous formulæ holding for charm and top quark decays;

$$\Gamma(H_\ell \to d\bar{d}) = \frac{g^2}{32\pi} N_c \frac{\sin^2\alpha}{\cos^2\beta} \left(\frac{m_d}{M_W}\right)^2 m_{H_\ell} \left(1 - \frac{4m_d^2}{m_{H_\ell}^2}\right)^{\frac{3}{2}} \quad , \tag{B.2}$$

with analogous formulæ holding for strange and bottom quark decays;

$$\Gamma(H_\ell \to \ell^-\ell^+) = \frac{g^2}{32\pi} \frac{\sin^2\alpha}{\cos^2\beta} \left(\frac{m_\ell}{M_W}\right)^2 m_{H_\ell} \left(1 - \frac{4m_\ell^2}{m_{H_\ell}^2}\right)^{\frac{3}{2}} \quad , \tag{B.3}$$

where $\ell^- = e^-$, μ^-, or τ^-. If neutrinos are massless, then $\Gamma(H \to \nu\bar{\nu}) = 0$ for $H = H_\ell$, H_h, and H_p. In the above equations $N_c = 3$ is the number of colors and g is the SU(2) gauge coupling, $g = \frac{e}{\sin\theta_W}$. The scalar Higgs mixing angle, α, is defined in Section A.3 of Appendix A. All partial widths are of course set to 0 if $m_H < 2m_f$.

The partial decay widths of the heavy Higgs boson into a pair of quarks or leptons at tree-level then follow from changing the MSSM angle factors as indicted in Tabll 1.2 of Chapter 1:

$$\Gamma(H_h \to u\bar{u}) = \frac{g^2}{32\pi} N_c \frac{\sin^2\alpha}{\sin^2\beta} \left(\frac{m_u}{M_W}\right)^2 m_{H_h} \left(1 - \frac{4m_u^2}{m_{H_h}^2}\right)^{\frac{3}{2}} \quad , \tag{B.4}$$

$$\Gamma(H_h \to d\bar{d}) = \frac{g^2}{32\pi} N_c \frac{\cos^2\alpha}{\cos^2\beta} \left(\frac{m_d}{M_W}\right)^2 m_{H_h} \left(1 - \frac{4m_d^2}{m_{H_h}^2}\right)^{\frac{3}{2}} \quad , \tag{B.5}$$

$$\Gamma(H_h \to \ell^-\ell^+) = \frac{g^2}{32\pi} \frac{\cos^2\alpha}{\cos^2\beta} \left(\frac{m_\ell}{M_W}\right)^2 m_{H_h} \left(1 - \frac{4m_\ell^2}{m_{H_h}^2}\right)^{\frac{3}{2}} \quad . \tag{B.6}$$

The partial decay widths of the pseudoscalar Higgs boson into a pair of quarks or leptons at tree-level are:

$$\Gamma(H_p \to u\bar{u}) = \frac{g^2}{32\pi} N_c \cot^2\beta \left(\frac{m_u}{M_W}\right)^2 m_{H_p} \left(1 - \frac{4m_u^2}{m_{H_p}^2}\right)^{\frac{1}{2}} \quad , \tag{B.7}$$

$$\Gamma(H_p \to d\bar{d}) = \frac{g^2}{32\pi} N_c \tan^2\beta \left(\frac{m_d}{M_W}\right)^2 m_{H_p} \left(1 - \frac{4m_d^2}{m_{H_p}^2}\right)^{\frac{1}{2}} \quad , \tag{B.8}$$

$$\Gamma(H_h \to \ell^-\ell^+) = \frac{g^2}{32\pi} \tan^2\beta \left(\frac{m_\ell}{M_W}\right)^2 m_{H_p} \left(1 - \frac{4m_\ell^2}{m_{H_p}^2}\right)^{\frac{1}{2}} \quad . \tag{B.9}$$

The MSSM angle factor can again be found from Table 1.2 of Ch. 1; note the kinematic mass-dependent factor's exponent differs from that for the CP-even Higgs bosons.

The running of the Yukawa couplings that enter into the $H \to q\bar{q}$ decays are incorporated by redefining the quark masses (m_q's) contained in the $(\frac{m_q}{M_W})^2$-factor of Eqns. (B.1), (B.2), (B.4), (B.5), (B.7), and (B.8). The changes are of the following form:

If $m_H < 2m_b$, then

$$m_q^{run} = m_q \times \frac{\log\left(\frac{4m_f^2}{\Lambda^2_{QCD4}}\right)^{\frac{12}{33-2\cdot 4}}}{\log\left(\frac{m_H^2}{\Lambda^2_{QCD4}}\right)} \quad ; \qquad (B.10a)$$

if $2m_b \leq m_H < 2m_t$, then

$$m_q^{run} = m_q \times \frac{\log\left(\frac{4m_f^2}{\Lambda^2_{QCD4}}\right)^{\frac{12}{33-2\cdot 4}}}{\log\left(\frac{4m_b^2}{\Lambda^2_{QCD4}}\right)} \times \frac{\log\left(\frac{4m_b^2}{\Lambda^2_{QCD5}}\right)^{\frac{12}{33-2\cdot 5}}}{\log\left(\frac{m_H^2}{\Lambda^2_{QCD5}}\right)} \quad ; \qquad (B.10b)$$

and if $m_H \geq 2m_t$, then

$$\frac{\log\left(\frac{4m_f^2}{\Lambda^2_{QCD4}}\right)^{\frac{12}{33-2\cdot 4}}}{\log\left(\frac{4m_b^2}{\Lambda^2_{QCD4}}\right)} \times \frac{\log\left(\frac{4m_b^2}{\Lambda^2_{QCD5}}\right)^{\frac{12}{33-2\cdot 5}}}{\log\left(\frac{4m_t^2}{\Lambda^2_{QCD5}}\right)} \times \frac{\log\left(\frac{4m_t^2}{\Lambda^2_{QCD6}}\right)^{\frac{12}{33-2\cdot 6}}}{\log\left(\frac{m_H^2}{\Lambda^2_{QCD6}}\right)} \quad . \qquad (B.10c)$$

The corrected partial width is then of the form

$$\Gamma' = \Gamma_{tree} \times \left(\frac{m_q^{run}}{m_q}\right)^2 \quad . \qquad (B.11)$$

In the above equations, the four-flavor QCD scale parameter is set to

$$\Lambda_{QCD4} = 0.177\,\text{GeV} \quad , \qquad (B.12)$$

and

$$\Lambda_{QCD5} = \exp\left(\frac{25\log(\Lambda_{QCD4}) - \log(4m_b^2)}{23}\right) \quad ; \qquad (B.13)$$

$$\Lambda_{QCD6} = \exp\left(\frac{25\log(\Lambda_{QCD4}) - \log(4m_b^2) - \log(4m_t^2)}{21}\right) \quad . \qquad (B.14)$$

Note also that the numbers 4, 5, and 6 in the denominators of the exponents of Eqns. (B.10) are the effective number of flavors.

Additional $\mathcal{O}(\alpha_s)$ QCD radiative corrections are added through the following formulæ from Drees and Hikasa [211] (see Eqn. (4.5) therein):

$$\Gamma = \Gamma' \times \left[1 + \frac{C_F \alpha_s}{\pi}\left(\Delta_H + \tfrac{3}{2}\log\frac{m_H^2}{m_q^2}\right)\right] \quad . \tag{B.15}$$

Here $C_F = \frac{4}{3}$ is a color factor and for CP-even neutral Higgs bosons (H_ℓ and H_h)

$$\Delta_H = \frac{\mathcal{A}(\beta_0)}{\beta_0} + \frac{3}{8\beta_0^2}(-1+7\beta_0^2) + \frac{1}{16\beta_0^3}(3+34\beta_0^2-13\beta_0^4)\log\left(\frac{1+\beta_0}{1-\beta_0}\right), \tag{B.16}$$

while for the CP-odd pseudoscalar Higgs boson (H_p)

$$\Delta_H = \frac{\mathcal{A}(\beta_0)}{\beta_0} + \frac{3}{8}(7-\beta_0^2) + \frac{1}{16\beta_0}(19+2\beta_0^2+3\beta_0^4)\log\left(\frac{1+\beta_0}{1-\beta_0}\right) . \tag{B.17}$$

In the above
$$\beta_0 = \left[1 - \frac{4m_q^2}{m_H^2}\right]^{\frac{1}{2}} \quad , \tag{B.18}$$

and
$$\begin{aligned}\mathcal{A}(\beta_0) = (1+\beta_0^2)\Bigg\{ & 4\mathrm{Li}_2\left(\frac{1-\beta_0}{1+\beta_0}\right) + 2\mathrm{Li}_2\left(-\frac{1-\beta_0}{1+\beta_0}\right) \\ & - 3\log\left(\frac{1}{1+\beta_0}\right)\log\left(\frac{1+\beta_0}{1-\beta_0}\right) - 2\log\beta_0\log\left(\frac{1+\beta_0}{1-\beta_0}\right)\Bigg\} \\ & - 3\beta_0\log\left(\frac{4}{1-\beta_0^2}\right) - 4\beta_0\log\beta_0 \quad ,\end{aligned} \tag{B.19}$$

where $\mathrm{Li}_2(x)$ is the dilogarithm or Spence function of x,

$$\mathrm{Li}_2 = -\int_0^x \frac{dt}{t}\log|1-t| \quad . \tag{B.20}$$

In calculating the production rate of Higgs bosons from $b\bar{b}$-fusion (see Eqn. (3.2)), the partial decay width employed, $\Gamma'(H \to b\bar{b})$, does not include this additional factor. This makes Γ' roughly 10% smaller than the full Γ used in Higgs boson decays, as shown in Fig. B.1c) and Fig. B.1d) on the next page. Also, no QCD corrections at all are included for Higgs boson decays to first generation quarks, $H \to u\bar{u}$ and $H \to d\bar{d}$; for such small quark masses the formulæ will yield invalid results, and these partial widths are insignificant anyway. Inter-flavor mixing via the CKM matrix is also neglected in all Higgs boson decays to quarks.

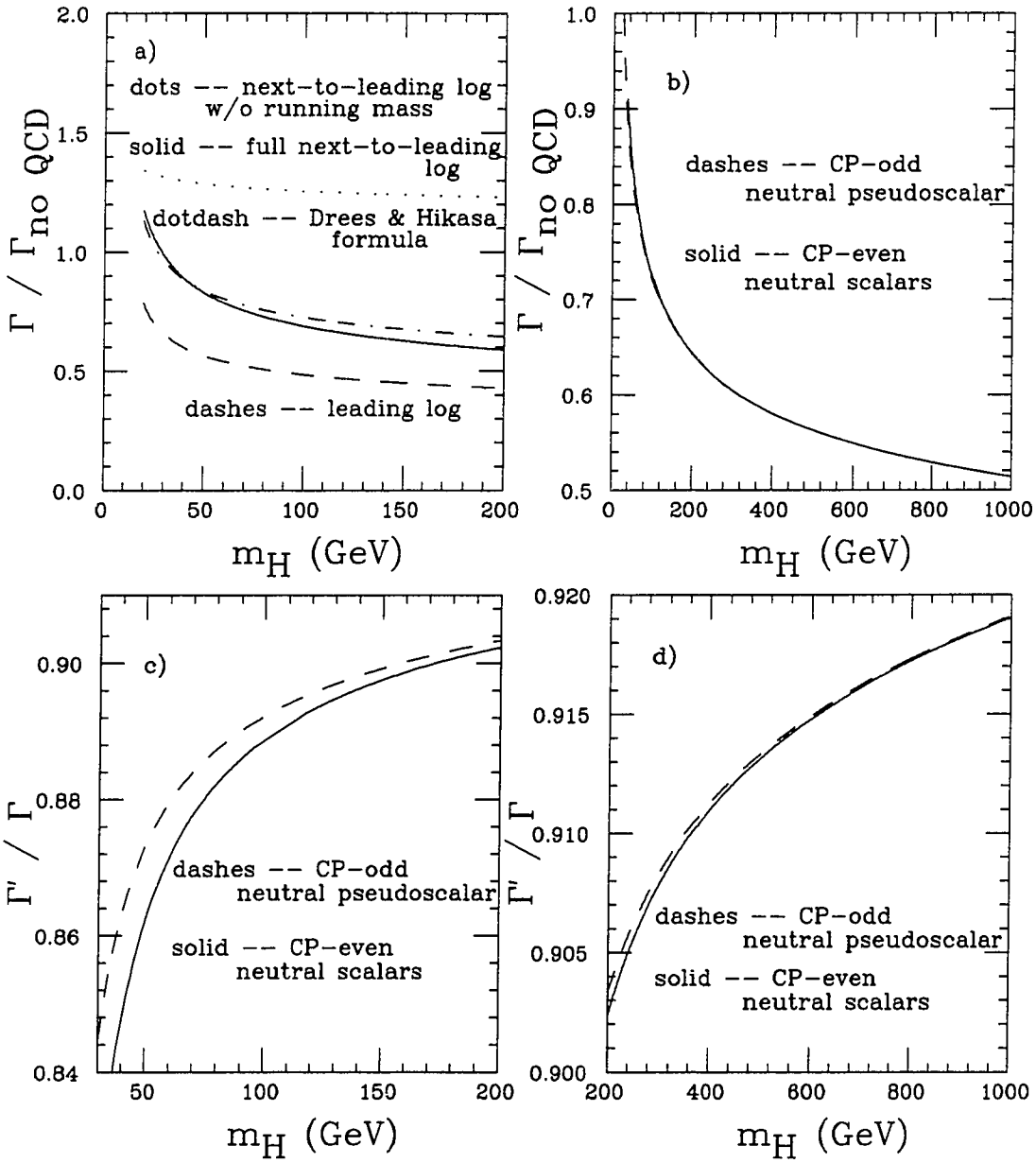

Figure B.1: QCD corrections to $\Gamma(H \to b\bar{b})$ a) comparison to Fig. 2.3 in HHG b) Γ / $\Gamma_{no\,QCD}$ c) and d) Γ' / Γ; $\Lambda_{QCD4} = 0.177$, $m_b = 5\,\mathrm{GeV}$, $m_t = 150\,\mathrm{GeV}$ in a) and $m_t = 165\,\mathrm{GeV}$ in b)-d) .

The question of how to treat the QCD corrections is important since these corrections do significantly reduce the $H \to b\bar{b}$ partial decay width, as is discussed in the *Higgs Hunter's Guide* (HHG) [64]. Figure B.1a above may be compared to Figure 2.3 in HHG. See also [212] for $\mathcal{O}(\alpha_s^2)$ corrections (not included in program).

The strong coupling constant used in the Higgs decay partial widths is determined from the following set of equations :

If $m_H < 2m_b$, then

$$\alpha_s = \frac{12\pi}{25\log\left(\frac{m_H^2}{\Lambda^2_{QCD4}}\right)} \quad ; \tag{B.21a}$$

if $2m_b \leq m_H < 2m_t$, then

$$\alpha_s = \frac{12\pi}{25\log\left(\frac{m_H^2}{\Lambda^2_{QCD4}}\right) - 2\log\left(\frac{m_H^2}{4m_b^2}\right)} \quad ; \tag{B.21b}$$

and if $m_H \geq 2m_t$, then

$$\alpha_s = \frac{12\pi}{25\log\left(\frac{m_H^2}{\Lambda^2_{QCD4}}\right) - 2\log\left(\frac{m_H^2}{4m_b^2}\right) - 2\log\left(\frac{m_H^2}{4m_t^2}\right)} \quad . \tag{B.21c}$$

On the other hand, a special value for the strong coupling constant at the Z^0 mass based on experimental results [213,214] is input in determining the neutralino and chargino masses (see Ch. 1):

$$\alpha_s(M_{Z^0}) = 0.118 \quad . \tag{B.22}$$

This is not consistent with the formulæ above; however, this should not seriously affect any of the results or conclusions. Another caveat that should be noted about the value in Eqn. (B.22) is that the renormalization scheme dependence may not have been taken into account correctly in the LEP analyses. Maxwell [215,216] argues that a more formalized treatment of this problem favors a lower value for $\alpha_s(M_{Z^0})$ of roughly 0.105 to 0.110 .

For the charged Higgs,

$$\begin{aligned}\Gamma(H^+ \rightarrow u\bar{d}) &= \Gamma(H^- \rightarrow d\bar{u}) \\ &= \frac{g^2}{32\pi} N_c \frac{(m_d^2 \tan^2\beta + m_u^2 \cot^2\beta)(m_{H_{ch}}^2 - m_u^2 - m_d^2) - 4m_u^2 m_d^2}{M_W^2\, m_{H_{ch}}} \\ &\quad \times \lambda^{\frac{1}{2}}\left(1, \frac{m_u^2}{m_{H_{ch}}^2}, \frac{m_d^2}{m_{H_{ch}}^2}\right) \quad ,\end{aligned} \tag{B.23}$$

where $\lambda(a,b,c) = a^2 + b^2 + c^2 - 2ab - 2bc - 2ac$ and $N_c = 3$. If $\lambda < 0$ in any equation, then the partial width is set to zero. Analogous equations hold for $\Gamma(H^+ \rightarrow \ell^+\nu_\ell)$, $\ell = e$, μ, or τ, except here $N_c = 1$.

For the heavier quarks (including s and c) QCD running masses [217] are employed using Eqns. (B.10), for instance,

$$\Gamma(H^+ \to t\bar{b}) = \frac{g^2}{32\pi} N_c \frac{((m_t^{run})^2 \tan^2\beta + (m_b^{run})^2 \cot^2\beta)(m_{H_{ch}}^2 - m_u^2 - m_d^2) - 4m_u^2 m_d^2}{M_W^2 m_{H_{ch}}} \times \lambda^{\frac{1}{2}}\left(1, \frac{m_u^2}{m_{H_{ch}}^2}, \frac{m_d^2}{m_{H_{ch}}^2}\right) \quad . \tag{B.24}$$

(See also [218] for electroweak corrections not included in program.)

B.3 Higgs Boson Tree-Level Decays to Gauge Bosons

The partial decay widths of the heavy Higgs boson into a pair of on mass-shell weak gauge bosons are given at tree-level by:

$$\Gamma(H_h \to Z^0 Z^0)_{on\ shell} = \frac{g^2 \cos^2(\alpha+\beta) M_W^2}{32\pi \cos^4\theta_w m_{H_h}} \left[3 - \frac{m_{H_h}^2}{M_{Z^0}^2} + \frac{m_{H_h}^4}{4M_{Z^0}^4}\right] \lambda^{\frac{1}{2}}\left(1, \frac{M_{Z^0}^2}{m_{H_h}^2}, \frac{M_{Z^0}^2}{m_{H_h}^2}\right) \tag{B.25}$$

$$\Gamma(H_h \to W^+ W^-)_{on\ shell} = \frac{g^2 \cos^2(\alpha+\beta) M_W^2}{16\pi m_{H_h}} \left[3 - \frac{m_{H_h}^2}{M_W^2} + \frac{m_{H_h}^4}{4M_W^4}\right] \lambda^{\frac{1}{2}}\left(1, \frac{M_W^2}{m_{H_h}^2}, \frac{M_W^2}{m_{H_h}^2}\right) \tag{B.26}$$

The light Higgs boson is not massive enought to decay into two on mass-shell weak gauge bosons and the pseudoscalar Higgs boson does not directly couple to gauge boson pairs. Again, this is as is summarized in Table 1.2 of Chapter 1. A coupling between the pseudoscalar Higgs and the gauge bosons can be generated a one-loop order; however, for the vast majority of the possible choices for the MSSM input parameters, the resulting partial decay width is quite small (see Chapter 4 and [65]), and can be neglected. Couplings between the neutral MSSM Higgs bosons and a pair of photons or gluons, which are absent at tree-level, are also generated through one-loop diagrams. This will be described in the next section.

If the mass of the Higgs boson is in the vicinity of $2M_{Z^0}$ or $2M_W$, then decays into one on mass-shell gauge boson and one off mass-shell gauge boson can become significant. An expression for this is found in Keung and Marciano [66],

for $m_{H_h} \geq M_{Z^0}$ we have

$$\Gamma(H_h \to Z^0 Z^{0*}) = \frac{g^4 \cos^2(\alpha+\beta) m_{H_h}}{2048\pi^3 \cos^4\theta_w}(7 - \tfrac{40}{3}\sin^2\theta_w + \tfrac{160}{9}\sin^4\theta_w) \times \int_{2\epsilon}^{1+\epsilon^2} \frac{x^2 - 12x\epsilon^2 + 8\epsilon^2 + 12\epsilon^4}{(1-x)^2 + \left(\frac{\epsilon\Gamma_{Z^0}}{m_{H_h}}\right)^2}(x^2 - 4\epsilon^2)^{\frac{1}{2}}\, dx\,, \quad \text{(B.27)}$$

where $\epsilon = \frac{M_{Z^0}}{m_{H_h}}$, and Γ_{Z^0} is the experimentally-determined total width of the Z^0 (see Ch. 2). An analgous formula holds for the partial decay width of a light Higgs boson into one on mass-shell Z^0 and one off mass-shell Z^0. This decay is now possible since radiative corrections can push the light Higgs boson mass above M_{Z^0}. The expression for $\Gamma(H_\ell \to Z^0 Z^{0*})$ (if $m_{H_\ell} \geq M_{Z^0}$) is the same as Eqn. (B.27) above except that

$$\left(m_{H_h},\, \cos^2(\alpha+\beta)\right) \longrightarrow \left(m_{H_\ell},\, \sin^2(\alpha+\beta)\right) \quad . \quad \text{(B.28)}$$

If $m_{h_h} \geq 2M_{Z^0}$, then to avoid double counting the on mass-shell result should be subtracted off,

$$\Gamma(H_h \to Z^0 Z^{0*}, Z^0 Z^0) = \Gamma(H_h \to Z^0 Z^{0*}) - \Gamma(H_h \to Z^0 Z^0)_{on\ shell} \quad . \text{(B.29)}$$

Similarly, for $m_{H_h} \geq M_W$ we have

$$\Gamma(H_h \to W^+W^{-*}, W^{+*}W^-) = \frac{3g^4\cos^2(\alpha+\beta)m_{H_h}}{512\pi^3} \times \int_{2\epsilon}^{1+\epsilon^2} \frac{x^2 - 12x\epsilon^2 + 8\epsilon^2 + 12\epsilon^4}{(1-x)^2 + \left(\frac{\epsilon\Gamma_W}{m_{H_h}}\right)^2}(x^2 - 4\epsilon^2)^{\frac{1}{2}}\, dx\,, \quad \text{(B.30)}$$

where now $\epsilon = \frac{M_W}{m_{H_h}}$, and Γ_W is the experimentally-determined total width of the W^+ (taken to be 2.076 GeV from the latest Tevatron value [219]). Again, the expression for $\Gamma(H_\ell \to W^+W^{-*}, W^{+*}W^-)$ (if $m_{H_\ell} \geq M_W$) is found from Eqn. (B.30) above via the set of substitutions (B.28), and again if $m_{H_h} \geq 2M_W$, then the on mass shell result must be subtracted from Eqn. (B.30) as was done in Eqn. (B.29).

It should be noted that the integral is highly peaked about $x = 1$ and so for the decays to W's (which are of particular interest since decays of the H_ℓ to W^+W^{-*} can significantly reduce the sought-after $H_\ell \to \gamma\gamma$ decay mode) the integral was

split up into up to three regions:
if $2\epsilon < 0.998$ and $1+\epsilon^2 > 1.001$, then from 2ϵ to 0.998, from 0.998 to 1.001, and from 1.001 to $1+\epsilon^2$;
if $2\epsilon < 0.998$ and $1+\epsilon^2 \leq 1.001$, then from 2ϵ to 0.998, and from 0.998 to $1+\epsilon^2$;
if $2\epsilon \geq 0.998$ and $1+\epsilon^2 > 1.001$, then from 2ϵ to 1.001, and from 1.001 to $1+\epsilon^2$;
and if $2\epsilon \geq 0.998$, $1+\epsilon^2 \leq 1.001$, or $2\epsilon \geq 1.001$, $1+\epsilon^2 > 1.001$, then just from 2ϵ to $1+\epsilon^2$.

Integrations are done using a Gaussian integration routine using 6, 12, 24, or 48 points (result from using a given number of points is tested against that using the the next smaller number of points until sufficient agreement is obtained).

B.4 Higgs Boson Loop Decays to Gauge Bosons

The $H \rightarrow g\,g$ partial decay widths are given by the formula

$$\Gamma(H \rightarrow gg) = \frac{\alpha_s(m_H)^2 g^2 m_H^3}{32\pi^3 M_W^2}\left|\sum_i \mathcal{I}_H^i\right|^2 \quad , \tag{B.31}$$

where the label i runs over the various loops contributing to the width and $\alpha_s(m_H)$ is given by Eqns. (B.21). For the light and heavy Higgs bosons this includes up-type and down-type squark loops in addition to up-type and down-type quark loops (as shown in Figure 3.1). For the pseudoscalar Higgs, squark loops do not contribute. If intraflavor squark mixing is neglected, this can easily be seen from the fact that the H_p-$\widetilde{q_L}$-$\widetilde{q_R}$ coupling of the pseudoscalar Higgs boson does not allow for three-vertex squark loops like that shown in Fig. 3.1b). It is also relatively easy to demonstrate that such three-vertex squark loops are still impossible even with intraflavor squark mixing.

The $\mathcal{I}_H^i$ factors are given by:

$$\mathcal{I}_H^q = R_q^H F_{1/2}^H(\tau_q) \qquad \text{(for quarks)} \tag{B.32a}$$

$$\mathcal{I}_H^{\tilde{q}} = R_{\tilde{q}}^H F_0^H(\tau_{\tilde{q}}) \frac{M_W^2}{8m_{\tilde{q}}^2} \qquad \text{(for squarks)} \tag{B.32b}$$

The squark loop contributions are seen to be suppressed if the squark mass is large. The quark loop angle factors are given by:

$$R^H_{u,c,t} = \begin{cases} \frac{\cos\alpha}{\sin\beta} & \text{for } H = H_\ell \\ -\frac{\sin\alpha}{\sin\beta} & H_h \\ \cot\beta & H_p \end{cases} \qquad R^H_{d,s,b} = \begin{cases} \frac{\sin\alpha}{\cos\beta} & \text{for } H = H_\ell \\ \frac{\cos\alpha}{\cos\beta} & H_h \\ \tan\beta & H_p \end{cases} \tag{B.33}$$

For the squark loops the angle factors are given by (recall $m_{\tilde{q}_1} \leq m_{\tilde{q}_2}$):

$$\begin{aligned} R^H_{\tilde{q}_1} &= R^H_{\tilde{q}_L}\cos\theta_{\tilde{q}} \; - \; R^H_{\tilde{q}_R}\sin\theta_{\tilde{q}} \\ R^H_{\tilde{q}_2} &= R^H_{\tilde{q}_L}\sin\theta_{\tilde{q}} \; + \; R^H_{\tilde{q}_R}\cos\theta_{\tilde{q}} \end{aligned} \tag{B.34}$$

Here $\theta_{\tilde{q}}$ is the intra-flavor squark mixing angle which will be described more thoroughly in the next section on Higgs boson to sfermion decays, and $R^H_{\tilde{q}_L}$ and $R^H_{\tilde{q}_L}$ are the angle factors for the supersymmetric partners of the left- and right-handed quark states, respectively, which in turn are given by

$$R^H_{\tilde{u}_L,\tilde{c}_L,\tilde{t}_L} = \begin{cases} (1-\frac{1}{3}\tan^2\theta_w)\sin(\beta-\alpha) \; - \; \frac{2m_q^2}{M_W^2}(\frac{\cos\alpha}{\sin\beta}) & \text{for } H = H_\ell \\ -(1-\frac{1}{3}\tan^2\theta_w)\cos(\beta-\alpha) \; - \; \frac{2m_q^2}{M_W^2}(\frac{-\sin\alpha}{\sin\beta}) & H_h \\ 0 & H_p \end{cases} \tag{B.35a}$$

$$R^H_{\tilde{d}_L,\tilde{s}_L,\tilde{b}_L} = \begin{cases} (-1-\frac{1}{3}\tan^2\theta_w)\sin(\beta-\alpha) \; - \; \frac{2m_q^2}{M_W^2}(\frac{\sin\alpha}{\cos\beta}) & \text{for } H = H_\ell \\ -(-1-\frac{1}{3}\tan^2\theta_w)\cos(\beta-\alpha) \; - \; \frac{2m_q^2}{M_W^2}(\frac{\cos\alpha}{\cos\beta}) & H_h \\ 0 & H_p \end{cases} \tag{B.35b}$$

$$R^H_{\tilde{u}_R,\tilde{c}_R,\tilde{t}_R} = \begin{cases} \frac{4}{3}\tan^2\theta_w\sin(\beta-\alpha) \; - \; \frac{2m_q^2}{M_W^2}(\frac{\cos\alpha}{\sin\beta}) & \text{for } H = H_\ell \\ -\frac{4}{3}\tan^2\theta_w\cos(\beta-\alpha) \; - \; \frac{2m_q^2}{M_W^2}(\frac{-\sin\alpha}{\sin\beta}) & H_h \\ 0 & H_p \end{cases} \tag{B.35c}$$

$$R^H_{\tilde{d}_R,\tilde{s}_R,\tilde{b}_R} = \begin{cases} -\frac{2}{3}\tan^2\theta_w\sin(\beta-\alpha) \; - \; \frac{2m_q^2}{M_W^2}(\frac{\sin\alpha}{\cos\beta}) & \text{for } H = H_\ell \\ \frac{2}{3}\tan^2\theta_w\cos(\beta-\alpha) \; - \; \frac{2m_q^2}{M_W^2}(\frac{\cos\alpha}{\cos\beta}) & H_h \\ 0 & H_p \end{cases} \tag{B.35d}$$

Note that the last bracketed quantity on each line is just the corresponding R^H_q from Eqns. (B.33).

The F functions are given by

$$F_{\frac{1}{2}}^{H}(\tau) = \tfrac{1}{2}\tau\Big[\eta_H \; + \; (1-\tau\eta_H)f(\tau)\Big] \tag{B.36a}$$

$$F_{0}^{H}(\tau) = \tau\Big(1-\tau f(\tau)\Big) \tag{B.36b}$$

$$\text{with } \eta_H = \begin{cases} 1 & \text{for } H = H_\ell \\ 1 & H_h \\ 0 & H_p \end{cases} \tag{B.37}$$

$$\text{and } f(\tau) = \begin{cases} \Big[\sin^{-1}\Big(\sqrt{1/\tau}\Big)\Big]^2 & \text{for } \tau \geq 1 \\ -\frac{1}{4}\Big[\log\frac{1+\sqrt{1-\tau}}{1-\sqrt{1-\tau}} \; - \; i\pi\Big]^2 & \text{for } \tau < 1 \end{cases} \tag{B.38}$$

$$\text{where} \quad \tau_i = \frac{4m_i^2}{m_H^2} \tag{B.39}$$

(Note: Refs. [50,90] use the variable λ rather than τ as used here and in Ref. [64] where $\tau = 4\lambda$, and $f(\lambda)$ of Ref. [50] is $-2 \times f(\tau)$ as written here.)

The $H \to \gamma\gamma$ partial decay widths are computed in a manner similar to that used to obtain the $H \to gg$ formulæ, except now there are more loop contributions that must be taken into account. In addition to quark and squark loops, there are also lepton, slepton, W-boson, charged Higgs, and chargino loops as illustrated in Fig. B.2 below.

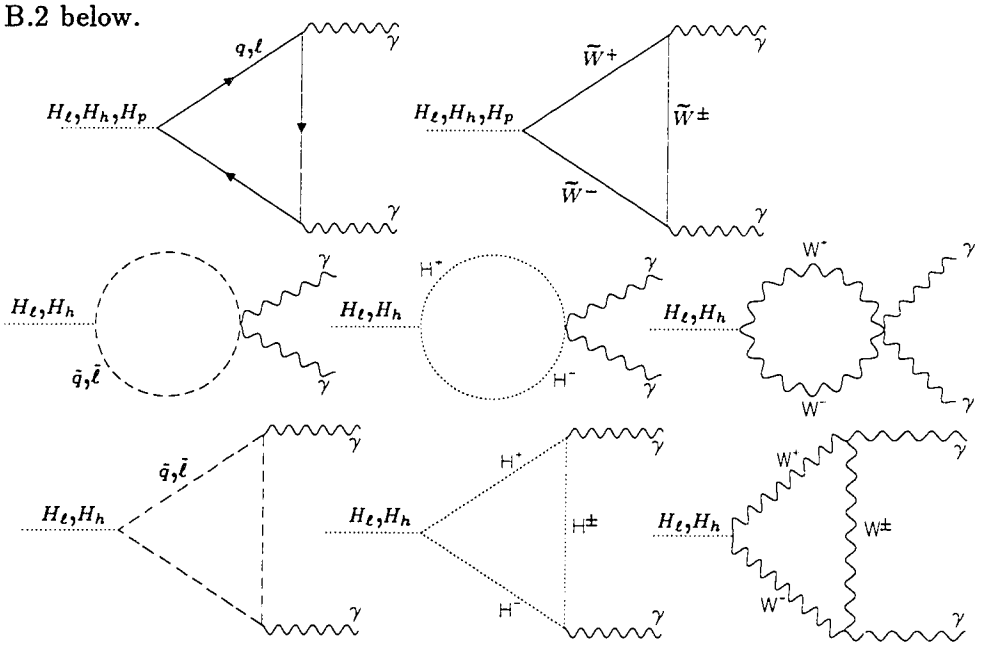

Figure B.2: One-loop Feynman diagrams contributing to $H \to \gamma\gamma$ decays.

The $H \to \gamma\gamma$ partial decay widths are given by the formula [50,64,90]

$$\Gamma(H \to \gamma\gamma) = \frac{\alpha_{em}^2 g^2 m_H^3}{1024\pi^3 M_W^2}\left|\sum_i \mathcal{I}_H^i\right|^2 \quad , \tag{B.40}$$

where $\alpha_{em} = 1/128$. The $\mathcal{I}_H^i$ factors are given by:

$$\mathcal{I}_H^f = N_c e_f^2 R_f^H F_{1/2}^H(\tau_f) \qquad \text{(for quarks and leptons)} \tag{B.41a}$$

$$\mathcal{I}_H^{\tilde{f}} = N_c e_f^2 R_{\tilde{f}}^H F_0^H(\tau_{\tilde{f}}) \frac{M_{Z^0}^2}{8m_{\tilde{f}}^2} \qquad \text{(for squarks and sleptons)} \tag{B.41b}$$

$$\mathcal{I}_H^W = R_W^H F_1^H(\tau_W) \qquad \text{(for the } W\text{-bosons)} \tag{B.41c}$$

$$\mathcal{I}_H^{H_{ch}} = R_{H_{ch}}^H F_0^H(\tau_{H_{ch}}) \frac{M_W^2}{m_{H_{ch}}^2} \qquad \text{(for the charged Higgs bosons)} \tag{B.41d}$$

$$\mathcal{I}_H^{\widetilde{W}} = R_{\widetilde{W}}^H F_{1/2}^H(\tau_{\widetilde{W}}) \frac{M_W}{m_{\widetilde{W}}} \qquad \text{(for charginos)} \tag{B.41e}$$

(Note that the squark and slepton formula is misprinted in Appendix C Eqn. (C.4) of HHG[64] – first edition.) Here $N_c = 3$ for quarks and squarks and $N_c = 1$ for leptons and sleptons; and e_f is the fermion electric charge in units of the absolute value of the electric charge of the electron. The quark loop angle factors are again given by Eqns. (B.33), and the electron, muon, and tau-lepton loops have the same angle factors as the down-type quarks. Since the loop contribution is proportional to the electric charge of the fermion or sfermion in the loop, there is no contribution from neutrinos or sneutrinos. The sfermion loop contributions are again suppressed if the sfermion mass is large. For the squark and slepton loops the angle factors are analogous to those of Eqns. (B.34) — an intra-flavor slepton mixing angle, $\theta_{\tilde{l}}$ can be defined in an analogous way to θ_q (again recall $m_{\tilde{f}_1} \leq m_{\tilde{f}_2}$):

$$\begin{aligned} R_{\tilde{f}_1}^H &= R_{\tilde{f}_L}^H \cos\theta_{\tilde{f}} \; - \; R_{\tilde{f}_R}^H \sin\theta_{\tilde{f}} \\ R_{\tilde{f}_2}^H &= R_{\tilde{f}_L}^H \sin\theta_{\tilde{f}} \; + \; R_{\tilde{f}_R}^H \cos\theta_{\tilde{f}} \end{aligned} \tag{B.42}$$

The supersymmetric partners of the left- and right-handed quarks and leptons have angle factors which may be written as:

$$R^H_{\tilde{u}_L,\tilde{c}_L,\tilde{t}_L} = \begin{cases} -(\frac{1}{2} - e_f \sin^2\theta_w)\sin(\beta-\alpha) + \frac{m_q^2}{M_{Z^0}^2}(\frac{\cos\alpha}{\sin\beta}) & \text{for } H = H_\ell \\ -(-\frac{1}{2} - e_f \sin^2\theta_w)\cos(\beta-\alpha) - \frac{m_q^2}{M_{Z^0}^2}(\frac{-\sin\alpha}{\sin\beta}) & H_h \\ 0 & H_p \end{cases} \quad \text{(B.43)}$$

$$R^H_{\substack{\tilde{d}_L,\tilde{s}_L,\tilde{b}_L,\\ \tilde{e}_L,\tilde{\mu}_L,\tilde{\tau}_L}} = \begin{cases} -(-\frac{1}{2} - e_f \sin^2\theta_w)\sin(\beta-\alpha) + \frac{m_l^2}{M_{Z^0}^2}(\frac{\sin\alpha}{\cos\beta}) & \text{for } H = H_\ell \\ -(-\frac{1}{2} - e_f \sin^2\theta_w)\cos(\beta-\alpha) + \frac{m_l^2}{M_{Z^0}^2}(\frac{\cos\alpha}{\cos\beta}) & H_h \\ 0 & H_p \end{cases} \quad \text{(B.44)}$$

$$R^H_{\tilde{u}_R,\tilde{c}_R,\tilde{t}_R} = \begin{cases} -e_f \sin^2\theta_w \sin(\beta-\alpha) + \frac{m_q^2}{M_{Z^0}^2}(\frac{\cos\alpha}{\sin\beta}) & \text{for } H = H_\ell \\ -e_f \sin^2\theta_w \cos(\beta-\alpha) + \frac{m_q^2}{M_{Z^0}^2}(\frac{-\sin\alpha}{\sin\beta}) & H_h \\ 0 & H_p \end{cases} \quad \text{(B.45)}$$

$$R^H_{\substack{\tilde{d}_R,\tilde{s}_R,\tilde{b}_R,\\ \tilde{e}_R,\tilde{\mu}_R,\tilde{\tau}_R}} = \begin{cases} -e_f \sin^2\theta_w \sin(\beta-\alpha) + \frac{m_l^2}{M_{Z^0}^2}(\frac{\sin\alpha}{\cos\beta}) & \text{for } H = H_\ell \\ -e_f \sin^2\theta_w \cos(\beta-\alpha) + \frac{m_l^2}{M_{Z^0}^2}(\frac{\cos\alpha}{\cos\beta}) & H_h \\ 0 & H_p \end{cases} \quad \text{(B.46)}$$

The angle factors for the W-boson loops are given by:

$$R^H_W = \begin{cases} \sin(\alpha+\beta) & \text{for } H = H_\ell \\ \cos(\alpha+\beta) & H_h \\ 0 & H_p \end{cases} \quad \text{(B.47)}$$

The angle factors for the charged Higgs boson loops are given by:

$$R^H_{H_{ch}} = \begin{cases} \sin(\alpha+\beta) + \frac{\sin(\beta-\alpha)\cos 2\beta}{2\cos^2\theta_w} & \text{for } H = H_\ell \\ \cos(\alpha+\beta) - \frac{\cos(\beta-\alpha)\cos 2\beta}{2\cos^2\theta_w} & H_h \\ 0 & H_p \end{cases} \quad \text{(B.48)}$$

And lastly, for the charginos, the angle factors are (recall $m_{\widetilde{W}_1} \leq m_{\widetilde{W}_2}$):

$$R^H_{\widetilde{W}_i} = \begin{cases} 2\left[S_{ii}\cos\alpha + Q_{ii}\sin\alpha\right] & \text{for } H = H_\ell \\ 2\left[S_{ii}\sin\alpha + Q_{ii}\cos\alpha\right] & H_h \\ 2\left[-S_{ii}\cos\beta - Q_{ii}\sin\beta\right] & H_p \end{cases} , \quad \text{(B.49)}$$

with S_{ij} and Q_{ij} defined in terms of the matrices U and V needed to diagonalize the chargino mass matrix

$$S_{ij} = \sqrt{\tfrac{1}{2}} U_{i1} V_{j2} \ , \qquad Q_{ij} = \sqrt{\tfrac{1}{2}} U_{i2} V_{j1} \ . \tag{B.50}$$

These matrix elements are in turn given by

$$\begin{aligned} U_{11} &= \sin\gamma_L \qquad & U_{12} &= -\cos\gamma_L \\ U_{21} &= \theta_x \cos\gamma_L \qquad & U_{22} &= \theta_x \sin\gamma_L \end{aligned} \tag{B.51}$$

$$\begin{aligned} \text{and} \quad U_{11} &= (-1)^{\theta_m} \sin\gamma_R \qquad & U_{12} &= -(-1)^{\theta_m} \cos\gamma_R \\ U_{21} &= (-1)^{\theta_p} \theta_y \cos\gamma_R \qquad & U_{22} &= (-1)^{\theta_p} \theta_y \sin\gamma_R \quad , \end{aligned} \tag{B.52}$$

where the angles γ_L and γ_R and the quantities θ_x, θ_y, θ_m, and θ_p are defined in the section of this appendix dealing with Higgs boson decays to pairs of charginos.

The F functions are given by

$$F_0^H(\tau) = \tau\Big(1 - \tau f(\tau)\Big) \tag{B.53a}$$

$$F_{\frac{1}{2}}^H(\tau) = -2\tau\Big[\eta_H \ + \ (1 - \tau\eta_H) f(\tau)\Big] \tag{B.53b}$$

$$F_1^H(\tau) = 2 + 3\tau + 3\tau(2 - \tau) f(\tau) \tag{B.53c}$$

where η_H, $f(\tau)$, and τ are given by Eqn. (B.37), Eqn. (B.38), and Eqn. (B.39), respectively.

The $H \to Z^0\gamma$ partial decay widths are generally comparable to or smaller than the $H \to \gamma\gamma$ partial decay widths. Then the Z^0 must decay leptonically to offer any good chance of detection; since the percentage of the time Z^0 decays into e^+e^- or $\mu^+\mu^-$ is only about 6-7%, this makes the $Z^0\gamma$ decay channel less useful than the $\gamma\gamma$ decay channel. Since the $H \to Z^0\gamma$ decays also give only a negligible contribution to the total decay widths of the Higgs bosons, it is acceptable to simply neglect these decays completely.

B.5 Higgs Boson Decays to Sfermions

The partial decay widths of the neutral Higgs bosons into a pair of squarks or sleptons are given by

$$\Gamma\Big(H \to \tilde{f}_i \bar{\tilde{f}}_j\Big) = \frac{|\mathcal{A}_{\tilde{f}_i \bar{\tilde{f}}_j}|^2}{16\pi m_{H_h}} N_c \, \lambda^{\frac{1}{2}}\left(1, \frac{m^2_{\tilde{f}_i}}{m^2_{H_h}}, \frac{m^2_{\tilde{f}_j}}{m^2_H}\right) \tag{B.54}$$

(assuming $m_H \geq m_{\tilde{f}_i} + m_{\tilde{f}_j}$, else set decay width equal to 0) where $i, j = 1, 2$; $N_c = 3$ for squarks and $N_c = 1$ for sleptons; and

$$\mathcal{A}_{\tilde{f}_1 \bar{\tilde{f}}_1} = \mathcal{A}_{\tilde{f}_L \bar{\tilde{f}}_L} \cos^2\theta_{\tilde{f}} + \mathcal{A}_{\tilde{f}_R \bar{\tilde{f}}_R} \sin^2\theta_{\tilde{f}} - 2\mathcal{A}_{\tilde{f}_L \bar{\tilde{f}}_R} \cos\theta_{\tilde{f}} \sin\theta_{\tilde{f}} \tag{B.55a}$$

$$\mathcal{A}_{\tilde{f}_2 \bar{\tilde{f}}_2} = \mathcal{A}_{\tilde{f}_L \bar{\tilde{f}}_L} \sin^2\theta_{\tilde{f}} + \mathcal{A}_{\tilde{f}_R \bar{\tilde{f}}_R} \cos^2\theta_{\tilde{f}} + 2\mathcal{A}_{\tilde{f}_L \bar{\tilde{f}}_R} \cos\theta_{\tilde{f}} \sin\theta_{\tilde{f}} \tag{B.55b}$$

$$\mathcal{A}_{\tilde{f}_1 \bar{\tilde{f}}_2} = \mathcal{A}_{\tilde{f}_L \bar{\tilde{f}}_L} \cos\theta_{\tilde{f}} \sin\theta_{\tilde{f}} - \mathcal{A}_{\tilde{f}_R \bar{\tilde{f}}_R} \cos\theta_{\tilde{f}} \sin\theta_{\tilde{f}} + \mathcal{A}_{\tilde{f}_L \bar{\tilde{f}}_R} \cos 2\theta_{\tilde{f}} \tag{B.55c}$$

$$\mathcal{A}_{\tilde{f}_2 \bar{\tilde{f}}_1} = \mathcal{A}_{\tilde{f}_1 \bar{\tilde{f}}_2} \tag{B.55d}$$

$$\mathcal{A}_{\tilde{u}_L \bar{\tilde{u}}_L, \tilde{c}_L \bar{\tilde{c}}_L, \tilde{t}_L \bar{\tilde{t}}_L} = \begin{cases} \frac{1}{2}(1 - \frac{1}{3}\tan^2\theta_w) g M_W \sin(\beta - \alpha) - \frac{g m_q^2}{M_W}(\frac{\cos\alpha}{\sin\beta}) & \text{for } H = H_\ell \\ -\frac{1}{2}(1 - \frac{1}{3}\tan^2\theta_w) g M_W \cos(\beta - \alpha) - \frac{g m_q^2}{M_W}(\frac{-\sin\alpha}{\sin\beta}) & H_h \\ 0 & H_p \end{cases} \tag{B.56a}$$

$$\mathcal{A}_{\substack{\tilde{d}_L \bar{\tilde{d}}_L, \tilde{s}_L \bar{\tilde{s}}_L, \tilde{b}_L \bar{\tilde{b}}_L, \\ \tilde{e}_L \bar{\tilde{e}}_L, \tilde{\mu}_L \bar{\tilde{\mu}}_L, \tilde{\tau}_L \bar{\tilde{\tau}}_L}} = \begin{cases} \frac{1}{2}(1 + \frac{1}{3}\tan^2\theta_w) g M_W \sin(\beta - \alpha) - \frac{g m_f^2}{M_W}(\frac{\sin\alpha}{\cos\beta}) & \text{for } H = H_\ell \\ -\frac{1}{2}(1 + \frac{1}{3}\tan^2\theta_w) g M_W \cos(\beta - \alpha) - \frac{g m_f^2}{M_W}(\frac{\cos\alpha}{\cos\beta}) & H_h \\ 0 & H_p \end{cases} \tag{B.56b}$$

$$\mathcal{A}_{\tilde{\nu}_L \bar{\tilde{\nu}}_L} = \begin{cases} \frac{1}{2}(1 + \tan^2\theta_w) g M_W \sin(\beta - \alpha) & \text{for } H = H_\ell \\ -\frac{1}{2}(1 + \tan^2\theta_w) g M_W \cos(\beta - \alpha) & H_h \\ 0 & H_p \end{cases} \tag{B.56c}$$

$$\mathcal{A}_{\tilde{u}_R\bar{\tilde{u}}_R,\tilde{c}_R\bar{\tilde{c}}_R,\tilde{t}_R\bar{\tilde{t}}_R} = \begin{cases} \frac{2}{3}\tan^2\theta_w g M_W \sin(\beta-\alpha) - \frac{gm_q^2}{M_W}\left(\frac{\cos\alpha}{\sin\beta}\right) & \text{for } H = H_\ell \\ -\frac{2}{3}\tan^2\theta_w g M_W \cos(\beta-\alpha) - \frac{gm_q^2}{M_W}\left(\frac{-\sin\alpha}{\sin\beta}\right) & H_h \\ 0 & H_p \end{cases} \tag{B.56d}$$

$$\mathcal{A}_{\substack{\tilde{d}_R\bar{\tilde{d}}_R,\tilde{s}_R\bar{\tilde{s}}_R,\tilde{b}_R\bar{\tilde{b}}_R, \\ \tilde{e}_R\bar{\tilde{e}}_R,\tilde{\mu}_R\bar{\tilde{\mu}}_R,\tilde{\tau}_R\bar{\tilde{\tau}}_R}} = \begin{cases} -\frac{1}{3}\tan^2\theta_w g M_W \sin(\beta-\alpha) - \frac{gm_q^2}{M_W}\left(\frac{\sin\alpha}{\cos\beta}\right) & \text{for } H = H_\ell \\ \frac{1}{3}\tan^2\theta_w g M_W \cos(\beta-\alpha) - \frac{gm_q^2}{M_W}\left(\frac{\cos\alpha}{\cos\beta}\right) & H_h \\ 0 & H_p \end{cases} \tag{B.56e}$$

$$\mathcal{A}_{\tilde{u}_L\bar{\tilde{u}}_R,\tilde{c}_L\bar{\tilde{c}}_R,\tilde{t}_L\bar{\tilde{t}}_R} = \begin{cases} (2m_1\sin\alpha + A_q\cos\alpha)\frac{gm_q}{2M_W\sin\beta} & \text{for } H = H_\ell \\ (2m_1\cos\alpha - A_q\sin\alpha)\frac{gm_q}{2M_W\sin\beta} & H_h \\ (2m_1 - \cot\beta A_q)\frac{gm_q}{2M_W} & H_p \end{cases} \tag{B.56f}$$

$$\mathcal{A}_{\substack{\tilde{d}_L\bar{\tilde{d}}_R,\tilde{s}_L\bar{\tilde{s}}_R,\tilde{b}_L\bar{\tilde{b}}_R, \\ \tilde{e}_L\bar{\tilde{e}}_R,\tilde{\mu}_L\bar{\tilde{\mu}}_R,\tilde{\tau}_L\bar{\tilde{\tau}}_R}} = \begin{cases} (2m_1\cos\alpha + A_f\sin\alpha)\frac{gm_f}{2M_W\cos\beta} & \text{for } H = H_\ell \\ (-2m_1\sin\alpha + A_f\cos\alpha)\frac{gm_f}{2M_W\cos\beta} & H_h \\ (2m_1 - \tan\beta A_f)\frac{gm_f}{2M_W} & H_p \end{cases} \tag{B.56g}$$

$$\mathcal{A}_{\tilde{\nu}_R\bar{\tilde{\nu}}_R} = \mathcal{A}_{\tilde{\nu}_L\bar{\tilde{\nu}}_R} = 0 \tag{B.56h}$$

The sfermion mixing angles used in Eqns. (B.55) and Eqns. (B.34) and (B.42) of Section B.4 are defined by

$$\begin{aligned} \widetilde{f_1} &= \widetilde{f_L}\cos\theta_{\tilde{f}} - \widetilde{f_R}\sin\theta_{\tilde{f}} \\ \widetilde{f_2} &= \widetilde{f_L}\sin\theta_{\tilde{f}} + \widetilde{f_R}\cos\theta_{\tilde{f}} \quad , \end{aligned} \tag{B.57}$$

where $\widetilde{f_L}$ and $\widetilde{f_R}$ are the supersymmetric partners of the left- and right-handed SM fermions (quarks or leptons), respectively, and $\widetilde{f_1}$ and $\widetilde{f_2}$ are the lighter and heavier mass eigenstates, respectively. From Eqns. (A.118)-(A.121) of Appendix A the

following formulæ may be derived:

For $\tilde{u}$, $\tilde{c}$, and $\tilde{t}$ squarks,

$$\tan\theta_{\tilde{q}} = \left\{ -(m^2_{\tilde{q}_L} - m^2_{\tilde{q}_R}) - \tfrac{1}{8}(g^2 - \tfrac{5}{3})(v'^2 - v^2) \right.$$
$$\left. - \left[\left((m^2_{\tilde{q}_L} - m^2_{\tilde{q}_R}) + \tfrac{1}{4}(g^2 - \tfrac{5}{3})(v'^2 - v^2) \right) + 4m_q^2(2m_1 \cot\beta + A_q)^2 \right]^{\frac{1}{2}} \right\}$$
$$\div\, m_q(2m_1 \cot\beta + A_q) \qquad \text{(B.58)}$$

If $2m_1 \cot\beta + A_q = 0$, then set $\theta_{\tilde{q}} = \frac{\pi}{2}$.

For $\tilde{d}$, $\tilde{s}$, and $\tilde{b}$ squarks and $\tilde{e}$, $\tilde{\mu}$, and $\tilde{\tau}$ sleptons,

$$\tan\theta_{\tilde{f}} = \left\{ -(m^2_{\tilde{f}_L} - m^2_{\tilde{f}_R}) + \tfrac{1}{8}(g^2 - \tfrac{1}{3})(v'^2 - v^2) \right.$$
$$\left. - \left[\left((m^2_{\tilde{f}_L} - m^2_{\tilde{f}_R}) - \tfrac{1}{4}(g^2 - \tfrac{1}{3})(v'^2 - v^2) \right) + 4m_f^2(2m_1 \tan\beta + A_f)^2 \right]^{\frac{1}{2}} \right\}$$
$$\div\, m_f(2m_1 \tan\beta + A_q) \qquad \text{(B.59)}$$

If $2m_1 \tan\beta + A_f = 0$, then set $\theta_{\tilde{f}} = \frac{\pi}{2}$.

The sneutrinos have no mixing angles (or alternatively one can say that $\theta_{\tilde{\nu}} = 0$) since there are no $\widetilde{\nu_R}$'s.

The partial decay widths of the charged Higgs bosons into squarks, $\Gamma\left(H^+ \to \tilde{q}_i \overline{\tilde{q}_j'}\right)$, where q is an up-type quark and q' is a down-type quark, are given by:

$$\Gamma\left(H^+ \to \tilde{q}_i \overline{\tilde{q}_j'}\right) = \Gamma\left(H^- \to \tilde{q}_j' \overline{\tilde{q}_i}\right) = \frac{\left(C_{\tilde{f}_i \overline{\tilde{f}_j'}}\right)^2}{16\pi m_{H_{ch}}} N_c\, \lambda^{\frac{1}{2}}\left(1, \frac{m^2_{\tilde{q}_1}}{m^2_{H_{ch}}}, \frac{m^2_{\tilde{q}_1'}}{m^2_{H_{ch}}}\right) \qquad \text{(B.60)}$$

(assuming $m_{H_{ch}} \geq m_{\tilde{f}_i} + m_{\tilde{f}_j'}$, else set decay width equal to 0) where $i, j = 1, 2$; $N_c = 3$ for squarks and $N_c = 1$ for sleptons; and for the squarks

$$C_{\tilde{f}_1 \overline{\tilde{f}_1'}} = C_{\tilde{f}_L \overline{\tilde{f}_L'}} \cos\theta_{\tilde{f}} \cos\theta_{\tilde{f}'} + C_{\tilde{f}_R \overline{\tilde{f}_R'}} \sin\theta_{\tilde{f}} \sin\theta_{\tilde{f}'}$$
$$- C_{\tilde{f}_L \overline{\tilde{f}_R'}} \cos\theta_{\tilde{f}} \sin\theta_{\tilde{f}'} - C_{\tilde{f}_R \overline{\tilde{f}_L'}} \sin\theta_{\tilde{f}} \cos\theta_{\tilde{f}'} \qquad \text{(B.61a)}$$

$$C_{\tilde{f}_2\bar{f}'_2} = C_{\tilde{f}_L\bar{f}'_L}\sin\theta_{\tilde{f}}\sin\theta_{\tilde{f}'} + C_{\tilde{f}_R\bar{f}'_R}\cos\theta_{\tilde{f}}\cos\theta_{\tilde{f}'} - C_{\tilde{f}_L\bar{f}'_R}\sin\theta_{\tilde{f}}\cos\theta_{\tilde{f}'} + C_{\tilde{f}_R\bar{f}'_L}\cos\theta_{\tilde{f}}\sin\theta_{\tilde{f}'} \quad \text{(B.61b)}$$

$$C_{\tilde{f}_1\bar{f}'_2} = C_{\tilde{f}_L\bar{f}'_L}\cos\theta_{\tilde{f}}\sin\theta_{\tilde{f}'} - C_{\tilde{f}_R\bar{f}'_R}\sin\theta_{\tilde{f}}\cos\theta_{\tilde{f}'} + C_{\tilde{f}_L\bar{f}'_R}\cos\theta_{\tilde{f}}\cos\theta_{\tilde{f}'} - C_{\tilde{f}_R\bar{f}'_L}\sin\theta_{\tilde{f}}\sin\theta_{\tilde{f}'} \quad \text{(B.61c)}$$

$$C_{\tilde{f}_2\bar{f}'_1} = C_{\tilde{f}_L\bar{f}'_L}\sin\theta_{\tilde{f}}\cos\theta_{\tilde{f}'} - C_{\tilde{f}_R\bar{f}'_R}\cos\theta_{\tilde{f}}\sin\theta_{\tilde{f}'} - C_{\tilde{f}_L\bar{f}'_R}\sin\theta_{\tilde{f}}\sin\theta_{\tilde{f}'} + C_{\tilde{f}_R\bar{f}'_L}\cos\theta_{\tilde{f}}\cos\theta_{\tilde{f}'} \quad \text{(B.61d)}$$

$$C_{\tilde{q}_L\bar{\tilde{q}}'_L} = C_{\tilde{u}_L\bar{\tilde{d}}_L,\tilde{c}_L\bar{\tilde{s}}_L,\tilde{t}_L\bar{\tilde{b}}_L} = \frac{g}{\sqrt{2}}\left[-M_W\sin 2\beta + \frac{m_q^2\cot\beta + m_{q'}^2\tan\beta}{M_W}\right] \quad \text{(B.62a)}$$

$$C_{\tilde{q}_R\bar{\tilde{q}}'_R} = C_{\tilde{u}_R\bar{\tilde{d}}_R,\tilde{c}_R\bar{\tilde{s}}_R,\tilde{t}_R\bar{\tilde{b}}_R} = \frac{g}{\sqrt{2}}\frac{m_q m_{q'}(\cot\beta + \tan\beta)}{M_W} \quad \text{(B.62b)}$$

$$C_{\tilde{q}_L\bar{\tilde{q}}'_R} = C_{\tilde{u}_L\bar{\tilde{d}}_R,\tilde{c}_L\bar{\tilde{s}}_R,\tilde{t}_L\bar{\tilde{b}}_R} = \frac{g}{\sqrt{2}}\frac{m_{q'}(2m_1 - A_{q'}\tan\beta)}{M_W} \quad \text{(B.62c)}$$

$$C_{\tilde{q}_R\bar{\tilde{q}}'_L} = C_{\tilde{u}_R\bar{\tilde{d}}_L,\tilde{c}_R\bar{\tilde{s}}_L,\tilde{t}_R\bar{\tilde{b}}_L} = \frac{g}{\sqrt{2}}\frac{m_q(2m_1 - A_q\cot\beta)}{M_W} \quad \text{(B.62d)}$$

For the sleptons, using the assumption that $m_\nu = 0$ (or at least that neutrino masses are negligibly small),

$$\begin{aligned} C_{\tilde{\nu}_1\bar{\tilde{\ell}}_1} &= C_{\tilde{\nu}_L\bar{\tilde{\ell}}_L}\cos\theta_{\tilde{\ell}} - C_{\tilde{\nu}_L\bar{\tilde{\ell}}_R}\sin\theta_{\tilde{f}} \ , \\ C_{\tilde{\nu}_1\bar{\tilde{\ell}}_2} &= C_{\tilde{\nu}_L\bar{\tilde{\ell}}_L}\sin\theta_{\tilde{\ell}} + C_{\tilde{\nu}_L\bar{\tilde{\ell}}_R}\cos\theta_{\tilde{\ell}} \ , \\ C_{\tilde{\nu}_2\bar{\tilde{\ell}}_1} &= C_{\tilde{\nu}_2\bar{\tilde{\ell}}_2} = 0 \ , \end{aligned} \quad \text{(B.63)}$$

which follow immediately from setting (in Eqn. (B.61)) $\theta_{\tilde{\nu}} = 0$ and $\widetilde{\nu_1} = \widetilde{\nu_L}$ with no $\widetilde{\nu_2} = \widetilde{\nu_R}$ state. The $C_{\tilde{\nu}\tilde{\ell}}$ coefficients also simplify, and are given by

$$C_{\tilde{\nu}_L\bar{\tilde{\ell}}_L} = C_{\widetilde{\nu_{e_L}}\bar{\tilde{e}}_L,\widetilde{\nu_{\mu_L}}\bar{\tilde{\mu}}_L,\widetilde{\nu_{\tau_L}}\bar{\tilde{\tau}}_L} = \frac{g}{\sqrt{2}}\left[-M_W\sin 2\beta + \frac{m_\ell^2\tan\beta}{M_W}\right] \quad \text{(B.64a)}$$

$$C_{\tilde{\nu}_L\bar{\tilde{\ell}}_R} = C_{\widetilde{\nu_{e_L}}\bar{\tilde{e}}_R,\widetilde{\nu_{\mu_L}}\bar{\tilde{\mu}}_R,\widetilde{\nu_{\tau_L}}\bar{\tilde{\tau}}_R} = \frac{g}{\sqrt{2}}\frac{m_\ell(2m_1 - A_\ell\tan\beta)}{M_W} \quad \text{(B.64b)}$$

$$C_{\tilde{\nu}_R\bar{\tilde{\ell}}_L} = C_{\tilde{\nu}_R\bar{\tilde{\ell}}_R} = 0 \quad \text{(B.64c)}$$

B.6 Higgs Boson Decays to Charginos and Neutralinos

Before giving expressions for the partial decay widths of the Higgs bosons into charginos and neutralinos, it will first be necessary to determine some parameters of the physical state combinations of the gauginos and higgsinos. The expressions given below are from Ref. [220], and have been corrected for a sign error in that paper. Beginning with the charged sector given by Eqns. (1.4)–(1.6) of Chapter 1, two distinct angles, γ_L and γ_R, can be defined (with $0 \leq \gamma_L, \gamma_R \leq 180°$) such that rotation of the left-handed components of the fields by γ_L and rotation of the right-handed components of the fields γ_R will diagonalize $\mathcal{M}_{charge}$. These angles are obtained from

$$\tan\gamma_L = 1/x_- \,, \qquad \tan\gamma_R = 1/y_- \,, \tag{B.65}$$

$$\text{where} \quad x_- = -\frac{\left[(2m_1)^2 - \mu_2^2 - 2M_W^2\cos 2\beta\right] - \zeta}{2\sqrt{2}M_W(\mu_2 \sin\beta + 2m_1\cos\beta)} \,, \tag{B.66}$$

$$\text{and} \quad y_- = -\frac{\left[(2m_1)^2 - \mu_2^2 + 2M_W^2\cos 2\beta\right] - \zeta}{2\sqrt{2}M_W(\mu_2 \cos\beta + 2m_1\sin\beta)} \,, \tag{B.67}$$

with μ_2 as given in Eqns. (1.9) and

$$\zeta^2 = \left[(2m_1)^2 - \mu_2^2\right]^2 \; + \; 4M_W^2\left[M_W^2\cos^2 2\beta + (2m_1)^2 + \mu_2^2 + 2(2m_1)\mu_2\sin 2\beta\right] \tag{B.68}$$

The masses of the charginos eigenstates are then given by

$$\begin{aligned} m_{\widetilde{W}_1} &= \theta_x\theta_y\left[\cos\gamma_R(\mu_2\cos\gamma_L + gv'\sin\gamma_L) \; - \; \sin\gamma_R(-gv\cos\gamma_L - 2m_1\sin\gamma_L)\right] \,, \\ m_{\widetilde{W}_2} &= \sin\gamma_R(\mu_2\sin\gamma_L - gv'\cos\gamma_L) \; + \; \cos\gamma_R(-gv\sin\gamma_L + 2m_1\cos\gamma_L)\Big] \,. \end{aligned} \tag{B.69}$$

Here $\theta_x = \text{sgn}(x_-)$ and $\theta_y = \text{sgn}(y_-)$. From the eigenvalues of $\mathcal{M}_{charge}\mathcal{M}_{charge}^T$, the squares of these masses can also be obtained:

$$m^2_{\widetilde{W}_1}, m^2_{\widetilde{W}_2} = \tfrac{1}{2}\left[(2m_1)^2 + \mu_2^2 + 2M_W^2 \pm \zeta\right] \tag{B.70}$$

The masses given by Eqns. (B.69) may be negative in which case the spinor $\gamma_5\widetilde{W}$ rather than $\widetilde{W}$ is used as the field with positive mass when computing couplings. The mass eigenstates for the left- and right-handed components of the charginos are

$$\begin{bmatrix}\widetilde{W_2}\\ \widetilde{W_1}\end{bmatrix}_L = \begin{bmatrix}\theta_x\cos\gamma_L & -\theta_x\sin\gamma_L\\ \sin\gamma_L & \cos\gamma_L\end{bmatrix}\begin{bmatrix}\tilde{\lambda}\\ \tilde{\chi}\end{bmatrix}_L \quad , \tag{B.71}$$

$$\text{and} \quad \begin{bmatrix}(-1)^{\theta_p}\widetilde{W_2}\\ (-1)^{\theta_m}\widetilde{W_1}\end{bmatrix}_R = \begin{bmatrix}\theta_y\cos\gamma_R & -\theta_y\sin\gamma_R\\ \sin\gamma_R & \cos\gamma_R\end{bmatrix}\begin{bmatrix}\tilde{\lambda}\\ \tilde{\chi}\end{bmatrix}_R , \tag{B.72}$$

$$\text{where} \quad \theta_m = \begin{cases} 0 & \text{if } m_{\widetilde{W_1}} > 0\\ 1 & \text{if } m_{\widetilde{W_1}} < 0\end{cases} \quad \text{and} \quad \theta_p = \begin{cases} 0 & \text{if } m_{\widetilde{W_2}} > 0\\ 1 & \text{if } m_{\widetilde{W_2}} < 0\end{cases} . \tag{B.73}$$

The neutral sector 4×4 mass matrix as given by Eqn. (1.8) is difficult to diagonalize analytically but can be solved numerically to give the neutralino mass eigenvalues and eigenvectors for a given set of input parameters. The unmixed gaugino and higgsino states are then defined as related to the mass eigenstates by the relations

$$\begin{bmatrix}\overline{\tilde{h}^0}\\ \overline{\tilde{h}'^0}\\ \overline{\tilde{\lambda}_3}\\ \overline{\tilde{\lambda}_0}\end{bmatrix} = \begin{bmatrix}v_1^{(1)} & v_1^{(2)} & v_1^{(3)} & v_1^{(4)}\\ v_2^{(1)} & v_2^{(2)} & v_2^{(3)} & v_2^{(4)}\\ v_3^{(1)} & v_3^{(2)} & v_3^{(3)} & v_3^{(4)}\\ v_4^{(1)} & v_4^{(2)} & v_4^{(3)} & v_4^{(4)}\end{bmatrix}\begin{bmatrix}(-i\gamma_5)^{\theta_1}\widetilde{Z}_1\\ (-i\gamma_5)^{\theta_2}\widetilde{Z}_2\\ (-i\gamma_5)^{\theta_3}\widetilde{Z}_3\\ (-i\gamma_5)^{\theta_4}\widetilde{Z}_4\end{bmatrix} , \tag{B.74}$$

where the coefficients $v_i^{(j)}$ are numerically calculated and $\theta_i = 0$ if the $\widetilde{Z}_i$ mass eigenvalue is positive and $\theta_i = 1$ if the $\widetilde{Z}_i$ mass eigenstate is negative ($i = 1,2,3,4$). The factor $(-i\gamma_5)^{\theta_i}$ in Eqn. (B.74) ensures the positive mass fields are self-conjugate Majorana fields. In the remainder of this section, and in all other sections and chapters of this work, $m_{\widetilde{W_i}}$ and $m_{\widetilde{Z}_i}$ are taken to be positive, *i.e.*, they are taken to be the absolute values of the eigenvalues resulting from diagonalizing the charged and neutral sector mass matrices, Eqns. (1.6) and (1.8).

Radiative corrections to the chargino and neutralino masses are not included in the program. These are small in general ($\lesssim$ 2-6%) [221-223], but can be larger for the lightest neutralino in certain restricted regions of parameter space (which are in or bordering upon the LEP excluded region) [223].

Using the above definitions, the partial decay widths of the Higgs bosons into charginos and neutralinos can now be presented. For the decays of the light Higgs boson, H_ℓ, into charginos the partial decay widths are given by

$$\Gamma(H_\ell \to \widetilde{W_1}^+ \widetilde{W_1}^-) = \frac{g^2}{4\pi} |S_1^\ell|^2 \, m_{H_\ell} \left(1 - \frac{m^2_{\widetilde{W_1}}}{m^2_{H_\ell}}\right)^{\frac{3}{2}} \quad , \tag{B.75}$$

$$\begin{aligned} \Gamma\left(H_\ell \to \widetilde{W_1}^+ \widetilde{W_2}^-\right) &= \Gamma\left(H_\ell \to \widetilde{W_2}^+ \widetilde{W_1}^-\right) \\ &= \frac{g^2}{16\pi m_{H_\ell}} \Big\{ \left(S_{12}^\ell\right)^2 \left[m^2_{H_\ell} - (m_{\widetilde{W_2}} + m_{\widetilde{W_1}})^2\right] \\ &\qquad + \left(P_{12}^\ell\right)^2 \left[m^2_{H_\ell} - (m_{\widetilde{W_2}} - m_{\widetilde{W_1}})^2\right] \Big\} \\ &\qquad \times \lambda^{\frac{1}{2}} \left(1, \frac{m^2_{\widetilde{W_1}}}{m^2_{H_\ell}}, \frac{m^2_{\widetilde{W_2}}}{m^2_{H_\ell}}\right) \quad , \end{aligned} \tag{B.76}$$

$$\Gamma(H_\ell \to \widetilde{W_2}^+ \widetilde{W_2}^-) = \frac{g^2}{4\pi} |S_2^\ell|^2 \, m_{H_\ell} \left(1 - \frac{m^2_{\widetilde{W_2}}}{m^2_{H_\ell}}\right)^{\frac{3}{2}} \quad , \tag{B.77}$$

where, again, $\lambda(a,b,c) = a^2 + b^2 + c^2 - 2ab - 2bc - 2ac$. Analogous formulæ hold for the heavy Higgs boson, H_h, and the pseudoscalar Higgs boson, H_p:

$$\Gamma(H_h \to \widetilde{W_1}^+ \widetilde{W_1}^-) = \frac{g^2}{4\pi} |S_1^h|^2 \, m_{H_h} \left(1 - \frac{m^2_{\widetilde{W_1}}}{m^2_{H_h}}\right)^{\frac{3}{2}} \quad , \tag{B.78}$$

$$\begin{aligned} \Gamma\left(H_h \to \widetilde{W_1}^+ \widetilde{W_2}^-\right) &= \Gamma\left(H_h \to \widetilde{W_2}^+ \widetilde{W_1}^-\right) \\ &= \frac{g^2}{16\pi m_{H_h}} \Big\{ \left(S_{12}^h\right)^2 \left[m^2_{H_h} - (m_{\widetilde{W_2}} + m_{\widetilde{W_1}})^2\right] \\ &\qquad + \left(P_{12}^h\right)^2 \left[m^2_{H_h} - (m_{\widetilde{W_2}} - m_{\widetilde{W_1}})^2\right] \Big\} \\ &\qquad \times \lambda^{\frac{1}{2}} \left(1, \frac{m^2_{\widetilde{W_1}}}{m^2_{H_h}}, \frac{m^2_{\widetilde{W_2}}}{m^2_{H_h}}\right) \quad , \end{aligned} \tag{B.79}$$

$$\Gamma(H_h \to \widetilde{W_2}^+ \widetilde{W_2}^-) = \frac{g^2}{4\pi} |S_2^h|^2 \, m_{H_h} \left(1 - \frac{m^2_{\widetilde{W_2}}}{m^2_{H_h}}\right)^{\frac{3}{2}} \quad , \tag{B.80}$$

$$\Gamma(H_p \to \widetilde{W_1}^+ \widetilde{W_1}^-) = \frac{g^2}{4\pi} |S_1^p|^2 \, m_{H_p} \left(1 - \frac{m^2_{\widetilde{W_1}}}{m^2_{H_p}}\right)^{\frac{3}{2}} \quad , \tag{B.81}$$

$$\Gamma\Big(H_p \to \widetilde{W_1}^+\widetilde{W_2}^-\Big) = \Gamma\Big(H_p \to \widetilde{W_2}^+\widetilde{W_1}^-\Big)$$
$$= \frac{g^2}{16\pi m_{H_p}}\Big\{\Big(S_{12}^p\Big)^2\Big[m_{H_p}^2 - (m_{\widetilde{W_2}} + m_{\widetilde{W_1}})^2\Big]$$
$$+ \Big(P_{12}^p\Big)^2\Big[m_{H_p}^2 - (m_{\widetilde{W_2}} - m_{\widetilde{W_1}})^2\Big]\Big\}$$
$$\times \lambda^{\frac{1}{2}}\left(1, \frac{m_{\widetilde{W_1}}^2}{m_{H_p}^2}, \frac{m_{\widetilde{W_2}}^2}{m_{H_p}^2}\right) \quad , \tag{B.82}$$

$$\Gamma(H_p \to \widetilde{W_2}^+\widetilde{W_2}^-) = \frac{g^2}{4\pi}|S_2^p|^2\, m_{H_p}\left(1 - \frac{m_{\widetilde{W_2}}^2}{m_{H_p}^2}\right)^{\frac{3}{2}} \quad . \tag{B.83}$$

If $m_H < m_{\widetilde{W_i}} + m_{\widetilde{W_j}}$, then the above partial decay widths, $\Gamma(H \to \widetilde{W_i}\widetilde{W_j})$, are set to zero. The functions S_1^ℓ, S_1^h, and S_1^p (which are found in Ref. [116]) are given by:

$$S_1^\ell = \tfrac{1}{2}(-1)^{\theta_m}\Big[\sin\alpha\cos\gamma_L\sin\gamma_R + \cos\alpha\sin\gamma_L\cos\gamma_R\Big] \ , \tag{B.84a}$$
$$S_1^h = \tfrac{1}{2}(-1)^{\theta_m}\Big[\cos\alpha\cos\gamma_L\sin\gamma_R - \sin\alpha\sin\gamma_L\cos\gamma_R\Big] \ , \tag{B.84b}$$
$$S_1^p = \tfrac{1}{2}(-1)^{\theta_m}\Big[\sin\beta\cos\gamma_L\sin\gamma_R + \cos\beta\sin\gamma_L\cos\gamma_R\Big] \ . \tag{B.84c}$$

The functions S_{12}^ℓ, S_{12}^h, and S_{12}^p are given by:

$$S_{12}^\ell = \tfrac{1}{2}\Big[-(-1)^{\theta_m}\theta_x\sin\alpha\sin\gamma_L\sin\gamma_R + (-1)^{\theta_m}\theta_x\cos\alpha\cos\gamma_L\cos\gamma_R$$
$$- (-1)^{\theta_p}\theta_y\cos\alpha\sin\gamma_L\sin\gamma_R + (-1)^{\theta_p}\theta_y\sin\alpha\cos\gamma_L\cos\gamma_R\Big] \ , \tag{B.85a}$$
$$S_{12}^h = \tfrac{1}{2}\Big[-(-1)^{\theta_m}\theta_x\cos\alpha\sin\gamma_L\sin\gamma_R - (-1)^{\theta_m}\theta_x\sin\alpha\cos\gamma_L\cos\gamma_R$$
$$+ (-1)^{\theta_p}\theta_y\sin\alpha\sin\gamma_L\sin\gamma_R + (-1)^{\theta_p}\theta_y\cos\alpha\cos\gamma_L\cos\gamma_R\Big] \ , \tag{B.85b}$$
$$S_{12}^p = \tfrac{1}{2}\Big[-(-1)^{\theta_m}\theta_x\sin\beta\sin\gamma_L\sin\gamma_R + (-1)^{\theta_m}\theta_x\cos\beta\cos\gamma_L\cos\gamma_R$$
$$+ (-1)^{\theta_p}\theta_y\cos\beta\sin\gamma_L\sin\gamma_R - (-1)^{\theta_p}\theta_y\sin\beta\cos\gamma_L\cos\gamma_R\Big] \ . \tag{B.85c}$$

The functions P_{12}^{ℓ}, P_{12}^{h}, and P_{12}^{p} are given by:

$$\begin{aligned} P_{12}^{\ell} = \tfrac{1}{2}\Big[&(-1)^{\theta_m}\theta_x \sin\alpha \sin\gamma_L \sin\gamma_R \;-\; (-1)^{\theta_m}\theta_x \cos\alpha \cos\gamma_L \cos\gamma_R \\ &- (-1)^{\theta_p}\theta_y \cos\alpha \sin\gamma_L \sin\gamma_R \;+\; (-1)^{\theta_p}\theta_y \sin\alpha \cos\gamma_L \cos\gamma_R\Big] , \end{aligned} \tag{B.86a}$$

$$\begin{aligned} P_{12}^{h} = \tfrac{1}{2}\Big[&(-1)^{\theta_m}\theta_x \cos\alpha \sin\gamma_L \sin\gamma_R \;+\; (-1)^{\theta_m}\theta_x \sin\alpha \cos\gamma_L \cos\gamma_R \\ &+ (-1)^{\theta_p}\theta_y \sin\alpha \sin\gamma_L \sin\gamma_R \;+\; (-1)^{\theta_p}\theta_y \cos\alpha \cos\gamma_L \cos\gamma_R\Big] , \end{aligned} \tag{B.86b}$$

$$\begin{aligned} P_{12}^{p} = \tfrac{1}{2}\Big[&(-1)^{\theta_m}\theta_x \sin\beta \sin\gamma_L \sin\gamma_R \;-\; (-1)^{\theta_m}\theta_x \cos\beta \cos\gamma_L \cos\gamma_R \\ &+ (-1)^{\theta_p}\theta_y \cos\beta \sin\gamma_L \sin\gamma_R \;-\; (-1)^{\theta_p}\theta_y \sin\beta \cos\gamma_L \cos\gamma_R\Big] . \end{aligned} \tag{B.86c}$$

And the functions S_2^{ℓ}, S_2^{h}, and S_2^{p} are given by:

$$S_2^{\ell} = \tfrac{1}{2}(-1)^{\theta_p+1}\theta_x\theta_y\Big[\sin\alpha \sin\gamma_L \cos\gamma_R \;+\; \cos\alpha \cos\gamma_L \sin\gamma_R\Big] , \tag{B.87a}$$

$$S_2^{h} = \tfrac{1}{2}(-1)^{\theta_p+1}\theta_x\theta_y\Big[\cos\alpha \sin\gamma_L \cos\gamma_R \;-\; \sin\alpha \cos\gamma_L \sin\gamma_R\Big] , \tag{B.87b}$$

$$S_2^{p} = -\tfrac{1}{2}(-1)^{\theta_p}\theta_x\theta_y\Big[\sin\beta \sin\gamma_L \cos\gamma_R \;+\; \cos\beta \cos\gamma_L \sin\gamma_R\Big] . \tag{B.87c}$$

For the decays of the light Higgs boson, H_ℓ, into neutralinos we have

$$\begin{aligned} \Gamma(H_\ell \to \widetilde{Z}_i\widetilde{Z}_j) = \frac{\triangle_{ij}}{8\pi m_{H_\ell}}\Big(X_{ij}^{\ell} + X_{ji}^{\ell}\Big)^2\Big[m_{H_\ell}^2 - (m_{\widetilde{Z}_i} + (-1)^{\theta_i+\theta_j}m_{\widetilde{Z}_j})^2\Big] \\ \times \lambda^{\frac{1}{2}}\left(1, \frac{m_{\widetilde{Z}_i}^2}{m_{H_\ell}^2}, \frac{m_{\widetilde{Z}_j}^2}{m_{H_\ell}^2}\right) , \end{aligned} \tag{B.88}$$

$$\text{where} \qquad \triangle_{ij} = \begin{cases} 1 & \text{if } i \neq j \\ \frac{1}{2} & \text{if } i = j \end{cases} . \tag{B.89}$$

Again, analogous formulæ hold for H_h and H_p:

$$\begin{aligned} \Gamma(H_h \to \widetilde{Z}_i\widetilde{Z}_j) = \frac{\triangle_{ij}}{8\pi m_{H_h}}\Big(X_{ij}^{\ell} + X_{ji}^{\ell}\Big)^2\Big[m_{H_h}^2 - (m_{\widetilde{Z}_i} + (-1)^{\theta_i+\theta_j}m_{\widetilde{Z}_j})^2\Big] \\ \times \lambda^{\frac{1}{2}}\left(1, \frac{m_{\widetilde{Z}_i}^2}{m_{H_h}^2}, \frac{m_{\widetilde{Z}_j}^2}{m_{H_h}^2}\right) ; \end{aligned} \tag{B.90}$$

$$\Gamma(H_p \to \widetilde{Z}_i\widetilde{Z}_j) = \frac{\triangle_{ij}}{8\pi m_{H_p}}\Big(X^{\ell}_{ij} + X^{\ell}_{ji}\Big)^2\Big[m^2_{H_p} - (m_{\widetilde{Z}_i} + (-1)^{\theta_i+\theta_j}m_{\widetilde{Z}_j})^2\Big]$$
$$\times\ \lambda^{\frac{1}{2}}\left(1, \frac{m^2_{\widetilde{Z}_i}}{m^2_{H_p}}, \frac{m^2_{\widetilde{Z}_j}}{m^2_{H_p}}\right) \quad . \tag{B.91}$$

Again, if $m_H < m_{\widetilde{Z}_i} + m_{\widetilde{Z}_j}$, then the partial decay width $\Gamma(H \to \widetilde{Z}_i\widetilde{Z}_j)$ is set to zero. The functions X^{ℓ}_{ij}, X^{h}_{ij}, and X^{p}_{ij} are given by

$$X^{\ell}_{ij} = -\tfrac{1}{2}(-1)^{\theta_i+\theta_j}\Big(v_2^{(i)}\sin\alpha - v_1^{(i)}\cos\alpha\Big)\Big(gv_3^{(j)} - g'v_4^{(j)}\Big) \ , \tag{B.92a}$$
$$X^{h}_{ij} = -\tfrac{1}{2}(-1)^{\theta_i+\theta_j}\Big(v_2^{(i)}\cos\alpha + v_1^{(i)}\sin\alpha\Big)\Big(gv_3^{(j)} - g'v_4^{(j)}\Big) \ , \tag{B.92b}$$
$$X^{p}_{ij} = \tfrac{1}{2}(-1)^{\theta_i+\theta_j}\Big(v_2^{(i)}\sin\beta - v_1^{(i)}\cos\beta\Big)\Big(gv_3^{(j)} - g'v_4^{(j)}\Big) \ . \tag{B.92c}$$

The partial decay widths for charged Higgs decays into a chargino and a neutralino are given by

$$\Gamma\Big(H^+ \to \widetilde{W_i}^+\widetilde{Z}_j\Big) = \Gamma\Big(H^- \to \widetilde{W_i}^-\widetilde{Z}_j\Big)$$
$$= \frac{1}{8\pi m_{H_{ch}}}\lambda^{\frac{1}{2}}\left(1, \frac{m^2_{\widetilde{W_i}}}{m^2_{H_{ch}}}, \frac{m^2_{\widetilde{Z}_j}}{m^2_{H_{ch}}}\right) \tag{B.93}$$
$$\times\left[\Big(\mathcal{R}ij^2 + \mathcal{S}^2_{ij}\Big)\Big(m^2_{H_{ch}} - m^2_{\widetilde{W_i}} - m^2_{\widetilde{Z}_j}\Big) - 2\Big(\mathcal{R}ij^2 - \mathcal{S}^2_{ij}\Big)m_{\widetilde{W_i}}m_{\widetilde{Z}_j}\right] \ ,$$

where $$\mathcal{R}_{1j} = \tfrac{1}{2}\Big[(-1)^{\theta_m}A_2^{(j)}\cos\beta \ - \ (-1)^{\theta_j}A_4^{(j)}\sin\beta\Big] \ , \tag{B.94a}$$
$$\mathcal{R}_{2j} = \tfrac{1}{2}\Big[(-1)^{\theta_p}\theta_y A_1^{(j)}\cos\beta \ - \ (-1)^{\theta_j}\theta_x A_3^{(j)}\sin\beta\Big] \ , \tag{B.94b}$$

and $$\mathcal{S}_{1j} = \tfrac{1}{2}\Big[(-1)^{\theta_m}A_2^{(j)}\cos\beta \ + \ (-1)^{\theta_j}A_4^{(j)}\sin\beta\Big] \ , \tag{B.95a}$$
$$\mathcal{S}_{2j} = \tfrac{1}{2}\Big[(-1)^{\theta_p}\theta_y A_1^{(j)}\cos\beta \ + \ (-1)^{\theta_j}\theta_x A_3^{(j)}\sin\beta\Big] \ . \tag{B.95b}$$

The functions $A_n^{(j)}$ are given by

$$A_1^{(j)} = -\tfrac{1}{\sqrt{2}}\Big(gv_3^{(j)} + g'v_4^{(j)}\Big)\sin\gamma_R \ - \ gv_1^{(j)}\cos\gamma_R \ , \tag{B.96a}$$
$$A_2^{(j)} = \tfrac{1}{\sqrt{2}}\Big(gv_3^{(j)} + g'v_4^{(j)}\Big)\cos\gamma_R \ - \ gv_1^{(j)}\sin\gamma_R \ , \tag{B.96b}$$
$$A_3^{(j)} = -\tfrac{1}{\sqrt{2}}\Big(gv_3^{(j)} + g'v_4^{(j)}\Big)\sin\gamma_L \ + \ gv_2^{(j)}\cos\gamma_L \ , \tag{B.96c}$$
$$A_4^{(j)} = \tfrac{1}{\sqrt{2}}\Big(gv_3^{(j)} + g'v_4^{(j)}\Big)\cos\gamma_L \ + \ gv_2^{(j)}\sin\gamma_L \ . \tag{B.96d}$$

B.7 Higgs Boson Decays to Other Higgs Bosons

It is possible for a heavy Higgs boson, H_h, to decay into a pair of charged Higgs bosons, $H^{\pm}$'s, a pair of pseudoscalar Higgs bosons, H_p's, or a pair of light Higgs bosons, H_ℓ's, *if such a decay is kinematically allowed* . The three Higgs vertex factors which are needed to calculate these partial decay widths may be expected to have significant radiative corrections. For the decay of a heavy Higgs boson into a pair of light Higgs bosons, both the tree-level H_h-H_ℓ-H_ℓ vertex factor, $\xi^{tree}_{h\ell\ell}$, and the radiative correction due to the third generation of quarks and squarks (top and bottom quarks and stop and sbottom squarks), $\Delta\xi_{h\ell\ell}$, in Appendix A in Sections A.10 and A.11, respectively (see Eqns (A.237) and Eqn. (A.252) therein). The complete partial decay width is then given by

$$\Gamma(H_h \to H_\ell H_\ell) = \frac{\xi^2_{h\ell\ell}}{8\pi m_{H_h}}\left(1 - \frac{4m^2_{H_\ell}}{m^2_{H_h}}\right)^{\frac{1}{2}} \tag{B.97}$$

$$\text{where} \qquad \xi_{h\ell\ell} = \xi^{tree}_{h\ell\ell} + \Delta\xi_{h\ell\ell} \tag{B.98}$$

(The partial decay width is of course set to zero if $m_{H_h} < 2m_{H_\ell}$.) The other two decays of the heavy Higgs boson mentioned above are kinematically inaccessible for most choices of the MSSM input parameters, and the few regions where they are allowed are either ruled out by LEP constraints or will be in the not-too-distant future. With this in mind, the radiative corrections to the three Higgs vertex factors involved in these decays have not been calculated in as much detail as has the H_h-H_ℓ-H_ℓ vertex: only corrections from top quarks and (unmixed) stop squarks were incorporated (corrections from bottom quarks and sbottom squarks are not included). These partial decay widths are given by

$$\Gamma(H_h \to H_p H_p) = \frac{\xi^2_{hpp}}{8\pi m_{H_h}}\left(1 - \frac{4m^2_{H_p}}{m^2_{H_h}}\right)^{\frac{1}{2}} \tag{B.99}$$

$$\text{where} \qquad \xi_{hpp} = \xi^{tree}_{hpp} + \Delta\xi_{hpp} \tag{B.100}$$

$$\text{with} \qquad \xi^{tree}_{hpp} = -\left(\frac{gM_{Z^0}}{4\cos\theta_w}\right)\cos(\beta-\alpha)\cos 2\beta \tag{B.101}$$

$$\text{and} \quad \Delta\xi_{hpp} = -\left(\frac{gM_{Z^0}}{4\cos\theta_w}\right)\frac{3g^2\cos^2\theta_w m_t^4 \sin\alpha\cos^2\beta}{16\pi^2 M_W^4 \sin^3\beta} \times \log\left[\left(1+\frac{m^2_{\tilde{t}_L}}{m_t^2}\right)\left(1+\frac{m^2_{\tilde{t}_R}}{m_t^2}\right)\right] \tag{B.102}$$

(set partial decay width to zero if $m_{H_h} < 2m_{H_p}$);

$$\Gamma(H_h \to H^+H^-) = \frac{\xi^2_{hcc}}{16\pi m_{H_h}}\left(1-\frac{4m^2_{H_{ch}}}{m^2_{H_h}}\right)^{\frac{1}{2}} \tag{B.103}$$

$$\text{where} \qquad \xi_{hcc} = \xi^{tree}_{hcc} + \Delta\xi_{hcc} \tag{B.104}$$

$$\text{with} \qquad \xi^{tree}_{hcc} = gM_W\left[\cos(\beta+\alpha) - \frac{\cos(\beta-\alpha)\cos 2\beta}{2\cos^2\theta_w}\right] \tag{B.105}$$

$$\text{and} \quad \Delta\xi_{hcc} = -gM_W\frac{3g^2 m_t^4 \sin\alpha\cos\beta}{32\pi^2 M_W^4 \sin^3\beta}\log\left[\left(1+\frac{m^2_{\tilde{t}_L}}{m_t^2}\right)\left(1+\frac{m^2_{\tilde{t}_R}}{m_t^2}\right)\right] \tag{B.106}$$

(set partial decay width to zero if $m_{H_h} < 2m_{H_{ch}}$).

With the inclusion of the radiative corrections, it becomes possible for the the light Higgs boson to be considerably heavier than the pseudoscalar Higgs boson. This can make the decay $H_\ell \to H_pH_p$ kinematically allowable in some limited regions of the MSSM parameter space, generally where the psudoscalar Higgs boson mass is quite low. The partial decay width for this decay is given by

$$\Gamma(H_\ell \to H_pH_p) = \frac{\xi^2_{\ell pp}}{8\pi m_{H_\ell}}\left(1-\frac{4m^2_{H_p}}{m^2_{H_\ell}}\right)^{\frac{1}{2}} \tag{B.107}$$

$$\text{where} \qquad \xi_{\ell pp} = \xi^{tree}_{\ell pp} + \Delta\xi_{\ell pp} \tag{B.108}$$

$$\text{with} \qquad \xi^{tree}_{\ell pp} = \left(\frac{gM_{Z^0}}{4\cos\theta_w}\right)\sin(\beta-\alpha)\cos 2\beta \tag{B.109}$$

$$\text{and} \quad \Delta\xi_{\ell pp} = \left(\frac{gM_{Z^0}}{4\cos\theta_w}\right)\frac{3g^2\cos^2\theta_w m_t^4 \cos\alpha\cos^2\beta}{16\pi^2 M_W^4 \sin^3\beta}\log\left[\left(1+\frac{m^2_{\tilde{t}_L}}{m_t^2}\right)\left(1+\frac{m^2_{\tilde{t}_R}}{m_t^2}\right)\right] \tag{B.110}$$

(set partial decay width to zero if $m_{H_\ell} < 2m_{H_p}$).

Lastly, there are the decays of one type of Higgs boson into another type of Higgs boson plus a gauge boson. At tree-level there are two such processes, $H_p \to H_\ell Z^0$ and $H^\pm \to H_\ell W^\pm$. Radiative corrections to a vertex with two Higgs bosons and one gauge boson (or with two gauge bosons and one Higgs boson, such as $H_h \to Z^0 Z^0, W^+W^-$) are not expected to be large and are not included here. The partial decay widths for these processes are given by

$$\Gamma(H_p \to H_\ell Z^0) = \frac{(g\cos\theta_w + g'\sin\theta_w)^2 \cos^2(\alpha+\beta)\, m_{H_p}^2}{64\pi M_{Z^0}^2}\, m_{H_p} \times \lambda^{\frac{3}{2}}\left(1, \frac{m_{H_\ell}^2}{m_{H_p}^2}, \frac{M_{Z^0}^2}{m_{H_p}^2}\right) , \tag{B.111}$$

which is set to zero if $m_{H_p} < m_{H_\ell} + M_{Z^0}$, and

$$\Gamma(H^\pm \to H_\ell W^\pm) = \frac{g^2 \cos^2(\alpha+\beta)\, m_{H_{ch}}^2}{64\pi M_W^2}\, m_{H_{ch}}\, \lambda^{\frac{3}{2}}\left(1, \frac{m_{H_\ell}^2}{m_{H_{ch}}^2}, \frac{M_W^2}{m_{H_{ch}}^2}\right) , \tag{B.112}$$

which is set to zero if $m_{H_{ch}} < m_{H_\ell} + M_W$.

Bibliography

[1] Douglas Adams, *The Restaurant at the End of the Universe*, Pocket Books, New York, 1980.

[2] S. Weinberg, "A model of leptons," Phys. Rev. Lett. 19 (1967): 1264-1266.

[3] A. Salam, "Weak and electromagnetic interactions," in: *Elementary Particle Theory: Relativistic Groups and Analycity, Proc. of the 8^{th} Nobel Symposium*, Lerum, Sweeden, May 19-25, 1968, N. Svartholm (ed.), Almqvist & Wiksell Stockholm (1968), pages 367-377.

[4] S. Glashow, "Partial-symmetries of weak interactions," Nucl. Phys. 22 (1961): 579-588.

[5] D. Dicus and V. Mathur, "Upper bounds on the values of masses in unified gauge theories," Phys. Rev. D 7 (1973): 3111-3114.

[6] B. Lee, C. Quigg, and H. Thacker, "Weak interactions at very high energies: the role of the Higgs-boson mass," Phys. Rev. D 16 (1977): 1519-1531.

[7] N. Cabibbo, L. Maiani, G. Parisi, and R. Petronzio, "Bounds on the fermions and Higgs boson masses in grand unified theories," Nucl. Phys. B 158 (1979): 295-305.

[8] M. Lindner, "Implications of triviality for the Standard Model," Z. Phys. C 31 (1986): 295-300.

[9] B.H. Wiik, "Future e^+e^- colliders," in: *Workshop on Physics and Experiments with Linear e^+e^- Colliders, Vol. II*, Waikaloa, Hawaii, Apr. 26-30, 1993, F.A. Harris, S.L. Olsen, S. Pakvasa, and X. Tata (eds.), World Scientific, Singapore (1993), pages 46-71.

[10] S. Weinberg, "Implications of dymanical symmetry breaking: an addendum," Phys. Rev. D 19 (1979): 1277-1280.

[11] L. Susskind, "Dynamics of spontaneous symmetry breaking in the Weinberg-Salam theory," Phys. Rev. D 20 (1979): 2619-2625.

[12] H.P. Nilles, "Supersymmetry, supergravity and particle physics," Phys. Rep. 110 (1984): 1-162.

[13] H. Haber and G. Kane, "The search for supersymmetry: probing physics beyond the Standard Model" Phys. Rep. 117 (1985): 75-263.

[14] R. Arnowitt and P. Nath, "Supersymmetry and supergravity: phenomenology and grand unification," in: *Properties of SUSY Particles; Proceedings of the VII J. A. Swieca Summer School*, Campos do Jordao, Brazil, 1993 CTP-TAMU-52/93, L. Cifarelli and V. Khoze (eds.), World Scientific, Singapore (1993), pages 3-63.

[15] X. Tata, "An introduction to supersymmetry and supersymmetry phenomenology," in: *The Standard Model and Beyond: the 9^{th} Symposium on Theoretical Physics*, Mt. Sorak, Korea, Aug. 20-25, 1990, J.E. Kim (ed.), World Scientific, Singapore (1991), pages 304-378.

[16] L. Girardello and M. Grisaru, "Soft breaking of supersymmetry," Nucl. Phys. B 194 (1982): 65-76.

[17] S.P. Martin and M.T. Vaughn, "Regularization dependence of running couplings in softly broken supersymmetry," Phys. Lett. B 318 (1993): 331-337.

[18] M. Drees and M. Nojiri, "Radiative symmetry breaking in minimal N=1 supergravity with large Yukawa couplings," Nucl. Phys. B 369 (1992): 54-98.

[19] V. Barger, J.L. Hewett, and R.J.N. Phillips, "New constraints on the charged Higgs sector in two-Higgs-doublet models," Phys. Rev. D 41 (1990): 3421-3441.

[20] A.J. Buras, P. Kawczyk, M.E. Lautenbacher, and C. Salazar, B^0-$\overline{B^0}$ mixing, CP violation, $K^+ \to \pi^+ \nu \bar{\nu}$ and $B \to K \gamma X$ in a two Higgs doublet model," Nucl. Phys. B 337 (1990): 248-312.

[21] J.F. Gunion and B. Grzadkowski, "Limits on the top quark mass and on the charged Higgs boson of a two-doublet model from K^0-$\overline{K^0}$ mixing, B_d-$\overline{B_d}$ mixing and $b \to u$ decays," Phys. Lett. B 243 (1990): 301-307.

[22] G. Ridolfi, G.G. Ross, and F. Zwirner, "Supersymmetry: Introduction" in: *Proceedings of the European Committee for Future Accelerators Large Hadron Collider Workshop, Vol. II*, Aachen, Germany, Oct. 4-9, 1990, G. Jarlskog and

D. Rein (eds.), CERN Rept. No. 90-10, Geneva, Switzerland (Dec. 1990), pages 608-615.

[23] A. Sopczak, *Search for Non-minimal Higgs Bosons in Z^0 Decays with the L3 Detector at LEP*, Ph. D. Thesis, University of California, San Diego, 1992, 243 pages. Summary in: *The Fermilab meeting. DPF 92. 7^{th} Meeting of the American Physical Society Division of Particles and Fields, Vol. I*, Fermilab, Batavia, Illinois, Nov. 10-14, 1992, C.H. Albright, P.H. Kasper, R. Raja, and J. Yoh (eds.), World Scientific, Singapore (1993), pages 470-473.

[24] G. Gopal. Talk given at Aspen Winter Conference on *Particle Physics Before the Year 2000*, Aspen, Colorado, January, 1994.

[25] K.G. Chetyrkin, J.H. Kühn, and A. Kwiatkowski, "Perturbative QCD corrections to the Z boson width and the Higgs decay rate," TTP-94-10, Jul 1994, 14 pages. Talk given at *Rencontre de Moriond on QCD*, Meribel, France, Mar 19-26, 1994 and *Workshop on QCD at LEP*, Aachen, Germany, Apr 11-14, 1994 and *Zeuthen Workshop on Elementary Particle Theory: Physics at LEP200 and Beyond*, Teupitz, Germany, Apr. 10-15, 1994.

[26] M. Davier, "Searches for new particles at LEP," in: *Proceedings of the Joint International Lepton-Photon Symposium & Europhysics Conference on High Energy Physics*, Geneva, Switzerland July 25 - August 1, 1991, Vol. 2 - Plenary Sessions, S. Hegarty, K. Potter, and E. Quercigh (eds.), World Scientific, Singapore (1992), pages 153-179.

[27] M. Drees and X. Tata, "How model dependent are sparticle mass bounds from CERN LEP?" Phys. Rev. D 43 (1991): 2971-2988.

[28] H. Baer, M. Drees, and X. Tata, "Constraints on supersymmetric particles from the LEP data on Z^0 decay properties," Phys. Rev. D 41 (1990): 3414-3420.

[29] J. Ellis, G. Ridolfi, and F. Zwirner, "Pursuing supersymmetry in Z^0 decays," Phys. Lett. B 237 (1990) 423-430.

[30] D. Decamp *et al.* (ALEPH Collaboration), "Search for neutralino production in Z decays," Phys. Lett. B 244 (1990): 541-550.

[31] D. Decamp *et al.* (ALEPH Collaboration), "Search for new particles in Z decays using the ALEPH detector," Phys. Rep. 216 (1992): 253-340.

[32] M.Z. Akrawy *et al.* (OPAL Collaboration), "A direct search for neutralino production at LEP," Phys. Lett. B 248 (1990): 211-219.

[33] A. Olchevski, "Electroweak data from LEP," from talk presented at *Physics in Collision Workshop* held at Florida State University in Talahassee, FL, June 1994.

[34] G. Altarelli, "The Standard electroweak theory and its experimental tests," CERN-TH.6867/93, April 1993, 62 pages, lectures given at *32. Internationale Universitätswochen für Kern- und Teilchenphysik*, Schladming, Austria, Feb. 24 - Mar. 5, 1993.

[35] S. Abachi *et al.* (DØ Collaboration), "Search for the top quark in $p\bar{p}$ collisions at $\sqrt{s} = 1.8\,\mathrm{TeV}$," Phys. Rev. Lett. 72 (1994): 2138-2142.

[36] F. Abe *et al.* (CDF Collaboration), "Evidence for top quark production in $\bar{p}p$ collisions at $\sqrt{s} = 1.8\,\mathrm{TeV}$," Phys. Rev. D 50 (1994): 2966-3026.

[37] D. Schaile, "Tests of the electroweak theory at LEP," CERN-PPE/93-213, Dec. 9, 1993, 71 pages.

[38] P. Langacker, "Precision tests of the Standard Model," in: *Recent Directions in Particle Theory: from Superstrings and Black Holes to the Standard Model, Proceedings of the 1992 Theoretical Advanced Study Institute in Elementary Particle Physics*, Boulder, Colorado, June 1-26, 1992, J. Harvey and J. Polchinski (eds.), World Scientific, Singapore (1992), pages 141-162.

[39] B. Adeva *et al.* (L3 Collaboration), "Mass limits for scalar muons, scalar electrons, and winos from e^+e^- collisions near $\sqrt{s} = 91\,\mathrm{GeV}$," Phys. Lett. B 233 (1989): 530-537.

[40] D. Decamp *et al.* (ALEPH Collaboration), "Search for supersymmetric particles using acoplanar charged-particle pairs from Z^0 decays," Phys. Lett. B 236 (1990): 86-94.

[41] M.Z. Akrawy *et al.* (OPAL Collaboration), "A search for acoplanar pairs of leptons or jets in Z^0 decays. Mass limits on supersymmetric particles," Phys. Lett. B 240 (1990): 261-270.

[42] P. Abreu *et al.* (DELPHI Collaboration), "A search for sleptons and gauginos in Z^0 decays," Phys. Lett. B 247 (1990): 157-166.

[43] O. Adriani *et al.* (L3 Collaboration), "Results from the L3 experiment at LEP," Phys. Rep. 236 (1993): 1-146.

[44] P. Abreu *et al.* (DELPHI Collaboration), "Search for scalar quarks in Z^0 decays," Phys. Lett. B 247 (1990): 148-156.

[45] R. Akers *et al.* (OPAL Collaboration), "Search for a scalar top quark using the OPAL detector," Phys. Lett. B 337 (1994): 207-218.

[46] G. Giacomelli and P. Giacomelli, "Particle searches at LEP," Riv. del Nuovo Cimento 16(3) (1993): 1-58.

[47] Z. Kunszt and F. Zwirner, "Testing the Higgs sector of the Minimal Supersymmetric Standard Model at large hadron colliders," Nucl. Phys. B 385 (1992): 3-75.

[48] J.-F. Grivaz, "Prospects for supersymmetry discoveries at future e^+e^- colliders," in: *Properties of SUSY Particles: Proceedings of the 23rd Workshop of the INFN Eloisatron Project*, Erice, Sicily, Italy, Sept. 28 - Oct. 4, 1992, L. Cifarelli and V.A. Khoze (eds.), World Scientific, Singapore (1993), pages 131-152.

[49] A. Bartl, H. Fraas, W. Majerotto, and B. Mößlacher," "Chargino production at LEP200," Z. Phys. C 55 (1992): 257-264.

[50] V.D. Barger and R.J.N. Phillips, *Collider Physics*, Addison-Wesley Publ. Co., Redwood City, CA, 1987.

[51] D.W. Duke and J.F. Owens, "Q^2-dependent parametrizations of parton distribution functions," Phys. Rev. D 30 (1984): 49-54.

[52] J.F. Owens, "An updated set of parton distribution parametrizations," Phys. Lett. B 266 (1991): 126-130.

[53] E. Eichten, I. Hinchliffe, K. Lane, and C. Quigg, "Supercollider physics," Rev. Mod. Phys. 56 (1984): 579-707. *Erratum*: Rev. Mod. Phys. 58 (1986): 1065-1073.

[54] P.N. Harriman, A.D. Martin, W.J. Stirling, and R.G. Roberts, "Parton distributions extracted from data on deep inelastic lepton scattering, prompt photon production and the Drell-Yan process," Phys. Rev. D 42 (1990): 798-810.

[55] J. Botts, J.G. Morfin, J.F. Owens, J. Qiu, W.K. Tung, and H. Weerts, "CTEQ parton distributions and flavor dependence of the sea quarks," Phys. Lett. B 304 (1993): 159-166.

[56] M. Spira, A. Djouadi, D. Graudenz, and P.M. Zerwas, "SUSY Higgs production at proton colliders," Phys. Lett. B 318 (1993): 347-353.

[57] D. Graudenz, M. Spira, and P.M. Zerwas "QCD corrections to Higgs-boson production at proton-proton colliders," Phys. Rev. Lett. 70(10) (1993): 1372-1375.

[58] S. Dawson, "Radiative corrections to Higgs boson production," Nucl. Phys. B 359 (1991): 283-300.

[59] S. Dawson and R. Kauffman, "QCD corrections to Higgs boson production," BNL-60769, Sept. 1994, 4 pages.

[60] S. Dawson and R. Kauffman, "QCD corrections to Higgs boson production: non-leading terms in the heavy quark limit," Phys. Rev. D 49 (1994): 2298-2309.

[61] R. P. Kauffman and W. Schaffer, "QCD corrections to production of Higgs pseudoscalars," Phys. Rev. D 49 (1994): 551-554.

[62] H. Baer, M. Bisset, C. Kao, and X. Tata, "Detecting Higgs boson decays to neutralinos at hadron supercolliders," Phys. Rev. D 50 (1994): 316-324.

[63] D.A. Dicus and S. Willenbrock, "Higgs-boson production from heavy-quark fusion," Phys. Rev.D 39 (1989): 751-757.

[64] J.F. Gunion, H.E. Haber, G. Kane, and S. Dawson, *The Higgs Hunter's Guide*, Addison-Wesley, Redwood City, CA, 1990. *Erratum*: Univ. of Calif., Santa Cruz, preprint SCIPP-92-58, Dec. 1992, 5 pages, hep-ph bull. board: 9302272.

[65] J.F. Gunion, H.E. Haber, and C. Kao, "Searching for the CP-odd Higgs boson of the minimal supersymmetric model at hadron supercolliders," Phys. Rev. D 46 (1992): 2907-2917.

[66] W.-Y. Keung and W.J. Marciano, "Higgs-scalar decays: $H \to W^{\pm} + X$," Phys. Rev. D 30 (1984): 248-250.

[67] M. Primiä, "The CMS experiment," in: *The Fourth Nordic LHC Meeting*, Helsinki, Finland, June 8-10, 1994, P. Eerola (ed.), Report Series, Univ. of Helsinki Res. Inst. for High Energy Phys., HU-SEFT R 1994-11, 47 pages.

[68] J. Gunion, R. Bork, H. Haber, and A Seiden, "Searching for CP-even Higgs bosons of the minimal supersymmetric model at hadron supercolliders," Phys. Rev. D 46 (1992): 2040-2051.

[69] E.L. Berger *et al.* (Solenoidal Detector Collaboration), *Expression of Interest by the Solenoidal Detector Collaboration to construct and operate a detector at the Superconducting Super Collider*, May 24, 1990 (corrected up to May 29, 1990), SDC Publ. No. SDC-90-00085, U.S. Govt. Printing Office (1990): 785-130-1016, 107 pages.

[70] E.L. Berger *et al.* (Solenoidal Detector Collaboration), *Letter of Intent by the Solenoidal Detector Collaboration to construct and operate a detector at the Superconducting Super Collider*, Nov. 30, 1990, SDC Publ. No. SDC-90-00151, 49 pages.

[71] E.L. Berger *et al.* (Solenoidal Detector Collaboration), *Technical Design of a detector to be operated at the Superconducting Super Collider*, April 1, 1992 (with corrections up to July 31, 1992), SDC Publ. No. SDC-92-00201, 532 pages.

[72] F. Abe *et al.* (CDF Collaboration), "Measurement of $\sigma B(W \to e\nu)$ and $\sigma B(Z^0 \to e^+e^-)$ in $\bar{p}p$ collisions at $\sqrt{s} = 1800\,\mathrm{GeV}$," Phys. Rev. D 44 (1991): 29-52.

[73] D.A. Dicus, C. Kao, and W.W. Repko, "Gluon production of gauge bosons," Phys. Rev. D 36 (1987): 1570-1572.

[74] N. Glover and J. van der Bij, "Z-boson pair production via gluon fusion," Nucl. Phys. B321 (1989): 561-590.

[75] J.F. Gunion, G.L. Kane, and J. Wudka, "Search techniques for charged and neutral intermediate-mass Higgs bosons," Nucl. Phys. B 299 (1988): 231-278.

[76] R. D. Kauffman and C.-P. Yuan, "Top-quark backgrounds to Higgs-boson decay to W^+W^-," Phys. Rev. D 42 (1990): 956-959.

[77] G. Kane and C.-P. Yuan, "How to study longitudinal W's in the TeV region," Phys. Rev. D 40 (1989): 2231-2244.

[78] J. Gunion, G.L. Kane, H.F.-W. Sadrozinski, A. Seiden, A.J. Weinstein, and C.P. Yuan, "Using the hadron multiplicity to distinguish real W's from QCD jet backgrounds," Phys. Rev. D 40 (1989): 2223-2230.

[79] M.H. Seymour, "Tagging a heavy Higgs boson," in: *proceedings of the European Committee for Future Accelerators Large Hadron Collider Workshop, Vol. II*, Aachen, Germany, Oct. 4-9, 1990, G. Jarlskog and D. Rein (eds.), CERN Rept. No. 90-10, Geneva, Switzerland (Dec. 1990), pages 557-569.

[80] D. Froidevaux, "Experimental review of the search for the Higgs boson," in: *proceedings of the European Committee for Future Accelerators Large Hadron Collider Workshop, Vol. II*, Aachen, Germany, Oct. 4-9, 1990, G. Jarlskog and D. Rein (eds.), CERN Rept. No. 90-10, Geneva, Switzerland (Dec. 1990), pages 444-473.

[81] C. Seez, T. Virdee, L. Dilella, R. Kleis, Z. Kunszt, and W.J. Stirling, "Photon decay modes of the intermediate mass Higgs," in: *Proceedings of the European Committee for Future Accelerators Large Hadron Collider Workshop, Vol. II*, Aachen, Germany, Oct. 4-9, 1990, G. Jarlskog and D. Rein (eds.), CERN Rept. No. 90-10, Geneva, Switzerland (Dec. 1990), pages 474-484.

[82] R.K. Ellis, I. Hinchliffe, M. Soldate, and J.J. van der Bij, "Higgs decay to $\tau^+\tau^-$: a possible signature of intermediate mass Higgs bosons at high energy hadron colliders," Nucl. Phys. B 297 (1988): 221-243.

[83] C. Barter, R. Partridge, A. Bay, A. Spadafora, S. Whitaker, A. Abashian, and R. Kass, "Detection of $H^0 \rightarrow \gamma\gamma$ at the SSC," in: *Proceedings of the Summer*

Study on High Energy Physics in the 1990's, Snowmass, Colorado, June 27-July 15, 1988, S. Jensen (ed.), World Scientific, Singapore (1989), pages 98-102.

[84] J.F. Gunion *et al.*, "Overview and progress in Higgs boson physics at the Superconducting Super Collider," in: *Research Directions for the Decade; Proceedings of the 1990 Summer Study on High Energy Physics*, Snowmass, Colorado, June 25 - July 13, 1990, World Scientific, Singapore (1992), pages 59-81.

[85] J.F. Gunion and G. Kane, "Motivation for an SSC detector with ultra-high resolution photon detection," in: *Research Directions for the Decade; Proceedings of the 1990 Summer Study on High Energy Physics*, Snowmass, Colorado, June 25 - July 13, 1990, World Scientific, Singapore (1992), pages 91-94.

[86] D. Gingrich *et al.* (ATLAS Collaboration), *ATLAS. Letter of Intent for a General-Purpose pp experiment at the Large Hadron Collider at CERN*, CERN/LHCC/92-4, LHCC/I 2, Oct. 1, 1992, 108 pages.

[87] R.-Y. Zhu, "Signal and background of $H \to \gamma\gamma$ with proposed GEM calorimeter systems," Cal Tech preprint CALT-68-1777, Mar. 1992, 25 pages; Y.-L. Ye and R.Y. Zhu, "γ/e discrimination with the proposed GEM central tracker," CALT-68-1908, Jan. 1994, 24 pages. See also: R. Steiner *et al.* (GEM Collaboration), *GEM Letter of Intent*, SSCL-SR-1184, GEM TN-92-49, Nov. 1991, 100 pages.

[88] P. Kalyniak, R. Bates, and J.N. Ng, "Two-photon decays of scalar and pseudoscalar bosons in supersymmetry," Phys. Rev. D 33 (1986): 755-762.

[89] R. Bates, J.N. Ng, and P. Kalyniak, "Two-photon decay widths of Higgs bosons in minimal broken supersymmetry," Phys. Rev. D 34 (1986): 172-181.

[90] J.F. Gunion, G. Gamberini, and S.F. Novaes, "Can the Higgs bosons of the minimal supersymmetric model be detected at a hadron collider via two-photon decays?" Phys. Rev. D 38 (1988): 3481-3487.

[91] T.J. Weiler and T.-C. Yuan, "Looking for SUSY virtually through loop-induced Higgs processes," Nucl. Phys. B318(1989): 337-374.

[92] H. Baer, M. Bisset, C. Kao, and X. Tata, "Observability of $\gamma\gamma$ decays of Higgs bosons from supersymmetry at hadron supercolliders," Phys. Rev. D 46 (1992): 1067-1075.

[93] J.F. Gunion and L.H. Orr, "Detecting the Higgs bosons of the minimal supersymmetric model," Phys. Rev. D 46 (1992): 2052-2067.

[94] V. Barger, M.S. Berger, A.L. Stange, and R.J.N. Phillips, "Supersymmetric Higgs boson hadroproduction and decays including radiative corrections," Phys. Rev. D 45 (1992): 4128-4147.

[95] V. Barger, K. Cheung, R.J.N. Phillips, and A.L. Stange, "Collider discovery limits for supersymmetric Higgs bosons," Phys. Rev. D 46 (1992): 4914-4929.

[96] J.F. Owens, "Large-momentum transfer production of direct photons, jets, and particles," Rev. Mod. Phys. 59 (1987): 465-503.

[97] D.A. Dicus and S.S.D. Willenbrock, "Photon pair production and the intermediate-mass Higgs boson," Phys. Rev. D 37 (1988): 1801-1809.

[98] B. Bailey and J.F. Owens, "Order-α_s two-photon background study for the intermediate mass Higgs boson," Phys. Rev. D 47 (1993): 2735-2738.

[99] H. Baer and J.F. Owens, "Two-photon backgrounds for the intermediate mass Higgs boson," Phys. Lett. B 205 (1988): 377-380.

[100] A. Djouadi, M. Spira, and P.M. Zerwas, "Two-photon decay widths of Higgs particles," Phys. Lett. B 311 (1993): 255-260.

[101] S. Dawson and R.P. Kauffman, "QCD corrections to the Higgs-boson decay $H \rightarrow \gamma\gamma$," Phys. Rev. D 47 (1993): 1264-1267.

[102] D. Pierce and A. Papadopoulos, "Radiative corrections tothe Higgs-boson decay rate $\Gamma(H \rightarrow ZZ)$ in the minimal supersymmetric model," Phys. Rev. D 47 (1993): 222-231.

[103] K. Melnikov, M. Spira, and O. Yakovlev, "Threshold effects in two-photon decays of Higgs particles," DESY 94-076, 14 pages.

[104] H. Baer, M. Bisset, D. Dicus, C. Kao, and X. Tata, "Search for Higgs bosons of minimal supersymmetry: impact of supersymmetric decay modes," Phys. Rev. D 47 (1993): 1062-1079.

[105] A.B. Lahanas and D.V. Nanopolous, "The road to no-scale supergravity," Phys. Rep. 145 (1987): 1-139.

[106] J. Ellis and F. Zwirner, "Experimental predictions from a minimal version of the supersymmetric standard model," Nucl. Phys. B 338 (1990): 317-348.

[107] R. Arnowitt and P. Nath, "Supersymmetric mass spectrum in $SU(5)$ supergravity grand unification," Phys. Rev. Lett. 69 (1992): 725-727.

[108] S. Kelly, J.L. Lopez, D.V. Nanopoulos, H. Pois, and K. Yuan, "Aspects of radiative electroweak breaking in supergravity models," Nucl. Phys. B 398 (1993): 3-51.

[109] J. Hisano, H. Murayama, and T. Yanagida, "Nucleon decay in the minimal supersymmetric $SU(5)$ grand unification," Nucl. Phys. B 402 (1993): 46-84.

[110] V. Barger, M.S. Berger, and P. Ohmann, "Supersymmetric particle spectrum," Phys. Rev. D 49 (1994): 4908-4930.

[111] G.L. Kane, C. Kolda, L. Roszkowski, and J.D. Wells, "Study of constrained minimal supersymmetry," Phys. Rev. D 49 (1994): 6173-6210.

[112] J.F. Gunion and H.E. Haber,

"Higgs bosons in supersymmetric models (I)," Nucl. Phys. B 272: 1-76; "Higgs bosons in supersymmetric models (II). Implications for phenomenology, Nucl. Phys. B 278 (1986): 449-492; "Higgs bosons in Supersymmetric models (III). Decays into neutralinos and charginos," Nucl. Phys. B 307 (1988): 445-475; *Errata*: Nucl. Phys. B 402 (1993): 567-569.

[113] J.F. Gunion, H.E. Haber, M. Drees, X. Tata, R. Godbole, D. Karatas, and N. Tracas, "Decays of the Higgs bosons to neutralinos and charginos in the minimal supersymmetric model: calculation and phenomenology," Int. J. Mod. Phys. 2 (1987): 1035-1053.

[114] H. Baer, D. Dicus, M. Drees, and X. Tata, "Higgs-boson signals in superstring-inspired models at hadron supercolliders," Phys. Rev. D 36 (1987): 1363-1377.

[115] K. Griest and H.E. Haber, "Invisible decays of Higgs bosons in supersymmetric models," Phys. Rev. D 37 (1988): 719-728.

[116] H. Baer, A. Bartl, D. Karakas, W. Majerotto, and X. Tata, "Searching for supersymmetry at e^+e^- supercolliders," Int. J. Mod. Phys. A4 (1989): 4111-4163.

[117] J.F. Gunion and H.E. Haber, "Two-body decays of neutralinos and charginos," Phys. Rev. D 37 (1988): 2515-2532.

[118] T. Schimert, C. Burgess, and X. Tata, "Lepton distributions from the decay of $\widetilde{W}$ pairs at e^+e^- supercolliders," Phys. Rev. D 32 (1985): 707-720.

[119] H. Baer, M. Drees, and X. Tata, "Phenomenology of light top squarks at the Fermilab Tevatron," Phys. Rev. D (1991): 725-740.

[120] M. Fukugita, H. Murayama, M. Yamaguchi, and T. Yanagida, "Case of the light scalar top quark," Phys. Rev. Lett. (1994): 3009-3012.

[121] H. Baer, J. Sender, and X. Tata, "The search for top squarks at the Fermilab Tevatron collider," Phys. Rev. D 50 (1994): 4517-4528.

[122] W. de Boer, R. Ehret, and D.I. Kazakov, "Is the stop mass below the top mass," Phys. Lett. B 334 (1994): 220-228.

[123] M. Felcini, "Search for top decays to charged Higgs bosons," in: *Proceedings of the European Committee for Future Accelerators Large Hadron Collider Workshop, Vol. II*, Aachen, Germany, Oct. 4-9, 1990, G. Jarlskog and D. Rein (eds.), CERN Rept. No. 90-10, Geneva, Switzerland (Dec. 1990), pages 414-417.

[124] J.L. Hewett, "Top ten models constrained by $b \to s\gamma$," presented at *21st SLAC Summer Inst. on Particle Physics: Spin Structure in High Energy Processes*, SLAC, July 26 - Aug. 6, 1993, SLAC-PUB-6521, 25 pages; and also, "Constraints on the charged Higgs sector from B physics," in: *The Fermilab meeting. DPF 92. 7th Meeting of the American Physical Society Division of Particles and Fields, Vol. I*, Fermilab, Batavia, Illinois, Nov. 10-14, 1992, C.H. Albright, P.H. Kasper, R. Raja, and J. Yoh (eds.), World Scientific, Singapore (1993), pages 496-500.

[125] J.L. Hewett, "Can the decay $b \to s\gamma$ close the supersymmetric Higgs boson production window?" Phys. Rev. Lett. 70 (1993): 1045-1048.

[126] R. Barbieri, F. Caravaglios, M. Frigeni, and M.L. Mangano, "Production and leptonic decays of charginos and neutralinos in hadronic collisions," Nucl. Phys. B 367 (1991): 28-59.

[127] H. Baer, F.E. Paige, S.D. Protopopescu, and X. Tata, "Simulating supersymmetry with ISAJET 7.0/ ISASUSY 1.0," Florida State preprint FSU-HEP-930329, Univ. of Hawaii preprint UH-511-764-93, April 1993, 17 pages, hep-ph bull. board: 9305342.

[128] V. Barger and T. Han, "Triple gauge boson production at e^+e^- and pp supercolliders," Phys. Lett. B 212 (1988): 117-122.

[129] V. Barger, A.L. Stange, and R.J.N. Phillips, "Four-heavy-quark hadroproduction," Phys. Rev. D 44 (1991): 1987-1996.

[130] H. Baer, X. Tata, and J. Woodside, "Multilepton signals from supersymmetry at hadron supercolliders," Phys. Rev. D 45 (1992): 142-160.

[131] G. Unal, D. Cavalli, L. Cozzi, and L. Perini, "Prospects for Higgs search with taus in the MSSM," EAGLE Internal Note, PHYS-NO-005, June 1992, 54 pages.

[132] T. Sjöstrand, "High-energy-physics event generation with PYTHIA 5.7 and JETSET 7.4," Computer Phys. Commun. 82 (1994): 74-90; and, "PYTHIA 5.7 and JETSET 7.4 physics and manual," CERN-TH.7112-93, Feb. 1994, 305 pages (revised version). References for older PYTHIA versions used in studies cited: H.-U. Bengtsson and T. Sjöstrand, "The LUND Monte Carlo for hadronic processes — PYTHIA version 4.8, Comp. Phys. Comm. 46 (1987): 43-82, "The LUND Monte Carlo for jet fragmentation and e^+e^- physics — JETSET version 6.3 — an update," Comp. Phys. Comm. 43 (1987): 367-379.

[133] I. Hinchliffe and S.F. Novaes, "Transverse-momentum distribution of Higgs bosons at the Superconducting Super Collider," Phys. Rev. D (1988): 3475-3480.

[134] L. DiLella, $H \rightarrow \tau^+\tau^-$ detection at the LHC," in: *Proceedings of the European Committee for Future Accelerators Large Hadron Collider Workshop, Vol. II*, Aachen, Germany, Oct. 4-9, 1990, G. Jarlskog and D. Rein (eds.), CERN Rept. No. 90-10, Geneva, Switzerland (Dec. 1990), pages 530-537.

[135] K. Bos, F. Anselmo, and B. van Eijk, $H^0 \rightarrow \tau^+\tau^-$ detection at the LHC," in: *Proceedings of the European Committee for Future Accelerators Large Hadron*

Collider Workshop, Vol. II, Aachen, Germany, Oct. 4-9, 1990, G. Jarlskog and D. Rein (eds.), CERN Rept. No. 90-10, Geneva, Switzerland (Dec. 1990), pages 538-546.

[136] C. Albajar *et al.* (UA1 Collaboration), "Events with large missing transverse energy at the CERN collider: I $W \to \tau\nu$ decay and test of τ-μ-e universality at $Q^2 = m_W^2$," Phys. Lett. B 185 (1987): 233-240.

[137] A. Savoy-Navarro, "The role of the τ lepton at pp colliders," in: *Proceedings of the Workshop on Tau Lepton Physics*, Orsay, France, Sept. 24-27, 1990, M. Davier and B. Jean-Marie (eds.), Gif-sur-Yvette, France, Ed. Frontieres (1991), pages 371-396.

[138] A. Rubbia, "Search for the Higgs boson at pp supercolliders," in: *Workshop on Physics and Experiments with Linear e^+e^- Colliders, Vol. II*, Waikaloa, Hawaii, Apr. 26-30, 1993, F.A. Harris, S.L. Olsen, S. Pakvasa, and X. Tata (eds.), World Scientific, Singapore (1993), pages 610-624.

[139] R. Kinnunen, "Higgs in CMS," in: *The Fourth Nordic LHC Meeting*, Helsinki, Finland, June 8-10, 1994, P. Eerola (ed.), Report Series, Univ. of Helsinki Res. Inst. for High Energy Phys., HU-SEFT R 1994-11, 37 pages.

[140] F. Pauss, lectures given in the CERN Academic Training Programme, Dec. 1991, and references therein.

[141] D.P. Roy, "Using τ polarization for the charged Higgs search at hadron colliders," Phys. Lett. B 277: 183-189.

[142] Y.-S. Tsai, "Decay correlations of heavy leptons in $e^+ + e^- \to \ell^+ + \ell^-$," Phys. Rev. D 4 (1971): 2821-2837.

[143] P. Aurenche and R. Kinnunen, "Missing energy sources at large p_T from standard QCD processes," Z. Phys. C 28 (1985): 261-268.

[144] A. Rougé, "Polarization observables in the $3\pi\nu$ decay mode of the τ," Z. Phys. C 48 (1990): 75-77.

[145] K. Hagiwara, A.D. Martin, and D. Zepprnfeld, "τ polarization measurements at LEP and SLC," Phys. Lett. B 235 (1990): 198-202.

[146] B. K. Bullock, K. Hagiwara, and A.D. Martin, "τ polarization as a signal of charged Higgs bosons," Phys. Rev. Lett. 67 (1991): 3055-3057.

[147] D. Decamp . *et al.* (ALEPH Collaboration), "Measurement of the polarization of τ leptons produced in Z decays," Phys. Lett. B 265 (1991): 430-444.

[148] D.P. Roy, "Discovery limit of the charged Higgs boson via top quark decay at future hadron colliders," Phys. Lett B 283 (1992): 403-410.

[149] R.M. Barnett, J.F. Gunion, H.E. Haber, I. Hinchliffe, B. Hubbard, and H.-J. Trost, "Searching for top decays to charged Higgs bosons with the SLD detector," in: *Research Directions for the Decade; Proceedings of the 1990 Summer Study on High Energy Physics*, Snowmass, Colorado, June 25 - July 13, 1990, World Scientific, Singapore (1992), pages 82-90.

[150] R.M. Barnett *et al.*, "Report of the subgroup on the top quark," in: *Research Directions for the Decade; Proceedings of the 1990 Summer Study on High Energy Physics*, Snowmass, Colorado, June 25 - July 13, 1990, World Scientific, Singapore (1992), pages 354-365.

[151] R.M. Barnett, R. Cruz, J.F. Gunion, and B. Hubbard, "Charged Higgs bosons at the Superconducting Super Collider," Phys. Rev. D 47 (1993): 1048-1061.

[152] Z. Kunszt, Z. Trócsányi, and J.W. Stirling, "Clear signal of intermediate mass Higgs boson production at LHC and SSC," Phys. Lett. B 271 (1991): 247-255.

[153] A. Ballestrero and E. Maina, "Prompt photon pair production in association with top-antitop pairs. An important background to intermediate mass Higgs detection," Phys. Lett. B 268 (1991): 437-440.

[154] M. L. Mangano *et al.* (SDC Collaboration),
"Production of $WH \to W\gamma\gamma \to e/\mu\,\gamma\gamma$," SDC Collaboration Note SSC-SDC-90-00113, Nov. 1990, 14 pages.

[155] A. Stange, W. Marciano, and S. Willenbrock, "Associated production of Higgs and weak bosons, with $H \to b\bar{b}$, at hadron colliders," Phys. Rev. D 50: 4491-4498.

[156] S. Mrenna and G.L. Kane, "Possible detection of a Higgs boson at higher luminosity hadron colliders," Cal Tech preprint CALT-68-1938, June 1994, 23 pages, hep-ph bull. board: 9406337.

[157] J. Dai, J.F. Gunion, and R. Vega, "Using b-tagging to detect $t\bar{t}$ Higgs production with $H \to b\bar{b}$," Phys. Rev. Lett. 71 (1993): 2699-2702.

[158] J. Dai, J.F. Gunion, and R. Vega, "Guaranteed detection of a Minimal Supersymmetric Model Higgs boson at hadron supercolliders," Phys. Lett. B 315 (1993): 355-359.

[159] J. Dai, J.F. Gunion, and R. Vega, "LHC detection of neutral MSSM Higgs bosons via $gg \to b\bar{b}h \to b\bar{b}b\bar{b}$," U.C. Davis preprint UCD-94-7, March 1994, 11 pages, hep-ph bull. board: 9403362.

[160] H. Baer, M. Bisset, X. Tata, and J. Woodside, "Supercollider signals from gluino and squark decays to Higgs bosons," Phys. Rev. D 46 (1992): 303-314.

[161] D. R. Claes *et al.* (DØ Collaboration), "Search for squarks and gluinos in DØ," Fermilab-Conf-94/290-E, Sept. 1994, 4 pages; presented at the 8^{th} *Meeting of the Division of Particles and Fields of the American Physical Society (DPF '94)*, Albuquerque, New Mexico, August 2-6, 1994.

[162] P. Janot, "Higgs boson search at a 500 GeV e^+e^- collider," in: *Workshop on Physics and Experiments with Linear e^+e^- Colliders, Vol. II*, Waikaloa, Hawaii, Apr. 26-30, 1993, F.A. Harris, S.L. Olsen, S. Pakvasa, and X. Tata (eds.), World Scientific, Singapore (1993), pages 46-71.

[163] H. Baer, C. Kao, and X. Tata, "Searching for the pseudoscalar Higgs boson of minimal supersymmetry via its ZH_ℓ decay mode at hadron supercolliders," Phys. Lett. B 303 (1993): 284-288.

[164] H. Baer, M. Drees, C. Kao, M. Nojiri, and X. Tata, "Supercollider signatures of supergravity models with Yukawa unification," Florida State preprint FSU-HEP-940311, Mar. 1994, 33 pages, hep-ph bull. board: 9403307.

[165] V. Barger, R.J.N. Phillips, and D.P. Roy, "Heavy charged Higgs signals at the LHC," Phys. Lett. B 324 (1994): 236-240.

[166] J.F. Gunion, "Detecting the tb decays of a charged Higgs boson at a hadron supercollider," Phys. Lett. B 322 (1994): 125-130.

[167] H. Baer and X. Tata, "Probing charginos and neutralinos beyond the reach of the CERN e^+e^- collider LEP at the Fermilab Tevatron collider," Phys. Rev. D 47 (1993): 2739-2745.

[168] P.H. Chankowski, S. Pokorski, and J. Rosiek, "Supersymmetric Higgs boson decays with radiative corrections," Nucl. Phys. B 423 (1994): 497-531. *Erratum:* Padova preprint DFPD 92/TH/60/ERR, Mar. 1993, 6 pages.

[169] P. Fayet and J. Iliopoulos, "Spontaneously broken supergauge symmetries and Goldstone spinors," Phys. Lett. B 51 (1974): 461-464.

[170] F. Halzen and A.D. Martin, *Quarks and Leptons: an Introductory Course in Modern Particle Physics*, John Wiley & Sons, New York, NY, 1984.

[171] T. Okada, H. Yamaguchi, and T. Tanagida, "Upper bound of the lightest Higgs boson mass in the minimal supersymmetric standard model," Prog. Theor. Phys. Lett. 85 (1991): 1-5.

[172] H.E. Haber and R. Hemfling, "Can the mass of the lightest Higgs boson of the minimal supersymmetric model be larger than m_Z?" Phys. Rev. Lett. 66 (1991): 1815-1818.

[173] J. Ellis, G. Ridolfi, and F. Zwirner, "Radiative corrections to the masses of supersymmetric Higgs bosons," Phys. Lett. B 257 (1991): 83-91.

[174] S.P. Li and M. Sher, "Upper limit to the lightest Higgs mass in supersymmetric models," Phys. Lett. B. 140 (1984): 339-343.

[175] J.F. Gunion and A.Turski, "Renormalization of Higgs boson mass sum rules and screening," Phys. Rev. D 39 (1989): 2701-2714; "Screening of large supersymmetric breaking in low-energy physics," Phys. Rev. D 40 (1989): 2325-2332; "Corrections to Higgs boson mass sum rules from the sfermion sector of a supersymmetric model," Phys. Rev. D 40 (1989): 2333-2339.

[176] M.S. Berger, "Radiative corrections to Higgs-boson-mass sum rules in the minimal supersymmetric extension to the standard model," Phys. Rev. D 41 (1990): 225-239.

[177] T. Okada, H. Yamaguchi, and T. Yanagida, "Renormalization group analysis on the Higgs mass in the softly broken supersymmetric model," Phys. Lett. 262 (1991): 54-58.

[178] J.R. Espinosa and M. Quirós, "Two loop radiative corrections to the mass of the lightest Higgs boson in supersymmetric standard models," Phys. Lett. B 266 (1991): 389-396.

[179] P.H. Chankowski, S. Pokorski, and J. Rosiek, "Is the lightest supersymmetric Higgs boson distinguishable from the minimal Standard Model one?" Phys. Lett. B 281 (1992): 100-105.

[180] M.A. Díaz and H.E. Haber, "One-loop radiative corrections to the charged-Higgs-boson mass of the minimal supersymmetric model," Phys. Rev. D 45 (1992): 4246-4260.

[181] M.A. Díaz and H.E. Haber, "Can the Higgs-boson mass be entirely due to radiative corrections?" Phys. Rev. D 46 (1992): 3086-3103.

[182] H.E. Haber and R. Hemfling, "Renormalization-group-improved Higgs sector of the Minimal Supersymmetric Model," Phys. Rev. D 48 (1993): 4280-4309.

[183] H.E. Haber, "Higgs bosons in the Minimal Supersymmetric Model: the influence of radiative corrections," in: *Perspectives on Higgs Physics*, G.L. Kane (ed.), World Scientific, Singapore (1993), pages 79-125.

[184] K. Susaki, M. Carena, and C.E.M. Wagner, "Renormalization-group analysis of the Higgs sector in the minimal supersymmetric standard model," Nucl. Phys. B 381 (1992): 66-86.

[185] P.H. Chankowski, S. Pokorski, and J. Rosiek, "Complete on-shell renormalization scheme for the minimal supersymmetric Higgs sector," Nucl. Phys. B 423 (1994): 437-496.

[186] P.H. Chankowski, S. Pokorski, and J. Rosiek, "Charged and neutral supersymmetric Higgs boson masses: complete one loop analysis," Phys. Lett. B 274 (1992): 191-198.

[187] P.H. Chankowski, S. Pokorski, and J. Rosiek, "One loop corrections to the supersymmetric Higgs boson couplings and LEP phenomenology," Phys. Lett. B 286 (1992): 307-314.

[188] S. Pokorski, J. Rosiek, and P.H. Chankowski, "Complete one-loop analysis of the minimal supersymmetric Higgs sector, in : *Proc. of the XXVI Internatl. Conf. on High Energy Physics Vol. II*, Dallas, Texas, August 6-12 1992, J.R. Sanford (ed.), American Institute of Physics Conference Proc. No. 272 (1993), pages 1368-1373.

[189] A. Brignole, "Radiative corrections to the supersymmetric charged Higgs boson mass," Phys. Lett. B 277 (1992): 313-323.

[190] A. Brignole, "Radiative corrections to the supersymmetric neutral Higgs boson masses," Phys. Lett. B 281 (1992): 284-294.

[191] A. Yamada, "Radiative corrections to the Higgs masses in the Minimal Supersymmetric Standard Model," Phys. Lett. B 263 (1991): 233-238.

[192] R.H. Hemfling, "Radiative corrections to the Higgs sector in the Minimal Supersymmetric Model," Ph.D. Thesis, University of California, Santa Cruz, SCIPP preprint 92-28, Dec. 1992, 99 pages.

[193] A. Dabelstein, "The one loop renormalization of the MSSM Higgs sector and its application to the neutral scalar Higgs masses," Karlsruhe U., ITP, preprint KA-THEP-5-1994, Sept. 1994, 37 pages, hep-ph bull. board: 9409375.

[194] A. Dabelstein "Radiative corrections to the Higgs sector in the standard model and in the minimal supersymmetric standard model," Ph.D. Thesis, Max-Planck-Institute, Munich, preprint MPI-PH/93-64, Dec. 1993, 141 pages.

[195] R. Barbieri, F. Caravaglio, and M. Frigeni, "The supersymmetric Higgs for heavy superpartners," Phys. Lett. B 258 (1991): 167-170.

[196] R. Barbieri and M. Frigeni, "The supersymmetric Higgs searches at LEP after radiative corrections," Phys. Lett. B 258 (1991): 395-398.

[197] J. Ellis, G. Ridolfi, and F. Zwirner, "On radiative corrections to the supersymmetric Higgs boson masses and their implications for LEP searches," Phys. Lett. B 262: (1991): 477-484.

[198] A. Brignole, J. Ellis, G. Ridolfi, and F. Zwirner, "The supersymmetric charged Higgs boson mass and LEP phenomenology", Phys. Lett. B 271 (1991): 123-132. *Erratum*: Phys. Lett. B 273 (1991): 550.

[199] F. Zwirner, "The hunt for supersymmetric Higgs bosons after the inclusion of radiative corrections," in: *Electroweak Interactions and Unified Theories. Proceedings, Leptonic Session of the 26th Rencontre de Moriond*, Les Arcs, France, Mar. 10-17, 1991, J. Tran Thanh Van (ed.), Gif-sur-Yvette, France Ed. Frontieres (1991), pages 425-434.

[200] H. Eberl and W. Majerotto, "Radiative corrections to the supersymmetric Higgs boson masses with the effective potential approximation," preprint HEPHY-PUB 593/93 Dec. 1993, 19 pages.

[201] D.M. Pierce, "Radiative corrections to the Higgs sector of the minimal supersymmetric model," Ph.D. Thesis, University of California, Berkeley, preprint LBL-33453, Jan. 1993, 55 pages.

[202] D.M. Pierce, A. Papadopoulos, and S.B. Johnson, "Limits on the CP-even Higgs-boson masses in the Minimal Supersymmetric Model," Phys. Rev. Lett. 68 (1992): 3678-3681.

[203] J.L. Lopez and D.V. Nanopoulos, "New theoretical lower bounds on the Higgs sector of minimal SUSY," Phys. Lett. B 266 (1991): 397-402.

[204] S. Coleman, "Secret symmetry: an introduction to spontaneous symmetry breakdown and gauge fields," in: *Laws of Hadronic Matter. Subnuclear Series Vol. 11 Part A*, A. Zichichi (ed.), Academic Press, New York (1975), pages 138-223; from lectures at the 1973 Internatl. School of Subnuclear Physics, Erice, Sicily, Italy, July 8-26, 1973. Reprinted in: *Aspects of Symmetry. Selected Erice Lectures of Sidney Coleman*, Cambridge University Press, Cambridge (1985), pages 113-184.

[205] S. Coleman and E. Weinberg, "Radiative corrections as the origin of spontaneous symmetry breaking," Phys. Rev. D (1973): 1888-1910.

[206] S. Weinberg, "Perturbative calculations of symmetry breaking," Phys. Rev. D 7 (1973): 2887-2910.

[207] A. Brignole and F. Zwirner, "Radiative corrections to the decay $H \rightarrow hh$ in the Minimal Supersymmetric Standard Model," Phys. Lett. B (1993): 72-82.

[208] H.E. Haber, R. Hempfling, and Y. Nir, "The decay $h^0 \rightarrow A^0 A^0$ in the Minimal Supersymmetric Model," Pyhs. Rev. D 46 (1992): 3015-3024.

[209] D. Decamp *et al.* (ALEPH Collaboration), "Search for neutral Higgs bosons of the MSSM and other two-doublet models," Phys. Lett. B 265 (1991): 475-486.

[210] F.E. Paige and S.D. Protopopescu, "ISAJET 5.30: a Monte Carlo event generator for pp and $p\bar{p}$ interactions," in: *Proceedings of the 1986 Summer Study on the Physics of the Superconducting Supercollider*, Snowmass, Colorado, June 23-July 11, 1986, R. Donaldson and J. Marx (eds.), Division of Particles and Fields of the American Physical Society, pages 320-325. Also: F.E. Paige, "Simulation of hadronic reactions," *Proceedings of the Oregon Meeting, Annuall Meeting of the Division of Particles and Fields of the American Physical Society*, Eugene, Oregon, August 12-15, 1985, R.C. Hwa (ed.), World Scientific, Singapore (1865), pages 566-574.

[211] M. Drees and K. Hikasa, "Note on QCD corrections to Hadronic Higgs decay," Phys. Lett. B 240 (1990): 455-464, *Erratum*: Phys. Lett. B 262 (1991): 497.

[212] L.R. Surguladze, "Quark mass effects in fermionic decays of the Higgs boson in $\mathcal{O}(\alpha_s^2)$ perturbative QCD, Phys. Lett. B 338 (1994): 229-234.

[213] S. Bethke, "Tests of QCD," in : *Proc. of the XXVI Internatl. Conf. on High Energy Physics Vol. I*, Dallas, Texas, August 6-12 1992, J.R. Sanford (ed.), American Institue of Physics Conference Proc. No. 272 (1993), pages 81-113.

[214] R.K. Ellis, "Status of QCD," in: *The Fermilab meeting. DPF 92. 7th Meeting of the American Physical Society Division of Particles and Fields, Vol. I*, Fermilab, Batavia, Illinois, Nov. 10-14, 1992, C.H. Albright, P.H. Kasper, R. Raja, and J. Yoh (eds.), World Scientific, Singapore (1993), pages 167-182.

[215] C.J. Maxwell, "Theoretical status of α_s determination, in : *Proc. of the XXVI Internatl. Conf. on High Energy Physics Vol. I*, Dallas, Texas, August 6-12 1992, J.R. Sanford (ed.), American Institute of Physics Conference Proc. No. 272 (1993), pages 905-909.

[217] M. Drees and D.P. Roy, "Effect of QCD correction on the charged Higgs signature in top quark decay," Phys. Lett. B 269 (1991): 155-160.

[218] M.A. Díaz, "Electroweak corrections to the supersymmetric charged Higgs fermionic decay," Phys. Rev. D 48 (1993): 2152-2159.

[219] D. Wood, "Electroweak physics results from hadronic interactions," from talk presented at *Physics in Collision Workshop* held at Florida State University in Talahassee, FL, June 15, 1994.

[220] H. Baer, V. Barger, D. Karatas, and X. Tata, "Detecting gluinos at hadron supercolliders," Phys. Rev. D 36 (1987): 96-108.

[221] A.B. Lahanas, K. Tamvakis, and N.D. Tracas, "One loop corrections to the neutralino sector and radiative electroweak breaking in the MSSM," Pyhs. Lett. B 324 (1994): 387-396.

[222] D. Pierce and A. Papadopoulos, "The complete radiative corrections to the gaugino and higgsino masses in the Minimal Supersymmetric Model," The Johns Hopkins Univ. preprint JHU-TIPAC-940001, Feb. 1994, 16 pages, hep-ph bull. board: 9403240.

[223] D. Pierce and A. Papadopoulos, "Radiative corrections to neutralino and chargino masses in the Minimal Supersymmetric Model," Phys. Rev. D 50 (1994): 567-570.

[224] Douglas Adams, *Life, the Universe and Everything*, Pocket Books, New York, 1982.

Epilogue

"It's just," he burst out at last, "that if we don't go soon, we might get caught in the middle of it again. And there's nothing that depresses me more than seeing a planet being destroyed. Except possibly still being on it when it happens. *Or*, " he added in an undertone, "*hanging around cricket matches.*" [224]